CHARLES UNIVERSITY

Faculty of Science, Department of Inorganic Chemistry

Study programme: Inorganic Chemistry

Mgr. Filip Horký

Electronically dissymmetric ferrocene bisphosphines

PhD Thesis

Supervisor: prof. RNDr. Petr Štěpnička, Ph.D., DSc.

Prague, 2021

Motto:

If you only do what you can do, you will never be more than you are now.

Master Shifu, Kung Fu panda

Declaration:

I declare that this Thesis is my original work except as cited in the references. The Thesis has not been submitted or is currently being considered for any other degree.

Prohlášení:

Prohlašuji, že jsem závěrečnou práci zpracoval samostatně a že jsem uvedl všechny použité informační zdroje a literaturu. Tato práce ani její podstatná část nebyla předložena k získání jiného nebo stejného akademického titulu.

V Praze, 29. 9. 2021

Mgr. Filip Horký

Acknowledgments

Throughout the working of this Thesis I have received a great deal of support and assistance.

It is my great pleasure to express my deep sense of thanks to my supervisor **Prof. RNDr. Petr Štěpnička, Ph.D., DSc**. Petr, thank you for the opportunity to join your group and stand on my own feet. Thank you for your patience when results were poor, theories wild and data incomplete. Thank you for your time in reading and tirelessly correcting my manuscripts.

I would like to thank **RNDr. Ivana Císařová, CSc.** for many single-crystal X-ray measurements. Especially, many thanks for trying to measure the unstable, smelly, ugly, small, broken and fused ones.

I want to thank all my respected teachers, namely **Mgr. Vladimíra Horáčková** and **PaedDr. Jana Drlíková**, for great impulses on my path of knowledge.

I wish to thank talented, smart, and hard-working friends and colleagues from **laboratory 316**: **Karel, Jirka, Martin, Ondra, Petr, Michal, Zdeněk, Věrka, David, Jakub**. You made my time at the lab very delightful.

I must thank my Scout brothers, **Peťulka**, **Rys**, and **Hanes**, for not forgetting me and for great moments every time I run away from my alma mater.

Lastly, I would like to thank my **family** and **Jaroslava**, my love, for their incredible support, encouragement and understanding.

In the end, I would like to dedicate this work to my grandfather **Emil** who passed away during my first year at University.

The research project presented in this Thesis was financially supported by the Charles University Grant Agency (project no. 920119) and the Charles University Research Centre program (project no. UNCE/SCI/014). In addition, computational resources were provided by the CESNET (project LM2015042) and by the CERIT Scientific Cloud (project LM2015085), supported within the program “Projects of Large Research, Development, and Innovations Infrastructures”.

Table of Contents

Abstract

This Thesis describes the synthesis, reactivity, coordination properties, and catalytic activity of novel electronically dissymmetric bisphosphines structurally related to 1,1'-bis(diphenylphosphino)ferrocene (dppf).

First, a methylene spaced congener containing a primary phosphine group, which is stable in the air, $Ph_2PfcCH_2PH_2$ (fc = ferrocene-1,1'-diyl), was prepared. While studying its reactivity, an unprecedented stable primary phosphine oxide, $Ph_2PfcCH_2P(O)H_2$, was isolated. The primary phosphine, the corresponding phosphine oxide, dppf and the known bis-tertiary phosphine $Ph_2PfcCH_2PPh_2$ were studied as ligands in Ru(II) complexes. The catalytic activity of the defined complexes was compared in two ruthenium-catalyzed reactions: cyclization of (*Z*)-3-methylpent-2-en-4-yn-1-ol into 2,3-dimethylfuran and isomerization of estragole to anethole.

Second, the remarkable stability of the prepared primary phosphine oxide called for a detailed investigation of this poorly described class of compounds. As a result, stable primary phosphine chalcogenides lacking steric protection $FcCH_2P(Y)H_2$ (Fc = ferrocenyl; Y = O, S, Se) were isolated for the first time. These compounds were studied as ligands in reactions with hard and soft Lewis acids (Zn(II) and Ru(II)), and the reactivity of the P-H hydrogens was examined via reactions with various unsaturated substrates (RCHO, R_2CO, PhNCE; R = Me, Ph; E = O, S).

Subsequently, $Ph_2PfcCH_2PH_2$ was employed in acid-catalysed condensation reaction with acetylacetone to produce the bulky bisphosphine Ph_2PfcCH_2PCg (PCg = 1,3,5,7-tetramethyl-2,4,6-trioxa-8-phosphaadamantyl). Together with $Ph_2PfcPCg$, these bisphosphine ligands were used to prepare defined Pd(0) and Pd(II) complexes, and tested in selected catalytic reactions compared to their analogs derived from dppf. Specifically, the Pd(0) complexes were applied to C-H arylation of benzoxazoles with aryl chlorides, in which they showed excellent catalytic activity and selectivity. Conversely, the Pd(II) complexes were employed in cyanation of aryl bromides using $K_4[Fe(CN)_6]$ as a non-toxic cyanide source and in the Suzuki-Miyaura reaction of benzoyl chlorides with arylboronic acids to give benzophenones.

Last but not least, a new polar bidentate ligand $Ph_2PfcPO_3H_2$ was prepared by hydrolysis of the corresponding ethyl ester. However, although the ligand, its ammonium salts, and even Pd(II) complexes were prepared and fully characterized, they gradually decomposed upon storage, which prevented further studies into the catalytic properties of these compounds.

Keywords: *bisphosphines, ferrocene ligands, homogeneous catalysis, primary phosphine chalcogenides, phosphonic acid.*

Shrnutí

Předkládaná disertační práce popisuje syntézu, reaktivitu, koordinační vlastnosti a katalytickou aktivitu nových elektronově nesymetrických bisfosfinů vycházející ze struktury známého 1,1'-bis(difenylfosfino)ferrocenu (dppf).

V rámci této práce byl připraven na vzduchu stabilní derivát dppf obsahující methylenový můstek a primární fosfinovou skupinu, $Ph_2PfcCH_2PH_2$ (fc = ferrocen-1,1'-diyl). Studium reaktivity této látky vedlo k syntéze neobvykle stabilního primárního fosfinoxidu $Ph_2PfcCH_2P(O)H_2$. Společně s dppf a bisfosfinem $Ph_2PfcCH_2PPh_2$ byly tyto nové ligandy studovány v reakcích s ruthenatými ionty. Katalytická aktivita definovaných ruthenatých komplexů byla poté porovnána v cyklizaci (*Z*)-3-methylpent-2-en-4-yn-1-olu poskytující 2,3-dimethylfuran a v isomerizaci estragolu na anethol.

Druhá část práce byla věnovaná přípravě a studiu vlastností primárního fosfinoxidu, jelikož v literatuře bylo popsano jen velmi málo podobných látek. Tak byla získána první série stabilních primárních chalkogenidů bez sterického bránění $FcCH_2P(Y)H_2$ (Fc = ferrocenyl, Y = O, S, Se). Koordinační vlastnosti těchto sloučenin byly studovány v reakcích se zinečnatými a ruthenatými ionty, zatímco reaktivita P-H vazeb fosfinoxidu $FcCH_2P(O)H_2$ byla sledována prostřednictvím adičních reakcí na nenasycené systémy (RCHO, R_2CO, PhNCE; R = Me, Ph; E = O, S).

V další části práce byl $Ph_2PfcCH_2PH_2$ pomocí kondensační reakce s acetylacetonem převeden na bisfosfin Ph_2PfcCH_2PCg (PCg = 1,3,5,7-tetramethyl-2,4,6-trioxa-8-fosfaadamantyl). Spolu s $Ph_2PfcPCg$ byla tato látka použita pro přípravu definovaných Pd(0) a Pd(II) komplexů. Katalytická aktivita získaných komplexů byla poté porovnána s analogickými komplexy obsahující dppf jako ligand. Pd(0) komplexy byly konkrétně testovány v C-H arylaci benzoxazolů s arylchloridy a prokázaly v ní vysokou katalytickou aktivitu i selektivitu. Pd(II) komplexy byly zase využity v kyanaci arylbromidů netoxickým $K_4[Fe(CN)_6]$ a dále v Suzukiho-Miyaurově reakci benzoylchloridů s arylboronovými kyselinami poskytující benzofenony.

V neposlední řadě práce představuje syntézů nového polárního bidentátního ligandu $Ph_2PfcPO_3H_2$. Ačkoli byl tento ligand, jeho amonná sůl a Pd(II) komplexy připraven a plně charakterizován, látky podléhají rozkladu a nehodí se tak pro další využití v katalýze.

Klíčová slova: *bisfosfiny, ferrocenové ligandy, homogení katalýza, primární fosfino-chalkogenidy, fosfonová kyselina.*

1. Introduction

1.1 The chemistry of phosphines and phosphine chalcogenides

Analogously to the ubiquitous amines (NR_3), which can be formally derived from the simplest pnictogen hydride, ammonia (NH_3), by replacing one or more of the three hydrogen atoms, the heavier congeners, phosphines (PR_3), are molecules analogous to phosphane (PH_3). Phosphines share many common properties with amines, such as the formation of high-boiling liquids or solids with often an unpleasant odor, a trigonal pyramidal molecular geometry, and properties of Brönsted and Lewis bases. However, in contrast to amines, phosphines do not occur in Nature, are easily oxidized in the air giving the corresponding phosphine oxides, and also have a considerably higher energy barrier of pyramidal inversion,[1] which in turn allows for isolation of individual enantiomers of $PR^1R^2R^3$ that differ by configuration at the stereogenic phosphorus atom (Figure 1.1).

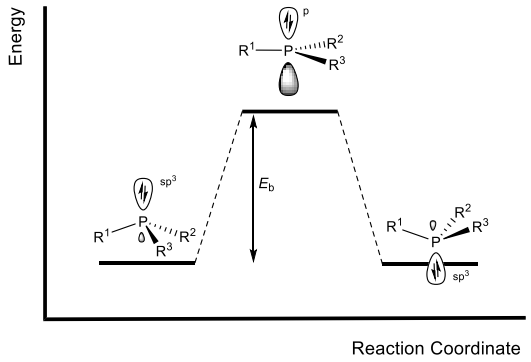

Figure 1.1. Reaction profile for pyramidal inversion (E_b = inversion energy barrier).

It should be pointed out that the complexity of organophosphorus compounds is considerable, so that there is an ample room for confusion even among specialists in the field. In this Introduction (focused only on "the tip of the iceberg"), attention will be given only to selected compounds relevant to the presented experimental work (Scheme 1.1).[2]

Phosphorus(III) compounds		Phosphorus(V) compounds	
H_3P	phosphane	$H_3P{=}O$	phosphine oxide
H_2PR	primare phosphine	$H_3P{=}S$	phosphine sulfide
HPR_2	secondary phosphine	$H_3P{=}Se$	phosphine selenide
PR_3	tertiary phosphine	$H_2P(O)(OH)$	phosphinic acid
$P(OR_3)$	phosphite	$HP(O)(OH)_2$	phosphonic acid

Scheme 1.1. Formulas and names of selected fundamental phosphorus compounds.

Primary phosphines are an exciting class of compounds with a notorious reputation of being toxic, extremely malodorous, volatile, and air-sensitive (Scheme 1.2). Primary phosphines with low molecular weights and without steric protection are often pyrophoric (spontaneously ignite in the air) or even explosive. These properties, and little applied chemistry to report, discouraged scientists from studying these molecules. Nevertheless, there are two main reasons why primary phosphines are receiving more attention nowadays. These include an increasing availability of inert atmosphere techniques and easy functionalization of P-H bonds leading to a range of products with wide potential applications, which are otherwise very difficult to achieve (Scheme1.3). In the current literature, one can even found the term "The primary phosphine renaissance".[3]

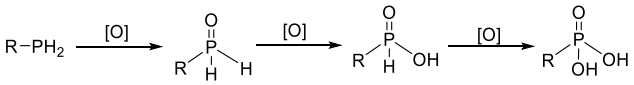

Scheme 1.2. Stepwise oxidation of primary phosphine to: phosphine oxide, phosphinic acid, and phosphonic acid.

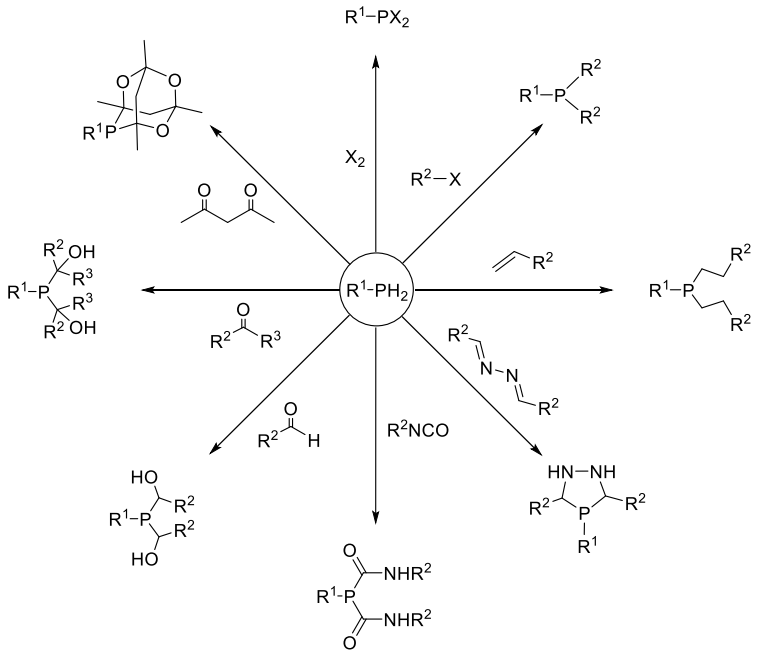

Scheme 1.3. Representative reactions of primary phosphines: substitution reactions and addition reactions with unsaturated molecules.

Primary phosphines are usually prepared by reduction of the appropriate halophosphines, alkyl phosphites, or phosphonates using lithium aluminum hydride. Alternative synthetic approaches are represented by reactions of organic halides with alkali metal phosphides or addition reactions between olefins and P-H reagents (Scheme 1.4).[4]

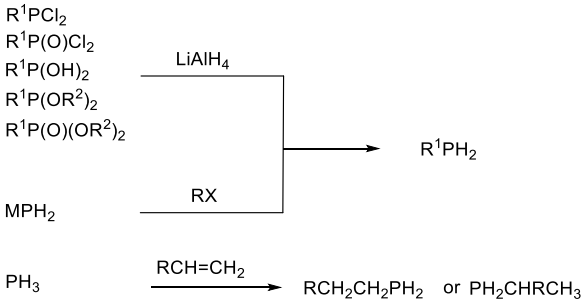

Scheme 1.4. Examples of common synthetic routes toward primary phosphines: reduction reactions, substitution reactions, and additions.

Indeed, some of the primary phosphines were found to be air-stable and were isolated. However, because of the lack of a general definition of air-stability, classification depends only on a subjective evaluation of the authors. Stable primary phosphines can be divided into two

classes. The first and more common are sterically protected compounds, in which the bulky substituent effectively improves oxidation resistance (Scheme 1.5, first line). The second, more exciting class of compounds, contains phosphines whose stability towards oxidation is difficult to rationalize (Scheme 1.5, second line). Typically, the backbone of these primary phosphines contains a heteroatom, conjugated system, or both. As far as steric hindrance cannot be the protecting factor in these compounds, stability must arise from electronic properties.[5] The prominent examples of air-stable primary phosphines are derived from ferrocene. However, only compounds containing a methylene or ethylene bridge, $Fc(CH_2)_nPH_2$ (n = 1, 2), are air-stable. If the phosphine moiety is directly bonded to the ferrocene backbone (e.g., $FcPH_2$), the molecule is air-sensitive. Even so, if the bridge is longer than two carbon atoms, the compounds are unstable again.[6]

In 2011, L. J. Higham *et al.* presented DFT calculations revealing a relationship between the stability of primary phosphines (18 examples) and the energy of singly occupied molecular orbital (SOMO) of their radical cation. The model universally predicted phosphines air stability/sensitivity and defined air-stability line at $E_{SOMO} = -10$ eV (Figure 1.2).[7]

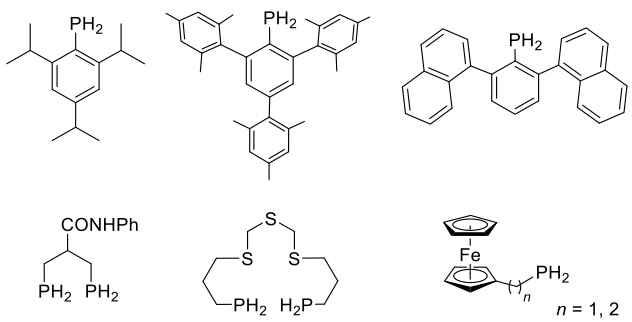

Scheme 1.5. Examples of air-stable primary phosphines. The first line: compounds with sterical encumbrance; second line: electronically stabilized molecules.

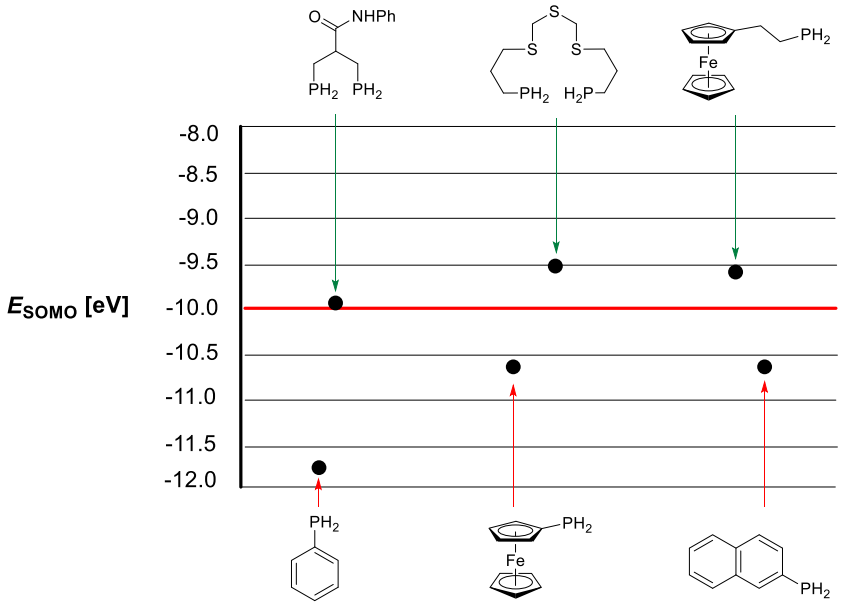

Figure 1.2. Plot of the calculated radical cation SOMO energies for the primary phosphines. The threshold at −10 eV separates air-sensitive and air-stable compounds (stable molecules have E_{SOMO} above or on this line).

Secondary phosphines, similar to their primary counterparts, are air-sensitive compounds (Scheme 1.6). Virtually all published synthetic procedures leading to these compounds involve the same general approach as mentioned in the previous paragraph focused on primary phosphines (Scheme 1.7). When the secondary phosphine is the synthetic target, the respective primary phosphine is the usual precursor, and where tertiary phosphine is the desired product, then secondary phosphine is often the entry point. An overalkylation of secondary phosphines is one of the main problems in their synthesis. The known reactivity of secondary phosphines results predominantly in the formation of new P-C bonds (Scheme 1.8). The current motivation for the synthesis of the secondary phosphines is the possibility to convert these molecules into chiral tertiary phosphines, which are valuable ligands for asymmetric homogeneous catalysis.[8]

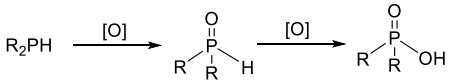

Scheme 1.6. Secondary phosphines can be oxidized to secondary phosphine oxides and phosphinic acids.

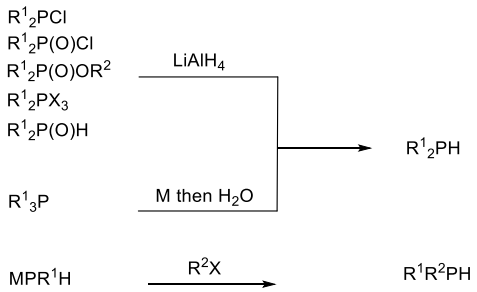

Scheme 1.7. Examples of common synthetic routes toward secondary phosphines. Reduction reactions and reactions involving phosphides.

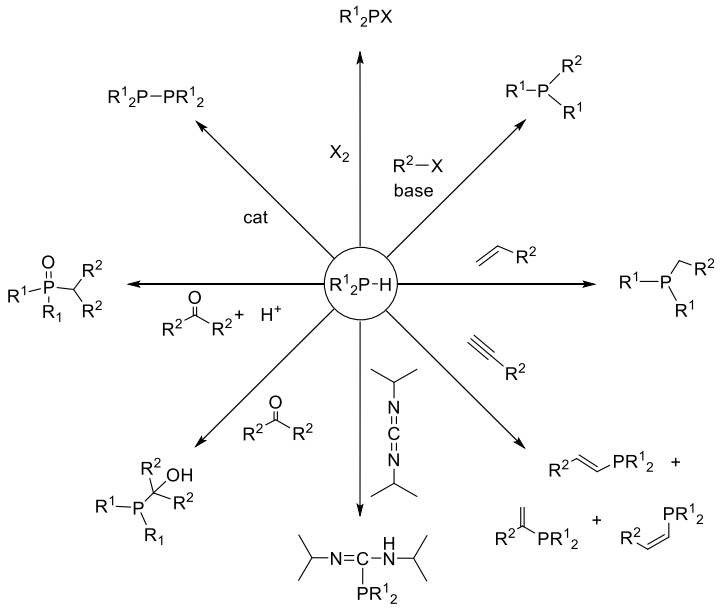

Scheme 1.8. Examples of reactions of secondary phosphines: substitution reactions, addition reactions with unsaturated molecules, and acidic-catalyzed oxygen transfer in the reaction of ketones.

Whereas primary and secondary phosphines are rarely isolated and serve only as reaction intermediates, tertiary phosphines are quite the opposite, with tremendous practical importance. From the whole series R_nPH_{3-n} (n = 0-3), tertiary phosphines are the strongest bases (Scheme 1.9). The most common methods employed for their preparation are outlined in Scheme 1.10. The archetypal representative, triphenylphosphine, is the reagent for Wittig, Staudinger, Mitsunobu, and Appel reactions and is also widely used as a ligand in homogenous catalysis (for examples see Section 1.2).[9]

$PR_3 > HPR_2 > H_2PR > PH_3$

Scheme 1.9. Phosphines are bases, and their basicity increases with the degree of substitution and the nature of substituents R.

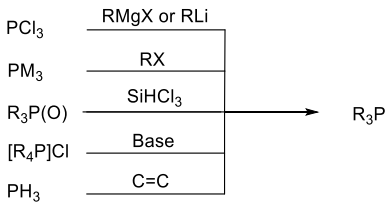

Scheme 1.10. Examples of common synthetic routes to tertiary phosphines: alkylation and reduction reactions, acid-base reactions, and addition reactions.

Primary phosphine chalcogenides $RP(Y)H_2$, where Y = O, S, Se, are compounds known only in very small numbers. The chalcogen atom in their structure carries a partial negative charge, whereas phosphorus has a partial positive charge, and the reactivity of these molecules reflects this polarization, which makes the phosphorus an electrophile. Overall, the reactivity of primary phosphine chalcogenides is similar to the reactivity of primary phosphines (Scheme 1.3). As shown in Scheme 1.11, tautomeric equilibria must be considered in these cases, albeit they have not been experimentally confirmed.

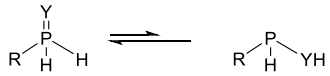

Scheme 1.11. Predicted tautomeric equilibria in molecules of primary phosphine chalcogenides. Enol form of the molecule has not yet been reported.

Primary phosphine oxides are prepared by controlled oxidation of primary phosphines (Scheme 1.2) or by reactions of ketones with phosphane in strongly acidic solutions (see Scheme 1.8, left). The thermal stability of primary phosphine oxides is much lower than the thermal stability of the secondary and tertiary phosphines, and the compounds readily undergo disproportionation (Scheme 1.12). In fact, the disproportionation is the main difficulty in synthesizing/isolating primary phosphine oxides, which will be demonstrated by a few examples (Scheme 1.13).[11] For instance, methylphosphine oxide was detected during hydrolysis of methylidenephosphine (in tetrahydrofuran at −50 °C) but immediately disproportionated into the corresponding phosphinic acid and primary phosphine, MeP(O)H(OH) and $MePH_2$.[12]

Phenylphosphine oxide has not yet been described in the literature. Octylphosphine oxide is considered to be one of the most stable simple phosphine oxides. It is reasonably stable in dilute solutions but decomposes upon concentration.[13] Finally, sterically protected 2,4,6-tri(*t*-butyl)phenylphosphine oxide is, to the best of my knowledge, the only known primary phosphine oxide, which is stable in the air and isolable as a solid.[14] Whereas using a large steric hindrance stabilizes the primary phosphine oxide, at the same time, it hinders their reactivity. Thus, although some reactivity was described when using *in situ* generated primary phosphine oxides, air-stable compounds without substantial steric protection continue to attract chemists.

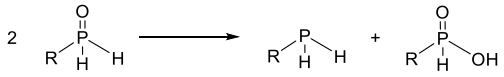

Scheme 1.12. Spontaneous disproportionation of primary phosphine oxide into primary phosphine and phosphinic acid.

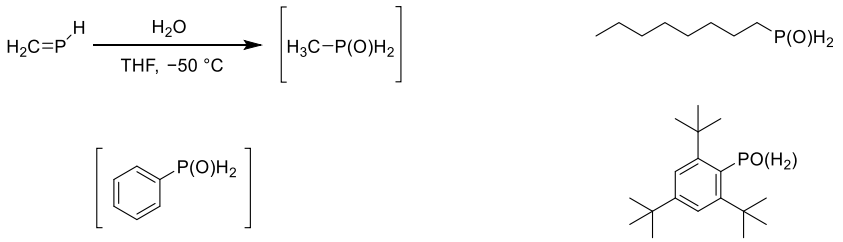

Scheme 1.13. Selected examples of primary phosphine oxides: methylphosphine oxide was observed in solution, phenylphosphine oxide is not yet known, octyl phosphine oxide is stable in dilute solutions, and 2,4,6-tri(*t*-butyl)phenylphosphine oxide is stable as a solid in the air.

The stability of heavier phosphine chalcogenides is even lower. Primary phosphine sulfides and selenides are formed upon treating primary phosphine with S_8 or Se, respectively. Although they were well characterized by ^{31}P NMR spectroscopy, with stable 2,4,6-tri(*t*-butyl)phenylphosphine sulfide as an exception, they cannot be isolated.[14, 15]

In contrast, secondary phosphine chalcogenides, $R_2P(Y)H$ (Y = O, S, Se), can be prepared easily by oxidation of secondary phosphines with oxygen, sulfur, or selenium. All these compounds were isolated, although they can be further oxidized, providing chalcogenophosphinic acids (Scheme 1.6). Secondary phosphine chalcogenides are in equilibrium with the respective phosphinous acids (Scheme 1.14).[16]

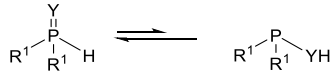

Scheme 1.14. Tautomeric equilibrium between secondary phosphine chalcogenide and phosphinous acid. The chalcogenide form usually predominates.

The thermodynamic stability of secondary phosphine oxides is significantly higher than that of their primary counterparts. In 1960, this was demonstrated by Sander, who observed only very slow disproportionation of (*n*-Bu)$_2$P(O)H above 150 °C (Scheme 1.15). The applicability of these compounds lies in using them as a versatile synthetic building block, and ligands for homogenous catalysis.[17] Secondary phosphine sulfides and selenides are also known (isolable) compounds and exert a higher oxidation stability than phosphines. Their reactivity was studied predominantly in addition reactions.[18]

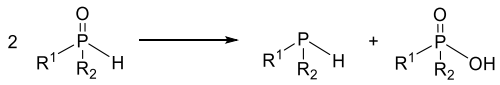

Scheme 1.15. Disproportionation of secondary phosphine oxides into secondary phosphine and phosphinic acid. The disproportionation occurs upon heating.

Tertiary phosphine chalcogenides are synthetically stable and generally easy to handle. Not surprisingly, therefore, they are known in large numbers.[19] They are all used during reversible protection of phosphine group in phosphine synthesis[20] and as directing groups in organic synthesis.[21] Besides, tertiary phosphine oxides are important for constructing optoelectronic and highly efficient light-emitting materials,[22] drugs with specific physicochemical properties and biological activity,[23] optically active compounds[24], and also as ligands in complexes with a wide range of metals.[25] The chemistry of tertiary phosphine sulfides and selenides has also gradually progressed.[26] The compounds were studied in several fields, being applied as organocatalysts,[27] extractants for actinides,[28] constituents of functional materials,[29] precursors of physiologically active compounds and as ligands for the design of multipurpose metal complexes. [30]

Recently, an impetus for the preparation of phosphine selenides arose from the possibility of determining electron-donating ability and basicity of the phosphorus atoms by measuring

the direct ^{31}P-^{77}Se scalar coupling constants in respective phosphine selenides ($^{1}J_{PSe}$, Figure 1.3). In general, the $^{1}J_{PSe}$ value increases with the substituents becoming more electron-withdrawing and covers a range wider than 100 Hz. However, it is necessary to note, the $^{1}J_{PSe}$ values are solvent-dependent and influenced by steric factors.[31]

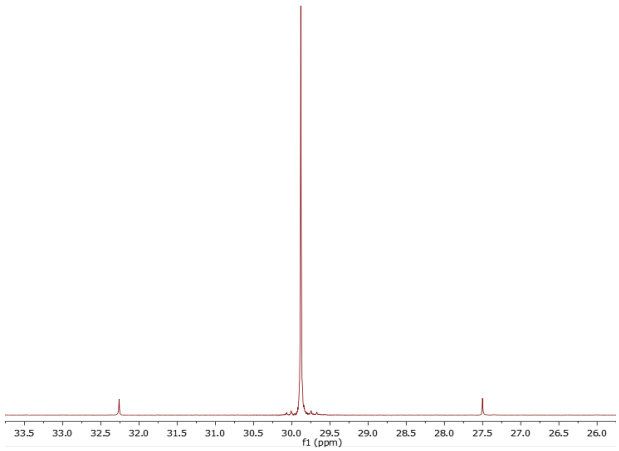

Figure 1.3. ^{31}P{^{1}H} NMR (CD_2Cl_2) spectrum of a model phosphine selenide FcP(Se)Ph_2, (Fc = ferrocene-1-yl). The main signal (singlet) is associated with a satellite doublet due to the ^{77}Se isotopomer. The natural abundance of ^{77}Se is only 7.6% (I = 1/2).

1.2 Phosphines and phosphine oxides: Ligands in homogenous catalysis

The most frequently exploited property of phosphorus derivatives is their ability to ligate transition metals. Phosphines and related trivalent phosphorus ligands are the most important ancillary ligands in homogenous catalysis (in both academic and industrial fields) and in coordination and organometallic chemistry. Many of the properties of these phosphine complexes were already summarized in books and review articles.[32] Phosphines are ligands whose electronic and steric properties (Figure 1.16) can be altered systematically over a very wide by varying substituents. However, practically, it is not so easy to affect one such parameter without affecting the other. Phosphines are σ-donors and π-acceptors, and the extent of these properties depends on the nature of the R group (Scheme 1.17).

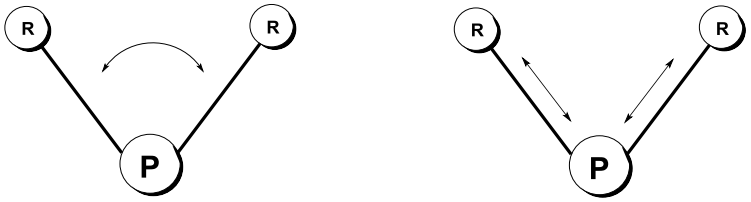

Scheme 1.16. Steric and electronic effect of substituents R at phosphorus atom. A steric effect results when the size or shape of the molecule changes. An electronic effect arises if a change to a part of the molecule results in a different electronic distribution within the molecule. Electronic and steric effects are interrelated and have a significant effect on the coordination and catalytic properties.

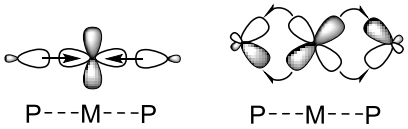

Scheme 1.17. Phosphine's electron-donating ability in coordination bond arises from two contributions: σ-donation (left) and π-acidity (right).

The catalytic performance of any phosphine-supported transition metal catalyst strongly depends on σ-donor and π-acceptor properties as well as on the steric properties. Although various methods were used to study and predict the electronic properties of phosphorus ligands, ligand design is still far from rational. Ligands of very different structures can provide similar catalytic activity in the same reaction, while ligands with very similar structures can behave very differently.

Due to the low chemical stability (and unfavorable sensory properties) of primary phosphines, transition-metal complexes of these ligands are relatively little studied.[33] Phosphines containing two hydrogen attoms are generally weaker donors to transition metal than their secondary/tertiary phosphine counterparts. Furthermore, characteristic difficulties in preparing defined complexes arise from the reactivity of P-H bonds, which often undergo a metal-mediated cleavage to form phosphide or phosphinidene ligands. Examples of primary phosphine complexes with the known structure are shown in Scheme 1.18. Complexes with primary phosphines have not been studied in catalysis. As an exception that proves the rule can

be mentioned palladium(II) catalyzed C-H arylation of unprotected indoles (Scheme 1.19) [34] or phenylacetylene hydrogenation (Scheme 1.20).[35]

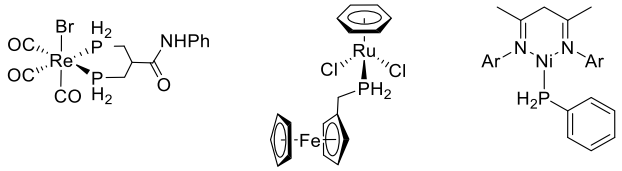

Scheme 1.18. Examples of primary phosphine complexes with the known structures (Ar = 2,6-diisopropylbenzene).

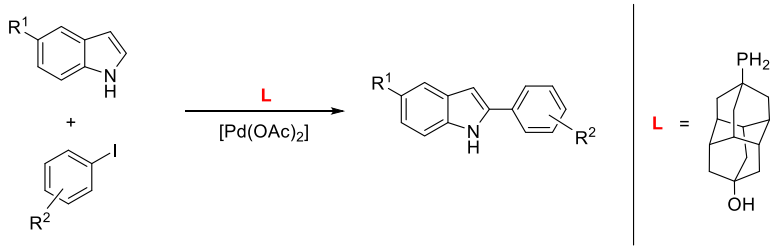

Scheme 1.19. Palladium(II) catalyzed C-H arylation of unprotected indoles using primary diamantyl phosphine.

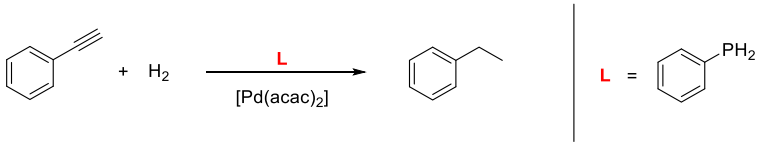

Scheme 1.20. Hydrogenation of phenylacetylene catalyzed by in-situ-formed palladium complex with primary phosphine.

The number of secondary phosphine complexes is also relatively small, and their applications in homogenous catalysis are limited because the complexes are generally unstable under the catalytic conditions (Scheme 1.21).[36] However, they can be important synthetic intermediates. As an example can be mentioned template synthesis of tetraphosphine macrocycles. After the coupling reaction, the cyclic ligand was liberated from the nickel(II) center using sodium cyanide (Scheme 1.22).[37] Further applications are represented

by the activation of secondary phosphines for stereoselective alkylation (Scheme 1.23).[36,38] For catalytic applications, secondary phosphines were incorporated into the first-generation Grubbs catalyst (Scheme 1.24). However, the catalyst showed poor activity, which was attributed to the *cis*-arrangement of the chloride ligands.[36,39]

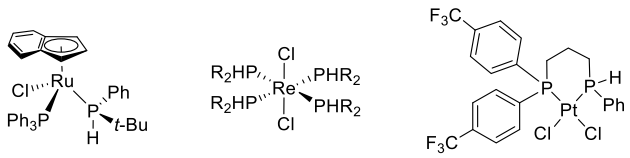

Scheme 1.21. Secondary phosphine complexes with the known structures (R = ferrocenyl).

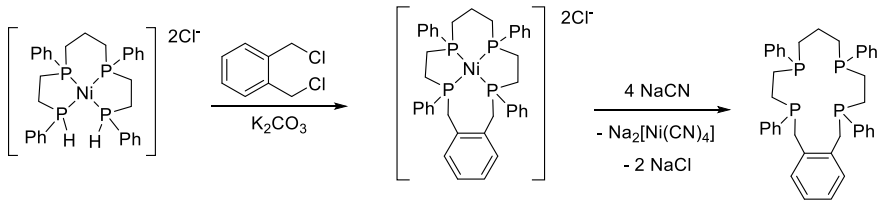

Scheme 1.22. Nickel(II)-template synthesis of a tetraphosphorus macrocycle.

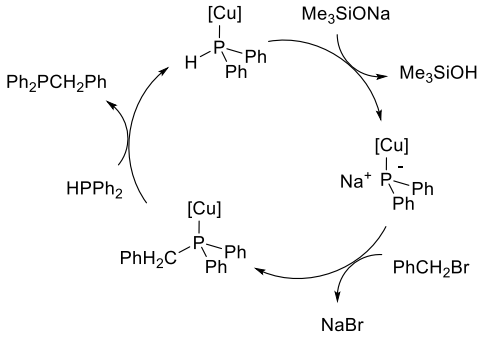

Scheme 1.23. Proposed mechanism for stereoselective alkylation of diphenylphosphine using copper(I) catalyst.

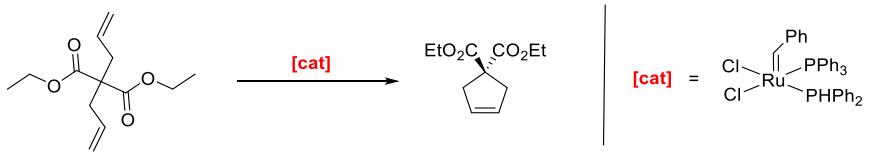

Scheme 1.24. Ring-closing metathesis using a modified Grubbs catalyst bearing a secondary phosphine ligand.

The coordination chemistry of tertiary phosphines has been widely studied. There are examples of tertiary phosphine ligands with virtually every transition metal. These stable complexes have found many catalytic applications in diverse chemical reactions such as hydrogenation, hydroformylation, hydrosilylation, formaldehyde hydrophosphination, polymerization reactions, coupling reactions and many others (Scheme 1.25).[40]

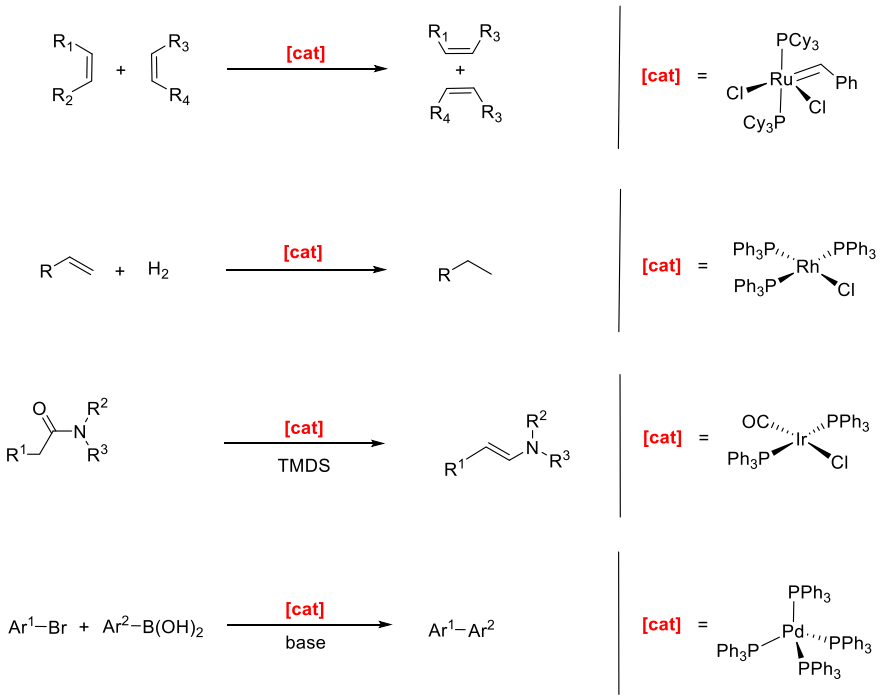

Scheme 1.25. Examples of tertiary phosphine complexes and their application as a catalyst: Grubbs catalyst for olefin metathesis, Wilkinson's catalyst for hydrogenation of olefins, Vaska's complex in reductive functionalization of tertiary amides[41] and tetrakis(triphenylphosphine)-palladium(0) catalyzing Suzuki-Miyaura reaction (TMDS = 1,1,3,3-tetramethyldisiloxane).

In contrast, a defined complex of primary phosphine oxide is not yet known. Nonetheless, it was recently assumed that primary phosphine oxide is formed *in situ* from primary diamantylphosphine during the catalytic test "on water" when heated at reflux (Scheme 1.19).[34] This assumption was then corroborated by the results obtained when diamantylphosphine oxide (obtained readily by bubbling air into a dichloromethane solution of the appropriate primary phosphine) was used as a defined ligand in the catalytic test and showed the same catalytic activity (Scheme 1.26). In an independent experiment, primary diamantylphosphine performed poorly under strictly anaerobic conditions.

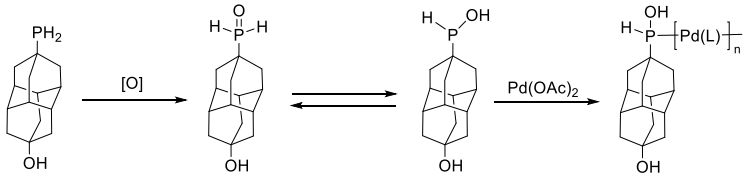

Scheme 1.26. Suggested formation of active catalytic species during the catalytic reaction inspired by the behaviour of secondary phosphine oxides.

Using secondary phosphine oxides as ligands is one of the modern courses in homogenous catalysis and has already been reviewed.[42] In the presence of late-transition metals, the equilibrium between "enol" and "keto" tautomers of the secondary phosphine oxide (Scheme 1.14) is shifted toward the phosphinous acid form (*via* coordination through the phosphorus atom). The coordination chemistry of secondary phosphines is very rich as they can coordinate as neutral or deprotonated P-bound ligands and form bridged structures (Scheme 1.27).

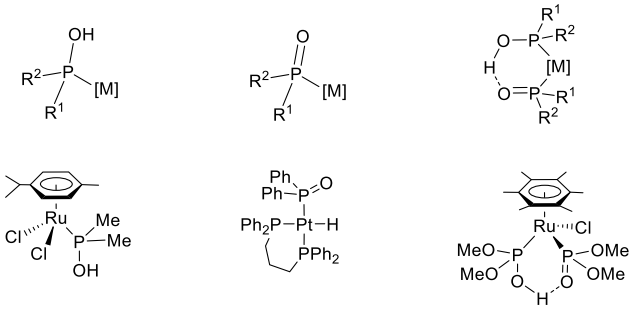

Scheme 1.27. Representative coordination modes of secondary phosphine oxides with specific examples.

There are also known several optically pure secondary phosphine oxides. JoSPOphos and SPO-Wudaphos are examples of these ligands bearing the ferrocenyl substituent producing excellent hydrogenation catalysts (Scheme 1.28). These ligands were studied in Ti, Cr, Mo, W, Mn, Re, and Ru complexes.[42a] In addition, in recent literature, the cooperative effect of the P-OH group on a metal during a catalytic cycle is discussed. For illustration, see the proposed mechanism of Ru-catalyzed nitrile hydration shown in (Scheme 1.29).[43]

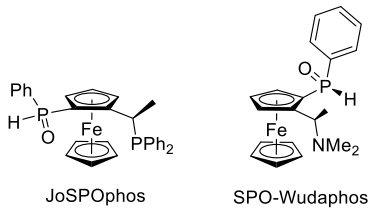

Scheme 1.28. Optically pure ligands bearing the ferrocenyl substituent.

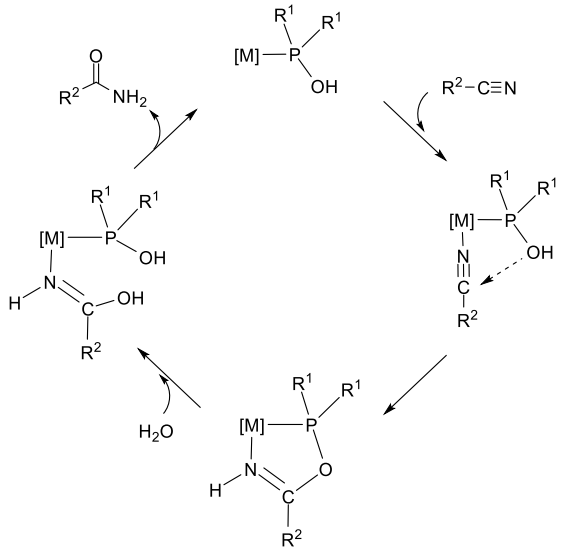

Scheme 1.29. Cooperative effect of phosphinous acid ligands in ruthenium(II)-catalyzed nitrile hydration.

Tertiary phosphine oxides bind late transition metals very weakly, as they can coordinate only *via* oxygen atom. Therefore, they were studied as hybrid ligands containing labile donor groups. For instance, this year, Grimaud *et al*. have presented that dppf shows worse catalytic

activity in palladium(II)-catalyzed Suzuki−Miyaura coupling reaction than hemilabile coordinated monoxide dppfO (Scheme 1.30).[44]

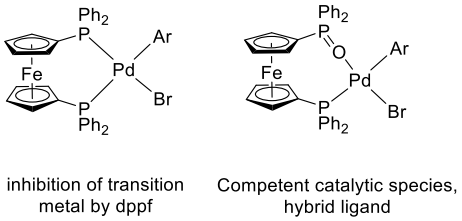

Scheme 1.30. Role of dppf and dppf monoxide in the transmetalation step of the Suzuki-Miyaura coupling reaction.

1.3 Ferrocene bisphoshphines

Ferrocene-based phosphorus ligands have emerged as one of the most powerful classes of ligands in chiral and achiral catalysis.[45] 1,1′-Bis(diphenylphosphino)ferrocene (dppf) is the archetype of this compound class (Scheme 1.31) and was studied in numerous metal complexes, mostly derived from the late transition metals (Scheme 1.32). Although the synthesis of dppf was reported in 1971,[45c] it took about two decades to prepare its analogues with varied electronic and steric properties. The basic route of the analogue synthesis involves stepwise lithiation and reaction with corresponding phosphine chloride (Scheme 1.33). Typical examples are modified ligands bearing bulky and electron-donating substituents.

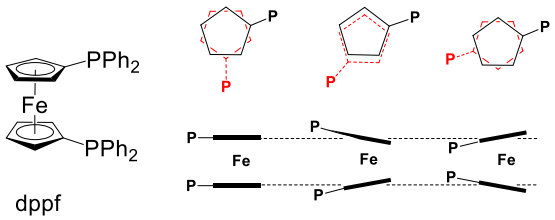

Scheme 1.31. 1,1′-Bis(diphenylphosphino)ferrocene (dppf), a successful donor in homogenous catalysis. Ferrocene provides a robust yet flexible backbone.

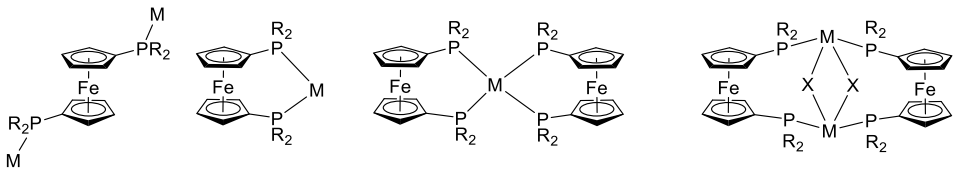

Scheme 1.32. Ferrocene backbone allows stabilizing a variety of metal centers by various coordination modes and conformation: bimetallic complex, chelate complex, and doubly-bridged complex.

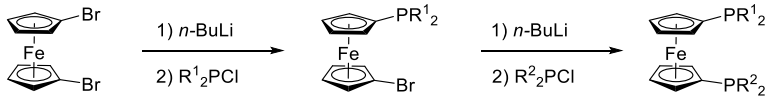

Scheme 1.33. General synthetic routes for dissymmetric 1,1′-bisphosphinoferrocene.

Another approach toward modifying the dppf molecule is represented by introducing a methylene spacer between one of the donor groups and the ferrocene moiety (Scheme 1.34). These ligands bind more flexibly than dppf, which is reflected mainly in the ligand bite angles. Consequently, their coordination behavior is more temperamental, which can be demonstrated on the example of palladium(II) complexes. While the reaction of dppf and bis(acetonitrile)-dichloropalladium(II) gives [$PdCl_2$(dppf)] chelate complex as a sole product, methylene spaced molecule provides a mixture of chelate and dinuclear products. The studies into catalytic activity of the last-mentioned ligands have been limited thus far.[46]

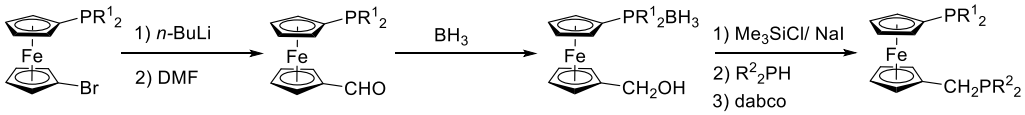

Scheme 1.34. Synthetic route to methylene spaced ferrocene bisphosphines (dabco = 1,4-diazabicyclo[2.2.2]octane).

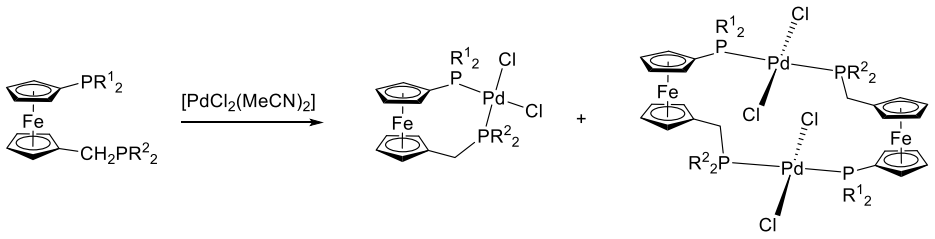

Scheme 1.35. The reaction of palladium(II) precursor and methylene spaced ferrocene bisphosphine gives a mixture of chelate complex (dominating) and symmetrical dinuclear complex.

1.4 Phosphatrioxa-adamantane ligands

Although the acid-catalyzed condensation of phosphane or primary phosphines with acetylacetone giving the corresponding 6-phospha-2,4,8-1,3,5,7-tetramethyladamantane (denoted often as phosphaadamantane, cage phosphine, and abbreviated as CgPH or CgPR) was first reported by Epstein and Buckler in 1961 (Scheme 1.36),[47] the main development of phospha-adamantane ligands with applications in homogenous catalysis occurred in the last two decades.

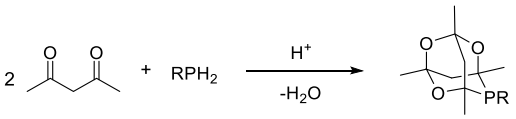

Scheme 1.36. Buckler-Epstein reaction: acid-catalyzed reaction of phosphine or primary phosphine with acetylacetone (R = H, alkyl, aryl).

The cage phosphines synthesis is straightforward, high yielding, and based on available reagents (Scheme 1.37). In addition, these compounds are generally air-stable, thermally robust, and resistant towards aqueous acids and bases. The CgP substituent can be categorized as very bulky, comparable with $(t\text{-Bu})_2$P, and electron-poor, comparable with $P(OR)_2$. Moreover, the CgP structure is very rigid, having an uncommonly small C-P-C angle close to 90°. The CgP group has C_1 symmetry and thus exists as enantiomeric forms (labels α and β in Scheme 1.38). The unique combination of the above-mentioned properties makes CgP phosphines a fascinating research target.[48]

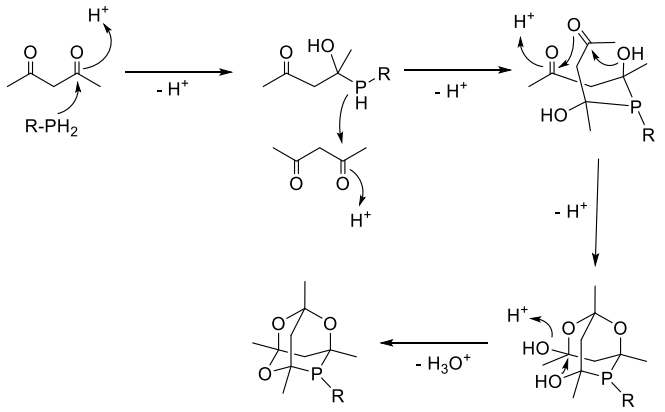

Scheme 1.37. A plausible mechanism of cage phosphine formation.

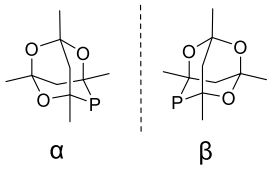

Scheme 1.38. The cage phosphines are racemic mixtures of enantiomers α and β.

After the pioneering work of Epstein and Buckler, the cage phosphine expansion was accelerated by the research of Pringle *et al.* describing in 2008 more general routes to these compounds.[49] First, they optimized the reaction conditions of the Buckler-Epstein reaction allowing the synthesis under atmospheric pressure at 0 °C. During the optimized reaction, HPCg is precipitated as a pure crystalline solid from an acidified aqueous solution of acetylacetone and was isolated in the air in the 50% yield. As a next step, they developed reliable synthetic approaches toward cage phosphines by discovering versatile alternative nucleophilic and electrophilic sources of the CgP group (Scheme 1.39, first line). These new molecules significantly extended the existing synthetic routes to RPCg, which were based on the reaction of RPH_2 with acetylacetone, a metal-catalyzed RBr substitution using CgPH, or radical initiated P-H addition of CgPH to alkene (Scheme 1.39, second line).

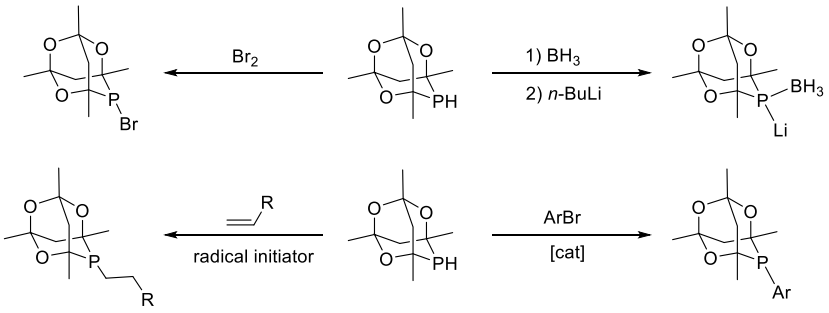

Scheme 1.39. Reactivity of HPCg. First line: lithiation of borane adduct of HPCg provides a nucleophilic source of the CgP fragment, but the controlled treatment of HPCg with bromine gave the electrophilic source of CgP. Second line: palladium-catalyzed arylation and P-H additions of HPCg.

Remarkably, about half of the articles focused on cage phosphines are patents, describing the application of these molecules in homogeneous catalysis. Many of them were inspired by the similarity of the steric bulkiness of CgP with the $(t\text{-Bu})_2$P group. Unlike di-*tert*-butylphosphine group, which is widely used in catalysis, cage phosphines are generally easier to handle as they are stable in air. Both types of phosphines, CgPR and $(t\text{-Bu})_2$PR, efficiently catalyzed alkoxycarbonation and C-C and C-N coupling reactions. Different electronic properties of the cage phosphines probably lie behind their success in hydroformylation and hydrocyanation reactions.[48] The versatility of cage phosphines as ligands for homogenous catalysis will be illustrated in few examples from the current literature.

Simple cage phosphine in a catalytic system with a palladium(0) precursor was shown to promote the Suzuki-Miyaura cross-coupling of aryl halides with a variety of aryl boronic acids at room temperature in a few hours with high yields (Scheme 1.40).[50]

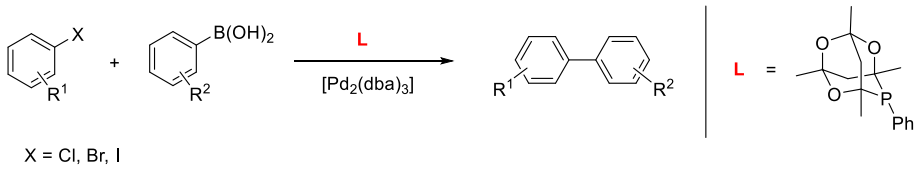

Scheme 1.40. Suzuki-Miyaura cross-coupling of aryl halides with arylboronic acid catalyzed by a cage phosphine/palladium(0) catalyst.

Another system consisting 1 mol% of allylpalladium(II) chloride and 2 mol % of $CgPPh_2$ showed the best results in palladium-catalyzed *anti*-Michael reductive Heck reaction of α,β-unsaturated esters (Scheme 1.41).[5]

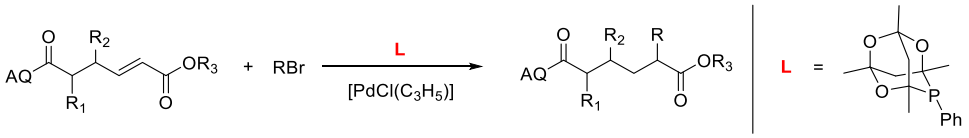

Scheme 1.41. Palladium-catalyzed *anti*-Michael reductive Heck reaction of α,β-unsaturated esters (AQ = 8-aminoquinolin-8-yl).

Stimulated by the favorable catalytic properties of RPCg-palladium(II) complexes in carbonylation reactions, a new series of CgPAr ligands was designed and studied in methoxycarbonylation of phenylacetylene (Scheme 1.42). From the series of aryl-functionalized phospha-adamantyl ligands, the ligand highlighted in red showed the best catalytic activity and selectivity for the branched product **B**.[52]

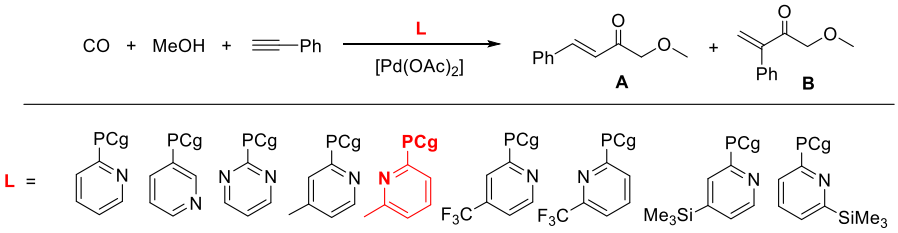

Scheme 1.42. CgPAr ligands tested in palladium(II)-catalyzed methoxycarbonylation of phenylacetylene.

Similarly, new PCg ligands bearing various aryl substituents were synthesized as catalyst components for palladium(II)-catalyzed telomerization of butadiene with methanol. The ligand highlighted in red converted 96% of butadiene into 1-methoxy-2,7-octadiene (Scheme 1.43) with 94% selectivity.[53]

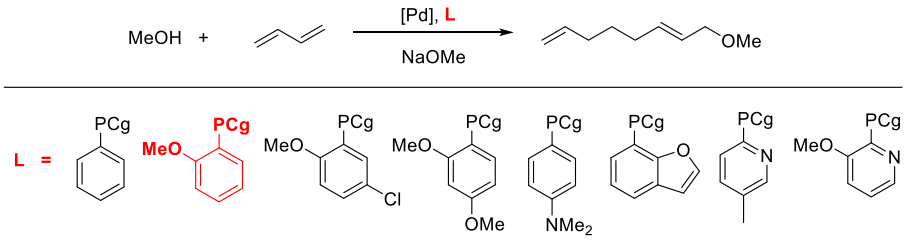

Scheme 1.43. In the presence of palladium(II) complex, butadiene undergoes a telomerization reaction in methanol to yield the desired linear product, 1-methoxy-2,7-octadiene.

More recently, Stradiotto showed that cage phosphines provide very good results in nickel(II)-catalyzed reactions. Thus, the compound in Scheme 1.44 is the first known complex of nickel efficiently catalyzing monoarylation of ammonia with arylchlorides.[54] The same complex was also studied in nickel(II)-catalyzed cross-coupling of sulfonamides with (hetero)aryl chlorides.[55]

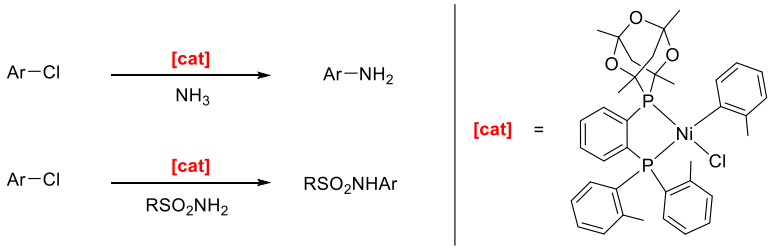

Scheme 1.44. Nickel(II)-catalyzed monoarylation of ammonia and cross-coupling of sulfonamides with (heteroaryl)aryl chlorides.

A new, double cage bisphosphine nickel(II) complex was successfully applied in the cross-coupling reaction of primary heteroaryl amines and heteroaryl chlorides (Scheme 1.45).[56]

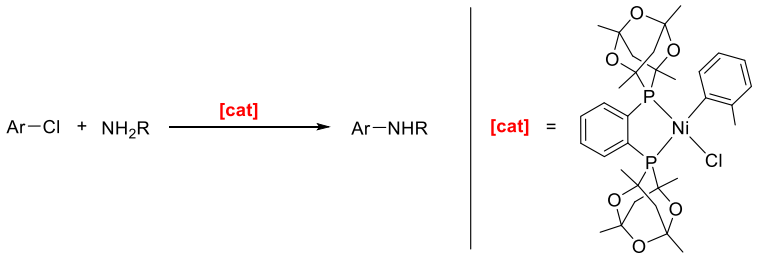

Scheme 1.45. Nickel(II)-catalyzed C-N cross-coupling of primary heteroaryl amines and (hetero)aryl chlorides.

Properties of bisphosphines combining ferrocene and CgP fragments are not known. However, they are claimed in patents as components of active catalysts for alkoxycarbonylation of vinylic substrates.[57]

1.5 Polar phosphine ligands

In recent years, the most important goal of chemistry became developing of resource-efficient and sustainable synthetic methodologies. Designing and developing of catalysts is identified as the heart of the greening of chemistry. In spite of the already achieved developments in catalysis, significant goals remain the same: expansion of substrate diversity, reduction of the amount of used catalysts, energy and, last but not least, replacing toxic reactants and solvents with their environmentally benign alternatives.[58] Thus, water as the cheapest, intrinsically safe, and environmentally friendly solvent, available in practically unlimited quantities on the Earth, attracted the research community.[59] For using this solvent in phosphine-catalyzed reactions, the lipophilic nature of phosphine ligand must be suppressed. An efficient and the most straightforward approach for designing a hydrophilic phosphine complex is introducing highly polar moiety into phosphine ligands. The advantages of using hydrophilic phosphines in catalysis lie in their solubility in the green solvent (water) and easy recovery by extracting into an aqueous phase after the reaction. Hence, a remarkable concept is using water-soluble phosphines for biphasic catalytic reactions. In these processes, the metal catalyst remains in the aqueous phase, whereas the substrate and product remain in another phase, facilitating their separation from the catalyst by simple decantation. The separation allows recycling of the complex and resolves the main disadvantage of homogeneous transition metal catalysis - difficulties with separating the catalyst from the products (Figure 1.4).[60] It is necessary to note that the introduction of water-solubilizing groups can also affect the steric and electronic properties of the known phosphine ligands and thus affect the activity of the resulting catalysts.

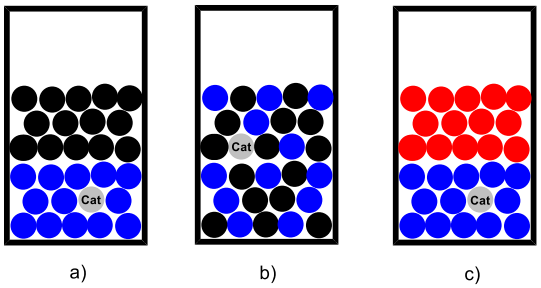

Figure 1.4. The biphasic system with a hydrophilic organometallic catalyst: a) reactant in the organic solvent is added to the aqueous phase containing catalyst; b) catalytic reaction is initiated, the mixture is stirred; c) reaction is complete, product in organic phase can be easily separated, catalyst stays in the water and can be used again - recycled.

Thanks to its synthetic accessibility and stability, the most commonly used water-solubilizing substituent is the sulfonate group. An archetypal example of such ligands is 3,3′,3″-phosphanetriyltris(benzenesulfonic acid) trisodium salt (TPPTS) prepared by direct sulfonation of PPh_3 by oleum and neutralization. TPPTS is probably the most wides used hydrophilic phosphine used in the industry. For example, highly water-soluble rhodium complexes are used for industrial production of butyraldehyde by hydroformylation of propylene or for [2+2+1] cycloaddition of alkyne, akene, and carbon monoxide (Pauson–Khand reaction, Scheme 1.46).[61] Recently, a new defined phosphinoferrocene sulfonate rhodium(I) complex was prepared and tested in the hydroformylation of vinyl acetate (Scheme 1.47). In the complex, one of the ligands coordinated as P,O-chelating ligand.[62]

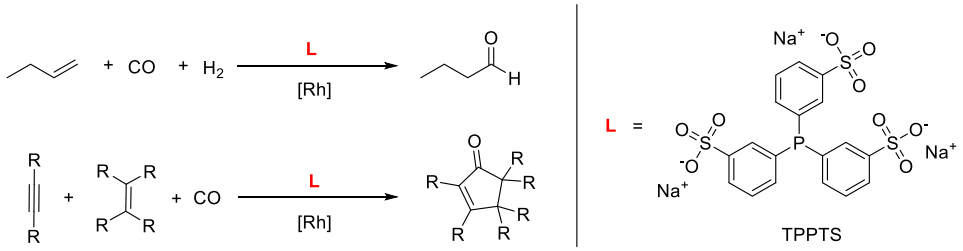

Scheme 1.46. Rhodium-catalyzed synthesis of butyraldehyde (top) and Pauson–Khand reaction (bottom).

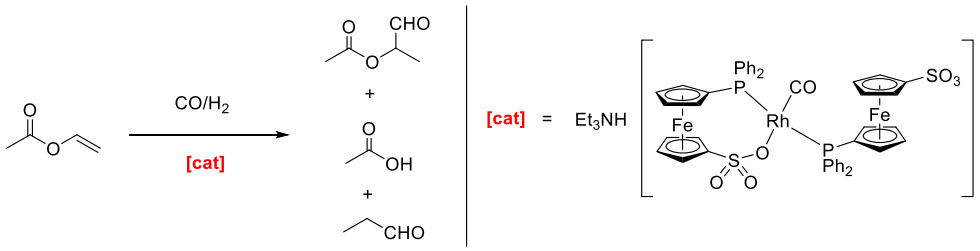

Scheme 1.47. Hydroformylation of vinyl acetate catalyzed by a rhodium(I) complexes with a polar phosphinoferrocene sulfonate ligand.

Polar phosphine ligands containing carboxylic acid moieties have been much less investigated as catalyst components. However (diphenylphosphino)acetic acid has already been applied at an early stage in the Shell Higher-Olefin Process (SHOP), the first large-scale industrial biphasic catalytic process (see complex in Scheme 1.48).[60c,63] A series of structurally similar palladium(II) complexes with phosphinoferrocene-carboxylate ligands were tested in CO-ethylene copolymerization (Scheme 1.49).[64]

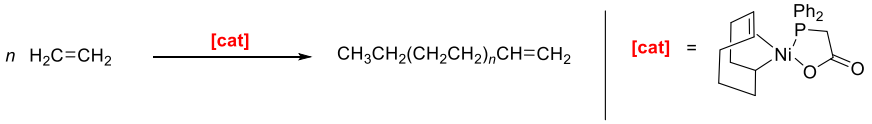

Scheme 1.48. Shell Higher Olefin Process for the production of linear α-olefins by ethylene oligomerization.

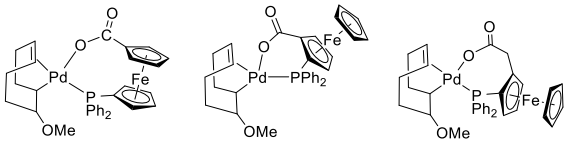

Scheme 1.49. Neutral palladium(II) complexes containing P,O-chelating phosphinoferrocene-carboxylate ligands tested in the CO-ethylene copolymerization.

Phosphines with cationic substituents represent another method to prepare hydrophilic phosphines. Although the most commonly used cationic functionalities are ammonium ions (e.g., $(R_2PCH_2CH_2NMe_3)X$ detonated as Amphos),[65] a hydrophilic group providing even higher water solubility is the guanidinium moiety ($HNC(NH_2)_2^+$). Recently, palladium(II)-guanidiniumphosphine system was reported to catalyze hydrocarboxylation of styrene in aqueous

media (Scheme 1.50).[66] Furthermore, ferrocene analogs are known and were tested in palladium-catalyzed Suzuki–Miyaura cross-coupling of aryl chlorides with arylboronic acids (Scheme 1.51).[67]

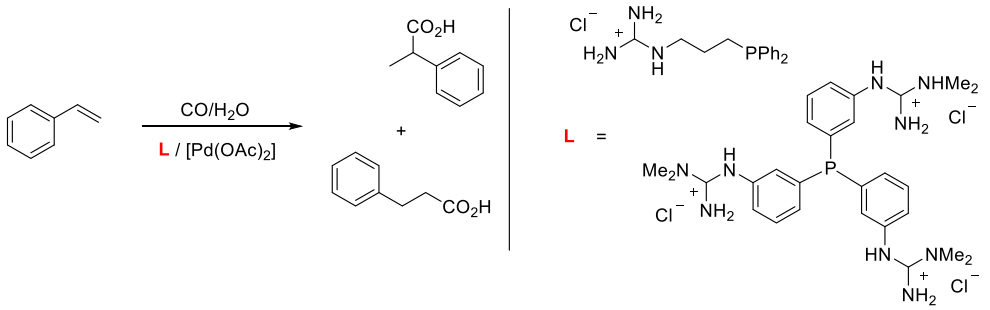

Scheme 1.50. Guanidinium phosphine ligands form water-soluble and selective catalysts for the hydrocarboxylation of styrene.

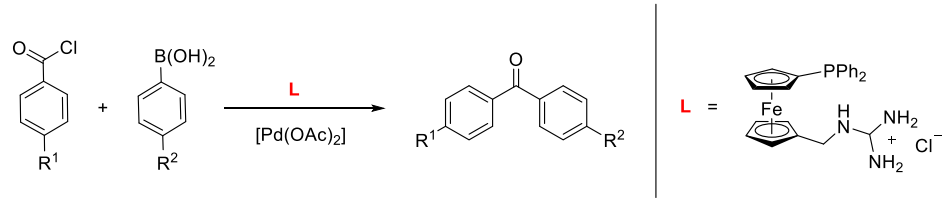

Scheme 1.51. Suzuki-Miyaura cross-couplings of aromatic acyl chlorides with arylboronic acids catalyzed by palladium(II) complexes with phosphinoferrocene ligands bearing cationic guanidinium tags.

Phosphines modified with phosphonic acid groups have been studied less extensively than other water-soluble ligands, probably because these compounds are difficult to access. Nevertheless, several of phosphonate-phosphines ligands (10 studied molecules) showed high solubilities in water and were used to immobilize rhodium(I) catalysts in the aqueous phase of biphasic systems for the hydroformylation of 1-octene and propene (Scheme 1.52).[68] Even though the obvious precursor of analogous ferrocene phosphonate-phosphine ligand $Ph_2PfcP(O)(OEt)_2$ has already been prepared,[69] 1-(diphenylphosphino)-1'-ferrocenephosphinic acid, $Ph_2PfcP(O)(OH)_2$, has not yet been reported.

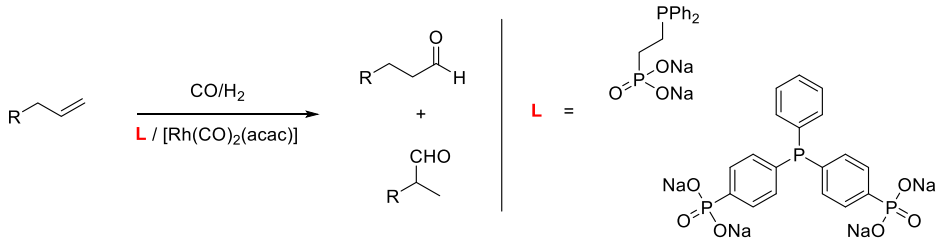

Scheme 1.52. Hydroformylation of alkyne catalyzed by catalysts generated from (acetylacetonato)dicarbonylrhodium(I) and phosphonate-phosphine ligands.

2. Aims of Thesis

The aim of this Thesis is to prepare and study electronically dissymmetric ferrocene bisphosphines derived from 1,1'-bis(diphenylphosphino)ferrocene (dppf), which contain a methylene spacer between one of the phosphine group and the ferrocene moiety, $Ph_2PfcCH_2PR_2$ (fc = ferrocene-1,1'-diyl). As a possible starting material for the syntheses, 1-(diphenylphosphino)-1'-(phosphinomethyl)ferrocene ($Ph_2PfcCH_2PH_2$) is considered. Investigation into the reactivity of the primary phosphine group in this molecule is one of the possible partial goals. In addition, new bisphoshines are studied as ligands in reactions with catalytically relevant transition metals. The main emphasis is put on comparing the coordination and catalytic properties of the prepared molecules with the properties of dppf.

The second objective of the Thesis is to synthesize 1'-(diphenylphosphino)ferrocene-1-phosphonic acid ($PPh_2fcPO_3H_2$) by hydrolysis of diethyl 1'-(diphenylphosphino)-ferrocene-1-phosphonate ($PPh_2fcPO_3Et_2$) and to compare its coordination and catalytic properties with known ferrocene hydrophilic ligands (PPh_2fcCO_2H, PPh_2fcSO_3H).

The prepared compounds will be characterized by nuclear magnetic resonance, infrared and mass spectroscopy, elemental analysis. If possible, the compound solid-state structures will be determined by single-crystal X-ray diffraction analysis.

3. Summary of the results

3.1 Dppf congeners bearing primary phosphine and primary phosphine oxide moieties

The unsymmetric bisphosphine **1**, which was one of the proposed synthetic targets, was prepared by a three-step synthesis starting from the known alcohol **4** (Scheme 3.1, from here onwards, the highlighting of the compound number in red indicates that the crystal structure has been determined). The first reaction step was the zinc iodide-mediated reaction of the alcohol with triethyl phosphite producing phosphonate **3** in a good 84% yield.[70] Next, the phosphonate group was reduced by *in situ* generated alane to produce primary phosphine **2** in quantitative yield. In the last step, the diphenylphosphine group was unprotected *via* reaction with a dabco as a stronger Lewis base. Subsequent crystallization gave bisphosphine **2** as an orange crystalline solid in 84% yield. Although compound **1** has a characteristic smell of phosphane, the ferrocenylmethyl substituent makes it air-stable, in accordance with the literature.[6]

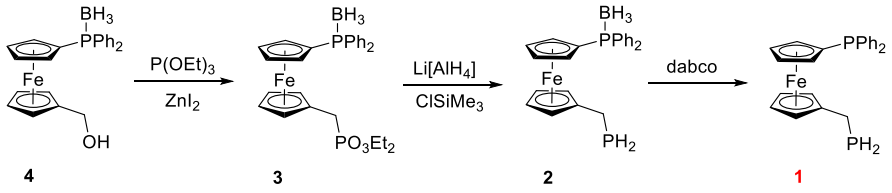

Scheme 3.1. Synthesis of bisphosphine **2** (dabco = 1,4-diazabicyclo[2.2.2]octane).

The stability of **1** against air oxidation is preserved in the crystalline state, in solution, and even upon heating in boiling heptane. Bisphosphine **1** can be thus readily purified by column chromatography in air. Moreover, the general reactivity of the primary phosphine group is low. For instance, no reaction was observed when treating the bisphosphine with acrylonitrile, 1,4-diphenyl-1,3-butadiyne, acetone, and phenyl iodide (without a catalyst). Subsequently, the reaction of **1** with PhI catalyzed with palladium(II) acetate or $[Pd_2(dba)_3]$ produced the known bisphosphine **5** in 78% yield (Scheme 3.2).

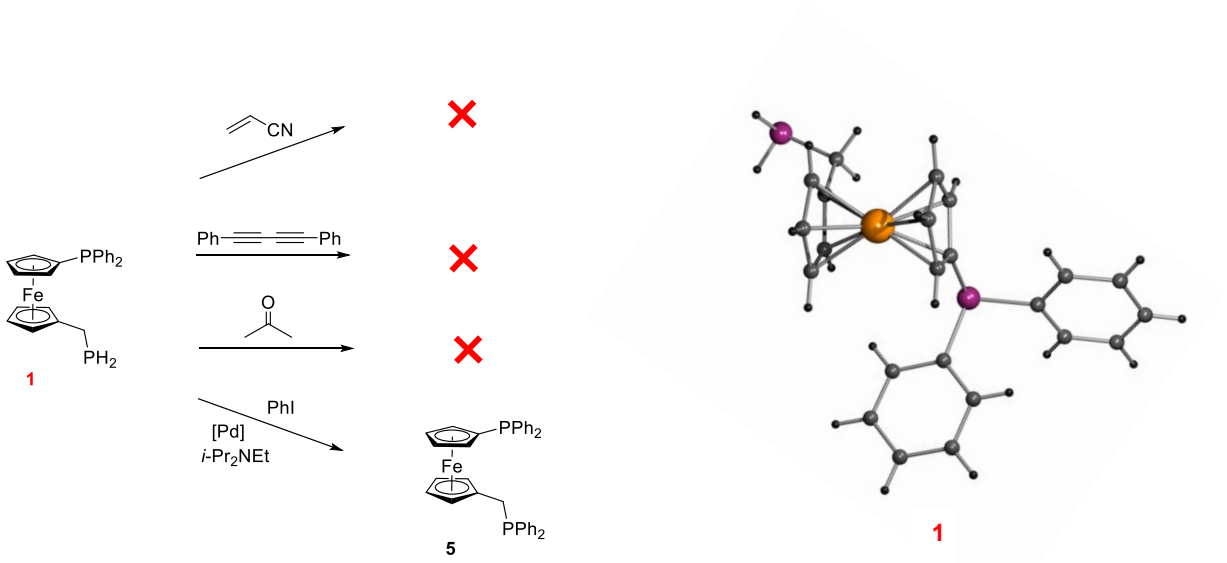

Scheme 3.2. Reactivity and molecular structure of bisphosphine **1**.

Next, the behavior of the primary phosphine **1** was tested in reactions with hydrogen peroxide. Even if using a large excess of the oxidizing agent (≈15 eqviv.), only the product with the primary oxidation step was isolated. The oxidation in methanol/dichloromethane mixture gave phosphine oxide **6** as the sole product (Scheme 3.3). When using acetone as a solvent for the same reaction, the addition product **8** was isolated instead. The subsequent deprotection with dabco afforded compounds **7** and **9**. Notably, the reactions of the phosphine oxide group with acetone suggest that primary phosphine oxide **7** is more reactive than primary phosphine **1**.

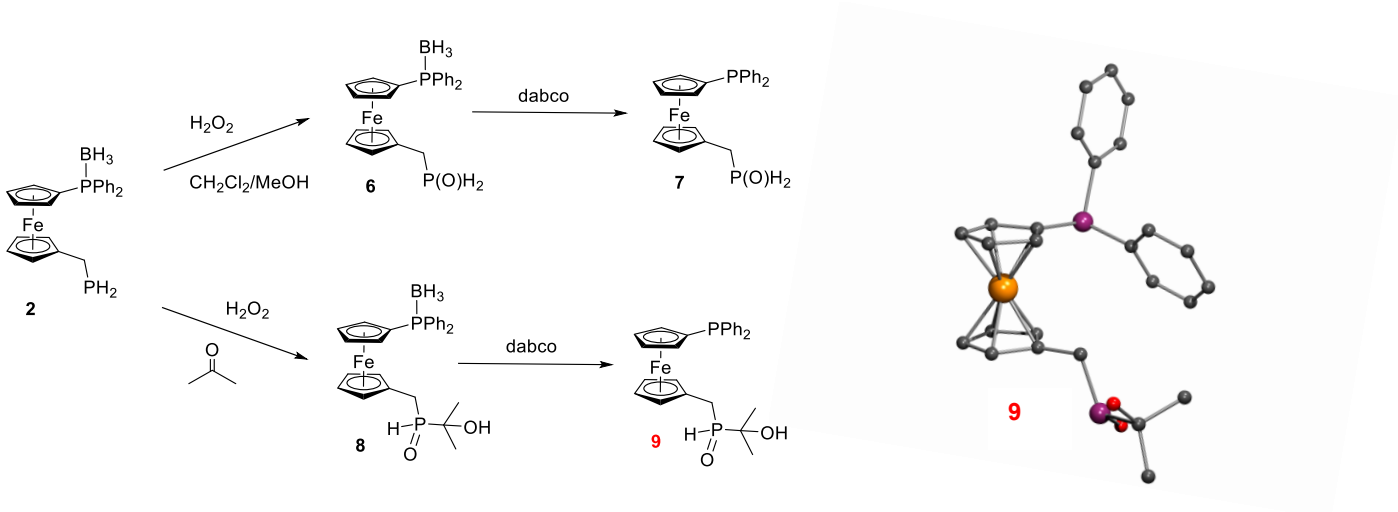

Scheme 3.3. Oxidation of bisphosphine **2** and the crystal structure of compound **9**.

Coordination properties of the new ligands were studied in ruthenium(II) complexes containing auxiliary π-arene ligands. Using half of the molar equivalent of $[(\eta^6\text{-mes})RuCl_2]_2$ as a ruthenium precursor (mes = mesitylene), the diphenylphosphine group in molecule **7** coordinated preferably giving **14** as a single product (Scheme 3.4). On the other hand, the reaction of borane adduct **6** produced complex **15** with a coordinated hydroxyphosphine group, which is the first defined complex of primary phosphine oxide. Efforts to prepare the complete series of chelate ruthenium(II) complexes from ligands of **1**, **5**, **7** and dppf failed as the ligands with methylene spacers (in contrast to dppf) provided complicated mixtures. The product mixtures could not be separated on a preparative scale. However, a few complexes were successfully structurally characterized (Scheme 3.5). A subsequent change of the target molecules yielded the complete series of dinuclear ruthenium(II) complexes **10-13** (Scheme 3.6). All prepared complexes were air-stable. In the case of complexes with ligands **1** and **7**, no P-H group activation was observed.

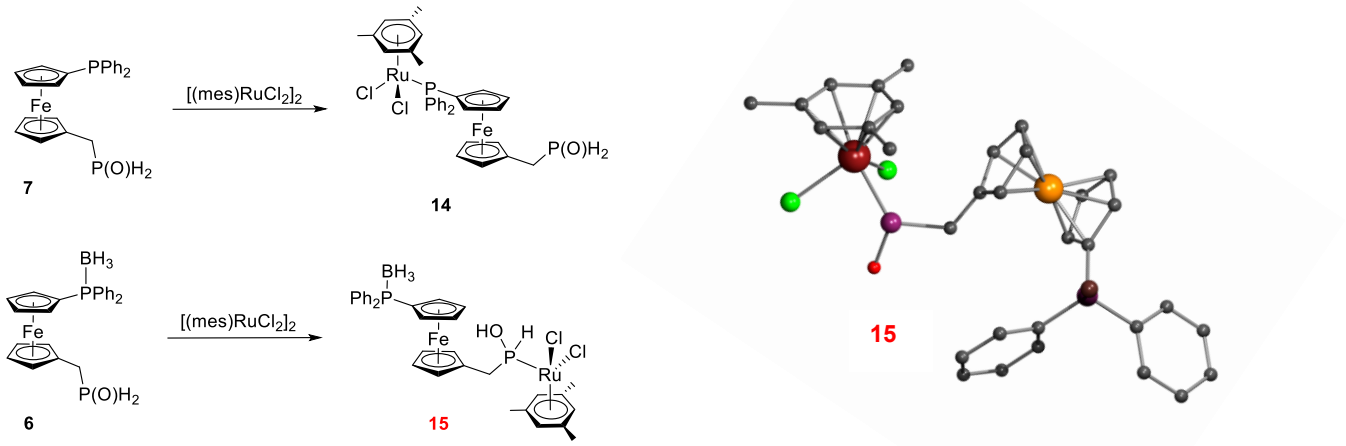

Scheme 3.4. Coordination study with ligands **6** and **7** and the crystal structure of complex **15**.

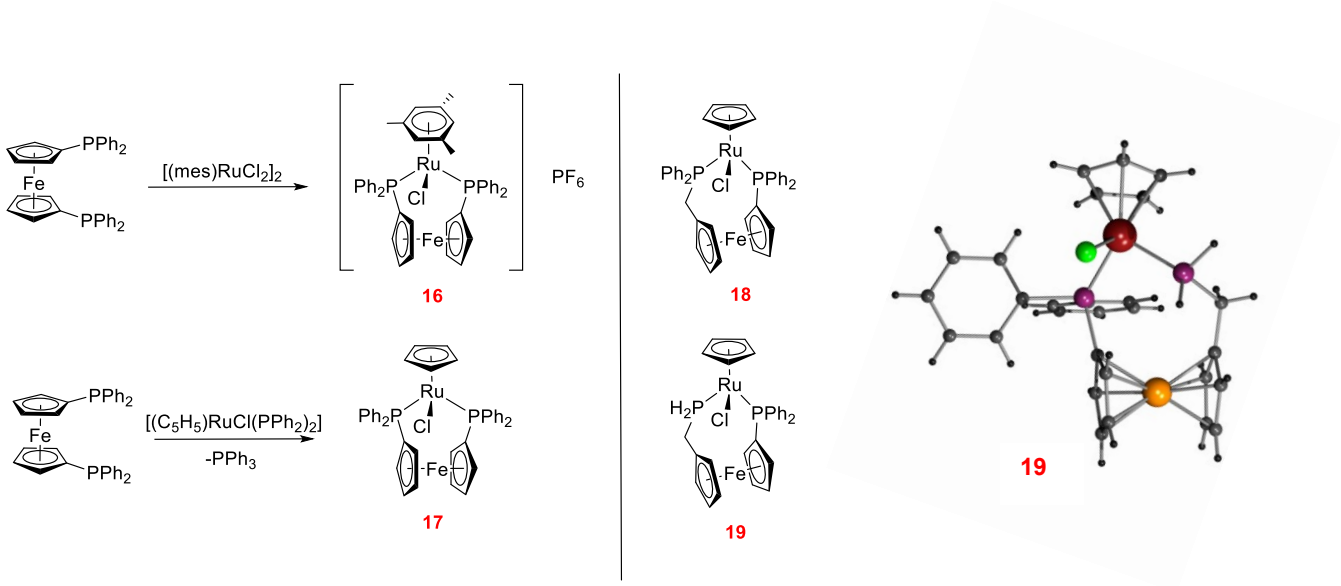

Scheme 3.5. Synthesis of chelate ruthenium(II) complexes. While the reaction with dppf yielded compounds **16** and **17**, ligands **1**, **2** and **7** produced complicated mixtures.

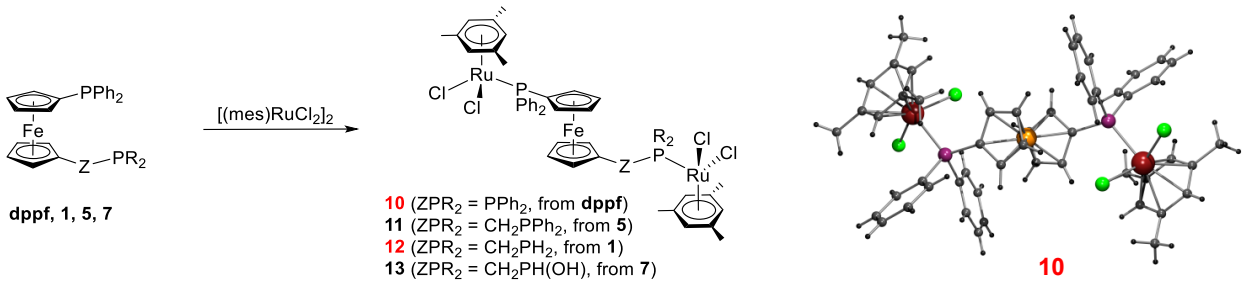

Scheme 3.6. Synthesis of the dinuclear ruthenium(II) complexes **10-13** and the structure of **10**.

The catalytic activity of all defined complexes was tested in two Ru-mediated reactions. The first reaction, catalytic double bond isomerization of estragole to anethole, was chosen considering the possible beneficial effect of the P-OH moiety.[43] Among the arene complexes (Table 3.1), the symmetric dppf-based complex **10** performed better than the dissymmetric complexes **11-13**. Unfortunately, no beneficial effect of the P-OH moiety in complex **13** was observed. Chelate complexes **17** and **18** with (η^5-C_5H_5) ligand showed no appreciable catalytic activity. The second testing reaction was the cyclization of (*Z*)-3-methylpent-2-en-4-yn-1-ol into 2,3-dimethylfuran (Table 3.2). Dinuclear complexes **10-13** showed a high catalytic activity even at room temperate. However, the effect of the different ligands in the complexes on the catalytic reactivity was rather marginal. Chelate complexes **17** and **18** were again catalytically inactive.

Table 3.1. Ruthenium-catalyzed isomerization of estragole to anethole.

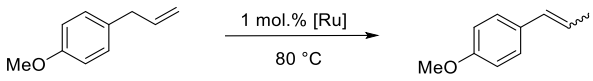

Catalyst	Conversion [%]	*E*/*Z*
10	97	90/10
11	85	78/22
12	68	76/24
13	25	70/30
17	<5	-
18	<5	-

Reaction conditions: ruthenium(II) catalyst (1 mol.%), K_2CO_3 (6 mol.%), H_2O (1 mL), 80 °C, 6 h. The conversions were determined by ^{1}H NMR spectroscopy and are an average of two independent runs.

Table 3.2. Ruthenium-catalyzed cyclization of (*Z*)-3-methylpent-2-en-4-yn-1-ol.

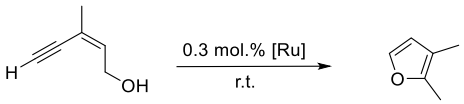

Catalyst	Conversion [%]
10	76
11	81
12	80
13	78
17	0
18	0

Reaction conditions: ruthenium(II) catalyst (0.3 mol.%), room temperature, solvent-free, 18 h. The conversions were determined by ^{1}H NMR spectroscopy and represent an average of two independent runs.

The collected results showed that **1** can serve as a practical precursor in the synthesis of dissymmetric bisphosphine ligands. However, the catalytic activity of the prepared Ru(II) complexes in the selected model reactions was only moderate. Therefore, the value of the presented research has to be seen in the pioneering synthesis of novel phosphine ligands equipped with primary phosphine oxide group.

3.2 A stable primary phosphine oxide and its heavier congeners

Encouraged by the extraordinary stability of the primary phosphine oxide **7**, we decided to further investigate the chemistry of these species. For this purpose, the known air-stable primary phosphine **20** was prepared as a starting material by an alternative synthesis in approximately 50% yield over three steps (Scheme 3.7).

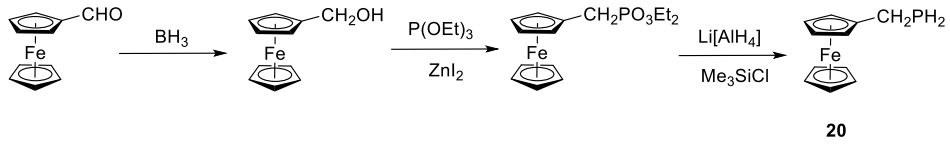

Scheme 3.7. Synthesis of primary phosphine **20**.

Gratifyingly, primary phosphine oxide **20O** was obtained as a single product from oxidation of **20** with hydrogen peroxide or 3-chloroperbenzoic acid (MCPBA) and isolated in 80% or 90% yield, respectively (Scheme 3.8). The compound is bench-stable in both the solution and the solid form. Spontaneous disproportionation, typical for primary phosphine oxides, was observed only upon heating of the compound in solution to 100 °C (Scheme 3.9). Although phosphine oxide **20O** is air-stable, it can be further oxidized to phosphinic acid **21** by a second equivalent of MCPBA.

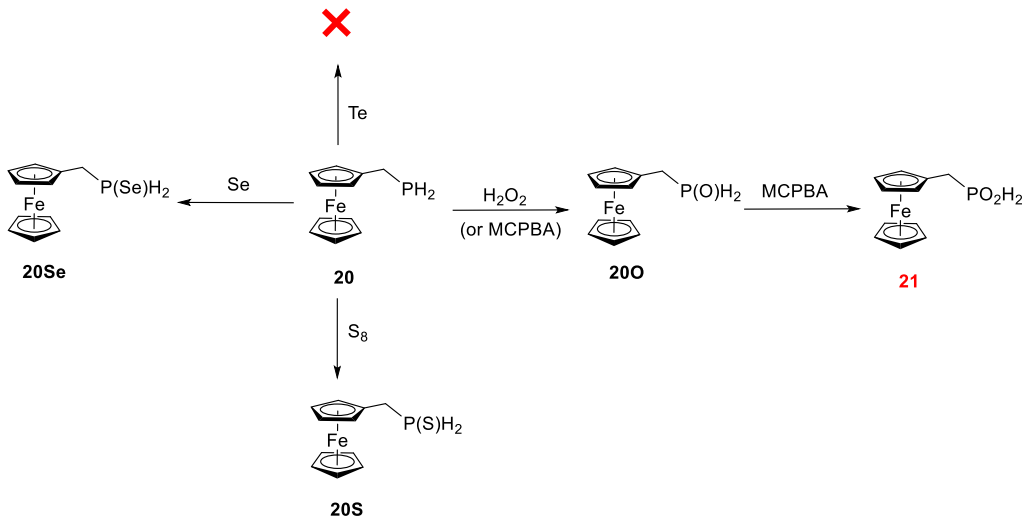

Scheme 3.8. Synthesis of primary phosphine chalcogenides.

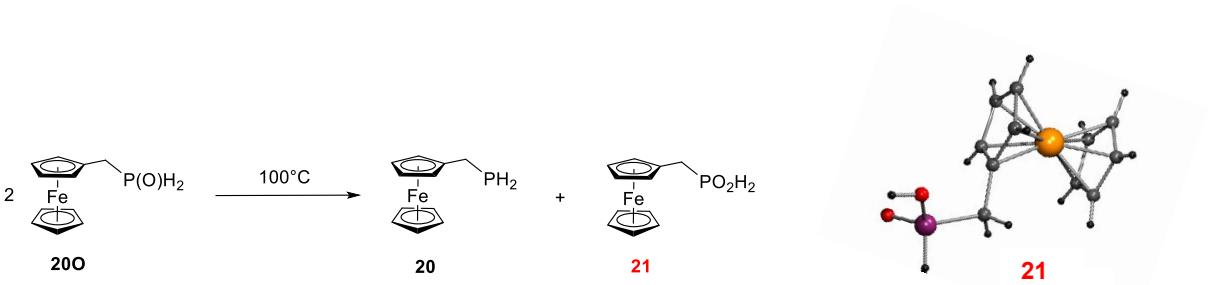

Scheme 3.9. Disproportionation of phosphine oxide **20O** and the structure of acid **21**.

The reaction of primary phosphine **20** with sulfur crucially depends on the reaction temperature (Scheme 3.8). Irrespective of the amount of sulfur, the reaction at low temperature gave only modest conversion. In contrast, higher temperatures led to degradation of the product into a mixture of polythionated compounds. When using 10 eq. of sulfur (in benzene at 50 °C overnight), product **20S** was isolated in 30% yield as a yellow solid, which is stable under an inert atmosphere.

Conversely, the reaction of **20** with grey selenium smoothly produced selenide **20Se** as the sole product. Compound **20Se** is thermally robust. Under strictly inert conditions, heating of the selenide in toluene at 100 °C did not lead to disproportionation or decomposition. Compound **20Se** is stable under an inert atmosphere, but in air it decomposes under release of red selenium. The $^{1}J_{PSe}$ coupling constant determined for the primary selenide **20Se** (733 Hz) is similar to the value of the corresponding tertiary phosphine selenide, $FcCH_2P(Se)Ph_2$ (728 Hz). Finally, no reaction occurred when treating the phosphine **20** with elemental tellurium. It is also noteworthy that in solutions as well as in the solid state, all prepared chalcogenides exit only as "keto" tautomers.

The reactivity and coordination properties of phosphine oxide **20O** were next examined through reaction with zinc(II) iodide, ruthenium(II) complex $[(\eta^6\text{-Mes})RuCl_2]_2$, borane and tris(pentafluorophenyl)borane (Scheme 3.10). Generally, the observed reactivity was similar to the reactivity of secondary phosphines.[42,71] Specifically, the reaction of zinc iodide with two equivalents of **20O** yielded phosphine oxide complex **22**, whereas a facile tautomerization occurred when treating **20O** with $[(\eta^6\text{-mes})RuCl_2]_2$ leading to complex **23**. The reaction of **20O** with tris(pentafluorophenyl)borane afforded the Lewis adduct **24**. Finally, the reaction of **20O** with borane led to a mixture of products. Based on the characteristic shifts in the ^{31}P NMR spectrum (Figure 3.1), few components were identified as the primary phosphine **20** and adducts

20·BH_3 and **20O**·BH_3. Rather surprisingly, the reaction of $[(\eta^6\text{-mes})RuCl_2]_2$ with chalcogenides **20S** or **20Se** resulted in a clean elimination of the chalcogen atom to produce complex **25**.

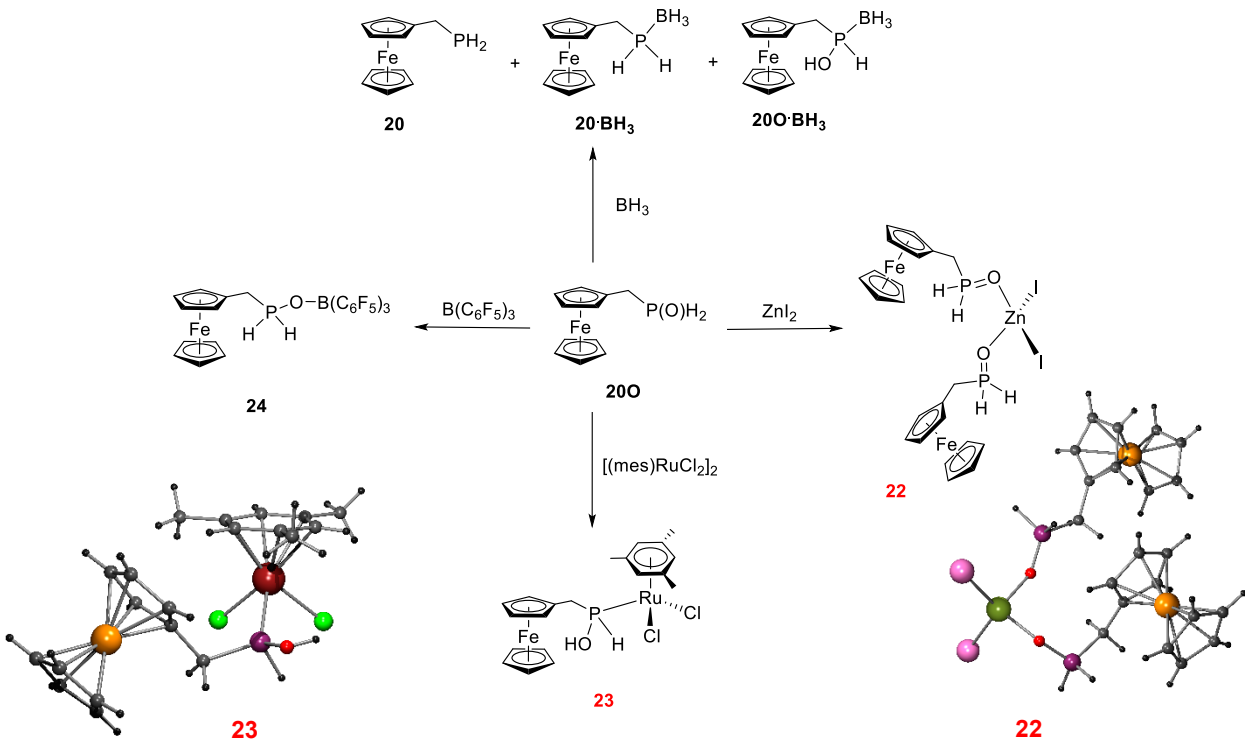

Scheme 3.10. Reactivity of phosphine oxide **20O** and the molecular structures of **22** and **23**.

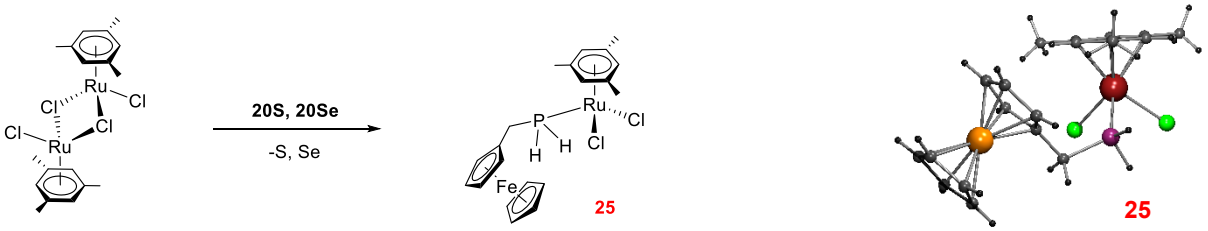

Scheme 3.11. The reaction of $[(\eta^6\text{-mes})RuCl_2]_2$ with chalcogenides **20S** or **20Se** leading to complex **25**.

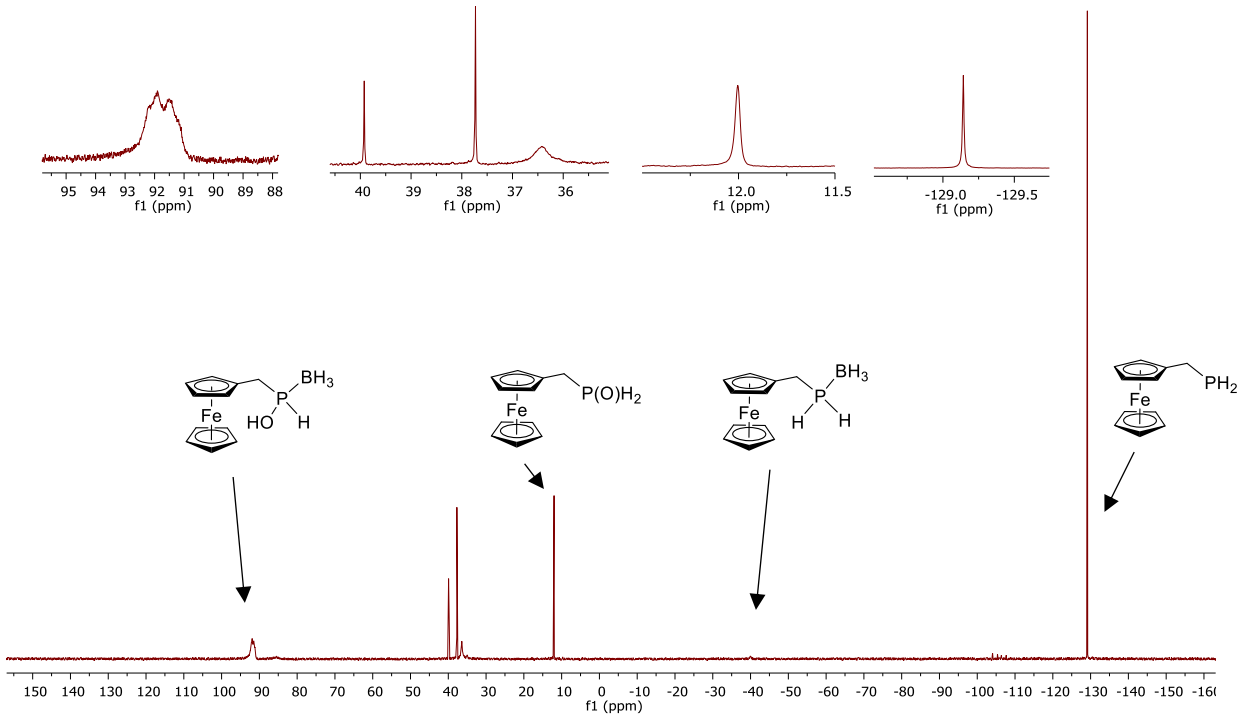

Figure 3.1. ^{31}P NMR spectrum (162 MHz, $CDCl_3$) of the mixture of products obtained by the reaction of **20O** with borane.

The reactivity of **20O** in addition reactions examined next, was found to truly depend on steric factor. Thus, the reactions with acetaldehyde and benzaldehyde afforded the products of two-fold addition **26a** and **26b**. Conversely, the reaction with acetone yielded mono-addition product **27a**, and the more sterically encumbered benzophenone furnished a mixture of the addition product **27b** and the starting materials in an equilibrium. The reaction of **20O** with phenyl isocyanate and isothiocyanate produced phospha-ureas **28a** and **28b**. Surprisingly, **20O** did not react with 4-ethynyltoluene.

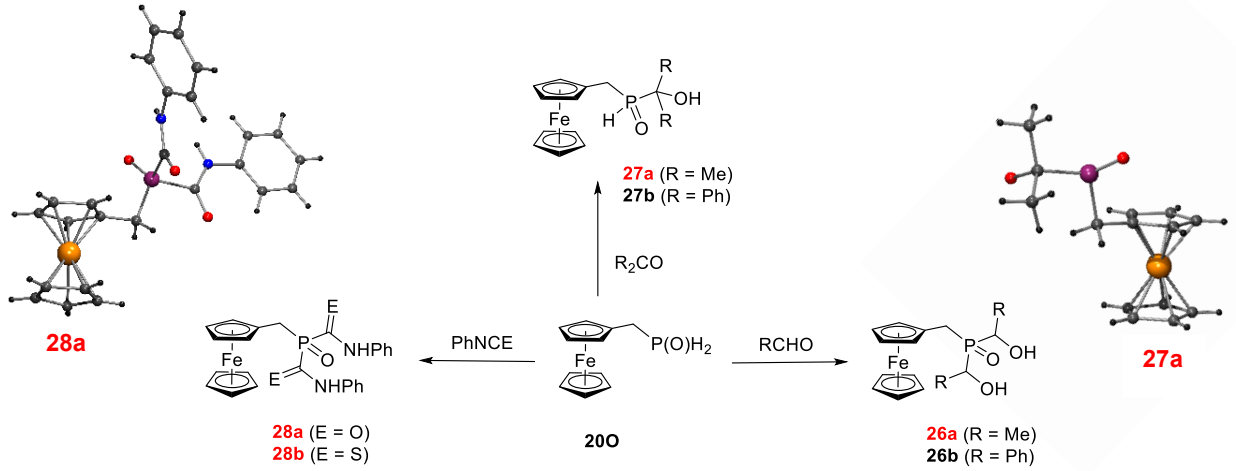

Scheme 3.12. Addition reactions of **20O** and selected structures of the addition products.

In summary, the presented work led to isolation of the first complete series of isolable primary phosphine chalcogenides. The fact that the structure of stable **20O** was inspired by the structure of the electronically stabilized primary phosphine **20** (Figure 1.2) allows to formulate a following hypothesis: the air-stable primary phosphines provide air-stable primary phosphine oxides. Confirmation of the hypothesis lies in future research. Coordination properties and fundamental reactivity of **20O** were also studied in this work. However, a more comprehensive study of the reactivity of primary phosphine oxides (comparable with the vast literature on the chemistry of secondary phosphine oxides) remains a great challenge.

3.3 Ferrocene bisphosphines bearing phosphatrioxaadamantyl substituents

With the stable primary/tertiary bisphosphine **1** in hands, we sought for further reactions that may provide new types of ferrocene phosphines. Thus, stable crystalline bisphosphine **29** was prepared in 61% yield by HCl-catalyzed Epstein-Buckler reaction[47] of bisphosphine **1** with acetylacetone (Scheme 3.13). Synthesis of the homologous compound **30**, lacking a suitable air-stable precursor, had followed a different synthetic strategy. Specifically, the published two-step synthesis of CgPBr was reproduced (Scheme 3.14) and the compound was used in stepwise lithiation/functionalization of 1,1'-dibromoferrocene (Scheme 3.15). The route employing phosphine **31** as an intermediate resulted in a better yield of **30** (48%) than the procedure where the order of introduction of the phosphine substituents was inverted. Phosphines **29**, **30** and **31** were further converted into the respective phosphine selenides. The CgP(Se) moieties expectedly

showed larger $^1J_{PSe}$ constants (757, 766, 766 Hz, respectively) than the PPh_2 group ($^1J_{PSe}$ ≈735 Hz), in line with lower basicity of cage phosphines.

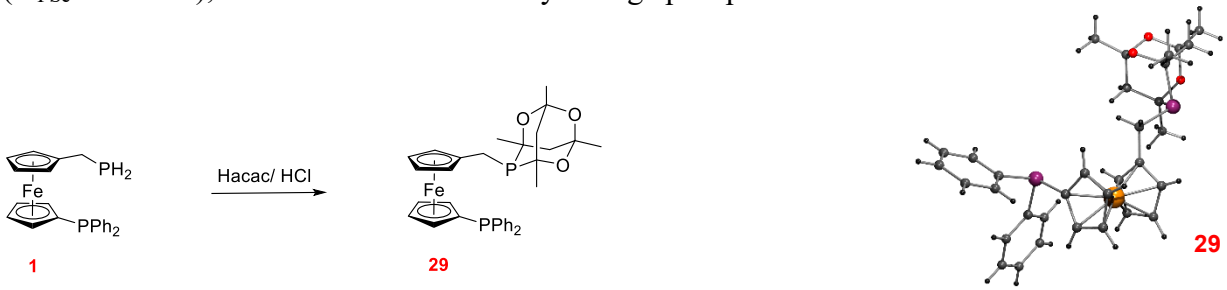

1 29

Scheme 3.13. Buckler-Epstein reaction of **1** and the structure of bisphosphine **29**.

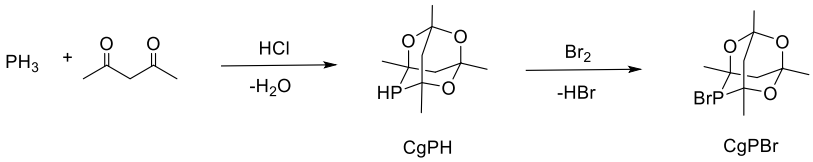

Scheme 3.14. Synthesis of CgPBr.

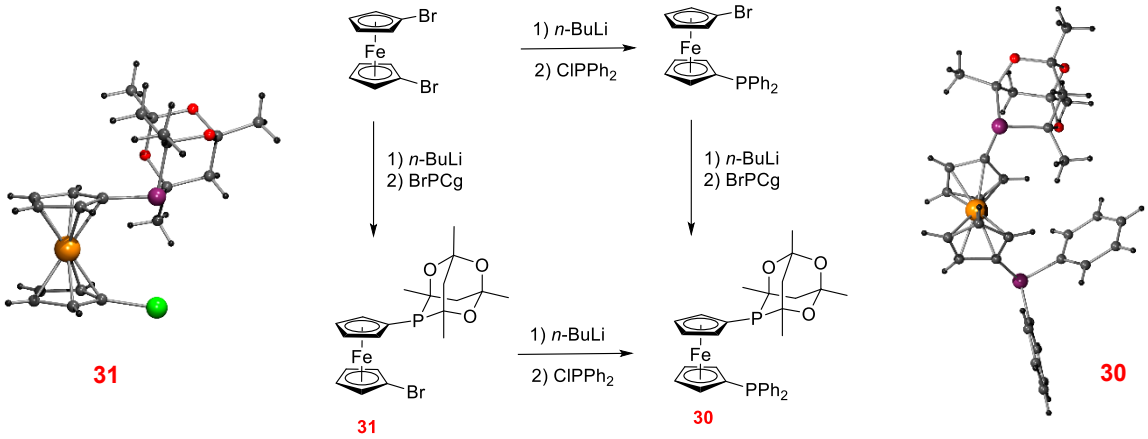

Scheme 3.15. Two routes toward synthesis of bisphosphine **30** and the molecular structures of **30** and **31**.

Coordination properties of bisphosphines **29** and **30** were probed in palladium(II) complexes. While bisphosphine **30** in the reaction with $[PdCl_2(MeCN)_2]$ produced selectively chelate complex **32,** ligand **29** afforded a complicated product mixture, wherein compounds **33a** and **33b** dominated. Upon refluxing the mixture overnight, the equilibrium shifted in favor of complex **33b**, which was crystallized.

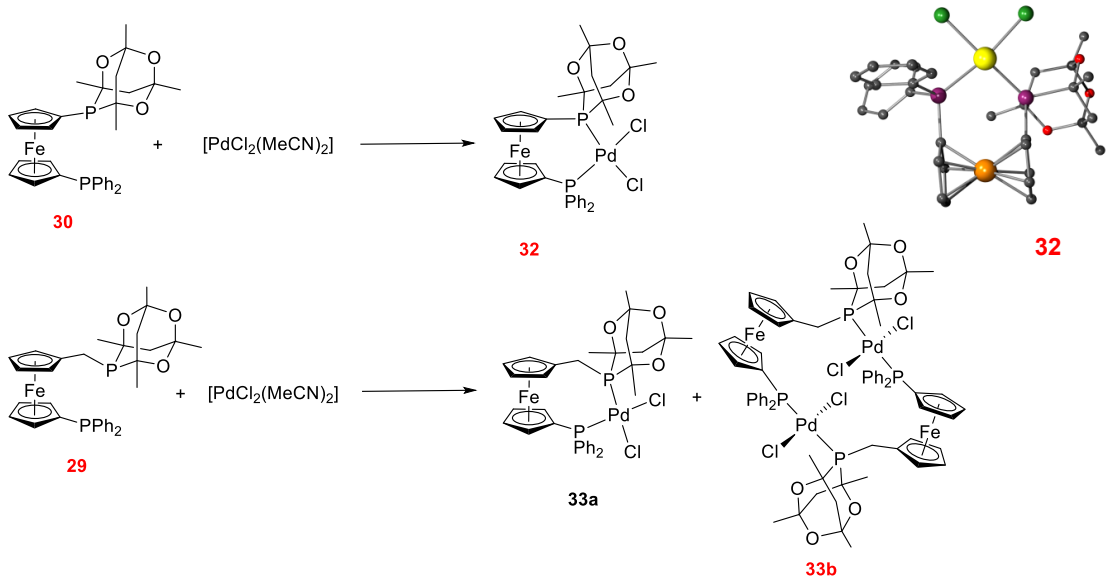

Scheme 3.16. Reactions of bisphosphines **30** and **29** with $[PdCl_2(MeCN)_2]$ and the structure of chelate complex **32**.

Catalytic properties of bisphosphines **29** and **30** were evaluated in two cross-coupling reactions and compared with those of dppf. Considering the complicated coordination behavior of ligand **29**, the palladium catalysts for the catalytic tests were generated *in situ* using two different palladium sources ($Pd(OAc)_2$ and $[PdCl_2(cod)]$).

Table 3.3. Palladium(II)-catalyzed cyanation of aryl bromides with $[K_4Fe(CN)_6]$.

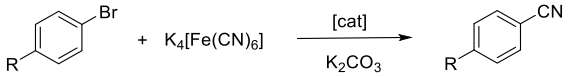

R = OMe, CF_3

Substrate/ligand	dppf	29	30
NMR yield of the coupling product [%] (palladium source = $Pd(OAc)_2$)			
MeO	60	62	100
CF_3	73	27	82
NMR yield of the coupling product [%] (palladium source = $[PdCl_2(cod)]$)			
MeO	62	81	100
CF_3	21	53	16

Reaction conditions: aryl bromide (2.0 mmol), palladium(II) catalyst (0.4 mol.%), $[K_4Fe(CN)_6]$ (1.0 mmol), K_2CO_3 (2.0 mmol), dioxane/water, 100 °C, 8 h. The conversions were determined by integrating ^1H NMR spectra and are an average of two independent runs.

For the first study reaction, palladium-catalyzed cyanation of aryl bromides with $K_4[Fe(CN)_6]$, the reaction conditions were adopted from my previous studies.[72] Two aryl bromides with electronically distinct substituents were investigated as substrates (Table 3.3). Independently on the palladium(II) source, ligand **30** showed the best results in the reaction of the electron-rich substrate. On the other hand, the substrate bearing the electron-withdrawing CF_3 group performed consistently better when using $Pd(OAc)_2$ precursor.

For the second study reaction, cross-coupling of benzoyl chlorides with phenylboronic acid, a similar array of experiments was used (Table 3.4).[73] Even in this case, the catalyst based on bisphosphine **30** afforded the best yields. In this case, the palladium source did not substantially affect the conversion.

Table 3.4. Palladium(II)-catalyzed cross-coupling of benzoyl chlorides with phenylboronic acid.

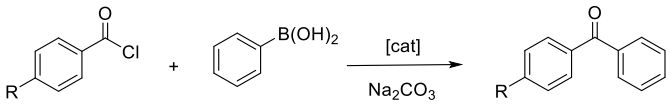

R = OMe, CF_3

Substrate/Ligand	dppf	29	30
NMR yield of the coupling product [%] (palladium source = $Pd(OAc)_2$)			
MeO	53	20	100
CF_3	92	100	100
NMR yield of the coupling product [%] (palladium source = $[PdCl_2(cod)]$)			
MeO	44	20	100
CF_3	53	93	100

Reaction conditions: benzoyl chloride (3.0 mmol), phenylboronic acid (2.5 mmol), palladium(II) catalyst (0.1 mol.%), Na_2CO_3 (2.5 mmol), anisole (2.5 mmol; internal standard) toluene/water, 50°C, 1 h. The conversions were determined by integration of ^1H NMR spectra and represent an average of two independent runs.

The catalytic results obtained with the new bisphosphines in palladium(II) complexes, more or less comparable with the reactivity of dppf and already published catalysts,[72,73] did not satisfy my desire to fully demonstrate the catalytic potential of the newly prepared ferrocene cage phosphines. In searching for challenging catalytic applications, I came across C-H arylations that offer an atom economic alternative to cross-coupling reactions and have decided to prepare defined Pd(0) precatalysts. For this purpose, palladium(0) precursor [Pd(ma)(N^N)] was synthesized according to the literature[74] and reacted with dppf, **29** and **30** (Scheme 3.17).

All bisphosphine ligands smoothly displaced the diimine ligand and produced bench stable chelate complexes **34**, **35** and **36** as the sole products.

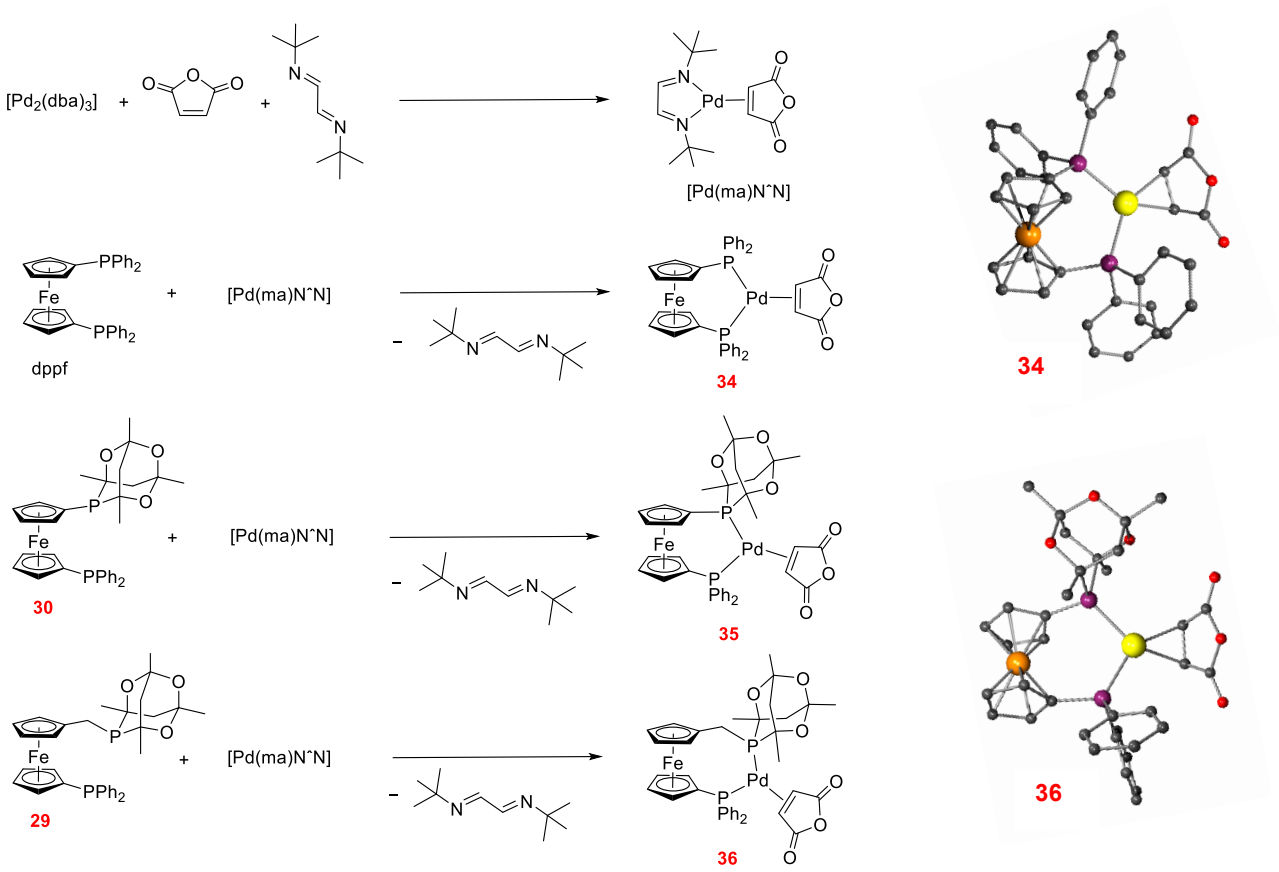

Scheme 3.17. Synthesis of palladium(0) complexes with dppf, **29** and **30** as the ligands and the molecular structures of **34** and **36**.

The isolated complexes were subsequently applied in C-H arylation of benzoxazoles with aryl chlorides. Reaction conditions for the first set of catalytic tests were adopted from the literature (Table 3.5).[75]

Table 3.5. Arylation of benzoxazole with chlorobenzene.

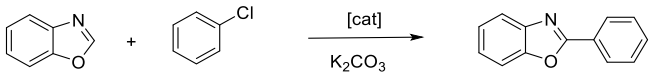

Catalyst	Conversion [%]
34	53
35	48
36	75
[Pd(ma)(N^N)]	25

Reaction conditions: benzoxazole (1.0 mmol), chlorobenzene (1.5 mmol), palladium(0) catalyst (1.5 mol.%), K_2CO_3 (2 mmol), *n*-BuOH, 125 °C, 18 h. The conversions were determined by integrating ^{1}H NMR spectra and are an average of two independent runs.

Catalyst **36** containing the homologated ligand **29** performed considering better than complexes based on the other bisphosphines and far better than the precursor [Pd(ma)(N^N)]. The base additive and reaction solvent were optimized in the following experiments (Table 3.6), which led to the "final" reaction conditions used for a substrate study (*n*-BuOH, 125 °C, 18 h, K_3PO_4, as the base, 1 mol.% of the catalyst, Table 3.7). Benzoxazole proceeds satisfactorily with electron-poor and electron-rich aryl chlorides except when sterically hindered.

Table 3.6. Optimization of the reaction conditions.

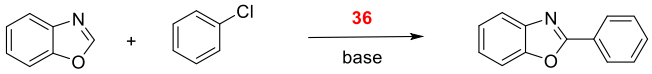

1.0 mol.% of complex **36**

base	conversion [%]	base	conversion [%]
Na_2CO_3	8	KOAc	<5
K_2CO_3	26	CsOAc	11
Cs_2CO_3	100	$KHCO_3$	34
NaOAc	0	K_3PO_4	100

0.5 mol.% of complex **36**

solvent	conversion [%]
n-BuOH	100
t-BuOH	73
toluene	13
toluene/H_2O	0
dmf	24

Reaction conditions: benzoxazole (1.0 mmol), chlorobenzene (1.5 mmol), complex **36** (1.0 or 0.5 mol.%), base (2 mmol), solvent, 125 °C, 18 h. The conversions were determined by integrating ^{1}H NMR spectra and are an average of two independent runs.

Table 3.7. Substrate scope experiments.

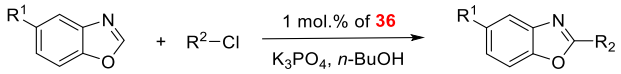

R^1	R^2	conversion (yield) [%]	R^1	R^2	conversion (yield) [%]
H	Ph	100 (76)	H	4-F-C_6H_4	100 (79)
H	4-Me-C_6H_4	100 (73)	H	4-CN-C_6H_4	88 (68)
H	4-CF_3-C_6H_4	100 (76)	H	pyridin-2-yl	100 (86)
H	2-Me-C_6H_4	85 (70)	Me	Ph	100 (82)
H	3-Me-C_6H_4	100 (82)	Me	4-Me-C_6H_4	100 (84)
H	napht-1-yl	90 (69)	Me	4-CF_3-C_6H_4	100 (79)
H	napht-2-yl	100 (76)	Cl	Ph	– (85)
H	4-MeO-C_6H_4	81 (62)	Cl	4-Me-C_6H_4	– (76)
H	4-Ac-C_6H_4	61 (37)	Cl	4-CF_3-C_6H_4	– (66)

Reaction conditions: heterocycle (1.0 mmol), chloroarene (1.5 mmol), complex **36** (1.0 mol.%), K_3PO_4 (1.5 mmol), *n*-BuOH, 125 °C, 18 h. The conversions were determined by integrating ^{1}H NMR spectra. The conversions and the yields are an average of two independent runs.

The collected results illustrate the favorable catalytic properties of the dissymmetric, methylene spaced ferrocene bisphosphines. The presented combination of the unexpensive base, environmentally benign solvent, and low catalyst loading with a high reaction selectivity in the C-H arylation of benzoxazoles is a challenge for future research studies. Unfortunately, the efforts to expand the substrate scope (oxazole, oxazoline, benzothiazole, 1-methylbenzimidazole) were unsuccessful. In addition, a question arises: is it complex **36** successful catalysts due to the presence of the methylene spacer between the ferrocene and PCg moieties, or because of the steric properties of the cage phosphine and its electronic properties? The answer should provide the following catalytic research focused on the corresponding palladium(0) complexes with electronically differentiated ligands, [Pd(η^2-ma)($Ph_2PfcCH_2PR_2$)], where R = Ph, 3,5-Me-C_6H_3, 3,5-CF_3-C_6H_3.

3.4 Ferrocene phosphine ligand bearing phosphonic acid group

A new hybrid ligand **37** with phosphonic acid group was obtained by hydrolysis of the corresponding diethyl phosphonate $Ph_2PfcPO_3Et_2$[69] in 67% yield (Scheme 3.18). Unfortunately, the compound slowly decomposed at room temperature or even when stored at 4 °C.

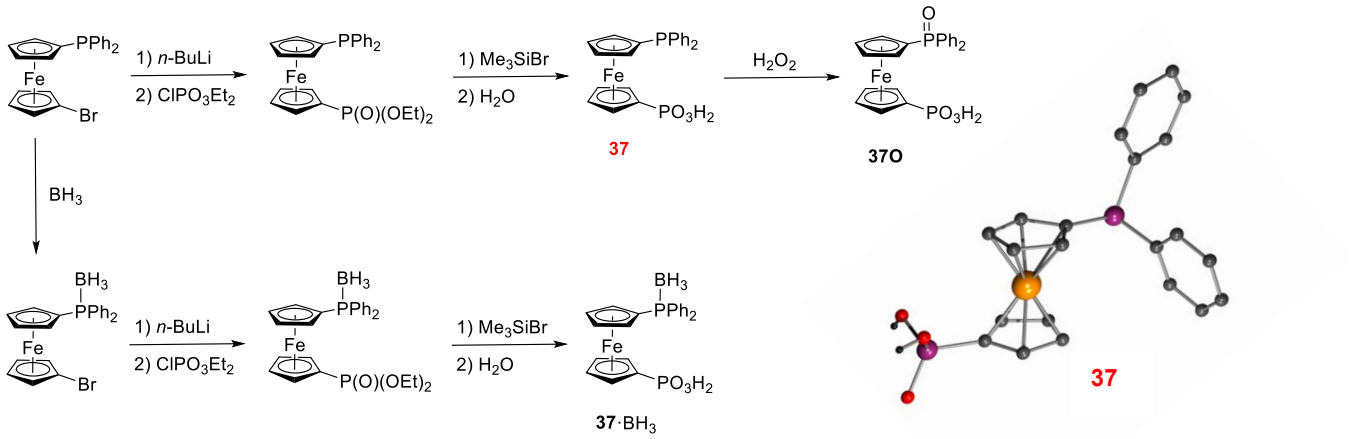

Scheme 3.18. Synthesis of hybrid ligand **37**, phosphine oxide **37O** and borane adduct **37·BH$_3$**; view of the molecular structure of **37**.

It has to be mention that spontaneous decomposition of ferrocenephosphonic acids has already been reported.[76] Thus, we decided to study the possible influence of the diphenylphosphine group on this process. For this purpose, compounds **37O** and **37·BH$_3$** with protected phosphine groups were prepared and proved bench stable. In contrast, attempts to stabilize acid **37** by neutralization were unsuccessful because the obtained salts **38** and **39** exerted the same level of lability as the free acid.

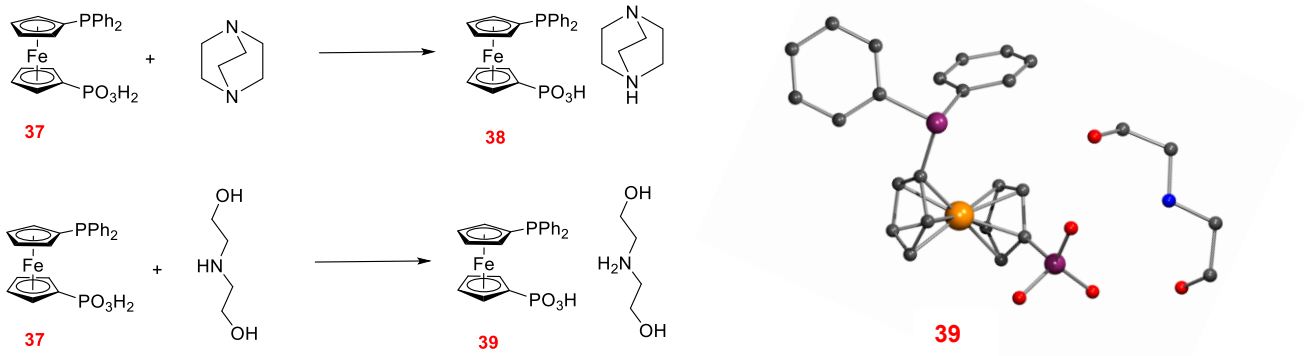

Scheme 3.19. Synthesis of salts **38** and **39** and the molecular structure of **39**.

The stability of compound **37·BH$_3$** suggested that transition metal complexes of **37** could be as well stable. Surprisingly, complex **40** was the most labile molecule in this study. In contrast, chelate complexes **41a** and **41b** containing deprotonated acid **37** were stable under ambient conditions.

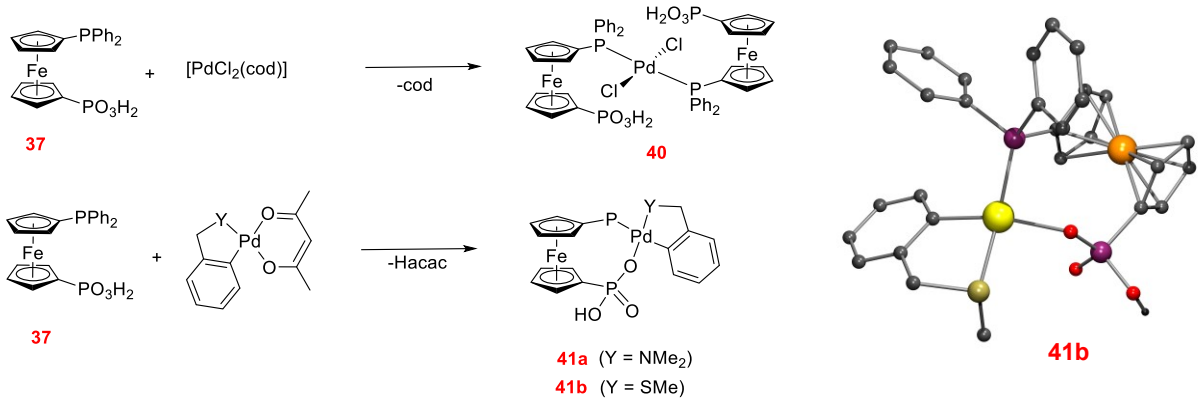

Scheme 3.20. Synthesis of palladium(II) complexes **40** and **41** and the molecular structure of **41b**.

Although the instability of **37** precluded its further utilization, the prepared and structurally characterized compounds revealed interesting hydrogen-bonded modes.

4. Conclusion

This Thesis aimed to synthesize and study in detail novel electronically dissymmetric ferrocene bisphosphines containing a methylene spacer between one of the phosphine groups and the ferrocene moiety. As a suitable precursor for the synthesis of these tertiary bisphosphines, 1-(diphenylphosphino)-1'-(phosphinomethyl)ferrocene $Ph_2PfcCH_2PH_2$ (fc = ferrocene-1,1'-diyl) was proposed. While studying the reactivity of the primary phosphine group in this compound, a unique molecule with a primary phosphine oxide group was isolated ($Ph_2PfcCH_2P(O)H_2$). Dissymetric bidentate ligands with primary phosphine, primary phosphine oxide, and tertiary phosphine group were then successfully compared in a coordination and catalytic study with ruthenium(II) complexes. However, in selected catalytic reactions, no beneficial effect of the dissymmetric bisphosphines was observed.

For a more detailed study of the properties of the stabilized primary phosphine group, ferrocenylmethylphosphine $FcCH_2PH_2$ (Fc = ferrocenyl) was synthesized and converted into a series of unexpectedly stable primary phosphine chalcogenides $FcCH_2P(Y)H_2$ (Y = O, S, Se). Comprehensive coordination study, description of their stability and fundamental reactivity studies are the cornerstone of a future research on these compounds.

Defined palladium(II) and palladium(0) complexes with new dissymmetric bisphosphines bearing cage phosphine groups ($Ph_2PfcPCg$ and $PhPfcCH_2PCg$; PCg = 6-phospha-2,4,8-1,3,5,7-tetramethyladamantane) were compared with the widely studied dppf in selected catalytic reactions. Palladium(II) complexes of the new dissymmetric bisphosphines showed catalytic activity in the same ranges as dppf complexes in Suzuki-Miyuara reaction of benzoyl chlorides with arylboronic acids and in cyanation of aryl bromides with $K_4[Fe(CN)_6]$. On the other hand, palladium(0) complex with the methylene spaced bisphosphine **36** showed excellent catalytic activity in selective C-H arylation of benzoxazoles with aryl chlorides.

Lastly, a new polar ligand, 1'-(diphenylphosphino)ferrocene-1-phosphonic acid ($PPh_2fcPO_3H_2$), was prepared and studied in palladium(II) complexes. However, the acid decomposed upon prolonged storage, which prevented further studies into catalytic properties of these compounds.

5. References

(1) a) Kölmel, C.; Ochsenfeld, C.; Ahlrichs, R. *Theor. Chim. Acta* **1991**, *82*, 271-284; b) Montgomery, C. D. *J. Chem. Educ.* **2013**, *90*, 661-664; c) Rauk, A.; Allen, L. C.; Mislow, K. *Angew. Chem., Int. Ed. Engl.* **1970**, *9*, 400-414.

(2) Gilheany D. G. *Structure and bonding in organophosphorus(III) compounds* in *The chemistry of organophosphorus compounds*, ed. Hartley, F. R.; John Wiley & Sons, Chichester, 1990, ch. 2, pp. 9-49.

(3) a) Fleming, J. T.; Higham, L. J. *Coord. Chem. Rev.* **2015**, *297*, 127-145; b) Higham, L. J. *The primary Phosphine Renaissance* in *Phosphorus Compounds Advanced Tools in Catalysis and Material Sciences*, ed. Peruzzini, M.; Gonsalvi, L.; Springer, Dordrecht, 2011, ch. 1, pp. 1-19.

(4) a) Lever, A. B. P. *Fundamentals: Ligands, Complexes, Synthesis, Purification, and Structure* in *Comprehensive Coordination Chemistry II: From Biology to Nanotechnology*, eds. McCleverty, J. A.; Meyer, T. J.; Elsevier Science, 2004, vol 1, ch. 1, pp 256-259; b) Katti, K. V.; Pillarsetty, N.; Raghuraman, K. *New Vistas in Chemistry and Applications of Primary Phosphines* in *New Aspects in Phosphorus Chemistry III*, ed. Majoral, J.-P.; Springer, Berlin, 2003, pp. 121-141.

(5) a) Hiney, R. M.; Higham, L. J.; Müller-Brunz, H.; Gilheany, D. G. *Angew. Chem. Int. Ed.* **2006**, *45*, 7248-7251; b) Goodwin, N. J.; Henderson, W.; Nicholson, B. K.; Fawcett, J.; Russell, D. R. *J. Chem. Soc. Dalton Trans.* **1999**, 1785-1793; c) Brynda, M. *Coord. Chem. Rev.* **2005**, *249*, 2013-2034.

(6) a) Goodwin, N. J.; Henderson, W.; Nicholson B. K. *Chem. Commun*. **1997**, 31-32; b) Goodwin, N. J.; Henderson, W.; Nicholson B. K.; Fawcett, J.; Russell, D. R. *Chem. Soc. Dalton Trans.* **1999**, 1785-1794.

(7) Stewart, B.; Harriman, A.; Higham, L. J. *Organometallics* **2011**, *30*, 5338–5343.

(8) a) a) Lever, A. B. P. *Fundamentals: Ligands, Complexes, Synthesis, Purification, and Structure* in *Comprehensive Coordination Chemistry II: From Biology to Nanotechnology*, eds. McCleverty, J. A.; Meyer, T. J.; Elsevier Science, 2004, vol 1, ch. 1, pp 256-259; c) Pomer, H. Angew. *Chem. Int. Ed. Engl*. 1977, 423-424.; b) Nell, B. P.; Tyler, D.R. *Coord. Chem. Rev*. **2014**, *279*, 23–42; c) Honaker, M. T.; Hovland, J. M.;

Salvatore, R. N. *Curr. Org. Synth.* **2007**, *4*, 31-45; d) Troev, K. D. *Reactivity of P-H Group of phosphines* in *Reactivity of P-H Group of phosphorus Based Compounds*, ed. Troev, K. D.; Elsevier, London, 2018, ch. 2, 19-144.

(9) a) Svara, J.; Weferling, N.; Hofmann, T. *Phosphorus Compounds, Organic* in *Ullmann's Encyclopedia of Industrial Chemistry*, Wiley-VCH, Weinheim, 2012, pp. 20-26; b) Lever, A. B. P. *Fundamentals: Ligands, Complexes, Synthesis, Purification, and Structure* in *Comprehensive Coordination Chemistry II: From Biology to Nanotechnology*, eds. McCleverty, J. A.; Meyer, T. J.; Elsevier Science, 2004, vol 1, ch. 1, pp 256-259; c) Pomer, H. *Angew. Chem. Int. Ed. Engl*. 1977, 423-424.

(10) a) Bucker, S. A.; Epstein, M. *Tetrahedron* **1962**, *18*, 1211-1219; b) Buckler, S. A; Epstein, M. *Tetrahedron* **1962**, *18*, 1221-1230; c) Quin, L. D. *A Guide to Organophosphorus Chemistry*, John Wiley & Sons, New York, 2000, pp. 96-118; d) Troev, K. D. *Reactivity of P-H Group of phosphine oxides* in *Reactivity of P-H Group of Phosphorus Based Compounds*, ed. Troev, K. D.; Elsevier, London, 2018, ch. 3, pp. 145-198.

(11) Pellerin, B.; Guenot, P.; Denis, J.-M. *Tetrahedron Lett.* **1987**, *28*, 5811-5814.

(12) Buckler, S. A.; Epstein, M. *J. Am. Chem. Soc.* **1960**, *82*, 2076-2077.

(13) Yoshifuji, M.; Shibayama, K.; Toyota, K.; Inamoto N. *Tetrahedron Letters* **1983**, *24*, 4227.

(14) Uhlig, F.; Herrmann, E.; Schaedler, D.; Ohms, G.; Grosmann, G.; Besser, S.; Herbst-Irmer, R. *Z. Anorg Allg. Chem.*, **1993**, *619*, 1962-1970.

(15) a) Walther, B. *Coord. Chem. Rev.* **1984**, *60*, 67-105; b) Peters, G. *J. Am. Chem. Soc*. **1960**, *82*, 4751; c) Peters, G. *J. Org. Chem.* **1962**, *27*, 2198–2201; d) Gusarova, N. K.; Malysheva, S. F.; Belogorlova, N. A.; Sukhov, B. G.; Trofimov, B. A. *Synthesis* **2007**, 2849-2852.

(16) Sander, M. *Chem. Ber.* **1960**, *93*, 1220-1230.

(17) a) Peters, G.; *J. Am. Chem. Soc.* **1960**, 82, 4751; b) Malysheva, S. F.; Artem'ev, A. V.; Gusarova, N. K.; Timokhin, B. V.; Tatarinova, A. A.; Trofimov, B. A. *Russ. J. Gen. Chem.* **2009**, *79*, 1617-1621; c) Verkhoturova, S. I.; Kazantseva, T. I.; Arbuzova, S. N.; Albanov, A. I.; Gusarova, N. K., Trofimov, B. A. *Russ. J. Gen. Chem.* **2014**, *84*, 1742-1747.

(18) a) Edmundson, R. S. *Chemical properties and reactions of Phospline chalcogenides* in *The chemistry of organophosphorus compounds*, ed. Hartley, F. R.; Wiley & Sons, Chichester, 1992, ch. 7, pp. 287-408; b) Hayashi, M. *Chem. Lett*. **2021**, *50*, 1-6.

(19) a) Routaboul, L.; Vincendeau, S.; Daran, J.-C.; Manoury, E. *Tetrahedron* **2005**, *16*, 2685-2690; b) Škoch, K. Císařová, I.; Schulz, J.; Siemeling, U.; Štěpnička, P. *Dalton Trans*. **2017**, *46*, 10339-10354.

(20) Sambiagio, C.; Schönbauer, D.; Blieck, B.; Dao-Huy, T.; Pototschnig, G.; Schaaf, P.; Wiesinger, T.; Zia, M. F.; Wencel-Delord, J.; Besset, T.; Maes, B. U. W.; Schnürch M. *Chem. Soc. Rev*. **2018**, *47*, 6603-6743.

(21) Song, X.; Xu, H. *J. Inf. Disp*. **2020**, *21*, 149-172.

(22) Finkbeiner, P.; Hehn, J. P.; Gnamm C. *J. Med. Chem.* **2020**, *63*, 7081-7107.

(23) a) Chrzanowski, J.; Krasowska, D.; Drabowicz, J. *Heteroatom Chem*. **2018**, 29, e21476; b) *Tetrahedron Lett*, **2020**, *61*, 151421.

(24) Platt, A. W. G. *Coord. Chem. Rev*. **2017**, *340*, 62-78.

(25) Malysheva, S. F.; Belogorlova, N. A. Vereshchagina, Y. A.; Alimova, A. Z.; Ishmaeva, E. A.; Chachkov, D. V. *Russ. J. Gen. Chem.,* **2016***, 86,* 590-601.

(26) Maddox, S. M.; Dinh, A. N.; Armenta, F. Um, J.; Gustafson, J. L. *Org. Lett*. **2016**, *18*, 5476-5479.

(27) Zakirova, G. G.; Matveev, P. I.; Mladentsev, D. Y.; Evsiunina, M. V.; Tafeenko, V. A.; Borisova, N. E.; *Mendeleev Commun*. **2019**, *29*, 463-465.

(28) a) Hifumi, R.; Tomita, I. *Polymer* **2020**, *186*, 121855; b) Li, H.; Jiang, Y.; Wang, J.; Zhi, Y.; Dai, Y.; Tao, Y.; Li, M.; Chen, R.; Zheng, C.; Huang, W. *ACS Sustainable Chem. Eng*. **2019**, *7*, 15723-15728.

(29) Xu, Q. Zhou, Y.-B.; Zhao, C.-Q.; Yin, S.-F.; Han, L.-B. *Mini Rev. Med. Chem*. **2013**, *13*, 824-835. a) Malysheva, S. F.; Belogorlova, N. A.; Vereshchagina, Y. A.; Alimova, A. Z.; Ishmaeva, E. A.; Chachkov, D. V. Russ. J. of Gen. Chem. **2016**, *86*, 590-601.

(30) Pop, A.; Silvestru, A.; Gimeno, M. C.; Laguna, A.; Kulcsar, B.; Arca, M.; Lippolis, V.; Pintus, A. *Dalton Trans*., **2011**, *40*, 12479-12490.

(31) a) Beckmann, U.; Süslüyan, D.; Kunz, P. C. *Phosphorus Sulfur Silicon Relat. Elem.* **2011**, *186*, 2061-2070; b) Glueck, D. S. *Modern Aspects of ^{31}P NMR Spectroscopy* in *Organophosphorus Chemistry: From Molecules to Applications*, ed. Iaroshenko, V.;

Wiley-VCH, Weinheim, 2019, ch. 9, pp. 468-469; c) Kroshefsky, R. D.; Weiss, R.; Verkade, J. G. *Inorg. Chem*. **1979**, *18*, 469-72.

(32) a) Achard, T. *CHIMIA* **2016**, *70*, No ½; b) García-Melchor, M.; Ujaque, G.; Maseras, F. Lledos, A. *Theoretical Evaluation of Phosphine Effects in Cross-Coupling* in *Phosphorus Compounds Advanced Tools in Catalysis and Material Sciences*, ed. Peruzzini, M.; Gonsalvi, L.; Springer, Dordrecht, 2011, vol. 37, ch. 3, pp. 57-84; c) Gillespie, J. A.; Zuidema, E.; van Leeuwen, P. W. N. M.; Kamer, P. C. J. *Phosphorus Ligand Effects in Homogeneous Catalysis and Rational Catalyst Design* in *Phosphorus(III) Ligands in Homogenous Catalysis: Design and Synthesis*, eds. van Leeuwen, P. W. N. M.; Kamer, P. C. J.; Wiley & Sons, Chichester, 2012, ch. 1, pp. 1-25; d) Hartwig, J. F. *Organotransition metal chemistry from bonding to catalysis*, University Science Books, US, 2009, pp. 1-1047; e) Crabtree, R. H. *The organometallic chemistry of the transition metals* (*Fourth edition),* Wiley & Sons, Hoboken, 2005, pp. 1-546.

(33) a) Fleming, J. T.; Higham, L. J. *Coord. Chem. Rev.* **2015**, 127-145; b) Brynda, M. *Coord. Chem. Rev.* **2005**, 2013-2034.

(34) Moncea, O.; Poinsot, D.; Fokin, A. A.; Schreiner, P. R.; Hierso J. C. *ChemCatChem* **2018**, *10*, 2915-2922.

(35) Belykh, L. B.; Goremyka, T. V.; Shmidt F. K. *Russ. J. Appl. Chem.* **2004**, *77,* 770-774.

(36) Nell, B. P.; Tyler, D. R. *Coord. Chem. Rev.* **2014**, *279*, 23-42.

(37) a) DelDonno, T. A.; Rosen, W. *J. Am. Chem. Soc.* **1977**, *99*, 8051-8052; b) DelDonno, T. A.; Rosen, W. *Inorg. Chem.* **1978**, *17*, 3714-3716.

(38) Cain, M. F.; Hughes, R. P.; Glueck, D. S.; Golen, J. A.; Moore, C. E.; Rheingold, A. L. *Inorg. Chem.* **2010**, *49*, 7650-7662.

(39) van Lierop, B. J.; Fogg, D. E. *Organometallics* **2013**, *32*, 7245-7248.

(40) a) Raj, J. G. J. *Rev. Inorg. Chem.* **2015**, *35*, 25-56; b) Guo, H, Fan, Y. C.; Sun, Z.; Wu, Y.; Kwon, O. *Chem. Rev.* **2018**, *118*, 10049-10293.

(41) Matheau-Raven, D.; Gabriel, P.; Leitch, J. A.; Almehmadi, Y. A.; Yamazaki, K.; Dixon, D. J. *ACS Catal*. **2020**, *10*, 8880-8897.

(42) a) Gallen, A.; Riera, A.; Verdaguer, X.; Grabulosa, A. *Catal. Sci. Technol*. **2019**, *9*, 5504-5561. b) Shaikh, T. M.; Weng, C.-M.; Hong, F.-E. *Coodr. Chem. Rev.* **2012**, *256*, 771-803; c) Ackermann, L. *Synthesis* **2006**, *10*, 1557-1571; d) Achard, T. *Chimia* **2016**, *70*, 8-

19; e) van Leeuwen, P. W. N. M.; Cano, I.; Freixa, Z. *ChemCatChem* **2020**, *12*, 3982-3994.

(43) González-Fernández, R.; Crochet, P.; Cadierno, V. *Organometallics* **2019**, *38*, 3696-3706.

(44) Payard, P.-A.; Bohn, A.; Tocqueville, D.; Jaouadi, K.; Escoude, E.; Ajig, S.; Dethoor, A.; Gontard, G.; Perego, L. A.; Vitale, M.; Ciofini, I.; Wagschal, S.; Grimaud, L. *Organometallics* **2021**, *40*, 1120-1128.

(45) a) Dai, L.-X.; Hou, X.-L. *Chiral Ferrocenes in Asymmetric Catalysis*, Wiley, Weinheim, **2010**, pp. 1-414; b) Cunningham, L.; Benson, A.; Guiry, P. J. *Org. Biomol. Chem.* **2020**, *18*, 9329-9370; c) Colacot, T. J.; Parisel, S. *Synthesis, Coordination Chemistry and Catalytic Use of dppf Analogs* in *Ferrocenes: ligands, materials and Biomolecules*, ed. Štěpnička, P.; John Wiley & Sons, Chichester, **2008**, ch. 3, 117-140, d) Dey, S.; Pietschnig, R. *Coord. Chem. Rev.* **2021**, *437*, 213850.

(46) a) Štěpnička, P.; Císařová, I.; Schulz, J. *Organometallics* **2011,** 30, 4393-4403; b) Siemeling, U.; Klemann, T.; Bruhn, C.; Schulz, J.; Štěpnička. P.; *Dalton Trans*. **2011**, *40*, 4722-4740. c) Vosáhlo, P.; Císařová, I.; Štěpnička, P. *J. Organomet. Chem.* **2018**, *860,* 14-29.

(47) Epstein, M.; Buckler, A. *J. Am. Chem. Soc.* **1961**, *83*, 3279-3282.

(48) Pringle, P. G.; Smith, M. B. *Phosphatrioxa-adamantane Ligands* in *Phosphorus(III) Ligands in Homogenous Catalysis: Design and Synthesis*, eds. Kamer, P. C. J.; van Leeuwen, P. W. N. M.; John Wiley & Sons, Chichester, 2012, ch. 13, pp. 391-404.

(49) Downing, J. H.; Floure, J.; Heslop, K.; Haddow, M. F.; Hopewell J.; Lusi, M.; Phetmung, H.; Orpen, A. G.; Pringle, P. G.; Pugh, R. I.; Zambrano-Williams, D. *Organometallics* **2008**, *27*, 3216-3224.

(50) Adjabeng, G.; Brenstrum,T.; Wilson, J.; Frampton, C.; Robertson, A.; Hillhouse, J.; McNulty, J.; Capretta, A. *Org. Lett.* **2003**, *5*, 953-955.

(51) Guo, T.; Ding, Y.; Zhou, L.; Xu, H.; Loh, T.-P.; Wu, X. *ACS Catal* **2020**, *10*, 7262-7268.

(52) Shuttleworth, T. A.; Miles-Hobbs, A. M.; Pringle, P. G.; Sparkes, H. A. *Dalton Trans.* **2017**, *46*, 125-137.

(53) Klinkenberg, J. L.; Lawry, K. P. *Org. Process Res. Dev.* **2019**, *23*, 1654-1658.

(54) Lavoie, C. M.; MacQueen, P. M.; Rotta-Loria, N. L.; Sawatzky, R. S.; Borzenko, A.; Chisholm, A. J.; Hargreaves, B. K. V.; McDonald, R.; Ferguson, M. J.; Stradiotto, M. *Nat. Commun.* **2016**, *7*, 11073.

(55) McGuire, R. T.; Simon, C. M.; Yadav, A. A.; Ferguson, M. J. Ferguson, M. J.; Stradiotto, M. *Angew. Chem. Int. Ed.* **2020**, *59*, 8952-8956.

(56) Clark, J. S. K.; Ferguson, M. J.; McDonald, R.; Stradiotto, M. *Angew. Chem. Int. Ed.* **2019**, *58*, 6391-6395.

(57) a) Eastham, G. World Patent WO 2004024322, **2004**; b) Eastham, G. World Patent WO 2005079981, **2005**; c) Eastham, G. World Patent WO 2005118519, **2005**.

(58) Dubey, R.; Pandey, J. *IJPSR* **2019**, *10*, 5311-5317.

(59) Schlatzer, T.; Breinbauer, R. *Adv. Synth. Catal.* **2021**, *363*, 668-687.

(60) a) van Zyl, V. L.; Muller, A.; Williams, B. G. *Tetrahedron Lett.* **2018**, *59*, 918-921; b) Peral, D.; Herrera, D.; Real, J.; Flor, T.; Baon, J. C. *Catal. Sci. Technol*. **2016**, *6*, 800-808; c) Shaughnessy, K. H. *Chem. Rev.* **2009,** *109,* 643-710.

(61) Fuji, K.; Morimoto, T.; Tsutsumi, K.; Kakiuchi, K. *Angew. Chem., Int. Ed.* **2003**, *42*, 2409-2411.

(62) Zábranský, M.; Císařová,I.; Trzeciak, A. M.; Alsalahi, W.; Štěpnička, P. *Organometallics* **2019**, *38*, 479-488.

(63) Peuckertt, M.; Keim, W. *Organometallics* **1983**, *2*, 594-597.

(64) Bianchini, C.; Meli, A.; Oberhauser, W. Segarra, A. M.; Passaglia, E.; Lamac, M.; Štěpnička, P. *Eur. J. Inorg. Chem.* **2008**, 441-452.

(65) Smith, R. T.; Ungar, R. K.; Sanderson, L. J.; Baird, M. C. *Organometallics* **1983**, *2*, 1138-1144.

(66) Aghmiz, A.; Gimenez-Pedros, M.; Masdeu-Bulto, A. M.; Schmidtchen, F. P. *Catalysis Letters* **2005**, *103*, 191-193.

(67) Bárta, O.; Císařová, I.; Mieczyńska, E.; Trzeciak, A. M.; Štěpnička, P *Eur. J. Inorg. Chem*. **2019**, 4846-4854.

(68) Bischoff, S.; Kant. M. *Catalysis Today* **2001**, *66*, 183-189.

(69) a) Basra, S.; de Vries, J. G.; Hyett, D. J. Harrison, G.; Heslop, K. M.; Orpen A. G.; Pringle, P. G.; von der Luehe, K. *Dalton Trans.* **2004**, 1901-1905; b) Štěpnička, P.; Císařová I.; Gyepes, R. *Eur. J. Inorg. Chem.* **2006**, 926-938.

(70) a) Barney, R. J.; Richardson, R. M.; Wiemer, D. F. *J. Org. Chem.* **2011**, *76*, 2875-2879; b) Richardson, R. M.; Barney, R. J.; Wiemer, D. F. *Tetrahedron Lett.* **2012**, *53*, 6682-6684.

(71) a) Becket, M. A.; Brassington, D. S.; Light, M. E.; Hursthouse, M. B. *J. Chem. Soc. Dalton trans* **2001**, 1768-1772; b) Regulska, E.; Christ, S.; Zimmermann, J.; Rominger, F.; Hernandez-Sosa, G.; Romero-Nieto, C. *Dalton. Trans.* **2019**, *48*, 12803-12807.

(72) a) Schulz, J.; Horký, F.; Štěpnička, P. *Catalysts* **2016**, *6*, 182; b) Schulz, J.; Horký, F.; Císařová, I.; Štěpnička, P. *Catalysts* **2017**, *7*, 167.

(73) a) Bárta, O.; Císařová, I.; Mieczyńska, E.; Trzeciak, A. M.; Štěpnička, P. *Eur. J. Inorg. Chem.* **2019**, 4846-4854; b) Zábranský, M.; Císařová, I.; Štěpnička, P. *Organometallics* **2018**, *37*, 1615-1626.

(74) Cavell, K. J.; Stufkens, D. J.; Vrieze, K. *Inorg. Chim. Acta.* **1981**, *47*, 67-76.

(75) Chiong, H. A.; Daugulis, O. *Org. Lett*. **2007**, 9, 1449-1451.

(76) Alley, S. R.; Henderson, W.; *J. Organomnet. Chem.* **2001**, *216*, 637-639.

6. List of appendices

Appendix A

Horký, F.; Císařová, I.; Štěpnička, P. Synthesis, Reactivity, and Coordination of Semihomologous dppf Congeners Bearing Primary Phosphine and Primary Phosphine Oxide Groups. *Organometallics* **2021**, *40*, 427.

Appendix B

Horký, F.; Císařová, I.; Štěpnička, P. A stable primary phosphane oxide and its heavier congeners. *Chem. Eur. J.* **2021**, *27*, 1282.

Appendix C

Horký, F.; Císařová, I.; Štěpnička, P. Stable Pd(0) Complexes with Ferrocene Bisphosphanes Bearing Phosphatrioxaadamantyl Substituents Efficiently Catalyze Selective C-H Arylation of Benzoxazoles by Aryl Chlorides. *ChemCatchem* **2021**, accepted manuscript, https://doi.org/10.1002/cctc.202101013.

Appendix D

Horký, F.; Císařová, I.; Štěpnička, P. Synthesis, coordination and catalytic use of phosphinoferrocene ligands bearing 6-phospha-2,4,6-trioxaadamantane P-donor moieties. *J. Organomet. Chem.* **2021**, submitted manuscript.

Appendix E

Horký, F.; Císařová, I.; Schulz, J.; Štěpnička, P. Synthesis and structural characterization of 1'-(diphenylphosphino)ferrocene-1-phosphonic acid, its ammonium salts and Pd(II) complexes. *J. Organomet. Chem.* **2019**, *891*, 44.

Appendix A

Horký, F.; Císařová, I.; Štěpnička, P. Synthesis, Reactivity, and Coordination of Semihomologous dppf Congeners Bearing Primary Phosphine and Primary Phosphine Oxide Groups. *Organometallics* **2021**, *40*, 427.

ORGANOMETALLICS

pubs.acs.org/Organometallics Article

Synthesis, Reactivity, and Coordination of Semihomologous dppf Congeners Bearing Primary Phosphine and Primary Phosphine Oxide Groups

Filip Horký, Ivana Císařová, and Petr Štěpnička*

Cite This: *Organometallics* 2021, 40, 427−441 Read Online

ACCESS | Metrics & More | Article Recommendations | Supporting Information

ABSTRACT: This contribution reports the synthesis of two phosphinoferrocene ligands desymmetrized by an inserted methylene spacer, viz., a bis-phosphine combining primary and tertiary phosphine moieties in its structure, $Ph_2PfcCH_2PH_2$ (**2**), and a structurally unique, stable phosphine-primary phosphine oxide $Ph_2PfcCH_2P(O)H_2$ (**7**; fc = ferrocene-1,1′-diyl). Compounds **2** and **7**, together with 1,1′-bis(diphenylphosphino)ferrocene (dppf), the bis-tertiary phosphine $Ph_2PfcCH_2PPh_2$, and the adduct $Ph_2P(BH_3)fcCH_2PH_2$ (**6**), were studied as ligands in Ru(II) complexes bearing auxiliary η^6-arene ligands and both free ligands and the isolated complexes were structurally authenticated, using spectroscopic methods and X-ray crystallography, and further investigated by cyclic voltammetry. The results suggest that distinct donor moieties in the unsymmetric ligands differentiate the otherwise identical coordinated metal centers and that the phosphine moiety in phosphine-phosphine oxide ligand **7** is preferably coordinated to Ru(II), before the phosphine oxide group, which must tautomerize into the hydroxyphosphine form prior to coordination.

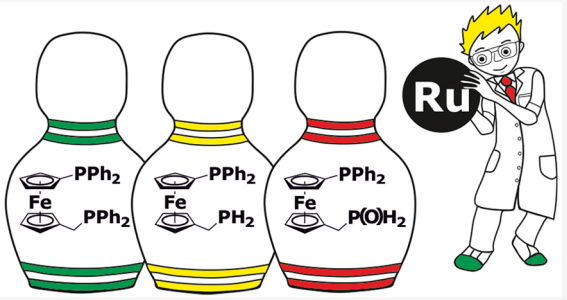

INTRODUCTION

1,1′-Bis(diphenylphosphino)ferrocene (Chart 1), commonly abbreviated as dppf and first reported in 1965,[1] has become an indispensable ligand for coordination chemistry and catalysis.[2] Its enormous practical success has prompted the search for purpose-tailored dppf analogs. To date, several dppf derivatives have been reported with varied substituents at the phosphorus atoms,[3] among which 1,1′-bis(di-*tert*-butylphosphino)-ferrocene has attracted particular attention for its favorable catalytic properties.[4]

In contrast, other approaches toward dppf modification that only partly retain the parent structure have been studied less often. These approaches include replacing one phosphine moiety by another group, which provides access to a vast family of functional phosphinoferrocene ligands and organometallic synthetic building blocks,[5] or inserting a spacer into the cyclopentadienyl-phosphorus bonds. The latter approach has so far resulted in the preparation of symmetrical homologous ligands **A**[6] and **B**,[7] their analogs with chiral phospholane substituents[8] and rigid phenylene spacers,[9] and C-chiral bis-phosphines **C**[10] (Chart 1).[11]

In our research, we desymmetrized the parent dppf structure by introducing a spacer group into *one* of the equivalent C(ferrocene)−P bonds and synthesized semihomologous dppf congener **1**.[12] The current data on **1** and related compounds[13] have shown that such a structural modification differentiates the two coordination sites (both sterically and electronically) and increases the structural flexibility of these ligands, thereby altering their coordination behavior with respect to the more rigid dppf.

Inspired by the structure of the simple, air-stable primary phosphine $FcCH_2PH_2$ (Fc = ferrocenyl),[14] we decided to synthesize and study a novel ferrocene bis-phosphine, **2** (Chart 1), containing tertiary and primary phosphine moieties and the flexible methylene linker. Compound **2** is a homologue of

Chart 1

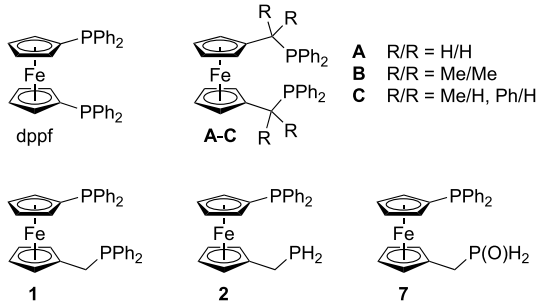

Received: December 4, 2020
Published: January 22, 2021

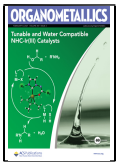

https://dx.doi.org/10.1021/acs.organomet.0c00767
Organometallics 2021, 40, 427−441

Ph_2PfcPH_2 (fc = ferrocene-1,1′-diyl), which has been used as an intermediate in the synthesis of chiral phosphines for catalytic C−C bond hydrogenation[15] and is an isomer of the somewhat overlooked, planar-chiral 1-(diphenylphosphino)-2-(phosphinomethyl)ferrocene.[16]

Furthermore, building upon our recent discovery that the ferrrocenymethyl group can stabilize even the hitherto elusive primary phosphine oxides,[17] we also describe the synthesis of compound **7** (Chart 1) as the first primary phosphine oxide functionalized by an additional phosphine moiety.

The coordination preferences of the newly prepared ligands are probed through reactions with Ru^{II} precursors with aromatic π-ligands and compared with those of dppf and **1**. The complexes are further studied by cyclic voltammetry and catalytically evaluated in Ru-catalyzed double bond isomerization using anethole as a model substrate and in Ru-mediated cyclization of (*Z*)-3-methylpent-2-en-4-yn-1-ol into 2,3-dimethylfuran.

RESULTS AND DISCUSSION

Synthesis of the Ligands. Bis-phosphine **2** was obtained by manipulating the hydroxyl group in borane-protected phosphinoalcohol **3**[13d] (Scheme 1). Specifically, the alcohol

Scheme 1. Synthesis and Arylation of Bis-phosphine 2[a]

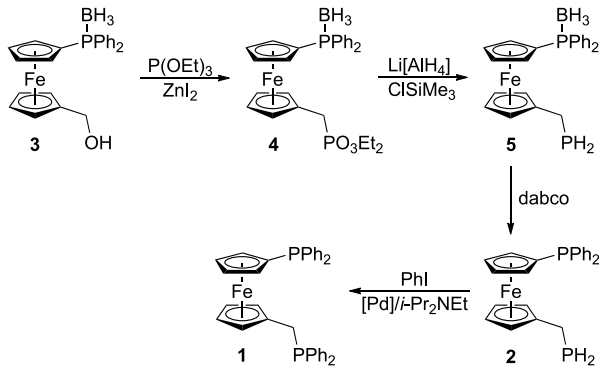

[a]Legend: dabco = 1,4-bicyclo[2.2.2]octane, [Pd] = $Pd(OAc)_2$.

was converted into phosphonic acid ester **4** via a reaction with triethyl phosphite/ZnI_2,[18] and the ester was reduced with $Li[AlH_4]/ClSiMe_3$[19] to give semiprotected bis-phosphine **5**. Subsequent deprotection with 1,4-diazabicyclo[2.2.2]octane (dabco)[20] in THF produced target compound **2** in approximately 60% yield over the three steps after a final crystallization.

Compound **2** was isolated as an air-stable and thermally robust, crystalline solid (mp 114 °C) with a characteristic yet only faint smell of phosphane. It did not react with acetone (at 40 °C; see below) but could be arylated[21] with iodobenzene in the presence of palladium(II) acetate (5 mol %) and an amine additive, giving known[12] bis-tertiary phosphine **1** in 78% yield (Scheme 1). Similar results were found when using $[Pd_2(dba)_3]$ as the catalyst (dba = dibenzylideneacetone).

To synthesize a ferrocene-based, hybrid phosphine-primary phosphine oxide ligand, we further oxidized P-protected intermediate **5** with aqueous hydrogen peroxide at 0 °C (Scheme 2). The oxidation proceeded rapidly and selectively, producing phosphine oxide **6** in 84% yield. Upon treatment with dabco, this compound was converted into phosphine oxide **7** in a virtually quantitative yield (95%). Similarly to

Scheme 2. Synthesis of Phosphine Oxides 6−9[a]

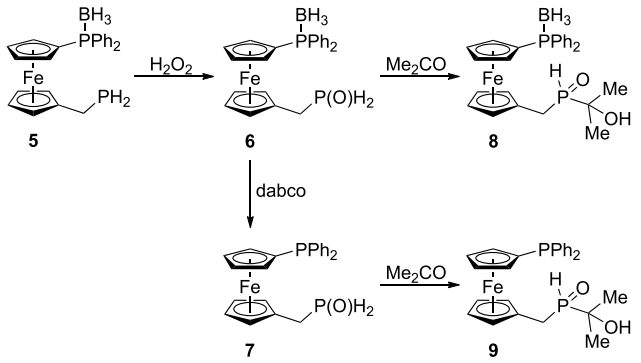

[a]Legend: dabco = 1,4-bicyclo[2.2.2]octane

$FcCH_2P(O)H_2$,[17] compounds **6** and **7** reacted with acetone at slightly elevated temperature (40 °C; the reaction proceeds even at room temperature but only slowly), providing the corresponding addition products **8** and **9** in good yields. Phosphine oxides **6**−**9** were stable under ambient conditions (we noted, however, that compounds **8** and **9** slowly and partly regenerated **6** and **7**, respectively, in a dichloromethane solution[17,22]).

^{31}P NMR spectra of **2** and **5** displayed diagnostic triplets of triplets ($^1J_{PH}$ = 194 Hz, $^2J_{PH}$ = 4−5 Hz) due to the primary phosphine moieties at $\delta_P \approx -126$ (Figure 1). The signal of the

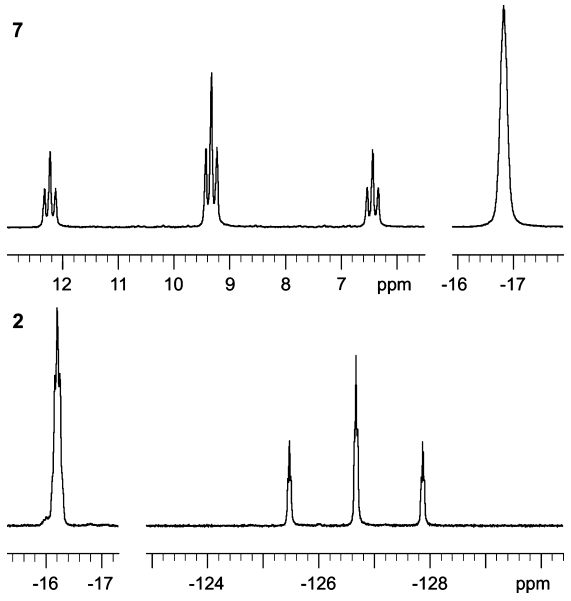

Figure 1. ^{31}P NMR spectra of **2** and **7**. Spectra are shown with identical scaling at both axes.

PPh_2 group was observed as a singlet at δ_P −16.2 for **2** and as a broad multiplet at δ_P 16.4 for BH_3-adduct **5**. Correspondingly, the PH_2 groups gave rise to doublets of multiplets at $\delta_H \approx 2.8$ in the ^1H NMR spectra, whereas the signals of the CH_2 linker were observed as doublets of triplets at $\delta_H \approx 2.3$. The presence of the PH_2 moieties was further manifested as intense bands in the ≈2300−2360 cm^{-1} range of IR spectra, attributable to P−H stretching modes.

Oxidation of the PH_2 group in **6** and **7** shifted the ^{31}P NMR signal downfield ($\delta_P \approx 9$) and increased the $^1J_{PH}$ coupling constant (≈ 470 Hz; see Figure 1). The signal of the $P(O)H_2$

https://dx.doi.org/10.1021/acs.organomet.0c00767
Organometallics 2021, 40, 427−441

hydrogens also shifted ($\delta_H \approx 6.8$), reflecting the stronger electron-withdrawing nature of the phosphinyl moiety. Even so, replacing one PH hydrogen with the 2-hydroxyprop-2-yl moiety in **8** and **9** was clearly indicated in the NMR spectra: The ^{31}P NMR spectra displayed doublets of multiplets with a large $^{1}J_{PH}$ coupling constant ($\approx$ 455 Hz), whereas the PH signals were observed at $\delta_H \approx 2.3$ in the ^{1}H NMR spectrum, split into a more complicated pattern (ddd for **8** and dt for **9**) due to the diastereotopic nature of the CH_2 hydrogens attached to the stereogenic phosphorus atom. For the same reason, two separate signals were found for the chemically equivalent methyl groups. No signals attributable to hydroxyphosphine tautomers were observed in the NMR spectra of phosphine oxides **6**–**9**.

The crystal structures of **2** and **9** are shown in Figure 2 (for additional diagrams and parameters, see the Supporting Information). Both compounds comprised regular ferrocene units with similar Fe–C distances (2.035(2)–2.055(2) Å for **2**; 2.028(3)–2.056(3) Å for **9**) and negligible tilting (4.86(9) and 2.1(2)°, respectively). The cyclopentadienyls in **2** adopted an approximate 1,2′-conformation[23] with the torsion angle C1–Cg1–Cg2–C6 (hencefort denoted as τ; Cg1 and Cg2 are the centroids of the cyclopentadienyl rings C(1–5) and C(6–10), respectively) of −81.8(1)°. A similar, though more compact, arrangement was identified in **9** (τ = 69.7(2)°). In the crystal, the molecules of **9** assembled into infinite chains through O–H···O=P hydrogen bonds (O1···O2 = 2.645(4) Å; see the Supporting Information).

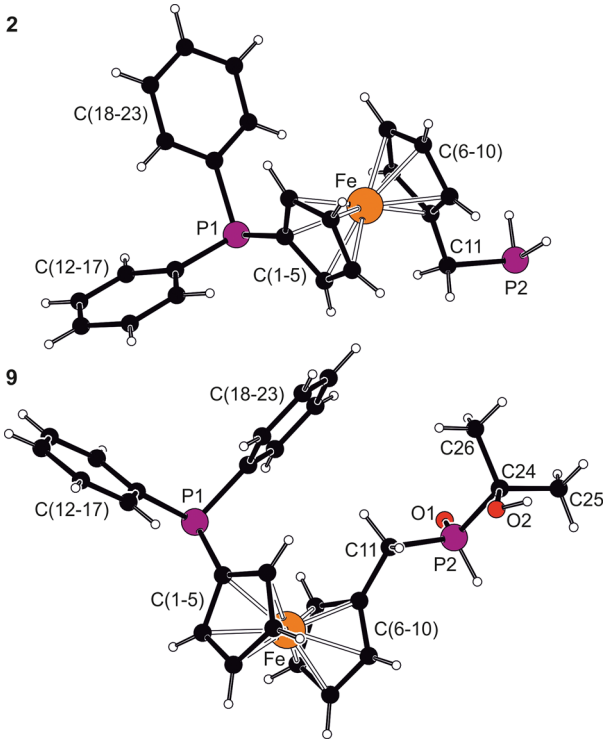

Figure 2. Molecular structures of **2** and **9**. Selected distances and angles (in Å and deg): for **2**: P1–C1 1.806(2), P1–C12 1.844(2), P1–C18 1.844(2), P2–C11 1.853(2), C6–C11–P2 114.9(1); for **9**: P1–C1 1.812(3), P1–C12 1.838(3), P1–C18 1.836(3), P2–O1 1.486(3), P2–C11 1.803(3), C6–C11–P2 111.8(2), C11–P2–O1 114.4(2). Parameters pertaining to the disordered $CH_2P(O)$ arm are given for the more populated orientation.

Synthesis of Ru(II) Complexes. The coordination behavior of compounds **1**, **2**, **6**, and **7** was evaluated through reactions with Ru(II) precursors bearing auxiliary π-ligands. The prototypical ligand dppf was also included in these studies for comparison purposes. Initially, we focused on (η^6-mes)Ru(II) complexes featuring the ligands in a P,P′-bridging mode. The reactions of $[\{(\eta^6\text{-mes})RuCl(\mu\text{-Cl})\}_2]$ (mes = mesitylene) with dppf, **1**, and **2** proceeded cleanly, producing respective diruthenium complexes **10**, **11**, and **12** as the sole products (Scheme 3).

Scheme 3. Synthesis of (η^6-mes)Ru(II) Complexes 10–15[a]

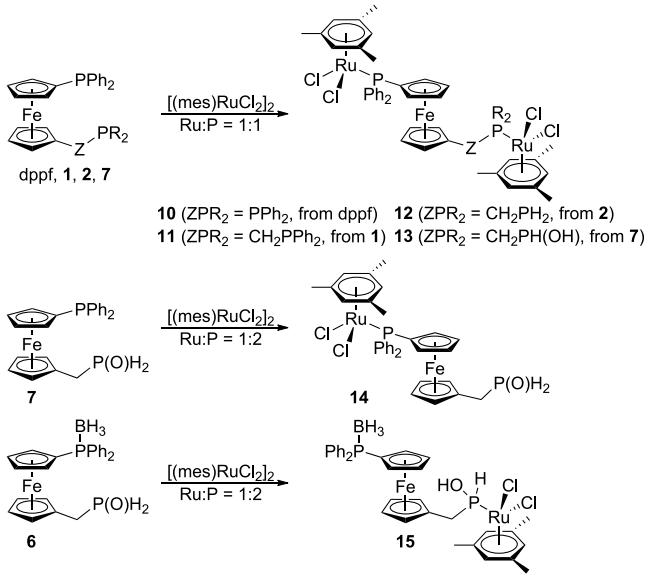

[a]mes = mesitylene.

When using hybrid ligand **7**, the reaction was accompanied by tautomerization of the primary phosphine oxide moiety, leading to phosphine-hydroxyphosphine complex **13**. Upon reducing the amount of the Ru precursor by half, the analogous reaction selectively produced phosphine complex **14** featuring uncoordinated phosphine oxide moiety. Conversely, the reaction of $[(\eta^6\text{-mes})RuCl_2]_2$ with ligand **6**, whose tertiary phosphine group was unavailable for coordination, led to hydroxyphosphine complex **15** (Scheme 3).

Generally, complexes **10**–**15** were relatively poorly soluble and exerted structural dynamics which complicated their characterization by NMR spectroscopy. The coordination of the PPh_2 moiety led to a rather uniform downfield shift of the ^{31}P NMR signal by 37–38 ppm (≈42 ppm for CH_2PPh_2 in **1**), whereas the coordination of the PH_2 group in **2** *or* tautomerization/coordination of the $P(O)H_2$ groups in **6** and **7** resulted in a considerably larger shift of approximately 107 ppm (the tautomerization was further indicated by changes in the non-decoupled ^{31}P NMR spectra, wherein the triplets due to P–H interactions in the $P(O)H_2$ groups were replaced by doublets of the PH(OH) fragments).

The molecular structures of **10**·THF·$2CH_2Cl_2$ and **12**·$2CHCl_3$ determined by X-ray crystallography (Figure 3) were generally similar to that of $[(L\text{^}L)\{(\eta^6\text{-arene})RuCl_2\}_2]$ (L^L = dppf and $fc(CH_2PPh_2)_2$)[24] and $[(\eta^6\text{-}p\text{-cymene})RuCl_2(FcCH_2PH_2\text{-}\kappa P)]$.[25] The complex molecule in the structure of **10**·THF·$2CH_2Cl_2$ was situated on the crystallographic inversion center, which rendered the ferrocene

https://dx.doi.org/10.1021/acs.organomet.0c00767
Organometallics 2021, 40, 427–441

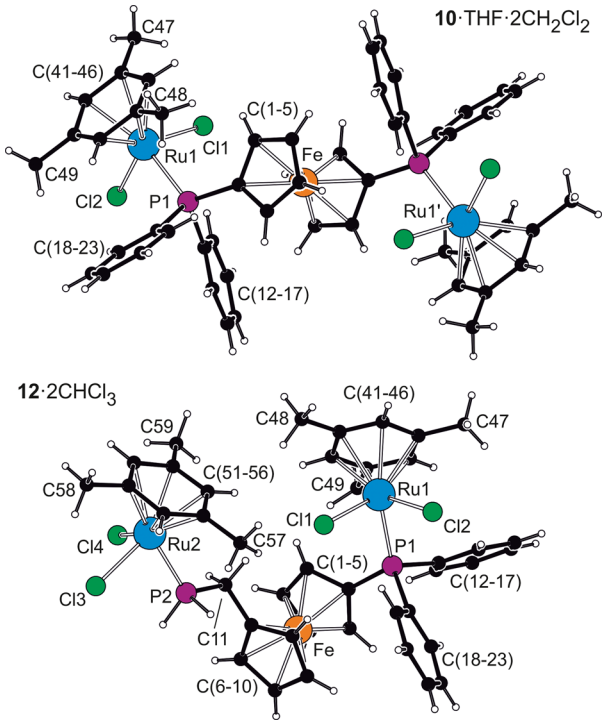

Figure 3. Views of the complex molecules in the structures of **10**·THF·$2CH_2Cl_2$ and **12**·$2CHCl_3$. Selected distances (in Å): for **10**·THF·$2CH_2Cl_2$: Ru1−P1 2.3598(5), Ru1−Cl1 2.4082(5), Ru1−Cl2 2.4113(5), Ru1−C(arene) 2.198(2)−2.270(2), Fe1−C(1−5) 2.039(2)−2.064(2); for **12**: Ru1−P1 2.3620(7), Ru1−Cl1 2.4160(7), Ru1−Cl2 2.4122(8), Ru1−C(arene) 2.205(3)−2.271(3), Ru2−P2 2.2770(7), Ru2−Cl3 2.4097(9), Ru2−Cl4 2.4027(9), Ru2−C(arene) 2.176(3)−2.263(3), Fe1−C(1−10) 2.025(3)−2.053(3).

cyclopentadienyls exactly parallel and brought their phosphine substituents and the ligated ruthenium fragments into anti positions. Ferrocene cyclopentadienyls in unsymmetric complex **12**·$2CHCl_3$ were mutually rotated by τ = 90.5(2)° and tilted by 4.4(2)°. In both complexes, the ruthenium atoms adopted the usual "piano stool" geometry, wherein the basal planes (Cl_2P) were oriented parallel to the π-coordinated arene ring (interplanar angles: 2.89(7)° for **10** and 1.6(1)° (Ru1) and 2.6(1)° (Ru2) for **12**). Notably, the Ru−PPh_2 bonds (≈2.36 Å) were significantly elongated with respect to the Ru−PH_2 bond in **12** (≈2.28 Å), most likely for steric reasons.

The structure of **15** (Figure 4) corroborated that the phosphine oxide moiety underwent tautomerization upon coordination. The P−H and P−OH bonds of the Ru-bound PH(OH) unit, located between the bulky (η^6-mes)Ru and ferrocene fragments, alternated in their positions, thereby resulting in positional disorder. The length of the Ru−P bond in **15** was very similar to the Ru−PH_2 bond distance in complex **12**, and the geometry of the fcPPh_2·BH_3 fragment matched that of dppf·$2BH_3$.[26]

Next, we focused on cationic (η^6-mes)Ru(II) complexes accommodating the studied ferrocene phosphines as chelating donors. The reaction[24a,b] of [{(η^6-mes)RuCl(μ-Cl)}$_2$] with dppf in the presence of Na[PF_6] produced [(η^6-mes)RuCl(dppf-κ^2*P*,*P*′)][PF_6] (**16**) in 89% yield (Scheme 4). Attempts to similarly prepare complexes with ligands **1** and **2** only led to equilibrium mixtures containing the respective compounds [(η^6-mes)RuCl(L^L)][PF_6], based on ^{31}P NMR analysis,[27] which could not be separated by crystallization or chromatography. Practically identical mixtures were obtained in the reaction of stoichiometric amounts of **1** or **2** with [(η^6-mes)RuCl(MeCN-κN)$_2$][PF_6] in dichloromethane (for the synthesis of the Ru-precursor, see the Supporting Information). Reactions with ligand **7** were also unsuccessful, albeit mainly due to extensive decomposition of the ligand in the reaction mixtures (compound **7** seems to decompose in the presence of the PF_6^- anion).

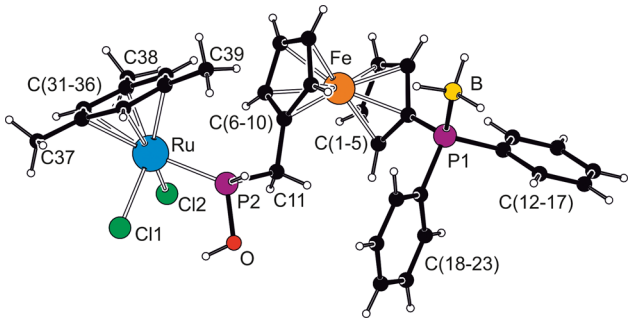

Figure 4. Molecular structure of complex **15**. Selected distances (in Å): Ru−P2 2.2815(8), Ru−Cl1 2.416(2) (dominant position), Ru−Cl2 2.4052(9), Ru−C(arene) 2.193(3)−2.275(3), P2−O 1.637(3), P1−B 1.924(4), Fe1−C(1−10) 2.025(3)−2.045(3).

Scheme 4. Synthesis of Complex 16

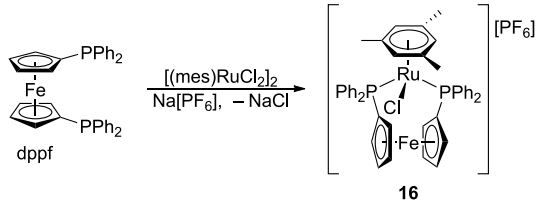

The crystal structure of **16**·CH_2Cl_2 (Figure 5) was unexceptional in view of the data reported for [(η^6-arene)RuCl(dppf-κ^2*P*,*P*′)][PF_6], where arene = C_6Me_6[24a,b] and *p*-cymene.[28] The complex cation had a three-legged piano stool structure symmetrically capped with the η^6-benzene ring (Ru1−C(41−46) = 2.251(3)−2.310(3) Å). The Ru−Cl and Ru−P distances were similar to those determined for **10**·

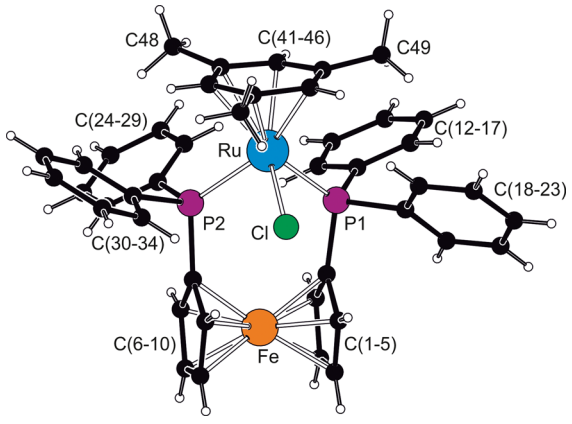

Figure 5. View of the complex cation in the structure of **16**·CH_2Cl_2. Selected distances and angles (in Å and deg): Ru−P1 2.3636(9), Ru−P2 2.3619(9), Ru−Cl 2.4030(8), P1−Ru−P2 95.10(3), Cl−Ru−P1/2 81.21(3)/88.64(3), Fe−C(1−10) 2.024(3)−2.062(3); the angle subtended by the C(41−46) and the {P1,P2,Cl} basal plane is 3.9(1)°.

https://dx.doi.org/10.1021/acs.organomet.0c00767
Organometallics 2021, 40, 427−441

$2CH_2Cl_2$·THF and did not differ much even from each other. Nevertheless, an asymmetry arose around the Ru atom, most likely resulting from the dissimilar steric demands of the Ru-bound ligands, with the largest interligand angle associated with the chelating dppf ligand. Because of chelate coordination, the ferrocene cyclopentadienyls were practically eclipsed (τ = 6.0(2)°) and, additionally, exerted negligible tilting (2.1(2)°).

To eliminate the problem with compound isolation, we replaced the (η^6-mes)Ru(II) moiety by the iso-π-electronic fragment (η^5-C_5H_5)Ru(II) toward synthesizing charge-neutral compounds analogous to the known dppf complex [(η^5-C_5H_5)RuCl(dppf-κ^2P,P')] (**17**).[29] Indeed, a modified method for preparing **17** based on thermally assisted replacement of triphenylphosphine ligands in [(η^5-C_5H_5)RuCl(PPh_3)$_2$] employing bis-phosphine **1** produced the corresponding chelate complex [(η^5-C_5H_5)RuCl(**1**-κ^2P,P')] (**18**), which was isolated as a rusty brown, air-stable solid in a 82% yield (Scheme 5).

Scheme 5. Synthesis of (η^5-C_5H_5)Ru(II) Complexes 18 and 19

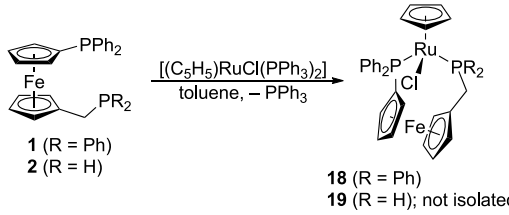

Regrettably, repeated attempts to similarly prepare complex [(η^5-C_5H_5)RuCl(**2**-κ^2P,P')] (**19**) were unsuccessful. The reactions of bis-phosphine **2** with [(η^5-C_5H_5)RuCl(PPh_3)$_2$] or, alternatively, [(η^5-C_5H_5)RuCl(cod)] (cod = η^2:η^2-cycloocta-1,5-diene) afforded mixtures in which complex **19** was detected as the main product[30] but could not be isolated in pure form. Even more complicated reaction mixtures were obtained when sequentially adding **2** and (Bu_4N)Cl as a chloride source (1 equiv of each) to [(η^5-C_5H_5)Ru(MeCN-κN)$_3$][PF_6] in dichloromethane. Analogous reactions with **7** were hampered by the decomposition of the ligand in the reaction mixtures at elevated temperatures or in the presence of PF_6^-.

The formation of complexes **18** and **19** was clearly indicated by ^{31}P NMR spectra showing a pair of doublets due to interacting nonequivalent Ru-bound phosphorus atoms. In addition, ^{1}H and ^{13}C NMR spectra of isolated complex **18** displayed eight resonances for the diastereotopic ferrocene CH groups (the Ru atom in **18** becomes a stereogenic center). Although we could not isolate pure bulk samples of **19**, we serendipitously obtained a few single crystals of this compound (as solvate **19**·CH_2Cl_2) and were thus able to structurally authenticate both **18** and **19** by X-ray diffraction analysis (Figure 6).

Complexes **18** and **19** adopted the typical piano stool structures similar to those of **16** and **17** (the Ru–C distances in **18** and **19** were slightly shorter than in arene complex **16**, presumably strengthened by a stronger interaction with the anionic cyclopentadienyl ligand). In both compounds, the Ru–P bond involving the ferrocene-bound PPh_2 group was longer than the Ru–P bond with the CH_2PR_2 (R = H and Ph) moiety. Both homologated ligands **1** and **2** forced wider bite angles than did dppf in **17** (95.01(4)°).[31] The dihedral angles between the ferrocene cyclopentadienyl rings were 2.4(2)° in

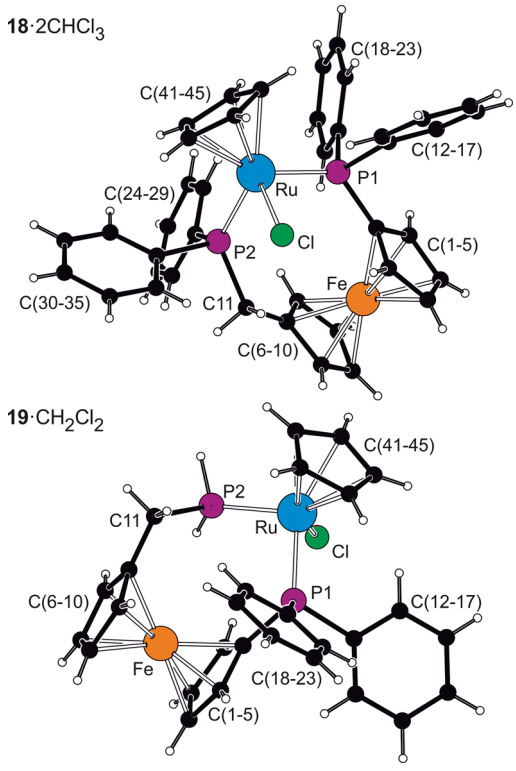

Figure 6. Views of the complex molecules in the structures of **18**·$2CHCl_3$ and **19**·CH_2Cl_2. Selected distances and angles (in Å and deg): for **18**: Ru–P1 2.311(1), Ru–P2 2.296(1), Ru–Cl 2.4473(9), P1–Ru–P2 101.66(4), Cl–Ru1–P1/2 89.28(2)/85.53(2), Ru–C(41–45) 2.187(5)–2.218(4), Fe–C(1–10) 2.040(3)–2.057(5); for **19**: Ru–P1 2.2858(8), Ru1–P2 2.2698(5), Ru–Cl 2.4439(6), P1–Ru–P2 96.19(6), Cl–Ru1–P1/2 89.28(2)/85.53(2), Ru–C(41–45) 2.179(2)–2.225(2), Fe–(C1–10) 2.046(2)–2.074(2).

18 and 5.6(1)° in **19**, and the rings appeared rotated from an ideal eclipsed conformation by −37.8(3)° in **18** and by 20.6(1)° in **19**.

Electrochemistry. The electrochemical behavior of the phosphine ligands and their neutral (η^6-mes)Ru(II) complexes that form a more complete series was investigated by cyclic voltammetry at a glassy carbon disc electrode in dichloromethane containing $Bu_4N[PF_6]$ as the supporting electrolyte, with particular focus on the anodic region where the oxidation of the metal centers was expected.

In line with previous reports,[32] dppf underwent an oxidation at 0.18 V versus ferrocene/ferrocenium reference (Figure 7). This redox process, attributable to the ferrocene/ferrocenium couple, was followed by chemical reactions that made it quasireversible within the usual time scale of cyclic voltammetry: Relatively faster scanning rendered the oxidation virtually reversible, whereas slower scan rates or scanning toward more positive potentials made it practically irreversible (additional ill-defined oxidative waves due to newly formed species could be observed at higher potentials; see Figure 7). The redox response[33] of semihomologous bis-phosphine **1** was practically identical except that the redox wave was shifted to less positive potentials (E = 0.08 V) because the influence of one of the electron-withdrawing phosphine moieties was lessened by the nonconjugated methylene spacer (σ_p for PPh_2 is 0.19).[34]

For bis-phosphine **2**, the ferrocene-centered oxidation was essentially reversible at a 0.10 V s^{-1} scan rate and occurred at E

https://dx.doi.org/10.1021/acs.organomet.0c00767
Organometallics 2021, 40, 427–441

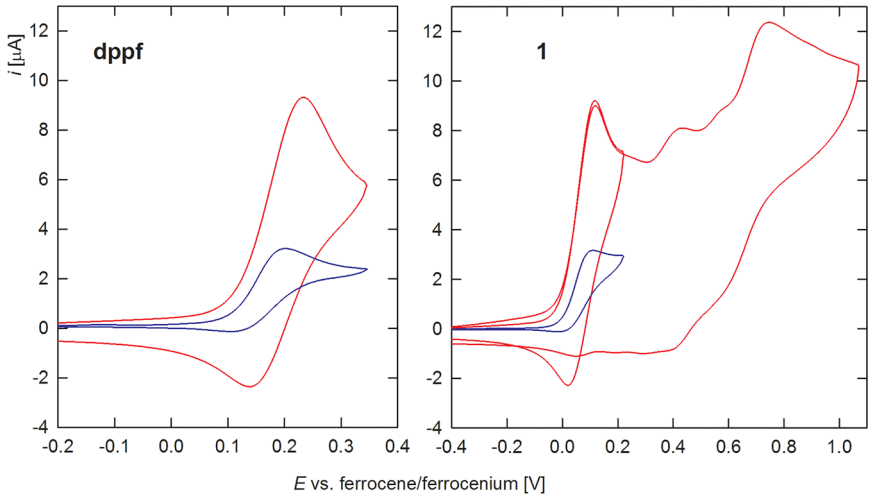

Figure 7. Cyclic voltammograms of dppf and **1**. The voltammograms recorded at a scan rate of 0.10 V s^{-1} are shown in red, and those at 0.010 V s^{-1} are shown in blue. The ratio of the anodic peak currents determined at 0.10 and 0.010 V s^{-1} scan rates, $i_{pa}(0.10)/i_{pa}(0.010)$, was 2.9 for both compounds (the theoretical value is $\sqrt{10} \approx 3.16$).

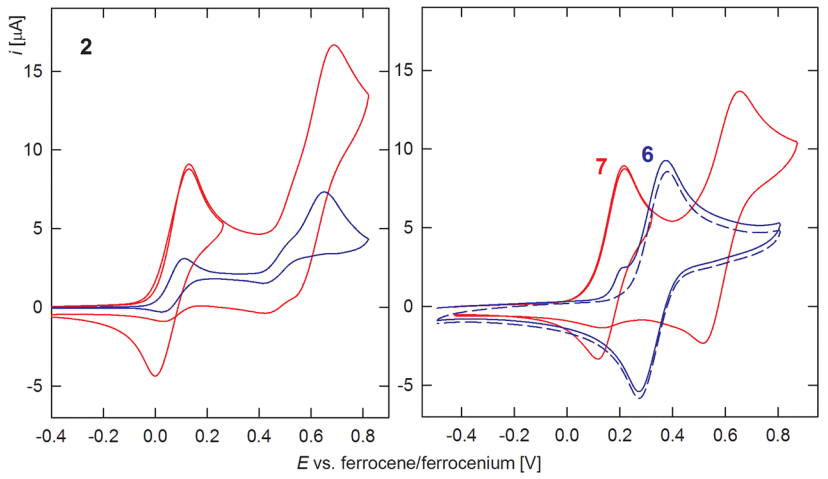

Figure 8. (left) Cyclic voltammograms of **2**. The voltammograms recorded in dichloromethane at a scan rate 0.10 V s^{-1} are shown in red, and those recorded at 0.010 V s^{-1} are shown in blue. (right) Cyclic voltammograms of **6** (blue) and **7** (red). The second scan is shown as a dashed line.

= 0.08 V, thus reflecting the presence of the methylene linker that minimizes the influence of the attached moiety (PPh_2 vs PH_2; Figure 7). At more positive potentials, an additional redox event was observed, consisting of two closely spaced, irreversible oxidations that convoluted into a composite wave peaking at $E \approx 0.70$ V and associated with a counter wave at approximately 0.43 V (peak potentials at 0.10 V s^{-1} are given). The cyclic voltammogram of phosphine oxide **7** also displayed two redox changes in the anodic region (Figure 8). Initially, the compound underwent a reversible oxidation presumably located at the ferrocene core. The redox wave occurred at more positive potentials ($E = 0.17$ V) with respect to that of **2**, in line with the electron-withdrawing nature of the $CH_2P(O)H_2$ moiety. The second oxidation at $E = 0.59$ V was also reversible but affected the preceding redox step during reverse scan. Finally, adduct **6** showed a single reversible oxidation in the accessible potential range (Figure 7). The position of the wave ($E = 0.32$ V) suggested further electron density removal from the ferrocene core associated with P → B donation. In its anodic branch, the redox wave was preceded by a prepeak, which disappeared (or decreased in intensity) upon repeated scanning and was explained by adsorption phenomena.

Overall, the initial oxidation of the studied phosphine ligands can be ascribed to oxidation of the ferrocene unit, as expected because the HOMO orbital of dppf is prevalently localized at the ferrocene core.[35] In some cases, the reversibility of the ferrocene/ferrocenium redox transition is affected by follow-up reactions in which the electro-generated product is converted into other species (typically redox-active) and can be linked to electron density relocations within the conjugated ferrocene−phosphine system.[36] The subsequent oxidative steps are difficult to explain because they are often of a composite nature and can be affected by chemical processes coupled with the preceding redox step.

Complex **10**, combining redox sites of two types (i.e., the ferrocene unit and two equivalent (η^6-arene)Ru(II) fragments), underwent two successive oxidations.[37] The first reversible oxidation, which occurred at $E = 0.16$ V due to the ferrocene ligand, was followed by an irreversible oxidation at 0.75 V (peak potential at 0.10 V s^{-1} is given), corresponding to a simultaneous one-electron irreversible oxidation of the two chemically equivalent Ru(II) centers. Similar behavior was reported for the analogous (η^6-arene)Ru(II) complexes featuring dppf and **A** as the bridging ligands[24a,b] and was

https://dx.doi.org/10.1021/acs.organomet.0c00767
Organometallics 2021, 40, 427−441

also observed for **11**–**13** (Figure 9). The ferrocene units in **11**, **12**, and **13** were oxidized reversibly at E = 0.06, 0.11, and 0.11

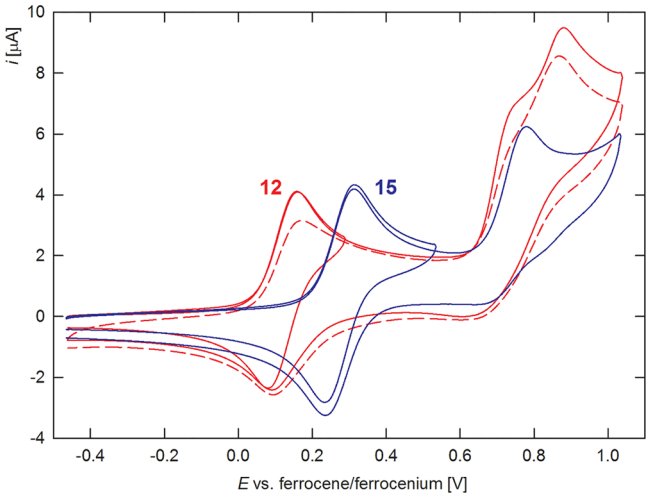

Figure 9. Cyclic voltammograms of **12** (red) and **15** (blue) as recorded in dichloromethane at scan rate 0.10 V s^{-1}. The second scan is shown by dashed line.

V, respectively, whereas the two nonequivalent Ru(II) centers, distinguished by the asymmetric bis-phosphine ligands, were oxidized in two closely separated irreversible redox steps in the 0.70–0.87 V range. Similar to the respective free ligand, the first oxidation of complex **15** was shifted to 0.27 V, reflecting the presence of the BH_3 unit (see above), followed by an additional one-electron irreversible oxidation of the Ru^{II} center at 0.77 V (peak potential determined at 0.10 V s^{-1}). Complex **14** could not be analyzed due to its instability in the presence of the PF_6^- anion.

Catalytic Testing. Considering the wide applications of ruthenium compounds in transition metal catalysis,[38] we evaluated the diruthenium(II) complexes, choosing two reactions that manipulate unsaturated C–C bonds and focusing on the possible influence of the different P-donor moieties. The first series of experiments was performed using a model catalytic double bond isomerization of estragole (**20**) to anethole (**21**; see Table 1),[39] in which the beneficial effect of the P–OH moiety has been recently established.[40] The reaction was performed in water[41] using potassium carbonate as a base in the presence of 1 mol % Ru (i.e., 0.5 mol %

Table 1. Ru-Catalyzed Isomerization of Estragole in Water[a]

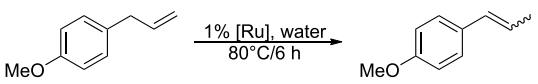

20 **21**

catalyst	conversion (%)	E/Z
10	97	90/10
11	85	78/22
12	68	76/24
13	25	70/30
17	<5	
18	<5	

[a]Reaction conditions: 1 mol % [Ru], K_2CO_3 (6 mol %), and estragole (2.0 mmol) were reacted in 1 mL of water at 80 °C for 6 h. The conversion was determined by ^{1}H NMR spectroscopy.

dirutenium complex). The results outlined in Table 1 indicate the superior performance of the (η^6-mes)Ru(II) complexes, which can be related to their easier catalytic activation, presumably by removal of the Ru-bound chloride ligand that provides a vacant coordination at Ru. Among the arene complexes, the compound with tertiary phosphine ligands performed better than "hydroxyphosphine" complex **13**, and the most active dppf-based catalyst (**10**) also showed the highest selectivity to (*E*)-alkene.

The other testing reaction was the cycloisomerization of (*Z*)-3-methylpent-2-en-4-yn-1-ol (**22**) into 2,3-dimethylfuran (**23**; Table 2).[42] In these experiments, the Ru catalyst (0.3 mol

Table 2. Ru-Catalyzed Cyclization of Enynol 22

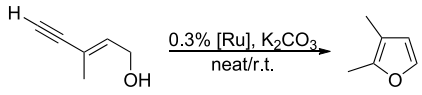

22 **23**

catalyst	yield of **23** (%)	catalyst	yield of **23** (%)
10	76	**13**	78
11	81	**17**	0
12	80	**18**	0

[a]Neat substrate **22** and Ru-catalysts (0.3 mol %) were reacted at room temperature (23–25 °C) in the air for 18 h. The yield was determined by ^{1}H NMR spectroscopy.

%) was added directly to the neat substrate, and the reaction was allowed to proceed in the air for 18 h. To our delight, arene complexes **10**–**13** were catalytically active, even at room temperature, without requiring a high temperature to initiate the cyclization reaction, in contrast to other Ru catalysts.[42,43] However, the product yields achieved with **10**–**13** varied only slightly. The (η^5-C_5H_5)Ru(II) complexes, **17** and **18**, showed no appreciable activity.

CONCLUSION

The findings of this study further demonstrate that the "homologation" approach is a viable route toward new unsymmetric ligands with modified steric and electronic properties. Newly prepared bis-phosphine **2**, combining primary and tertiary phosphine moieties in its structure, and phosphine-phosphine oxide **7**, which is the first phosphine ligand bearing an additional *primary* phosphine oxide moiety, are remarkably stable and hence suitable for further synthesis (this was already exemplified by the **2** → **1** conversion reported herein) and for other applications (e.g., catalytic). Moreover, both structural and electrochemical data indicate that the two different donor moieties available in these ligands differentiate the coordinated metal fragments, which can further affect catalytic applications of these ligands.

EXPERIMENTAL SECTION

Materials and Methods. All syntheses were performed in argon or nitrogen atmosphere using standard Schlenk techniques and oven-dried glassware. Compounds **3**,[13d] [(η^5-C_5H_5)RuCl(PPh_3)$_2$],[44] [(η^5-C_5H_5)Ru(MeCN-κN)$_3$][PF_6],[45] and [(η^5-C_5H_5)RuCl(cod)][46] (cod = η^2:η^2-cycloocta-1,5-diene) were prepared according to literature procedures. Other chemicals were purchased from commercial suppliers (Sigma-Aldrich or Alfa-Aesar) and used as received. Anhydrous dichloromethane, tetrahydrofuran and methanol used for syntheses were prepared using a PureSolv MD5 solvent purification system (Innovative Technology). Acetonitrile and toluene were dried over anhydrous potassium carbonate and sodium metal, respectively,

https://dx.doi.org/10.1021/acs.organomet.0c00767
Organometallics 2021, 40, 427–441

and distilled prior to use. Solvents used for crystallizations and for chromatography (reagent-grade; Lach-Ner, Czech Republic) were utilized without additional purification.

NMR spectra were recorded at 25 °C on a Varian Unity Inova 400 spectrometer operating at 400, 101, and 162 MHz for ^{1}H, ^{13}C, and ^{31}P, respectively. Chemical shifts (δ in ppm) are given relative to internal tetramethylsilane (^{1}H and ^{13}C) and to external 85% aqueous H_3PO_4 (^{31}P). FTIR spectra were acquired with a Thermo Nicolet 6700 instrument over the 400−4000 cm^{-1} range. Electrospray ionization (ESI) mass spectra were recorded on a Compact QTOF-MS spectrometer (Bruker Daltonics). Elemental analyses were conducted using a PE 2400 Series II CHNS/O Elemental Analyzer (PerkinElmer). The amount of residual solvent(s) was verified by NMR analysis.

Electrochemical measurements were recorded using a mAUTOLAB III multipurpose apparatus (Eco Chemie, Netherlands) at room temperature and a standard three-electrode cell equipped with a glassy carbon disc (2 mm diameter) working electrode, a platinum sheet auxiliary electrode, and a double-junction Ag/AgCl (3 M KCl) reference electrode. The compounds were dissolved in anhydrous dichloromethane to give a solution containing 1 mM analyte and 0.1 M $Bu_4N[PF_6]$ (Fluka, puriss grade for electrochemistry) as the supporting electrolyte. The solutions were deaerated with argon before the measurements and then kept under an argon blanket. Decamethylferrocene (Alfa-Aesar) was added as an internal standard for the final scans, and the redox potentials were converted into the ferrocene/ferrocenium scale by subtracting 0.548 V.[47]

Synthesis of 1-(Diphenylphosphino)-1′-[(diethoxyphosphinyl)methyl]ferrocene−borane (1:1) (4). A reaction flask equipped with a large stirring bar was charged with alcohol **3** (4.14 g, 10.0 mmol), zinc(II) iodide (3.50 g, 11.0 mmol), and triethyl phosphite (17 mL, 100 mol) under argon (the content of the reaction flask gently warmed upon mixing). The resulting mixture was stirred at room temperature overnight and then diluted with chloroform (180 mL) and 3 M aqueous hydrochloric acid (80 mL). The organic layer was separated, washed with brine (200 mL), dried over anhydrous magnesium sulfate, and evaporated under reduced pressure. The oily residue was kept under oil pump vacuum (3×10^{-3} Torr at 50 °C) to remove the excess of triethyl phosphite and subsequently purified by column chromatography (silica gel, ethyl acetate). A second orange band was collected, which afforded ester **4** after evaporation. Yield: 4.48 g (84%), orange oil. The compound may be contaminated with up to 10% of diethyl phosphite. However, this impurity does not hamper the subsequent reduction, after which it can be easily removed during the crystallization step.

^{1}H NMR (400 MHz, $CDCl_3$): δ 0.8−1.7 (br m, 3H, BH_3), 1.25 (t, $^{3}J_{HH}$ = 7.1 Hz, 6H, Me), 2.59 (d, $^{2}J_{PH}$ = 19.7 Hz, 2H, CH_2P), 3.96 (qd, J = 7.1, 0.9 Hz, 4H, CH_2O), 4.02 (vt, J' = 2.0 Hz, 2H, fc), 4.25 (d vt, J' = 1.0, 1.1 Hz, 2H, fc), 4.32 (vq, J' = 2.0 Hz, 2H, fc), 4.48 (d vt, J' = 1.1, 0.7 Hz, 2H, fc), 7.38−7.50 (m, 6H, PPh_2), 7.55−7.61 (m, 4H, PPh_2). ^{13}C{^{1}H} NMR (101 MHz, $CDCl_3$): δ 16.43 (d, $^{3}J_{PC}$ = 6 Hz, Me), 27.33 (d, $^{1}J_{PC}$ = 139 Hz, CH_2P), 61.93 (d, $^{2}J_{PC}$ = 7 Hz, CH_2O), 69.22 (d, J_{PC} = 68 Hz, C^{ipso} of fc), 69.78 (s, CH of fc), 71.22 (d,J_{PC} = 4 Hz, CH of fc), 72.81 (d, J_{PC} = 7 Hz, CH of fc), 73.73 (d, J_{PC} = 10 Hz, CH of fc), 79.77 (d,J_{PC} = 3 Hz, C^{ipso} of fc), 128.44 (d, J_{PC} = 10 Hz, CH of PPh_2), 130.92 (d, J_{PC} = 3 Hz, CH of PPh_2), 131.53 (s, C^{ipso} of PPh_2), 132.62 (d, J_{PC} = 10 Hz, CH of PPh_2). ^{31}P{^{1}H} NMR (162 MHz, $CDCl_3$): δ 16.4 (br s, PPh_2BH_3), 25.3 (s, $PO(OEt)_2$). IR (Nujol) ν_{max}: 3075 w, 3056 w, 2724 w, 2349 s, 2344 s, 2255 m, 1701 m, 1588 w, 1572 w, 1483 w, 1438 s, 1415 w, 1311 w, 1251 s, 1237 m, 1217 m, 1205 w, 1182 m, 1174 m, 1130 m, 1110 s, 1059 s, 1029 s, 959 s, 928 m, 896 w, 865 m, 841 m, 823 m, 814 m, 800 m, 784 m, 764 m, 744 s, 670 s, 669 w, 639 s, 624 s, 610 s, 531 m, 495 s, 476 s, 467 m, 439 m cm^{-1}. ESI-HRMS (m/z): calcd for $C_{27}H_{32}BFeO_3P_2$ ([M − H]$^{+}$), 533.1269. Found, 533.1262. Anal. Calcd for $C_{27}H_{33}BFeO_3P_2$ (534.2): C, 60.71; H, 6.23. Found: C, 60.58; H, 6.07.

Synthesis of 1-(Diphenylphosphino)-1′-(phosphinomethyl)ferrocene−borane (1:1) (5). Neat trimethyl-chlorosilane (3.8 mL, 30 mmol) was slowly introduced to a suspension of Li[AlH_4] (1.14 g, 30 mmol) in dry THF (150 mL) while stirring and cooling on ice. The resulting mixture was stirred for 10 min before adding a solution of ester **4** (3.20 g, 6.0 mmol in 100 mL of THF). After completing the addition, the cooling bath was removed, and the reaction mixture was stirred at room temperature overnight. Then, the reaction flask was cooled in an ice bath, and methanol (200 mL) was cautiously added to terminate the reaction. The resulting mixture was evaporated under vacuum, leaving an orange residue, which was taken up with hexane (300 mL), filtered, and evaporated. The residue was redissolved in chloroform, filtered, and evaporated to give pure phosphine **5** as an orange oil. Yield: 2.53 g (98%).

^{1}H NMR (400 MHz, $CDCl_3$): δ 0.8−1.7 (br m, 3H, BH_3), 2.27 (td, $^{3}J_{HH}$ = 7.5 Hz, $^{2}J_{PH}$ = 4.6 Hz, 2H, CH_2), 2.78 (dm, $^{1}J_{PH}$ = 194.0 Hz, 2H, PH_2), 3.99 (vt, J' = 1.8 Hz, 2H, fc), 4.08 (vt, J' = 1.8 Hz, 2H, fc), 4.35 (vq, J' = 2.0 Hz, 2H, fc), 4.48−4.50 (m, 2H, fc), 7.38−7.49 (m, 6H, PPh_2), 7.55−7.62 (m, 4H, PPh_2). ^{13}C{^{1}H} NMR (101 MHz, $CDCl_3$): δ 13.86 (d, J_{PC} = 9 Hz, CH_2), 68.85 (d, J_{PC} = 69 Hz, C^{ipso} of fc), 69.26 (s, CH of fc), 69.60 (d, J_{PC} = 3 Hz, CH of fc), 72.64 (d, J_{PC} = 8 Hz, CH of fc), 73.58 (d, J_{PC} = 10 Hz, CH of fc), 90.84 (d, J_{PC} = 3 Hz, C^{ipso} of fc), 128.40 (d, J_{PC} = 10 Hz, CH of PPh_2), 130.86 (d, J_{PC} = 2 Hz, CH of PPh_2), 131.38 (d, $^{1}J_{PC}$ = 59 Hz, C^{ipso} of PPh_2), 132.64 (d, J_{PC} = 10 Hz, CH of PPh_2). ^{31}P{^{1}H} NMR (162 MHz, $CDCl_3$): δ −125.9 (s, PH_2), 16.4 (br d, J = 74 Hz, PPh_2BH_3). ^{31}P NMR (162 MHz, $CDCl_3$): δ −125.9 (tt, $^{1}J_{PH}$ = 194 Hz, $^{2}J_{PH}$ = 5 Hz, PH_2), 16.4 (br m, PPh_2BH_3). IR (Nujol) ν_{max}: 3078 m, 3056 m, 2366 s, 2336 s, 2293 w, 1981 w, 1792 w, 1749 w, 1734 w, 1717 w, 1697 w, 1684 w, 1670 w, 1653w, 1647 w, 1636 w, 1584 w, 1576 w, 1559 w, 1540 w, 1521 w, 1507 w, 1457 s, 1435 s, 1418 w, 1313 m, 1198 w, 1182 m, 1174 m, 1134 m, 1109 s, 1059 s, 1027 s, 998 w, 928 m, 896 w, 830 s, 759 m, 741 s, 701 s, 669 m, 637 s, 622 m, 610 m, 531 m, 496 s, 466 s, 439 m, 419 w cm^{-1}. ESI-MS (m/z): 429 ([M − H]$^{+}$). Anal. Calcd for $C_{23}H_{22}FeP_2$ (430.0): C, 64.24; H, 5.86. Found: C, 64.25; H, 5.67.

Synthesis of 1-(Diphenylphosphino)-1′-(phosphinomethyl)ferrocene (2). A reaction flask was charged with adduct **5** (2.58 g, 6.0 mmol) and 1,4-diazabicyclo[2.2.2]octane (1.35 g, 12.0 mmol). Dry tetrahydrofuran (50 mL) was introduced under argon, and the resulting solution was stirred at 45 °C overnight. Subsequent evaporation produced an orange residue, which was purified by chromatography over silica gel, eluting with diethyl ether−hexane (1:1). A single broad orange band was collected and evaporated, affording **2** as an orange solid. The compound was further crystallized from hot heptane. Yield: 1.80 g (72%), orange crystalline solid. Mp 114 °C (heptane).

^{1}H NMR (400 MHz, $CDCl_3$): δ 2.34 (td, $^{3}J_{HH}$ = 7.3 Hz, $^{2}J_{PH}$ = 4.7 Hz, 2H, CH_2), 2.82 (dm, $^{1}J_{PH}$ = 194.2 Hz, 2H, PH_2), 4.00 (vt, J' = 1.8 Hz, 2H, fc), 4.03 (vt, J' = 1.7 Hz, 2H, fc), 4.04 (vq, J' = 1.8 Hz, 2H, fc), 4.34 (vt, J' = 1.7 Hz, 2H, fc), 7.28−7.40 (m, 10H, PPh_2). ^{13}C{^{1}H} NMR (101 MHz, $CDCl_3$): δ 14.07 (d, $^{1}J_{PC}$ = 9 Hz, CH_2), 68.61 (s, CH of fc), 68.77 (d, J_{PC} = 2 Hz, CH of fc), 71.62 (d, J_{PC} = 4 Hz, CH of fc), 73.62 (d, J_{PC} = 15 Hz, CH of fc), 75.79 (d, J_{PC} = 5 Hz, C^{ipso} of fc), 89.89 (d, J_{PC} = 3 Hz, C^{ipso} of fc), 128.10 (d, J_{PC} = 7 Hz, CH of PPh_2), 128.48 (s, CH of PPh_2), 133.49 (d, J_{PC} = 19 Hz, CH of PPh_2), 139.07 (d, $^{1}J_{PC}$ = 19 Hz, C^{ipso} of PPh_2). ^{31}P{^{1}H} NMR (162 MHz, $CDCl_3$): δ −126.7 (s, PH_2), −16.2 (s, PPh_2). ^{31}P NMR (162 MHz, $CDCl_3$): δ −126.7 (tt, $^{1}J_{PH}$ = 194 Hz, $^{2}J_{PH}$ = 4 Hz, PH_2), −16.2 (m, PPh_2). IR (Nujol) ν_{max}: 3097 w, 3083 w, 3069 w, 3054 w, 3041 w, 3030 w, 3015 w, 2726 w, 2359 w, 2303 s, 2296 s, 1974 w, 1901 w, 1829 w, 1767 w, 1733 w, 1679 m, 1646 m, 1584 s, 1569 w, 1775 s, 1433 s, 1414 w, 1395 w, 1381 m, 1325 w, 1312 m, 1305 m, 1279 w, 1236 m, 1210 w, 1193 m, 1163 s, 1124 m, 1091 m, 1078 w, 1036 s, 1026 s, 998 m, 977 w, 936 w, 924 w, 916 w, 863 w, 856 m, 827 s, 812 s, 749 s, 699 s, 668 w, 661 w cm^{-1}. ESI-HRMS: calcd for $C_{23}H_{23}FeOP_2$ ([M + H + O]$^{+}$), 433.0568. Found, 433.0565. Anal. Calcd for $C_{23}H_{22}FeP_2$ (416.2): C, 66.37; H, 5.33. Found: C, 66.40; H, 5.27.

Synthesis of 1-(Diphenylphosphino)-1′-[(diphenylphosphino)methyl]ferrocene (1). An oven-dried Schlenk flask was charged (in this order) with phosphine **2** (205 mg, 0.5 mmol), iodobenzene (204 mg, 1.0 mmol), *N*,*N*-diisopropylethylamine (162 mg, 1.25 mmol), and palladium(II) acetate (5.6 mg, 25 μmol) under argon. Dry acetonitrile (5 mL) was

https://dx.doi.org/10.1021/acs.organomet.0c00767
Organometallics 2021, 40, 427−441

introduced, and the reaction mixture was stirred at 80 °C overnight. Then, the mixture was cooled to room temperature and evaporated under vacuum with chromatographic silica gel. The crude, preadsorbed product was transferred onto the top of a chromatographic column and eluted with a diethyl ether−hexane mixture (1:1). A single orange band was collected and evaporated, leaving phosphine **1** as orange oil, which solidifies when stored in a fridge. Yield: 220 mg (78%).

^{1}H NMR (400 MHz, $CDCl_3$): δ 2.86 (s, 2H, CH_2), 3.84 (vt, J' = 1.8 Hz, 2H, fc), 3.89 (vt, J' = 1.8 Hz, 2H, fc), 4.01 (vq, J' = 1.9 Hz, 2H, fc), 4.32 (vt, J' = 1.8 Hz, 2H, fc), 7.24−7.37 (m, 20H, PPh_2). ^{31}P{^{1}H} NMR (162 MHz, $CDCl_3$): δ −16.2 (s, PPh_2), −11.4 (s, CH_2PPh_2). The data match those in the literature.[12a]

Synthesis of 1-(Diphenylphosphino)-1′-(phosphinylmethyl)ferrocene−borane (1:1) (6). In air, phosphine **5** (0.70 g, 3.0 mmol) was dissolved in a mixture of methanol (20 mL) and dichloromethane (30 mL), and the reaction flask, equipped with stirring bar, was cooled in an ice bath. Hydrogen peroxide solution (3 mL of 30% aqueous solution, 58 mmol) was added over 5 min while stirring, and the resulting mixture was stirred and cooled for another 5 min. Then, the excess of hydrogen peroxide was destroyed by *slowly* adding saturated aqueous sodium thiosulfate (30 mL). ***Caution!****Rapid addition can result in overheating of the reaction mixture and decomposition!* The mixture was transferred to a separatory funnel and diluted with dichloromethane (20 mL) and brine (30 mL). The organic phase was separated, and the aqueous residue was extracted with dichloromethane (20 mL). The combined organic layers were dried over magnesium sulfate, filtered, and evaporated under vacuum. The crude product was purified by flash chromatography over silica gel eluting with a dichloromethane−methanol mixture (10:1). Evaporation of the first orange band afforded phosphine oxide **6** as a yellow solid. Yield: 613 g (84%).

^{1}H NMR (400 MHz, $CDCl_3$): δ 0.8−1.7 (br m, 3H, BH_3), 2.78 (dt, $^2J_{PH}$ = 16.0 Hz, $^3J_{HH}$ = 4.6 Hz, 2H, CH_2), 4.09 (t, J' = 1.9 Hz, 2H, fc), 4.19 (dt, J' = 0.9, 1.9 Hz, 2H, fc), 4.38 (q, J' = 1.8 Hz, 2H, fc), 4.56 (dt, J' = 1.1, 1.9 Hz, 2H, fc), 6.79 (dt, $^1J_{PH}$ = 470.0 Hz, $^3J_{HH}$ = 4.6 Hz, 2H, $P(O)H_2$), 7.40−7.52 (m, 6H, PPh_2), 7.56−7.62 (m, 4H, PPh_2). ^{13}C{^{1}H} NMR (101 MHz, $CDCl_3$): δ 28.20 (d, $^1J_{PC}$ = 62 Hz, CH_2), 69.72 (d, J_{PC} = 68 Hz, C^{ipso} of fc), 70.25 (s, CH of fc), 70.84 (d, J_{PC} = 4 Hz, CH of fc), 72.74 (d, J_{PC} = 8 Hz, CH of fc), 73.98 (d, J_{PC} = 9 Hz, CH of fc), 128.54 (d, J_{PC} = 10 Hz, CH of PPh_2), 130.97 (d, $^1J_{PC}$ = 60 Hz, C^{ipso} of PPh_2), 131.12 (d, J_{PC} = 2 Hz, CH of PPh_2), 132.62 (d, J_{PC} = 10 Hz, CH of PPh_2); the signal due to C^{ipso} of fc is obscured by the solvent resonance. ^{31}P{^{1}H} NMR (162 MHz, $CDCl_3$): δ 8.5 (s, $P(O)H_2$), 16.2 (br m, PPh_2). ^{31}P NMR (162 MHz, $CDCl_3$): δ 8.5 (tt, $^1J_{PH}$ = 470 Hz, $^2J_{PH}$ = 16 Hz, $P(O)H_2$), 16.2 (br m, PPh_2). IR (DRIFTS) ν_{max}: 3074 m, 2383 s, 2344 s, 2247 w, 1587 w, 1485 m, 1466 m, 1434 s, 1387 w, 1363 w, 1363 w, 1311 w, 1250 w, 1220 s, 1201 s, 1182 s, 1172 s, 1129 m, 1109 s, 1060 s, 1025 s, 999 m, 924 w, 911 w, 870 w, 861 w, 837 s, 822 w, 810 w, 779 w, 762 w, 743 s, 700 s, 639 m, 624 s, 612 m, 531 m, 511 m, 496 s, 473 s, 441 w cm^{-1}. ESI-MS (m/z): 469 ([M + Na]$^+$), 915 ([2 M + Na]$^+$). Anal. Calcd for $C_{23}H_{25}BFeOP_2$ (446.0): C, 61.93; H, 5.65. Found: C, 61.74; H, 5.61.

Synthesis of 1-(Diphenylphosphino)-1′-(phosphinylmethyl)ferrocene (7). Compound **6** (89.2 mg, 0.20 mmol), 1,4-diazabicyclo[2.2.2]octane (26.9, 0.24 mmol), and tetrahydrofuran (5 mL) were mixed in a reaction flask under argon, and the mixture was stirred at 50 °C overnight. Subsequent evaporation afforded an orange residue, which was purified by chromatography over silica gel, eluting with a dichloromethane−methanol mixture (10:1). The first orange band was collected and evaporated to give phosphine **7** as orange oil, which gradually solidified. Yield: 82 mg (95%). Mp 107 °C (amorphous sample).

^{1}H NMR (400 MHz, $CDCl_3$): δ 2.78 (dt, $^2J_{PH}$ = 16.2 Hz, $^3J_{HH}$ = 4.7 Hz, 2H, CH_2), 4.08−4.11 (m, 6H, fc), 4.40 (vt, J' = 1.8 Hz, 2H, fc), 6.77 (dt, $^1J_{PH}$ = 469.3 Hz, $^3J_{HH}$ = 4.7 Hz, 2H, $P(O)H_2$), 7.31−7.40 (m, 10H, PPh_2). ^{13}C{^{1}H} NMR (101 MHz, $CDCl_3$): δ 28.24 (d, $^1J_{PC}$ = 62 Hz, CH_2), 69.04 (d, J_{PC} = 84 Hz, C^{ipso} of fc), 69.74 (s, CH of fc), 70.03 (d, J_{PC} = 4 Hz, CH of fc), 71.79 (d, J_{PC} = 4 Hz, CH of fc), 73.99 (d, J_{PC} = 15 Hz, CH of fc), 75.91 (s, C^{ipso} of fc), 128.25 (d, J_{PC} = 7 Hz, CH of PPh_2), 128.75 (s, CH of PPh_2), 133.51 (d, J_{PC} = 20 Hz, CH of PPh_2), 138.75 (d, $^1J_{PC}$ = 9 Hz, C^{ipso} of PPh_2). ^{31}P{^{1}H} NMR (162 MHz, $CDCl_3$): δ −16.8 (s, PPh_2), 9.3 (s, $P(O)H_2$). ^{31}P NMR (162 MHz, $CDCl_3$): δ −16.8 (s, $PPh_2{\cdot}BH_3$), 9.3 (tt, $^1J_{PH}$ = 469 Hz, $^2J_{PH}$ = 16 Hz, $P(O)H_2$). IR (Nujol) ν_{max}: 3089 w, 3073 m, 3051 m, 2669 w, 2347 m, 2324 m, 1719 w, 1583 w, 1568 w, 1435 s, 1239 w, 1214 s, 1201 s, 1115 m, 1096 m, 1028 s, 1018 m, 998 w, 975 w, 914 w, 847 w, 834 m, 818 m, 752 s, 729 m, 700 s, 632 w, 489 s, 455 w, 437 w cm^{-1}. ESI-MS (m/z): 455 ([M + Na]$^+$), 887 ([2 M + Na]$^+$). Anal. Calcd for $C_{23}H_{22}FeOP_2{\cdot}0.1CH_2Cl_2$ (440.7): C, 62.96; H, 5.08. Found: C, 62.93; H, 5.04.

Synthesis of 1-(Diphenylphosphino)-1′-{[(2-hydroxyprop-2-yl)phosphinyl]methyl}ferrocene−borane (1:1) (8). A solution of phosphine **6** (223 mg, 0.50 mmol) in reagent-grade acetone (5 mL) was heated at 40 °C under argon overnight. The resulting mixture was evaporated, and the crude product was purified by chromatography over silica gel with a dichloromethane−methanol mixture (10:1) as the eluent. Subsequent evaporation produced **8** as an orange powder. Yield: 218 mg (87%).

^{1}H NMR (400 MHz, $CDCl_3$): δ 0.8−1.7 (br s, 3H, BH_3), 1.35 (d, $^3J_{PH}$ = 14.7 Hz, 3H, Me), 1.37 (d, $^3J_{PH}$ = 14.9 Hz, 3H, Me), 2.65−2.82 (m, 2H, CH_2), 3.79 (br s, 1H, OH), 4.03 (d vt, J' = 1.3, 2.6 Hz, 1H, fc), 4.05 (d vt, J' = 1.4, 2.5 Hz, 1H, fc), 4.25−4.28 (m, 2H, fc), 4.33−4.36 (m, 2H, fc), 4.52−4.54 (m, 2H, fc), 6.33 (ddd, $^1J_{PH}$ = 454.9 Hz, J_{HH} = 5.1, 1.9 Hz, 1H, PH), 7.38−7.50 (m, 6H, PPh_2), 7.54−7.62 (m, 4H, PPh_2). ^{13}C{^{1}H} NMR (101 MHz, $CDCl_3$): δ 23.85 (d, $^2J_{PC}$ = 8 Hz, Me), 24.59 (d, $^2J_{PC}$ = 9 Hz, Me), 25.65 (d, $^1J_{PC}$ = 56 Hz, CH_2), 69.11 (s, C−OH), 69.84 (d, J_{PC} = 9 Hz, C^{ipso} of fc), 69.91 (s, CH of fc), 70.06 (s, CH of fc), 70.91 (d, J_{PC} = 3 Hz, CH of fc), 71.21 (d, J_{PC} = 3 Hz, CH of fc), 72.80 (d, J_{PC} = 7 Hz, CH of fc), 72.88 (d, J_{PC} = 7 Hz, CH of fc), 73.70 (d, J_{PC} = 9 Hz, CH of fc), 74.10 (d, J_{PC} = 10 Hz, CH of fc), 79.91 (d, J_{PC} = 4 Hz, C^{ipso} of fc), 128.49 (d, J_{PC} = 10 Hz, CH of PPh_2), 128.50 (d, J_{PC} = 10 Hz, CH of PPh_2), 130.98 (d, J_{PC} = 2 Hz, CH of PPh_2), 131.02 (d, $^1J_{PC}$ = 59 Hz, C^{ipso} of PPh_2), 131.05 (d, J_{PC} = 2 Hz, CH of PPh_2), 131.13 (d, $^1J_{PC}$ = 59 Hz, C^{ipso} of PPh_2), 132.60 (d, J_{PC} = 9 Hz, CH of PPh_2), 132.62 (d, J_{PC} = 9 Hz, CH of PPh_2). ^{31}P{^{1}H} NMR (162 MHz, $CDCl_3$): δ 16.3 (br s, PPh_2BH_3), 46.0 (s, P(O)H). ^{31}P NMR (162 MHz, $CDCl_3$): δ 16.3 (br m, PPh_2BH_3), 46.0 (dm, $^1J_{PH}$ = 455 Hz, P(O)H). IR (Nujol) ν_{max}: 3177 br m, 2332 m, 1629 w, 1309 w, 1202 s, 1172 m, 1157 w, 1135 m, 1109 m, 1059 m, 1029 m, 998 w, 974 w, 942 m, 929 m, 836 m, 819 m, 804 m, 764 m, 739 s, 702 s, 638 m, 608 m, 531 w, 499 m, 471 m, 442 w cm^{-1}. ESI-MS (m/z): 527 ([M + Na]$^+$), 1031 ([2 M + Na]$^+$). Anal. Calcd for $C_{26}H_{31}BFeO_2P_2{\cdot}0.25CH_2Cl_2$ (525.4): C, 60.01; H, 6.04. Found: C, 59.84; H, 5.95.

Synthesis of 1-(Diphenylphosphino)-1′-{[(2-hydroxyprop-2-yl)phosphinyl]methyl}ferrocene (9). Phosphine **7** (173 mg, 0.40 mmol) was dissolved in reagent-grade acetone (5 mL), and the solution was stirred at 40 °C under argon overnight. The mixture was cooled to room temperature and evaporated under vacuum, leaving a crude product, which was purified over silica gel using a dichloromethane−methanol mixture (10:1) as the eluent. Evaporation of the second orange band afforded **9** as an orange solid. Yield: 155 mg (79%). Crystals suitable for structure determination were obtained by recrystallization from ethyl acetate/hexane.

^{1}H NMR (400 MHz, $CDCl_3$): δ 1.34 (d, $^3J_{PH}$ = 12.9 Hz, 3H, Me), 1.38 (d, $^3J_{PH}$ = 13.0 Hz, 3H, Me), 2.72 (d, $^3J_{HH}$ = 3.5 Hz, 1H, CH_2), 2.75 (d, $^3J_{HH}$ = 3.5 Hz, 1H, CH_2), 3.25 (d, $^3J_{PH}$ = 3.8 Hz, 1H, OH), 4.04−4.08 (m, 4H, fc), 4.15 (vd, J' = 1.4 Hz, 1H, fc), 4.20 (vd, J' = 1.3 Hz, 1H, fc), 4.37 (vt, J' = 1.8 Hz, 2H, fc), 6.35 (dt, $^1J_{PH}$ = 454.1 Hz, $^3J_{HH}$ = 3.5 Hz, 1H, PH), 7.30−7.39 (m, 10H, PPh_2). ^{13}C{^{1}H} NMR (101 MHz, $CDCl_3$): δ 23.87 (d, $^2J_{PH}$ = 7 Hz, Me), 24.75 (d, $^2J_{PH}$ = 8 Hz, Me), 26.26 (d, $^1J_{PH}$ = 53 Hz, CH_2), 69.40 (s, CH of fc), 69.69 (s, CH of fc), 70.08 (br s, CH of fc), 70.47 (br s, CH of fc), 71.89 (br s, 2CH of fc), 73.90 (d, J_{PC} = 11 Hz, CH of fc), 74.04 (d, J_{PC} = 11 Hz, CH of fc), 78.87 (br s, C^{ipso} of fc), 128.22 (s, CH of PPh_2), 128.65 (s, CH of PPh_2), 133.57 (d, J_{PH} = 17 Hz, CH of PPh_2), 138.91 (s, C^{ipso} of PPh_2). Signals due to C−OH and C^{ipso} fc were not observed, presumably due to overlaps. ^{31}P{^{1}H} NMR (162 MHz, $CDCl_3$): δ −16.8 (s, PPh_2), 45.9 (s, P(O)H). ^{31}P NMR (162 MHz,

https://dx.doi.org/10.1021/acs.organomet.0c00767
Organometallics 2021, 40, 427−441

$CDCl_3$): δ 16.8 (s, PPh_2), 45.9 (d of septets, $^1J_{PH}$ = 454 Hz, $^2J_{PH}$ = 13 Hz, P(O)H). IR (Nujol) ν_{max}: 3146 br s, 3066 m, 2326 s, 2170 w, 2066 w, 1435 s, 1210 w, 1192 m, 1119 s, 1097 m, 1030 m, 999 w, 975 m, 925 w, 908 m, 846 m, 804 s, 751 s, 743 s, 699 s, 568 w, 527 w, 503 s, 484 m, 462 w cm^{-1}. ESI-MS (m/z): 529 ($[M + O + Na]^+$), 1003 ($[2 M + Na]^+$). Anal. Calcd for $C_{26}H_{28}FeO_2P_2 \cdot 0.2CH_2Cl_2$ (507.3): C, 62.03; H, 5.64. Found: C, 62.01; H, 5.41.

Synthesis of [μ-1κP:2$\kappa P'$-1,1′-Bis(diphenylphosphino)-ferrocene]bis[dichloro(η^6-mesitylene)ruthenium(II)] (10). [{(η^6-Mesitylene)RuCl(μ-Cl)}$_2$] (58 mg, 0.10 mmol) and dppf (55 mg, 0.10 mmol) were dissolved in dichloromethane (40 mL) under argon, and the solution was stirred overnight. Subsequent evaporation afforded analytically pure complex **10** as a red solid in quantitative yield. Crystals suitable for structure determination were grown from a dichloromethane/hexane mixture. The yield of crystalline material was 58 mg (50%).

^{1}H NMR (400 MHz, $CDCl_3$): δ 1.87 (s, 18H, Me), 4.10 (very br s, 8H, CH of fc), 4.40 (s, 6H, C_6H_3), 7.27−7.37 (m, 12H, PPh_2), 7.63−7.72 (m, 8H, PPh_2). ^{31}P{^{1}H} NMR (162 MHz, $CDCl_3$): δ 20.7 (s). IR (Nujol) ν_{max}: 3567 br m, 3053 s, 1992 w, 1586 w, 1570 w, 1559 w, 1540 m, 1528 m, 1507 w, 1482 m, 1265 m, 1190 m, 1092 m, 1073 m, 1026 s, 879 w, 839 s, 751 s, 728 m, 698 s, 669 w, 623 w, 570 w, 542 s, 523 s, 487 m, 471 s, 445 m cm^{-1}. ESI-MS (m/z): 811 ($[M - (mes)RuCl_2 - Cl)]^+$). Anal. Calcd for $C_{52}H_{52}Cl_4FeRu_2P_2 \cdot 1.5CH_2Cl_2$ (1266.1): C, 50.75; H, 4.38. Found: C, 50.86; H, 4.29.

Synthesis of {μ-1κP:2$\kappa P'$-1-(Diphenylphosphino)-1′-[(diphenylphosphino)methyl]ferrocene}bis[dichloro(η^6-mesitylene)ruthenium(II)] (11). [{(η^6-Mesitylene)RuCl(μ-Cl)}$_2$] (41 mg, 0.070 mmol) and phosphine **1** (40 mg, 0.070 mmol) were dissolved in dichloromethane (20 mL) under argon, and the mixture was stirred overnight. Subsequent evaporation produced a red solid, which was redissolved in dichloromethane (3 mL), precipitated with pentane, and isolated by suction. Yield of 11:64 mg (68%), red solid.

^{1}H NMR (400 MHz, $CDCl_3$): δ 1.84 (s, 9H, Me), 1.89 (s, 9H, Me), 3.02 (br s, 2H, fc), 3.34 (br s, 2H, fc), 3.54 (br d, $^2J_{PH}$ = 7.1 Hz, 2H, CH_2), 4.33 (br vq, J' = 1.2 Hz, 2H, fc), 4.42 (br s, 2H, fc), 4.44 (s, 3H, C_6H_3), 4.65 (s, 3H, C_6H_3), 7.24−7.36 (m, 10H, PPh_2), 7.38−7.44 (m, 2H, PPh_2), 7.60−7.68 (m, 4H, PPh_2), 7.68−7.76 (m, 4H, PPh_2). ^{13}C{^{1}H} NMR (101 MHz, $CDCl_3$): δ 18.23 (s, Me), 18.36 (s, Me), 26.89 (d, $^1J_{PC}$ = 24 Hz, CH_2), 71.41 (s, CH of fc), 71.86 (s, CH of fc), 72.01 (d, J_{PC} = 8 Hz, CH of fc), 75.27 (br s, CH of fc), 82.24 (d, J_{PC} = 8.5 Hz, C^{ipso} of fc), 86.17 (d, J_{PC} = 4 Hz, CH of C_6H_3), 87.20 (d, J_{PC} = 3 Hz, CH of C_6H_3), 100.90 (d, J_{PC} = 3 Hz, C^{ipso} of C_6H_3), 102.86 (d, J_{PC} = 2 Hz, C^{ipso} of C_6H_3), 126.96 (d, J_{PC} = 10 Hz, CH of PPh_2), 127.73 (d, J_{PC} = 9 Hz, CH of PPh_2), 129.69 (br s, CH of PPh_2), 130.46 (d, J_{PC} = 2 Hz, CH of PPh_2), 130.73 (d, J_{PC} = 42 Hz, C^{ipso} of PPh_2), 133.88 (d, J_{PC} = 9 Hz, CH of PPh_2), 134.25 (br d, J_{PC} = 6 Hz, CH of PPh_2). The signals due to C^{ipso} of fc and PPh_2 were not observed, presumably due to overlaps. ^{31}P{^{1}H} NMR (162 MHz, $CDCl_3$): δ 21.8 (s, PPh_2), 30.4 (s, CH_2PPh_2). IR (Nujol) ν_{max}: 2726 w, 1992 w, 1541 w, 1507 w, 1299 m, 1096 m, 1030 m, 922 w, 841 s, 746 m, 698 m, 669 w, 558 m, 537 w, 497 m cm^{-1}. ESI-MSI (m/z): 789 ($[M - (mes)RuCl_2 - HCl - Cl]^+$). Anal. Calcd for $C_{54}H_{54}Cl_4FeRu_2P_2 \cdot 0.5CH_2Cl_2$ (1195.2): C, 53.76; H, 4.64. Found: C, 53.73; H, 4.55.

Synthesis of [μ-1κP:2$\kappa P'$-1-(Diphenylphosphino)-1′-(phosphinomethyl)ferrocene]bis[dichloro(η^6-mesitylene)-ruthenium(II)] (12). [{(η^6-Mesitylene)RuCl(μ-Cl)}$_2$] (32 mg, 0.10 mmol) and phosphine **2** (58 mg, 0.10 mmol) were dissolved in dry dichloromethane (40 mL), and the resulting solution was stirred overnight. The reaction mixture was evaporated, and the residue was crystallized from chloroform/hexane. The resulting crystals were isolated by suction and dried under vacuum. Yield: 64 mg (64%), red crystals.

^{1}H NMR (400 MHz, $CDCl_3$): δ 1.93 (s, 9H, Me), 2.17 (d, J_{PH} = 1.0 Hz, 9H, Me), 3.12 (br s, 2H, CH_2), 3.52 (br s, 2H, fc), 3.89 (br s, 2H, fc), 4.46 (br s, 2H, fc), 4.50 (br s, 3H of C_6H_3 and 2H of fc), 4.60 (dt, $^1J_{PH}$ = 361.5 Hz, $^3J_{PH}$ = 6.6 Hz, 2H, PH_2), 4.98 (s, 3H, C_6H_3), 7.32−7.43 (m, 6H, PPh_2), 7.77−7.85 (m, 4H, PPh_2). ^{13}C{^{1}H} NMR (101 MHz, $CDCl_3$): δ 18.24 (d, J_{PC} = 1 Hz, Me), 19.00 (d, J_{PC} = 1 Hz, Me), 19.26 (d, $^1J_{PC}$ = 19 Hz, CH_2), 70.40 (s, CH of fc), 70.97 (s, CH of fc), 71.05 (s, CH of fc), 76.38 (d, J_{PC} = 25 Hz, C^{ipso} of fc), 82.06 (d, J_{PC} = 5 Hz, CH of C_6H_3), 85.98 (d, J_{PC} = 6 Hz, CH of fc), 86.57 (d, J_{PC} = 4 Hz, CH of C_6H_3), 103.02 (br s, C^{ipso} of C_6H_3), 104.48 (d, J_{PC} = 2 Hz, C^{ipso} of C_6H_3), 127.27 (d, J_{PC} = 10 Hz, CH of PPh_2), 129.91 (d, J_{PC} = 2 Hz, CH of PPh_2), 133.95 (br s, CH of PPh_2). The signals due to C^{ipso} of fc and PPh_2 were not observed. ^{31}P{^{1}H} NMR (162 MHz, $CDCl_3$): δ −19.4 (s, PH_2), 20.8 (s, PPh_2). ^{31}P NMR (162 MHz, $CDCl_3$): δ −19.4 (t, $^1J_{PH}$ = 361 Hz, PH_2), 20.8 (s, PPh_2). IR (Nujol) ν_{max}: 1933 w, 1526 m, 1298 m, 1192 w, 1161 m, 1085 m, 1031 s, 930 m, 884 s, 837 m, 814 w, 760 s, 749 m, 698 s, 543 m, 524 m, 490 m, 469 m, 444 w, 426 w cm^{-1}. ESI-MS (m/z): 669 ($[(M - RuCl_2(mes) - 2Cl + OMe]^+$). Anal. Calcd for $C_{41}H_{46}Cl_4FeP_2Ru_2 \cdot 0.25CHCl_3$ (1030.4): C, 48.08; H, 4.52. Found: C, 48.49; H, 4.44.

Synthesis of {μ-1κP:2$\kappa P'$-1-(Diphenylphosphino)-1′-[(hydroxyphosphino)methyl]ferrocene}bis[dichloro(η^6-mesitylene)ruthenium(II)] (13). Ligand **7** (43 mg, 0.10 mmol) and [{(η^6-mesitylene)RuCl(μ-Cl)}$_2$] (58 mg, 0.10 mmol) were dissolved in dichloromethane (10 mL), and the resulting mixture was stirred overnight. Subsequent evaporation afforded pure complex **13** as a red solid in an essentially quantitative yield (102 mg).

^{1}H NMR (400 MHz, $CDCl_3$): δ 1.94 (s, 9H, Me), 2.08 (d, J_{PC} = 0.8 Hz, 9H, Me), 3.22−3.50 (m, 2H, CH_2), 3.41 (br s, 1H, fc), 3.69 (br s, 1H, fc), 4.00 (br s, 2H, fc), 4.45−4.55 (m, 7H, 3H of C_6H_3 and 4H of fc), 4.88 (s, 3H, C_6H_3), 6.80 (dt, $^1J_{PH}$ = 377.9 Hz, $^3J_{HH}$ = 5.4 Hz, 1H, PH), 7.34−7.42 (m, 6H, PPh_2), 7.74−7.87 (m, 4H, PPh_2). ^{13}C{^{1}H} NMR (101 MHz, $CDCl_3$): δ 18.26 (s, Me), 18.73 (s, Me), 30.35 (br s, CH_2), 70.29 (s, CH of fc), 70.91 (s, CH of fc), 71.26 (s, CH of fc), 71.62 (s, CH of fc), 72.89 (s, C^{ipso} of fc), 82.20 (s, C^{ipso} of fc), 82.77 (s, CH of C_6H_3), 86.55 (s, CH of C_6H_3), 103.05 (s, C^{ipso} of C_6H_3), 105.85 (s, C^{ipso} of C_6H_3), 127.15 (d, J_{PC} = 16 Hz, CH of PPh_2), 127.38 (d, J_{PC} = 10 Hz, CH of PPh_2), 129.94 (d, J_{PC} = 9.0 Hz, CH of PPh_2), 133.97 (br d, $^1J_{PH}$ = 112 Hz, C^{ipso} of PPh_2). ^{31}P{^{1}H} NMR (162 MHz, $CDCl_3$): δ 20.7 (s, PPh_2), 117.1 (br s, P(OH)H). ^{31}P NMR (162 MHz, $CDCl_3$): δ 20.7 (s, PPh_2), 117.1 (d, $^1J_{PH}$ = 378 Hz, P(OH)H). IR (Nujol) ν_{max}: 1524 m, 1094 m, 1031 m, 931 w, 878 s, 836 w, 748 m, 699 m, 543 m, 523 m, 487 m, 471 m, 434 w cm^{-1}. ESI-MS (m/z): 945 ($[M - HCl - Cl]^+$), 1237 ($[M + RuCl_2(mes) - HCl - Cl]^+$). Anal. Calcd for $C_{41}H_{46}Cl_4FeOP_2Ru_2$ (1016.5): C, 48.44; H, 4.56. Found: C, 48.16; H, 4.58.

Synthesis of {1-(Diphenylphosphino-κP)-1′-[(phosphinyl)-methyl]ferrocene}[dichloro(η^6-mesitylene)ruthenium(II)] (14). Phosphine **7** (95 mg, 0.22 mmol) and [{(η^6-mesitylene)RuCl(μ-Cl)}$_2$] (64 mg, 0.11 mmol) were dissolved in dichloromethane (15 mL). The resulting mixture was stirred overnight and then evaporated, leaving complex **14** as an orange powdery solid in a quantitate yield.

^{1}H NMR (400 MHz, $CDCl_3$): δ 1.91 (br s, 9H, Me), 2.96 (br d, $^2J_{PH}$ = 16.0 Hz, 2H, CH_2), 3.58 (br s, 2H, fc), 3.86 (br s, 2H, fc), 4.44 (br s, 2H, fc), 4.54 (br s, 5H, 3H of C_6H_3 and 2H of fc), 6.79 (dt, $^1J_{PH}$ = 470 Hz, $^3J_{PH}$ = 4.5 Hz, 2H, $P(O)H_2$), 7.35−7.45 (m, 6H, PPh_2), 7.78−7.85 (m, 4H, PPh_2). ^{13}C{^{1}H} NMR (101 MHz, $CDCl_3$): δ 18.23 (s, Me), 28.04 (d, $^1J_{PC}$ = 62 Hz, CH_2), 70.73 (s, CH of fc), 70.83 (br s, 2 × CH of fc), 71.70 (s, CH of fc), 77.22 (s, CH of fc), 86.98 (s, CH of C_6H_3), 102.56 (s, C^{ipso} of C_6H_3), 127.05 (d, J_{PC} = 10 Hz, CH of PPh_2), 130.01 (d, J_{PC} = 2 Hz, CH of PPh_2), 133.88 (br s, CH of PPh_2). The signals due to C^{ipso} of fc and PPh_2 were not observed. ^{31}P{^{1}H} NMR (162 MHz, $CDCl_3$): δ 9.4 (s, $P(O)H_2$), 21.1 (br s, PPh_2). ^{31}P NMR (162 MHz, $CDCl_3$): δ 9.4 (tt, $^1J_{PH}$ = 470 Hz, $^2J_{PH}$ = 16 Hz, $P(O)H_2$), 21.1 (br s, PPh_2). IR (Nujol) ν_{max}: 1541 w, 1250 w, 1221 w, 1193 w, 1027 s, 835 w, 822 w, 762 w, 746 w, 697 w, 545 m, 523 w, 483 w, 474 w, 458 w, 444 w, 420 w cm^{-1}. ESI-MS (m/z): 685 ($[M - 2Cl + OMe]^+$), 1369 ($[2M - HCl-3Cl + 2OMe]^+$). Anal. Calcd for $C_{32}H_{34}Cl_2FeOP_2Ru \cdot 0.2CH_2Cl_2$ (741.4): C, 52.17; H, 4.68. Found: C, 52.30; H, 4.64.

Synthesis of {1-(Diphenylphosphino)-1′-[(hydroxy-phosphino-κP)methyl]ferrocene}[dichloro(η^6-mesitylene)-ruthenium(II)]−borane (1:1) (15). Complex **6** (67 mg, 0.15 mmol) and [{(η^6-mesitylene)RuCl(μ-Cl)}$_2$] (44 mg, 0.075 mmol) were

https://dx.doi.org/10.1021/acs.organomet.0c00767
Organometallics 2021, 40, 427−441

dissolved in dichloromethane (10 mL), and the resulting solution was stirred overnight. Subsequent evaporation left complex **15** as a red-orange powder in quantitative yield. Crystals used for structure determination were obtained from chloroform/hexane.

^{1}H NMR (400 MHz, $CDCl_3$): δ 0.8−1.7 (br s, 3H, BH_3), 2.05 (d, J_{PH} = 1.2 Hz, 9H, Me), 2.95−3.04 (m, 1H, CH_2), 3.27−3.34 (m, 1H, CH_2), 4.10 (d vt, J = 1.3, 2.4 Hz, 1H, fc), 4.19 (d vt, J = 1.3, 2.4 Hz, 1H, fc), 4.30−4.32 (m, 3H, fc), 4.40−4.42 (m, 1H, fc), 4.52−4.54 (m, 2H, fc), 4.79 (s, 3H, C_6H_3), 6.77 (dtd, $^1J_{PH}$ = 375.3 Hz, $^3J_{HH}$ = 5.5, 1.4 Hz, 1H, PH), 7.39−7.66 (m, 10H, PPh_2). ^{13}C{^{1}H} NMR (101 MHz, $CDCl_3$): δ 18.71 (d, J_{PC} = 1 Hz, Me), 29.53 (d, $^1J_{PC}$ = 38 Hz, CH_2), 69.58 (d, J_{PC} = 68 Hz, C^{ipso} of fc), 69.75 (s, CH of fc), 70.34 (s, CH of fc), 71.27 (d, J_{PC} = 2 H, CH of fc), 71.88 (d, J_{PC} = 2 H, CH of fc), 73.00 (d, J_{PC} = 8 H, CH of fc), 73.21(d, J_{PC} = 7 H, CH of fc), 73.90 (s, CH of fc), 74.00 (d, J_{PC} = 2 H, CH of fc), 81.09 (d, J_{PC} = 3 Hz, C^{ipso} of fc), 82.53 (d, J_{PC} = 5 Hz, CH of C_6H_3), 106.19 (d, J_{PC} = 2 Hz, C^{ipso} of C_6H_3), 128.50 (d, J_{PC} = 2 Hz, CH of PPh_2), 128.61 (d, J_{PC} = 2 Hz, CH of PPh_2), 130.72 (d, $^1J_{PC}$ = 60 Hz, C^{ipso} of PPh_2), 131.00 (d, J_{PC} = 2 Hz, CH of PPh_2), 131.09 (d, $^1J_{PC}$ = 60 Hz, C^{ipso} of PPh_2), 131.33 (d, J_{PC} = 2 Hz, CH of PPh_2), 132.44 (d, J_{PC} = 9 Hz, CH of PPh_2), 132.74 (d, J_{PC} = 9 Hz, CH of PPh_2). ^{31}P{^{1}H} NMR (162 MHz, $CDCl_3$): δ 16.3 (br s, PPh_2BH_3), 115.3 (s, P(OH)H). ^{31}P NMR (162 MHz, $CDCl_3$): δ 16.3 (br s, PPh_2BH_3), 115.3 (ddd, $^1J_{PH}$ = 375 Hz, $^2J_{PH}$ = 18, 8 Hz, P(OH)H). IR (nujol) ν_{max}: 3180 br m, 3079 m, 3053 m, 2914 w, 2379 m, 2341 m, 2326 m, 1572 w, 1528 m, 1483 w, 1455 w, 1436 m, 1399 w, 1383 w, 1371 m, 1311 w, 1298 w, 1266 w, 1240 w, 1185 w, 1173 s, 1127 m, 1108 s, 1053 s, 1030 s, 999 m, 986 m, 961 m, 923 s, 872 s, 840 m, 829 m, 806 w, 753 m, 737 s, 700 s, 638 m, 624 m, 530 m, 500 s, 477 m, 442 m, 404 m cm^{-1}. ESI-MS (m/z): 958 ([M + $RuCl_2$(mes) − HCl − Cl]$^+$). Anal. Calcd for $C_{32}H_{37}BCl_2FeOP_2Ru$ (738.2): C, 52.06; H, 5.05. Found: C, 51.82; H, 4.99.

Synthesis of [1,1′-Bis(diphenylphosphino)ferrocene-κ^2P,P']-[chloro(η^6-mesitylene)ruthenium(II)] hexafluorophosphate (16). dppf (55 mg, 0.10 mmol), [{(η^6-mesitylene)RuCl(μ-Cl)}$_2$] (29 mg, 0.05 mmol), and sodium hexafluorophosphate (84 mg, 0.5 mmol) were mixed in methanol and dichloromethane (10 mL each) under argon, and the suspension was stirred overnight and then evaporated. The solid residue was extracted with dichloromethane (15 mL), and the extract was filtered (PTFE syringe filter, 45 μm pore size). The filtrate was evaporated, and the crude solid was further purified by chromatography over a short silica gel column, eluting with a dichloromethane−methanol mixture (10:1). Finally, the product was dissolved in dichloromethane (approximately 5 mL) and precipitated with cold pentane (ca. 40 mL). Separated solid was isolated by suction and dried under vacuum. Yield of **16**: 85 mg (89%), orange powdery solid. Crystals suitable for structure determination were obtained by liquid-phase diffusion of hexane into a dichloromethane solution of the complex.

^{1}H NMR (400 MHz, $CDCl_3$): δ 1.74 (s, 9H, Me), 4.00−4.01 (m, 2H, fc), 4.09−4.11 (m, 2H, fc), 4.31−4.33 (m, 2H, fc), 4.85 (s, 3H, C_6H_3), 5.10−5.11 (m, 2H, fc), 7.40−7.50 (m, 6H, PPh_2), 7.52−7.60 (m, 4H, PPh_2), 7.64−7.72 (m, 6H, PPh_2), 7.86−7.94 (m, 4H, PPh_2). ^{13}C{^{1}H} NMR (101 MHz, $CDCl_3$): δ 19.38 (s, Me), 68.74 (t, J_{PC} = 3 Hz, CH of fc), 73.82 (t, J_{PC} = 3 Hz, CH of fc), 74.77 (t, J_{PC} = 2 Hz, CH of fc), 79.17 (t, J_{PC} = 5 Hz, CH of fc), 84.38 (t, $^1J_{PC}$ = 28 Hz, C^{ipso} of fc), 92.65 (t, J_{PC} = 3 Hz, CH of C_6H_3), 114.28 (t, J_{PC} = 2 Hz, C^{ipso} of C_6H_3), 128.20 (t, J_{PC} = 5 Hz, CH of PPh_2), 128.25 (t, J_{PC} = 5 Hz, CH of PPh_2), 130.48 (t, J_{PC} = 24 Hz, C^{ipso} of PPh_2), 130.84 (s, CH of PPh_2), 132.47 (s, CH of PPh_2), 132.91 (t, J_{PC} = 4 Hz, CH of PPh_2), 135.83 (t, J_{PC} = 6 Hz, CH of PPh_2), 137.81 (t, $^1J_{PC}$ = 24 Hz, C^{ipso} of PPh_2). ^{31}P{^{1}H} NMR (162 MHz, $CDCl_3$): δ −143.9 (hept, $^1J_{PF}$ = 713 Hz, PF_6), 35.6 (s, PPh_2). IR (Nujol) ν_{max}: 1541 w, 1298 m, 1090 m, 1035 m, 842 v s, 743 m, 703 s, 631 w, 558 s, 546 w, 517 s, 508 m, 479 m, 440 w cm^{-1}. ESI-MS (m/z): 811 ([M − PF_6]$^+$). Anal. Calcd for $C_{43}H_{40}ClF_6FeRuP_3$ (956.1): C, 54.02; H, 4.22. Found: C, 54.08; H, 4.32.

Synthesis of [1,1′-Bis(diphenylphosphino)ferrocene κ^2P,P']-chloro(η^5-cyclopentadienyl)ruthenium(II) (17). The procedure was adopted from ref 29. Chloro(cyclopentadienyl)bis(triphenylphosphine)ruthenium(II) (80 mg, 0.11 mmol) and dppf (61 mg, 0.11 mmol) were mixed in toluene (20 mL) under argon, and the mixture was heated at reflux for 24 h. After cooling, the solvent was evaporated under vacuum, and the residue was triturated with diethyl ether (50 mL). The remaining solid was filtered off, washed with diethyl ether (50 mL), and dried under vacuum to produce complex **17** as an orange solid. Yield: 61 mg (73%).

^{1}H NMR (400 MHz, $CDCl_3$): δ 4.02 (v td, J' = 1.3 Hz, 2H, fc), 4.11 (s, 5H, C_5H_5), 4.24 (br s, 2H, fc), 4.32 (br s, 2H, fc), 5.19 (br s, 2H, fc), 7.27−7.44 (m, 16H, PPh_2), 7.76−7.83 (m, 4H, PPh_2). ^{31}P{^{1}H} NMR (162 MHz, $CDCl_3$): δ 45.7 (s). The data match those in the original report.[29]

Synthesis of {1-(Diphenylphosphino)-1′-[(diphenylphosphino)methyl]ferrocene-κ^2P,P'}chloro(η^5-cyclopentadienyl)ruthenium(II) (18). Analogously to the previous synthesis, chloro(cyclopentadienyl)bis(triphenylphosphine)-ruthenium(II) (72.5 mg, 0.10 mmol) and **1** (59 mg, 0.10 mmol) were mixed in anhydrous toluene (8 mL), and the mixture was heated under gentle reflux (in an oil bath) for 6 h. The clear reaction mixture was cooled, diluted with hexane (12 mL), and filtered through a PTFE syringe filter (0.45 μm pore size). The filtrate was evaporated, and the residue was redissolved in chloroform (2.5 mL) and crystallized by layering with hexane (5 mL). The crystals, which separated during several days, were filtered off, washed with pentane, and dried under vacuum. Yield of **18**·1.8$CHCl_3$: 81 mg (82%), orange-brown crystalline solid.

^{1}H NMR (400 MHz, $CDCl_3$): δ 3.11 (br m, 1H, fc), 3.37 (ddd, J = 15.5, 13.8, 1.2 Hz, 1H, CH_2), 3.94−3.96 (m, 1H, fc), 3.95 (s, 5H, C_5H_5), 3.91−4.00 (m, 1H, fc), 4.12−4.13 (m, 3H, fc), 4.22−4.24 (m, 1H, fc), 4.34 (dd, J = 16.0, 7.5 Hz, 1H, CH_2), 5.51−5.52 (m, 1H, fc), 7.12−7.92 (m, 20H, PPh_2). ^{13}C{^{1}H} NMR (101 MHz, $CDCl_3$): δ 26.53 (d, $^1J_{PC}$ = 20 Hz, CH_2), 67.84 (s, CH of fc), 68.38 (s, CH of fc), 69.45 (s, CH of fc), 69.78 (d, J_{PC} = 4 Hz, CH of fc), 70.39 (d, J_{PC} = 3 Hz, CH of fc), 71.51 (d, J_{PC} = 10 Hz, CH of fc), 72.66 (d, J_{PC} = 7 Hz, CH of fc), 76.43 (d, J_{PC} = 16 Hz, CH of fc), 81.33 (t, J_{PC} = 2 Hz, C_5H_5), 82.12 (s, C^{ipso} of fc), 84.43 (d, J_{PC} = 35 Hz, C^{ipso} of fc), 127.38 (d, J_{PC} = 9 Hz, CH of PPh_2), 127.56 (d, J_{PC} = 9 Hz, 2CH of PPh_2), 128.12 (s, 2CH of PPh_2), 128.21 (s, CH of PPh_2), 128.55 (s, CH of PPh_2), 129.96 (br d, J_{PC} = 7 Hz, CH of PPh_2), 130.25 (br s, CH of PPh_2), 132.05 (d, J_{PC} = 9 Hz, CH of PPh_2), 134.04 (d, J_{PC} = 11 Hz, CH of PPh_2), 134.97 (d, J_{PC} = 12 Hz, CH of PPh_2), 135.94 (br d, J_{PC} = 37 Hz, C^{ipso} of PPh_2), 140.63 (d, J_{PC} = 44 Hz, C^{ipso} of PPh_2), 143.21 (dd, J_{PC} = 38, 4 Hz, C^{ipso} of PPh_2), 141.15 (br d, J_{PC} = 40 Hz, C^{ipso} of PPh_2). ^{31}P{^{1}H} NMR (162 MHz, $CDCl_3$): δ 33.7 (d, $^2J_{PP}$ = 34 Hz, PPh_2), 34.6 (d, $^2J_{PP}$ = 35 Hz, PPh_2). IR (DRIFTS) ν_{max}: 3078 m, 3053 m, 3002 w, 2879 w, 1586 w, 1480 m, 1432 s, 1411 m, 1309 w, 1222 w, 1186 w, 1165 m, 1094 s, 1070 m, 1046 w, 1031 s, 1000 m, 920 w, 860 w, 827 s, 806 m, 794 m, 743 s, 696 s, 662 m, 629 w, 618 w, 602 w, 542 s, 523 s, 513 s, 494 s, 479 s, 462 s, 444 s, 427 s cm^{-1}. ESI-MS (m/z): 735 ([M − Cl]$^+$). Anal. Calcd for $C_{40}H_{35}ClFeRuP_2$·1.8$CHCl_3$ (984.9): C, 50.97; H, 3.77. Found: C, 50.82; H, 3.82.

Catalytic Estragole to Anethole Isomerization. A Schlenk tube was charged with the catalyst (0.010 mmol, 1.0 mol % of [Ru]), potassium carbonate (8.0 mg, 0.060 mmol), and estragole (296 mg, 2.0 mmol) and flushed with nitrogen. Degassed deionized water was introduced (1 mL), and the flask was stoppered and transferred into an oil bath maintained at 80 °C. After heating for 6 h, the reaction mixture was cooled to room temperature and diluted with diethyl ether (15 mL) and brine (15 mL). The organic layer was separated, and the aqueous residue was extracted with ether (15 mL). The combined organic layers were dried over $MgSO_4$ and evaporated. The conversion and (E/Z) ratios were determined by ^{1}H NMR.

(E)-1-(4-Methoxyphenyl)prop-1-ene. ^{1}H NMR (400 MHz, $CDCl_3$): δ 1.86 (d, $^3J_{HH}$ = 7.2 Hz, 3H, Me), 3.82 (s, 3H, OMe), 6.06−6.14 (m, 1H, CHCH), 6.34 (d, $^3J_{HH}$ = 11.6 Hz, 1H, CHCH) 6.84 (d, $^3J_{HH}$ = 8.4 Hz, 2H, C_6H_4), 7.27 (d, $^3J_{HH}$ = 8.4 Hz, 2H, C_6H_4).

(Z)-1-(4-Methoxyphenyl)prop-1-ene. ^{1}H NMR (400 MHz, $CDCl_3$): δ 1.88 (d, $^3J_{HH}$ = 7.2 Hz, 3H, Me), 3.77 (s, 3H, OMe), 5.66−5.71 (m, 1H, CHCH), 6.36 (d, $^3J_{HH}$ = 11.6 Hz, 1H, CHCH),

https://dx.doi.org/10.1021/acs.organomet.0c00767
Organometallics 2021, 40, 427−441

6.87 (d, $^3J_{HH}$ = 8.4 Hz, 2H, C_6H_4), 7.23 (d, $^3J_{HH}$ = 8.4 Hz, 2H, C_6H_4). The spectroscopic data are in accordance with the literature.[48]

Catalytic Cycloisomerization of (*Z*)-3-Methylpent-2-en-4-yn-1-ol into 2,3-Dimethylfuran. A vial was charged with a stirring bar, catalyst (4.5 μmol, 0.3 mmol % [Ru]), (*Z*)-3-methylpent-2-en-4-yn-1-ol (90%; 288 mg, 3.0 mmol), and anisole (324 mg, 3.0 mmol) as an inert standard and sealed. The mixture was stirred 18 h at room temperature under ambient atmosphere and then analyzed by ^{1}H NMR. The (*E*)-isomer of the starting enynol remains unchanged in the reaction mixture.

2,3-Dimethylfuran. ^{1}H NMR (400 MHz, $CDCl_3$): δ 1.94 (br s, 3H, Me), 2.19 (br s, 3H, Me), 6.15 (d, $^3J_{HH}$ = 1.8 Hz, 1H, CH), 7.20 (d, $^3J_{HH}$ = 1.8 Hz, 1H, CH). $^{13}C\{^1H\}$ NMR (101 MHz, $CDCl_3$): δ 9.82 (Me), 11.27 (Me), 112.78 (CH), 113.74 (C^{ipso}), 139.56 (CH), 147.36 (C^{ipso}). The NMR data match those in the literature.[49]

X-ray Crystallography. Diffraction data ($\pm h \pm k \pm l$, θ_{max} = 27.5°) were collected with a Bruker Apex II CCD (**2**, **9**, and **18**) or a Bruker D8 VENTURE Kappa Duo diffractometer with a PHOTON detector (all other compounds), both equipped with a Cryostream Cooler (Oxford Cryosystems), using Mo Kα radiation (λ = 0.71073 Å). The structures were solved using direct methods (SHELXT-2014[50] or SIR-97)[51] and then refined by full-matrix least-squares routine based on F^2 (SHELXL-2014).[52] Non-hydrogen atoms were refined with anisotropic displacement parameters. The PH hydrogens were identified on the difference electron density maps and refined as riding atoms with U_{iso}(H) set to 1.2U_{eq}(P). Hydrogens residing on carbon atoms were included in their theoretical positions and refined similarly. The phosphorus atom P2 in the structure of **9** is disordered over two positions and was modeled accordingly. In the structure of **15**, the H and OH groups bonding to phosphorus atom P2 alternated in their positions with practically equal occupancies (the compound is thus racemic), which also affected one of the Ru-bound chlorine atoms. The positions of the disordered hydrogen atoms were based not only on the difference Fourier maps but also on their surroundings and crystal packing (mainly hydrogen bonding interactions). Finally, the solvent molecules in the structure of **10**·THF·$2CH_2Cl_2$ were extensively disordered and could not be satisfactorily included in the structure model. Hence, their contribution to the overall scattering was numerically eliminated using PLATON SQUEEZE.[53] Relevant crystallographic data and refinement parameters are presented in Table S1.

All geometric data and structural diagrams were obtained using a recent version of the PLATON program.[54] The numerical values were rounded to one decimal place with respect to their estimated standard deviations (ESDs). Parameters pertaining to atoms in geometrically constrained positions (hydrogens) are given without ESDs.

■ ASSOCIATED CONTENT

Supporting Information

The Supporting Information is available free of charge at https://pubs.acs.org/doi/10.1021/acs.organomet.0c00767.

Synthesis and crystal structure of [(η^6-mesitylene)RuCl-(MeCN-κ*N*)$_2$][PF_6], additional structural diagrams, a summary of crystallographic parameters, and copies of the NMR spectra (PDF)

Accession Codes

CCDC 2047814−2047822 contain the supplementary crystallographic data for this paper. These data can be obtained free of charge via www.ccdc.cam.ac.uk/data_request/cif, or by emailing data_request@ccdc.cam.ac.uk, or by contacting The Cambridge Crystallographic Data Centre, 12 Union Road, Cambridge CB2 1EZ, UK; fax: +44 1223 336033.

■ AUTHOR INFORMATION

Corresponding Author

Petr Štěpnička − *Department of Inorganic Chemistry, Faculty of Science, Charles University, 128 40 Prague, Czech Republic;* orcid.org/0000-0002-5966-0578; Email: petr.stepnicka@natur.cuni.cz

Authors

Filip Horký − *Department of Inorganic Chemistry, Faculty of Science, Charles University, 128 40 Prague, Czech Republic*

Ivana Císařová − *Department of Inorganic Chemistry, Faculty of Science, Charles University, 128 40 Prague, Czech Republic*

Complete contact information is available at: https://pubs.acs.org/10.1021/acs.organomet.0c00767

Notes

The authors declare no competing financial interest.

■ ACKNOWLEDGMENTS

This work was supported by the Grant Agency of Charles University (project no. 920119) and by the Charles University Research Centre program (project UNCE/SCI/014).

■ REFERENCES

(1) (a) Sollott, G. P.; Snead, J. L.; Portnoy, S.; Peterson, W. R.; Mertwoy, H. E.*Phosphorus, Arsenic, and Boron-Containing Ferrocene Derivatives*; U.S. Dept. Com., Office Technol. Serv., 1965; Vol. *II*, pp 441−452. *Chem. Abstr.* **1965**, *63*, 98559. (b) Marr, G.; Hunt, T. Unsymmetrically disubstituted ferrocenes. Part VIII. Synthesis and reactivity of some 2-substituted ferrocenylphosphines. *J. Chem. Soc. C* **1969**, 1070−1072. (c) Bishop, J. J.; Davison, A.; Katcher, M. L.; Lichtenberg, D. W.; Merrill, R. E.; Smart, J. C. Symmetrically disubstituted ferrocenes: I. The synthesis of potential bidentate ligands. *J. Organomet. Chem.* **1971**, *27*, 241−249.

(2) (a) Gan, K.-S.; Hor, T. S. A. 1,1′-Bis(diphenylphosphino)-ferrocene. Coordination Chemistry, Organic Syntheses, and Catalysis. In *Ferrocenes: Homogeneous Catalysis, Organic Synthesis Materials Science*; Togni, A., Hayashi, T., Eds.; Wiley-VCH: Weinheim, Germany, 1995; Chapter 1, pp 3−104. (b) Chien, S. W.; Hor, T. S. A. The Coordination and Homogeneous Catalytic Chemistry of 1,1′-Bis(diphenylphosphino)ferrocene and its Chalcogenide Derivatives. In *Ferrocenes: Ligands, Materials and Biomolecules*; Štěpnička, P., Ed.; Wiley: Chichester, 2008; Chapter 2, pp 33−116. (c) Bandoli, G.; Dolmella, A. Ligating ability of 1,1′-bis(diphenylphosphino)ferrocene: a structural survey (1994−1998). *Coord. Chem. Rev.* **2000**, *209*, 161−196.

(3) (a) Colacot, T. J.; Parisel, S. Synthesis, Coordination Chemistry and Catalytic Use of dppf Analogs. In *Ferrocenes: Ligands, Materials and Biomolecules*; Štěpnička, P., Ed.; Wiley: Chichester, U.K., 2008; Chapter 3, pp 117−140. For selected recent examples, see (b) Qin, L.; Ren, X.; Lu, Y.; Li, Y.; Zhou, J. Intermolecular Mizoroki-Heck Reaction of Aliphatic Olefins with High Selectivity for Substitution at the Internal Position. *Angew. Chem., Int. Ed.* **2012**, *51*, 5915−5919. (c) Dong, K.; Sang, R.; Fang, X.; Franke, R.; Spannenberg, A.; Neumann, H.; Jackstell, R.; Beller, M. Efficient Palladium-Catalyzed Alkoxycarbonylationof Bulk Industrial Olefins Using Ferrocenyl Phosphine Ligands. *Angew. Chem., Int. Ed.* **2017**, *56*, 5267−5271. (d) Cooper, P.; Crisenza, G. E. M.; Feron, L.; Bower, J. F. Iridium-Catalyzed α-Selective Arylation of Styrenes by Dual C-H Functionalization. *Angew. Chem., Int. Ed.* **2018**, *57*, 14198−14202. (e) Dey, S.; Buzsaki, D.; Bruhn, C.; Kelemen, Z.; Pietschnig, R. Bulky 1,1′-bisphosphanoferrocenes and their coordination behavior towards Cu(I). *Dalton Trans.* **2020**, *49*, 6668−6681.

(4) (a) Gildner, P. G.; Colacot, T. J. Reactions of the 21st Century: Two Decades of Innovative Catalyst Design for Palladium-Catalyzed Cross-Couplings. *Organometallics* **2015**, *34*, 5497−5508. (b) DeAngelis, A.; Colacot, T. J. Prominent Ligand Types in Modern Cross-Coupling Reactions. *RSC Catal. Ser.* **2014**, 20−90.

(5) Selected recent examples (a) Škoch, K.; Císařová, I.; Schulz, J.; Siemeling, U.; Štěpnička, P. Synthesis and characterization of 1′-

(diphenylphosphino)-1-isocyanoferrocene, an organometallic ligand combining two different soft donor moieties, and its Group 11 metal complexes. *Dalton Trans.* **2017**, *46*, 10339−10354. (b) Štěpnička, P.; Zábranský, M.; Císařová, I. Synthesis and structural characterization of phosphinoferrocene carboxylic acids with extended carboxyl pendants and their palladium(II) phosphinocarboxylate complexes. *J. Organomet. Chem.* **2017**, *846*, 193−200. (c) Zábranský, M.; Císařová, I.; Štěpnička, P. Synthesis, coordination, and catalytic use of 1′-(diphenylphosphino)ferrocene-1-sulfonate anion. *Organometallics* **2018**, *37*, 1615−1626. (d) Škoch, K.; Císařová, I.; Uhlík, F.; Štěpnička, P. Comparing the reactivity of isomeric phosphinoferrocene nitrile and isocyanide in Pd(II) complexes: synthesis of simple coordination compounds *vs.* preparation of P-chelated insertion products and Fischer-type carbeness. *Dalton Trans.* **2018**, *47*, 16082−16101. (e) Vosáhlo, P.; Schulz, J.; Škoch, K.; Císařová, I.; Štěpnička, P. Synthesis and structural characterisation of palladium(II) complexes with hybrid phosphinoferrocene ligands bearing additional O-donor substituents. *New J. Chem.* **2019**, *43*, 4463−4470. (f) Horký, F.; Císařová, I.; Schulz, J.; Štěpnička, P. Synthesis and structural characterisation of 1′-(diphenylphosphino)ferrocene-1-phosphonic acid, its ammonium salts and Pd(II) complexes. *J. Organomet. Chem.* **2019**, *891*, 44−53. (g) Škoch, K.; Schulz, J.; Císařová, I.; Štěpnička, P. Pd(II) Complexes with chelating phosphinoferrocene diaminocarbene ligands: synthesis, characterization, and catalytic use in Pd-catalyzed borylation of aryl bromides. *Organometallics* **2019**, *38*, 3060−3073. (h) Škoch, K.; Vosáhlo, P.; Císařová, I.; Štěpnička, P. Synthesis and characterisation of Pd(II) and Au(I) complexes with mesoionic carbene ligands bearing phosphinoferrocene substituents and isomeric carbene moieites. *Dalton Trans.* **2020**, *49*, 1011−1021. (i) Bárta, O.; Gyepes, R.; Císařová, I.; Alemayehu, A.; Štěpnička, P. Synthesis and study of Fe k Pd interactions in unsymmetric Pd(II) complexes with phosphinoferrocene guanidine ligands. *Dalton Trans.* **2020**, *49*, 4225−4229.

(6) (a) Yamamoto, Y.; Tanase, T.; Mori, I.; Nakamura, Y. Preparation of 1,1′-bis[(diphenylphosphino)methyl]ferrocene and its transition-metal complexes. *J. Chem. Soc., Dalton Trans.* **1994**, 3191−3192. (b) Mai, J.-F.; Yamamoto, Y. Preparations and structures of (η^6-arene)ruthenium(II) complexes bearing 1,1′-bis(diphenylphosphinomethyl)ferrocene or 1,1′-bis(diphenylphosphino)-ferrocene. *J. Organomet. Chem.* **1998**, *560*, 223−232. (c) Ma, J.-F.; Yamamoto, Y. Reaction of di-μ-dichloro-bis(*N*,*N*-dimethylbenzylamine-C^2,*N*)dipalladium(II) with diphosphines. Six-membered ring complexes bearing spiro rings. *Inorg. Chim. Acta* **2000**, *299*, 164−171.

(7) Roy, D.; Mom, S.; Royer, S.; Lucas, D.; Hierso, J.-C.; Doucet, H. Palladium-Catalyzed Direct Arylation of Heteroaromatics with Activated Aryl Chlorides Using a Sterically Relieved Ferrocenyl-Diphosphane. *ACS Catal.* **2012**, *2*, 1033−1041.

(8) Oisaki, K.; Zhao, D.; Suto, Y.; Kanai, M.; Shibasaki, M. New chiral bis(diphenylphospholane) ligands: design, synthesis, and application to catalytic enantioselective aldol reaction to ketones. *Tetrahedron Lett.* **2005**, *46*, 4325−4329.

(9) Stead, R.; Xiao, J. A New Class of Ferrocenyl Phosphines. *Lett. Org. Chem.* **2004**, *1*, 148−150.

(10) (a) Watanabe, M. Asymmetric synthesis of 1,1′-bis(1-hydroxyalkyl)metallocenes and their derivatization to the novel chiral metallocenes with C_2 symmetry. *Tetrahedron Lett.* **1995**, *36*, 8991−8994. (b) Lu, Y.; Plocher, E.; Hu, Q.-S. Synthesis of Novel Bisphosphine-Containing Polymers and Their Applications as Bidentate Ligands for Nickel(0)-Catalyzed Cross-Coupling Reactions. *Adv. Synth. Catal.* **2006**, *348*, 841−845. (c) Ling, L.; Hu, J.; Huo, Y.; Zhang, H. Synthesis of ferrocene-based phosphine ligands via Cu-catalyzed reductive coupling of ferrocenyl ketone-derived tosylhydrazones and H-phosphorus oxides. *Tetrahedron* **2017**, *73*, 86−97.

(11) (a) For the preparation of **A**- and **B**-type compounds from fulvenes, see Bellabarba, R. M.; Clancy, G. P.; Gomes, P. T.; Martins, A. M.; Rees, L. H.; Green, M. L. H. Synthesis of metallocenes of zirconium, hafnium, manganese, iron, tin, lead and half-sandwich complexes of rhodium and iridium containing the ligands (η-$C_5R_4CR'_2PMe_2$), where R and R' may be H or Me. *J. Organomet. Chem.* **2001**, *640*, 93−112. (b) The preparation of homologoues with longer aliphatic spacers has been reported in Kettenbach, R. T.; Bonrath, W.; Buttenschön, H. [ω-(Phosphanyl)alkyl]cyclopentadienyl Complexes. *Chem. Ber.* **1993**, *126*, 1657−1669.

(12) (a) Štěpnička, P.; Císařová, I.; Schulz, J. Coordination and Catalytic Properties of a Semihomologous Dppf Congener, 1-(Diphenylphosphino)-1′-[(diphenylphosphino)methyl]ferrocene. *Organometallics* **2011**, *30*, 4393−4403. (b) Štěpnička, P.; Císařová, I. Synthesis, molecular structure and electrochemistry of gold(I) complexes with 1-(diphenylphosphino)-1′-[(diphenylphosphino)-methyl]ferrocene. *J. Organomet. Chem.* **2012**, *716*, 110−119. (c) Vosáhlo, P.; Císařová, I.; Štěpnička, P. Comparing the asymmetric dppf-type ligands with their semi-homologous counterparts. *J. Organomet. Chem.* **2018**, *860*, 14−29.

(13) (a) Štěpnička, P.; Schulz, J.; Klemann, T.; Siemeling, U.; Císařová, I. Synthesis, Structural Characterization, and Catalytic Evaluation of Palladium Complexes with Homologous Ferrocene-Based Pyridylphosphine Ligands. *Organometallics* **2010**, *29*, 3187−3200. (b) Siemeling, U.; Klemann, T.; Bruhn, C.; Schulz, J.; Štěpnička, P. The coordination behaviour of ferrocene-based pyridylphosphine ligands towards Zn^{II}, Cd^{II} and Hg^{II}. *Dalton Trans.* **2011**, *40*, 4722−4740. (c) Siemeling, U.; Klemann, T.; Bruhn, C.; Schulz, J.; Štěpnička, P. The Coordination Behaviour of Ferrocene-based Pyridylphosphine Ligands towards Ag^{I} and Au^{I}. *Z. Anorg. Allg. Chem.* **2011**, *637*, 1824−1833. (d) Štěpnička, P.; Císařová, I. Selective borane reduction of phosphinoferrocene carbaldehydes to phosphinoalcohol-borane adducts. The coordination behaviour of 1-(diphenylphosphino)-1′-(methoxymethyl)ferrocene, a new ferrocene O,P-hybrid donor prepared from such an adduct. *Dalton Trans.* **2013**, *42*, 3373−3389. (e) Zábranský, M.; Machara, A.; Císařová, I.; Štěpnička, P. Palladium(II) complexes of homologated ferrocene phosphanylether and thioether ligands. *Eur. J. Inorg. Chem.* **2017**, *2017*, 4850−4860. (f) Bárta, O.; Císařová, I.; Štěpnička, P. Synthesis, palladium(II) complexes, and catalytic use of a phosphanylferrocene ligand bearing a guanidinium pendant. *Eur. J. Inorg. Chem.* **2017**, *2017*, 489−495. (g) Zábranský, M.; Císařová, I.; Štěpnička, P. Synthesis of two isomeric ferrocene phosphanylcarboxylic acids and their Pd^{II} complexes with and without auxiliary ortho-metalated C,E-ligands (E = N and S). *Eur. J. Inorg. Chem.* **2017**, *2017*, 2557−2572. (h) Bárta, O.; Císařová, I.; Štěpnička, P. Phosphinomethylation of [1′-(diphenylphosphino)ferrocenyl]methylamines as a route to unsymmetric ferrocene diphosphine ligands. *J. Organomet. Chem.* **2018**, *855*, 26−32. (i) Bárta, O.; Císařová, I.; Mieczyńska, E.; Trzeciak, A. M.; Štěpnička, P. Synthesis and catalytic evaluation of phosphanylferrocene ligands with cationic guanidinium pendants and varied phosphane substituents. *Eur. J. Inorg. Chem.* **2019**, *2019*, 4846−4854.

(14) (a) Goodwin, N. J.; Henderson, W.; Nicholson, B. K. An air-stable, primary alkylphosphine: $FcCH_2PH_2$ [Fc = (η^5-C_5H_5)Fe(η^5-C_5H_4)]. *Chem. Commun.* **1997**, 31−32. (b) Goodwin, N. J.; Henderson, W.; Nicholson, B. K.; Fawcett, J.; Russell, D. R. (Ferrocenylmethyl)phosphine, an air-stable primary phosphine. *J. Chem. Soc., Dalton Trans.* **1999**, 1785−1794.

(15) Basra, S.; de Vries, J. G.; Hyett, D. J.; Harrison, G.; Heslop, K. M.; Orpen, A. G.; Pringle, P. G.; von der Luehe, K. Efficient asymmetric hydrogenation with rhodium complexes of C_1-symmetric 2,5-dimethylphospholane-diphenylphosphines. *Dalton Trans.* **2004**, 1901−1905.

(16) Labrue, F.; Pons, B.; Ricard, L.; Marinetti, A. Synthesis and X-ray crystal structure of [2-(phosphinomethyl)ferrocenyl]-diphenylphosphine. *J. Organomet. Chem.* **2005**, *690*, 2285−2290.

(17) Horký, F.; Císařová, I.; Štěpnička, P. A stable primary phosphane oxide and its heavier congeners. *Chem. - Eur. J.* **2021**, *27*, 1282−1285.

(18) (a) Barney, R. J.; Richardson, R. M.; Wiemer, D. F. Direct Conversion of Benzylic and Allylic Alcohols to Phosphonates. *J. Org. Chem.* **2011**, *76*, 2875−2879. (b) Richardson, R. M.; Barney, R. J.; Wiemer, D. F. Synthesis of dialkyl and diaryl benzylphosphonates through a ZnI_2-mediated reaction. *Tetrahedron Lett.* **2012**, *53*, 6682−6684.

https://dx.doi.org/10.1021/acs.organomet.0c00767
Organometallics 2021, 40, 427−441

(19) (a) Kyba, E. P.; Liu, S.-T.; Harris, R. L. A Facile Synthesis of 1,2-Bis(phosphino)benzene and Related Alkylated Species. *Organometallics* **1983**, *2*, 1877−1879. (b) Kyba, E. P.; Liu, S.-T. Synthesis of Unusual Phosphine Ligands. Use of 1-Naphthylmethyl Moiety as a P-H Protecting Groups in the Synthesis of a Phosphino Macrocycle That Contains a Secondary-Phosphino Ligating Site. *Inorg. Chem.* **1985**, *24*, 1613−1616.
(20) Brisset, H.; Gourdel, Y.; Pellon, P.; Le Corre, M. Phosphine-borane complexes; direct use in asymmetric catalysis. *Tetrahedron Lett.* **1993**, *34*, 4523−4526.
(21) Herd, O.; Hessler, A.; Hingst, M.; Tepper, M.; Stelzer, O. Water soluble phosphines. VIII. Palladium-catalyzed P-C cross coupling reactions between primary or secondary phosphines and functional aryl iodides - a novel synthetic route to water soluble phosphines. *J. Organomet. Chem.* **1996**, *522*, 69−76.
(22) (a) Miller, R. C.; Miller, C. D.; Rogers, W., Jr.; Hamilton, L. A. Disubstituted Phosphine Oxides. IV. Addition Reactions with Aldehydes and Ketones. *J. Am. Chem. Soc.* **1957**, *79*, 424−427. (b) Dvorko, M. Yu.; Glotova, T. E.; Ushakov, I. A.; Gusarova, N. K. Reaction of secondary phosphine oxides with acylacetylenes. *Russ. J. Org. Chem.* **2010**, *46*, 485−490.
(23) Kirin, S. I.; Kraatz, H.-B.; Metzler-Nolte, N. Systematizing structural motifs and nomenclature in 1,*n*>-disubstituted ferrocene peptides. *Chem. Soc. Rev.* **2006**, *35*, 348−354.
(24) (a) Ma, J.-F.; Yamamoto, Y. Dimeric complexes of ruthenium(II) and rhodium(III) bridged by 1,1′-bis(diphenylphosphinomethyl) ferrocene. *J. Organomet. Chem.* **1997**, *545*−*546*, 577−579. (b) Mai, J.-F.; Yamamoto, Y. Preparations and structures of (η^6-arene)-ruthenium(II) complexes bearing 1,1′-bis-(diphenylphosphinomethyl)ferrocene or 1,1′-bis-(diphenylphosphino)ferrocene. *J. Organomet. Chem.* **1998**, *560*, 223−232. (c) Rodríguez-Bárzano, A.; Fonseca, J. D. A.; Blacker, A. J.; McGowan, P. C. Ruthenium Halide Complexes as *N*-Alkylation Catalysts. *Eur. J. Inorg. Chem.* **2014**, *2014*, 1974−1983.
(25) Paris, S. I. M.; Lemke, F. R.; Sommer, R.; Lonnecke, P.; Hey-Hawkins, E. Molecular structures of ruthenium half-sandwich complexes with primary and secondary phosphines: [(η^6-*p*-cymene)-$RuCl_2(PR_3)$] [*p*-cymene = 1-Me-4-Pr^{i}C$_6$H$_4$; PR_3 = PH_2Fc, PH_2CH_2Fc, $PH(CH_2Fc)_2$; Fc = Fe(η^5-C_5H_4)(η^5-C_5H_5)]. *J. Organomet. Chem.* **2005**, *690*, 1807−1813.
(26) Donaghy, K. J.; Carroll, P. J.; Sneddon, L. G. Reactions of 1,1′-Bis(diphenylphosphino)ferrocene with Boranes, Thiaboranes, and Carboranes. *Inorg. Chem.* **1997**, *36*, 547−553.
(27) Data for [(η^6-mes)RuCl(**1**-κ^2*P*,*P*′)][PF_6]: ^{31}P{^{1}H} NMR (162 MHz, acetone-d_6): δ 34.9 (d, $^2J_{PP}$ = 34 Hz, PPh_2), 49.0 (d, $^2J_{PP}$ = 34 Hz, PPh_2). Data for [(η^6-mes)RuCl(**2**-κ^2*P*,*P*′)][PF_6]: ^{31}P{^{1}H} NMR (162 MHz, acetone-d_6): δ −36.1 (d, $^2J_{PP}$ = 62 Hz, PH_2), 29.5 (d, $^2J_{PP}$ = 62 Hz, PPh_2).
(28) Jensen, S. B.; Rodger, S. J.; Spicer, M. D. Facile preparation of η^6-*p*-cymene ruthenium diphosphine complexes. Crystal structure of [(η^6-*p*-cymene)Ru(dppf)Cl]PF_6. *J. Organomet. Chem.* **1998**, *556*, 151−158.
(29) Bruce, M. I.; Butler, I. R.; Cullen, W. R.; Koutsantonis, G. A.; Snow, M. R.; Tiekink, E. R. T. Cyclopentadienyl-Ruthenium and -Osmium Chemistry. XXXI. Preparation of Some Complexes Containing 1,1′-Bis(diphenylphosphino)ferrocene (dppf): X-Ray Structure of RuH(dppf)(η-C_5H_5). *Aust. J. Chem.* **1988**, *41*, 963−969.
(30) Data for **19**: ^{31}P{^{1}H} NMR (162 MHz, $CDCl_3$): δ −52.0 (d, $^2J_{PP}$ = 58 Hz, PH_2), 37.5 (d, $^2J_{PP}$ = 58 Hz, PPh_2).
(31) Lu, X. L.; Vittal, J. J.; Tiekink, E. R. T.; Tan, G. K.; Kuan, S. L.; Goh, L. Y.; Hor, T. S. A. Comparative reactivity studies of dppf-containing $CpRu^{II}$ and $(C_6Me_6)Ru^{II}$ complexes towards different donor ligands (dppf = 1,11-bis(diphenylphosphino)ferrocene). *J. Organomet. Chem.* **2004**, *689*, 1978−1990.
(32) (a) Corain, B.; Longato, B.; Favero, G.; Ajò, D.; Pilloni, G.; Russo, U.; Kreissl, F. R. Heteropolymetallic complexes of 1,1′-Bis(diphenylphosphino)ferrocene (dppf). III. Comparative physicochemical properties of (dppf)MCl_2 (M = Co, Ni, Pd, Pt, Zn, Cd, Hg). *Inorg. Chim. Acta* **1989**, *157*, 259−266. (b) Pilloni, G.; Longato, B.; Corain, B. Heteropolymetallic complexes of 1,1′-bis-(diphenylphosphino)ferrocene (dppf): VII. Redox behaviour of dppf. *J. Organomet. Chem.* **1991**, *420*, 57−65. (c) Zanello, P.; Opromolla, G.; Giorgi, G.; Sasso, G.; Togni, A. Redox behaviour of ferrocene derivatives VIII. 1,1′-Bis(diphenylphosphino)ferrocenes. *J. Organomet. Chem.* **1996**, *506*, 61−65. (d) Nataro, C.; Campbell, A. N.; Ferguson, M. A.; Incarvito, C. D.; Rheingold, A. L. Group 10 metal compounds of 1,1′-bis(diphenylphosphino)ferrocene (dppf) and 1,1′-bis(diphenylphosphino)ruthenocene: a structural and electrochemical investigation. X-ray structures of [MCl_2(dppr)] (M = Ni, Pd). *J. Organomet. Chem.* **2003**, *673*, 47−55.
(33) For an electrochemical characterization of $FcCH_2PR_2$ (R = Ph, CH_2OH, and CH_2CH_2CN), see Downard, A. J.; Goodwin, N. J.; Henderson, W. Electrochemistry of ferrocenylphosphines $FcCH_2PR_2$ (Fc = (η^5-C_5H_5)Fe(η^5-C_5H_4); R = Ph, CH_2OH and CH_2CH_2CN), and some phosphine oxide, phosphine sulfide, phosphonium and metal complex derivatives. *J. Organomet. Chem.* **2003**, *676*, 62−72.
(34) Hansch, C.; Leo, A.; Taft, R. W. A survey of Hammett substituent constants and resonance and field parameters. *Chem. Rev.* **1991**, *91*, 165−195.
(35) See, for instance, (a) Rosa, V.; Realista, S.; Mourato, A.; Abrantes, L. M.; Henriques, J.; Calhorda, M. J.; Avilés, T.; Drew, M. G. B.; Félix, V. 1,1′-Bis(diphenylphosphino)ferrocene bridging two mono(cyclopentadienyl) cobalt moieties: Synthesis, structure, electrochemistry and DFT studies. *J. Organomet. Chem.* **2012**, *712*, 52−56. (b) Fernandes, T. A.; Solařová, H.; Císařová, I.; Uhlík, F.; Štícha, M.; Štěpnička, P. Synthesis of phosphinoferrocene amides and thioamides from carbamoyl chlorides and the structural chemistry of Group 11 metal complexes with these mixed-donor ligands. *Dalton Trans.* **2015**, *44*, 3092−3108. Our recent electrochemical and DFT studies focused on phosphinoferrocene ligands and their complexes with Pd(II) and group 11 metals also suggested that the HOMO in these compounds is localized on the ferrocene unit and that the first oxidation affects predominantly the ferrocene moiety: (c) Škoch, K.; Císařová, I.; Uhlík, F.; Štěpnička, P. Comparing the reactivity of isomeric phosphinoferrocene nitrile and isocyanide in Pd(II) complexes: synthesis of simple coordination compounds vs. preparation of P-chelated insertion products and Fischer-type carbenes. *Dalton Trans.* **2018**, *47*, 16082−16101. (d) Škoch, K.; Schulz, J.; Císařová, I.; Štěpnička, P. Pd(II) Complexes with Chelating Phosphinoferrocene Diaminocarbene Ligands: Synthesis, Characterization, and Catalytic Use in Pd-Catalyzed Borylation of Aryl Bromides. *Organometallics* **2019**, *38*, 3060−3073.
(36) Podlaha, J.; Štěpnička, P.; Ludvík, J.; Císařová, I. 1.-(Diphenylphosphino)ferrocenecarboxylic acid, its P-oxide and methylester: Synthesis, characterization, crystal structure, and electrochemistry. *Organometallics* **1996**, *15*, 543−550.
(37) (a) Štěpnička, P.; Gyepes, R.; Lavastre, O.; Dixneuf, P. H. Ferrocene-Containing (η^6-Hexamethylbenzene)Ruthenium(II) Methoxycarbenes: Synthesis, Structure, and Electrochemistry. *Organometallics* **1997**, *16*, 5089−5095. (b) Sixt, T.; Sieger, M.; Krafft, M. J.; Bubrin, D.; Fiedler, J.; Kaim, W. Ambi-Valence Taken Literally: Ruthenium vs Iron Oxidation in (1,1′-Diphosphinoferrocene)-ruthenium(II) Hydride and Chloride Complexes as Deduced from Spectroelectrochemistry of the Heterodimetallic "Mixed-Valent" Intermediates. *Organometallics* **2010**, *29*, 5511−5516. (c) Tauchman, J.; Therrien, B.; Süss-Fink, G.; Štěpnička, P. Heterodinuclear Arene Ruthenium Complexes Containing a Glycine-Derived Phosphinoferrocene Carboxamide: Synthesis, Molecular Structure, Electrochemistry, and Catalytic Oxidation Activity in Aqueous Media. *Organometallics* **2012**, *31*, 3985−3994. (d) Paim, L. A.; Dias, F. M.; Siebald, H. G. L.; Ellena, J.; Ardisson, J. D.; da Silva, M. M.; Batista, A. A. Synthesis and characterization of [$Ru(\eta^6$-$C_{10}H_{14})$(dppf)X][PF_6] (X = Cl, Br, I, SnF_3) compounds: The X-ray structure of [$Ru(\eta^6$-$C_{10}H_{14})$(dppf)Cl][$SnCl_3$]·0.45CH_2Cl_2. *Polyhedron* **2012**, *42*, 110−117.
(38) (a) Dixneuf, P. H., Bruneau, C., Eds. *Ruthenium Catalysts and Fine Chemistry*; Topics in Organometallics Chemistry Series, Vol. *11*; Springer: Berlin, 2004. (b) Dixneuf, P. H., Bruneau, C., Eds.

https://dx.doi.org/10.1021/acs.organomet.0c00767
Organometallics 2021, 40, 427−441

Ruthenium in Catalysis; Topics in Organometallics Chemistry Series, Vol. *38*; Springer, Cham, 2014.
(39) Hassam, M.; Taher, A.; Arnott, G. E.; Green, I. R.; van Otterlo, W. A. L. Isomerization of Allylbenzenes. *Chem. Rev.* **2015**, *115*, 5462−5569.
(40) Gonzalez-Fernandez, R.; Crochet, P.; Cadierno, V. Hydrophilic (η^6-Arene)-Ruthenium(II) Complexes with P-OH Ligands as Catalysts for the Isomerization of Allylbenzenes and C-H Bond Arylation Reactions in Water. *Organometallics* **2019**, *38*, 3696−3706.
(41) (a) Butler, R. N.; Coyne, A. G. Water: Nature's Reaction Enforcer—Comparative Effects for Organic Synthesis "In-Water" and "On-Water. *Chem. Rev.* **2010**, *110*, 6302−6337. (b) Kitanosono, T.; Kobayashi, S. Reactions in Water Involving the "On-Water" Mechanism. *Chem. - Eur. J.* **2020**, *26*, 9408−9429.
(42) Seiller, B.; Bruneau, C.; Dixneuf, P. H. Novel Ruthenium-catalysed Synthesis of Furan Derivatives *via* Intramolecular Cyclization of Hydroxy Enynes. *J. Chem. Soc., Chem. Commun.* **1994**, 493−494.
(43) Selected examples: (a) Kücükbay, H.; Çetinkaya, B.; Guesmi, S.; Dixneuf, P. H. New (Carbene)ruthenium-Arene Complexes: Preparation and Uses in Catalytic Synthesis of Furans. *Organometallics* **1996**, *15*, 2434−2439. (b) Çetinkaya, B.; Özdemir, I.; Bruneau, C.; Dixneuf, P. H. Ruthenium-carbene catalysts for the synthesis of 2,3-dimethylfuran. *J. Mol. Catal. A: Chem.* **1997**, *118*, L1−L4. (c) Özdemir, I.; Yigit, B.; Çetinkaya, B.; Ulku, D.; Tahir, M. N.; Arici, C. Synthesis of a water-soluble carbene complex and its use a scatalyst for the synthesis of 2,3-dimethylfuran. *J. Organomet. Chem.* **2001**, *633*, 27−32. (d) Díaz-Álvarez, A. E.; Crochet, P.; Zablocka, M.; Duhayon, C.; Cadierno, V.; Gimeno, J.; Majoral, J. P. Water-Soluble Group 8 and 9 Transition Metal Complexes Containing a Trihydrazinophosphaadamantane Ligand: Catalytic Applications in Isomerization of Allylic Alcohols and Cycloisomerization of (*Z*)-Enynols in Aqueous Medium. *Adv. Synth. Catal.* **2006**, *348*, 1671−1679. (e) Albers, J.; Cadierno, V.; Crochet, P.; García-Garrido, S. E.; Gimeno, J. Octahedral ruthenium(II) complexes *cis, cis*-[RuX_2(CNR)-(CO)(PP)] and *cis, cis, cis*-[$RuX_2(CO)_2$(PP)] (X = Cl, Br; PP = 1,1ô-bis(diphenylphosphino)ferrocene, 1,1′-bis (diisopropylphosphino)-ferrocene): Synthesis and catalytic applications in transfer hydrogenation of acetophenone and cycloisomerizationof (*Z*)-3-methyl-pent-2-en-4-yn-1-ol. *J. Organomet. Chem.* **2007**, *692* (23), 5234−5244.
(44) Bruce, M. I.; Hameister, C.; Swincer, A. G.; Wallis, R. C.; Ittel, S. D. Some η^5-Cyclopentadienylruthenium(II) Complexes Containing Triphenylphosphine. *Inorg. Synth.* **2007**, *21*, 78−84.
(45) Kündig, P. E.; Monnier, F. R. Efficient Synthesis of Tris(acetonitrile)-(η^5-cyclopentadienyl)-ruthenium(II) Hexafluorophosphate *via* Ruthenocene. *Adv. Synth. Catal.* **2004**, *346*, 901−904.
(46) Takemoto, S.; Ishii, H.; Yamaguchi, M.; Teramoto, A.; Tsujita, M.; Ozeki, D.; Matsuzaka, H. Parent Cyclopentadienyl Ruthenium(II) Chloride Synthon: Derivatization to CpRu Amido, Imido, and Oxo Complexes. *Organometallics* **2019**, *38*, 4298−4306.
(47) Barrière, F.; Geiger, W. E. Use of Weakly Coordinating Anions to Develop an Integrated Approach to the Tuning of $\Delta E_{1/2}$ Values by Medium Effects. *J. Am. Chem. Soc.* **2006**, *128*, 3980−3989.
(48) Thimmaiah, M.; Zhang, X.; Fang, S. Palladium-catalyzed cross-coupling of aryl chlorides with alkenylboronic acids with low *E*/*Z* isomerization. *Tetrahedron Lett.* **2008**, *49*, 5605−5607.
(49) Škoch, K.; Císařová, I.; Štěpnička, P. Synthesis and Catalytic Use of Gold(I) Complexes Containing a Hemilabile Phosphanylferrocene Nitrile Donor. *Chem. - Eur. J.* **2015**, *21*, 15998−16004.
(50) Sheldrick, G. M. *SHELXT* - Integrated space-group and crystal-structure determination. *Acta Crystallogr., Sect. A: Found. Adv.* **2015**, *71*, 3−8.
(51) Altomare, A.; Burla, M. C.; Camalli, M.; Cascarano, G. L.; Giacovazzo, C.; Guagliardi, A.; Moliterni, A. G. G.; Polidori, G.; Spagna, P. *SIR97*: a new tool for crystal structure determination and refinement. *J. Appl. Crystallogr.* **1999**, *32*, 115−119.
(52) Sheldrick, G. M. Crystal structure refinement with *SHELXL*. *Acta Crystallogr., Sect. C: Struct. Chem.* **2015**, *71*, 3−8.
(53) Spek, A. L. *PLATON SQUEEZE*: a tool for the calculation of the disordered solvent contribution to the calculated structure factors. *Acta Crystallogr., Sect. C: Struct. Chem.* **2015**, *71*, 9−18.
(54) (a) Spek, A. L. Single-crystal structure validation with the program *PLATON*. *J. Appl. Crystallogr.* **2003**, *36*, 7−13. (b) Spek, A. L. Structure validation in chemical crystallography. *Acta Crystallogr., Sect. D: Biol. Crystallogr.* **2009**, *65*, 148−155.

https://dx.doi.org/10.1021/acs.organomet.0c00767
Organometallics 2021, 40, 427−441

Supporting Information

for

Synthesis, Reactivity and Coordination of Semi-Homologous Dppf Congeners Bearing Primary Phosphine and Primary Phosphine Oxide Groups

Filip Horký, Ivana Císařová, Petr Štěpnička*

Department of Inorganic Chemistry, Faculty of Science, Charles University, Hlavova 2030, 128 40 Prague, Czech Republic

Contents

Additional structural diagrams

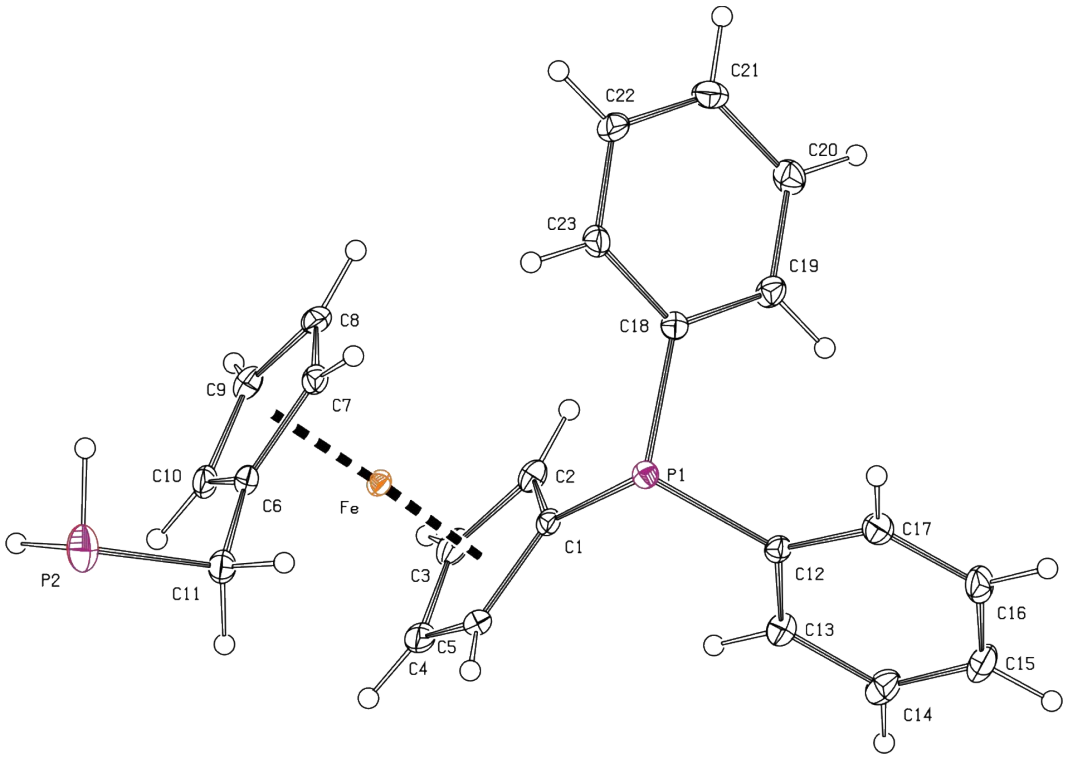

Figure S1. PLATON plot of the molecular structure of **2** showing displacement ellipsoids at the 30% probability level.

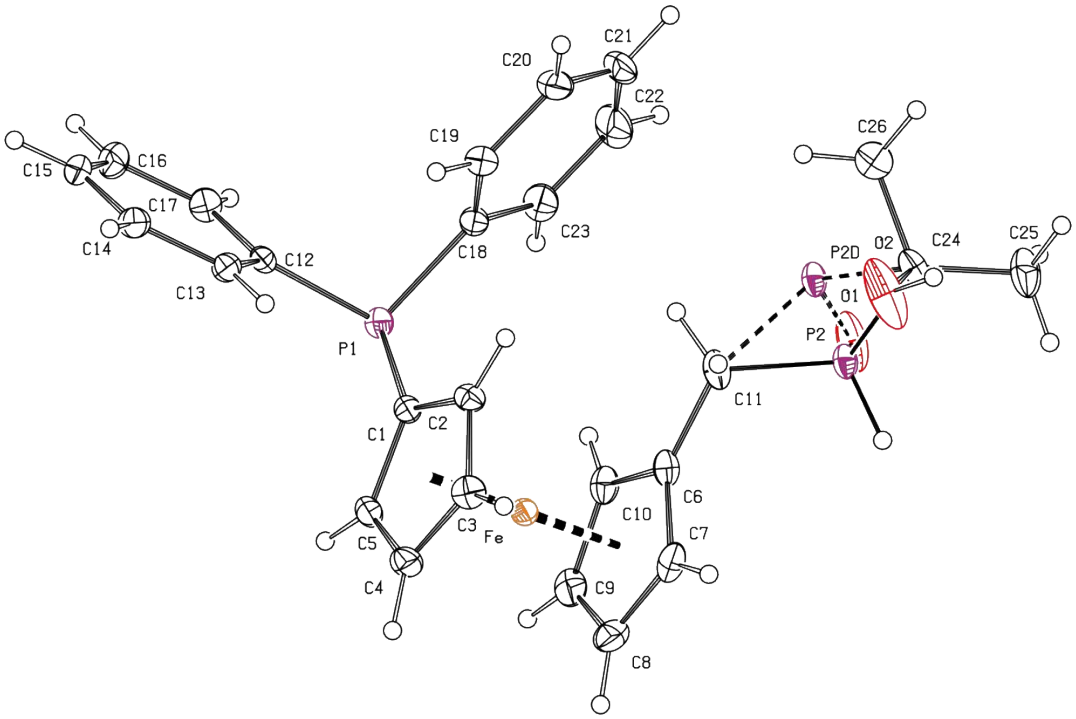

Figure S2. PLATON plot of the molecular structure of **9** with displacement ellipsoids at the 30% probability level.

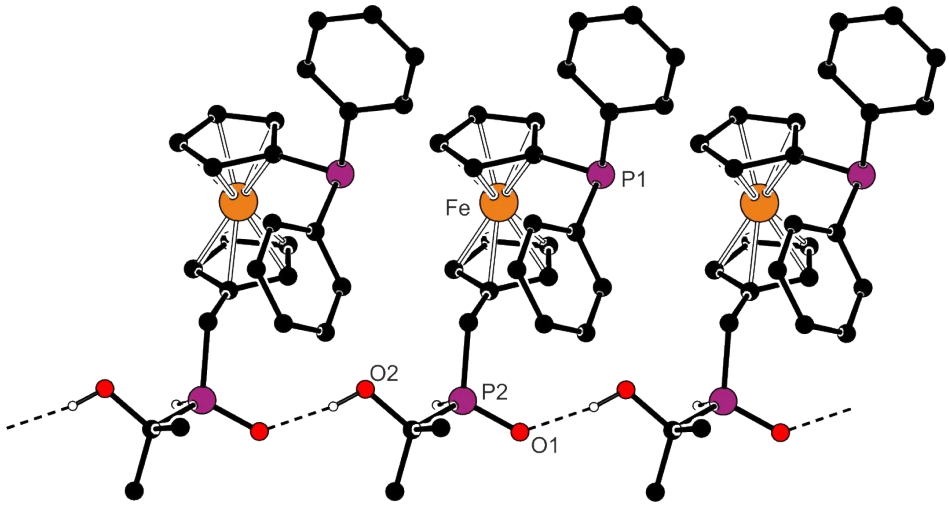

Figure S3. Section of the infinite hydrogen-bonded chain in the structure of **9**.

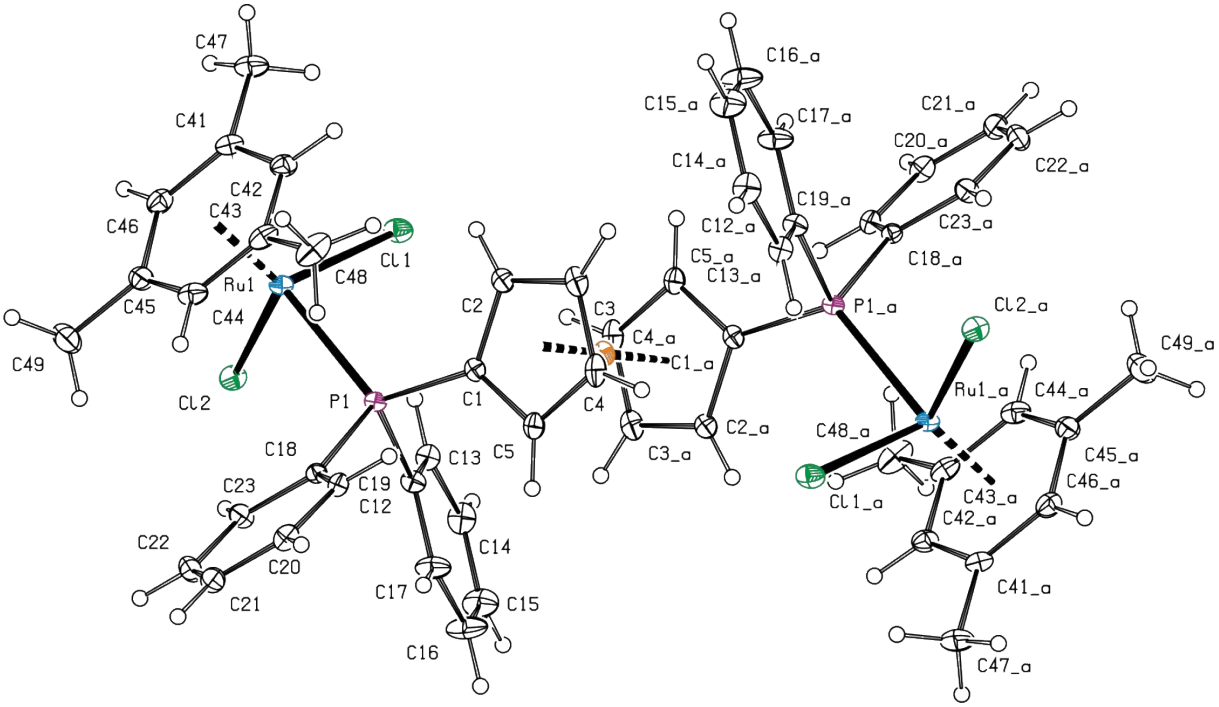

Figure S4. PLATON plot of the complex molecule in the structure of **10**·2CH_2Cl_2·THF showing displacement ellipsoids at the 30% probability level.

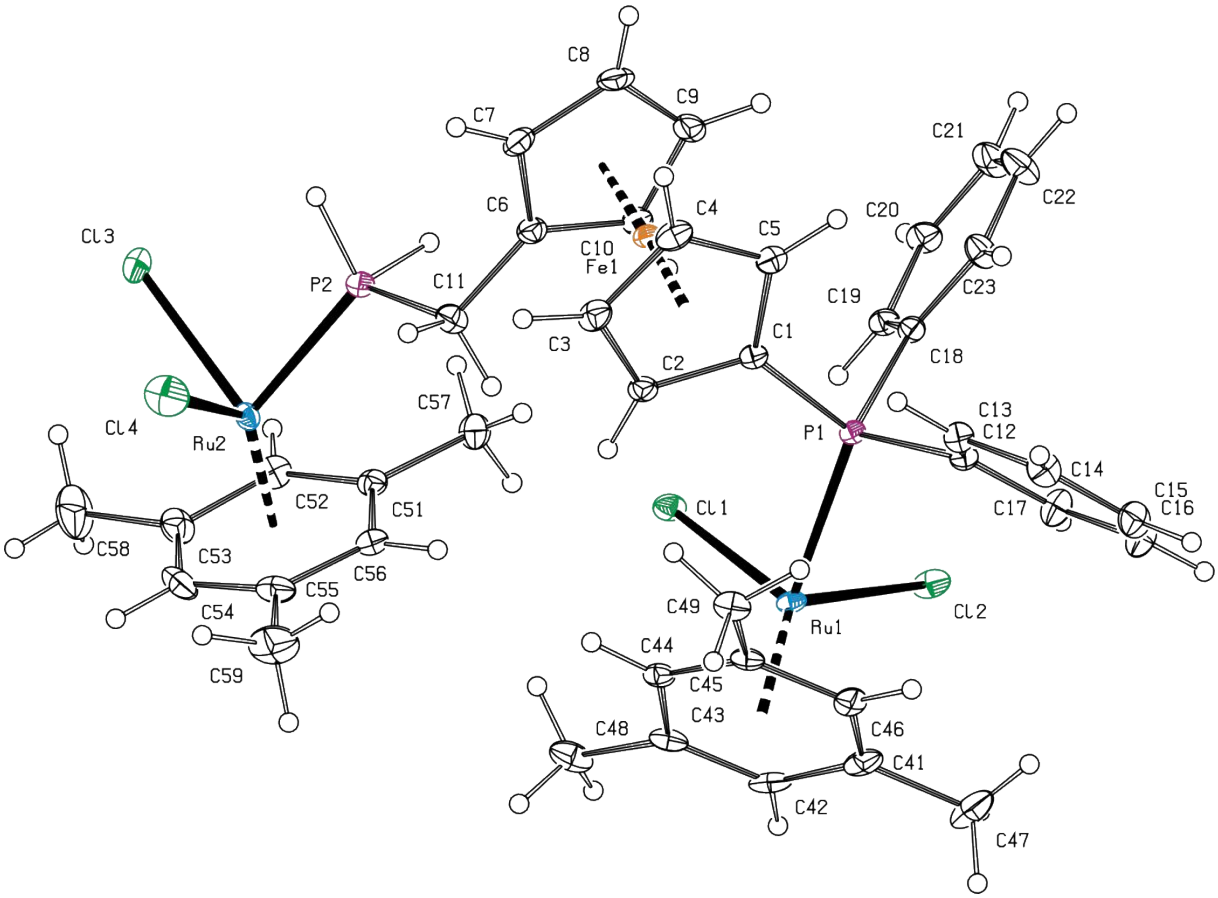

Figure S5. PLATON plot of the complex molecule in the structure of **12**·2$CHCl_3$ showing displacement ellipsoids at the 30% probability level.

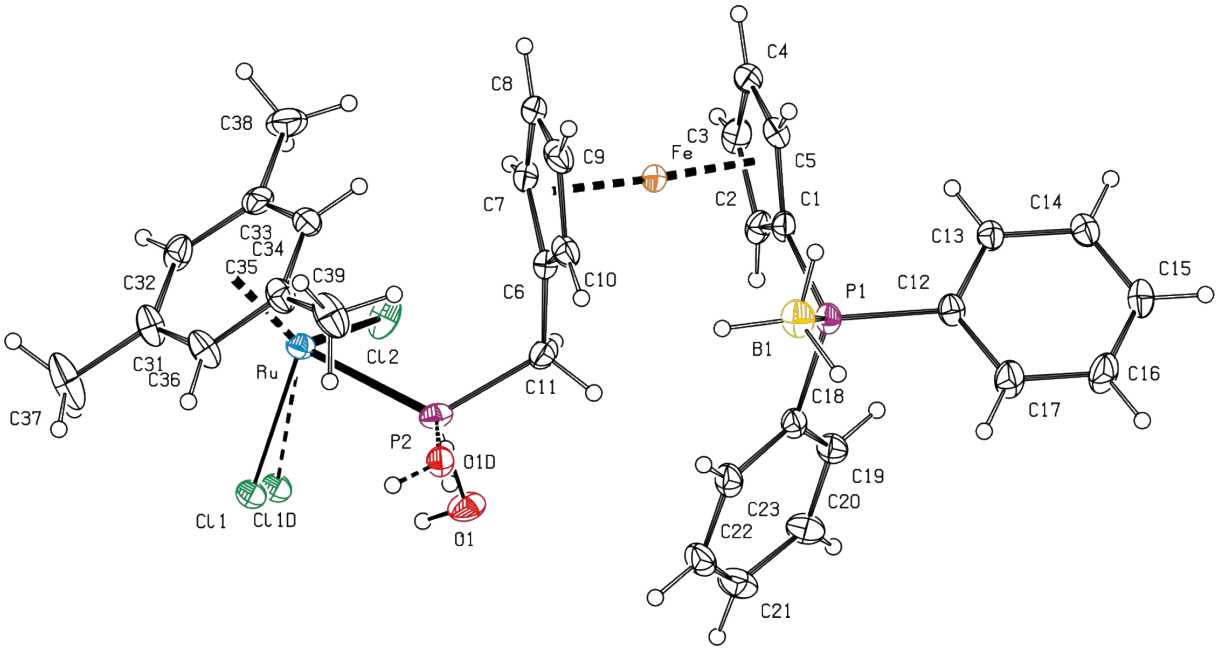

Figure S6. PLATON plot of the molecular structure of **15** showing displacement ellipsoids at the 30% probability level and both positions of the disordered OH group and the chloride ligand.

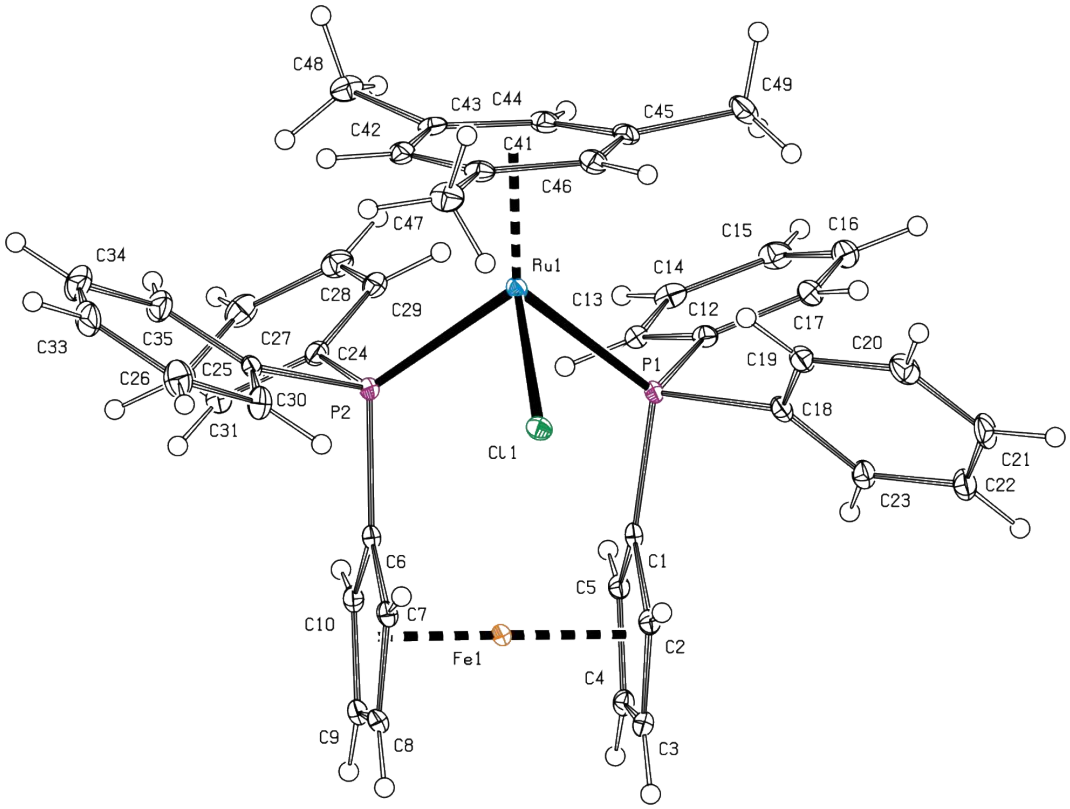

Figure S7. PLATON plot of the complex cation in the structure of **16**·CH_2Cl_2 with displacement ellipsoids at the 30% probability level.

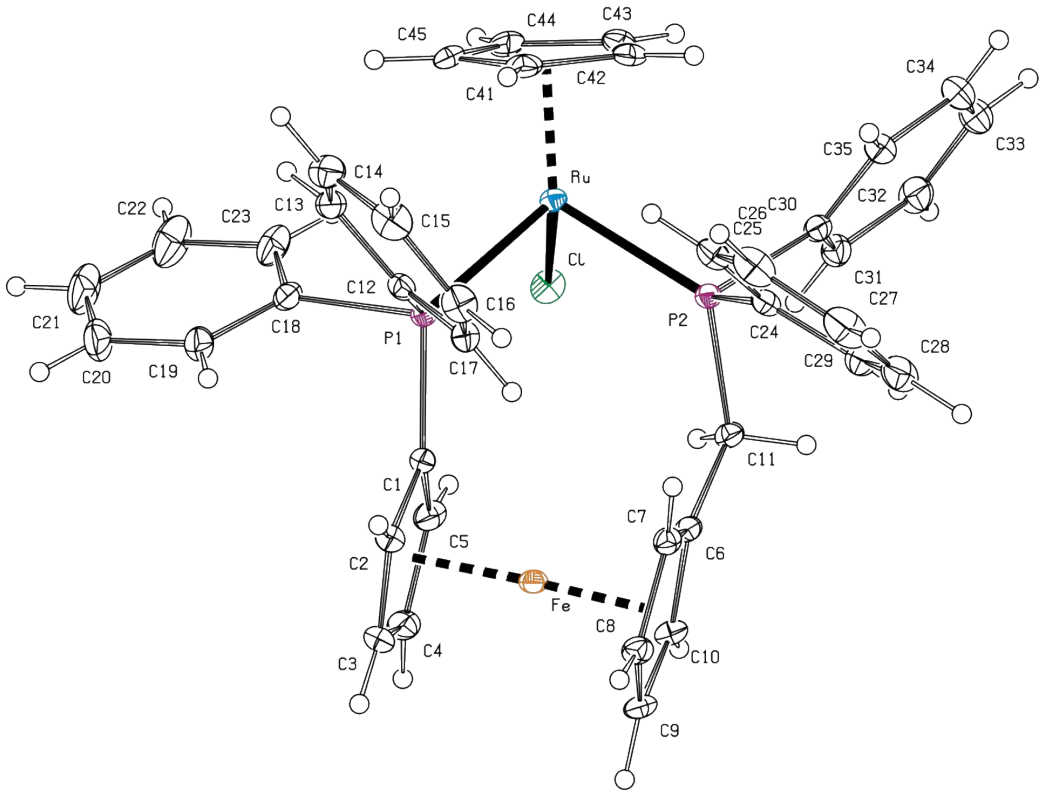

Figure S8. PLATON plot of the complex molecule in the structure of **18**·$2CH_2Cl_2$ showing displacement ellipsoids at the 30% probability level.

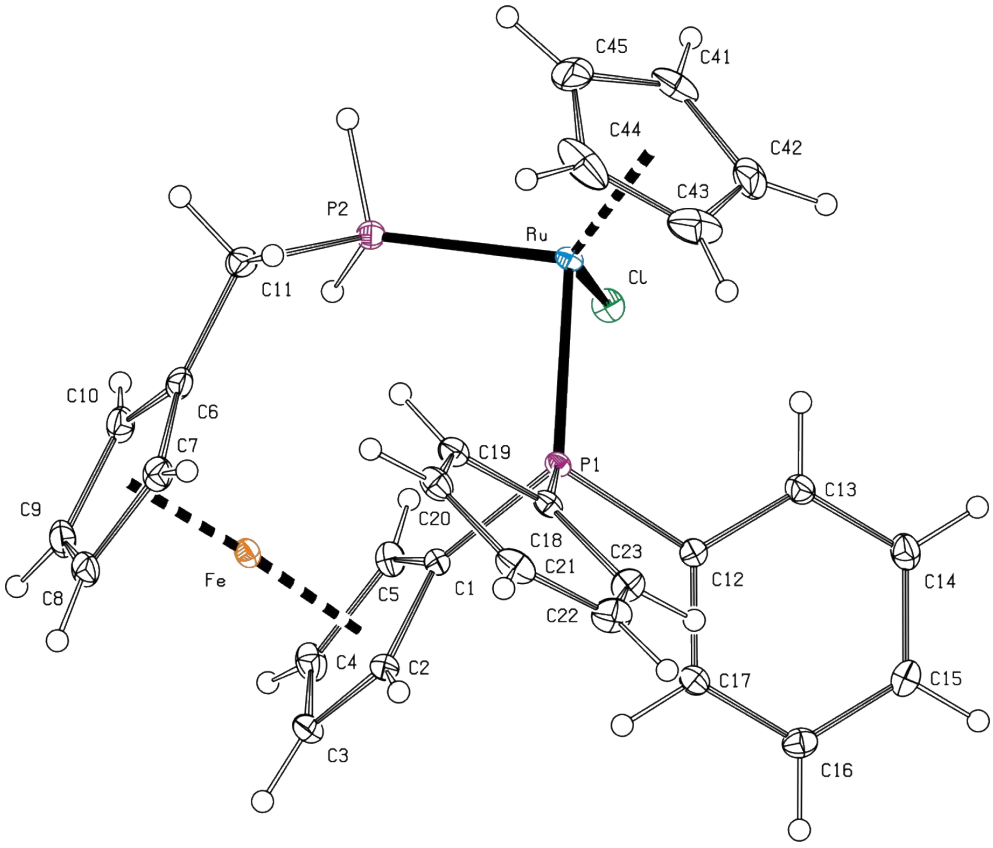

Figure S9. PLATON plot of the molecular structure of **19** showing displacement ellipsoids at the 30% probability level.

Synthesis and Crystal Structure of Bis(acetonitrile-κ*N*)chloro(η⁶-mesitylene)ruthenium(II) hexafluorophosphate

Solution of silver(I) hexafluorophosphate (101 mg, 0.40 mmol) in acetonitrile (6 mL) was introduced to a suspension of [{(η⁶-mesitylene)RuCl(μ-Cl)}$_2$] (117 mg, 0.20 mmol) in the same solvent (4 mL), and the resulting mixture was stirred overnight and then evaporated. The solid residue was dissolved in a small amount of acetonitrile (4 mL) and filtered. The filtrate was layered with diethyl ether-hexane (1:1 mixture, approximately 16 mL) and set aside for crystallization by liquid-phase diffusion. Orange crystals of [(η⁶-mesitylene)RuCl(MeCN-κ*N*)$_2$][PF_6], which formed during several days, were filtered off and dried under vacuum. Yield 87 mg (45%). Single-crystals were selected from the reaction batch.

^{1}H NMR (400 MHz, CD_3CN): δ 1.96 (s, 6H, MeCN), 2.19 (s, 9H, Me), 5.28 (s, 3H, C_6H_3). $^{13}C\{^1H\}$ NMR (101 MHz, CD_3CN): δ 19.46 (s, Me), 78.62 (s, CH of C_6H_3), 107.91 (C^{ipso} of C_6H_3). $^{31}P\{^1H\}$ NMR (162 MHz, CD_3CN): δ –143.1 (septet, $^1J_{PF}$ = 707 Hz, PF_6^-). IR (Nujol): ν_{max} 2327 w, 2300 w, 1527 m, 1323 w, 1300 w, 1133 w, 1033 m, 1008 w, 988 w, 850 s, 826 s, 722 w, 647 w, 559 s, 519 w cm^{-1}. ESI– MS: 298 ([M – PF_6 – MeCN]$^+$), 339 ([M – PF_6]$^+$). Anal. Calcd for $C_{13}H_{18}ClF_6N_2RuP$ (483.8): C, 32.27; H, 3.75; N, 5.79. Found: C, 32.39; H, 3.55; N, 5.79.

The molecular structure of [(η⁶-mesitylene)RuCl(MeCN)$_3$][PF_6] is shown in Figure S10. Details on structure determination and relevant crystallographic data are provided below. The cation adopts the expected piano-stool geometry as determined before for the cations in [(η⁶-arene)RuCl(MeCN-κ*N*)$_2$][PF_6] (arene = C_6H_6[1] and C_6Me_6[2]), and in [(η⁶-mesitylene)RuCl(MeCN-κ*N*)$_2$][BF_4].[3] The Ru1-C(1-6) distances vary 2.181(2)-2.205(2) Å and the mesitylene ligands is oriented so that its C-Me bonds are practically eclipsed with the Ru-donor bonds, when viewed along the Cg···Ru direction (Cg is the centroid of the arene ring). Even though the Ru-N distances (Ru1-N1 = 2.068(2) Å, Ru1-N2 = 2.065(2) Å) are substantially shorter than the Ru1-Cl1 distance (2.4038(5) Å), the π-coordinated arene ring is practically coplanar with the basal plane {Cl1, N1, N2} (interplanar angle: 4.44(7)°). The nitrile ligands are linearly coordinated (Ru1-N1-C10 = 177.7(1)°, N1-C10-C11 = 179.4(2)°, Ru1-N2-C12 = 176.0(1)°, N2-C12-C13 = 179.0(2)°) and retain their usual geometry[4] (N1-C10 = 1.136(2) Å, N2-C12 = 1.135(2) Å). In the crystal, the individual complex cations interact *via* π···π interactions of the parallel but offset (by ca. 0.6 Å) aromatic rings at the centroid···centroid distance 3.3904(7) Å.

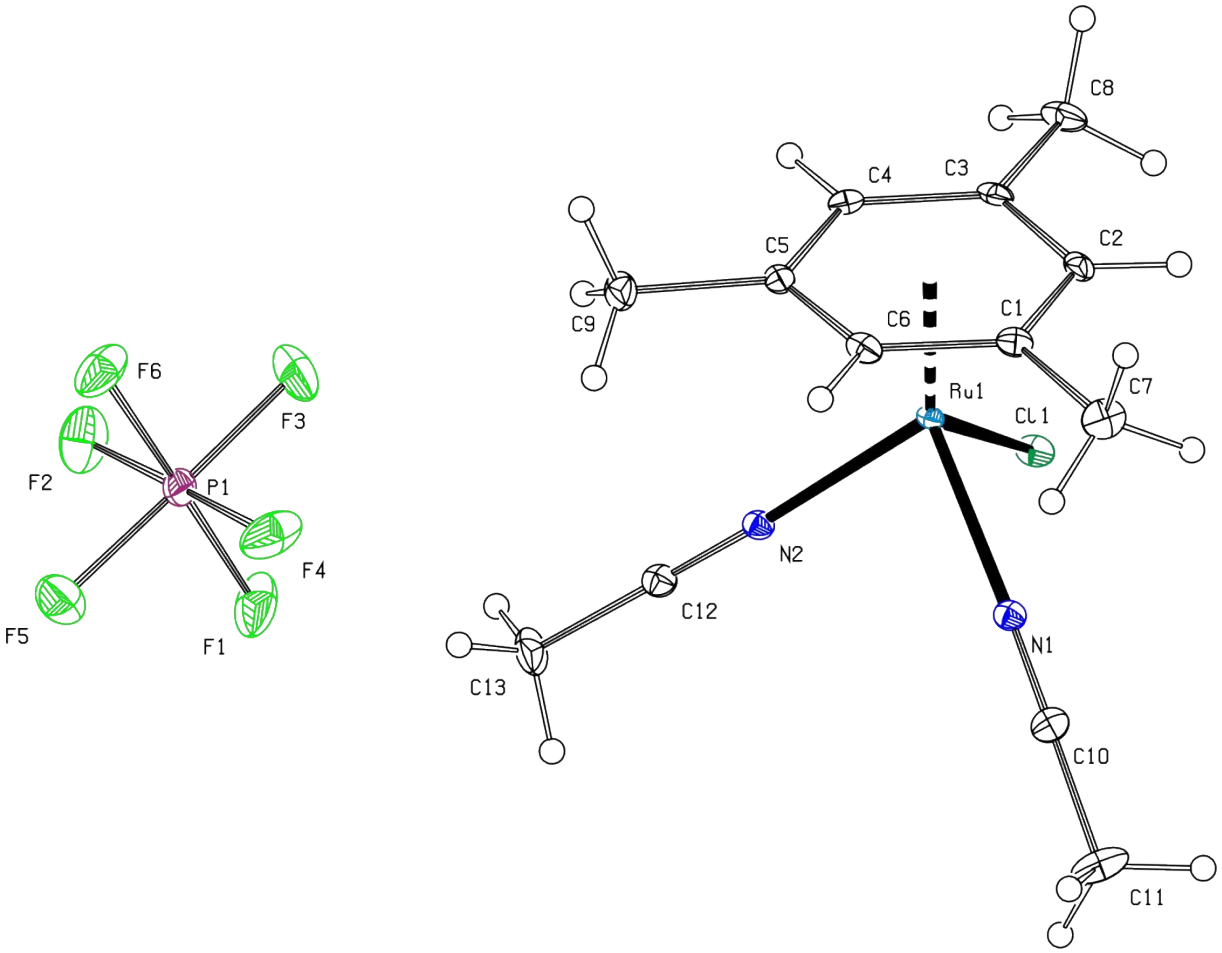

Figure S10. PLATON plot of the molecular structure of [(η⁶-mesitylene)RuCl(MeCN)$_3$][PF_6] with displacement ellipsoids scaled to the 30% probability level.

Selected Crystallographic Parameters

Table S1. Selected crystallographic data and structure refinement parameters.[a]

Compound	**2**	**9**	**10**·THF·2CH_2Cl_2
Formula	$C_{23}H_{22}FeP_2$	$C_{26}H_{28}FeO_2P_2$	$C_{58}H_{64}Cl_8FeOP_2Ru_2$
M	416.19	490.27	1364.62
Crystal system	monoclinic	triclinic	triclinic
Space group	$P2_1/c$ (no. 14)	$P\bar{1}$ (no. 2)	$P\bar{1}$ (no. 2)
a [Å]	7.8610(2)	6.1950(3)	9.4576(5)
b [Å]	11.2670(2)	13.8270(7)	10.8679(5)
c [Å]	22.1549(5)	14.0117(8)	15.0898(7)
α [°]	90	98.950(2)	83.951(2)
β [°]	96.336(1)	94.727(2)	74.811(2)
γ [°]	90	99.625(2)	84.697(2)
V [Å]^3	1950.27(7)	1161.7(1)	1485.1(1)
Z	4	2	1
μ(Mo Kα) [mm^{-1}]	1.179	0.808	1.193
Diffrns collected	13031	16140	33716
Independent diffrns	4475	5314	6829
Observed[a] diffrns	3994	4084	6310
R_{int}[b] [%]	2.19	3.84	2.11
No. of parameters	235	287	280
R[b] obsd diffrns [%]	2.75	5.07	2.41
R, wR[b] all data [%]	3.23, 7.01	7.48, 11.94	2.69, 5.95
Δρ [e Å^{-3}]	0.41, −0.68	1.35, −0.47	0.39, −0.76

[a] Diffractions with $I > 2\sigma(I)$. [b] Definitions: $R_{int} = \Sigma \left| F_o^2 - F_o^2(\text{mean}) \right| / \Sigma F_o^2$, where F_o^2(mean) is the average intensity of symmetry-equivalent diffractions. $R = \Sigma \left| \left| F_o \right| - \left| F_c \right| \right| / \Sigma \left| F_o \right|$, $wR = [\Sigma\{w(F_o^2 - F_c^2)^2\}/\Sigma w(F_o^2)^2]^{1/2}$.

Table S1 continued

Compound	**12**·2$CHCl_3$	**15**	**16**·CH_2Cl_2
Formula	$C_{43}H_{48}Cl_{10}FeP_2Ru_2$	$C_{32}H_{37}BCl_2FeOP_2Ru$	$C_{44}H_{42}Cl_3F_6FeP_3Ru$
M	1239.24	738.18	1040.95
Crystal system	triclinic	monoclinic	monoclinic
Space group	*P*–1 (no. 2)	$P2_1/n$ (no. 14)	$C2/c$ (no. 15)
a [Å]	10.2348(6)	9.4223(3)	29.799(2)
b [Å]	15.3753(8)	16.9051(7)	10.7602(7)
c [Å]	16.5514(8)	19.8836(8)	26.685(2)
α [°]	74.283(2)	90	90
β [°]	85.961(2)	93.541(1)	103.043(2)
γ [°]	74.855(2)	90	90
V [Å]^3	2420.1(2)	3161.1(2)	8335(1)
Z	2	4	8
μ(Mo Kα) [mm^{-1}]	1.561	1.232	1.078
Diffrns collected	51167	42521	37097
Independent diffrns	11062	7260	9538
Observed[a] diffrns	10279	6488	8170
R_{int}[b] [%]	2.11	3.52	4.14
No. of parameters	529	377	526
R[b] obsd diffrns [%]	3.27	3.45	4.08
R, wR[b] all data [%]	3.55, 8.29	3.99, 8.08	5.13, 9.66
Δρ [e Å^{-3}]	2.22, −1.39	0.74, −0.69	1.66, −1.03

Table S1 continued

Compound	**18**·2$CHCl_3$	**19**	[(η^6-$C_6H_3Me_3$)RuCl(MeCN)$_2$][PF_6]
Formula	$C_{42}H_{37}Cl_7FeP_2Ru$	$C_{28}H_{27}ClFeP_2Ru$	$C_{13}H_{18}ClF_6N_2PRu$
M	1008.72	617.80	483.78
Crystal system	monoclinic	monoclinic	orthorhombic
Space group	$P2_1/n$ (no. 14)	$P2_1/c$ (no. 14)	*Pbca* (no. 61)
a [Å]	10.8280(1)	7.8926(7)	13.8820(7)
b [Å]	22.6590(2)	10.3590(8)	12.9415(7)
c [Å]	17.1504(2)	28.986(3)	19.779(1)
α [°]	90	90	90
β [°]	101.0016(6)	90.019(3)	90
γ [°]	90	90	90
V [Å]^3	4130.55(7)	2369.9(4)	3553.3(3)
Z	4	4	8
μ(Mo Kα) [mm^{-1}]	1.278	1.513	1.179
Diffrns collected	88097	27956	22472
Independent diffrns	9453	5444	4071
Observed[a] diffrns	7987	5100	3677
R_{int}[b] [%]	5.06	2.00	1.88
No. of parameters	478	298	222
R[b] obsd diffrns [%]	4.71	2.12	2.13
R, *wR*[b] all data [%]	5.79, 13.39	2.35, 5.26	2.45, 5.54
$\Delta\rho$ [e Å^{-3}]	1.60, −2.00	0.58, −0.48	0.70, −0.59

Copies of the NMR Spectra

(Note: solvent signals in the NMR spectra are denoted by an asterisk.)

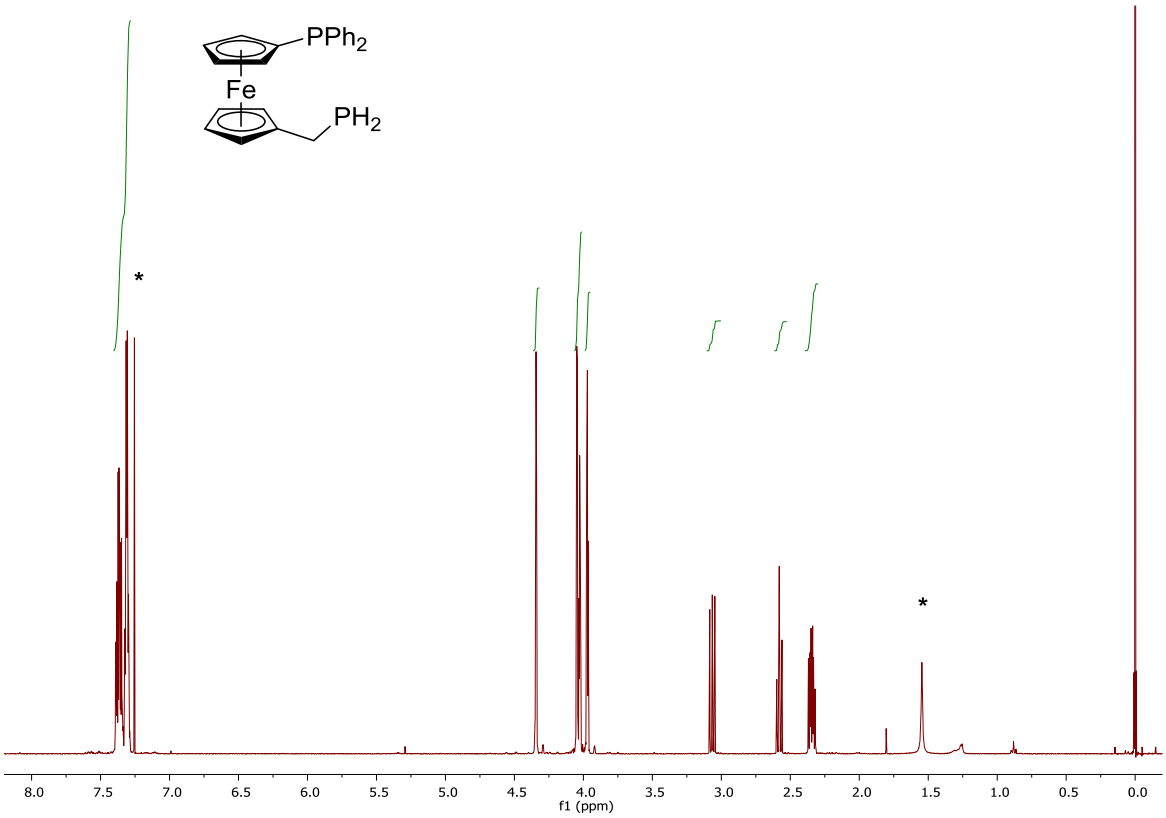

Figure S11. ^{1}H NMR spectrum (400 MHz, $CDCl_3$) of **2**.

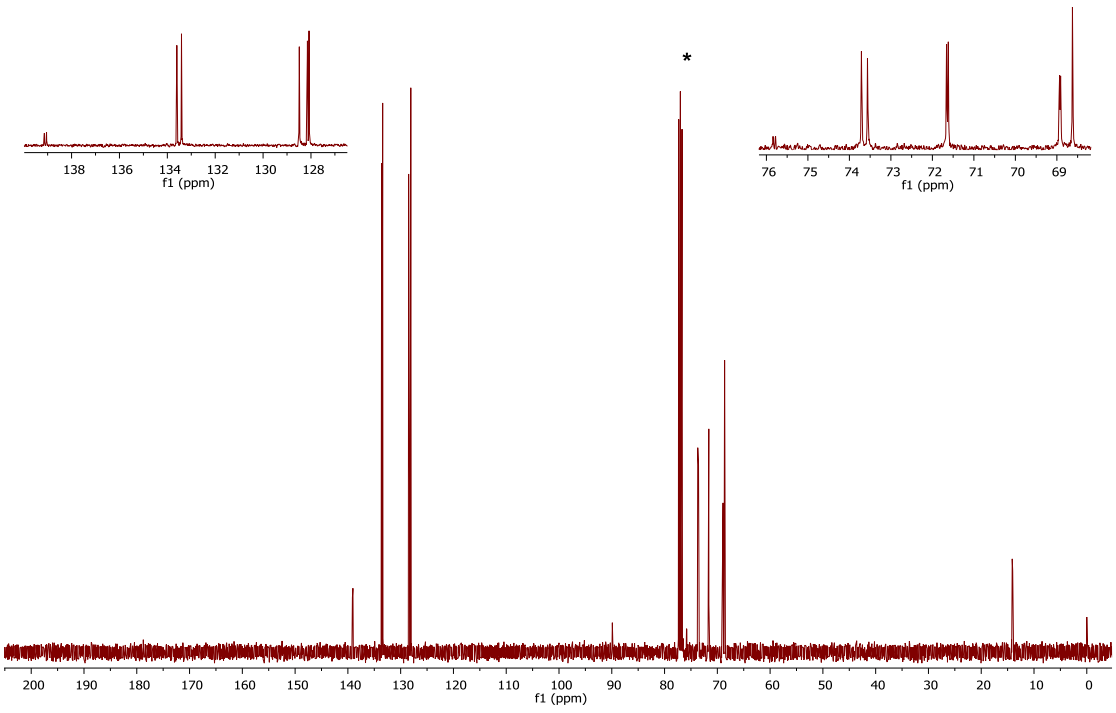

Figure S12. $^{13}C\{^{1}H\}$ NMR spectrum (101 MHz, $CDCl_3$) of **2**.

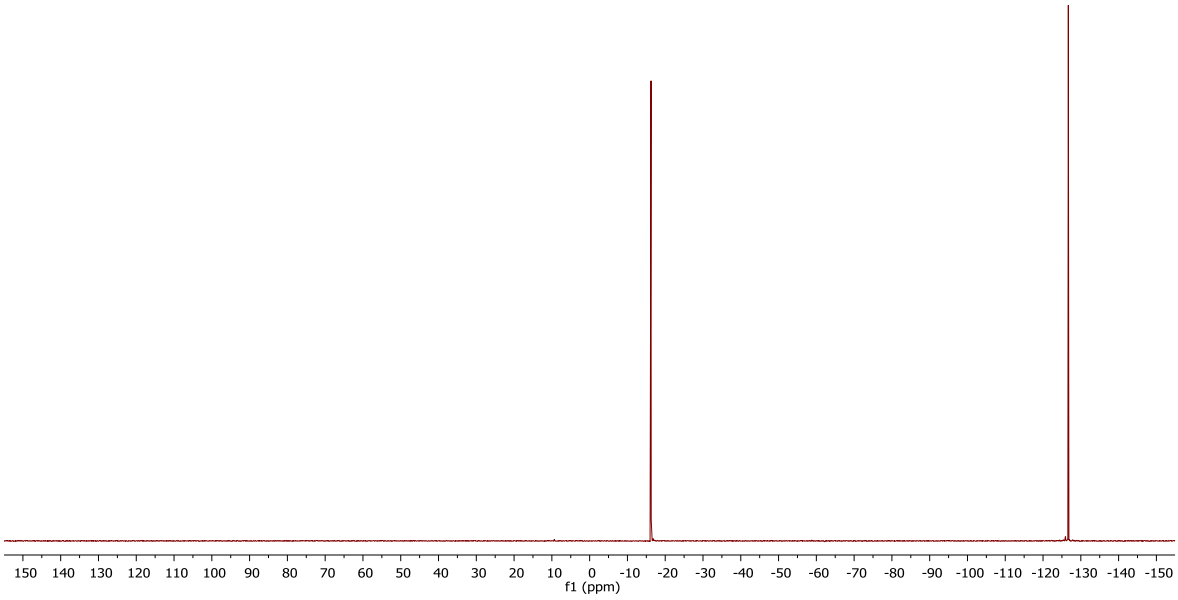

Figure S13. $^{31}P\{^{1}H\}$ NMR spectrum (162 MHz, $CDCl_3$) of **2**.

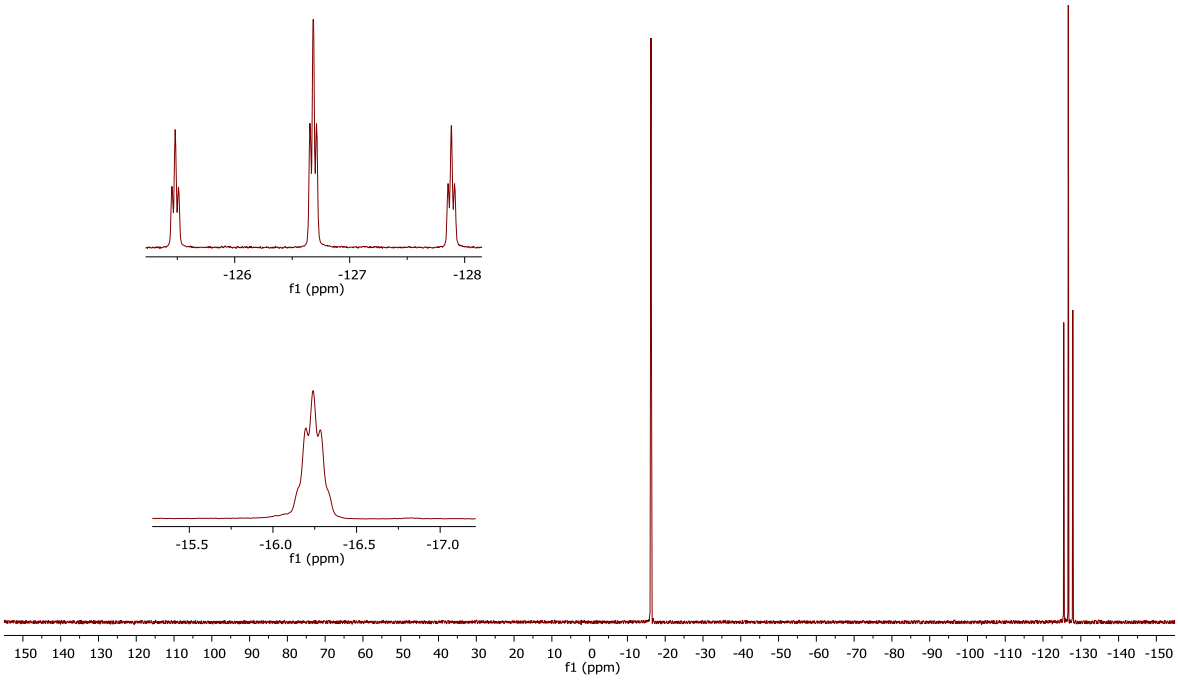

Figure S14. ^{31}P NMR spectrum (162 MHz, $CDCl_3$) of **2**.

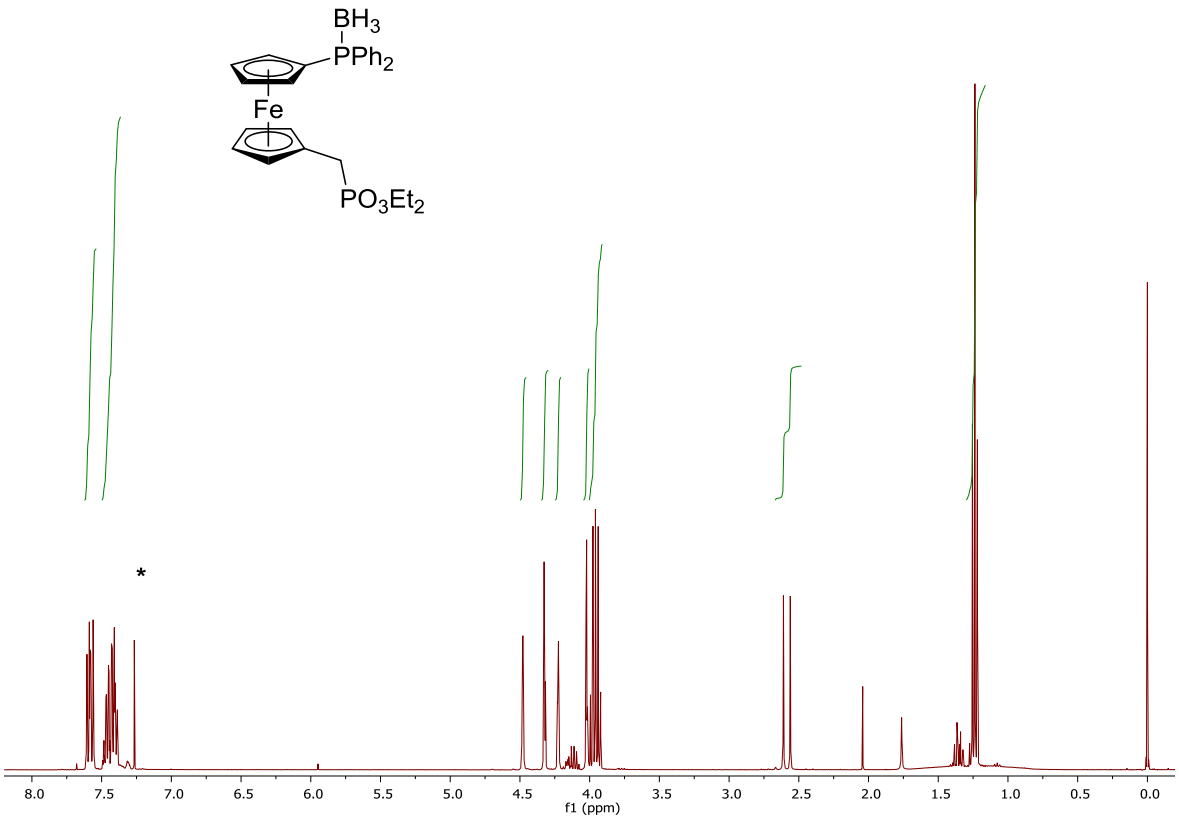

Figure S15. ^{1}H NMR spectrum (400 MHz, $CDCl_3$) of **4**.

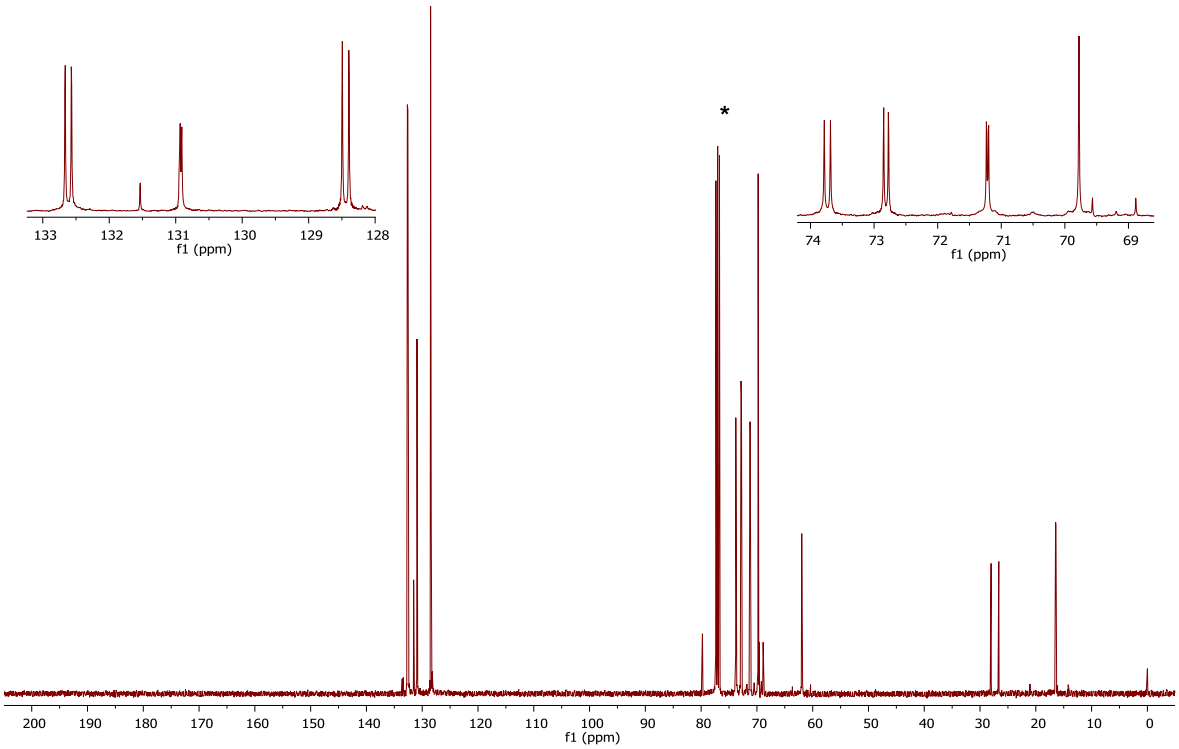

Figure S16. $^{13}C\{^{1}H\}$ NMR spectrum (101 MHz, $CDCl_3$) of **4**.

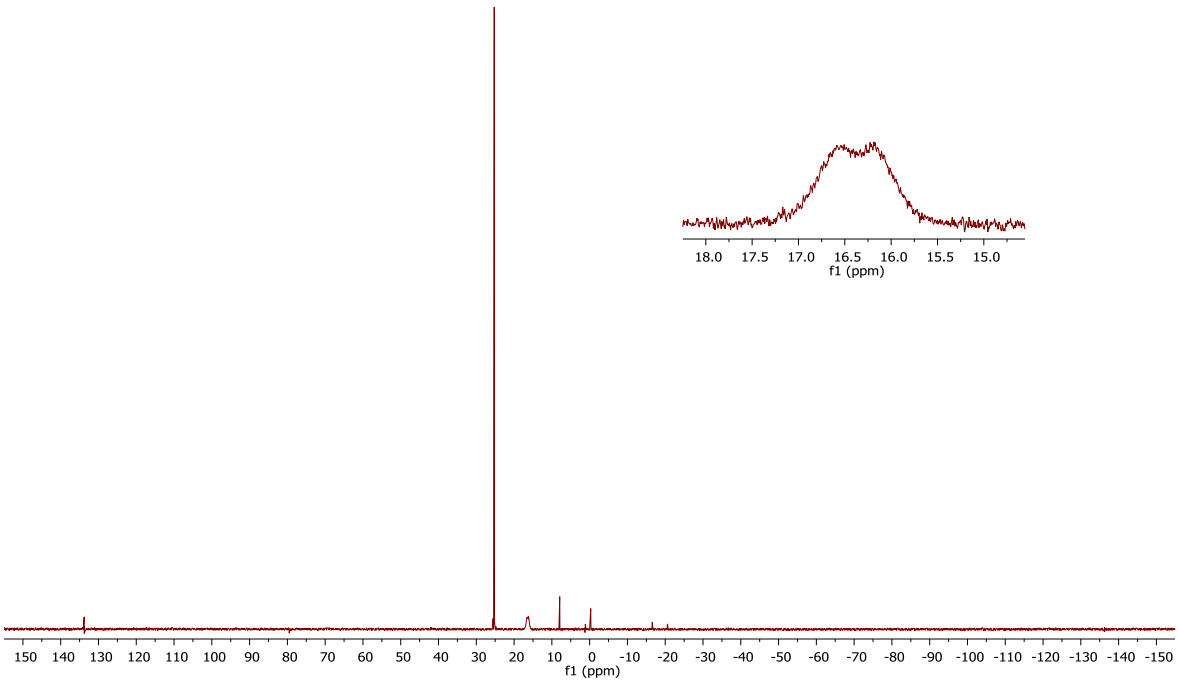

Figure S17. $^{31}P\{^{1}H\}$ NMR spectrum (162 MHz, $CDCl_3$) of **4**.

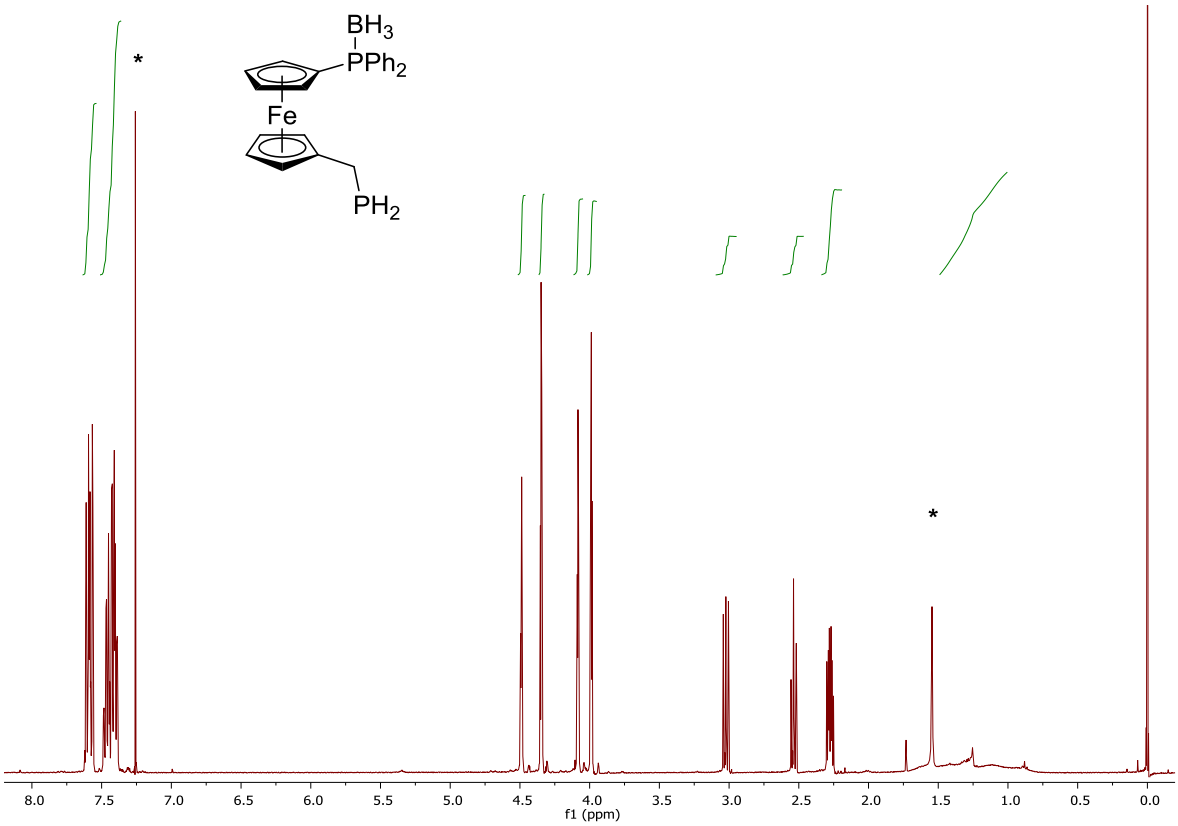

Figure S18. ^{1}H NMR spectrum (400 MHz, $CDCl_3$) of **5**.

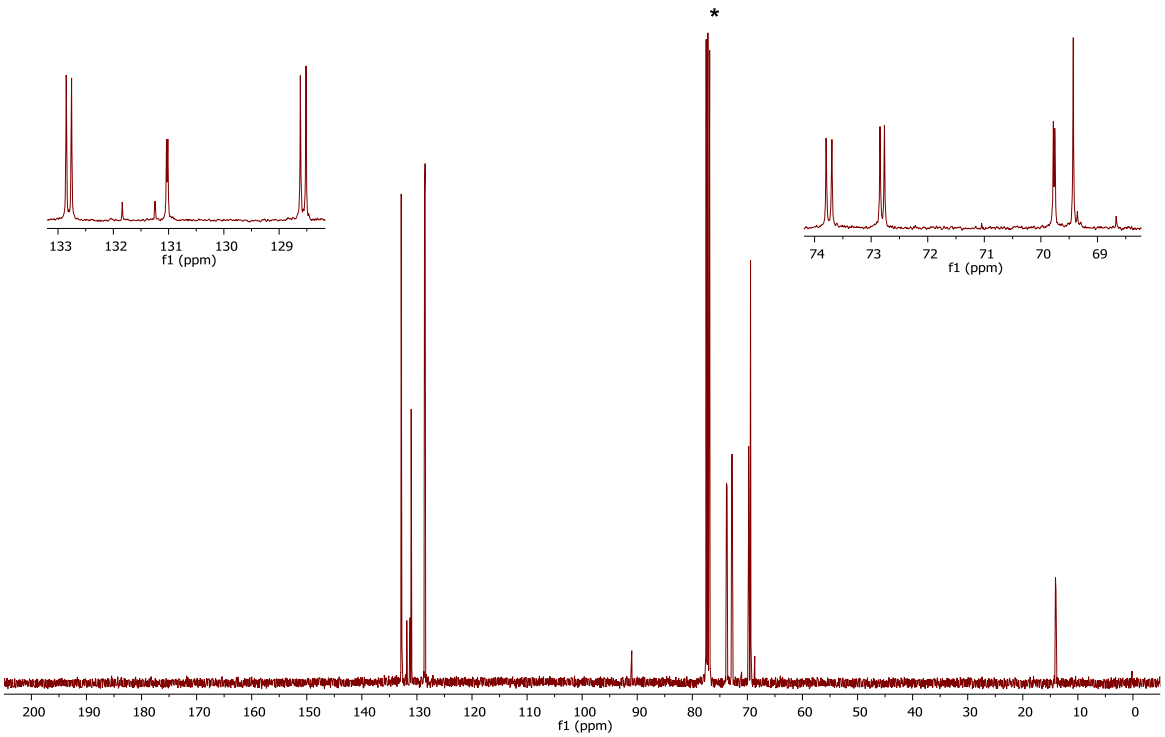

Figure S19. $^{13}C\{^{1}H\}$ NMR spectrum (101 MHz, $CDCl_3$) of **5**.

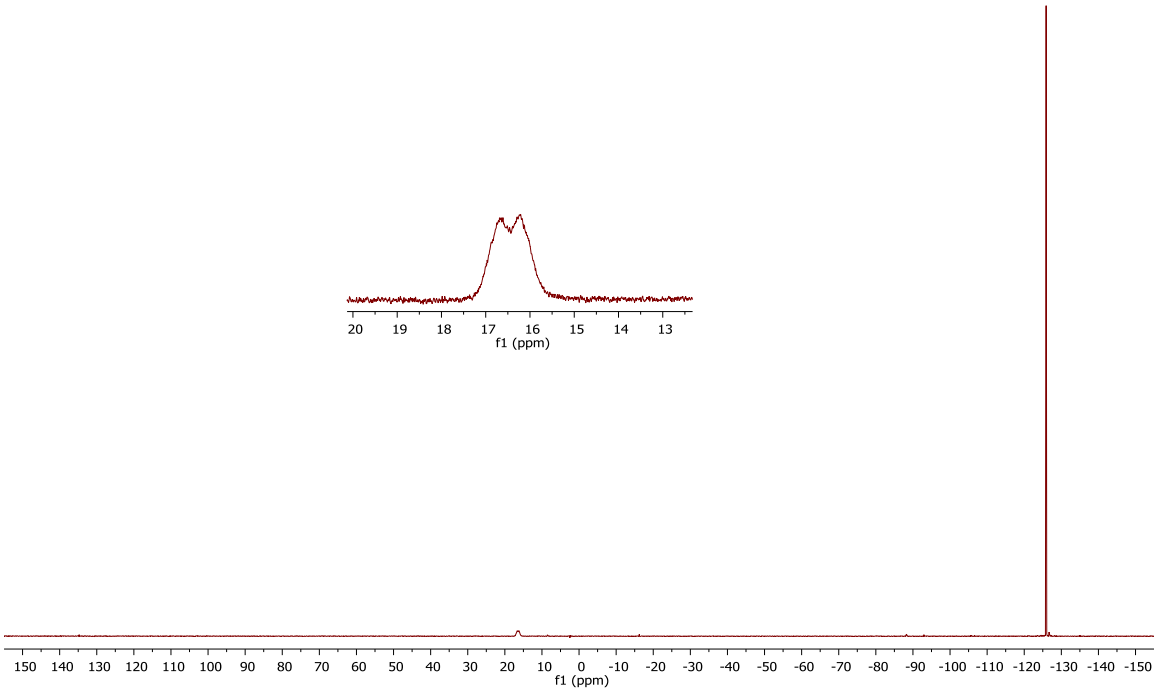

Figure S20. $^{31}P\{^{1}H\}$ NMR spectrum (162 MHz, $CDCl_3$) of **5**.

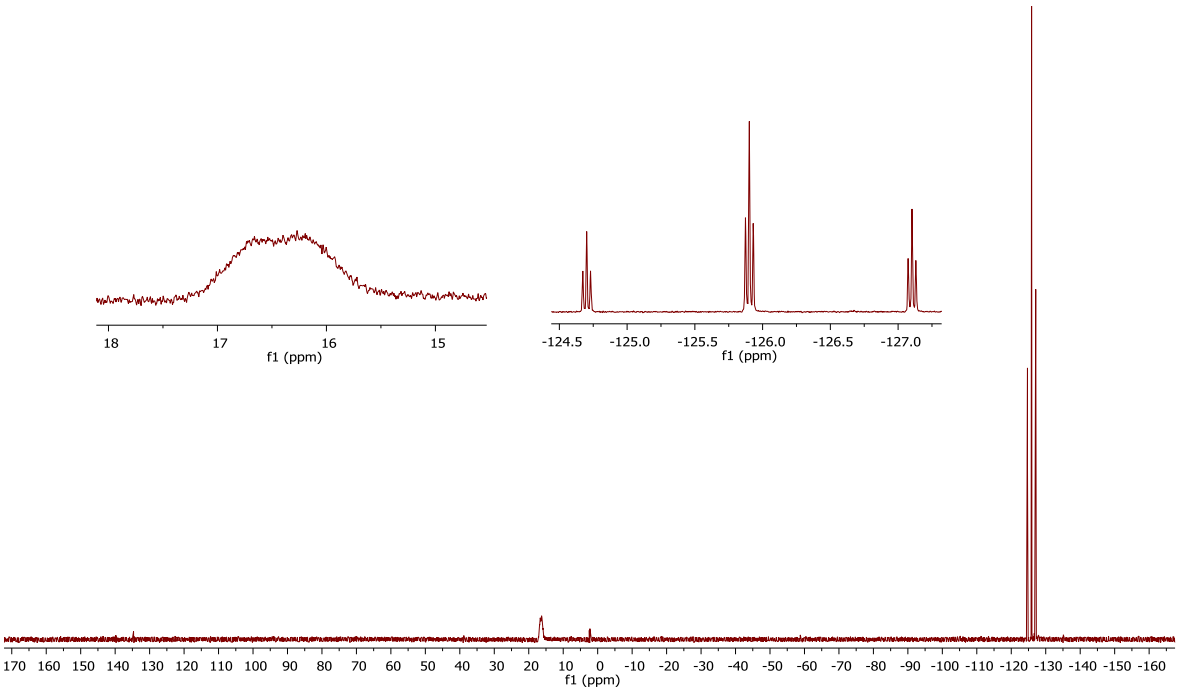

Figure S21. ^{31}P NMR spectrum (162 MHz, $CDCl_3$) of **5**.

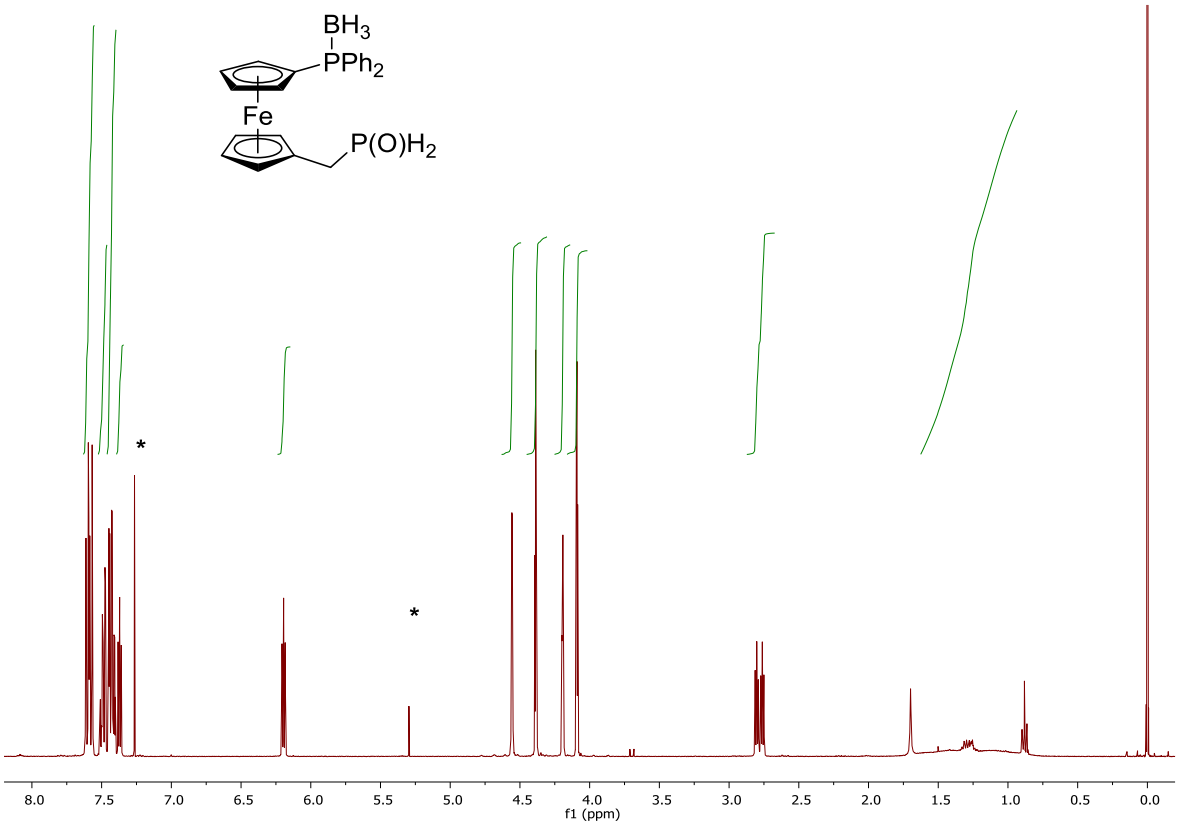

Figure S22. ^{1}H NMR spectrum (400 MHz, $CDCl_3$) of **6**.

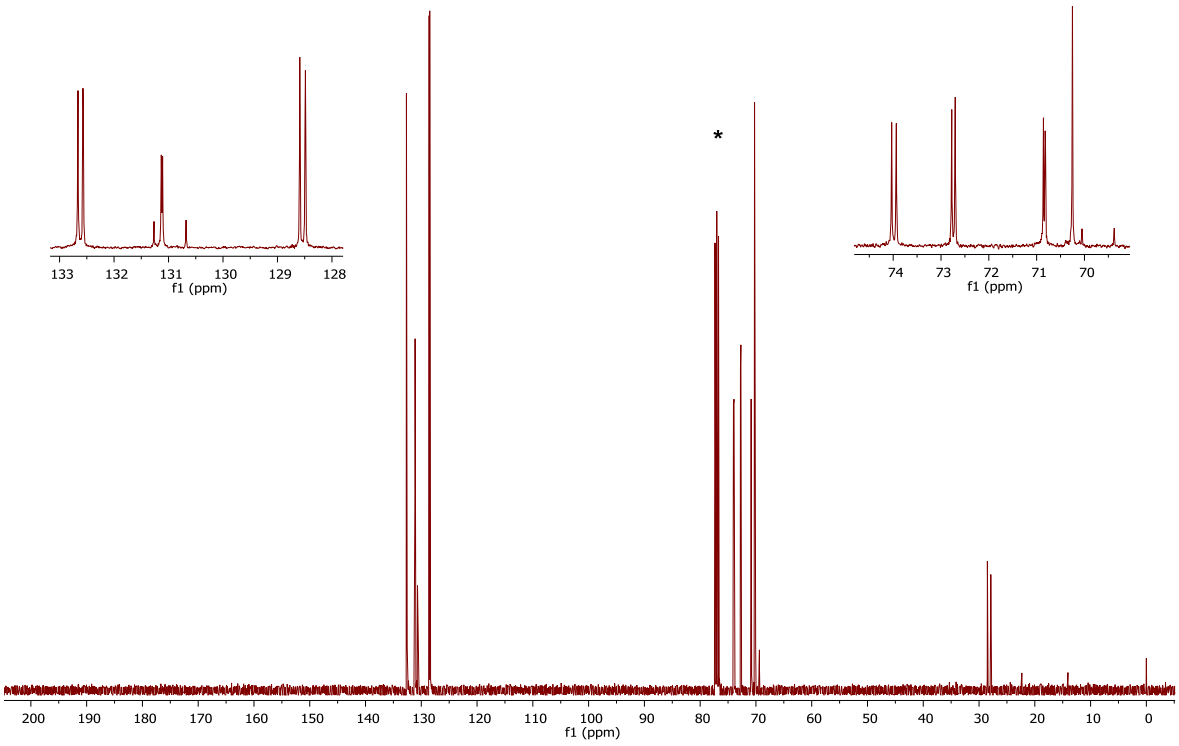

Figure S23. $^{13}C\{^{1}H\}$ NMR spectrum (101 MHz, $CDCl_3$) of **6**.

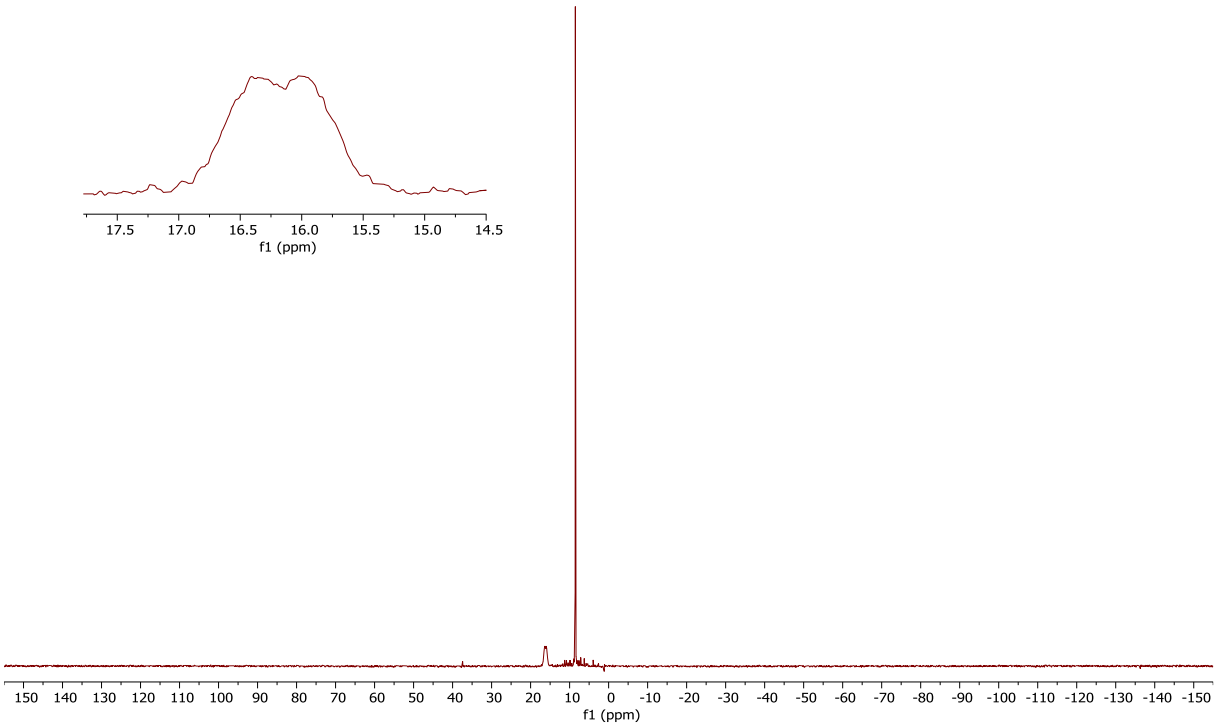

Figure S24. $^{31}P\{^{1}H\}$ NMR spectrum (162 MHz, $CDCl_3$) of **6**.

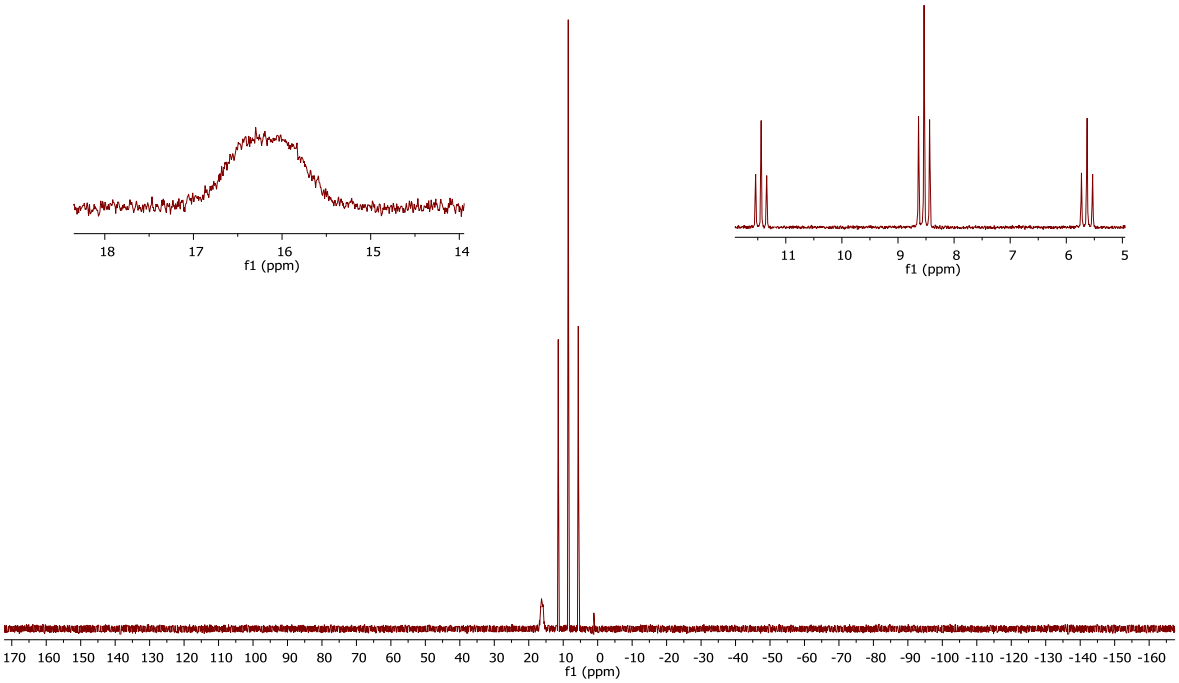

Figure S25. ^{31}P NMR spectrum (162 MHz, $CDCl_3$) of **6**.

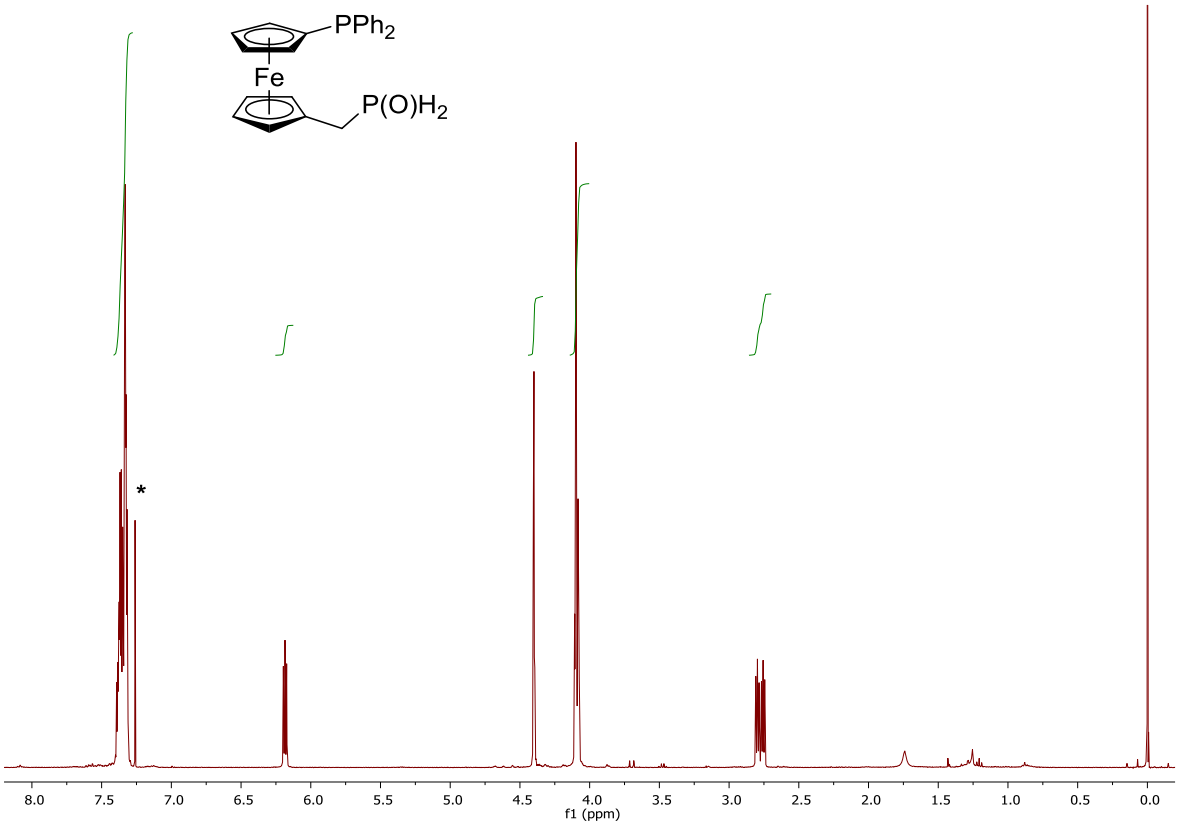

Figure S26. ^{1}H NMR spectrum (400 MHz, $CDCl_3$) of **7**.

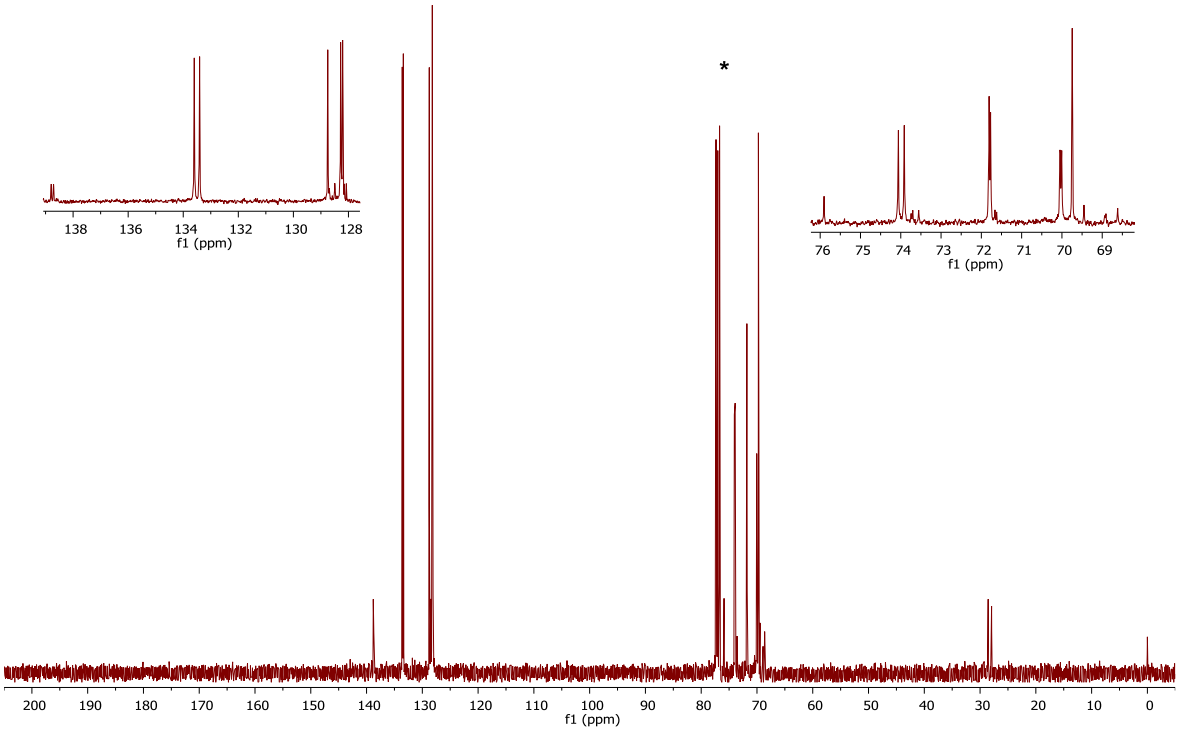

Figure S27. $^{13}C\{^{1}H\}$ NMR spectrum (101 MHz, $CDCl_3$) of **7**.

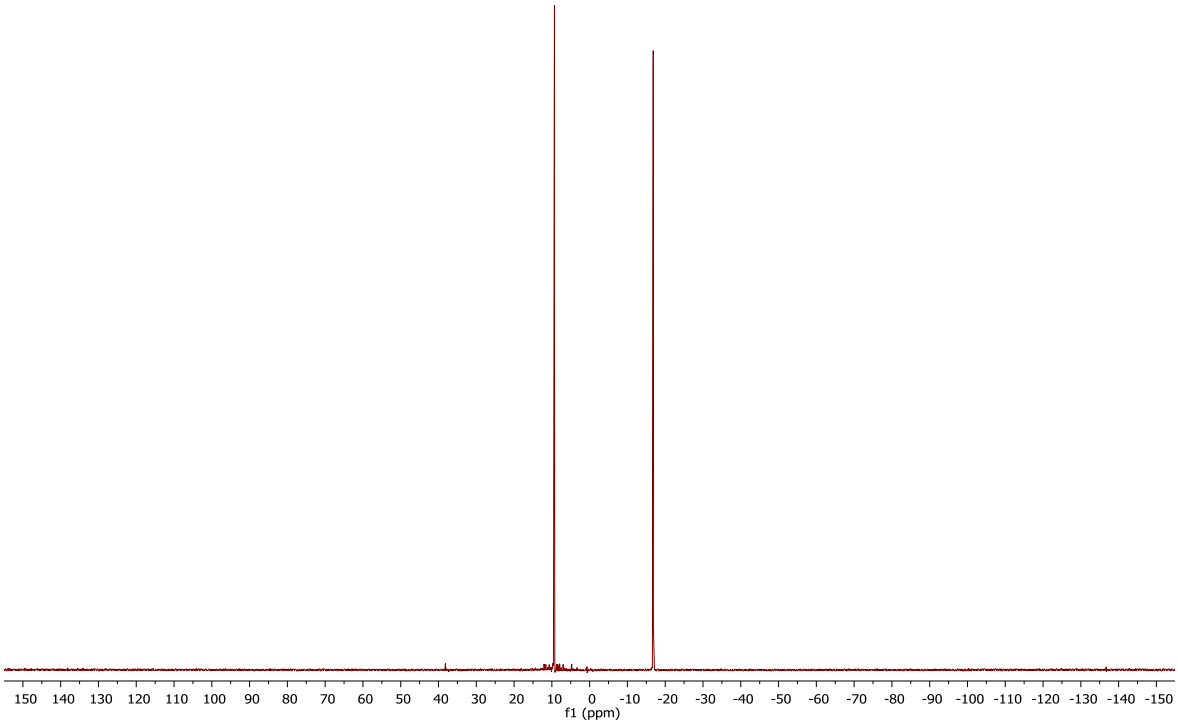

Figure S28. $^{31}P\{^{1}H\}$ NMR spectrum (162 MHz, $CDCl_3$) of **7**.

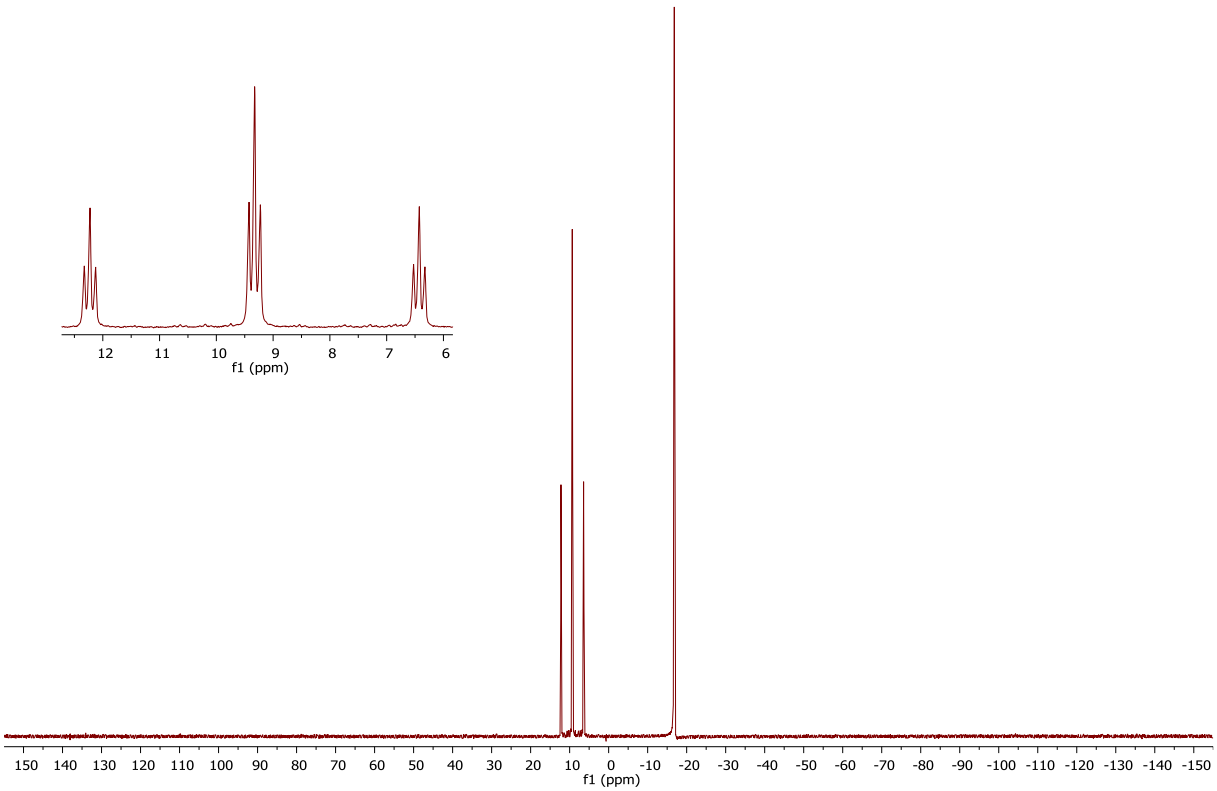

Figure S29. ^{31}P NMR spectrum (162 MHz, $CDCl_3$) of **7**.

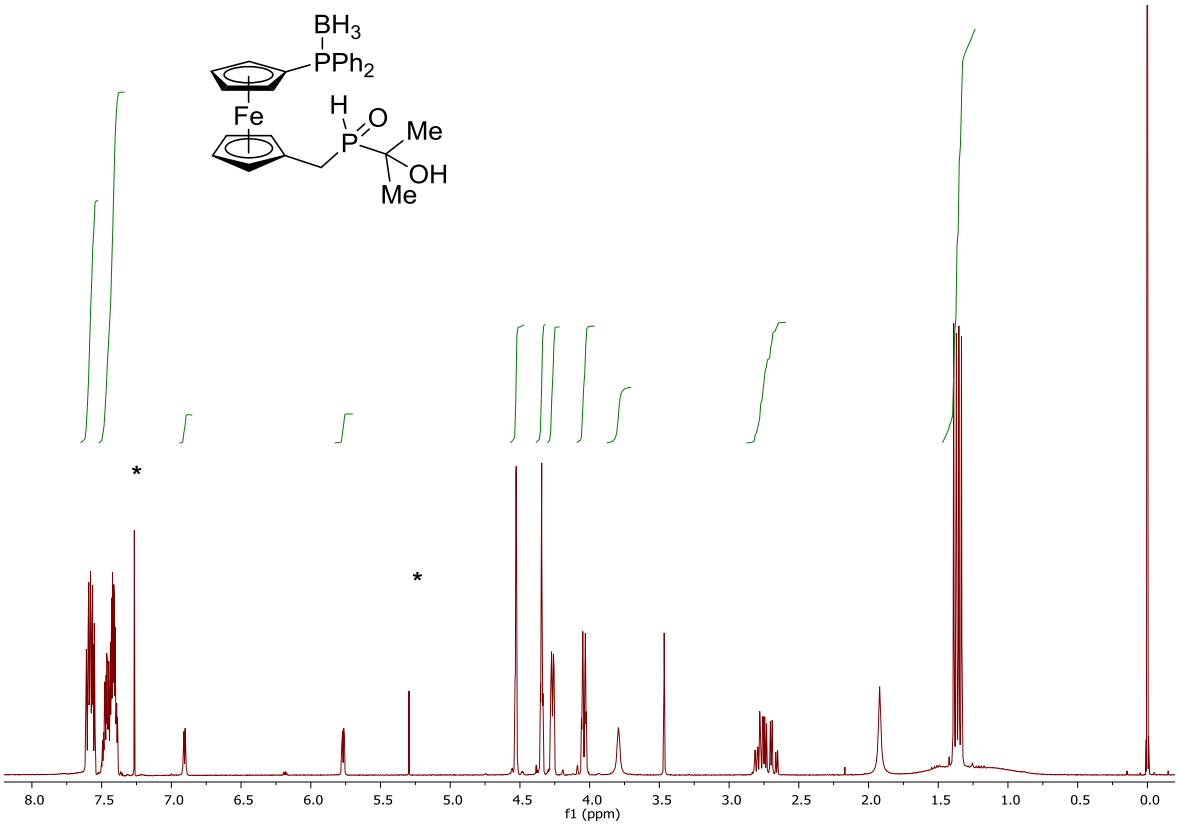

Figure S30. ^{1}H NMR spectrum (400 MHz, $CDCl_3$) of **8**.

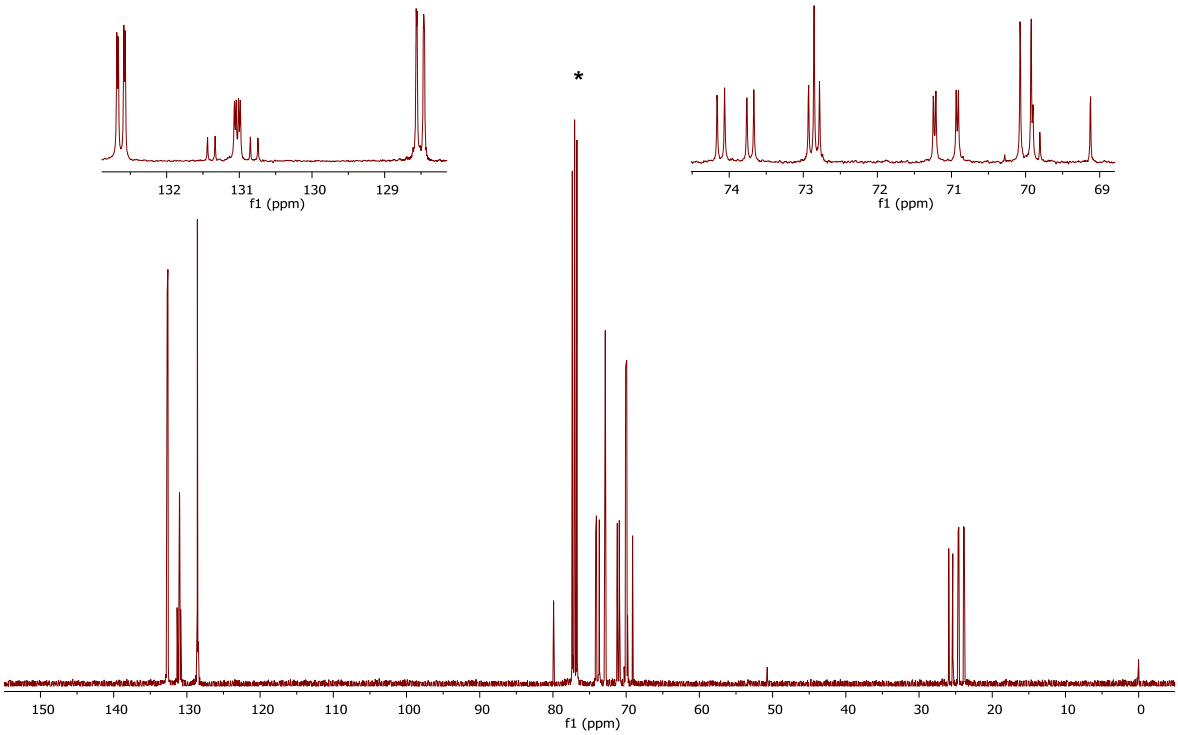

Figure S31. $^{13}C\{^{1}H\}$ NMR spectrum (101 MHz, $CDCl_3$) of **8**.

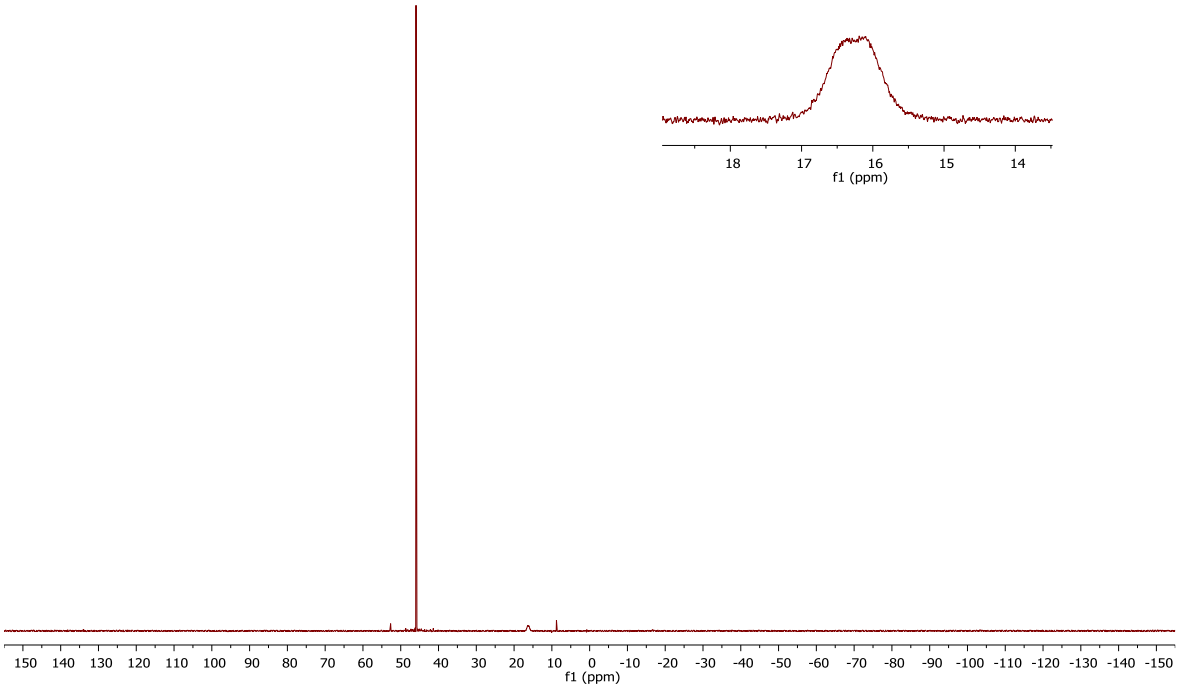

Figure S32. $^{31}P\{^{1}H\}$ NMR spectrum (162 MHz, $CDCl_3$) of **8**.

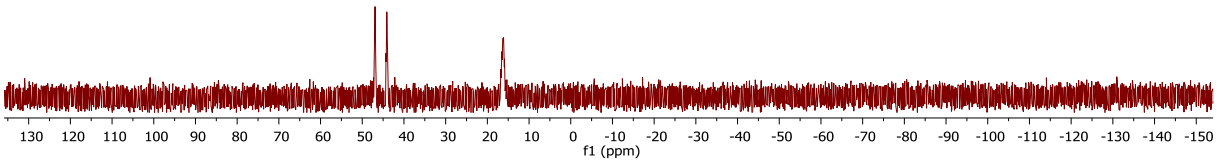

Figure S33. ^{31}P NMR spectrum (162 MHz, $CDCl_3$) of **8**.

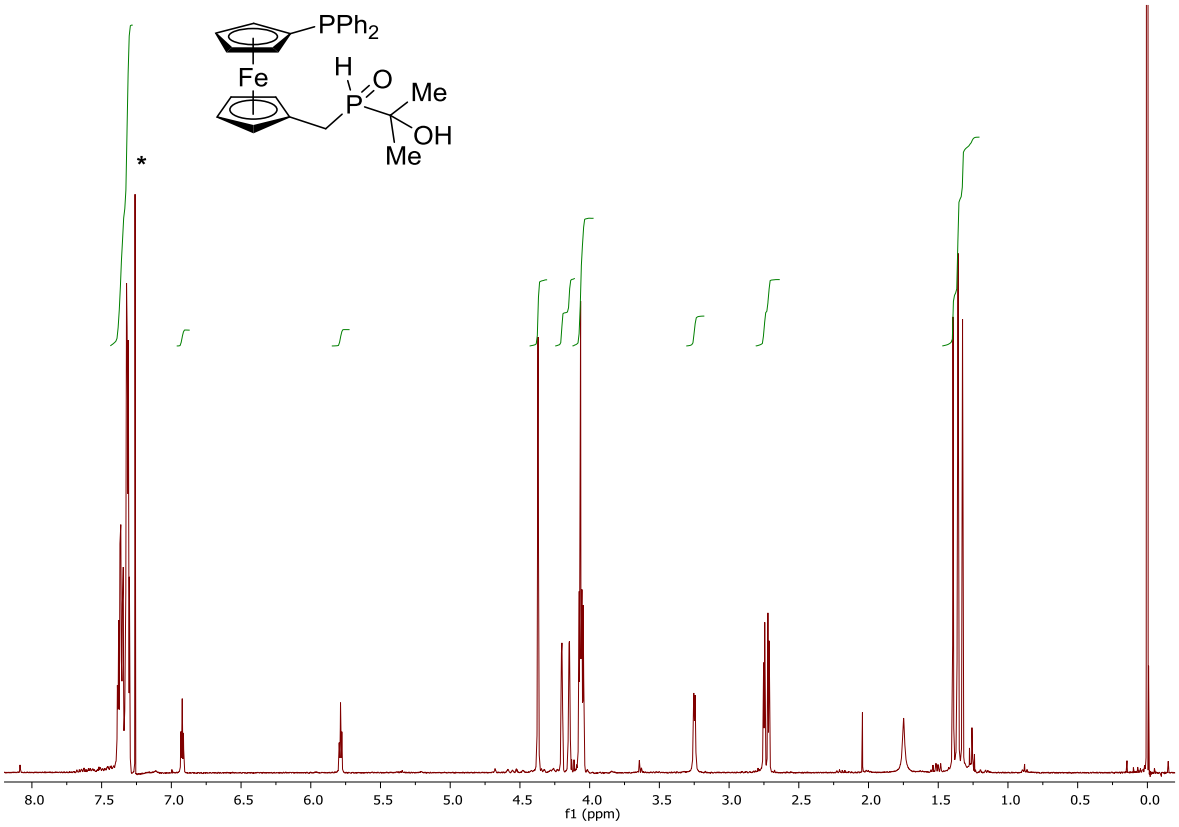

Figure S34. ^{1}H NMR spectrum (400 MHz, $CDCl_3$) of **9**.

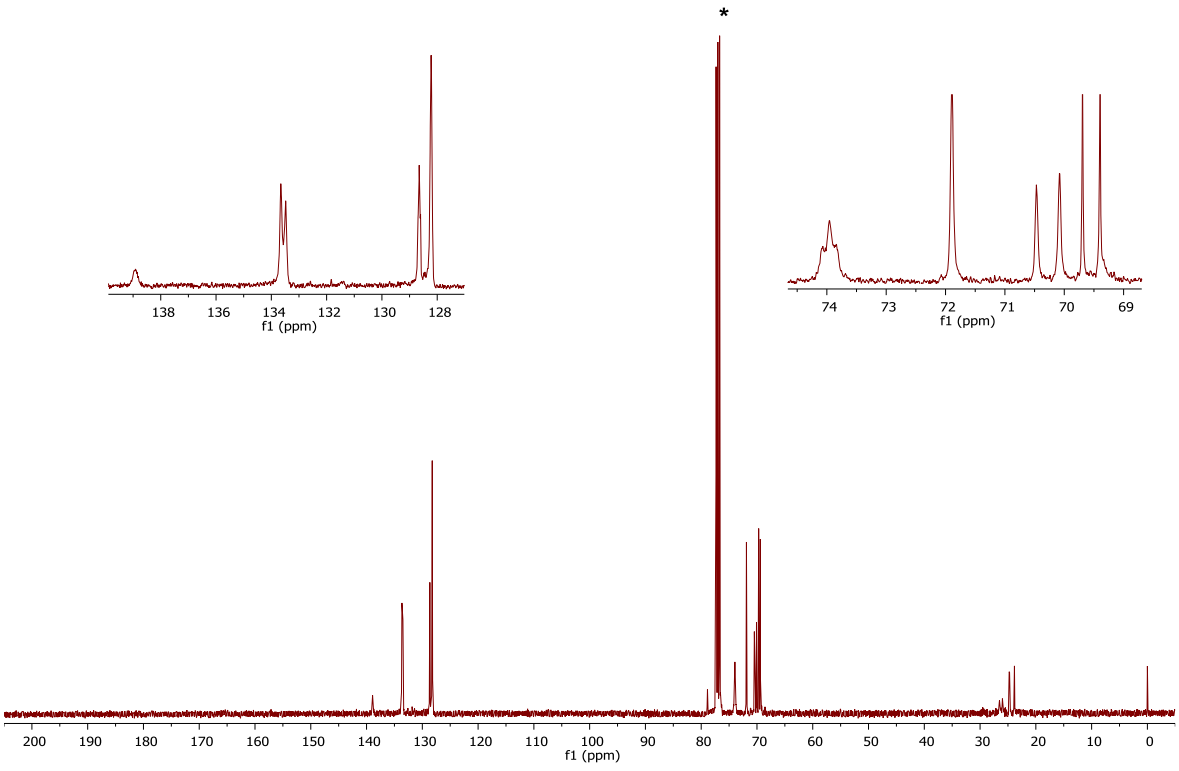

Figure S35. $^{13}C\{^{1}H\}$ NMR spectrum (101 MHz, $CDCl_3$) of **9**.

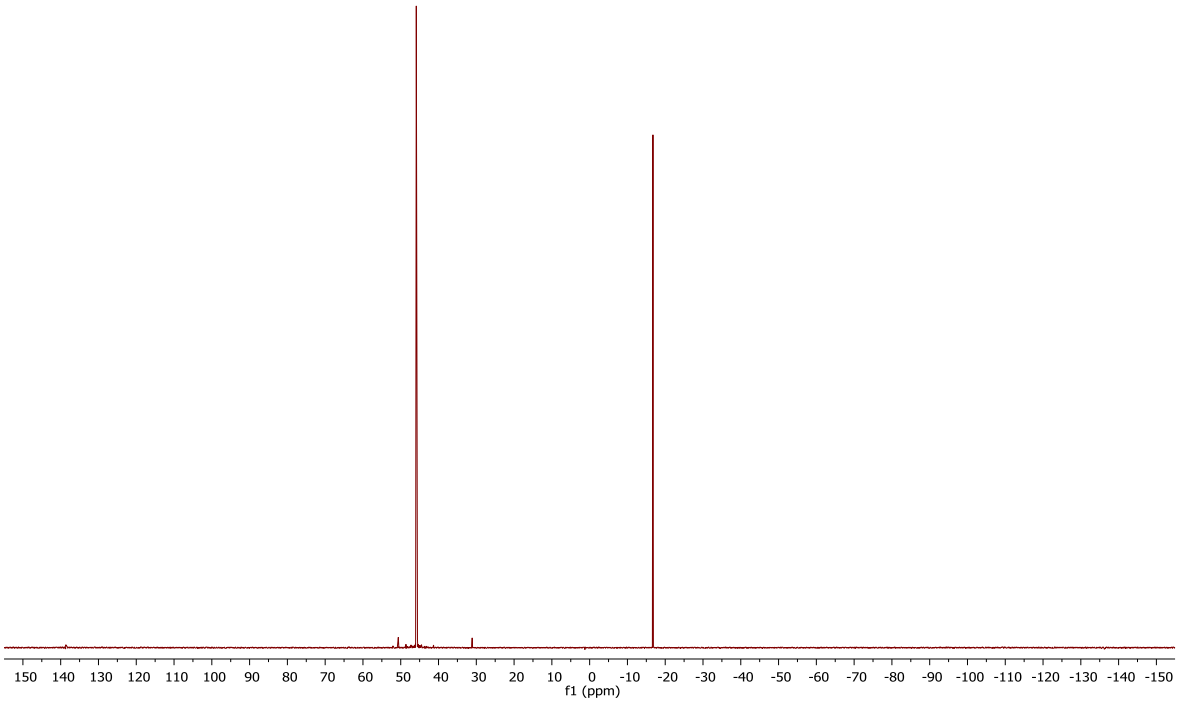

Figure S36. $^{31}P\{^{1}H\}$ NMR spectrum (162 MHz, $CDCl_3$) of **9**.

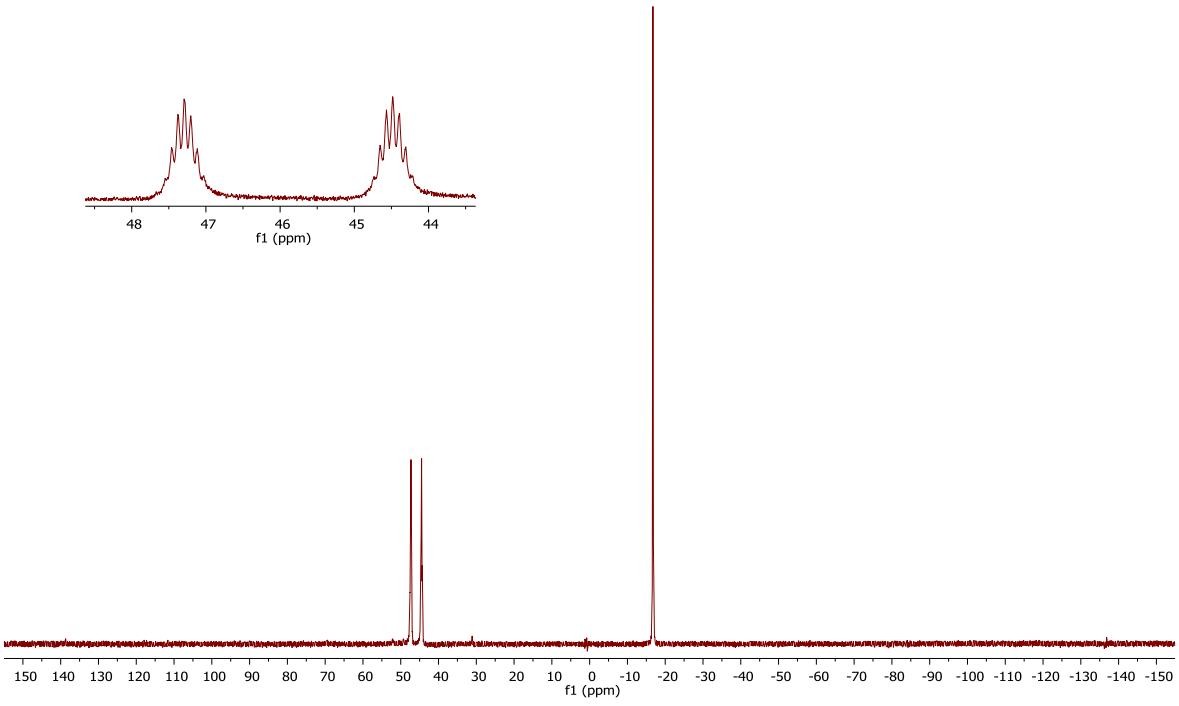

Figure S37. ^{31}P NMR spectrum (162 MHz, $CDCl_3$) of **9**.

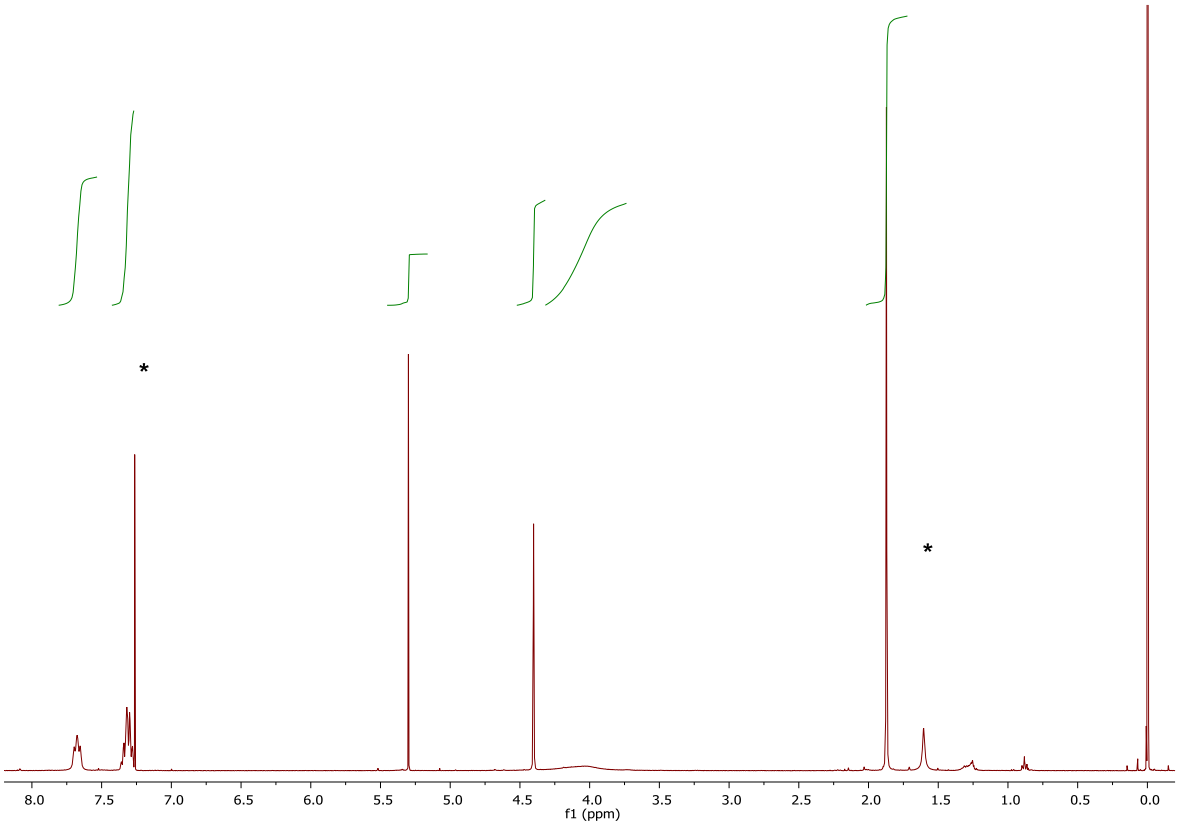

Figure S38. ^{1}H NMR spectrum (400 MHz, $CDCl_3$) of **10**.

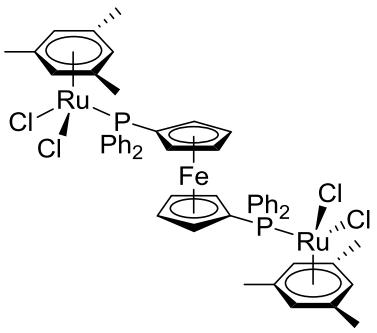

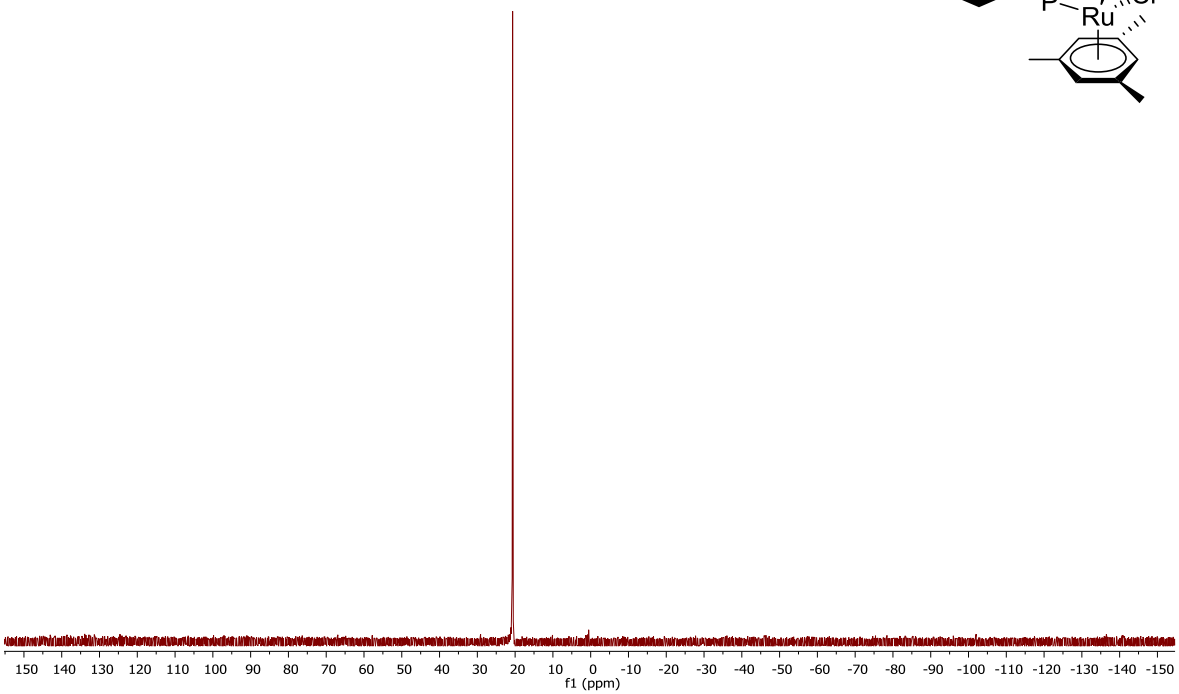

Figure S39. $^{31}P\{^{1}H\}$ NMR spectrum (162 MHz, $CDCl_3$) of **10**.

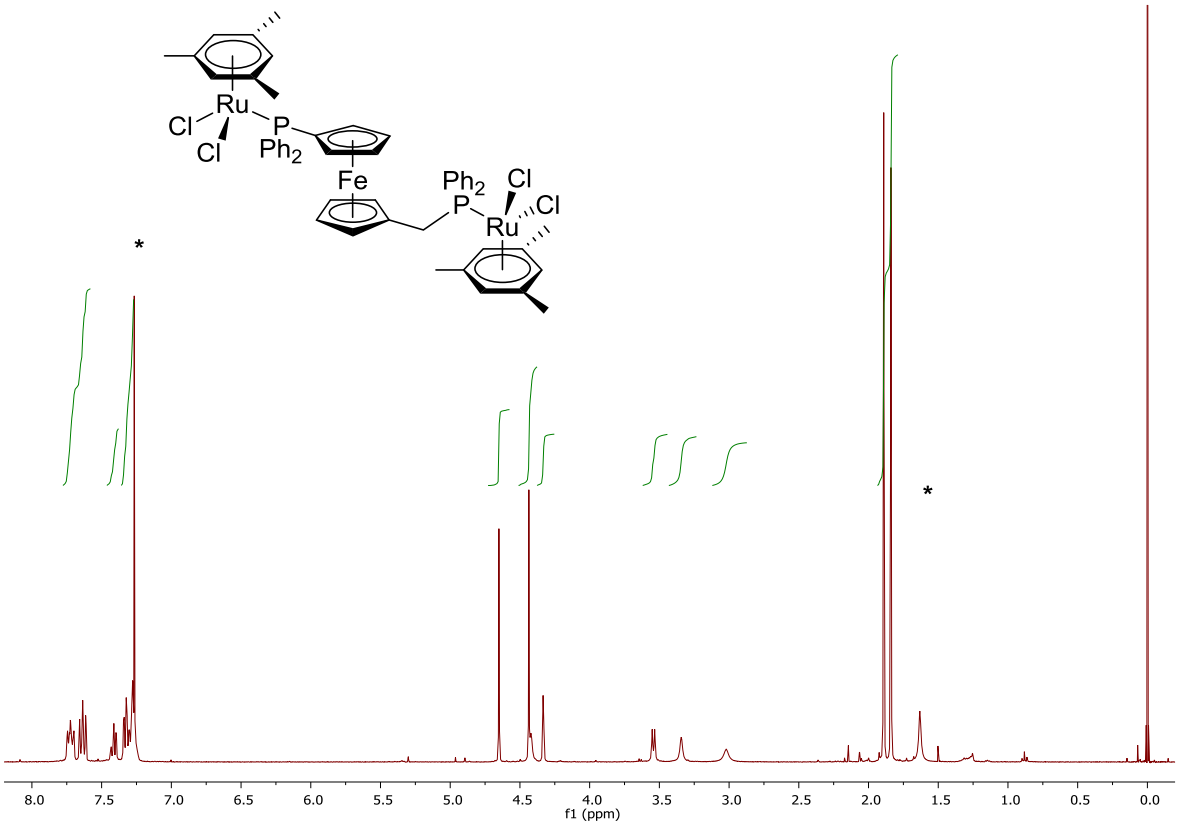

Figure S40. ^{1}H NMR spectrum (400 MHz, $CDCl_3$) of **11**.

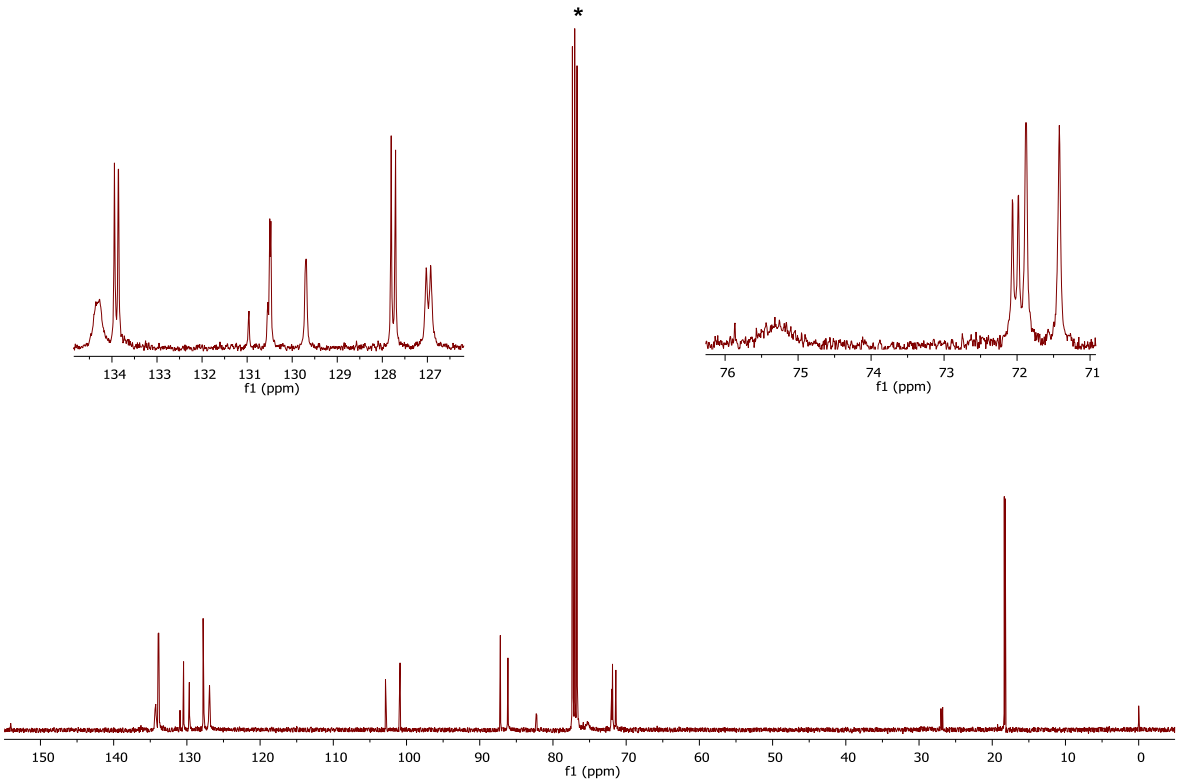

Figure S41. $^{13}C\{^{1}H\}$ NMR spectrum (101 MHz, $CDCl_3$) of **11**.

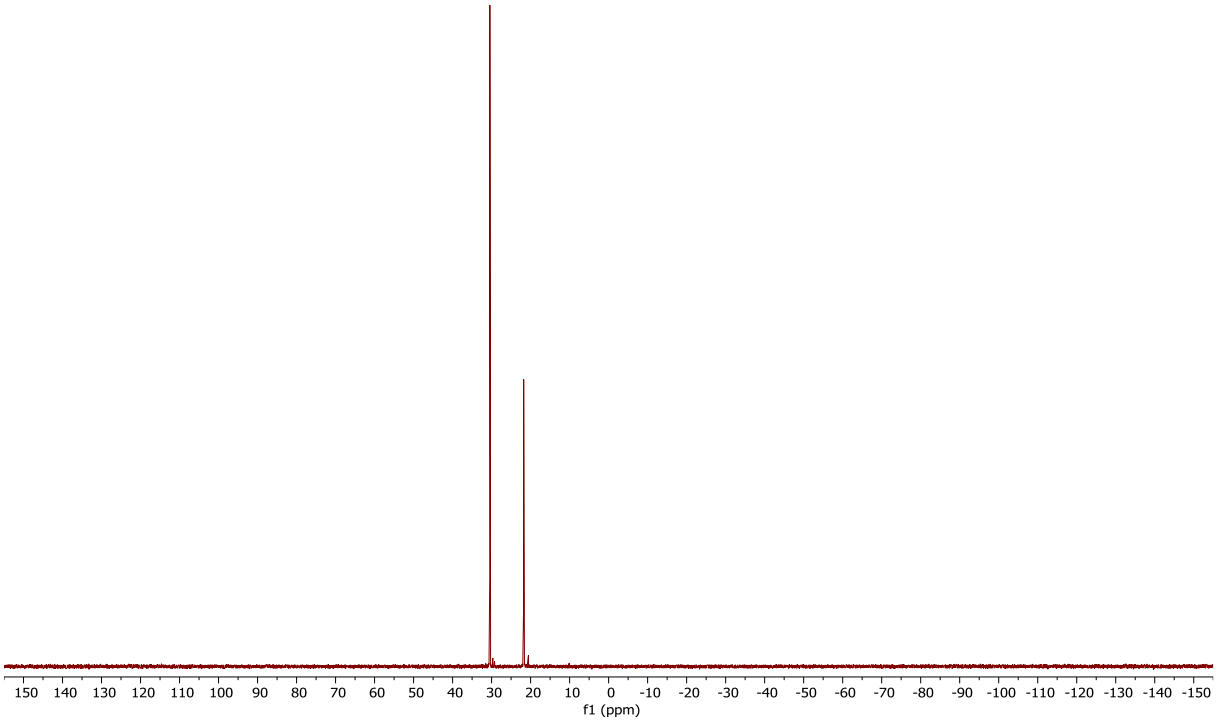

Figure S42. $^{31}P\{^{1}H\}$ NMR spectrum (162 MHz, $CDCl_3$) of **11**.

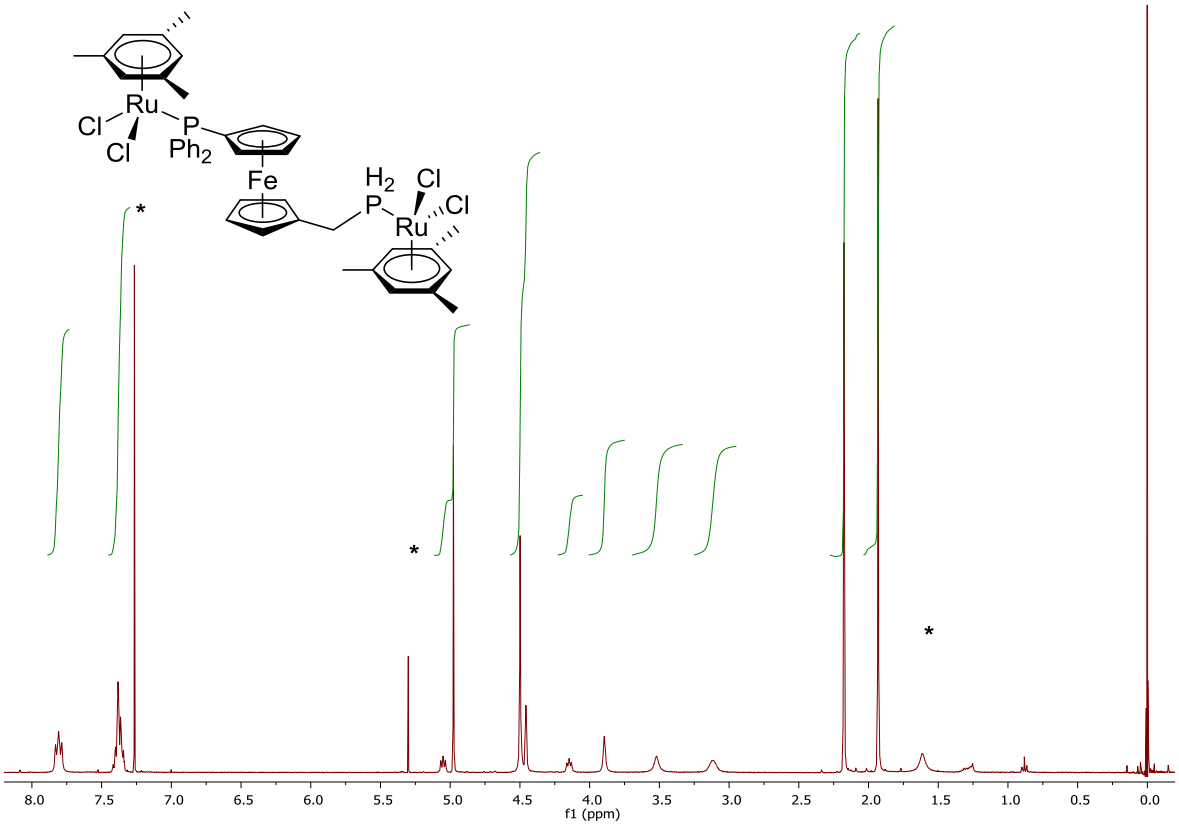

Figure S43. ^{1}H NMR spectrum (400 MHz, $CDCl_3$) of **12**.

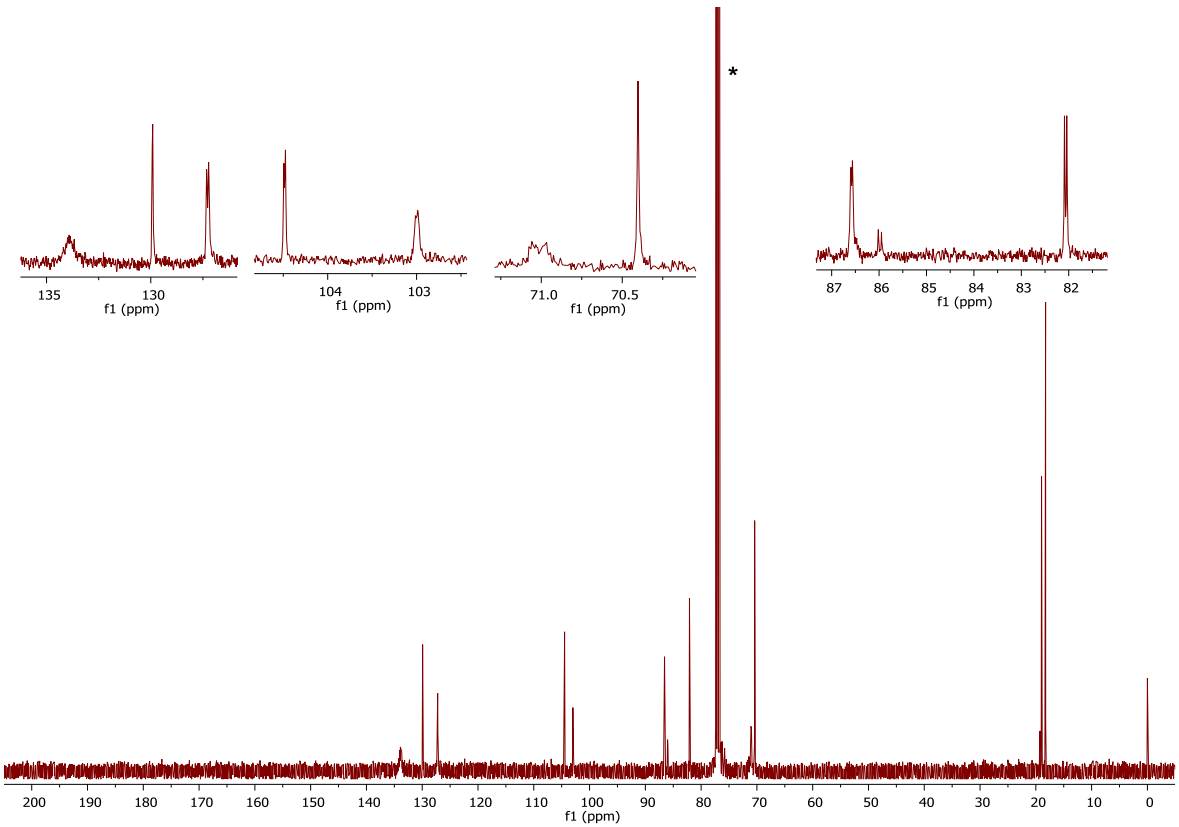

Figure S44. $^{13}C\{^{1}H\}$ NMR spectrum (101 MHz, $CDCl_3$) of **12**.

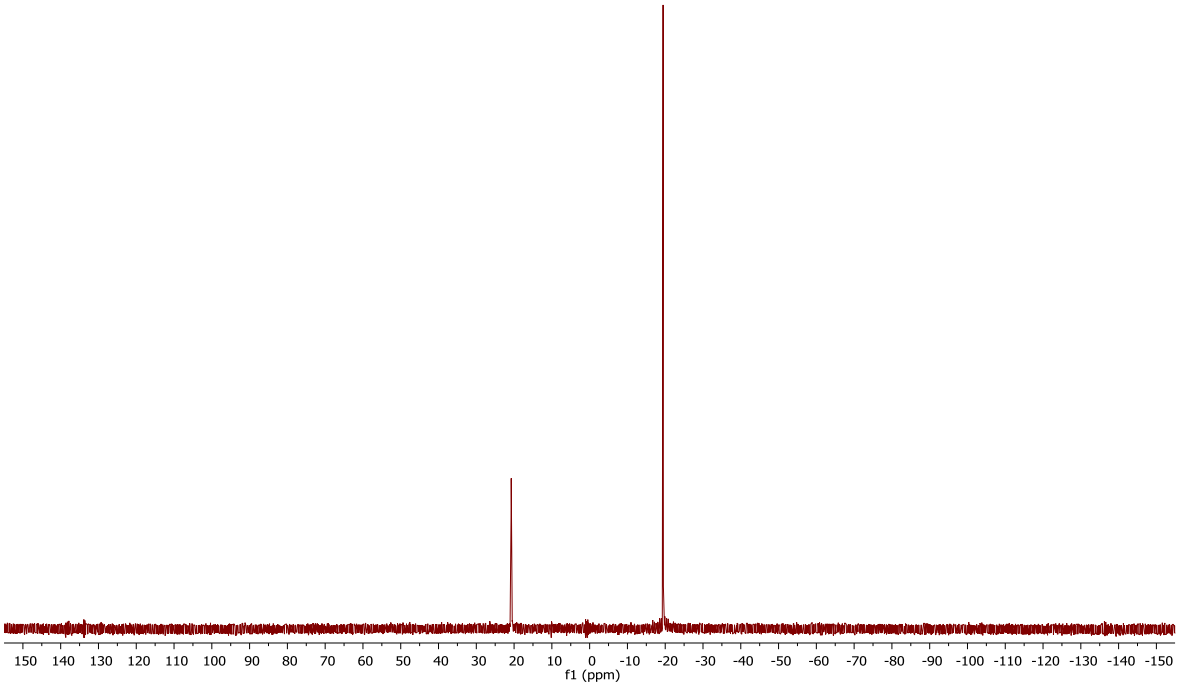

Figure S45. $^{31}P\{^{1}H\}$ NMR spectrum (162 MHz, $CDCl_3$) of **12**.

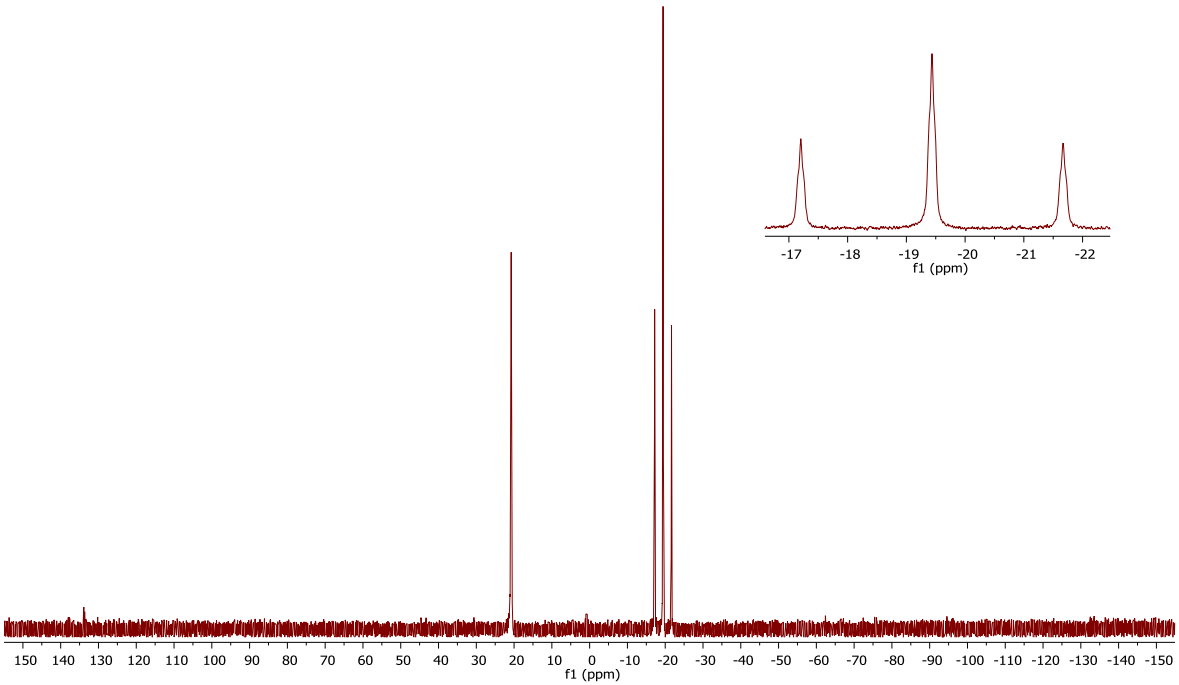

Figure S46. ^{31}P NMR spectrum (162 MHz, $CDCl_3$) of **12**.

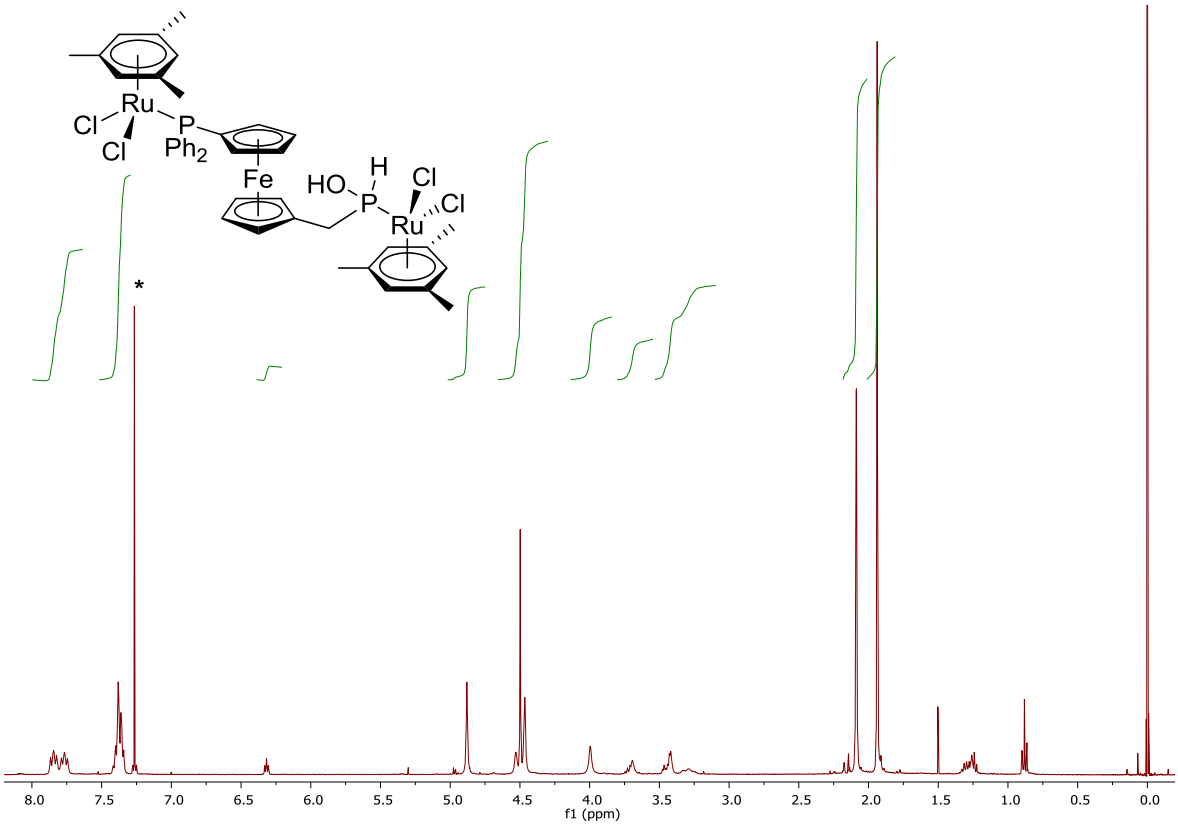

Figure S47. ^{1}H NMR spectrum (400 MHz, $CDCl_3$) of **13**.

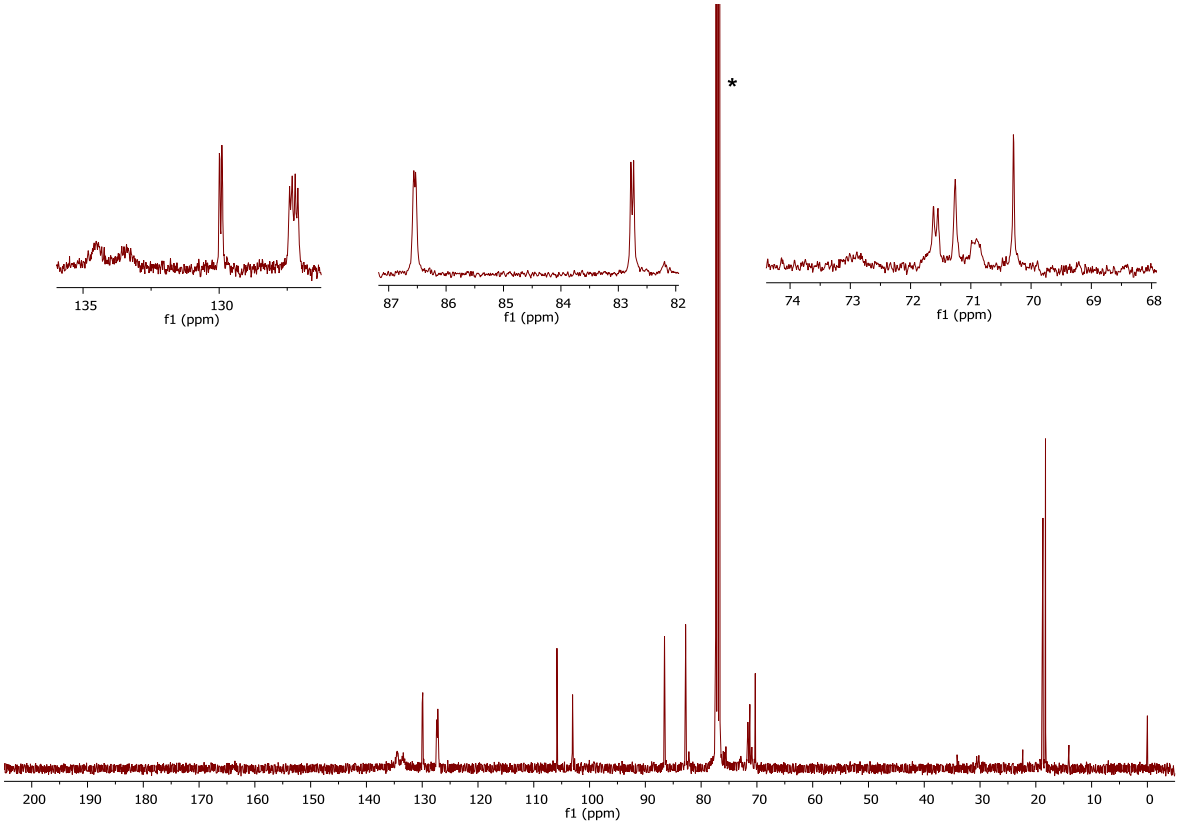

Figure S48. $^{13}C\{^{1}H\}$ NMR spectrum (101 MHz, $CDCl_3$) of **13**.

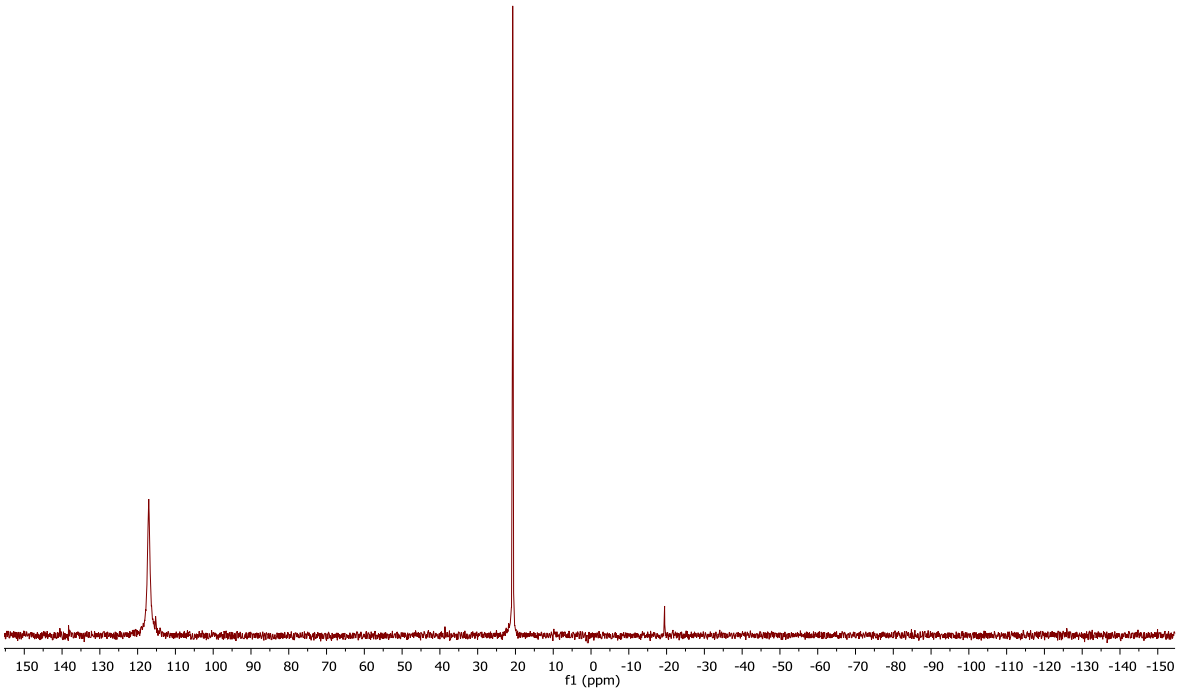

Figure S49. $^{31}P\{^{1}H\}$ NMR spectrum (162 MHz, $CDCl_3$) of **13**.

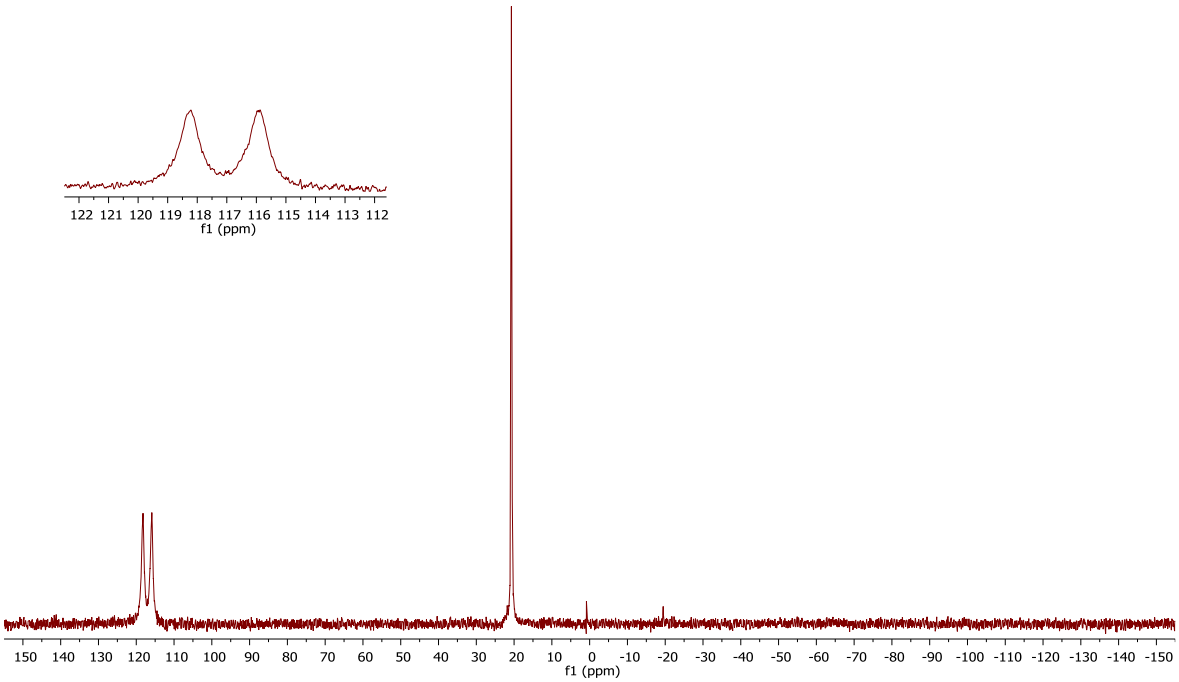

Figure S50. ^{31}P NMR spectrum (162 MHz, $CDCl_3$) of **13**.

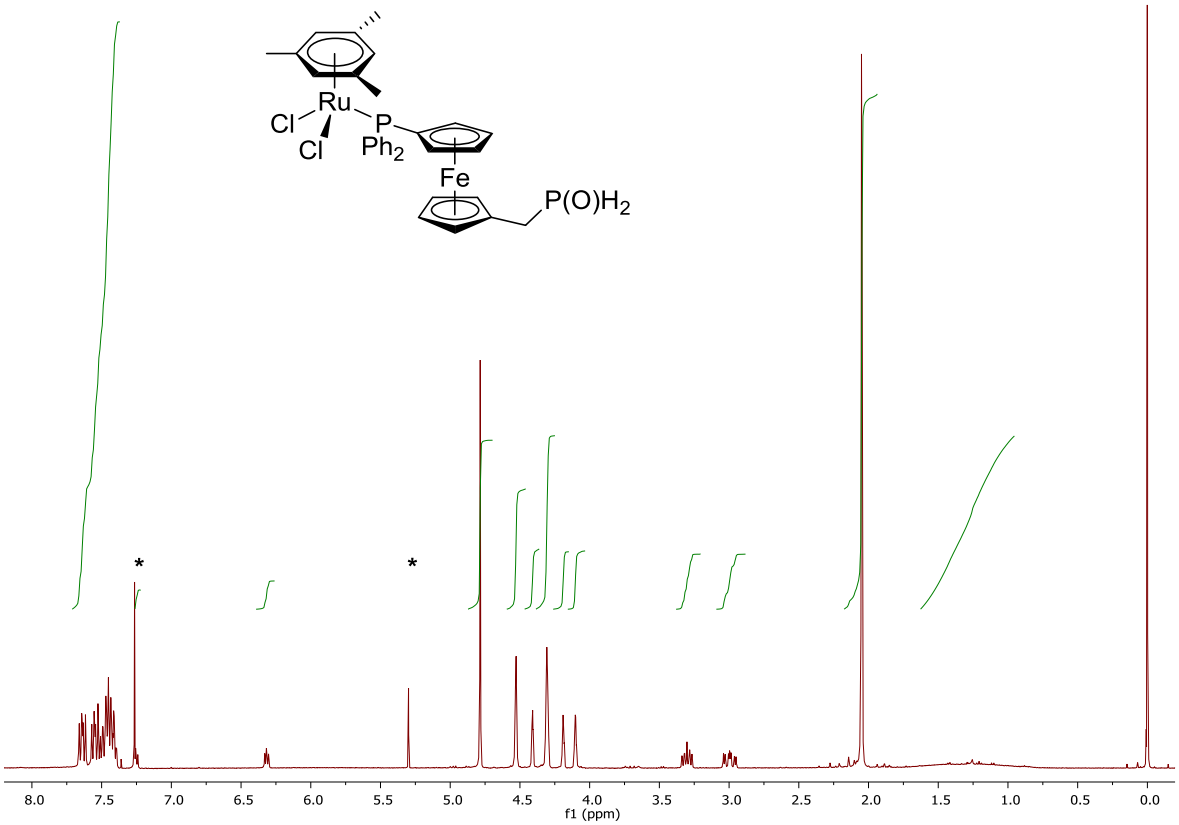

Figure S51. ^{1}H NMR spectrum (400 MHz, $CDCl_3$) of **14**.

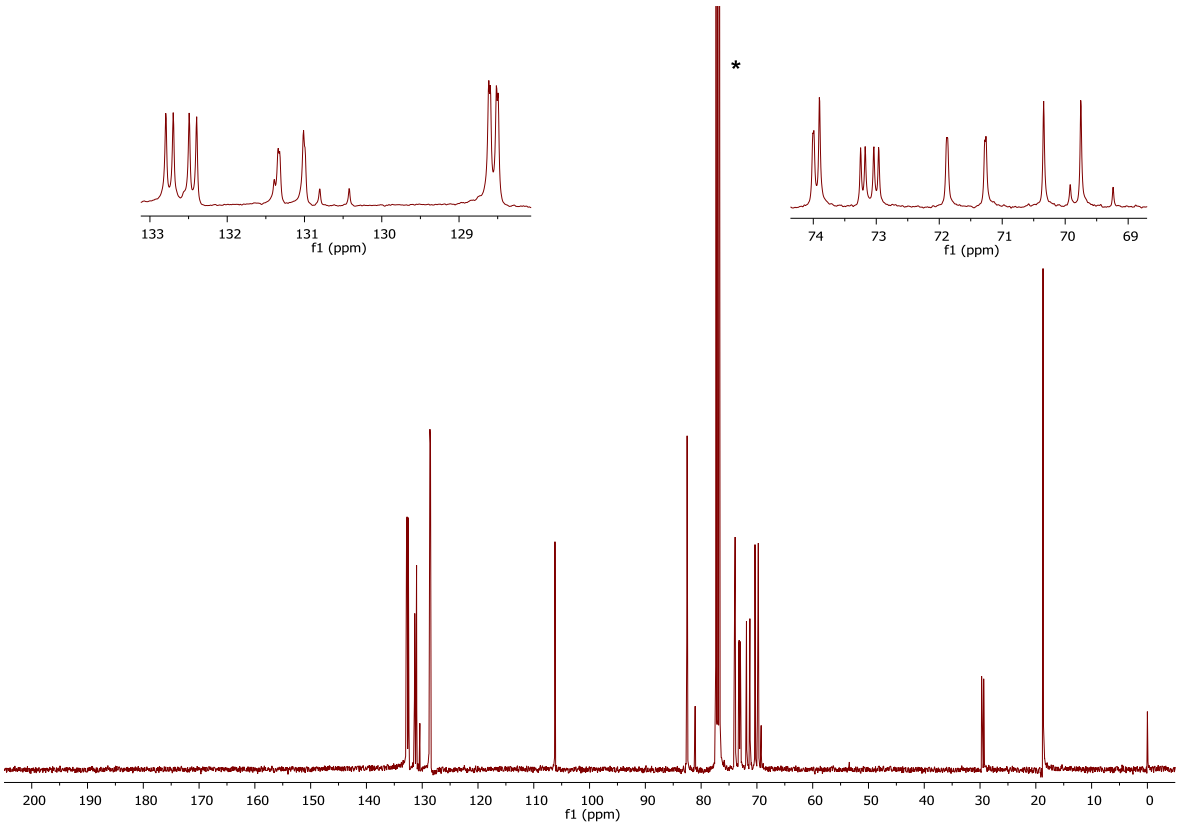

Figure S52. $^{13}C\{^{1}H\}$ NMR spectrum (101 MHz, $CDCl_3$) of **14**.

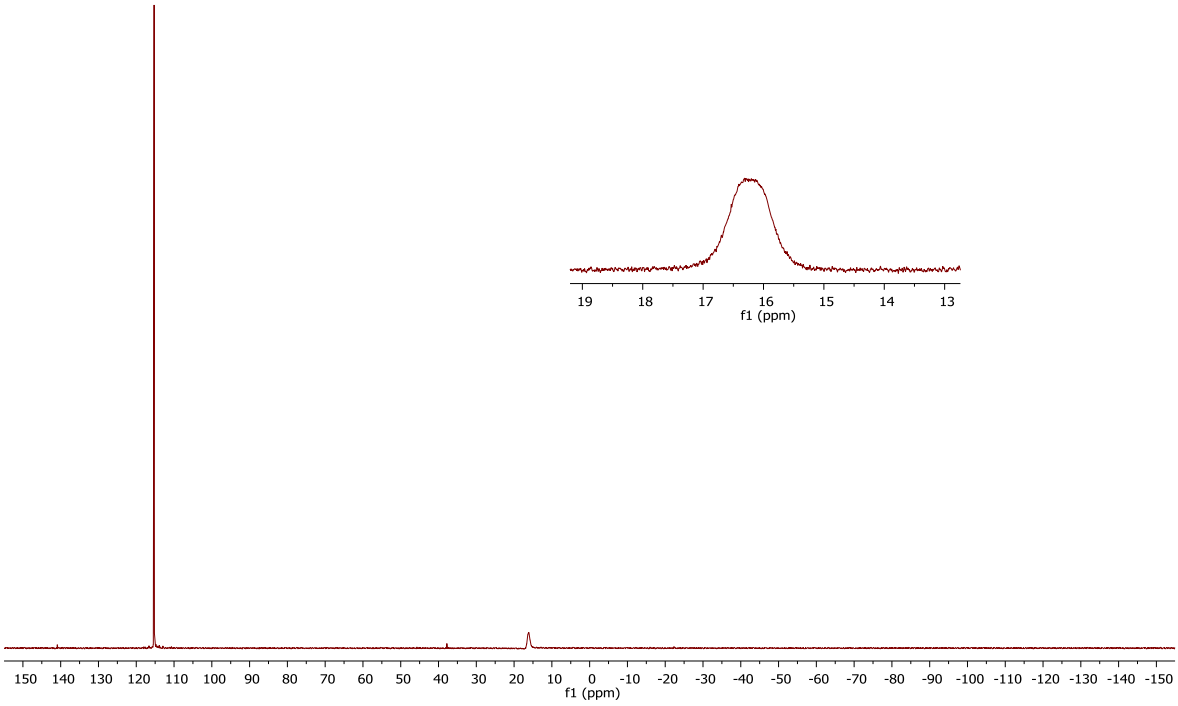

Figure S53. $^{31}P\{^{1}H\}$ NMR spectrum (162 MHz, $CDCl_3$) of **14**.

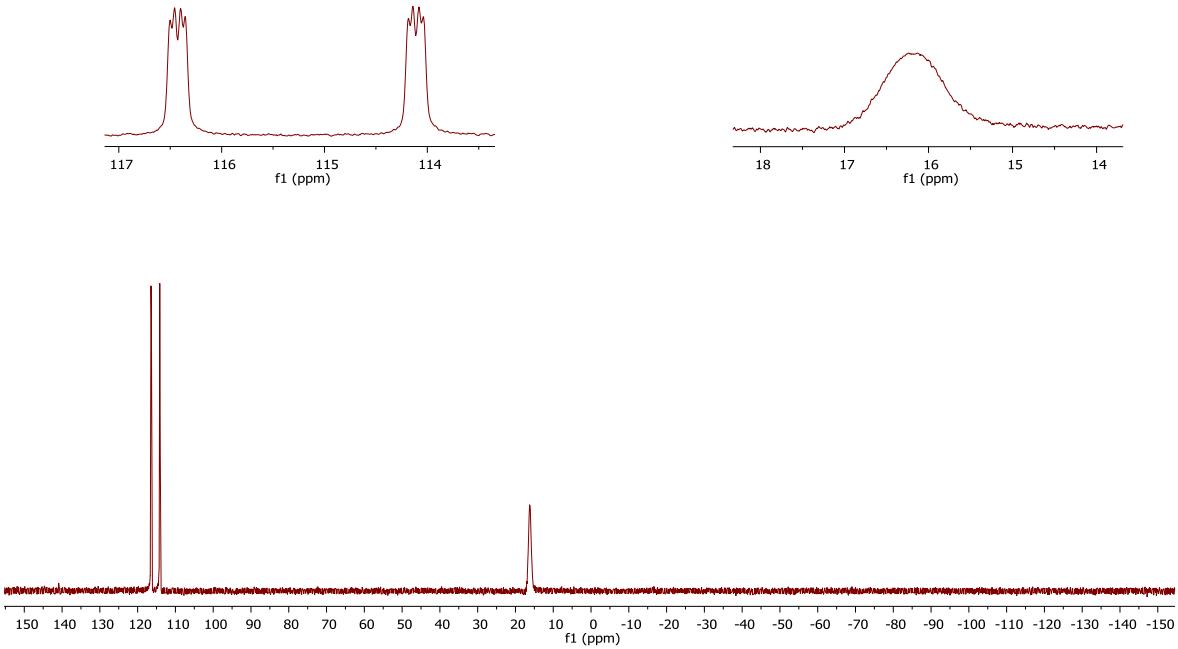

Figure S54. ^{31}P NMR spectrum (162 MHz, $CDCl_3$) of **14**.

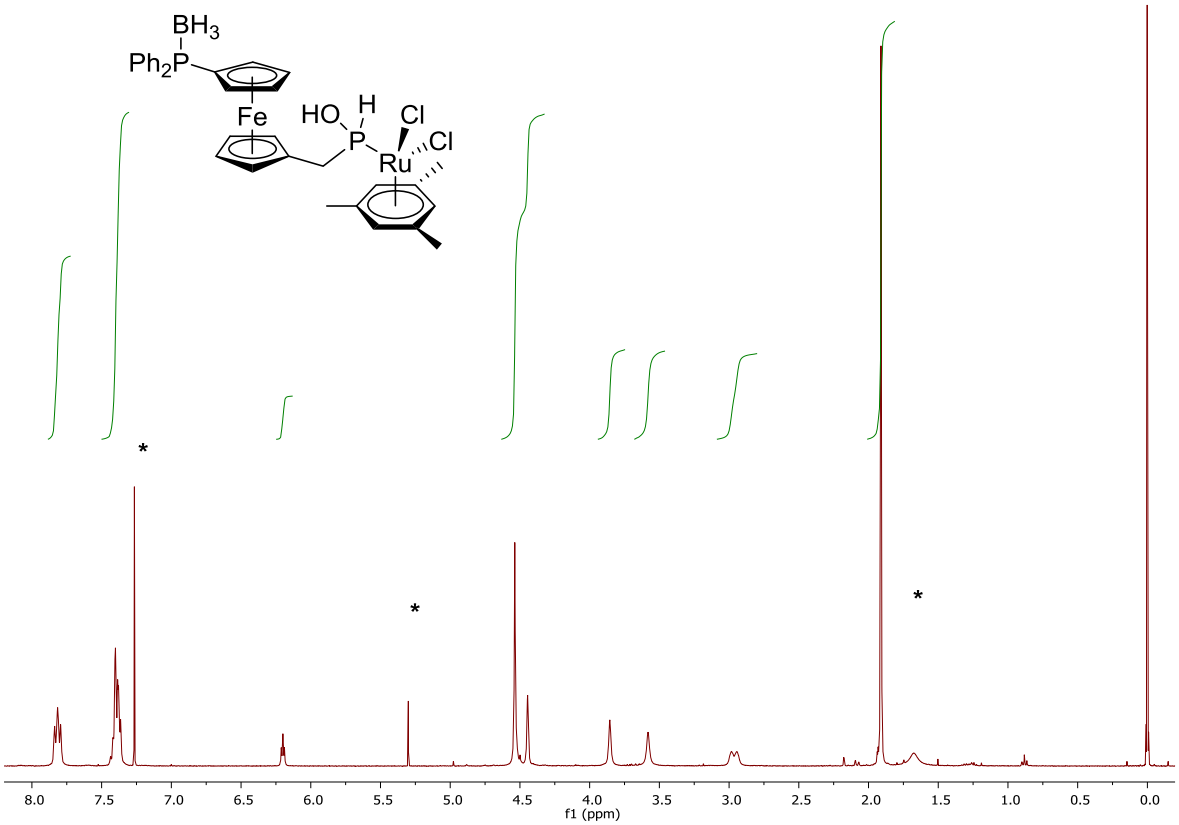

Figure S55. ^{1}H NMR spectrum (400 MHz, $CDCl_3$) of **15**.

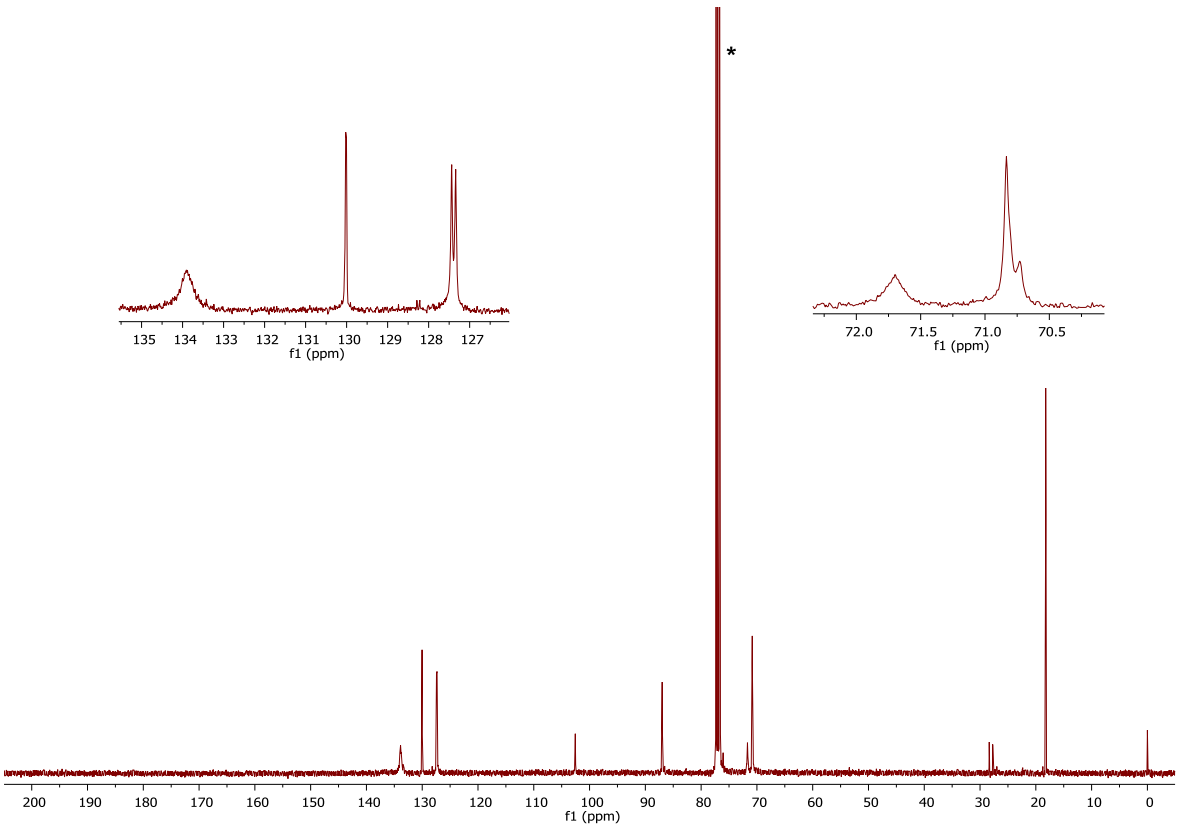

Figure S56. $^{13}C\{^{1}H\}$ NMR spectrum (101 MHz, $CDCl_3$) of **15**.

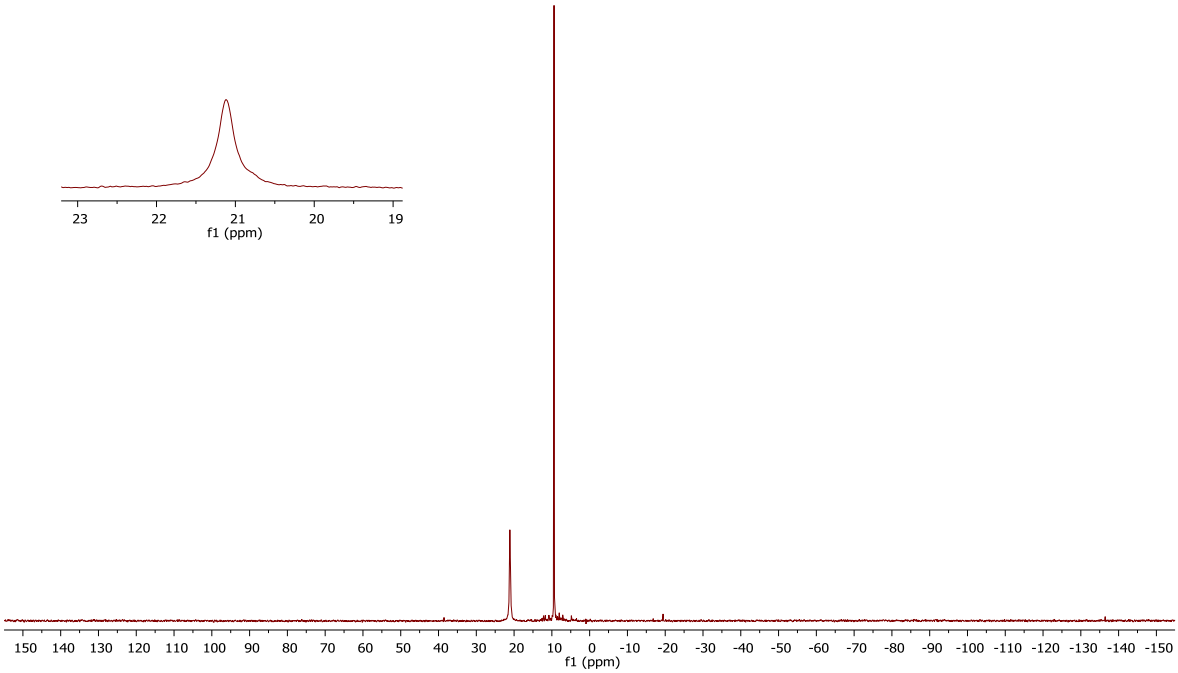

Figure S57. $^{31}P\{^{1}H\}$ NMR spectrum (162 MHz, $CDCl_3$) of **15**.

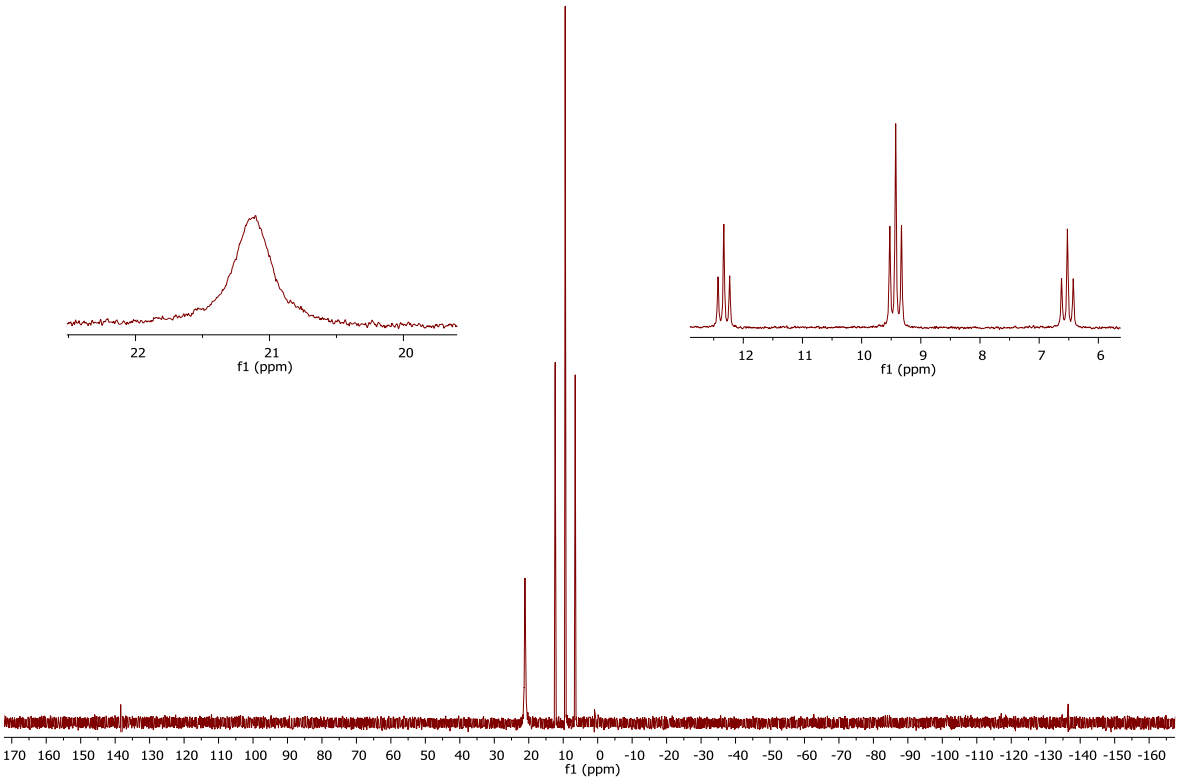

Figure S58. ^{31}P NMR spectrum (162 MHz, $CDCl_3$) of **15**.

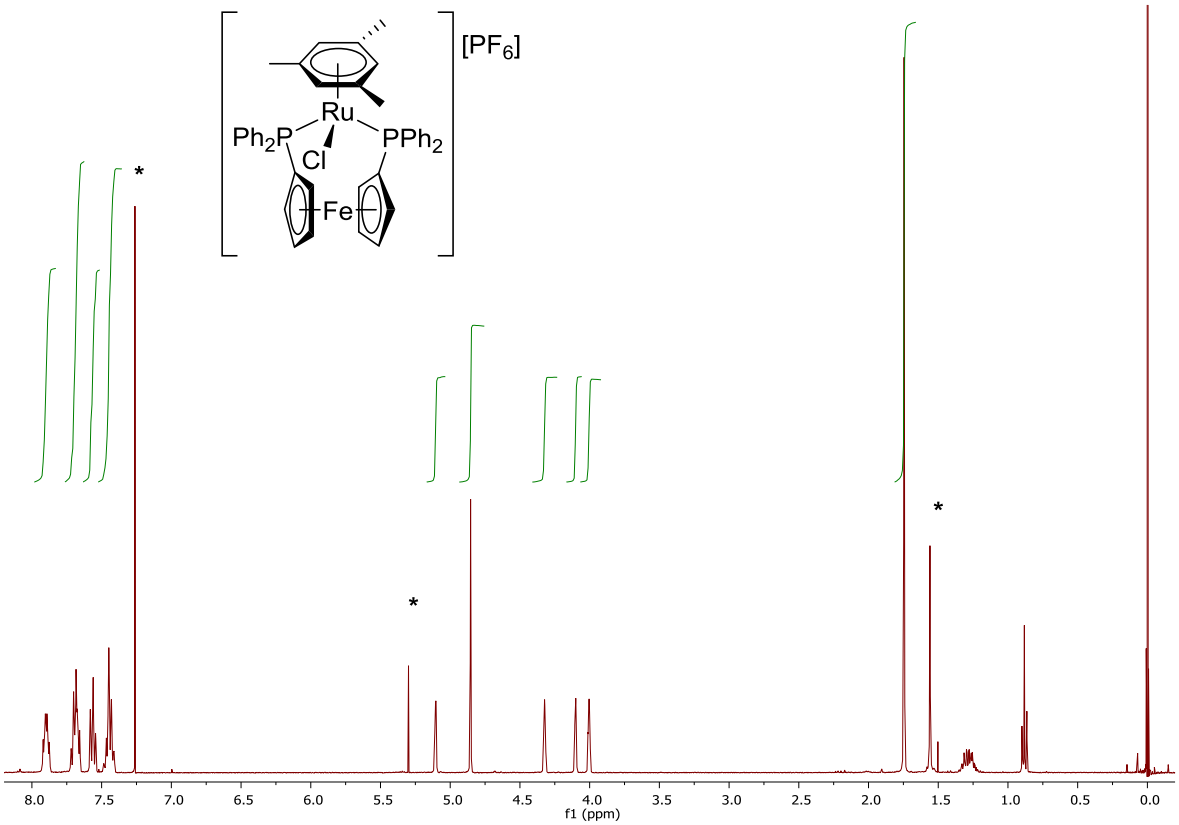

Figure S59. ^{1}H NMR spectrum (400 MHz, $CDCl_3$) of **16**.

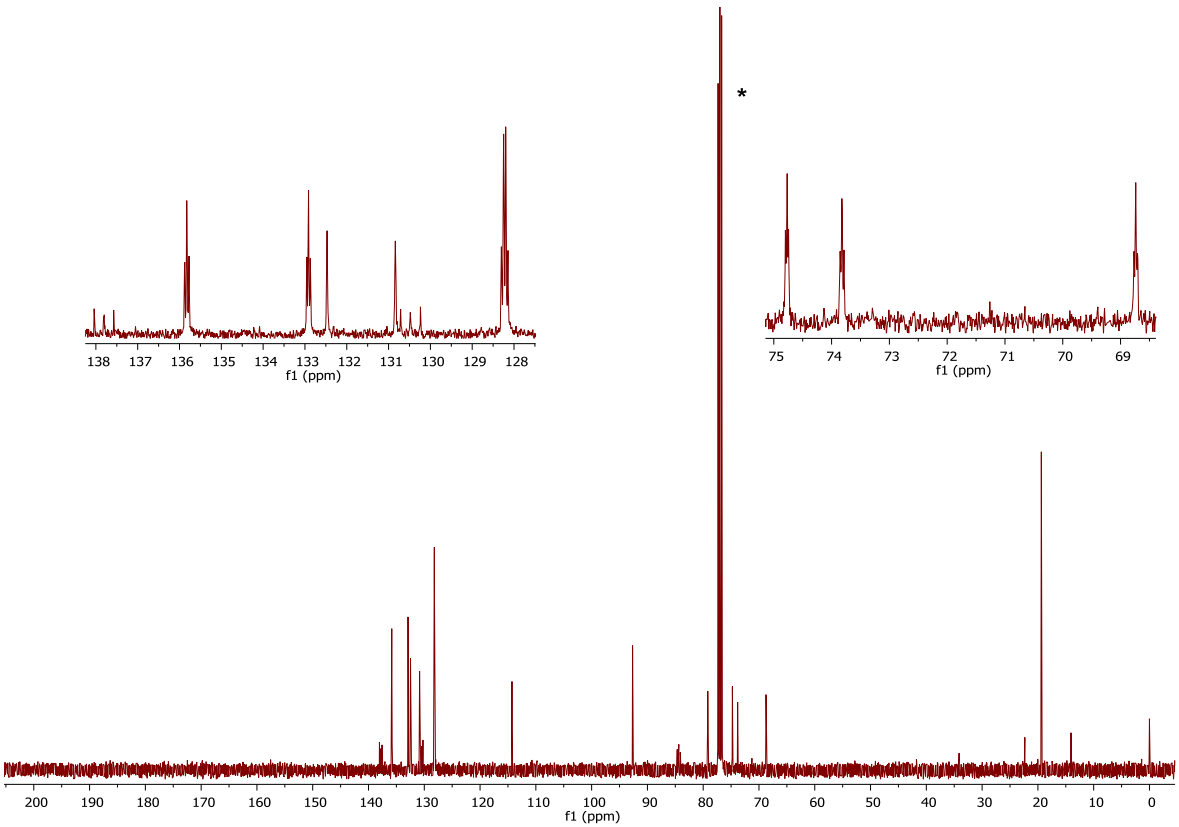

Figure S60. $^{13}C\{^{1}H\}$ NMR spectrum (101 MHz, $CDCl_3$) of **16**.

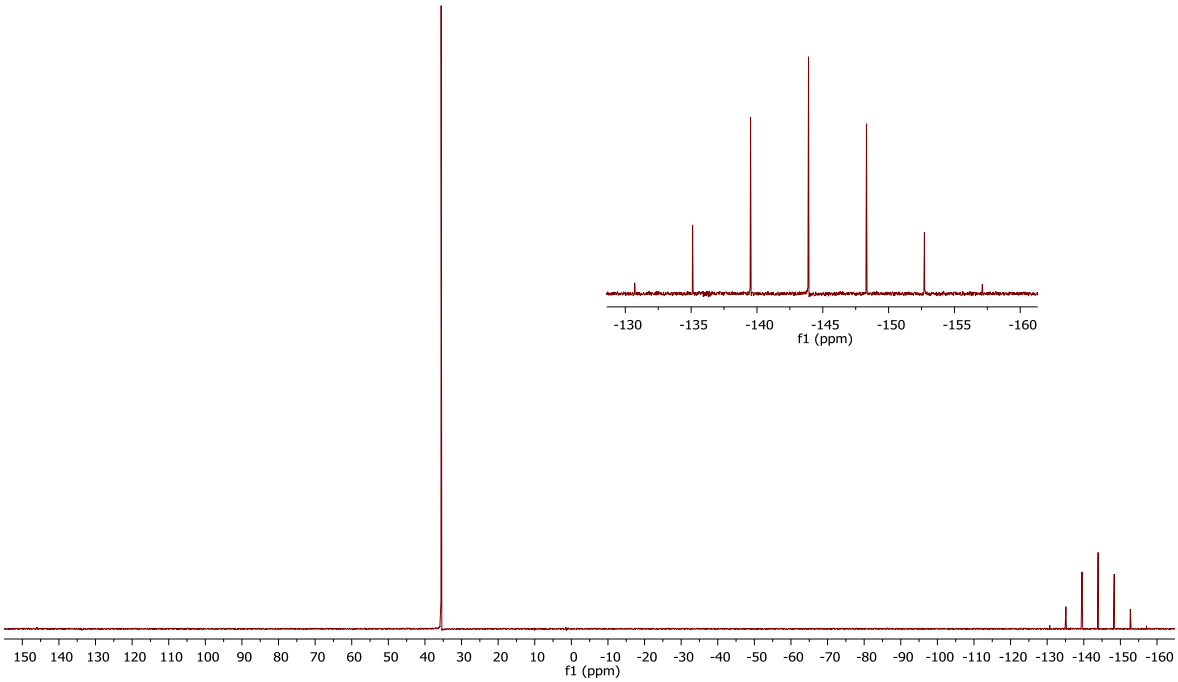

Figure S61. $^{31}P\{^{1}H\}$ NMR spectrum (162 MHz, $CDCl_3$) of **16**.

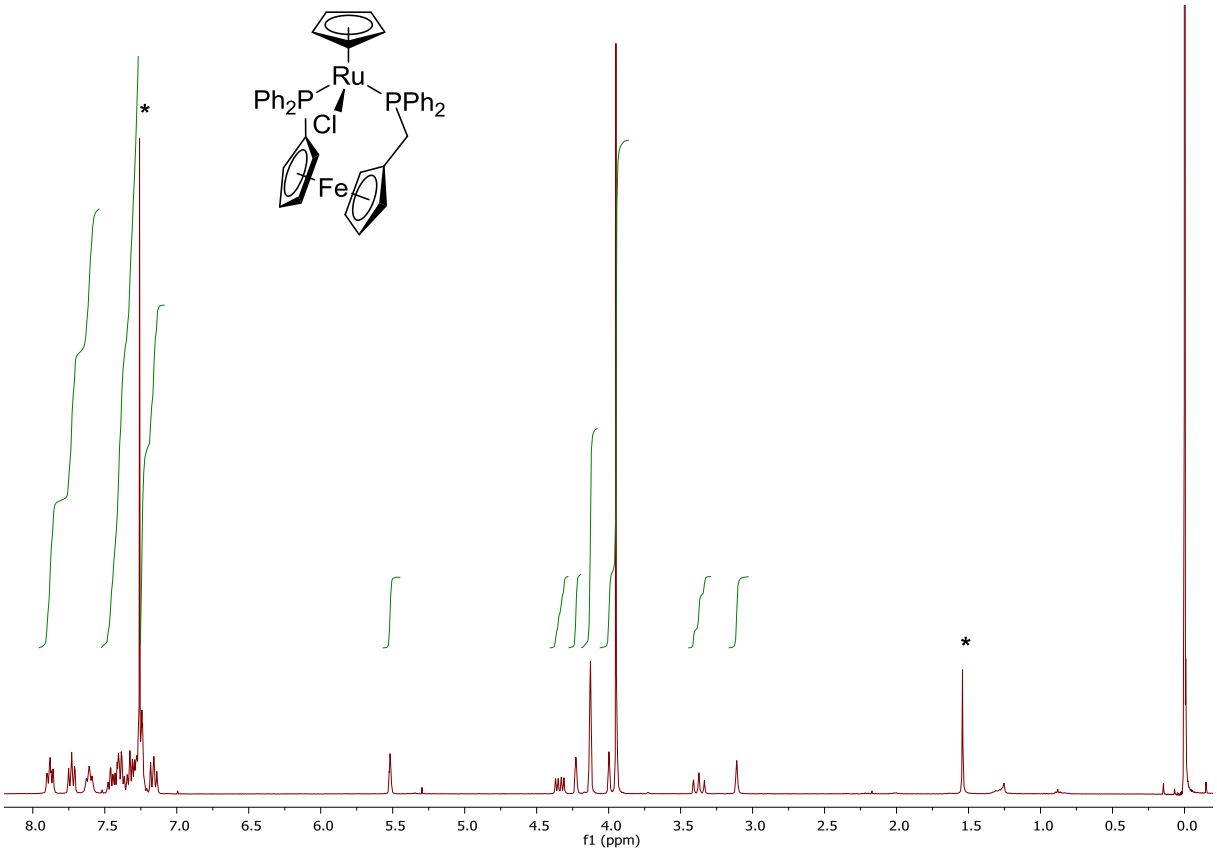

Figure S62. ^{1}H NMR spectrum (400 MHz, $CDCl_3$) of **18.**

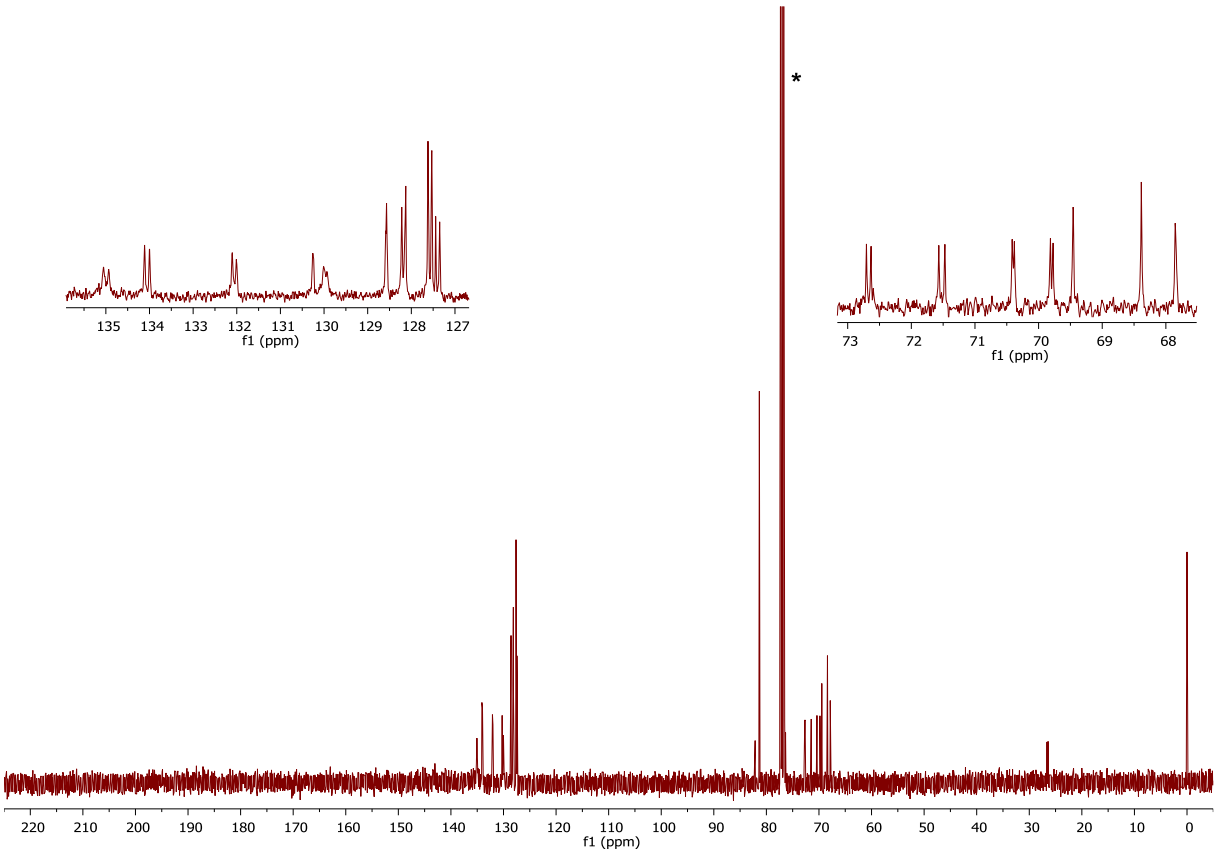

Figure S63. $^{13}C\{^{1}H\}$ NMR spectrum (101 MHz, $CDCl_3$) of **18**.

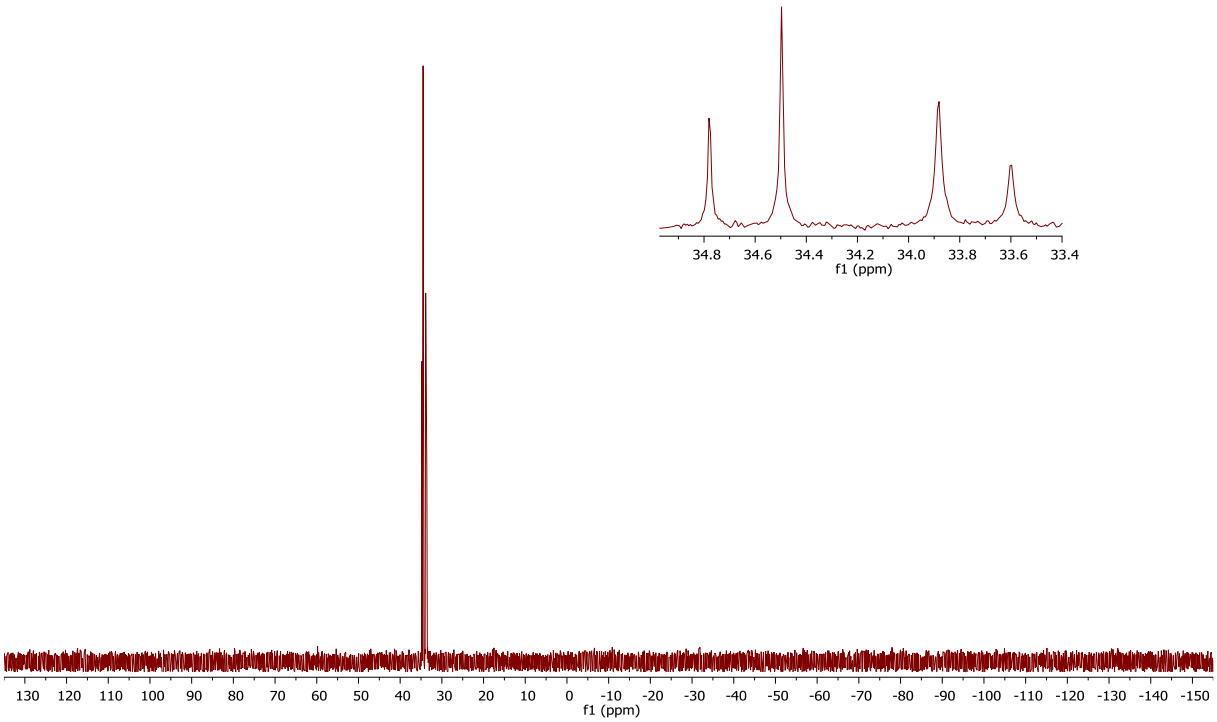

Figure S64. $^{31}P\{^{1}H\}$ NMR spectrum (162 MHz, $CDCl_3$) of **18**.

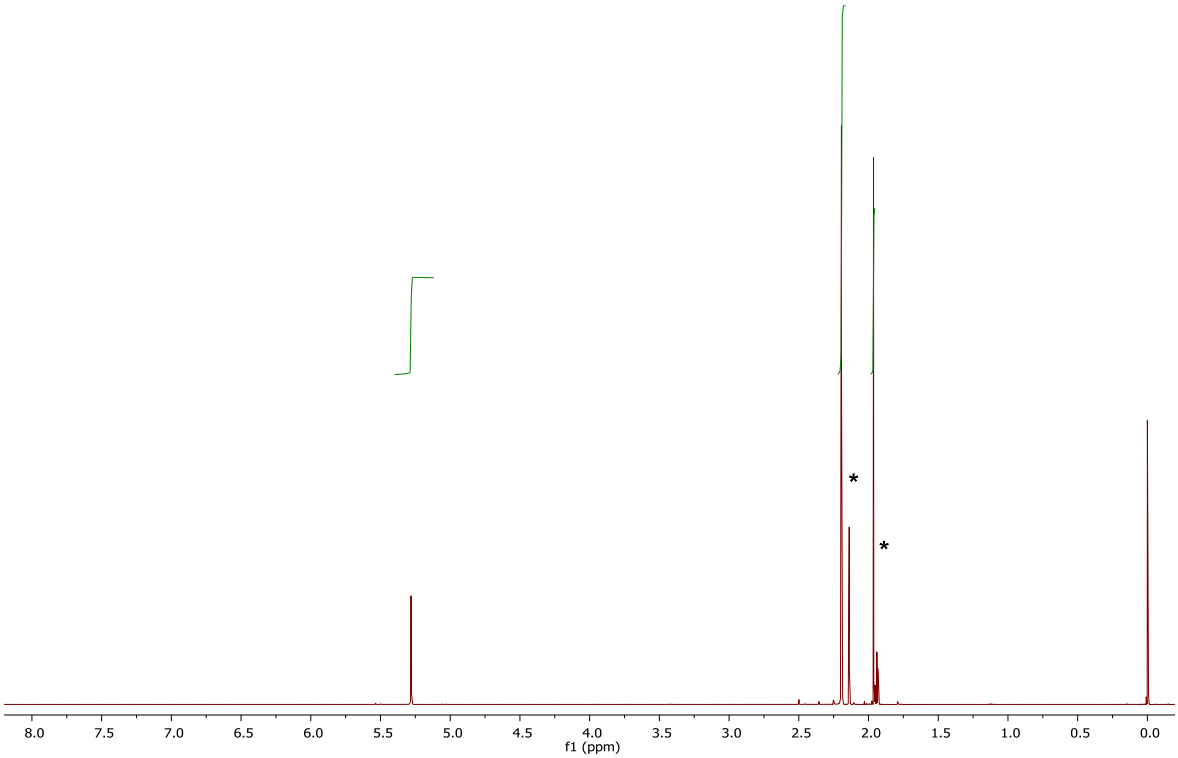

Figure S65. ^{1}H NMR spectrum (400 MHz, CD_3CN) of $[(\eta^6\text{-mesitylene})RuCl(MeCN)_3][PF_6]$.

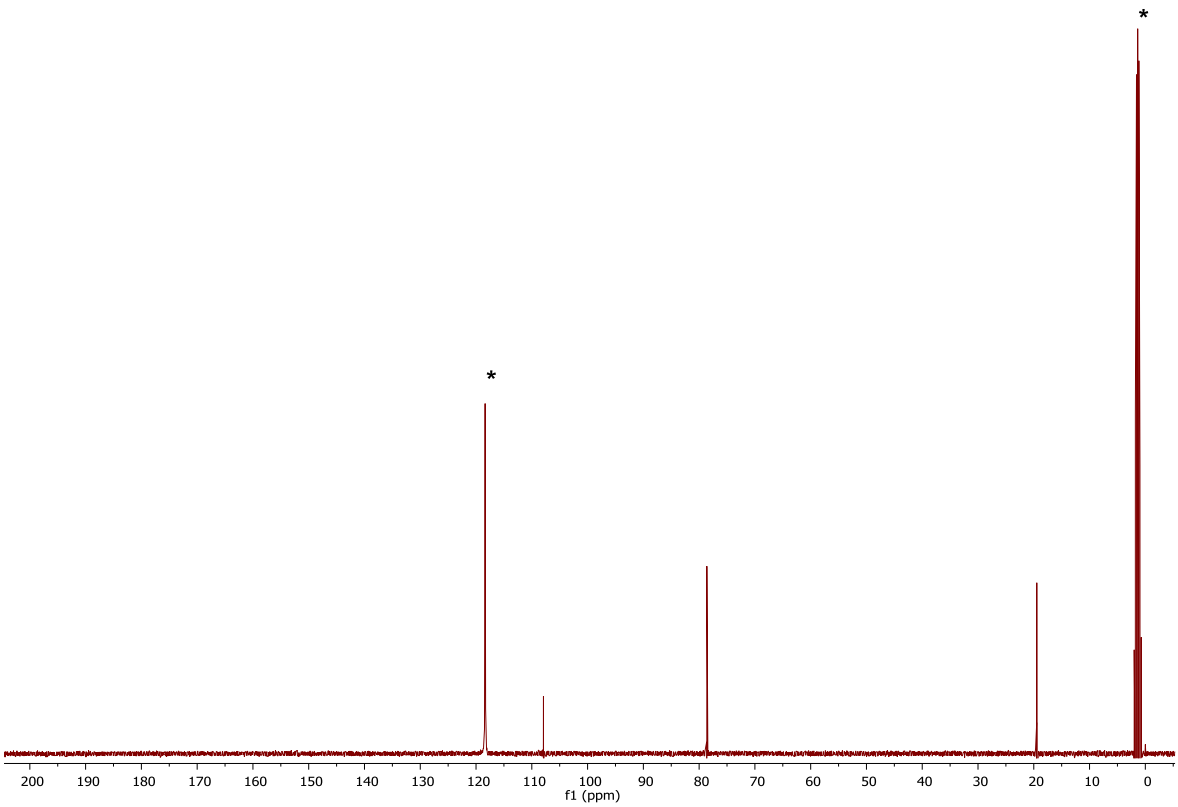

Figure S66. $^{13}C\{^{1}H\}$ NMR spectrum (101 MHz, CD_3CN) of $[(\eta^6\text{-mesitylene})RuCl(MeCN)_3][PF_6]$.

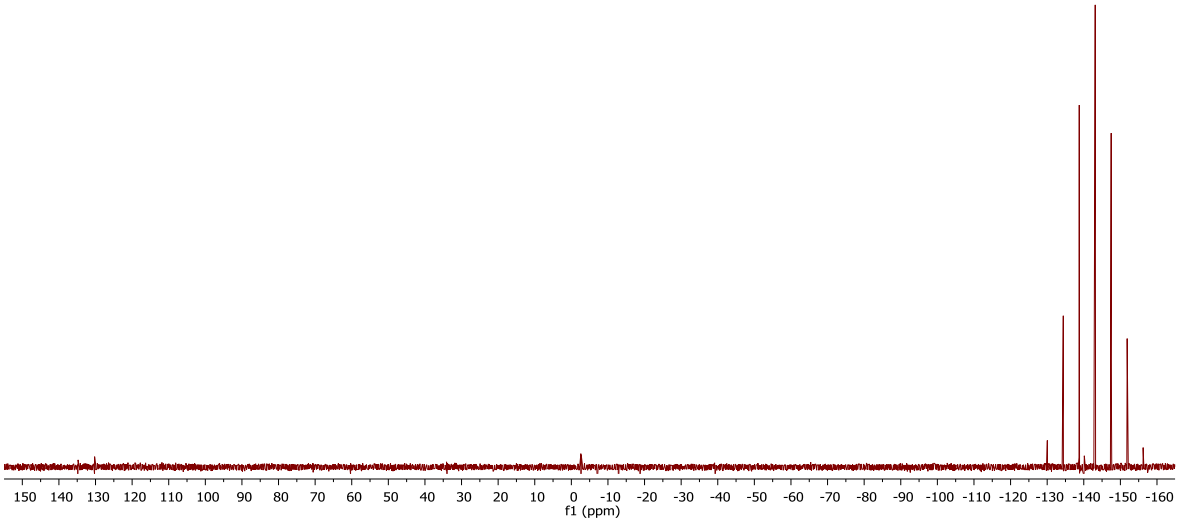

Figure S67. $^{31}P\{^{1}H\}$ NMR spectrum (162 MHz, CD_3CN) of $[(\eta^6\text{-mesitylene})RuCl(MeCN)_3][PF_6]$.

References

1. Azhar, M. R.; Bailey, P.; White, F. *CSD Private communication*, **2015**; refcode: OHOBEU.
2. Lu, X. L.; Vittal, J. J.; Tiekink, E. R. T.; Tan, G. K.; Kuan, S. L.; Goh, L. Y.; Hor, T. S. A. Comparative reactivity studies of dppf-containing $CpRu^{II}$ and $(C_6Me_6)Ru^{II}$ complexes towards different donor ligands (dppf = 1,1′-bis(diphenylphosphino)ferrocene). *J. Organomet. Chem.* **2004**, *689*, 1978-1990.
3. McCormick, F. B.; Cox, D. D.; Gleason, W. B. Synthesis, Structure, and Disproportionation of Labile $(\eta^6\text{-}C_6H_6)Ru(CH_3CN)_2Cl^+$ Salts. *Organometallics* **1993**, *12*, 610-612.
4. a) Brackemeyer, T.; Erker, G.; Fröhlich, R.; Prigge, J.; Peuchert, U. $Cp_3Zr(acetonitrile)^+$: Structure of an Electron-Rich Organometallic d^0-Cation. *Chem. Ber.* **1997**, *130*, 899-902; b) Enjalbert, R.; Gally, R. CH_3CN: X-ray structural investigation of a unique single crystal. $\beta \rightarrow \alpha$ phase transition and crystal structure. *Acta Crystallogr., Sect. B: Struct. Sci.* **2002**, *58*, 1005-1010.

Appendix B

Horký, F.; Císařová, I.; Štěpnička, P. A stable primary phosphane oxide and its heavier congeners. *Chem. Eur. J*. **2021**, *27*, 1282.

Chemistry A European Journal

Chemistry Europe
European Chemical Societies Publishing

Cover Feature:
P. Štěpnička et al.
A Stable Primary Phosphane Oxide and Its Heavier Congeners

4/2021

WILEY-VCH

Chemistry–A European Journal | Communication
doi.org/10.1002/chem.202003702

Phosphane Chemistry | *Hot Paper*

A Stable Primary Phosphane Oxide and Its Heavier Congeners

Filip Horký, Ivana Císařová, and Petr Štěpnička*[a]

Abstract: (Ferrocenylmethyl)phosphane (**1**) oxidation with hydrogen peroxide, elemental sulfur and grey selenium produced (ferrocenylmethyl)phosphane oxide **1O**, sulfide **1S** and selenide **1Se**, respectively, as the first *isolable* primary phosphane chalcogenides lacking steric protection. At elevated temperatures, compound **1O** disproportionated into **1** and (ferrocenylmethyl)phosphinic acid. In reactions with $[(\eta^6\text{-mes})RuCl_2]_2$, **1O** underwent tautomerization into a phosphane complex $[(\eta^6\text{-mes})RuCl_2\{FcCH_2PH(OH)\text{-}\kappa P\}]$, whereas **1S** and **1Se** lost their P-bound chalcogen atoms, giving rise to the phosphane complex $[(\eta^6\text{-mes})RuCl_2(FcCH_2PH_2\text{-}\kappa P)]$ (Fc = ferrocenyl, mes = mesitylene). No tautomerization was observed in the reaction of **1O** with $B(C_6F_5)_3$, which instead produced a Lewis pair $FcCH_2P(O)H_2\text{-}B(C_6F_5)_3$. Phosphane oxide **1O** added to C=O bonds of aldehydes and ketones and even to cumulenes PhNCE (E = O and S). However, both PH hydrogens were only employed in the reactions with aldehydes and cyanates.

Despite unrelenting research efforts, the chemistry of organophosphorus compounds still poses major challenges. For instance, although the long-sought air-stable and isolable primary phosphanes without substantial steric protection have been already reported,[1,2] the corresponding *primary* phosphane chalcogenides continue to elude chemists.[3,4] To the best of our knowledge, primary phosphane oxides have only been generated or postulated in reaction mixtures so far,[5] with the sole exception of the highly unstable *n*-octylphosphane oxide,[6] and their stable congeners with heavier chalcogen atoms have never been reported at all.[7] Yet, considering the remarkable influence of the ferrocenylmethyl group on the overall chemical stability[8] of the primary phosphane $FcCH_2PH_2$ (**1**; Fc = ferrocenyl),[9] we hypothesized that the corresponding phosphane oxide, $FcCH_2P(O)H_2$ (**1O**), could be stabilized and even isolated. Accordingly, in this contribution, we describe the isolation of the bench-stable primary phosphane oxide **1O**, the analogous phosphane sulfide (**1S**) and the first primary phosphane selenide (**1Se**).

For this purpose, the starting phosphane **1** was synthesized by an alternative, three-step procedure from ferrocene carboxaldehyde (see the Supporting Information). Subsequent oxidation of **1** with hydrogen peroxide (10 equiv of H_2O_2, methanol/CH_2Cl_2 at 0 °C for less than 10 min, 80% yield; Scheme 1) or with 3-chloroperoxybenzoic acid (MCPBA; 1 equiv in dichloromethane at 0 °C; 90% yield) cleanly and swiftly produced the phosphane oxide **1O**. This compound was isolated by a conventional chromatography as an air-stable, yellow solid with a characteristic though not intense smell of phosphane. Compound **1O** could be stored under ambient conditions but, upon heating to 100 °C in a solution, it disproportionated into **1** and (ferrocenylmethyl)phosphinic acid (**2**) (see Equation (1)):

$$2FcCH_2P(O)H_2\ (\mathbf{1O}) \rightarrow \mathbf{1} + FcCH_2PH(O)OH\ (\mathbf{2}) \qquad (1)$$

Acid **2** also formed when **1** was treated with an excess of MCPBA (2 equiv); similar over-oxidation with H_2O_2 was only noted over extended reaction times.

The synthesis of the corresponding phosphane sulfide **1S** was rather difficult due to the thermal sensitivity of **1S** (decomposition above 50 °C) and to its tendency to enter into follow-up reactions, producing mixtures of polythionated compounds. When using 10 equiv of sulfur (in benzene at 50 °C for 1 day), the reaction mixture contained 8% of the starting phosphane, 61% of **1S** and 31% of other unidentified products. From this mixture, nevertheless, **1S** could be isolated in a 30% yield as a yellow solid, which was stable under inert atmosphere but gradually decomposed when exposed to air. Thionation of **1** or **1O** with Lawesson reagent proceeded similarly. In contrast, **1Se** was obtained smoothly as the sole product of the reaction between **1** and grey selenium (1.5 equiv of Se in toluene at 50 °C overnight) and isolated in a 93% yield as a yellow, extremely malodorous solid. Under inert atmosphere, the compound could be stored practically indefinitely, albeit gradually converting into **1**, **2** and red selenium when exposed to air and moisture. Unlike its lighter congeners, **1Se** did not decompose when heated to 100 °C for 2 days (in CH_2Cl_2/hexane under argon), but failed to provide crystalline samples. Our attempts at chalcogenation of **1** with elemental tellurium under otherwise similar conditions failed, only producing some **2**.

[a] F. Horký, Dr. I. Císařová, Prof. Dr. P. Štěpnička
Department of Inorganic Chemistry, Faculty of Science, Charles University
Hlavova 2030, 128 40 Prague (Czech Republic)
E-mail: petr.stepnicka@natur.cuni.cz
Supporting information and the ORCID identification numbers for the authors of this article can be found under: https://doi.org/10.1002/chem.202003702.

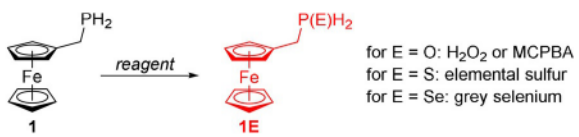

Scheme 1. Synthesis of P-chalcogenides **1E**.

Compounds **1O**, **1S** and **1Se** are reluctant to crystallize, and their formulation was thus mostly based on spectroscopic methods. In their ^{31}P NMR spectra, they displayed triplets of triplets due to interactions of the phosphorus atom with two directly bonded hydrogen atoms and with the protons of the adjacent CH_2 group. In proton-decoupled spectra, these signals collapsed into singlets (for parameters, see Table S5). The presence of PH hydrogens was also indicated by ^{1}H NMR spectra, showing a doublet of triplets resulting from their interaction with ^{31}P and with the methylene protons. The spectra of **1Se** further contained characteristic ^{77}Se satellites (Figure 1). The $^{1}J_{PSe}$ coupling constant (733 Hz) of **1Se** was larger than that of the tertiary phosphane selenide $FcCH_2P(Se)Ph_2$ (728 Hz), hence suggesting that the basicity of **1** is lower than that of $FcCH_2PPh_2$.[10]

Notably, no signs of phosphinous acid tautomer were observed in the NMR spectra of **1O** recorded in common deuterated solvents (even after adding 1,8-bis(dimethylamino)naphthalene as a proton scavenger). Nonetheless, a facile tautomerization[11] occurred during the reaction of **1O** with $[(\eta^6\text{-mesitylene})RuCl(\mu\text{-}Cl)]_2$, producing complex **3** as the sole product (Scheme 2).[12] Unexpectedly, similar reactions with **1S** and **1Se** took an different course, with the elimination of the P-bound chalcogen atom and the formation of complex **4**, which was alternatively obtained by conventional cleavage of the Ru^{II} precursor with a stoichiometric amount of phosphane **1**.

The ^{31}P NMR signatures of compounds **3** and **4** markedly differed in the magnitude of the upfield-shift and fine structure according to the substitution at the phosphorus atom [**3**: δ_P 115.0 (ddt, $^{1}J_{PH}=110$ Hz, $^{2}J_{PH}=15$ and 6 Hz), **4**: δ_P −24.0 (tt, $^{1}J_{PH}=355$ Hz, $^{2}J_{PH}=8$ Hz)]. Both complexes were unequivocally authenticated by X-ray diffraction analysis (see the Supporting Information).

In a reaction with ZnI_2, **1O** produced a phosphine oxide complex, compound **5** (Scheme 3). Although the solution NMR spectra indicated that **1O** was coordinated to Zn^{II} ions, they also suggested fluxional nature of the species formed in this reaction, corresponding with the rather weak (predominantly electrostatic) interaction of the O-donor ligand **1O** with the hard Lewis acid Zn^{II}.

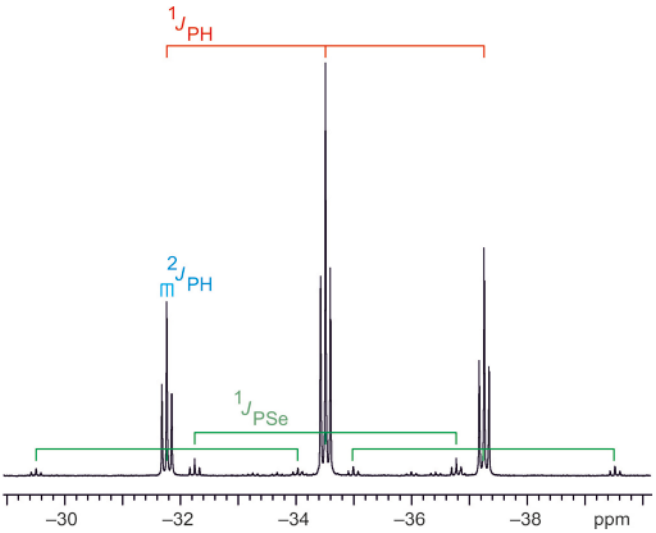

Figure 1. ^{31}P NMR spectrum of **1Se** (162 MHz, $CDCl_3$).

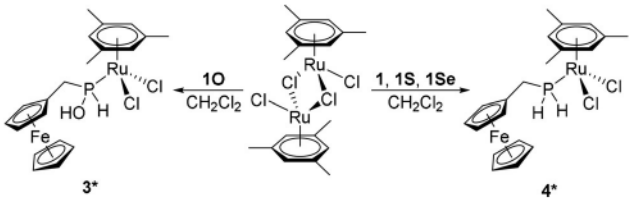

Scheme 2. Reactions of $[(\eta^6\text{-mesitylene})RuCl(\mu\text{-}Cl)]_2$ with **1E** (the asterisk indicates that the crystal structure was determined; see the Supporting Information).

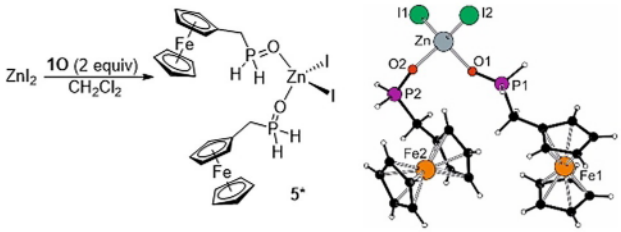

Scheme 3. Reaction of **1O** with ZnI_2 (left) and the crystal structure of complex **5** (right; for details, see the Supporting Information).

Already during the initial experiments, we noted that phosphane oxide **1O** adds across the C=O bond of the solvent when performing the oxidation of **1** by H_2O_2 in acetone. In this respect, **1O** is more reactive than its parent phosphane. This result led us to investigate addition reactions of **1O** in more detail (Scheme 4).

Thus, in a clean reaction of compound **1O** with acetaldehyde and benzaldehyde, the respective products of two-fold addition, **6a** and **6b**,[7a] were formed as a mixture of three diastereoisomers in a statistical 1:2:1 ratio. These isomers differed in the configuration at the two stereogenic carbon centres and at the phosphorus atom (for a detailed discussion and crystal structures, see the Supporting Information). Conversely, the reaction with ketones only led to the monoaddition products **7**, even when using an excess of the carbonyl compound.[7a] Of these compounds, only **7a** resulting from **1O** and acetone could be isolated in pure form. The more sterically congested

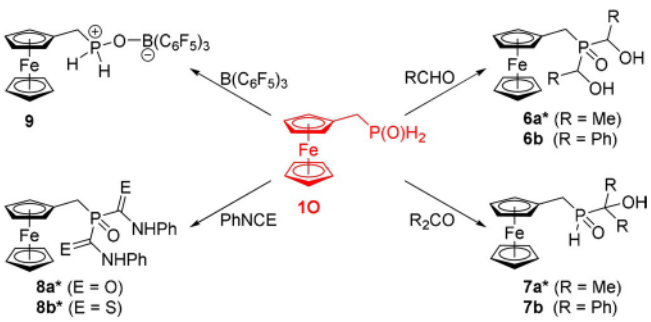

Scheme 4. Reactions of **1O** (asterisk indicates that the crystal structure was determined; for details, see the Supporting Information).

compound **7b** was in equilibrium with the starting materials,[13] which precluded its isolation by chromatography or crystallization because **1O** and Ph_2CO were partly regenerated during the purification. Lastly, in the reaction of the phosphane oxide **1O** with phenyl isocyanate[14] and isothiocyanate, the respective phosphabiurets **8a** and **8b** were formed in good yields.[15] In contrast, when treated with neat 4-ethynyltoluene (80 °C/overnight), **1O** disproportionated into a mixture of **1** and **2** (vide supra) rather than adding to the alkyne triple bond, as expected for secondary phosphane oxides.[16]

Considering the possibility of tautomerization, we also investigated the interaction of **1O** with borane and tris(pentafluorophenyl)borane. Similarly to diphenylphosphane oxide,[17] when mixing **1O** with $B(C_6F_5)_3$, a bipolar Lewis pair $FcCH_2P^{(+)}(O)H_2$-$B^{(-)}(C_6F_5)_3$ (**9**) formed instead of the „conventional" Lewis adduct $FcCH_2PH(OH)\cdot B(C_6F_5)_3$. Although **9** readily decomposed and could not be crystallized, its formulation was unambiguously established from the spectroscopic data. Specifically, the signal observed in the $^{31}P\{^1H\}$ NMR spectrum of **9** was observed at a position close to that of complex **5** (δ_P 17.8) and was split into a septet by a scalar interaction with six fluorine atoms of $B(C_6F_5)_3$ in *ortho* positions. The non-decoupled ^{31}P NMR and ^1H NMR spectra confirmed the presence of two equivalent hydrogen atoms at phosphorus, whereas the position of the ^{11}B NMR resonance (δ_B 0.7) corresponded with that reported for the similar adduct resulting from $Ph_2P(O)H$.[17a] In contrast, BH_3 (1 equiv of THF solution) addition to **1O** produced a complex mixture. ^{31}P NMR analysis allowed us to identify the parent phosphane **1** as the dominant product, in addition to unreacted **1O**, adducts $1\cdot BH_3$ and $FcCH_2PH(OH)\cdot BH_3$ and some unidentified minor by-products (see the Supporting Information).

In summary, we reported the synthesis of the first bench-stable phosphane oxide. Although this compound can be conveniently synthesized, purified by chromatography and stored under ambient conditions without precautions, it retains the reactivity typical of phosphane oxides. Together with the corresponding phosphane sulfide and selenide, these compounds are the first isolable primary phosphane chalcogenides with a conventional albeit somewhat exotic „organic" substituent at the phosphorus atom.[18] With their parent compound **1**, they form a unique family of homologous compounds with a high potential for comparative studies. The first results from such studies are also presented herein. Although no signs of phosphinous acid tautomer were detected in solutions of **1O**, the phosphane oxide undergoes facile tautomerization upon coordination to a soft metal ion but binds to relatively harder metal ions in its native P-oxide form. This P-oxide form also seems to be the active species in additions of **1O** to various unsaturated systems.

Acknowledgements

We acknowledge the support from the Grant Agency of Charles University (project no. 920119) and from the Charles University Research Centre program (project UNCE/SCI/014).

Conflict of interest

The authors declare no conflict of interest.

Keywords: metallocenes · phosphanes · primary phosphane chalcogenides · structure elucidation · synthesis

[1] a) M. Brynda, *Coord. Chem. Rev.* **2005**, *249*, 2013–2034; b) J. T. Fleming, L. J. Higham, *Coord. Chem. Rev.* **2015**, *297–298*, 127–145.
[2] For a sterically shielded, primary phosphane oxide and sulfide, see: M. Yoshifuji, K. Shibayama, K. Toyota, N. Inamoto, *Tetrahedron Lett.* **1983**, *24*, 4227–4228.
[3] a) L. D. Quin, *A Guide to Organophosphorus Chemistry*, Wiley-Interscience, New York, **2000**, pp. 95–113.
[4] By contrast, the more stable *secondary* phosphane oxides found attractive applications as ligands for catalysis: a) L. Ackermann, *Synthesis* **2000**, 1557–1571; b) T. M. Shaikh, C.-M. Weng, F.-E. Hong, *Coord. Chem. Rev.* **2012**, *256*, 771–803; c) A. Gallen, A. Riera, X. Verdauger, A. Grabulosa, *Catal. Sci. Technol.* **2019**, *9*, 5504–5561.
[5] a) S. A. Buckler, M. Epstein, *Tetrahedron* **1962**, *18*, 1211–1219; b) B. Pellerin, P. Guenot, J.-M. Denis, *Tetrahedron Lett.* **1987**, *28*, 5811–5814; c) M. Scherer, D. Stein, F. Breher, J. Geier, H. Schönberg, H. Grützmacher, *Z. Anorg. Allg. Chem.* **2005**, *631*, 2770–2774; d) E. V. Gorbachuk, E. K. Badeeva, S. A. Katsyuba, P. O. Pavlov, K. R. Khayarov, O. G. Sinyashin, D. G. Yakhvarov, *Phosphorus Sulfur Silicon Relat. Elem.* **2016**, *191*, 1480–1481; e) M. A. Gunawan, O. Moncea, D. Poinsot, M. Keskes, B. Domenichini, O. Heintz, R. Chassagnon, F. Herbst, R. M. K. Carlson, J. E. P. Dahl, A. A. Fokin, P. R. Schreiner, J.-C. Hierso, *Adv. Funct. Mater.* **2018**, *28*, 1705786; f) O. Moncea, D. Poinsot, A. A. Fokin, P. R. Schreiner, J.-C. Hierso, *ChemPlusChem* **2018**, *83*, 2915–2922; g) American Cyanamid Company, *Organic Phosphine Oxides and Method of Preparing Same*, GB Patent 912269A, 1960.
[6] S. A. Buckler, M. Epstein, *Tetrahedron* **1962**, *18*, 1221–1230.
[7] a) F. Uhlig, E. Herrmann, D. Schädler, G. Ohms, G. Grossmann, S. Besser, R. Herbst-Irmer, *Z. Anorg. Allg. Chem.* **1993**, *619*, 1962–1970; b) S. Stadlbauer, A. Torvisco, F. Uhlig, *Phosphorus, Sulfur, Silicon, Relat. Elem.* **2014**, *189*, 1084–1093.
[8] B. Stewart, A. Harriman, L. J. Higham, *Organometallics* **2011**, *30*, 5338–5343.
[9] N. J. Goodwin, W. Henderson, B. K. Nicholson, *Chem. Commun.* **1997**, 31–32.
[10] a) C. A. Tolman, *Chem. Rev.* **1977**, *77*, 313–348; b) U. Beckmann, D. Süslüyan, P. C. Kunz, *Phosphorus Sulfur Silicon Relat. Elem.* **2011**, *186*, 2061–2070.
[11] a) B. G. Janesko, H. C. Fisher, M. J. Brindle, J.-L. Montchamp, *J. Org. Chem.* **2015**, *80*, 10025–10032; b) D. Vincze, P. Ábrányi-Balogh, P. Bagi, G. Kegevich, *Molecules* **2019**, *24*, 3859. For a similar reaction of in situ generated $H_3P{=}O$, see: c) D. Yakhvarov, M. Caporali, L. Gonsalvi, S. Latypov, V. Mirabello, I. Rizvanov, O. Sinyashin, P. Stoppioni, M. Peruzzini, *Angew. Chem. Int. Ed.* **2011**, *50*, 5370–5373; *Angew. Chem.* **2011**, *123*, 5482–5485.
[12] a) R. Krafczyk, H. Thönnessen, P. G. Jones, R. Schmutzler, *J. Fluorine Chem.* **1997**, *83*, 159–166; b) S. M. M. Knapp, T. J. Sherbow, R. B. Yelle, J. J. Juliette, D. R. Tyler, *Organometallics* **2013**, *32*, 3744–3752; c) L. V. Graux, M. Giorgi, G. Buono, H. Clavier, *Dalton Trans.* **2016**, *45*, 6491–6502.
[13] M. Y. Dvorko, T. E. Glotova, I. A. Ushakov, N. K. Gusarova, *Russ. J. Org. Chem.* **2010**, *46*, 485–490.
[14] The reaction of **1O** with PhNCO required the presence of a base catalyst (5 mol.% dabco) and stepwise addition of the isocyanate to avoid the formation of a 1:1 addition product. See ref. [7a].
[15] D. H. M. W. Thewissen, H. P. M. M. Ambrosius, *Rec. Trav. Chim. Pays-Bas* **1980**, *99*, 344–345 and references cited therein.
[16] A. C. Gaumont, M. Gulea, *Science of Synthesis Vol. 33* (Ed.: G. A. Molander), Thieme, Stuttgart, **2006**, pp. 701–710.
[17] a) R. Kather, E. Lork, J. Beckmann, *Eur. J. Inorg. Chem.* **2017**, 2595–2599. For examples of $B(C_6F_5)_3$ adducts with tertiary phosphanes, see: b) M. A. Beckett, D. S. Brassington, M. E. Light, M. B. Hursthouse, *J. Chem. Soc.*

Dalton Trans. **2001**, 1768 – 1772; c) E. Regulska, S. Christ, J. Zimmermann, F. Rominger, G. Hernandez-Sosa, C. Romero-Nieto, *Dalton Trans.* **2019**, *48*, 12803 – 12807.

[18] For a complete series of phosphanylborane chalcogenides, see: C. Marquardt, O. Hegen, T. Kahoun, M. Scheer, *Chem. Eur. J.* **2017**, *23*, 4397 – 4404.

Manuscript received: August 9, 2020
Accepted manuscript online: August 26, 2020
Version of record online: November 18, 2020

Chemistry–A European Journal

Supporting Information

A Stable Primary Phosphane Oxide and Its Heavier Congeners

Filip Horký, Ivana Císařová, and Petr Štěpnička*[a]

CONTENTS

SYNTHESES

Materials and methods

Unless stated otherwise, all syntheses were performed under an argon atmosphere using standard Schlenk techniques. Anhydrous tetrahydrofuran, dichloromethane and methanol were dried using a PureSolv MD5 Solvent Purification System (Innovative Technology, Inc., USA). Benzene and toluene were dried over sodium/benzophenone ketyl and freshly distilled under argon. Reagent-grade solvents used for chromatography and for crystallizations were purchased from Lach-Ner (Czech Republic) and used without additional purification. All other reagents were purchased from commercial suppliers (Sigma-Aldrich, Alfa-Aesar or TCI) and used as received.

NMR spectra were recorded at 25°C on Varian UNITY Inova 400 or Bruker Avance III 400 spectrometers. Chemical shifts (δ in ppm) are expressed relative to internal tetramethylsilane (^{1}H and ^{13}C NMR), to external 85% aqueous H_3PO_4 (^{31}P NMR), to external $BF_3{\cdot}OEt_2$ (^{11}B NMR), and to external neat $CFCl_3$ (^{19}F NMR), all se to 0 ppm. Electrospray ionization (ESI) mass spectra were recorded on Shimadzu LCMS-2020 (low-resolution spectra) and Compact QTOF-MS (high-resolution spectra) spectrometers. Elemental analyses were performed using a Perkin-Elmer PE 2400 CHN elemental analyzer. The amount of residual solvent (if any) was verified by NMR analysis.

Syntheses

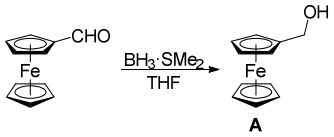

A

Synthesis of ferrocenylmethanol (A). The procedure was modified from ref.[1] A reaction flask equipped with a stirring bar was charged with ferrocenecarboxaldehyde (8.562 g, 40.0 mmol), flushed with argon and sealed with a rubber septum. The solid educt was dissolved in THF (300 mL), and the solution was cooled on ice. Neat borane–dimethyl sulfide (1/1) (4.55 mL, 48.0 mmol) was added, and the reaction mixture was stirred for 2 h before quenching by slowly adding methanol (30 mL; *Caution! Gas evolution.*) and by stirring for 10 min. Following evaporation under vacuum, the dark crude product was dissolved in dichloromethane (≈100 mL), pre-adsorbed onto silica gel (ca. 50 mL) and purified by chromatography over a silica gel column using ethyl acetate-hexane (1:1) as the eluent. The second, major orange band was collected and evaporated to provide alcohol **A** as an orange solid. Yield: 7.60 g (88%).

^{1}H NMR (400 MHz, $CDCl_3$): δ = 1.53 (br t, $^{3}J_{HH}$ = 5.4 Hz, 1H, OH), 4.17 (vt, J' = 1.9 Hz, 2H, C_5H_4), 4.18 (s, 5H, C_5H_5), 4.24 (vt, J'= 1.8 Hz, 2H, C_5H_4), 4.33 (d, $^{3}J_{HH}$ = 5.4 Hz, 2H, CH_2) ppm. The data match those published in literature.[2]

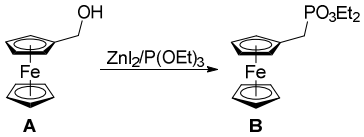

Synthesis of diethyl (ferrocenylmethyl)phosphonate (B). The procedure was adopted from ref.[3] A reaction flask equipped with a large stirring bar was charged with alcohol **A** (8.642 g, 40.0 mmol), zinc(II) iodide (14.05 g, 44.0 mmol) and triethyl phosphite (34.3 ml, 0.20 mol) under argon (the content of the reaction flask gently warmed upon mixing), and the resulting mixture was stirred at room temperature overnight. Then, it was diluted with chloroform (300 mL) and 3 M aqueous hydrochloric acid (100 mL) and transferred to a separatory funnel. The organic layer was separated, washed with brine, dried over magnesium sulfate and evaporated under reduced pressure. The oily residue was kept under oil pump vacuum (3×10^{-3} Torr at 50°C) to remove the excess of triethyl phosphite and subsequently purified by column chromatography (silica gel, ethyl acetate). A second orange band was collected, which afforded the phosphonate ester **B** as a deep orange oil. The compound was contaminated with *ca*. 10 mol.% of diethyl phosphite, which is, however, easily removed during the following synthetic step. Yield: 12.2 g (ca. 80%).

^{1}H NMR (400 MHz, $CDCl_3$): δ = 1.25 (t, $^{3}J_{HH}$ = 7.0 Hz, 6H, CH_3), 2.91 (d, $^{2}J_{PH}$ = 19.2 Hz, 2H, PCH_2), 3.95-4.04 (m, 4H, OCH_2), 4.10-4.12 (m, 7H, C_5H_5 and C_5H_4), 4.23 (br s, 2H, C_5H_4) ppm. ^{31}P{^{1}H} NMR (162 MHz, $CDCl_3$): δ = 26.5 (s) ppm. The data are in line with the literature values.[4]

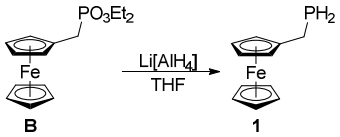

Synthesis of (ferrocenylmethyl)phosphane (1). Neat trimethyl-chlorosilane (16.3 mL, 0.128 mol) was slowly introduced to a suspension of $Li[AlH_4]$ (4.86 g, 0.128 mol) in dry THF (250 mL) while stirring and cooling on ice. The resulting mixture was stirred for 10 min before adding a solution of phosphonate ester **B** (10.77 g, 32.0 mmol in 250 mL of THF). After completing the addition, the cooling bath was removed, and the reaction mixture was stirred at room temperature overnight. Then, the reaction flask was cooled in an ice bath, adding methanol (200 mL) to terminate the reaction before evaporating under vacuum. The residue was taken up with hexane (500 mL), and the extract was filtered and evaporated (Note: the filtration is time-consuming, albeit with no complications because the product is air-stable). The crude product

was pre-adsorbed by co-evaporation with silica gel (ca. 75 mL) and purified by column chromatography (silica gel, diethyl ether-hexane 1:1). Evaporation of the first orange band gave phosphane **1** as an orange solid. Yield: 5.35 g (72%).

^{1}H NMR (400 MHz, $CDCl_3$): δ = 2.58-2.72 (m, 2H, CH_2), 2.94 (dt, $^{1}J_{PH}$ = 192 Hz, $^{3}J_{HH}$ = 7.3 Hz, 2H, PH_2), 4.07 (vt, J' = 1.8 Hz, 2H, C_5H_4), 4.11 (vt, J' = 1.8 Hz, 2H, C_5H_4), 4.13 (s, 5H, C_5H_5) ppm. ^{13}C{H} NMR (101 MHz, $CDCl_3$): δ 14.45 (d, $^{1}J_{PC}$ = 9 Hz, CH_2), 67.32 (s, CH of C_5H_4), 67.82 (d, J_{PC} = 3 Hz, CH of C_5H_4), 68.65 (s, C_5H_5), 89.07 (d, $^{2}J_{PC}$ = 3 Hz, C^{ipso} of C_5H_4) ppm. ^{31}P{^{1}H} NMR (162 MHz, $CDCl_3$): δ = −129.7 (s) ppm. ^{31}P NMR (162 MHz, $CDCl_3$): δ −129.7 (tt, $^{1}J_{PH}$ = 194 Hz, $^{2}J_{PH}$ = 5 Hz) ppm. The data are in agreement with the literature.[5]

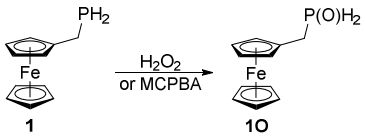

Synthesis of (ferrocenylmethyl)phosphane oxide (1O). Method A. In air, phosphane **1** (0.70 g, 3.0 mmol) was dissolved in a mixture of methanol (8 mL) and dichloromethane (20 mL), and the reaction flask, equipped with stirring bar, was cooled in an ice bath. Hydrogen peroxide solution (3 mL of 30% aqueous solution, 29 mmol) was added during 5 min while stirring, and the resulting mixture was stirred and cooled for another 3 min. The excess of hydrogen peroxide was destroyed by *slowly* adding saturated aqueous sodium thiosulfate (20 mL; *Caution! Rapid addition can result in overheating of the reaction mixture!*). The mixture was transferred to a separatory funnel and diluted with dichloromethane (50 mL) and brine (30 mL). The organic phase was separated, and the aqueous residue was extracted with dichloromethane (20 mL). The combined organic layers were dried over magnesium sulfate, filtered and evaporated under vacuum. The crude product was purified by flash column chromatography over silica gel using dichloromethane-methanol mixture (10:1) as the eluent. Evaporation of the first yellow band afforded phosphane oxide **1O** as a yellow solid. Yield: 0.60 g, 80%.

Method B. Under argon, a dichloromethane solution of 3-chloroperoxybenozic acid (86%, 112 mg, 0.5 mmol in 5 mL of the solvent) was introduced to a solution of **1** (116 mg, 0.50 mmol) in the same solvent (5 mL) while stirring and cooling in an ice bath. After stirring for 10 min, the cooling bath was removed and the stirring was continued overnight. On the following day, the mixture was concentrated under vacuum, and the residue was purified by chromatography over silica gel column with dichloromethane-methanol (10:1). Subsequent evaporation of the single yellow band afforded pure **1O** as a yellow powdery solid. Yield: 111 mg (90%).

^{1}H NMR (400 MHz, $CDCl_3$): δ = 3.14 (dt, $^{2}J_{PH}$ = 16.4 Hz, $^{3}J_{HH}$ = 4.8 Hz, 2H, CH_2), 4.16-4.19 (m, 4H, C_5H_4), 4.17 (s, 5H, C_5H_5), 6.91 (dt, $^{1}J_{PH}$ = 469.7 Hz, $^{3}J_{HH}$ = 4.9 Hz, 2H, $P(O)H_2$) ppm. ^{13}C{^{1}H} NMR (101 MHz, $CDCl_3$): δ = 28.82 (d, $^{1}J_{PC}$ = 63 Hz, CH_2), 68.61 (s, CH of C_5H_4), 68.87 (d, J_{PC} = 4 Hz,

CH of C_5H_4), 69.01 (s, C_5H_5), 75.14 (s, C^{ipso} of C_5H_4) ppm. $^{31}P\{^1H\}$ NMR (162 MHz, $CDCl_3$): δ = 9.6 (s) ppm. ^{31}P NMR (162 MHz, $CDCl_3$): δ = 9.6 (tt, $^1J_{PH}$ = 469 Hz, $^2J_{PH}$ = 16 Hz) ppm. IR (DRIFTS): ν = 3101 w, 3069 m, 2373 s, 1668 w, 1459 w, 1414 m, 1401 m, 1339 w, 1262 m, 1229 m, 1192 s, 1173 s, 1131 m, 1103 m, 1054 w, 1041 m, 1028 s, 1009 m, 925 w, 912 w, 853 s, 824 s, 809 s, 744 w, 729 m, 506 m, 486 s cm^{-1}. HRMS (ESI+) calc. for $C_{11}H_{13}FeNaOP$ ($[M + Na]^+$): 270.9946, found: 270.9950. Anal. Calc. for $C_{11}H_{13}FeOP$ (248.0): C 53.26, H 5.28%. Found: C 53.59, H 5.18%.

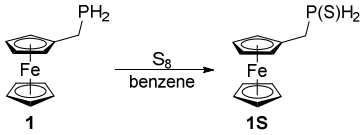

Synthesis of (ferrocenylmethyl)phosphane sulfide (1S). Phosphane **1** (232 mg, 1.0 mmol) and sulfur (320 mg, 10.0 mmol) were mixed in dry benzene under argon, and the resulting mixture was stirred at 50°C overnight (the sulfur completely dissolved upon warming). On the following day, the mixture was concentrated under vacuum, and the residue was purified by chromatography over silica gel, eluting with dry dichloromethane. The first, light yellow band containing the starting phosphane and sulfur was discarded, and the following darker band due to the product was collected and evaporated to afford **1S** as a yellow solid. Yield: 80 mg (30%).

^1H NMR (400 MHz, $CDCl_3$): δ = 3.21-3.29 (m, 2H, CH_2), 4.17 (s, 5H, C_5H_5), 4.18 (br s, 4H, C_5H_4), 6.57 (dm, $^1J_{PH}$ = 453.7 Hz, 2H, $P(S)H_2$) ppm. $^{13}C\{^1H\}$ NMR (101 MHz, $CDCl_3$): δ = 31.62 (d, $^1J_{PC}$ = 49 Hz, CH_2), 68.62 (d, J_{PC} = 4 Hz, CH of C_5H_4), 68.69 (s, CH of C_5H_4), 69.07 (s, C_5H_5), 77.73 (d, $^2J_{PC}$ = 2 Hz, C^{ipso} of C_5H_4). $^{31}P\{^1H\}$ NMR (162 MHz, $CDCl_3$): δ = −7.2 (s) ppm. ^{31}P NMR (162 MHz, $CDCl_3$): δ = −7.2 (tt, $^1J_{PH}$ = 453 Hz, $^2J_{PH}$ = 14 Hz) ppm. IR (DRIFTS): ν = 3104 w, 3081 w, 2914 w, 2343 w, 2324 m, 1738 w, 1463 w, 1410 m, 1389 m, 1242 w, 1209 w, 1105 s, 1085 m, 1042 m, 1028 m, 999 m, 952 s, 914 m, 864 w, 835 m, 814 s, 759 m, 738 w, 698 w, 638 s, 596 m, 498 s, 483 s cm^{-1}. HRMS (ESI−) calc. for $C_{11}H_{12}FeOPS$ ($[M + O - H]^-$): 278.9701, found: 278.9705. Anal. Calc. for $C_{11}H_{13}FePS$ (264.1): C 50.02, H 4.96%. Found: C 49.65, H 4.77%.

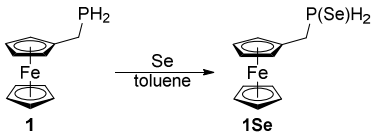

Synthesis of (ferrocenylmethyl)phosphane selenide (1Se). A dry Schlenk tube was charged with phosphane **1** (300 mg, 1.29 mmol), grey selenium (153 mg, 1.94 mmol) and dry toluene (15 mL), and the resulting mixture was stirred at 50°C overnight. The volatiles were removed under vacuum, and the residue was taken up with anhydrous dichloromethane (10 mL) and filtered through a PTFE syringe filter (0.45 μm pore size) to remove unreacted selenium. The filtrate was evaporated, leaving **1Se** as an orange, foul smelling solid. Yield: 373 mg (93%). When

insufficiently pure, the product can be further purified by chromatography over silica gel with dry dichloromethane (in air).

^{1}H NMR (400 MHz, $CDCl_3$): δ = 3.32-3.40 (m, 2H, CH_2), 4.17 (s, 5H, C_5H_5), 4.18 (br s, 4H, C_5H_4), 6.00 (dm, $^{1}J_{PH}$ = 444.4 Hz, 2H, P(Se)H_2) ppm. ^{13}C{^{1}H} NMR (101 MHz, $CDCl_3$): δ = 30.22 (d, $^{1}J_{PC}$ = 42 Hz, CH_2), 68.42 (d, J_{PC} = 3 Hz, CH of C_5H_4), 68.72 (s, CH of C_5H_4), 69.07 (s, C_5H_5), 79.12 (d, $^{2}J_{PC}$ = 3 Hz, C^{ipso} of C_5H_4) ppm. ^{31}P{^{1}H} NMR (162 MHz, $CDCl_3$): δ = −34.5 (s with ^{77}Se satellites $^{1}J_{SeP}$ = 734 Hz) ppm. ^{31}P NMR (162 MHz, $CDCl_3$): δ = −34.5 (tt with ^{77}Se satellites, $^{1}J_{PH}$ = 444 Hz, $^{2}J_{PH}$ = 13 Hz, $^{1}J_{SeP}$ = 734 Hz) ppm. IR (DRIFTS): ν = 3090 br m, 2911 br m, 2360 s, 2324 s, 1734 w, 1459 m, 1410 m, 1387 m, 1241 m, 1209 w, 1105 s, 1084 s, 1042 m, 1028 m, 999 m, 929 s, 915 s, 862 w, 832 m, 814 s, 751 w, 599 w, 475 s cm^{-1}. HRMS (ESI−) calc. for $C_{11}H_{12}FeOPSe$ ($[M + O - H]^-$): 326.9146, found: 326.9147. Anal. Calc. for $C_{11}H_{13}FePSe$ (311.0): C 42.48, H 4.21%. Found: C 42.93, H 4.29%.

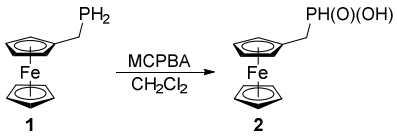

Overoxidation of 1 with 3-chloroperoxybenzoic acid (MCPBA). A solution of phosphane **1** (116 mg, 0.50 mmol) in dichloromethane (10 mL) was added to a dichloromethane solution of 3-chloroperoxybenzoic acid (86%, 224 mg, 1 mmol in 5 mL) while stirring and cooling on ice. The cooling bath was removed, and the stirring continued overnight. Subsequent evaporation afforded an inseparable mixture of (ferrocenylmethyl)phosphinic acid (**2**) and 3-chlorobenzoic acid. The conversion of **1** into **2** estimated from the NMR data was approximately 70%.

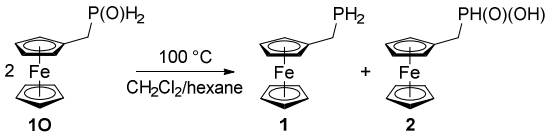

Thermal disproportionation of 1O. A pressure tube was charged with phosphane oxide **1O** (124 mg, 0.50 mmol), anhydrous dichloromethane and hexane (3 mL each), and tightly sealed. The resulting solution was maintained at 100°C for 48 h and then for another day at 40°C. On the fourth day, the reaction mixture was cooled to room temperature, and the separated orange crystalline solid was filtered off and washed with pentane to produce (ferrocenylmethyl)-phosphinic acid (**2**) (35 mg, 53%). The filtrate was evaporated with added silica gel, and the preadsorbed residue was purified by column chromatography (silica gel, hexane-diethyl ether 1:1). The first orange band was collected and evaporated, affording phosphane **1** (52 mg, 90% of the theoretic amount). Residual acid **2** remained adsorbed on the column.

Analytical data for **2**. ^{1}H NMR (400 MHz, dmso-d_6): δ = 2.77 (dd, $^{2}J_{PH}$ = 16.9, $^{3}J_{HH}$ = 1.9 Hz, 2H, CH_2), 4.10 (vt, J' = 1.8 Hz, 2H, C_5H_4), 4.15 (s, 5H, C_5H_5), 4.20 (br s, 2H, C_5H_4), 6.84 (dt, $^{1}J_{PH}$ = 528.1 Hz, $^{3}J_{HH}$ = 2.0 Hz, 1H, PH) ppm. ^{13}C{^{1}H} NMR (101 MHz, dmso-d_6): δ 31.83 (d, $^{1}J_{PC}$ = 88 Hz, CH_2), 67.46 (s, CH of C_5H_4), 68.65 (s, C_5H_5), 68.93 (d, J_{PC} = 4 Hz, CH of C_5H_4), 78.08 (s, C^{ipso} of C_5H_4) ppm. ^{31}P{^{1}H} NMR (162 MHz, dmso-d_6): δ = 28.2 (s) ppm. ^{31}P NMR (162 MHz, dmso-d_6): δ = 28.2 (dt, $^{1}J_{PH}$ = 528 Hz, $^{2}J_{PH}$ = 17 Hz) ppm. IR (Nujol): ν = 3088 w, 2954 s, 2379 m, 1701 br m, 1258 w, 1217 w, 1180 m, 1105 m, 997 s, 963 m, 920 s, 828 m, 814 m, 748 m, 590 w, 470 m, 452 w cm^{-1}. ESI− MS: *m/z* 464 ([M − H]$^-$). Anal. Calc. for $C_{11}H_{13}FeO_2P$ (264.0): C 50.04, H 4.96%. Found: C 49.80, H 4.74%.

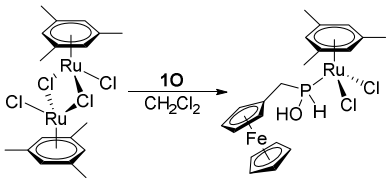

3

Synthesis of dichlorido[(ferrocenylmethyl)phosphinous acid-κ*P*](η^6-mesitylene)ruthenium(II) (3). [{(η^6-mesitylene)RuCl(μ-Cl)}$_2$] (58 mg, 0.10 mmol) and phosphane oxide **10** (50 mg, 0.20 mmol) were dissolved in dry dichloromethane (20 mL) under argon. The reaction mixture was stirred overnight and evaporated under vacuum, leaving complex **3** as red solid in a quantitative yield. Crystals for structure determination were obtained from chloroform/hexane.

^{1}H NMR (400 MHz, $CDCl_3$): δ = 2.04 (d, J_{PH} = 1.5 Hz, 9H, Me), 3.38-3.46 (m, 1H, CH_2), 3.57-3.65 (m, 1H, CH_2), 4.15-4.17 (m, 1H, C_5H_4), 4.16 (s, 5H, C_5H_5), 4.20-4.21 (m, 1H, C_5H_4), 4.27-4.29 (m, 1H, C_5H_4), 4.31-4.32 (m, 1H, C_5H_4), 4.76 (s, 3H, C_6H_3), 6.89 (ddd, $^{1}J_{PH}$ = 372.0 Hz, J_{HH} = 7.6, 3.9 Hz, 1H, PH) ppm. ^{13}C{^{1}H} NMR (101 MHz, $CDCl_3$): δ = 18.69 (d, J_{PH} = 1 Hz, Me), 29.65 (d, $^{1}J_{PC}$ = 38 Hz, CH_2), 67.97 (s, CH of C_5H_4), 68.45 (s, CH of C_5H_4), 69.00 (d, J_{PC} = 2 Hz, CH of C_5H_4), 69.17 (s, C_5H_5), 70.75 (br s, CH of C_5H_4), 78.91 (d, $^{2}J_{PC}$ = 5 Hz, C^{ipso} of C_5H_4), 82.34 (d, J_{PC} = 5 Hz, CH of C_6H_3), 106.32 (d, J_{PH} = 2 Hz, C of C_6H_3) ppm. ^{31}P{^{1}H} NMR (162 MHz, $CDCl_3$): δ = 115.0 (s) ppm. ^{31}P NMR (162 MHz, $CDCl_3$): δ = 115.0 (ddd, $^{1}J_{PH}$ = 372 Hz, $^{2}J_{PH}$ = 18 and 11 Hz) ppm. IR (DRIFTSl): ν = 3094 br m, 3029 m, 2968 m, 2917 m, 2869 m, 2333 m, 1652 w, 1538 w, 1523 w, 1455 m, 1383 m, 1298 m, 1248 m, 1119 s, 1105 s, 1036 m, 1019 w, 1002 w, 984 w, 965 m, 940 m, 904 s, 877 vs, 838 m, 812 m, 746 w, 659 w, 583 w, 499 m, 481 m, 432 m cm^{-1}. ESI+ MS: *m/z* 761 ([M + RuCl(mes) − HCl]$^+$). Anal. Calc. for $C_{20}H_{25}Cl_2FeOPRu{\cdot}0.3CH_2Cl_2$ (568.5): C 42.96, H 4.55%. Found: C 42.81, H 4.36%.

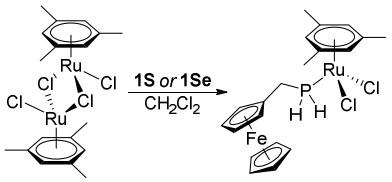

4

Reaction of [{(η⁶-mesitylene)RuCl(μ-Cl)}₂] with 1S and 1Se. [{(η⁶-mesitylene)RuCl(μ-Cl)}₂] (71 mg, 0.12 mmol) and **1S** (63 mg, 0.24 mmol) were dissolved in dichloromethane (20 mL) under argon, and the mixture was stirred for 2 days. Subsequent evaporation and chromatography (silica gel, dichloromethane-methanol 10:1) afforded [(η⁶-mesitylene)RuCl₂(**1**-κ*P*)] (**4**) (40 mg, 32%). The complex and the liberated chalcogen tend to co-elute during the chromatography, which significantly reduces the yield of the complex. The analogous reaction with **1Se** (75 mg, 0.24 mmol) proceeded similarly and with similar yield, except tht the reaction mixture became turbid shortly after adding the solvent, depositing elemental selenium.

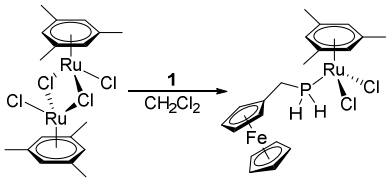

4

Synthesis of dichlorido[(ferrocenylmethyl)phosphane-κ*P*](η⁶-mesitylene)ruthenium(II) (4) from 1. [{(η⁶-mesitylene)RuCl(μ-Cl)}₂] (88 mg, 0.15 mmol) and phosphane **1** (70 mg, 0.30 mmol) were dissolved in dichloromethane (15 mL) under argon, and the solution was stirred overnight. Subsequent evaporation afforded analytically pure **4** as a red solid in quantitative yield (157 mg). Crystals suitable for structure determination was obtained from a ternary dichloromethane/ethyl acetate/hexane mixture.

^{1}H NMR (400 MHz, $CDCl_3$): δ = 2.13 (d, J_{PH} = 1.3 Hz, 9H, Me), 3.13-3.18 (m, 2H, CH_2), 4.14 (s, 5H, C_5H_5), 4.17 (vt, J' = 1.7 Hz, 2H, C_5H_4), 4.20 (vt, J' = 1.6 Hz, 2H, C_5H_4), 4.79 (ddt, $^{1}J_{PH}$ = 355.3 Hz, J_{HH} = 0.4, 6.3 Hz, 2H, PH_2), 4.88 (s, 3H, C_6H_3) ppm. ^{13}C{^{1}H} NMR (101 MHz, $CDCl_3$): δ = 18.19 (d, $^{1}J_{PC}$ = 29 Hz, CH_2), 18.87 (d, J_{PC} = 1 Hz, Me), 68.12 (s, CH of C_5H_4), 68.67 (d, J_{PC} = 2 Hz, CH of C_5H_4), 69.08 (s, C_5H_5), 81.74 (d, J_{PC} = 5 Hz, CH of C_6H_3), 83.87 (d, $^{2}J_{PC}$ = 5 Hz, C^{ipso} of C_5H_4), 104.80 (d, J_{PC} = 2 Hz, C^{ipso} of C_6H_3) ppm. ^{31}P{^{1}H} NMR (162 MHz, $CDCl_3$): δ = −24.0 (s) ppm. ^{31}P NMR (162 MHz, $CDCl_3$): δ = −24.0 (tt, $^{1}J_{PH}$ = 355 Hz, $^{3}J_{HH}$ = 8 Hz) ppm. IR (DRFITS): ν = 3071 w, 3028 w, 2917 w, 2377 w, 2326 w, 1528 m, 1453 m, 1399 m, 1389 m, 1371 m, 1299 w, 1240 m, 1208 w, 1157 w, 1114 s, 1104 s, 1083 s, 1036 s, 1018 m, 1002 m, 988 w, 930 s, 895 m, 878 s, 873 s, 836 m, 813 s, 753 m, 730 m, 678 w, 640 w, 592 w, 495 s, 477 s, 423 m cm^{-1}. ESI+ MS: *m/z* 489 ($[M - Cl]^+$), 547 ($[M + Na]^+$), 1073 ($[2M + Na]^+$). Anal. Calc. for $C_{20}H_{25}Cl_2FePRu$: C 45.82, H 4.81%. Found: C 45.56, H 4.62%.

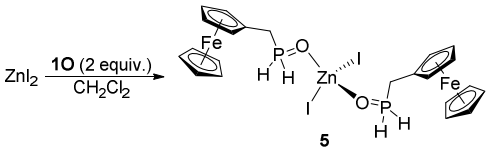

Synthesis of bis[(ferrocenylmethyl)phosphane oxide-κ*O*]diiodozinc(II) (5). A Schlenk flask was charged with zinc(II) iodide (32 mg, 0.10 mmol) and phosphane oxide **1O** (50 mg, 0.20 mmol). Dry dichloromethane (20 mL) was added, and the resulting suspension was stirred overnight. Evaporation of the clear reaction mixture gave **5** as an orange solid in quantitative yield (82 mg). Crystals suitable from X-ray diffraction analysis were obtained from chloroform/hexane.

^{1}H NMR (400 MHz, $CDCl_3$): δ = 3.41 (br dt, $^{2}J_{PH}$ = 17.2 Hz, $^{3}J_{HH}$ = 4.5 Hz, 2H, CH_2), 4.21 (br s, 9H, ferrocenyl), 6.89 (br d, $^{1}J_{PH}$ = 501.0 Hz, 2H, PH_2) ppm. ^{31}P{^{1}H} NMR (162 MHz, $CDCl_3$): δ = 18.4 (s) ppm. ^{31}P NMR (162 MHz, $CDCl_3$): δ = 18.4 (tt, $^{1}J_{PH}$ = 501 Hz, $^{2}J_{PH}$ = 17 Hz) ppm. IR (DRIFTS): ν = 3097 w, 2875 w, 2388 m, 2375 m, 1459 w, 1409 w, 1393 m, 1376 w, 1263 w, 1248 w, 1232 w, 1215 m, 1195 m, 1151 s, 1129 s, 1104 s, 1082 w, 1039 w, 1027 s, 1020 w, 1004 s, 922 m, 905 w, 868 w, 839 s, 813 s, 785 w, 745 w, 723 w, 608 w, 505 s, 485 s cm^{-1}. ESI+ MS: *m/z* 271 ([**1O** + Na]$^{+}$), 519 ([2(**1O**) + Na]$^{+}$), 687 ([M − I]$^{+}$), 935 ([M – I + **1O**]$^{+}$). Anal. Calc. for $C_{22}H_{26}Fe_2I_2O_2P_2Zn$ (815.3): C 32.41, H 3.21%. Found: C 32.32, H 3.03%.

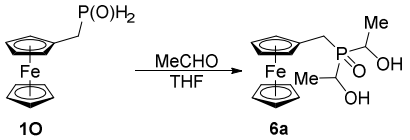

Synthesis of ferrocenylmethyl-bis(1-hydroxyethyl)phosphane oxide (6a). A Schlenk flask equipped with a stirring bar was charged with phosphane oxide **1O** (124 mg, 0.50 mmol) and acetaldehyde (84 µL, 1.5 mmol). Dry THF (10 mL) was introduced, and the reaction mixture was stirred at 50°C overnight and then evaporated under vacuum. The residue was purified by flash column chromatography over silica gel, eluting with dichloromethane-methanol (10:1). A single yellow band was collected and evaporated, leaving **6a** as a mixture of isomers. Yield: 128 mg (77%), yellow solid. The compound is a mixture of stereoisomers in 1:2:1 ratio (*vide infra*). A single crystal used for structure determination was obtained from chloroform/cyclohexane.

^{1}H NMR (400 MHz, dmso-d_6): δ = 1.12-1.28 (m, 6H, all Me), 2.81 (d, $^{2}J_{PH}$ = 10.9 Hz, 2H, minor CH_2), 2.89 (d, $^{2}J_{PH}$ = 11.8 Hz, 2H, major CH_2), 2.94 (d, $^{2}J_{PH}$ = 11.8 Hz, 2H, minor CH_2), 3.76-3.95 (m, 2H, all C*H*Me), 4.05-4.26 (m, 4H, all C_5H_4), 4.13 (s, 5H, minor C_5H_5), 4.14 (s, 5H, major C_5H_5), 4.14 (s, 5H, minor C_5H_5), 5.20-5.31 (m, 2H, all OH) ppm. ^{13}C{^{1}H} NMR (101 MHz, dmso-d_6): δ = 16.82 (s, minor Me), 16.84 (s, minor Me), 16.93 (s, major Me), 17.28 (s, major Me), 17.32 (s, minor Me), 17.33 (s, minor Me), 22.78 (d, $^{1}J_{PC}$ = 55 Hz, minor CH_2), 23.82 (d, $^{1}J_{PC}$ = 54 Hz, major CH_2), 24.23 (d, $^{1}J_{PC}$ = 53 Hz, minor CH_2), 61.43 (d, $^{1}J_{PC}$ = 77 Hz, minor *CH*Me), 62.44 (dd, *J* = 75, 9

Hz, major *CH*Me), 62.73 (d, $^{1}J_{PC}$ = 76 Hz, minor *CH*Me), 66.93 (s, minor CH of C_5H_4), 67.09 (s, minor CH of C_5H_4), 67.14 (d, J_{PC} = 2 Hz, major CH of C_5H_4), 68.52 (s, minor C_5H_5), 68.55 (s, major C_5H_5), 68.56 (s, minor C_5H_5), 69.19 (d, J_{PC} = 2 Hz, major CH of C_5H_4), 69.24 (d, J_{PC} = 2 Hz, major CH of C_5H_4), 69.46 (d, J_{PC} = 2 Hz, minor CH of C_5H_4), 69.55 (d, J_{PC} = 2 Hz, minor CH of C_5H_4), 79.04 (d, $^{2}J_{PC}$ = 4 Hz, minor C^{ipso} of C_5H_4), 79.24 (d, $^{2}J_{PC}$ = 4 Hz, major C^{ipso} of C_5H_4), 79.54 (d, $^{2}J_{PC}$ = 3 Hz, minor C^{ipso} of C_5H_4) ppm. $^{31}P\{^{1}H\}$ NMR (162 MHz, dmso-d_6): δ = 44.9 (s, minor), 46.5 (s, minor), 46.7 (s, major) ppm. IR (Nujol): ν = 3200 br m, 1718 w, 1140 m, 1105 m, 1085 m, 1024 w, 999 m, 926 w, 895 w, 816 m, 763 w, 494 m, 432 w cm^{-1}. ESI+ MS: *m/z* 359 ($[M + Na]^+$), 695 ($[2M + Na]^+$). Anal. Calc. for $C_{15}H_{21}FeO_3P$ (336.1): C 53.60, H 6.30%. Found: C 53.49, H 6.12%.

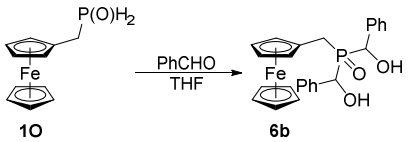

1O **6b**

Synthesis of ferrocenylmethyl-bis(1-hydroxybenzyl)phosphane oxide (6b). Phosphane oxide **1O** (124 mg, 0.50 mmol), benzaldehyde (159 mg, 1.5 mmol) and THF (5 mL) were mixed in a Schlenk flask, and the mixture was maintained at 40°C overnight. Subsequent evaporation afforded a yellow residue, which was purified by chromatography over silica gel, eluting firstly with dichloromethane-methanol (50:1) to remove the excess of benzaldehyde and then with dichloromethane-methanol (20:1) to elute the product as a yellow band. The yellow band was collected and evaporated to afford **6b** as a mixture of isomers. Yield: 159 mg (69%), yellow solid.

^{1}H NMR (400 MHz, dmso-d_6): δ = 2.60 (d, $^{2}J_{PH}$ = 10.6 Hz, 1H, minor CH_2), 2.74 (d, $^{2}J_{PH}$ = 13.1 Hz, 1H, minor CH_2), 2.78 (d, $^{2}J_{PH}$ = 12.8 Hz, 1H, major CH_2), 2.90 (d, $^{2}J_{PH}$ = 9.3 Hz, 1H, major CH_2), 2.94 (d, $^{2}J_{PH}$ = 9.1 Hz, 1H, minor CH_2), 2.98 (d, $^{2}J_{PH}$ = 11.5 Hz, 1H, minor CH_2), 3.67-4.03 (m, 4H, all C_5H_4), 3.98 (s, 5H, major C_5H_5), 4.02 (s, 5H, both minor C_5H_5), 4.82 (t, $^{2}J_{PH}$ = 5.8 Hz, 2H, minor C*H*Ph), 4.95 (t, $^{2}J_{PH}$ = 6.0 Hz, 2H, major C*H*Ph), 5.07 (dd, J = 8.9, 5.3 Hz, 2H, minor C*H*Ph), 6.00 (dd, J = 15.0, 6.0 Hz, 2H, minor OH), 6.18-6.31 (m, 2H, major and minor OH), 7.19-7.42 (m, 10H, all Ph) ppm. $^{13}C\{^{1}H\}$ NMR (101 MHz, dmso-d_6): δ = 22.87 (d, $^{1}J_{PC}$ = 56 Hz, major and minor CH_2), 25.77 (d, $^{1}J_{PC}$ = 56 Hz, minor CH_2), 66.50-70.20 (m, all *CH*Ph and CH of C_5H_4), 68.41 (s, major and minor C_5H_5), 68.49 (s, minor C_5H_5), 78.33 (d, $^{2}J_{PC}$ = 4 Hz, major C^{ipso} of C_5H_4), 78.42 (d, $^{2}J_{PC}$ = 4 Hz, minor C^{ipso} of C_5H_4), 79.02 (d, $^{2}J_{PC}$ = 3 Hz, minor C^{ipso} of C_5H_4), 126.60-127.70 (m, all CH of C_6H_5), 138.03 (d, $^{2}J_{PC}$ = 17 Hz, major and minor C^{ipso} of C_6H_5), 138.59 (s, minor C^{ipso} of C_6H_5) ppm. $^{31}P\{^{1}H\}$ NMR (162 MHz, dmso-d_6): δ = 41.6 (s, minor), 42.8 (s, minor), 42.9 (s, major) ppm. IR (Nujol): ν = 3438 w, 1491 w, 1193 w, 1140 m, 1103 w, 1046 m, 1024 m, 998 w, 925 m, 816 m, 698 m, 467 w cm^{-1}. ESI+ MS: *m/z* 483 ($[M + Na]^+$), 943 ($[2M + Na]^+$). Anal. Calc. for $C_{25}H_{25}FeO_3P$ (460.3): C 65.24, H 5.47%. Found: C 64.97, H 5.49%.

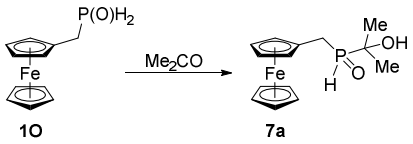

1O **7a**

Synthesis of (ferrocenylmethyl)(2-hydroxyprop-2-yl)phosphane oxide (7a). A pressure tube equipped with a stirring bar was charged phosphane oxide **1O** (150 mg, 0.6 mmol) and dry acetone (10 mL), flushed with argon and sealed. The reaction mixture was heated at 40°C with stirring overnight and then evaporated under vacuum. The residue was purified by flash column chromatography over silica gel using dichloromethane-methanol (10:1) as the eluent. A single yellow band was collected and evaporated, affording pure **7a** as a yellow solid. Yield: 170 mg (92%). Crystals used for structure analysis were grown from acetone/hexane.

^{1}H NMR (400 MHz, dmso-d_6): δ = 1.26 (d, $^{3}J_{PH}$ = 13.1 Hz, 3H, CH_3), 1.32 (d, $^{3}J_{PH}$ = 14.3 Hz, 3H, CH_3), 2.78 (dt, $^{2}J_{PH}$ = 16.5 Hz, $^{3}J_{HH}$ = 6.5 Hz, 1H, CH_2), 3.01 (dd, $^{2}J_{PH}$ = 15.3 Hz, $^{3}J_{HH}$ = 8.1 Hz, 1H, CH_2), 4.13 (dt, J' = 2.3, 1.2 Hz, 2H, C_5H_4), 4.18 (s, 5H, C_5H_5), 4.23 (br d, J' = 1.4 Hz, 1H, C_5H_4), 4.25 (br d, J' = 1.4 Hz, 1H, C_5H_4), 5.49 (d, $^{3}J_{PH}$ = 5.6 Hz, 1H, OH), 6.27 (dd, $^{1}J_{PH}$ = 446.8 Hz, J_{HH} = 6.4 Hz, 1H, P(O)H) ppm. ^{13}C{^{1}H} NMR (101 MHz, dmso-d_6): δ = 22.92 (d, $^{2}J_{PC}$ = 8 Hz, CH_3), 24.63 (d, $^{1}J_{PC}$ = 56 Hz, CH_2), 25.26 (d, $^{2}J_{PC}$ = 9 Hz, CH_3), 67.37 (s, CH of C_5H_4), 67.90 (d, $^{2}J_{PC}$ = 81 Hz, C^{ipso} of C_5H_4), 68.43 (d, J_{PC} = 3 Hz, CH of C_5H_4), 68.60 (s, C_5H_5), 69.11 (d, J_{PC} = 4 Hz, C_5H_4), 79.63 (d, $^{1}J_{CP}$ = 5 Hz, *C*Me_2) ppm. ^{31}P{^{1}H} NMR (162 MHz, dmso-d_6): δ = 46.8 (s) ppm. ^{31}P{^{1}H} NMR (162 MHz, dmso-d_6): δ = 46.8 (ddt, $^{1}J_{PH}$ = 446 Hz, J_{PH} = 13 and 7 Hz) ppm. IR (Nujol): ν = 3185 br m, 2343 m, 1393 m, 1361 m, 1250 w, 1213 w, 1199 m, 1156 w, 1124 s, 1103 m, 1036 w, 1027 w, 1002 w, 986 w, 975 w, 941 w, 928 m, 916 m, 847 w, 832 w, 812 w, 803 s, 660 w, 482 m, 447 m cm^{-1}. ESI+ MS: *m/z* 329 ([M + Na]$^{+}$), 635 ([2M + Na]$^{+}$). Anal. Calc. for $C_{14}H_{19}FeO_2P$ (306.1): C 54.93, H 6.29%. Found: C 55.02, H 6.09%.

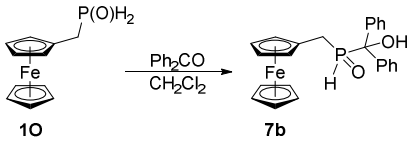

1O **7b**

Attempted synthesis of (ferrocenylmethyl)(diphenylhydroxymethyl)phosphane oxide (7b). A Schlenk flask was charged with phosphane oxide **1O** (124 mg, 0.50 mmol) and benzophenone (273 mg, 1.5 mmol) under argon. Dichloromethane (5 mL) was introduced, and the reaction mixture was heated at 50°C for 3 days with continuous stirring. NMR analysis of the crude product obtained after cooling and evaporation indicated that approximately 50 mol.% of the starting phosphane oxide was converted into **7b**. However, all attempts to isolate **7b** failed due to equilibrium between **7b** and the starting materials.

Analytical data of the crude product. ^{1}H NMR (400 MHz, $CDCl_3$): δ = 2.69-2.86 (m, 2H, CH_2), 4.04-4.15 (m, 4H, C_5H_4), 4.06 (s, 5H, C_5H_5), 6.28 (br s, 1H, PH), 7.30-7.70 (m, 10H, Ph) ppm.

$^{31}P\{^{1}H\}$ NMR (162 MHz, $CDCl_3$): δ = 44.3 (s) ppm. ESI+ MS: *m/z* 271 ([**10** + Na]$^+$), 453 ([M + Na]$^+$), 883 ([2M + Na]$^+$).

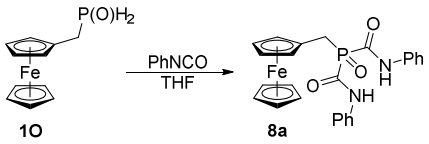

10 **8a**

Synthesis of ferrocenylmethyl-bis[(phenylamino)carbonyl]phosphane oxide (8a). Phosphane oxide **10** (124 mg, 0.50 mmol) and 1,4-diazabicyclo[2.2.2]octane (2.8 mg, 5 mol.%) were dissolved in dry THF (10 mL), subsequently adding neat phenyl isocyanate (72 mg, 0.60 mmol). After stirring for 12 h, additional phenyl isocayanate (72 mg, 0.60 mmol) was added, and the stirring was continued for another 12 h. The reaction mixture was concentrated under vacuum, and the crude product was purified by column chromatography over silica gel using dichloromethane-methanol (10:1) as the eluent. A single orange band was collected and evaporated. The residue was crystallized from dichloromethane-hexane (1:2, approximately 70 mL) to give analytically pure **8a** as an orange crystalline solid. Yield: 160 mg (66%). The crystal used for structure determination was selected from the reaction batch.

^{1}H NMR (400 MHz, $CDCl_3$): δ = 3.60 (d, $^{2}J_{PH}$ = 11.8 Hz, 2H, CH_2), 4.12 (vt, *J*′ = 1.8 Hz, 2H, C_5H_4), 4.14 (s, 5H, C_5H_5), 4.24 (dt, *J*′ = 0.9, 1.8 Hz, 2H, C_5H_4), 7.15-7.20 (m, 2H, Ph), 7.30-7.36 (m, 4H, Ph), 7.53-7.58 (m, 4H, Ph), 9.20 (s, 2H, NH) ppm. $^{13}C\{^{1}H\}$ NMR (101 MHz, $CDCl_3$): δ = 27.40 (d, $^{1}J_{PC}$ = 58 Hz, CH_2), 68.85 (s, CH of C_5H_4), 69.11 (s, C_5H_5), 69.40 (d, J_{PC} = 2 Hz, CH of C_5H_4), 74.98 (d, ^{2}J = 3 Hz, C^{ipso} of C_5H_4), 120.08 (s, CH of C_6H_5), 125.91 (s, CH of C_6H_5), 129.19 (s, CH of C_6H_5), 136.31 (d, $^{3}J_{PC}$ = 9 Hz, C^{ipso} of C_6H_5). $^{31}P\{^{1}H\}$ NMR (162 MHz, $CDCl_3$): δ = 14.2 (s) ppm. ^{31}P NMR (162 MHz, $CDCl_3$): δ = 14.2 (t, $^{2}J_{PH}$ = 12 Hz) ppm. IR (Nujol): ν = 3247 m, 3195 m, 3133 m, 3074 w, 1675 s, 1617 w, 1606 s, 1548 s, 1486 m, 1244 m, 1198 w, 1104 m, 1081 w, 1023 w, 998 w, 922 w, 846 w, 820 s, 756 s, 688 m, 620 w, 608 w, 509 w, 483 w, 446 s, 421 m cm^{-1}. ESI+ MS: *m/z* 509 ([M + Na]$^+$), 995 ([2M + Na]$^+$). Calc. for $C_{25}H_{23}FeN_2O_3P$ (486.3): C 61.75, H 4.77, N 5.76%. Found: C 61.65, H 4.77, N 5.47%.

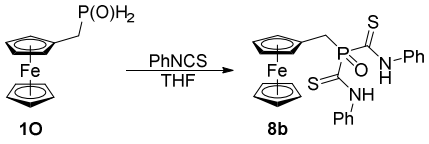

10 **8b**

Synthesis of ferrocenylmethyl-bis[(phenylamino)thiocarbonyl]phosphane oxide (8b). Phosphane oxide **10** (124 mg, 0.50 mmol) and phenyl isothiocyanate (270 mg, 2.0 mmol) were mixed in THF (6 mL) in a Schlenk flask under argon, and the resulting solution was stirred at 60°C overnight (the reaction mixture turned red during this time). The volatiles were removed under vacuum, and the residue was purified by chromatography (silica gel, dichloromethane-

methanol 10:1). Evaporation of the first band afforded thioamide **8b** as a red solid. Yield: 200 mg (77%). Crystal used for structure determination was obtained from ethyl acetate/hexane.

^{1}H NMR (400 MHz, CH_2Cl_2): δ = 3.84 (d, $^{2}J_{PH}$ = 12.6 Hz, 2H, CH_2), 4.12 (vt, *J′* = 1.8 Hz, 2H, C_5H_4), 4.14 (s, 5H, C_5H_5), 4.25 (vt, *J′* = 2.0 Hz, 1H, C_5H_4), 4.25 (vt, *J′* = 1.9 Hz, 1H, C_5H_4), 7.29-7.34 (m, 2H, Ph), 7.39-7.44 (m, 4H, Ph), 7.83-7.86 (m, 4H, Ph), 11.06 (br d, $^{3}J_{PC}$ = 6.3 Hz, 2H, NH) ppm. ^{13}C{^{1}H} NMR (101 MHz, CH_2Cl_2): δ = 30.46 (d, $^{1}J_{PC}$ = 73 Hz, CH_2), 68.61 (s, CH of C_5H_4), 69.18 (s, C_5H_5), 69.93 (d, *J* = 2 Hz, CH of C_5H_4), 75.87 (d, $^{2}J_{PC}$ = 2 Hz, C^{ipso} of C_5H_4), 122.43 (s, CH of C_6H_5), 127.75 (s, CH of C_6H_5), 129.11 (s, CH of C_5H_4), 138.08 (d, $^{3}J_{PC}$ = 10 Hz, C^{ipso} of C_6H_5), 191.99 (d, $^{1}J_{PC}$ = 74 Hz, CS) ppm. ^{31}P{^{1}H} NMR (162 MHz, CH_2Cl_2): δ = 17.8 (s) ppm. IR (Nujol): ν = 3242 m, 3176 m, 3117 m, 3092 m, 3070 m, 3027 m, 2957 s, 1596 m, 1538 m, 1493 s, 1446 m, 1356 m, 1331 w, 1312 w, 1292 w, 1239 w, 1212 w, 1200 w, 1156 s, 1152 s, 1104 w, 1090 w, 1075 w, 1036 w, 1026 w, 1020 w, 1009 m, 924 w, 839 w, 822 m, 768 m, 752 w, 699 m, 684 m, 614 w, 602 w, 583 w, 566 w, 537 w, 491 w, 429 w cm^{-1}. ESI− MS: *m/z* 517 ([M − H]$^{-}$). Anal. Calc. for $C_{25}H_{23}FeN_2OPS_2$ (518.4): C 57.92, H 4.47, N 5.40%. Found: C 57.81, H 4.28, N 5.27%.

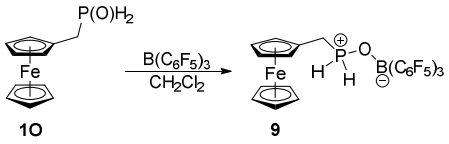

10 **9**

Synthesis of the 1O-B(C_6F_5)$_3$ adduct 9. A dry Schlenk flask was charged with phosphane oxide **1O** (62 mg, 0.25 mmol) and tris(pentafluorophenyl)borane (128 mg, 0.25 mmol) under argon. Dry dichloromethane (5 mL) was introduced, and the resulting solution was stirred for 1 h. Evaporation under vacuum left pure adduct **9** as a yellow solid in quantitative yield (190 mg).

^{1}H NMR (400 MHz, $CDCl_3$): δ = 3.42-3.49 (m, 2H, CH_2), 4.15 (vq, *J′* = 1.3 Hz, 2H, C_5H_4), 4.22 (s, 5H, C_5H_5), 4.28 (vt, *J′* = 1.8 Hz, 2H, C_5H_4), 6.68 (br dt, $^{1}J_{PH}$ = 523.6 Hz, $^{3}J_{HH}$ = 4.6 Hz, 2H, PH_2) ppm. ^{13}C{^{1}H} NMR (101 MHz, $CDCl_3$): δ = 24.21 (d, $^{1}J_{PC}$ = 67 Hz, CH_2), 69.04 (d, J_{PC} = 4 Hz, CH of C_5H_4), 69.45 (s, C_5H_5), 69.93 (s, CH of C_5H_4), 117.92 (br s, C^{ipso} of C_6F_5), 137.12 (dm, $^{1}J_{FC}$ = 251 Hz, CF), 140.02 (d of sextet, $^{1}J_{FC}$ = 252 Hz, J_{FC} = 7 Hz, CF), 147.74 (dm, $^{1}J_{FC}$ = 240 Hz, CF) ppm; the signal due to C^{ipso} of C_5H_4 was not detected. ^{11}B {^{1}H} NMR (128 MHz, $CDCl_3$): δ = −0.7 (br s) ppm. ^{19}F NMR (376, $CDCl_3$): δ = −135.6 (m, 6F, F^{orto} of C_6F_5), −157.1 (t, $^{3}J_{FF}$ = 21 Hz, 3F, F^{para} of C_6F_5), −163.6 (m, 6F, F^{meta} of C_6F_5) ppm. ^{31}P{^{1}H} NMR (162 MHz, $CDCl_3$): δ = 17.8 (heptet, $^{5}J_{PF}$ = 7 Hz) ppm. ^{31}P NMR (162 MHz, $CDCl_3$): δ = 17.8 (tt of heptet, $^{1}J_{PH}$ = 523 Hz, $^{2}J_{PH}$ = 9 Hz, $^{5}J_{PF}$ = 7 Hz) ppm. IR (Nujol): ν = 2954 s, 1647 m, 1521 m, 1460 vs, 1413 w, 1396 w, 1284 m, 1206 m, 1145 s, 1102 s, 1063 w, 1040 w, 1029 w, 1013 m, 982 m, 964 m, 945 w, 918 w, 893 w, 857 w, 850 w, 827 m, 793 m, 773 m, 740 w, 730 w, 697 w, 682 m, 676 m, 614 w, 575 w, 498 w, 482 w, 415 w cm^{-1}. HRMS (ESI−) Calc. for $C_{29}H_{12}F_{15}FeOP$ ([M − H]$^{-}$): 758.9840, found: 758.9837. Anal. Calc. for $C_{29}H_{13}BF_{15}FeOP$ (760.0): C 45.83, H 1.72%. Found: C 45.61, H 1.96%.

The reaction of 1O with borane. Borane in THF (0.5 mL of 1M solution, 0.50 mmol) was added to a solution of **1O** in the same solvent (124 mg, 0.50 mmol in 10 mL) while stirring and cooling in a dry ice/ethanol bath. The solution was stirred at −78°C for 2 h and then evaporated. Subsequent NMR analysis revealed the formation of a complex mixture, which contains unreacted **1O** (major), regenerated phoshane **1** (major) and its borane adduct **1**·BH_3 (traces), presumably the adduct $FcCH_2P(OH)H{\cdot}BH_3$ and other unidentified species with P–H bonds (see Figures S82 and S83). When the amount of BH_3 was increased to 5 equiv., the reaction mixture mostly consisted of **1** and **1**·BH_3.

Analytical data for **1**:[5] $^{31}P\{^1H\}$ NMR (162 MHz, $CDCl_3$): δ = −129.1 (s) ppm. ^{31}P NMR (162 MHz, $CDCl_3$): δ = −129.1 (t, $^1J_{PH}$ = 194 Hz) ppm. Analytical data for **1**·BH_3:[6] $^{31}P\{^1H\}$ NMR (162 MHz, $CDCl_3$): δ = −40.5 (br s) ppm. ^{31}P NMR (162 MHz, $CDCl_3$): −40.5 (br t, $^1J_{PH}$ = 357 Hz) ppm. Analytical data for $FcCH_2P(OH)H{\cdot}BH_3$: $^{31}P\{^1H\}$ NMR (162 MHz, $CDCl_3$): δ = 91.8 (br s) ppm. ^{31}P NMR (162 MHz, $CDCl_3$): δ = 91.8 (br d, $^1J_{PH}$ = 376) ppm.

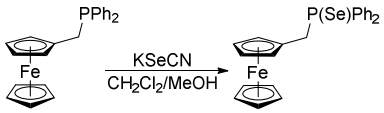

Synthesis of (ferrocenylmethyl)phosphane selenide, $FcCH_2P(Se)Ph_2$. (Ferrocenylmethyl)-diphenylphosphane (192 mg, 0.50 mmol)[7] and potassium selenocyanate (86 mg, 0.60 mmol) were mixed in dichloromethame and methanol (10 ml each), and the resulting mixture was stirred overnight and then evaporated with chromatographic silica gel (ca. 15 mL). The crude, preadsorbed product was transferred onto the top of a chromatographic column and eluted by ethyl acetate-hexane (1:1). A single yellow band was collected and evaporated, leaving **$FcCH_2P(Se)Ph_2$** as a yellow solid. Yield: 210 mg (91%).

^1H NMR (400 MHz, $CDCl_3$): δ = 3.79 (d, $^2J_{PH}$ = 11.7 Hz, 2H, CH_2), 3.95 (dt, J' = 1.0, 1.8 Hz, 2H, C_5H_4), 4.00 (t, J' = 1.8 Hz, 2H, C_5H_4), 4.09 (s, 5H, C_5H_5), 7.39-7.50 (m, 6H, PPh_2), 7.70-7.78 (m, 4H, PPh_2) ppm. $^{13}C\{^1H\}$ NMR (101 MHz, $CDCl_3$): δ = 37.88 (d, $^1J_{PC}$ = 44 Hz, CH_2), 68.03 (s, CH of C_5H_4), 68.82 (s, C_5H_5), 70.10 (d, J_{PC} = 2 Hz, CH of C_5H_4), 77.87 (s, C^{ipso} of C_5H_4), 128.35 (d, J_{PC} = 12 Hz, CH of PPh_2), 130.86 (d, $^1J_{PC}$ = 71 Hz, C^{ipso} of PPh_2), 131.50 (d, J_{PC} = 3 Hz, CH of PPh_2), 132.17 (d, J_{PC} = 10 Hz, CH of PPh_2) ppm. $^{31}P\{^1H\}$ NMR (162 MHz, $CDCl_3$): δ = 32.2 (s with ^{77}Se satellites, $^1J_{SeP}$ = 728 Hz) ppm. IR (Nujol): ν = 1438 m, 1410 w, 1339 w, 1309 w, 1106 m, 1099 m, 1071 w, 1038 w, 1026 m, 999 m, 923 m, 837 m, 831 m, 824 w, 808 m, 748 s, 737 s, 718 m, 701 m, 691 s, 611 w, 531 s, 489 m, 474 m, 450 m, 415 w cm^{-1}. ESI+ MS: *m/z* 464 (M^+), 487 ($[M + Na]^+$). Anal. Calc. for $C_{23}H_{21}FePSe$ (463.2): C 59.64, H 4.57%. Found: C 59.46, H 4.40%.

X-RAY CRYSTALLOGRAPHY

Full-sphere diffraction data were collected at 120 K using a Bruker D8 VENTURE Kappa Duo diffractometer equipped with a PHOTON detector and a Cryostream Cooler (Oxford Cryosystems). The data for **7a** were obtained using Cu Kα radiation (λ = 1.54178 Å); in all other cases, Mo Kα radiation (λ = 0.71073 Å) was employed.

The structures were solved using direct methods (SHELXT-2014[8]) and subsequently refined using a full-matrix least-squares procedure based on F^2 (SHELXL-2014 or 2017[9]). All non-hydrogen atoms were refined with anisotropic displacement parameters. Hydrogen atoms at the PH, NH and OH moieties were identified on the difference density maps and refined as riding atoms with U_{iso}(H) set to a multiple of U_{eq} of their bonding atom, except for complex **4**·CH_2Cl_2, whose the PH hydrogens were refined with unconstrained isotropic displacement parameters. Hydrogen atoms bonding to carbons were included in their theoretical positions and refined as riding atoms with constrained U_{iso}(H). Compound **3** crystallized as a twin (twin law: 1 0 0.118; 0 −1 0; 0 0 −1). The refined contributions of the two domains were 44:56. In the structure of **8a**, the unsubstituted cyclopentadienyl ring was affected by a disorder and modelled over two positions. Their relative occupancies refined to approximately 70:30.

Selected crystallographic data and refinement parameters are outlined in Table S1. All geometric data and structural diagrams were obtained using a recent version of the PLATON program.[10] The numerical values were rounded to one decimal place with respect to their estimated deviations (ESDs). Parameters pertaining to atoms in constrained positions (hydrogens) are presented without ESDs.

CCDC 2019338 (**2**), 2019339 (**3**), 2019340 (**4**·CH_2Cl_2), 2019341 (**5**), 2019342 (**6a**), 2019343 (**7a**), 2019344 (**8a**), and 2019345 (**8b**) contain the supplementary crystallographic data for this paper. These data can be obtained free of charge from the joint Cambridge Crystallographic Data Centre and Fachinformationszentrum Karlsruhe Access Structures service www.ccdc.cam.ac.uk/structures.

Table S1. Selected crystallographic data and structure refinement parameters.[a]

Compound	**2**	**3**	**4**·CH_2Cl_2
Formula	$C_{11}H_{13}FeO_2P$	$C_{20}H_{25}Cl_2FeOPRu$	$C_{21}H_{27}Cl_4FePRu$
M	264.03	540.19	609.11
Crystal system	monoclinic	monoclinic	monoclinic
Space group	$P2_1/c$	$P2_1/c$	$P2_1/n$
a [Å]	14.0630(4)	18.3049(8)	7.9310(2)
b [Å]	7.5795(2)	9.8837(4)	16.2223(3)
c [Å]	10.5937(3)	11.4100(4)	18.7335(4)
α [°]	90	90	90
β [°]	108.877(1)	92.093(1)	100.730(1)
γ [°]	90	90	90
V [Å]^3	1068.45(5)	2062.9(1)	2368.09(9)
Z	4	4	4
μ(Mo Kα) [mm^{-1}]	1.535	1.779	1.775
Diffrns collected	18572	4702	36271
Independent diffrns	2429	4702	5431
Observed[a] diffrns	2401	4533	5360
R_{int}[b] [%]	1.86	3.19	2.21
No. of parameters	136	239	258
R[b] obsd diffrns [%]	1.88	2.12	2.04
R, wR[b] all data [%]	1.90, 5.02	2.32, 4.92	2.07, 4.62
Δρ [e Å^{-3}]	0.366, -0.307	0.526, -0.385	0.654, -0.819

[a] Diffractions with $I > 2\sigma(I)$. [b] Definitions: $R_{int} = \Sigma \left| F_o^2 - F_o^2(\text{mean}) \right| / \Sigma F_o^2$, where F_o^2(mean) is the average intensity of symmetry-equivalent diffractions. $R = \Sigma \left| \left| F_o \right| - \left| F_c \right| \right| / \Sigma \left| F_o \right|$, $wR = [\Sigma\{w(F_o^2 - F_c^2)^2\}/\Sigma w(F_o^2)^2]^{1/2}$.

Table S1 continued

Compound	**5**	**6a**	**7a**
Formula	$C_{22}H_{26}Fe_2I_2O_2P_2Zn$	$C_{15}H_{21}FeO_3P$	$C_{14}H_{19}FeO_2P$
M	815.24	336.14	306.11
Crystal system	monoclinic	triclinic	monoclinic
Space group	$P2_1/c$	$P\bar{1}$	$P2_1/c$
a [Å]	8.9552(3)	10.8030(5)	12.3996(8)
b [Å]	9.4406(3)	11.8932(5)	10.6015(6)
c [Å]	30.808(1)	11.9674(5)	11.5940(6)
α [°]	90	80.249(2)	90
β [°]	91.680(1)	80.710(2)	112.090(3)
γ [°]	90	85.793(2)	90
V [Å]^3	2603.5(2)	1493.8(1)	1412.2(1)
Z	4	4	4
μ(Mo Kα) [mm^{-1}]	4.525	1.120	9.562
Diffrns collected	28018	38154	10610
Independent diffrns	5960	6856	2656
Observed[a] diffrns	5826	6120	2089
R_{int}[b] [%]	2.12	3.30	8.53
No. of parameters	280	369	165
R[b] obsd diffrns [%]	1.93	5.00	5.07
R, wR[b] all data [%]	1.98, 4.61	5.63, 11.83	6.56, 12.76
Δρ [e Å^{-3}]	0.992, -0.891	1.205, -0.566	0.514, -0.389

Table S1 continued

Compound	**8a**	**8b**
Formula	$C_{25}H_{23}FeN_2O_3P$	$C_{25}H_{23}FeN_2OPS_2$
M	486.27	518.39
Crystal system	monoclinic	monoclinic
Space group	$P2_1/c$	$P2_1/c$
a [Å]	11.2862(4)	10.8195(4)
b [Å]	9.2552(3)	20.2357(7)
c [Å]	21.9031(7)	10.9584(4)
α [°]	90	90
β [°]	104.805(1)	102.905(1)
γ [°]	90	90
V [Å]^3	2212.0(1)	2338.6(2)
Z	4	4
μ(Mo Kα) [mm^{-1}]	0.785	0.913
Diffrns collected	35525	22737
Independent diffrns	5048	5348
Observed[a] diffrns	4901	5098
R_{int}[b] [%]	2.08	1.72
No. of parameters	326	289
R[b] obsd diffrns [%]	2.62	2.22
R, *wR*[b] all data [%]	2.68, 6.74	2.34, 5.72
Δρ [e Å^{-3}]	0.492, -0.312	0.406, -0.249

DESCRIPTION OF THE CRYSTAL STRUCTURES

As the more polar product of thermally induced disproportionation of **1O**, **(ferrocenylmethyl)-phosphinic acid (2)** crystallized directly from the reaction mixture upon cooling. A view of the molecular structure is shown in Figure S1 along with the relevant geometric parameters.

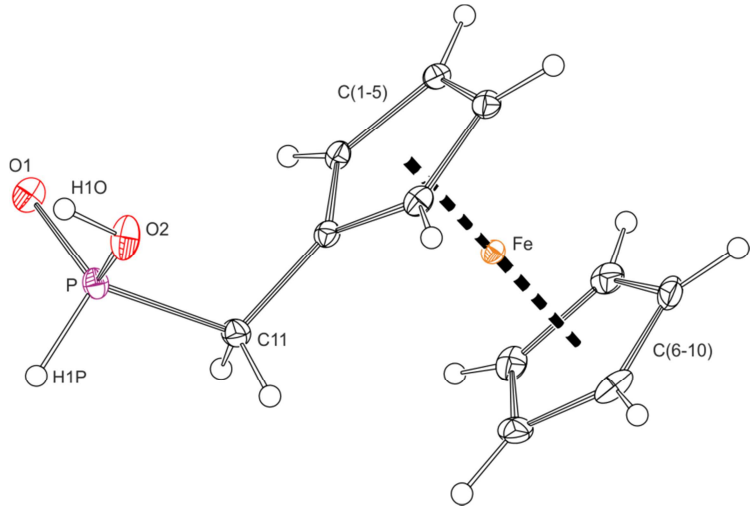

Figure S1. PLATON plot of the molecular structure of **2** showing atomic labels and displacement ellipsoids at the 30% probability level. Selected distances and angles (in Å and deg): P-O1 1.497(1), P-O2 1.544(1), P-C11 1.789(1); O1-P-O2 114.26(6), O1-P-C11 114.42(6), O2-P-C11 105.63(6), C1-C11-P 113.34(9).

The molecule of **2** comprises a regular ferrocene moiety with negligibly varying Fe-C distances (2.034(1)-2.046(1) Å) and, accordingly, planar and parallel cyclopentadienyl rings (the dihedral angle of the ring planes is only 1.22(8)°). The pivotal C1-C11 bond lies in the plane of the cyclopentadienyl ring C(1-5) (angle: 1.32(9)°) but the methylphosphinic moiety is directed above the ferrocene unit. Parameters pertaining to the terminal PH(O)(OH) group suggest a localized nature with clearly distinct P-O bond lengths similar to those in, *e.g.*, 1,2-ethylenebis(phosphonic acid).[11] In the crystal state, individual molecules of **2** assemble into the infinite zig-zag chains *via* P-OH···O=P bonds (O···O = 2.490(1) Å), oriented in the direction of the crystallographic *b* axis (Figure S2).

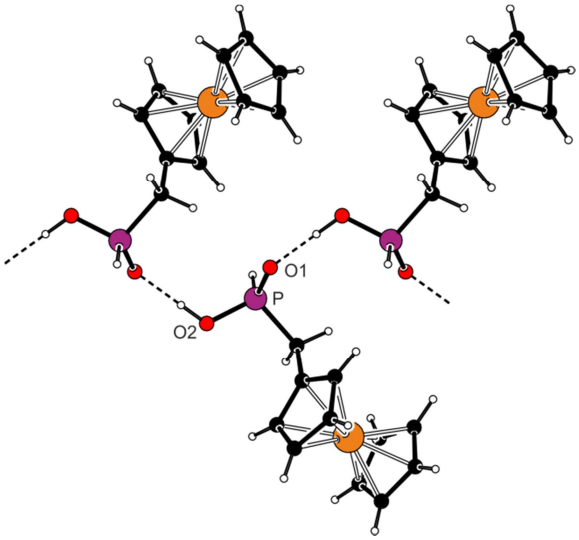

Figure S2. View of the hydrogen-bonded chain in the structure of **2**.

Apart from the presence of solvent of crystallization, the structures of **(η⁶-arene)Ru(II) complexes 3 and 4·CH_2Cl_2** differ only in substitution at the coordinated phosphorus atoms (Figure S3 and Table S2). Unsurprisingly, therefore, the geometric parameters describing the coordination sphere of the Ru(II) ions are very similar and match the data previously reported for complexes [(η⁶-*p*-cymene)$RuCl_2$($FcCH_2PR_2$-κ*P*)], where R = H[12] and Ph.[13] A minor, albeit statistically significant, difference was found in the Ru-P bond length, which is shorter in the hydroxyphosphine complex **3**. The arene ligands are somewhat twisted, as shown by the variation in Ru-C bonds, but remain oriented parallel to the basal planes {P,Cl1,Cl2} (*cf*. the dihedral angles 1.01(9)° and 1.72(6)° for **3** and **4**·CH_2Cl_2, respectively). Conversely, the ferrocene units retain their regular geometry, with marginally varying Fe-C distances and practically parallel cyclopentadienyl rings.

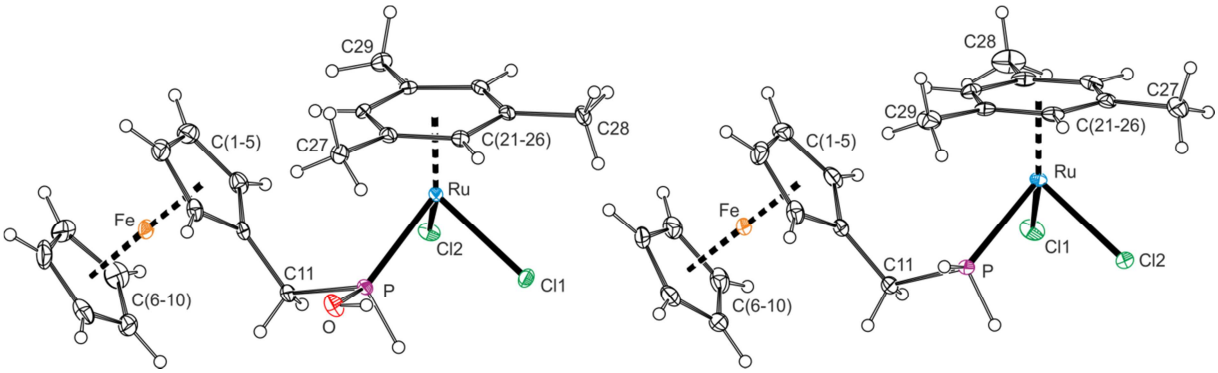

Figure S3. PLATON plot of the complex molecules in the structures of **3** (left) and **4**·CH_2Cl_2 (right). Displacement ellipsoids are scaled to the 30% probability level.

Table S2. Selected distances and angles for **3** and **4**·CH_2Cl_2 (in Å and deg).[a]

Parameter	**3**[b]	**4**·CH_2Cl_2
Ru-P	2.2831(7)	2.3186(5)
Ru-Cl1/2	2.4107(8)/2.4095(7)	2.4130(4)/2.4120(5)
P-Ru-Cl1/2	83.91(3)/79.02(3)	82.53(2)/83.48(2)
Cl1-Ru-Cl2	85.52(3)	87.97(2)
Ru-C (range)	2.13(3)-2.278(2)	2.190(2)-2.243(2)
Fe-C (range)	2.034(3)-2.047(3)	2.038(2)-2.049(2)
Cp1 *vs*. Cp2	1.5(2)	1.2(1)
arene *vs*. Cp1	49.2(2)	50.3(1)
P-C11	1.815(3)	1.837(2)
P-C11-C1	116.5(2)	112.2(1)

[a] Cp1 and Cp2 are the cyclopentadienyl rings C(1-5) and C(6-10), respectively; arene denotes the plane of the π-bound arene ring, C(21-26). [b] Additional data: P-O 1.594(2), Ru-P-O 119.44(8), C11-P-O 99.9(1).

In the crystal, the molecules of **3** associate *via* O-H···Cl hydrogen bonds into dimers located around the crystallographic inversion centers (O···Cl1 = 3.042(2) Å; Figure S4). In the structure of **4**·CH_2Cl_2, the solvent forms H-bonds with the chloride ligands (C1S-H1S1-Cl1 with C1S···Cl = 3.575(3) Å, and C1S-H1S2···Cl2 with C1S···H2S = 3.502(2) Å).

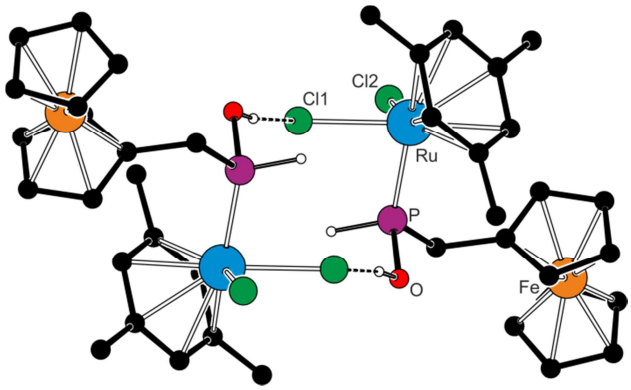

Figure S4. Simplified packing diagram of **3**. Only OH and PH hydrogen are shown for clarity.

Complex 5 crystallized with the symmetry of the monoclinic space group $P2_1/c$ directly from the reaction mixture. In its structure, the zinc(II) ion is tetracoordinate (Figure S5), ligated by two iodide anions and two O-bonded phosphane oxide ligands **1O**. The Zn-donor distances in **5** are similar to the corresponding parameters determined for $[ZnI_2(Ph_3PO)_2]$.[14] However, the coordination sphere of the zinc(II) ion is angularly distorted due to different steric demands of

the ligands. Among the interligand angles, the I1-Zn-I2 is the most acute and the O1-Zn-O2 the most opened. Other angles remain near the ideal tetrahedral value (≈106-108°). The departure from a regular geometry is also reflected in the τ_4 index,[15] which is 0.90 (*cf.* the values expected for an ideal square and tetrahedral geometry are 0 and 1, respectively).

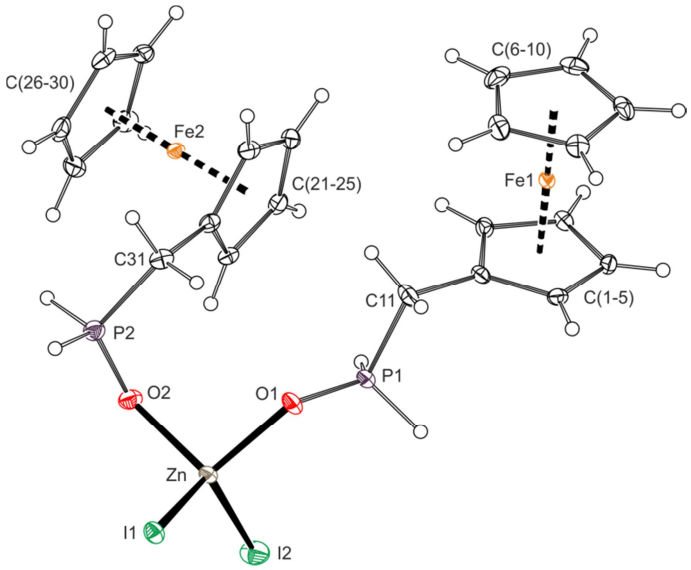

Figure S5. PLATON plot of the molecular structure of **5** showing atomic labels and displacement ellipsoids at the 30% probability level. Selected distances and angles (in Å and deg): Zn-I1 2.5337(8), Zn-I2 2.5542(4), Zn-O1 1.990(2), Zn-O2 1.982(2), I1-Zn-I2 124.82(2), I1-Zn-O1 106.63(5), I1-Zn-O2 106.10(5), I2-Zn-O1 108.42(5), I2-Zn-O2 108.31(5), O1-Zn-O2 99.72(7).

The ferrocene units in the two structurally independent ligands in **5** adopt their usual geometry (*cf*. Fe1-C(1-10): 2.023(2)-2.049(2) Å, Fe2-C(21-30): 2.032(2)-2.049(2) Å; tilt angles: 1.4(1)° for Fe1, and 1.4(1)° for Fe2) and are rotated to positions nearly perpendicular with respect to each other (the dihedral angle of the C(1-5) and C(21-25) lest-squares planes is 86.5(1)°). In addition, the organometallic ligands differ in the orientation of their phosphoryl donor substituents: the conformation at the C11-P1 bond in ligand 1 is *anti* (*cf*. O1-P1-C11-C1 = −178.8(1)°), whereas the P=O bond in ligand 2 is in a gauche position (O2-P2-C31-C21 = 60.7(2)°).

Depending on the configuration of the stereogenic carbon atoms, **compound 6a** contains two or three chirality centers. Isomers with the *same* configuration at both stereogenic carbon atoms, (S_C,S_C) and (R_C,R_C), do not contain an additional chirality element (the phosphorus atom is not stereogenic). Conversely, in isomers with *different* configuration at the carbon atoms, (S_C,R_C) and (R_C,S_C), the phosphorus atom becomes a stereogenic center, which in turn gives rise to two enantiomeric pairs, (R_P,R_C,S_C) − (S_P,S_C,R_C) and (R_P,S_C,R_C) − (S_P,R_C,S_C). In total, the addition of **1O** to

two acetone molecules produces **6a** as a mixture of *three* diastereoisomers in a statistical ratio of 1:2:1, which indeed matches the experimental observation.

This situation is also reflected in the solid-state structure. Compound **6a** crystallized with the symmetry of the triclinic space group *P*−1 and with two molecules *per* the asymmetric unit (Figure S6). The geometry of the molecules is very similar (Table 3). However, one of the molecules (Fe1) has the stereogenic carbon atoms C12 and C14 with the same configuration (S_C,S_C) and, hence, contains an achiral phosphorus atom. Because of the symmetry of the crystal lattice, this molecule has its inversion-related (enantiomeric) counterpart (R_C,R_C) in the crystal. The other molecule (Fe2) is affected by a positional disorder of one methyl substituent, corresponding to a configurational inversion (H and Me groups swap their positions). Thus, although the configuration at C32 remains the same (R_C), the configuration at C34 is (R_C) in 80% of cases and (S_C) in the remaining 20% of molecules in the crystal. Only the less populated, (R_C,S_C) isomeric molecules and their centrosymmetric (S_C,R_C) counterparts present in the crystal structure contain an additional chirality center at the phosphorus atom.

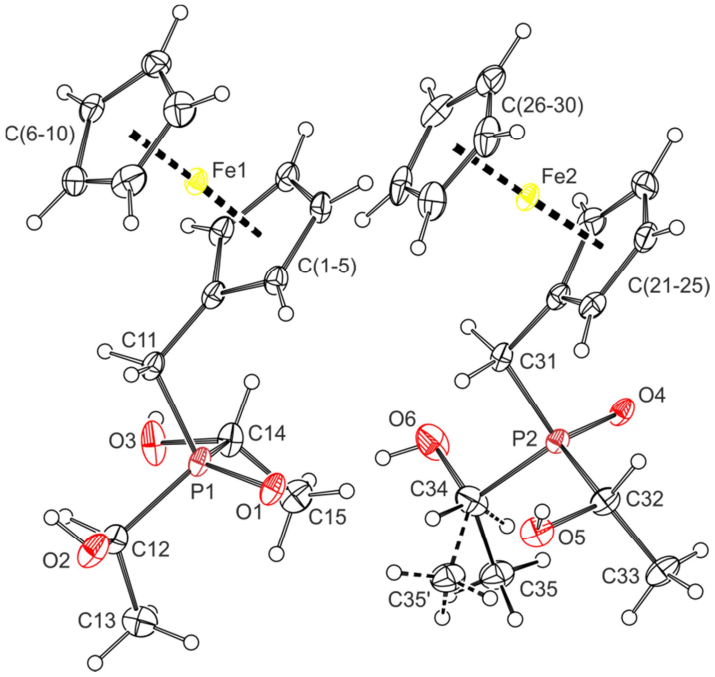

Figure S6. PLATON plot of the structure of **6a** with the displacement ellipsoids at the 30% probability level. Both positions of the disordered methyl group (C35) in molecule 2 are shown.

Table S3. Selected distances and angles for **6a** (in Å and deg).[a]

Parameter	Molecule 1	Parameter	Molecule 2
P1=O1	1.509(2)	P2=O4	1.506(2)
P1-C11	1.812(4)	P2-C31	1.814(4)
P1-C12	1.839(3)	P2-C32	1.834(3)
P1-C14	1.838(4)	P2-C34	1.829(4)
C1-C11-P1	112.2(2)	C21-C31-P2	112.7(2)
O1-P1-C11	112.2(1)	O4-P2-C31	113.5(1)
O1-P1-C12	111.4(2)	O4-P2-C32	112.0(1)
O1-P1-C14	112.5(1)	O4-P2-C34	114.0(2)
C12-O2	1.408(4)	C32-O5	1.433(4)
C14-O3	1.424(4)	C34-O6	1.421(5)
Fe1-C(1-10)	2.027(4)-2.049(3)	Fe2-C(21-30)	2.033(3)-2.047(3)
Cp1 *vs.* Cp2	3.7(2)	Cp3 *vs.* Cp4	1.1(2)

[a] Definition of the ring planes: Cp1 = C(1-5), Cp2 = C(6-10), Cp3 = C(21-25), Cp4 = C(26-30).

Individual molecules of **6a** associate into two-dimensional layers through O-H···O=P interactions in which the phoshoryl oxygen atoms acts as bifurcate H-bond acceptors (Figure S7). The layers are oriented parallel to the crystallographic *ab* planes and are separated by the bulky ferrocene moieties, which are located above and below the layers.

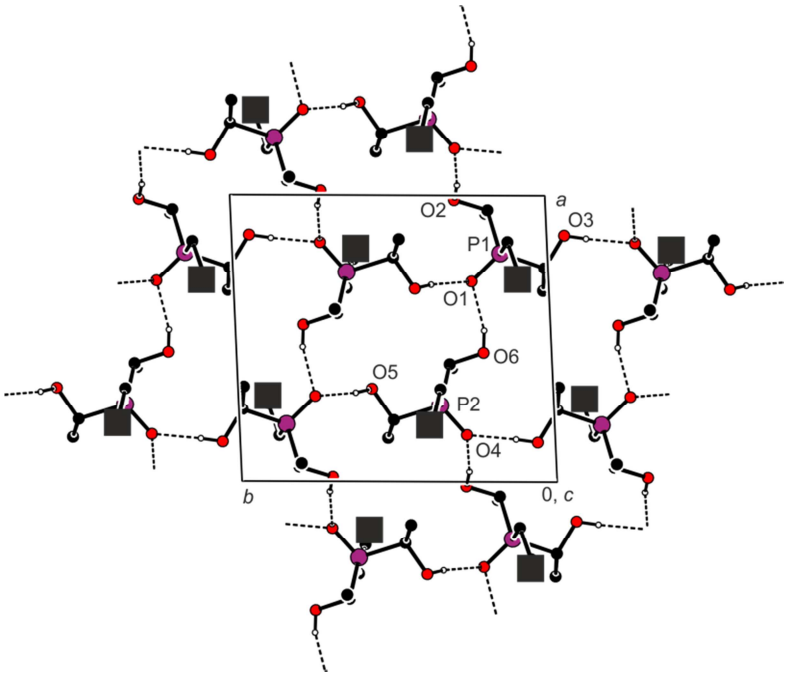

Figure S7. Depiction of the hydrogen-bonded assembly of **6a**. For clarity, the ferrocenyl moieties are replaced by black squares. Hydrogen bond lengths are as follows: O2···O4 = 2.738(3) Å, 03···O4 = 2.679(3) Å, O5···O1 = 2.715(3) Å, and O6···O1 = 2.698(4) Å.

Compound 7a crystallized with the symmetry of the monoclinic space group $P2_1/c$ and with one molecule *per* the asymmetric unit (Figure S8).

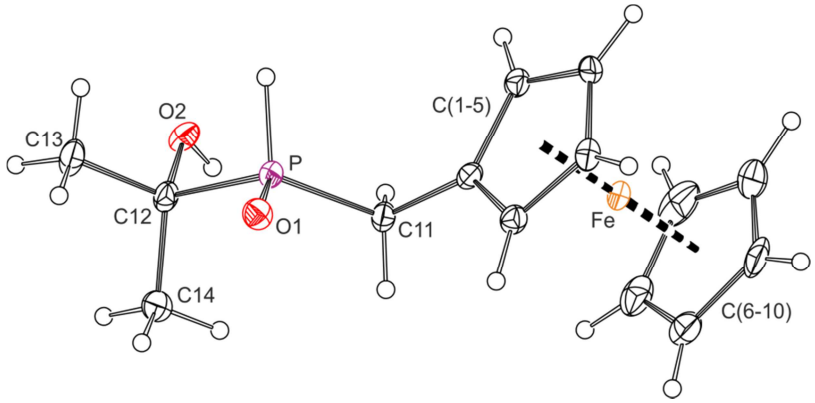

Figure S8. PLATON plot of the molecular structure of **7a** showing displacement ellipsoids at the 30% probability level. Selected distances and angles (in Å and deg): C1-C11 1.496(5), P-O1 1.496(2), P-C11 1.808(3), P-C12 1.829(3), C12-O2 1.429(4), C12-C13/C14 1.528(5)/1.522(5); C1-C11-P 107.9(2), C11-P-O1 113.9(1), C11-P-C12 109.0(2), P-C12-O2 105.5(2), C13-C12-C14 111.1(3).

The ferrocene unit in the structure of **7a** has a regular geometry (Fe-C distances in the range 2.030(5)-2.049(3) Å, tilt angle 1.6(2)°). Its phosphane oxide substituent is directed away from the iron atom with the pivotal C1-C11 bond diverted by 3.8(2)° from the plane of the parent cyclopentadienyl ring C(1-5). The terminal $CMe_2(OH)$ moiety is oriented to the side of the ferrocene scaffold with the two oxygen atoms assuming *anti* positons (*cf*. the torsion angle O1-P-C12-O2 = 168.2(2)°). The molecules in the crystal associate into one-dimensional chains through P=O···H-O hydrogen bonds (O1···O2 = 2.694(3) Å) oriented along the crystallographic *b* axis (Figure S9).

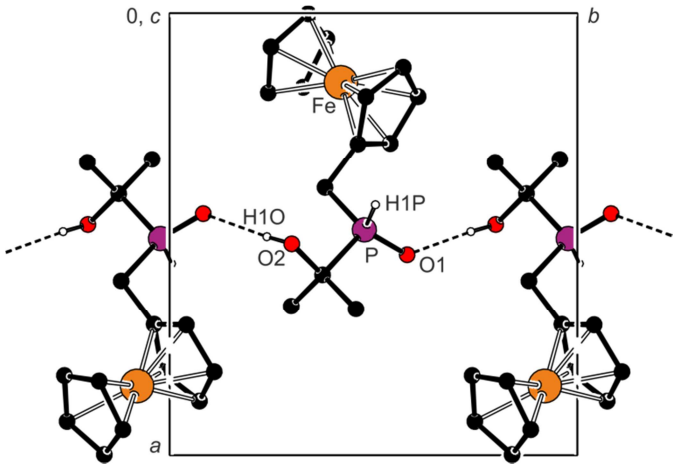

Figure S9. Section of a hydrogen-bonded chain in the structure of **7a**. Only the PH and OH hydrogens are shown for clarity.

Molecular structures of the **bis-amides 8a and 8b** are very similar and, hence, will be discussed jointly (Figure S10 and Table S4). For an easier comparison, parameters of **8b** are given in square brackets in the following text (the atomic labelling is the same with atoms S1 and S2 in **8b** respectively replacing O2 and O3 in **8a**).

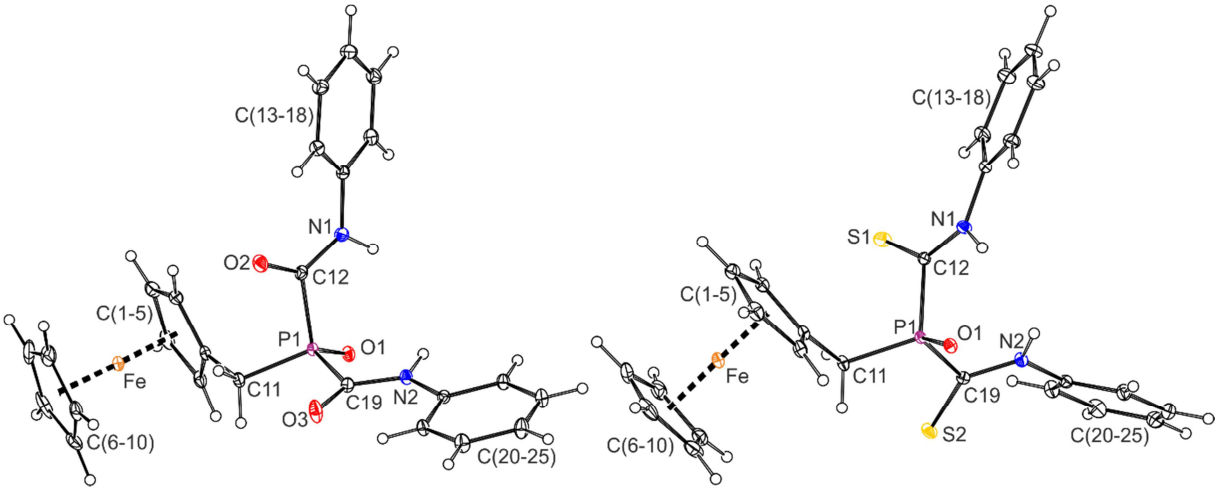

Figure S10. PLATON plots of **8a** (left) and **8b** (right) showing atomic labelling and displacement ellipsoids at the 30% probability level.

In both structures, the CH_2-P (C11-P1) bond is directed above the ferrocene unit (the angle at which the C11-P1 bond intersects the cyclopentadienyl plane is 71.47(7)° [63.44(7)°]) and slightly twisted, as shown by the torsion angles C2-C1-C11-P1 94.5(1)° [102.7(1)°] and C5-C1-C11-P1 −81.6(2)° [−79.4(1)°]. The P1=O1 bond is oriented to one side of the ferrocene moiety (C1-C11-P1-O1 = −53.4(1)° [56.5(1)]), whereas the two amide fragments are directed to the other side in an arrangement resembling open arms and with the C=O (C=S) bonds oriented approximately *anti* with respect to the central P1=O1 bond (**8a**: O1-P1-C12-O2 = 159.3(1)°, O1-P1-C19-O3 = −141.4(1)°; **8b**: O1-P1-C12-S1 = −168.34(7)°, O1-P1-C19-S2 = 120.78(7)°). Both amide units are essentially planar (**8a**: O2-C12-N1-C13 = −4.2(2)°, O3-C19-N2-C20 = −2.1(2)°; **8b**: S1-C12-N1-C13 = −2.9(2)°, S2-C19-N2-C20 = 4.2(2)°) and with their usual bond lengths and angles.[16]

Table S4. Selected distances and angles for **8a** and **8b** (in Å and deg).[a]

Parameter	**8a**	Parameter	**8b**
P1=O1	1.497(1)	P1=O1	1.4977(8)
P1-C11	1.806(1)	P1-C11	1.797(1)
C1-C11-P1	109.79(9)	C1-C11-P1	112.21(8)
O1-P1-C11	117.23(6)	O1-P1-C11	115.20(5)
O1-P1-C12/C19	114.79(6)/113.98(6)	O1-P1-C12/C19	111.72(5)/110.77(5)
C11-P1-C12/C19	103.51(6)/104.44(6)	C11-P1-C12/C19	108.92(6)/107.57(5)
C12=O2	1.215(2)	C12=S1	1.646(1)
C12-N1	1.346(2)	C12-N1	1.337(2)
O2=C12-N1	127.7(1)	S1=C12-N	130.7(1)
P1-C12-N1	114.1(1)	P1-C12-N1	111.43(9)
C19=O3	1.221(2)	C19=S2	1.650(1)
C19-N2	1.349(2)	C19-N2	1.340(2)
O3=C19-N2	127.0(1)	S2=C19-N2	128.01(9)
P1-C19-N2	114.92(9)	P1-C19-N2	112.62(8)
Ph1 *vs*. Ph2	88.46(7)	Ph1 *vs*. Ph2	84.73(7)
Cp1 *vs*. Ph1/Ph2	57.18(7)/84.70(7)	Cp1 *vs*. Ph1/Ph2	71.50(8)/39.48(7)
Fe1-C(1-10)	2.039(2)-2.053(1)[b]	Fe1-C(1-10)	2.039(1)-2.052(1)
Cp1 *vs*. Cp2	2.8(2)[b]	Cp1 *vs*. Cp2	1.34(8)

[a] Definition of the ring planes: Cp1 = C(1-5), Cp2 = C(6-10), Ph1 = C(13-18), Ph2 = C(20-25). [b] Only the data for the more populated position of the disordered cyclopentadienyl ring C(6-10) are considered.

In the crystal, the molecules of **8a** associate into centrosymmetric dimers by pairs of N-H···O=P hydrogen bonds (Figure S11), wherein the fosforyl oxygen serves as an acceptor for both NH moieties of the other molecule (N1···O1 = 2.965(2) Å, N2···O1 = 2.916(1) Å). These dimers are further interlinked through soft C-H···O=C interactions involving the amide oxygens O2 and O3. The molecules of **8b** form similar dimers around the inversion centers, albeit with shorter hydrogen bond distances (N1···O1 = 2.910(1) Å, N2···O1 = 2.877(1) Å) because their conformation is more compact. The changed conformation is also manifested by a close intramolecular contact between the N1-H1N group and the phosphoryl oxygen O1 (N1···O1 = 2.904(1) Å), but at a rather acute angle at H1N (122°) (indicated by a blue dotted line in Figure S11). Soft intra- and intermolecular N-H···S=C interactions are also detected in the structure of the thioamide.

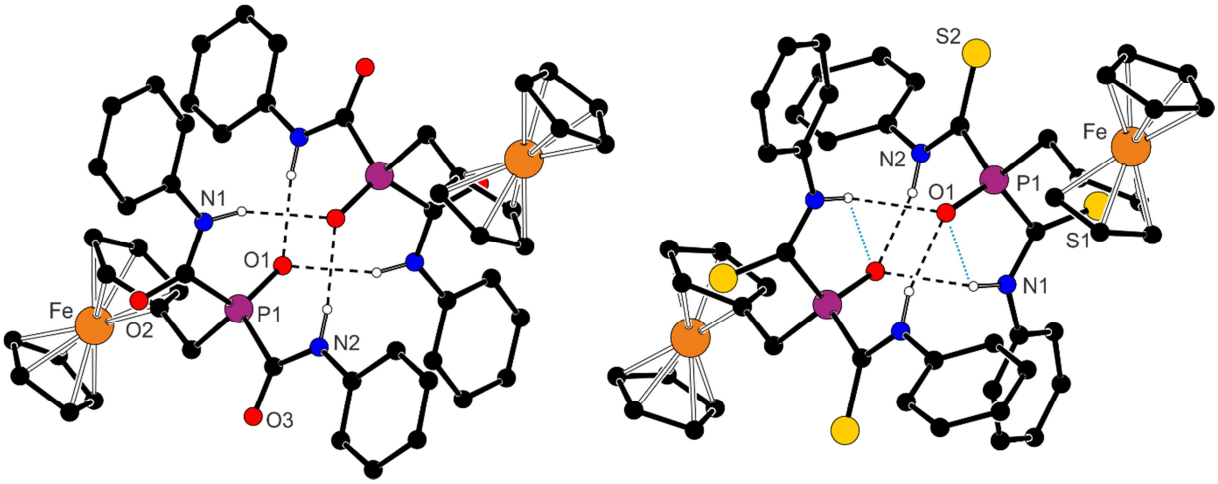

Figure S11. Hydrogen-bonded dimers in the structure of **8a** (left) and **8b** (right). Hydrogen bonds are indicated by dashed lines.

COMPARISON OF THE NMR PARAMETERS

Table S5. A tabular summary of selected NMR parameters.[a]

Compound	^{31}P NMR				^{1}H NMR	^{13}C NMR	
	δ_P	$^{1}J_{PSe}$	$^{1}J_{PH}$	$^{2}J_{PH}$	$\delta_H(PH_2)$	$\delta_H(CH_2)$	$^{1}J_{PC}$ (CH_2)
1[b]	−129.7	–	194	5	2.94	14.45	9
1O[b]	9.6	–	469	16	6.91	28.82	63
1S[b]	−7.2	–	453	14	6.57	31.62	49
1Se[b]	−34.5	733	444	13	6.00	30.22	42
$FcCH_2P(Se)Ph_2$[b]	32.2	728	–	12	–	37.88	44
3[b]	115.0	–	372	18, 11	6.86	29.65	38
4[b]	−24.0	–	355	8	4.79	18.19	29
5[b]	18.4	–	501	17	6.89	–	–
7a[c]	46.8	–	446	13	6.27	24.63	56
8a[b]	14.2	–	–	12	–	27.40	58
8b[d]	17.8	–	–	13	–	30.46	73
9[b]	17.8	–	523	9	6.68	24.21	67

[a] Chemical shifts (δ) and coupling constants (J) are given in ppm and Hz, respectively. Compounds, which could not be isolated or result as isomers with different NMR signature were excluded from the Table. [b] Recorded in $CDCl_3$. [c] Recorded in $(CD_3)_2SO$. [d] Recorded in CD_2Cl_2.

IR SPECTRA

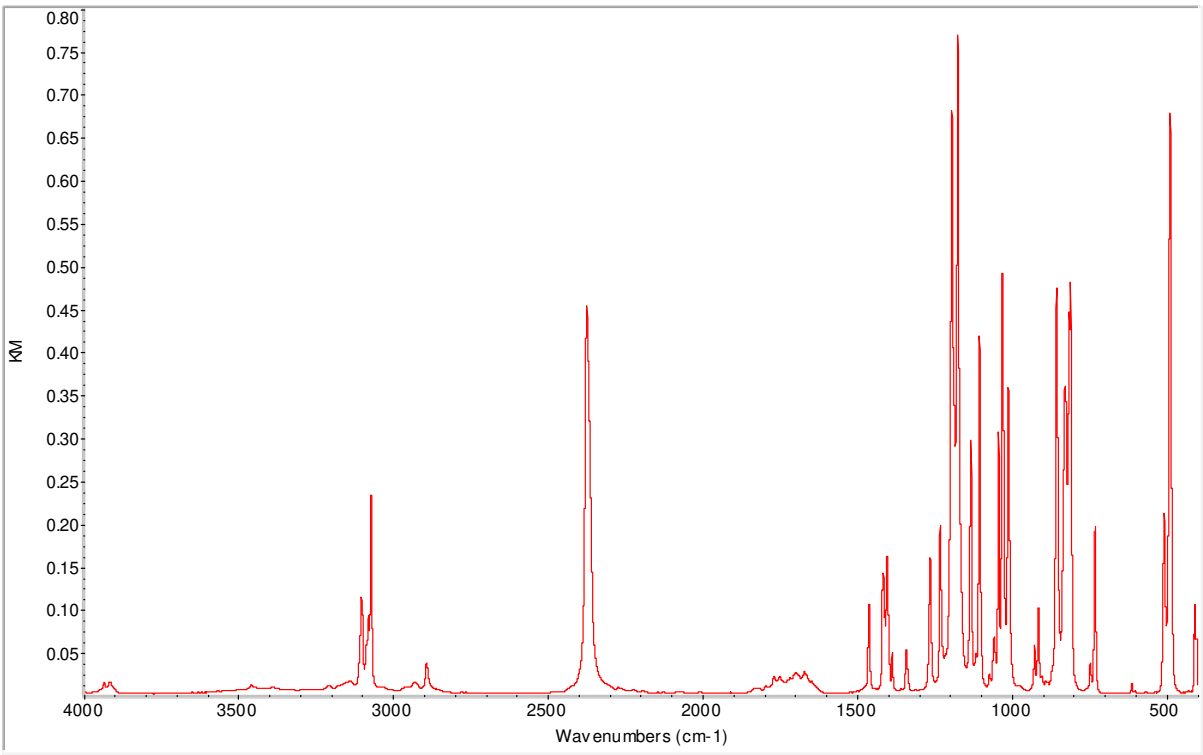

Figure S12. FTIR spectrum of **1O** (neat sample, diffuse reflectance mode).

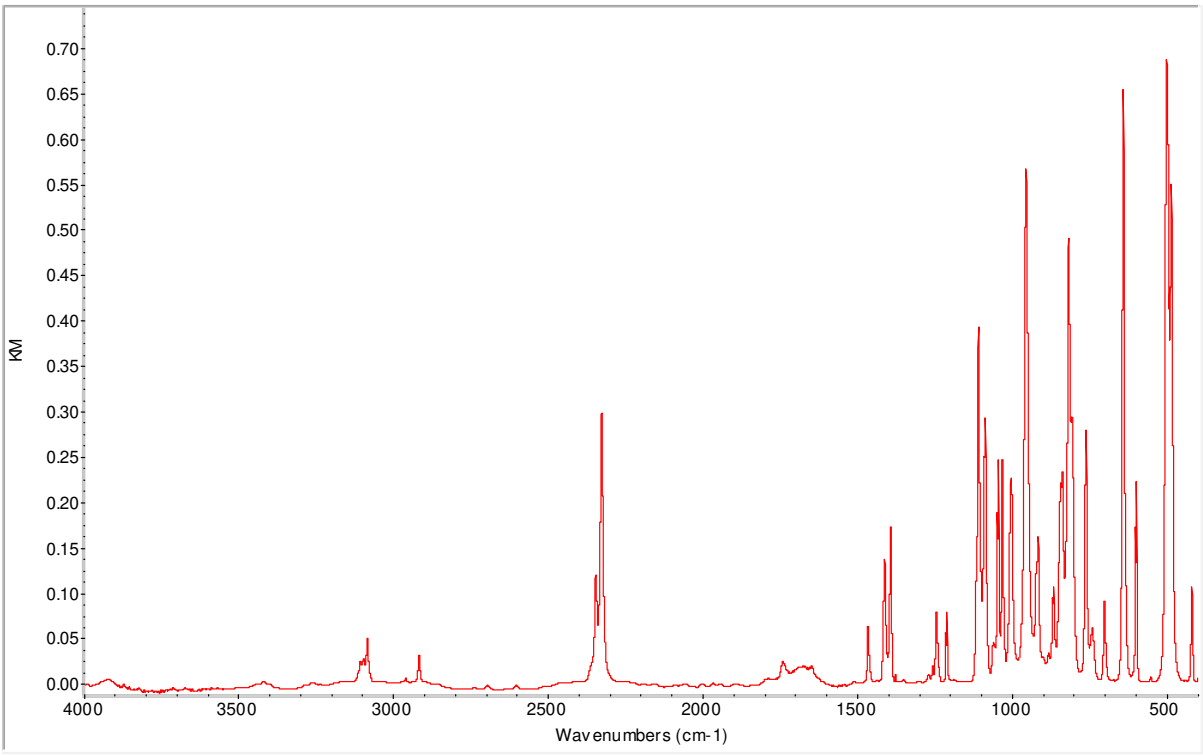

Figure S13. FTIR spectrum of **1S** (neat sample, diffuse reflectance mode).

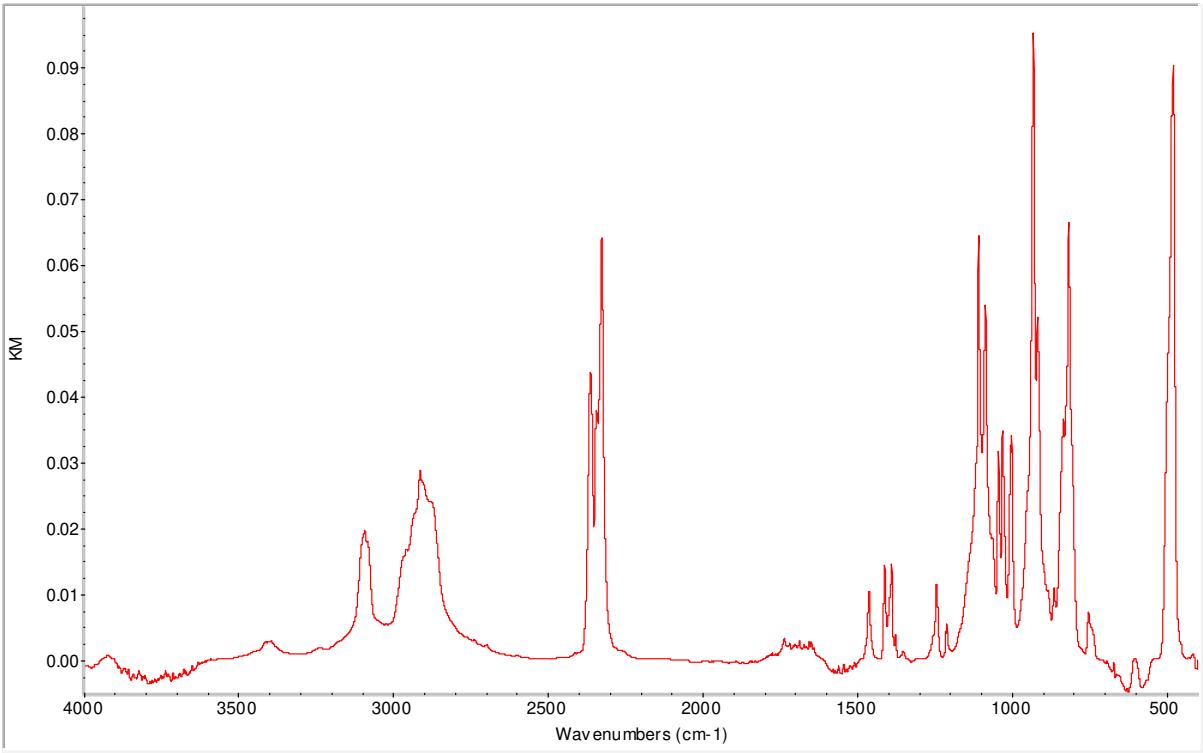

Figure S14. FTIR spectrum of **1Se** (neat sample, diffuse reflectance mode).

Table S6. Positions of the selected bands in the IR spectra of chalcogenides **1E**.[a]

assignment	**1O**	**1S**	**1Se**
P-H symmetric stretching vibration	2373 s	2343 m	2360 s
P-H asymmetric stretching vibration	2373 s	2324 s	2324 s
P-H scissoring vibration	1173 s	1105 s	1105 s
P-H wagging vibration	1028 s	952 s	929 s
P=E stretching vibration	1192 s	638 s	475 s

[a] The spectra were recorded in diffuse reflectance mode. The assignment is based on the results of preliminary DFT calculations at the PBE0[17]-D3[18]/def2-TZVP[19]:sdd[20](Fe) level of theory using the Gaussian 16 program package.[21]

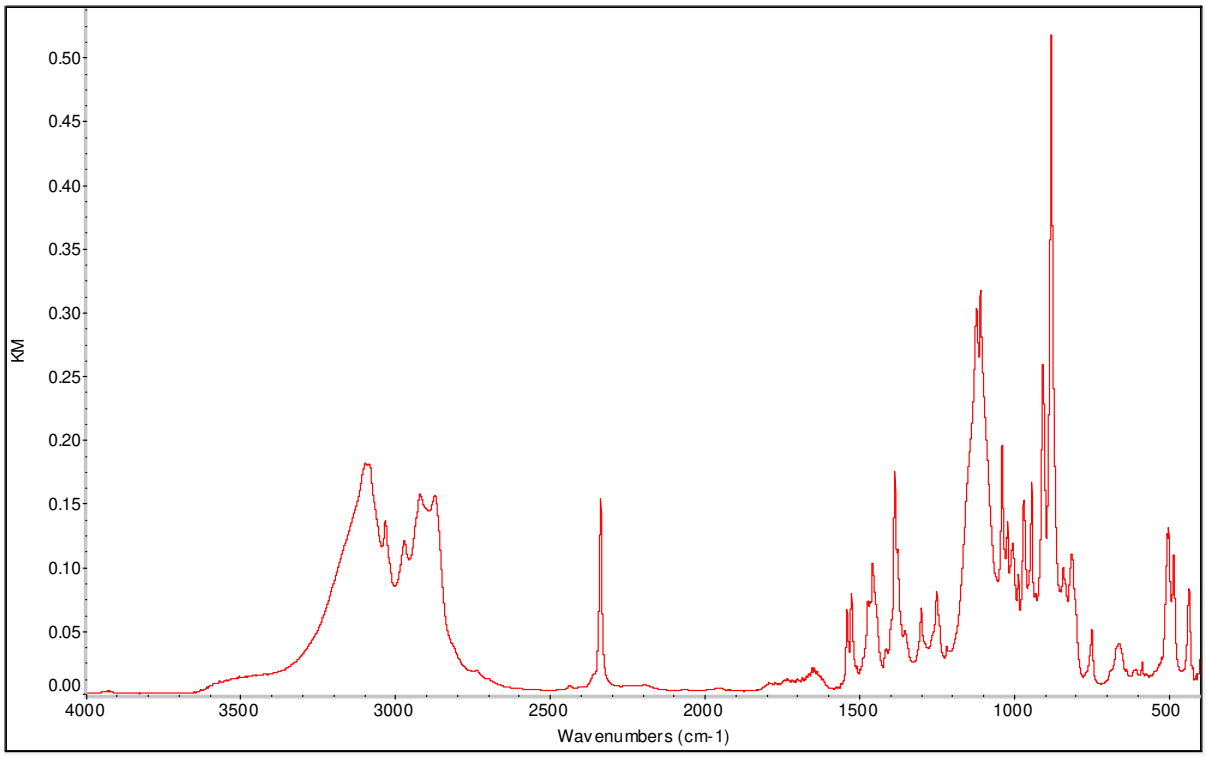

Figure S15. FTIR spectrum of **3** (neat sample, diffuse reflectance mode).

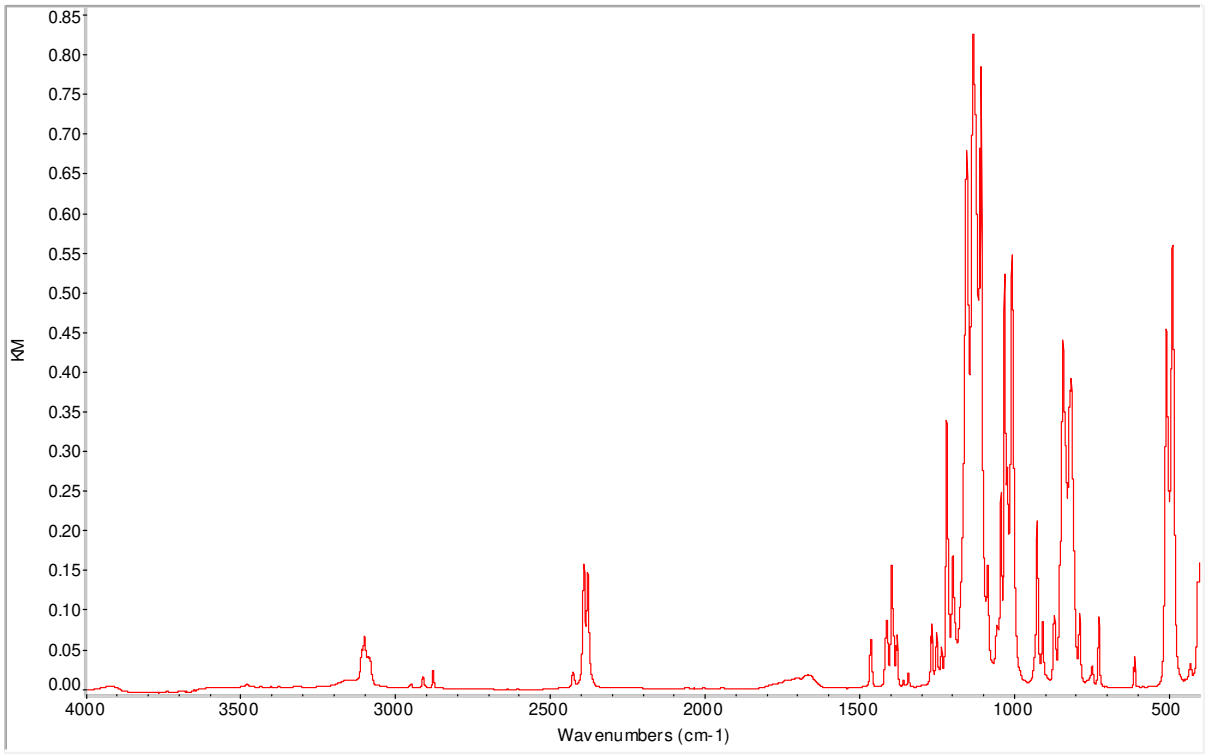

Figure S16. FTIR spectrum of **5** (neat sample, diffuse reflectance mode).

ELECTROCHEMISTRY

Cyclic voltammograms were recorded on a computer-controlled potentiostat μAUTOLAB III (EcoChemie, The Netherlands) at room temperature using a standard Metrohm cell with a glassy carbon disc working electrode (2 mm diameter), a platinum auxiliary electrode, and Ag/AgCl (KCl) reference electrode. The samples were dissolved in anhydrous dichloromethane containing 0.1 M $Bu_4N[PF_6]$ (Fluka, purissimum for electrochemistry) as the supporting electrolyte to make a 1 mM solution. The solutions were deaerated by argon bubbling before the measurements and then kept under an argon atmosphere. Decamethylferrocene (Alfa-Aesar) was added as an internal standard during the final scans, and the redox potentials were converted into the ferrocene/ferrocenium scale by subtracting 0.548 V.[22] The formal redox potentials $E°'$ for reversible redox events were determined as an average of the anodic and cathodic peak potentials in the cyclic voltammograms recorded at 0.1 V s^{-1} scan rate, $E°' = ½(E_{pa} + E_{pc})$. Due to the higher resistance of the analyzed solutions, the separations of the counter-waves in cyclic voltammograms, $\Delta E_p = E_{pa} - E_{pc}$, exceeded the theoretical value (59 mV for a reversible one-electron transfer at 25°C); the typical value was near 100 mV.

The redox behavior of all chalcogenides **1E** was complicated by adsorption phenomena that distorted peak shapes and led to the development of stripping peaks, as shown in the cyclic voltammograms of **1O** (Figure S17), with a reversible redox transition at 0.08 V *vs.* the ferrocene/ferrocenium reference, attributable to the oxidation of the ferrocene unit. This redox process was accompanied by a small pre-wave and a distinct cathodic stripping peak when the scan range was extended toward more positive potentials.

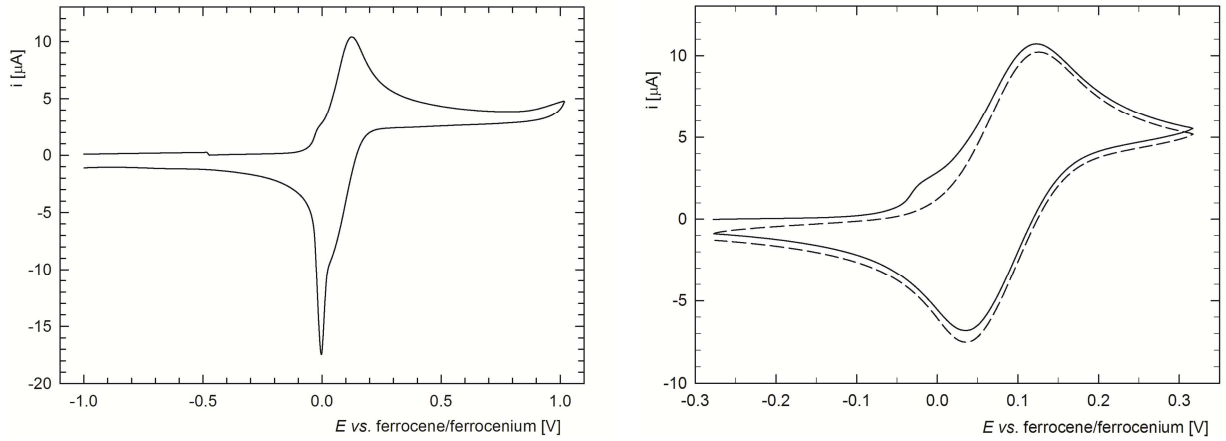

Figure S17. "Full" (left) and partial (right) cyclic voltammogram of **1O** as recorded on a glassy carbon electrode in dichloromethane solution containing 0.1 M $Bu_4N[PF_6]$ (scan rate: 0.1 V s^{-1}). The second scan is shown by a dashed line.

The redox response of phosphane sulfide **1S** and phosphane selenide **1Se** as reflected in the cyclic voltammograms was similar to that of **1O** (Figure S18). The compounds showed reversible redox events at essentially the same potential as **1O** ($E^{\circ\prime}$ 0.07-0.09 V). Unfortunately, the precision of potential determination was lowered by the adsorption phenomena. Especially in the case of **1Se**, the redox wave was markedly tilted, had widely separated counter peaks and was followed by an ill-defined, irreversible oxidation at more positive potentials.

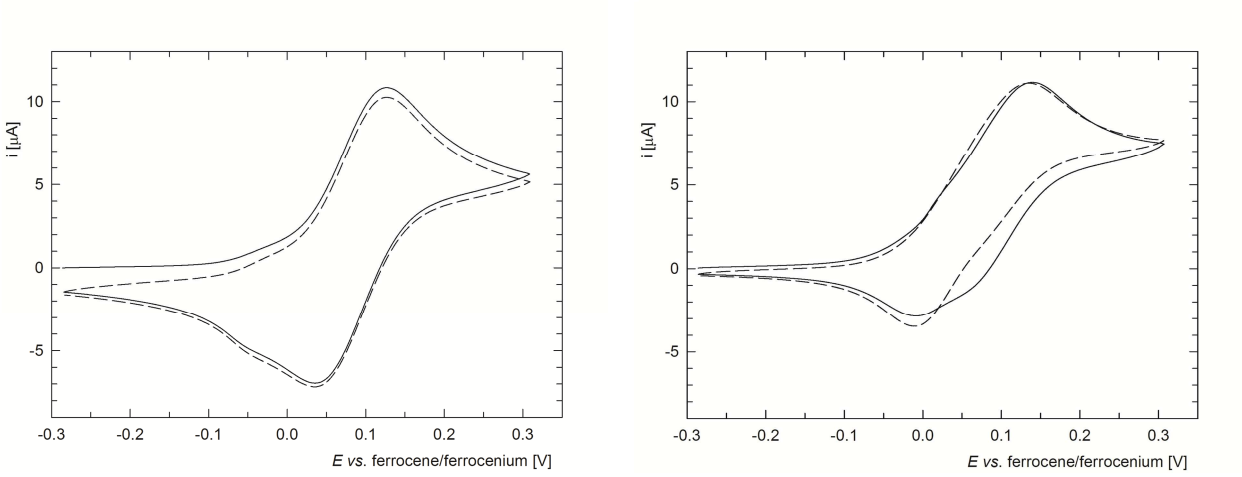

Figure S18. Cyclic voltammograms of **1S** (left) and **1Se** (righ). For conditions, see caption to Figure 17. The second scans are shown by dashed lines.

The redox behavior of complex **3** reflected the presence of an additional redox-active moiety (Ru^{II}/Ru^{III}). Specifically, the cyclic voltammogram (Figure 17) showed a reversible oxidation due to the ferrocene unit at 0.03 V and an irreversible oxidation at 0.76 V (peak potential), presumably occurring at the Ru center, which is followed by a post wave ($E_{pa} \approx 0.91$ V). In addition, there is observed an irreversible reduction at approximately −1.8 V.

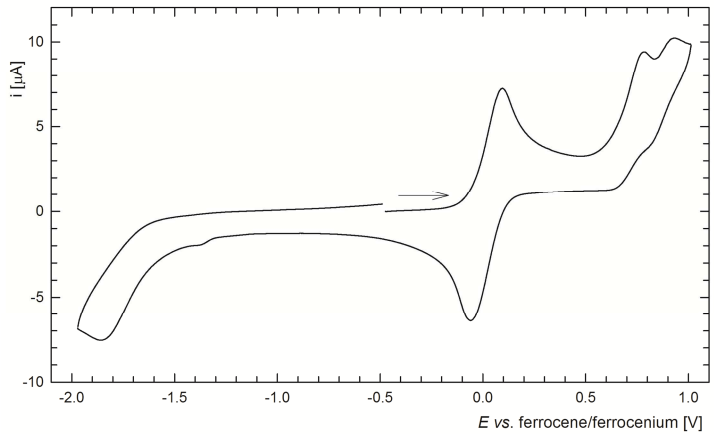

Figure S19. Cyclic voltammogram of complex **3** (for conditions see caption to Figure S17). The scan direction is indicated with an arrow.

COPIES OF THE NMR SPECTRA

(Note: solvent signals in the NMR spectra are denoted by an asterisk.)

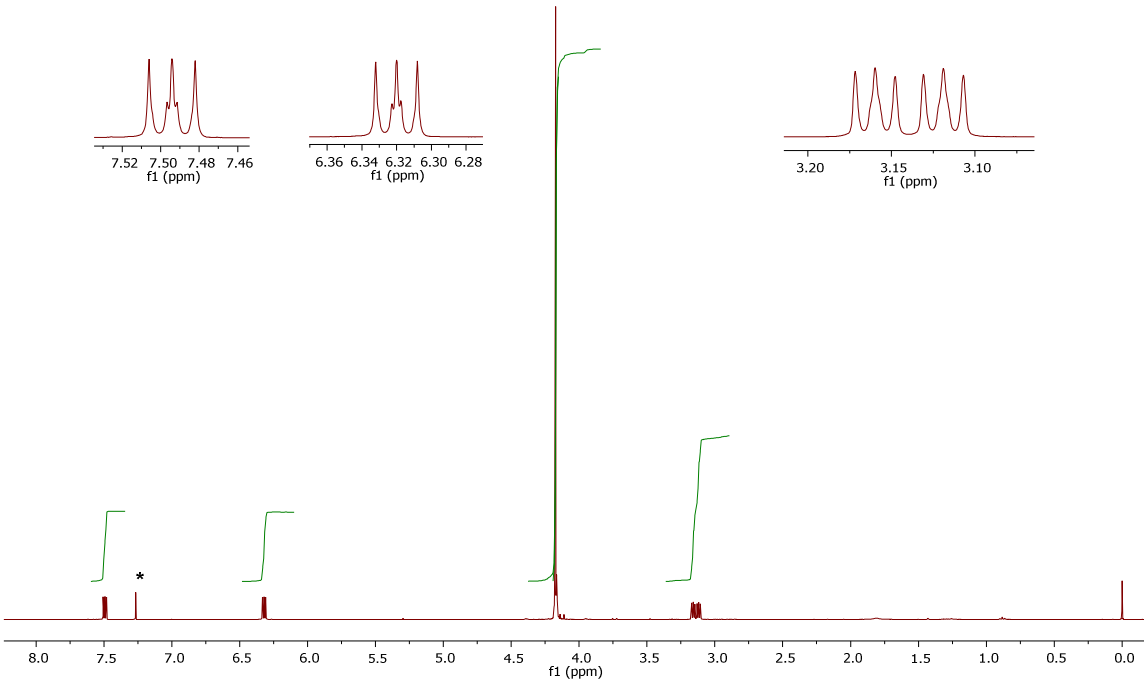

Figure S20. ^{1}H NMR spectrum (400 MHz, $CDCl_3$) of **1O**.

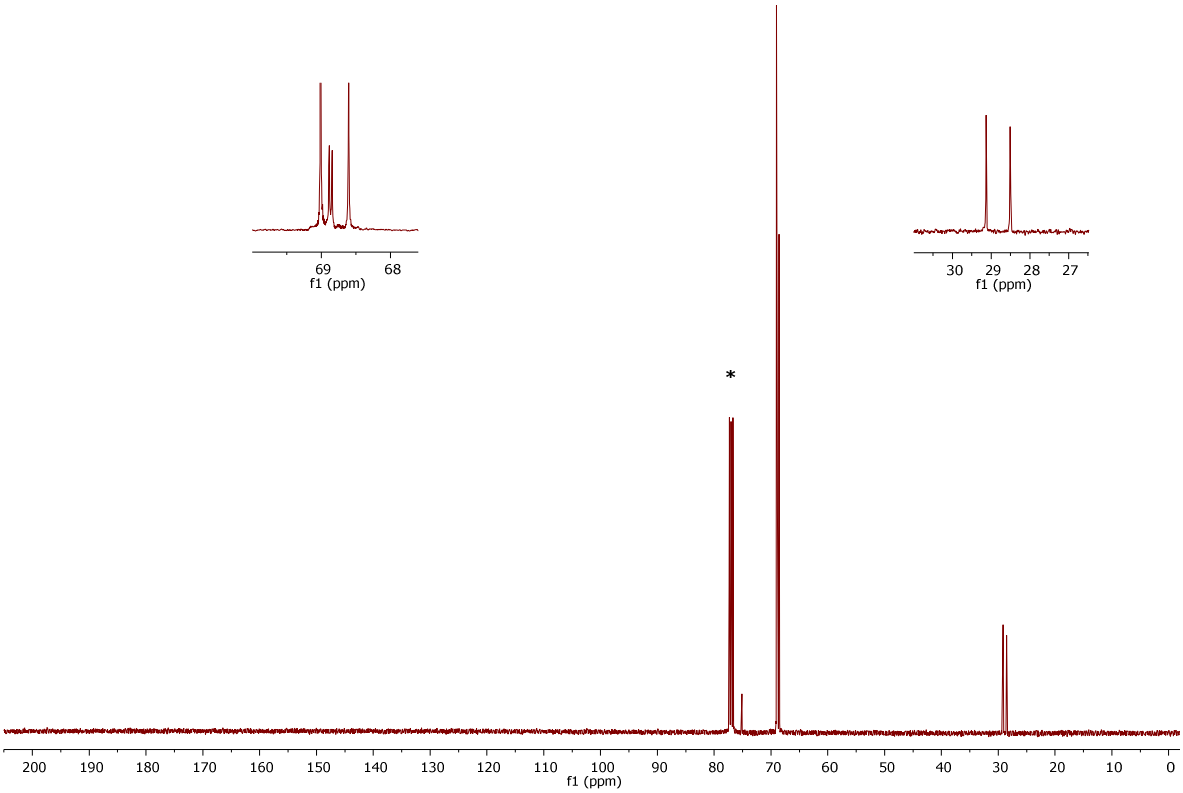

Figure S21. $^{13}C\{^{1}H\}$ NMR spectrum (101 MHz, $CDCl_3$) of **1O**.

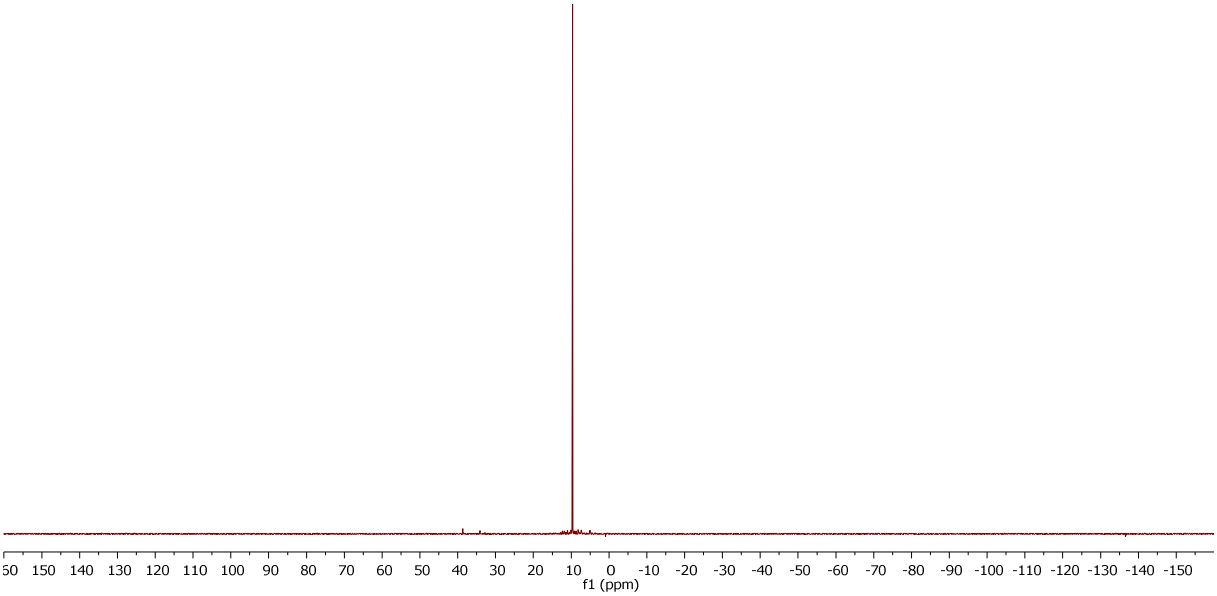

Figure S22. $^{31}P\{^{1}H\}$ NMR spectrum (162 MHz, $CDCl_3$) of **1O**.

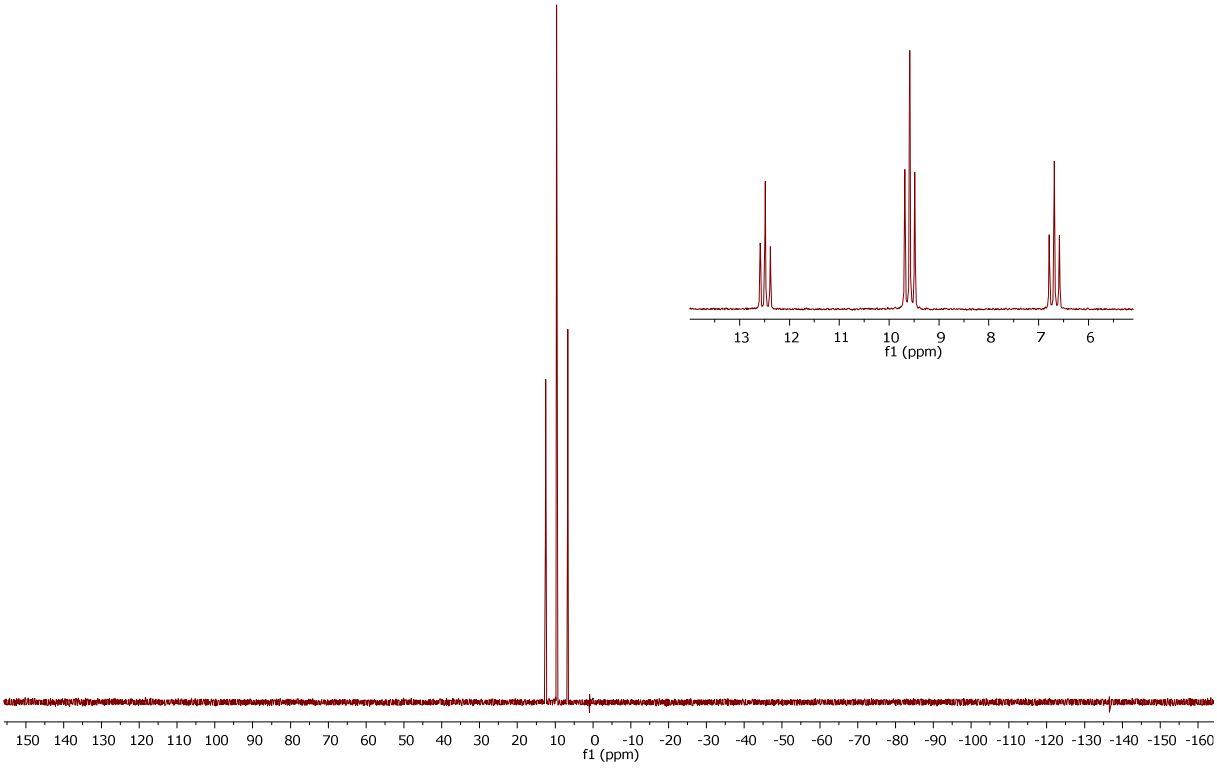

Figure S23. ^{31}P NMR spectrum (162 MHz, $CDCl_3$) of **1O**.

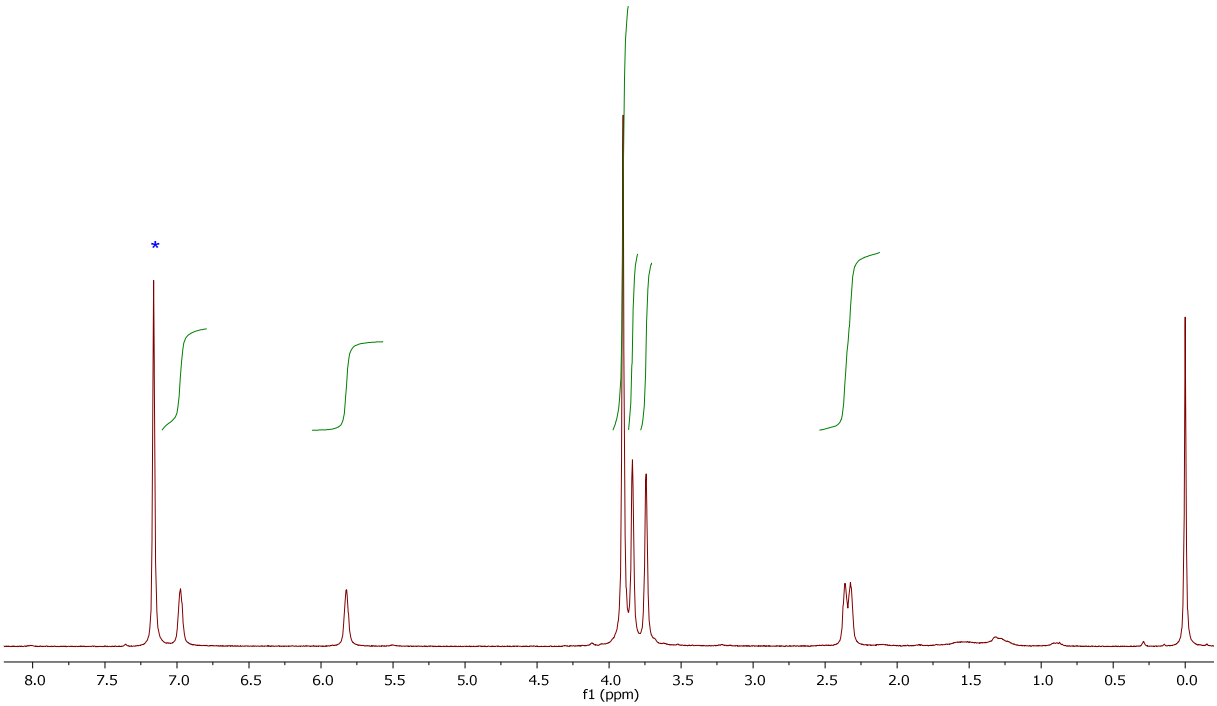

Figure S24. ^{1}H NMR spectrum (400 MHz, C_6D_6) of **1O**.

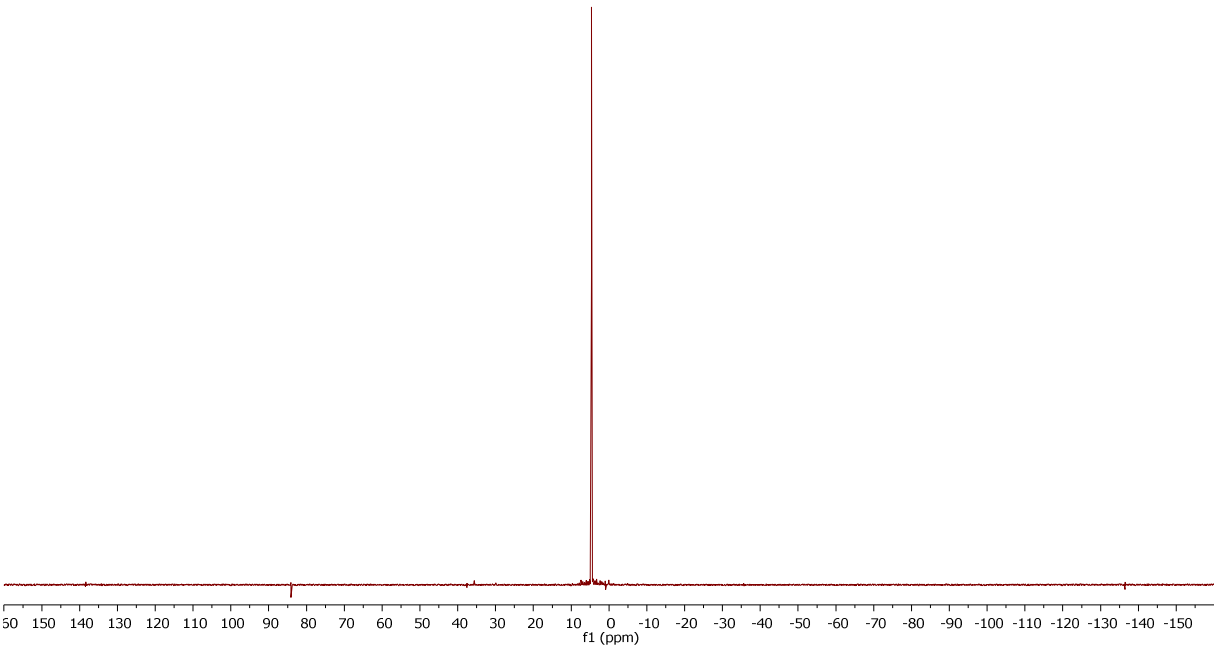

Figure S25. $^{31}P\{^{1}H\}$ NMR spectrum (162 MHz, C_6D_6) of **1O**.

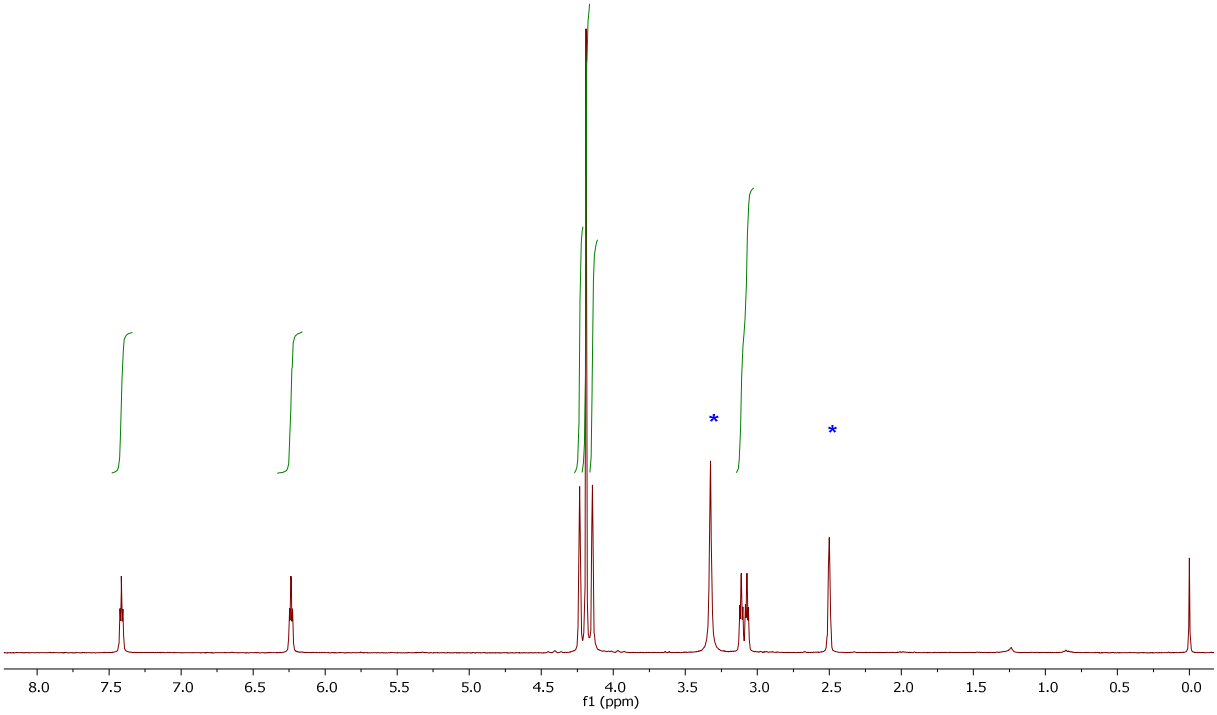

Figure S26. ^{1}H NMR spectrum (400 MHz, dmso-d_6) of **1O**.

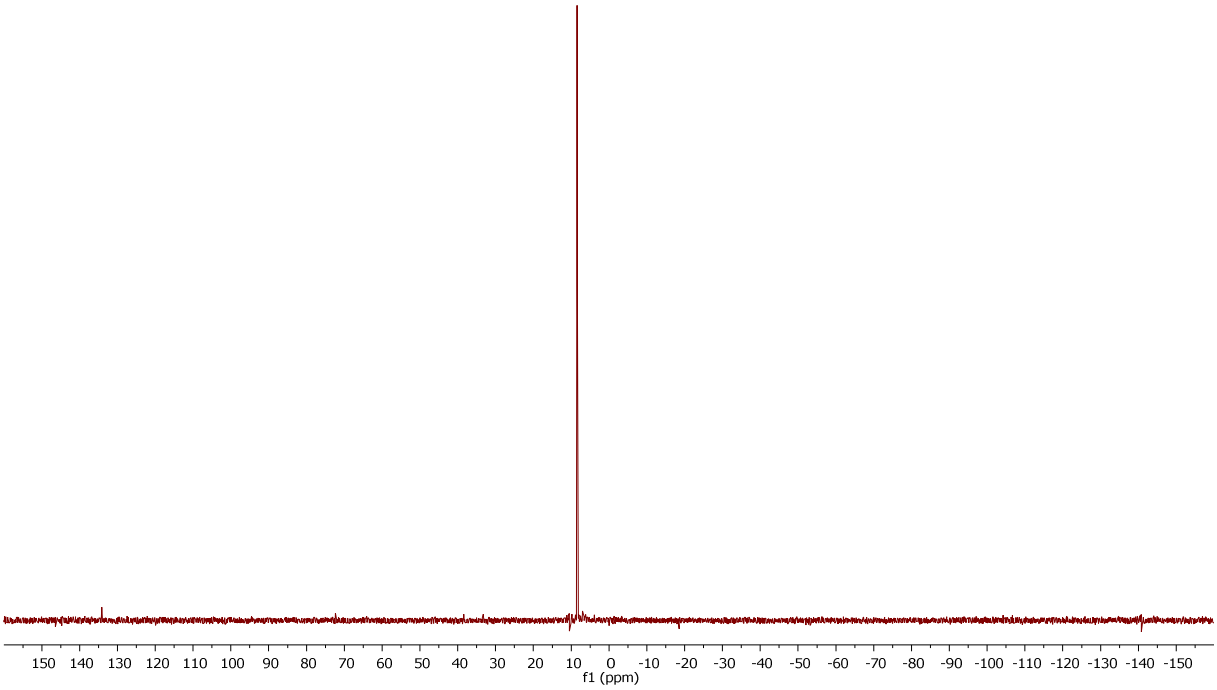

Figure S27. $^{31}P\{^{1}H\}$ NMR spectrum (162 MHz, dmso-d_6) of **1O**.

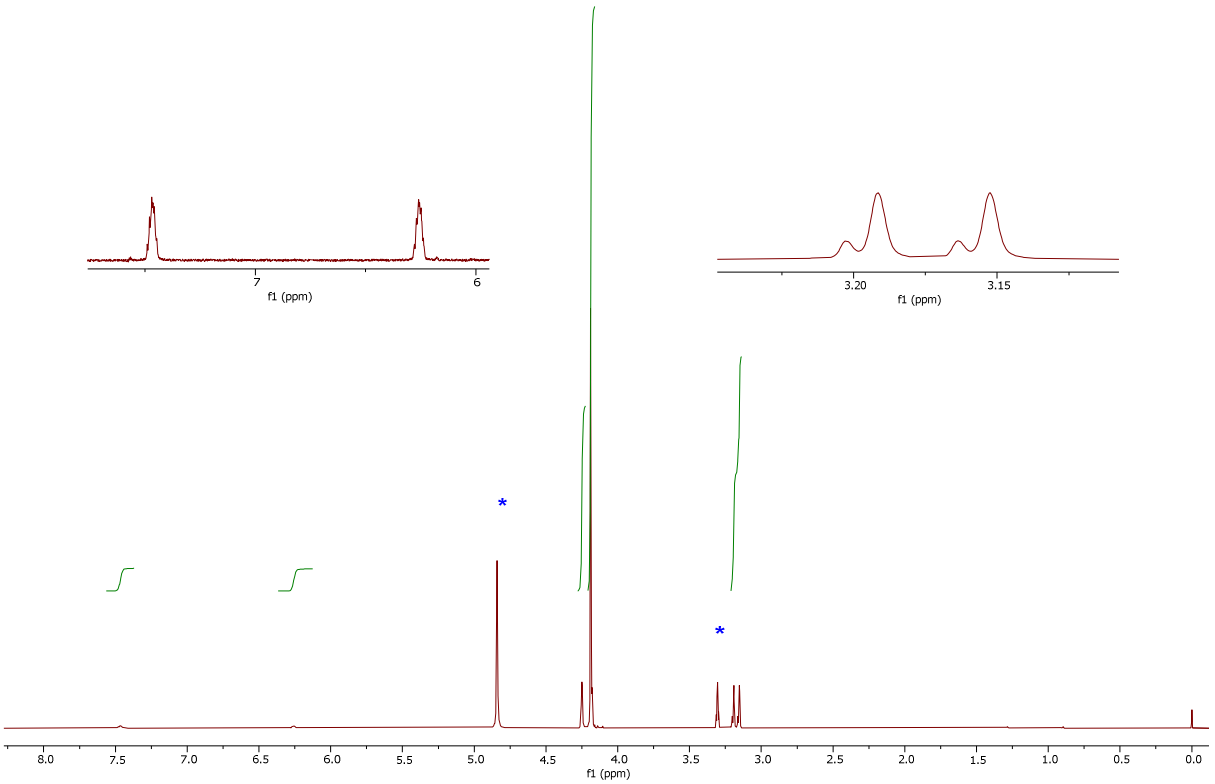

Figure S28. ^{1}H NMR spectrum (400 MHz, CD_3OD) of **1O**.

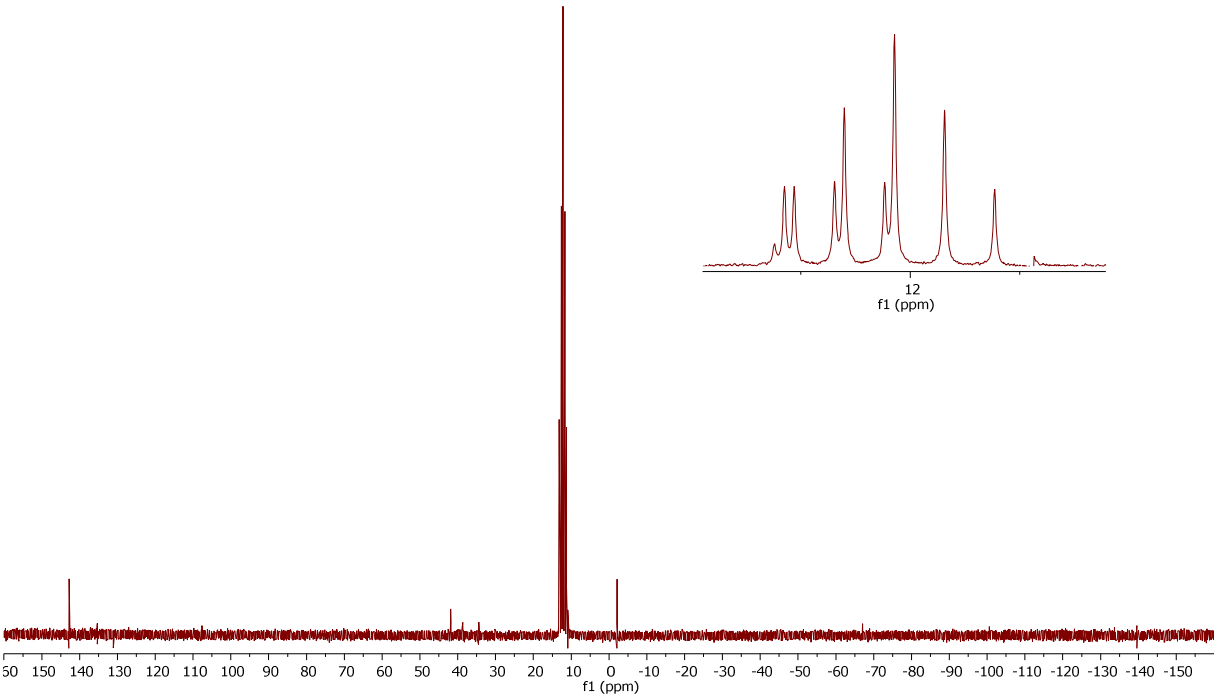

Figure S29. $^{31}P\{^{1}H\}$ NMR spectrum (162 MHz, CD_3OD) of **1O** (the spectrum corresponds to a mixture of $FcCH_2P(O)HD$ and $FcCH_2P(O)D_2$).

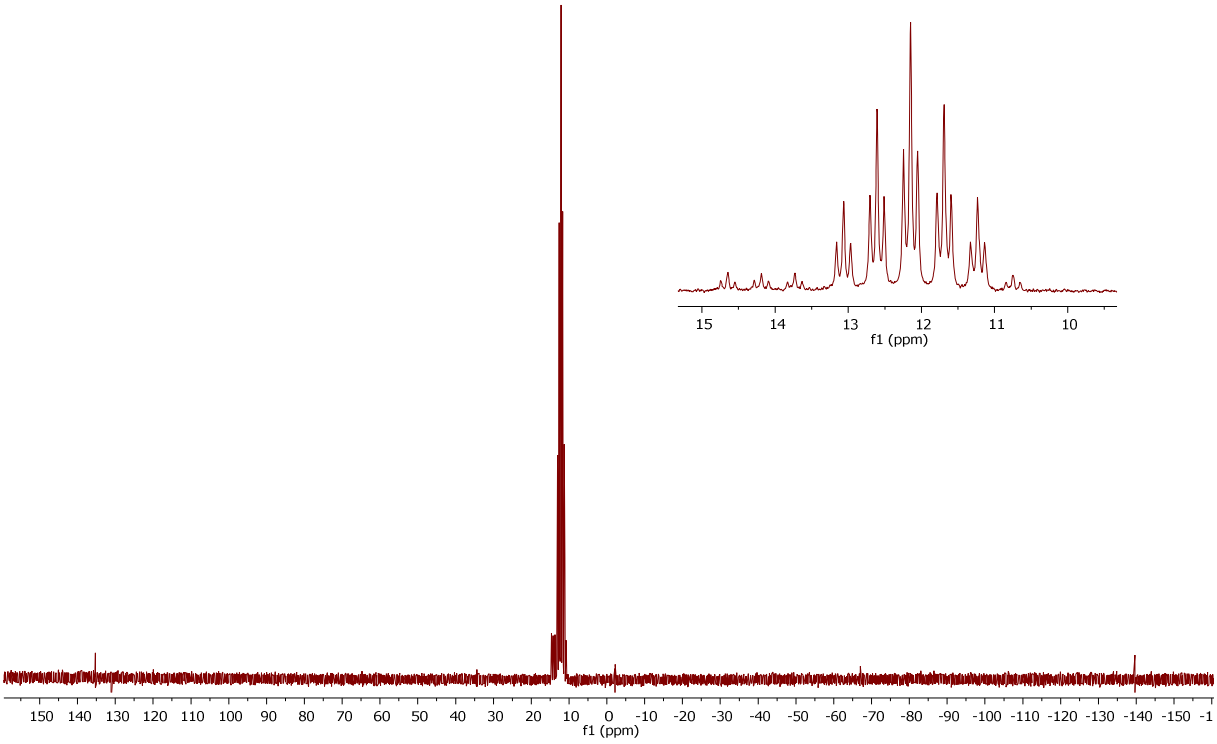

Figure S30. ^{31}P NMR spectrum (162 MHz, CD_3OD) of **1O** (the spectrum corresponds to a mixture of $FcCH_2P(O)HD$ and $FcCH_2P(O)D_2$).

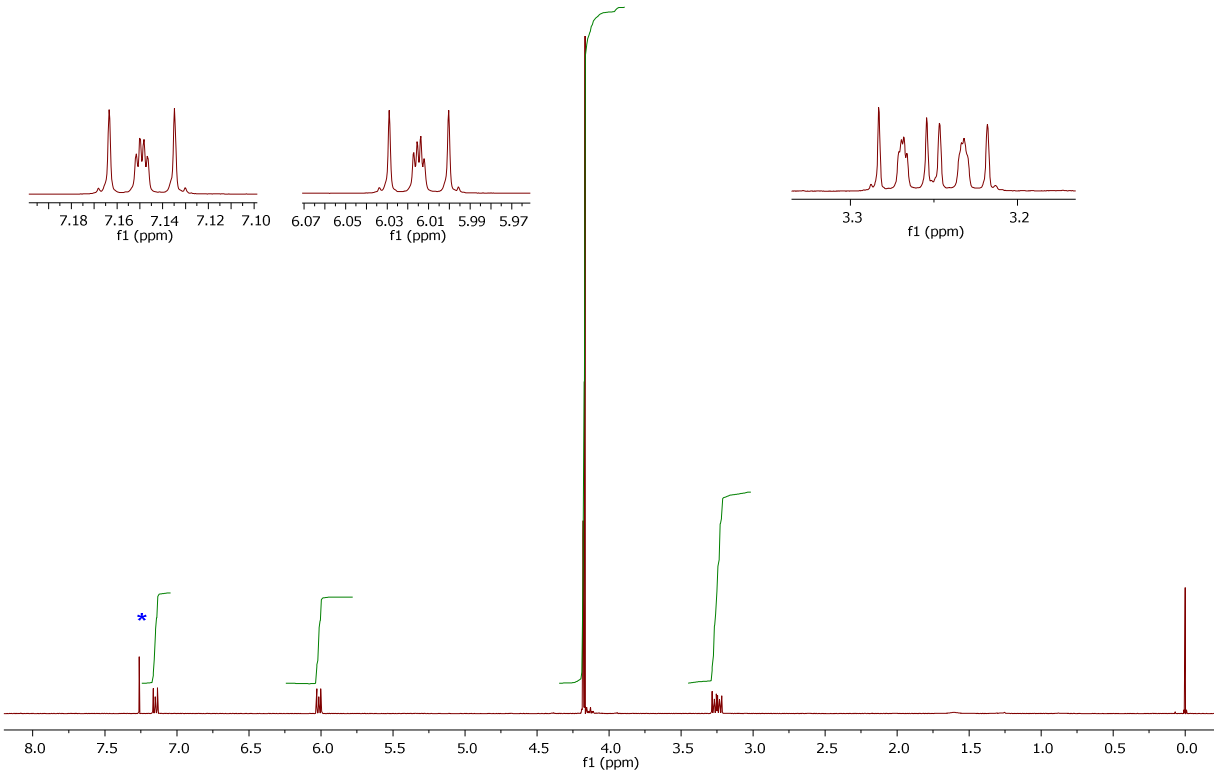

Figure S31. ^{1}H NMR spectrum (400 MHz, $CDCl_3$) of **1S**.

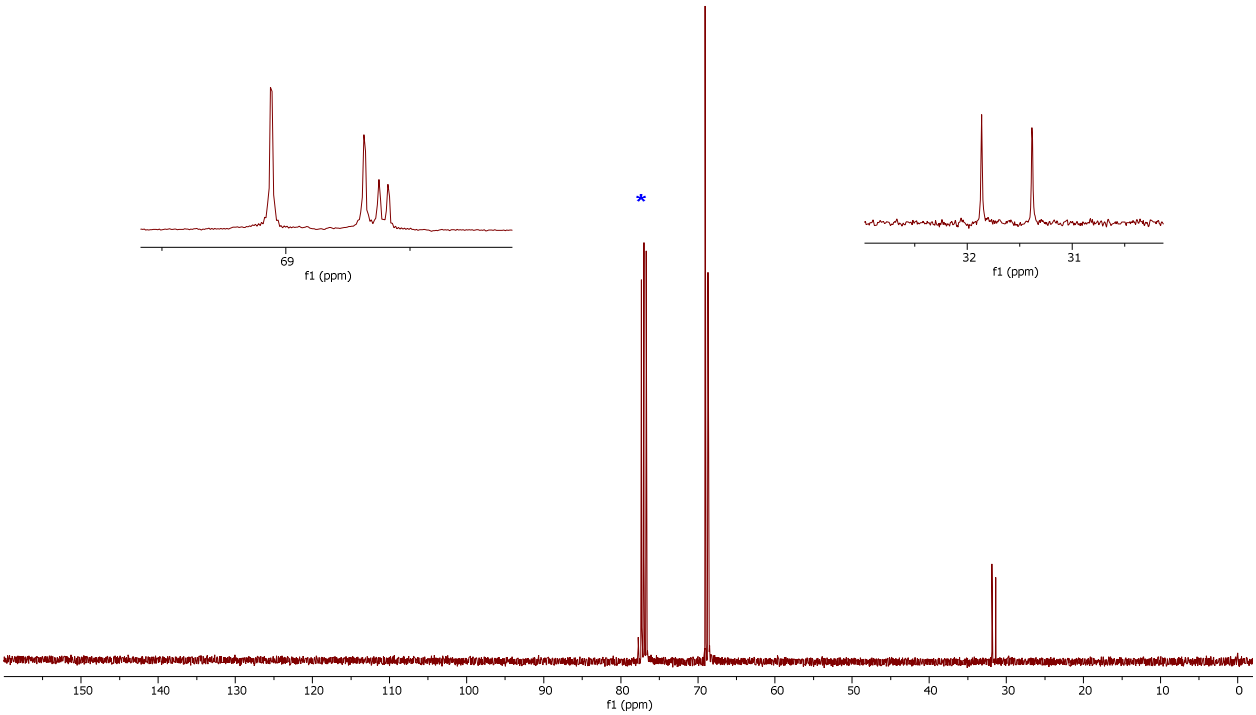

Figure S32. $^{13}C\{^{1}H\}$ NMR spectrum (101 MHz, $CDCl_3$) of **1S**.

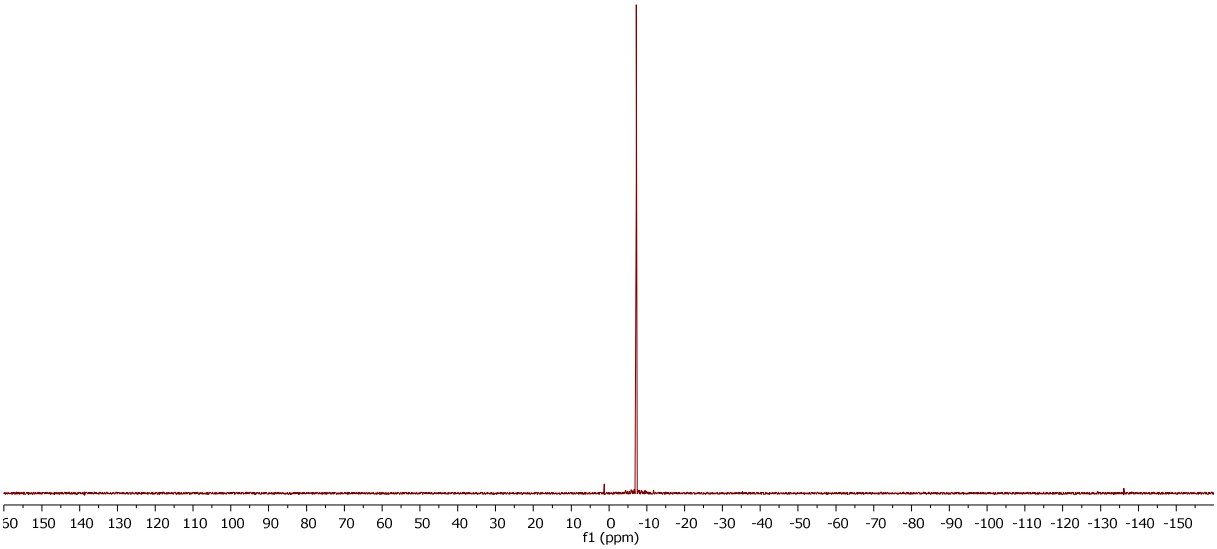

Figure S33. $^{31}P\{^{1}H\}$ NMR spectrum (162 MHz, $CDCl_3$) of **1S**.

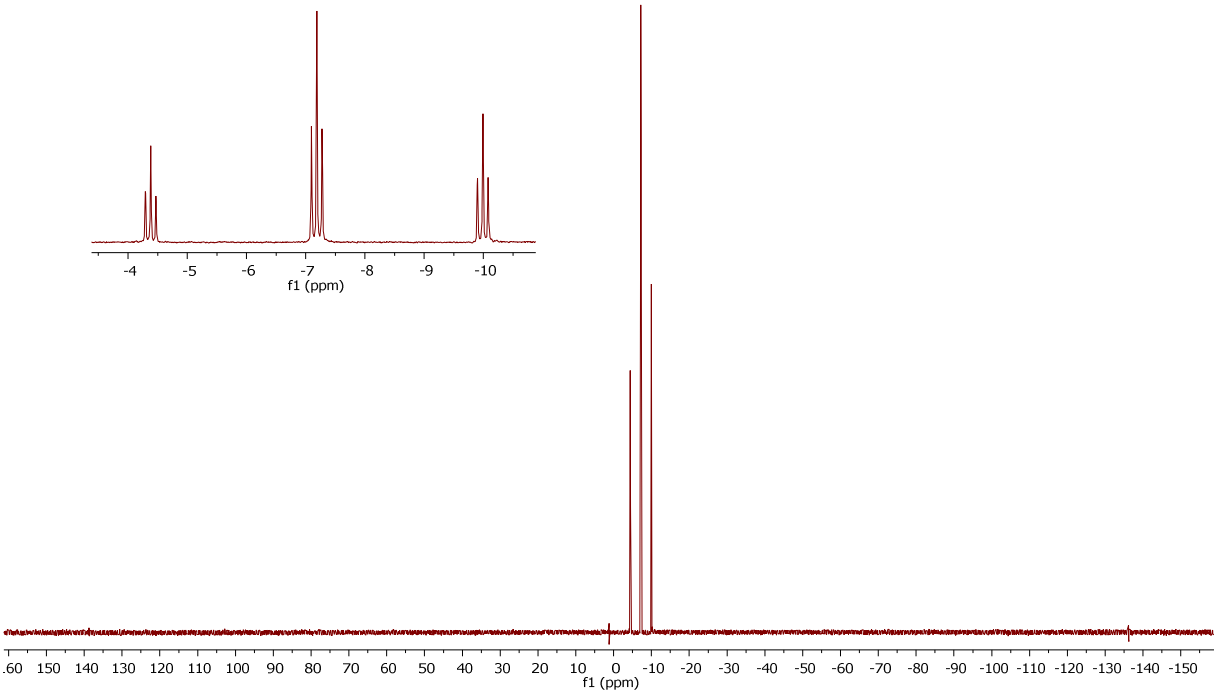

Figure S34. ^{31}P NMR spectrum (162 MHz, $CDCl_3$) of **1S**.

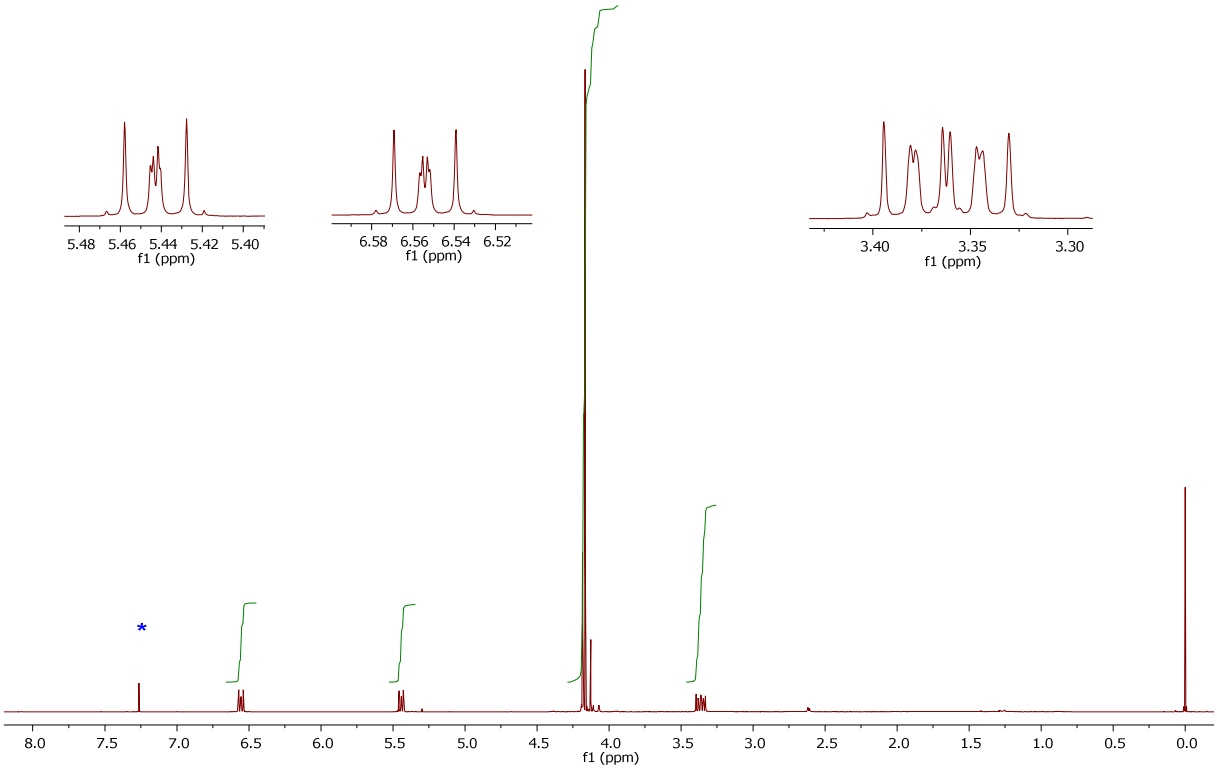

Figure S35. ^{1}H NMR spectrum (400 MHz, $CDCl_3$) of **1Se**.

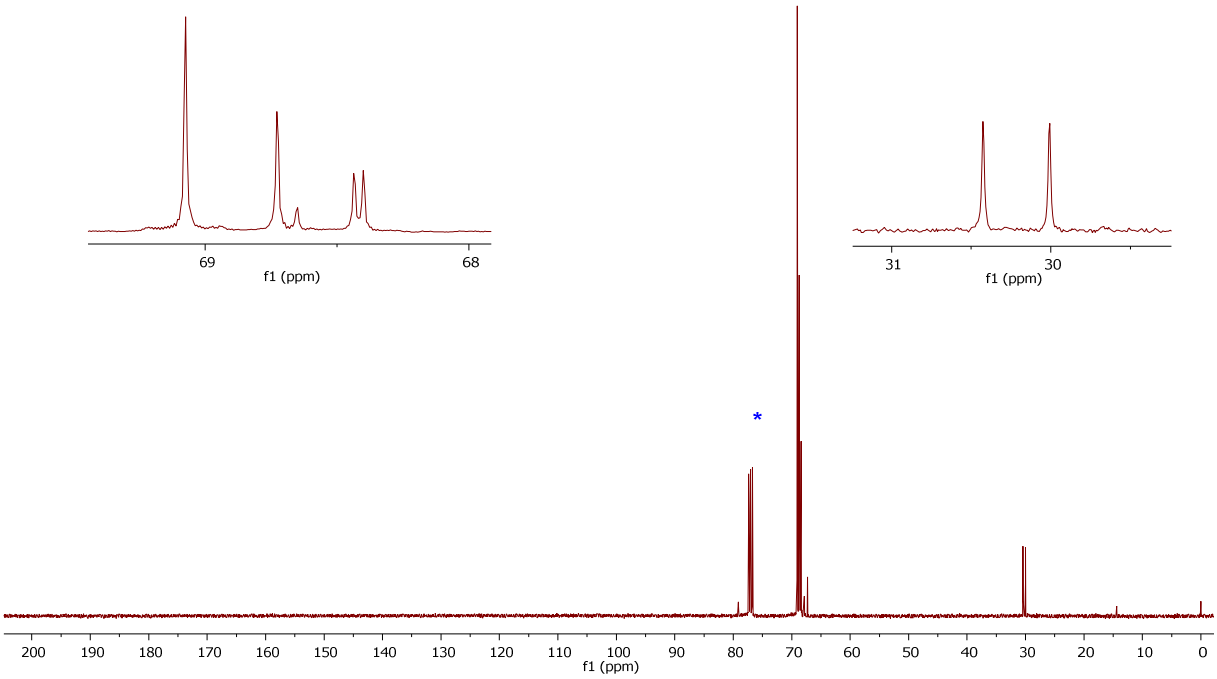

Figure S36. $^{13}C\{^{1}H\}$ NMR spectrum (101 MHz, $CDCl_3$) of **1Se**.

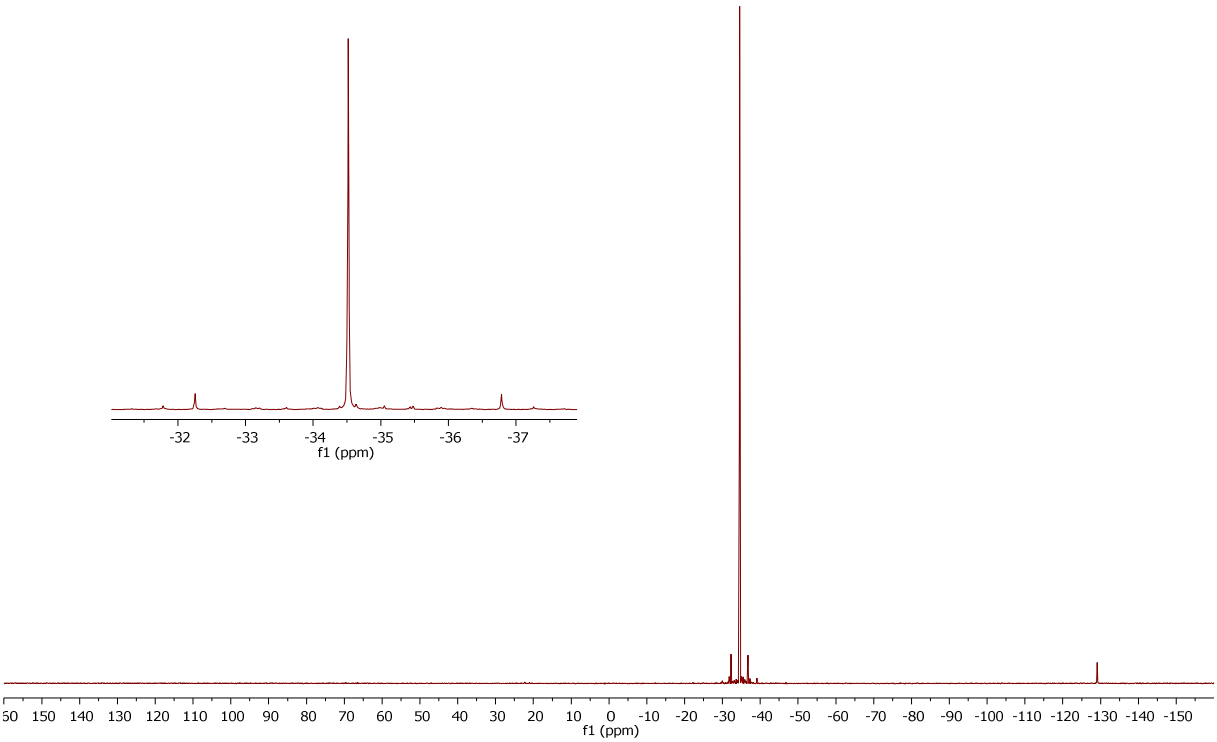

Figure S37. $^{31}P\{^{1}H\}$ NMR spectrum (162 MHz, $CDCl_3$) of **1Se**.

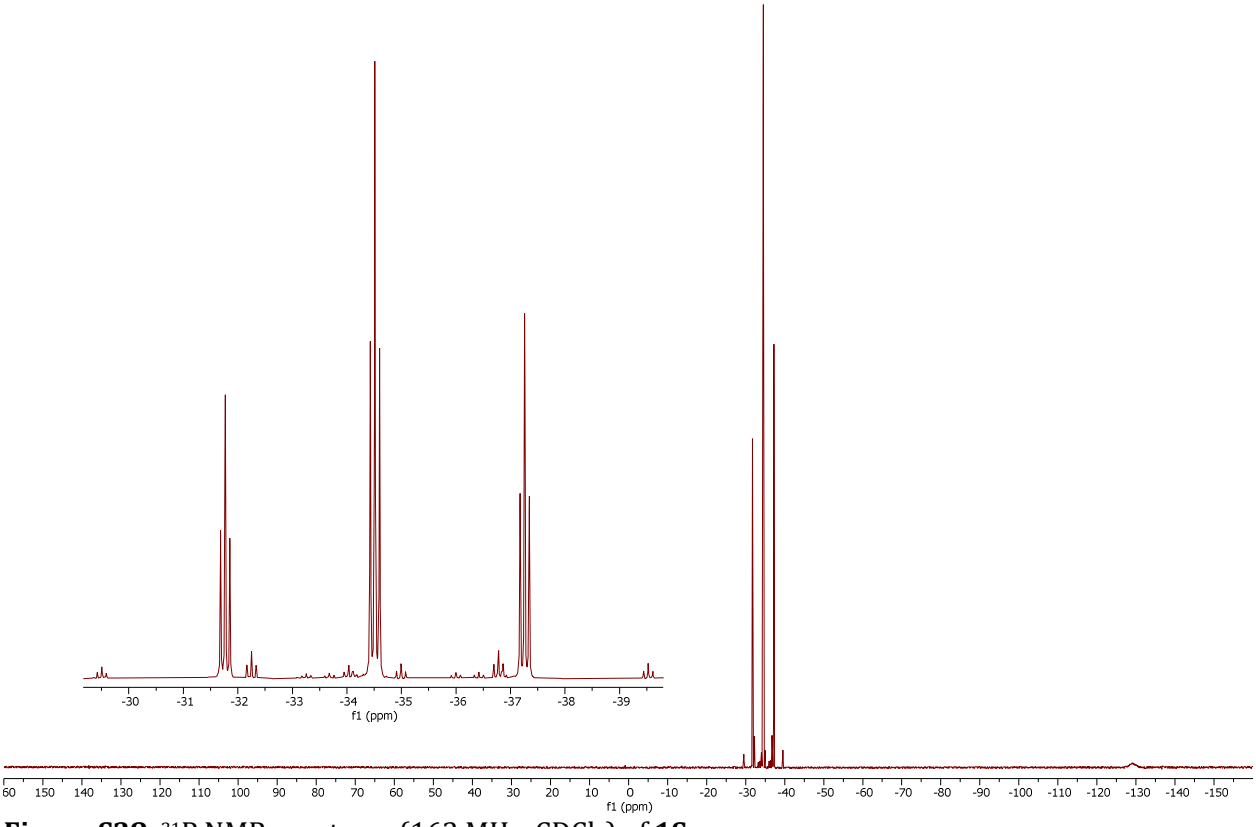

Figure S38. ^{31}P NMR spectrum (162 MHz, $CDCl_3$) of **1Se**.

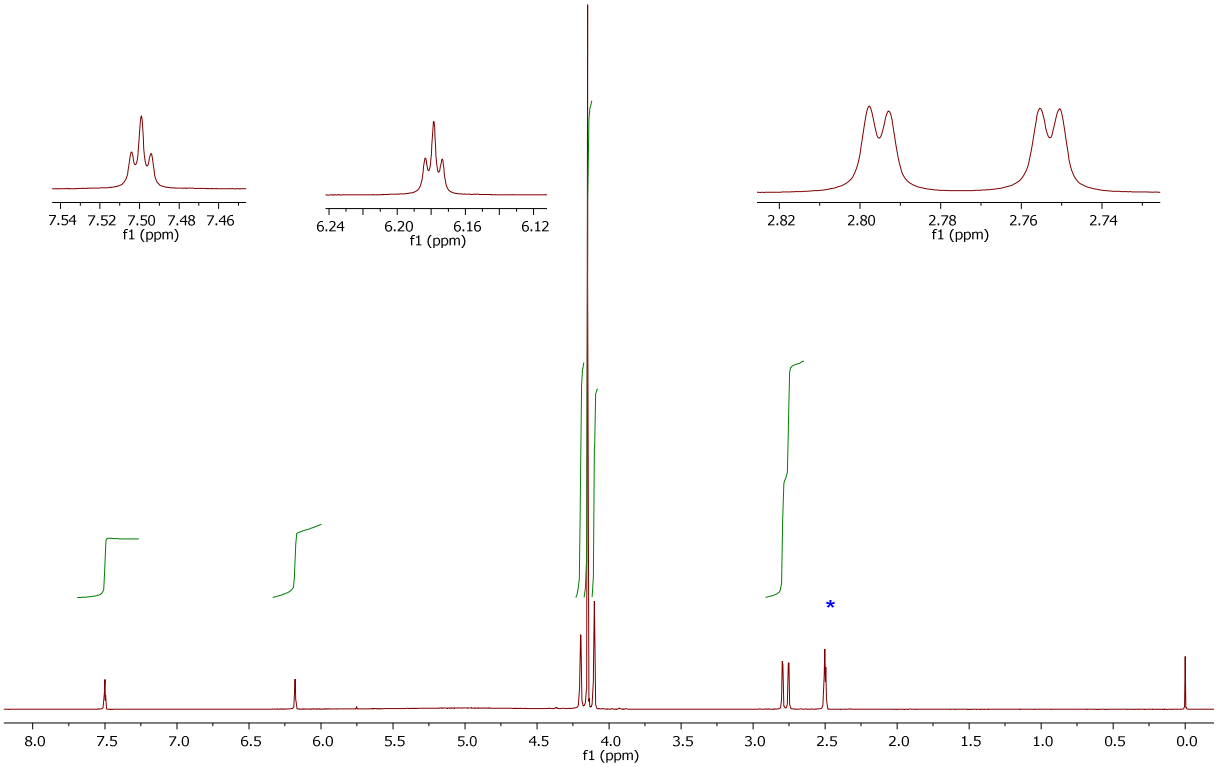

Figure S39. ^{1}H NMR spectrum (400 MHz, dmso-d_6) of **2**.

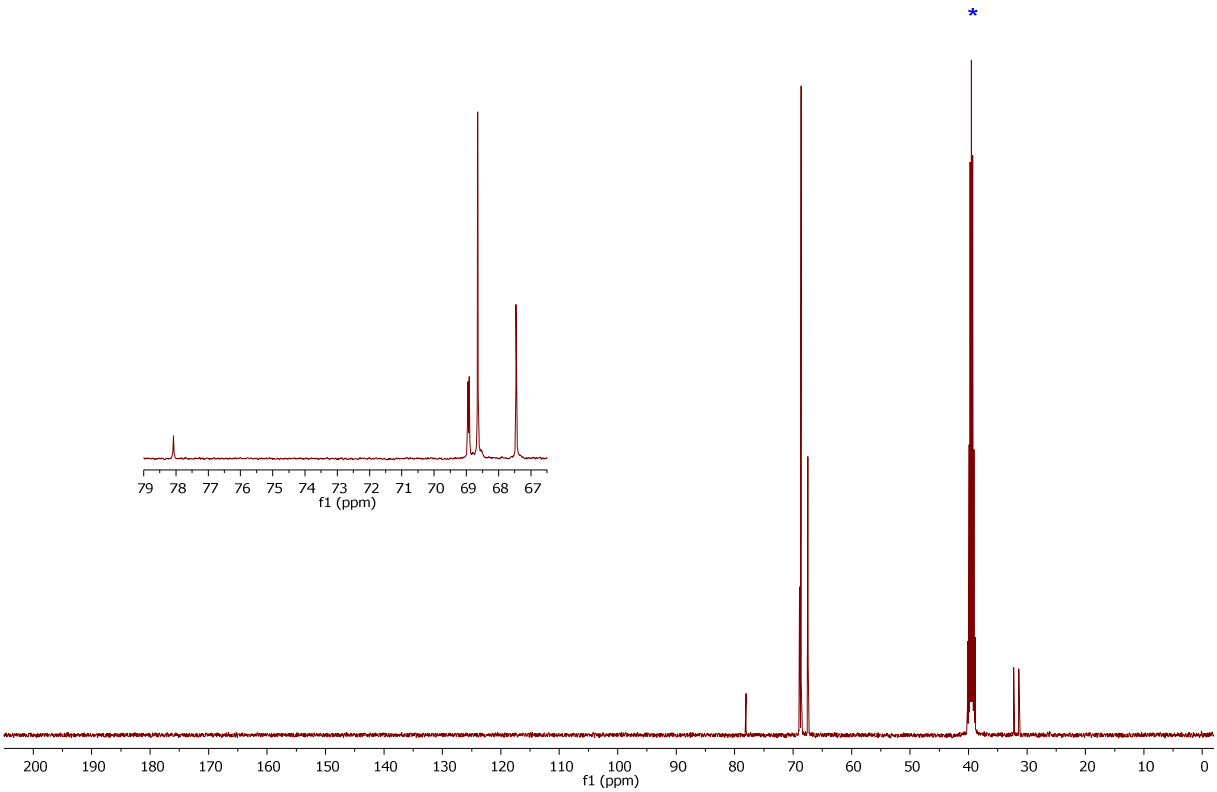

Figure S40. $^{13}C\{^{1}H\}$ NMR spectrum (101 MHz, dmso-d_6) of **2**.

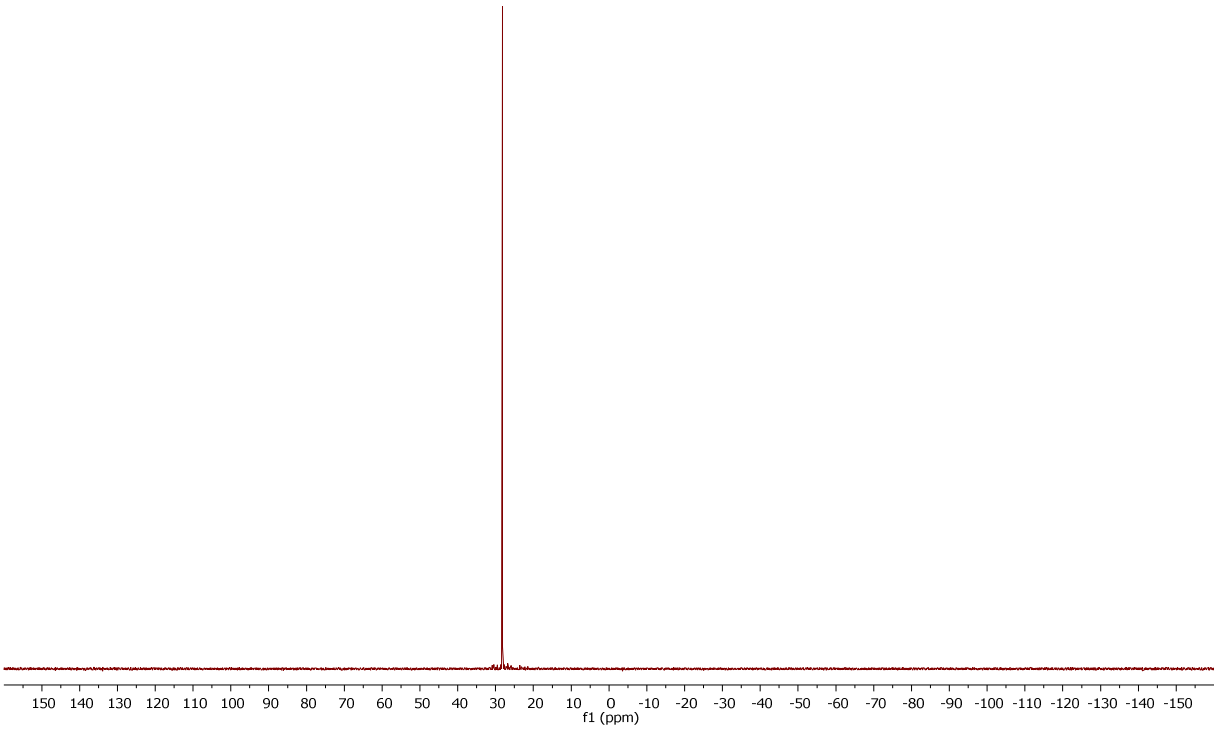

Figure S41. $^{31}P\{^{1}H\}$ NMR spectrum (162 MHz, dmso-d_6) of **2**.

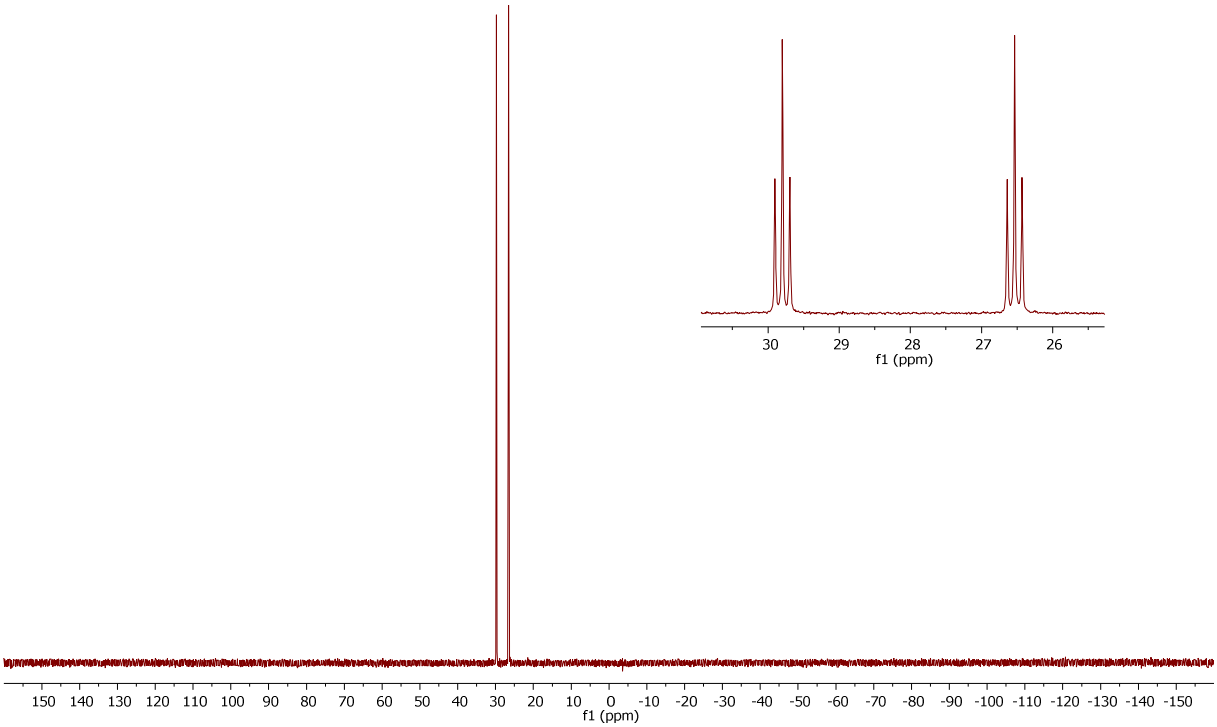

Figure S42. ^{31}P NMR spectrum (162 MHz, dmso-d_6) of **2**.

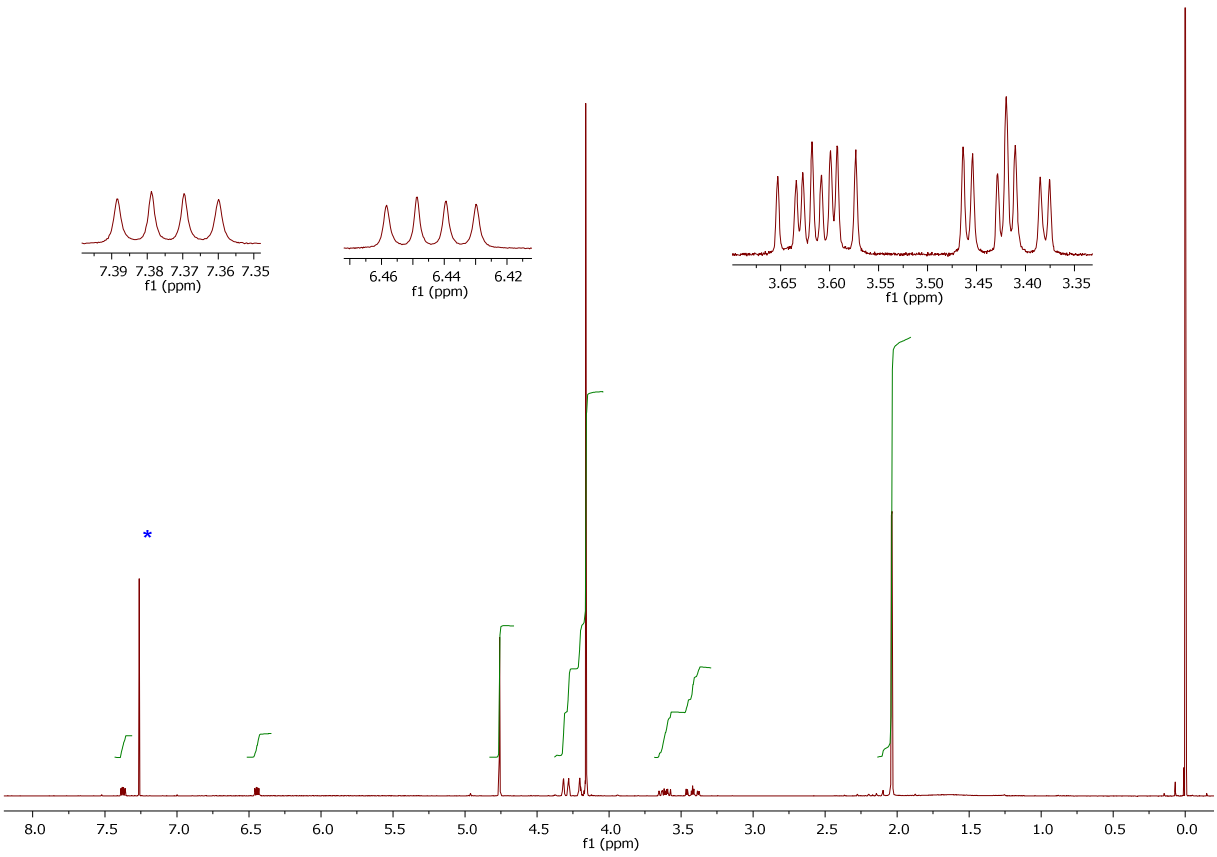

Figure S43. ^{1}H NMR spectrum (400 MHz, $CDCl_3$) of **3**.

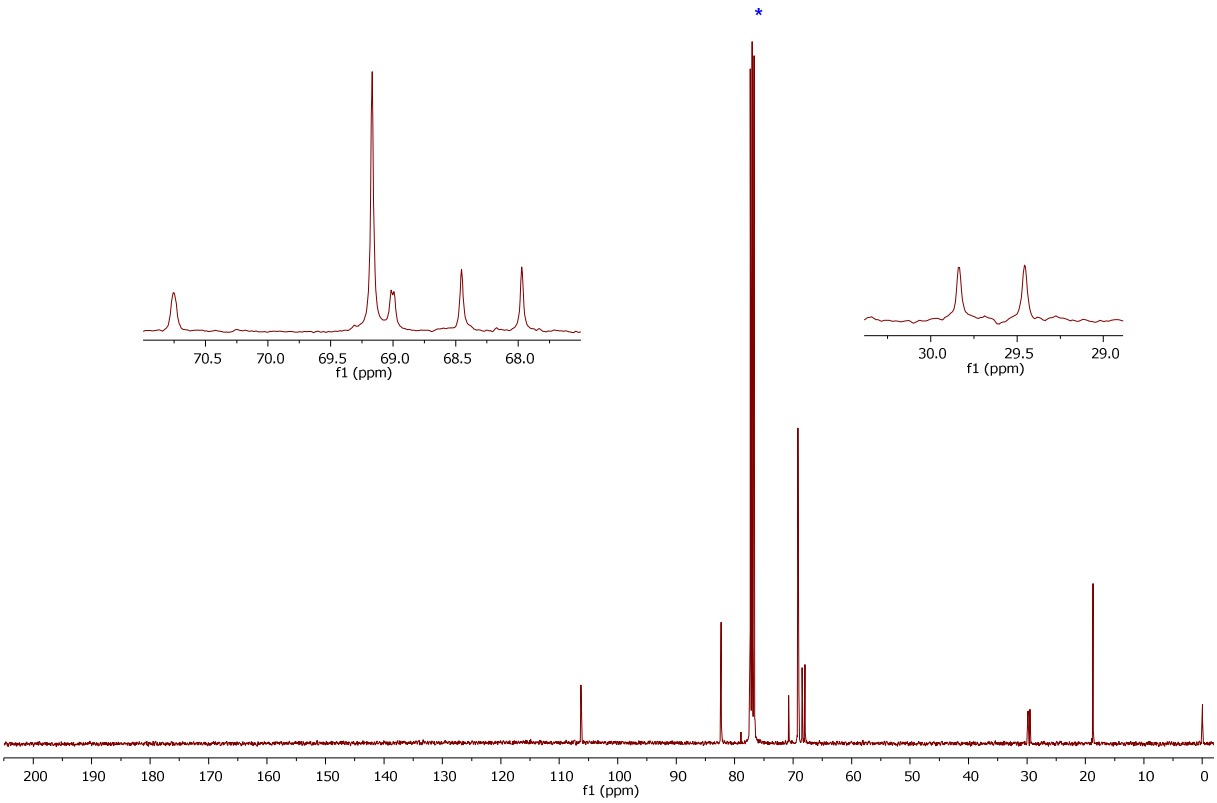

Figure S44. $^{13}C\{^{1}H\}$ NMR spectrum (101 MHz, $CDCl_3$) of **3**.

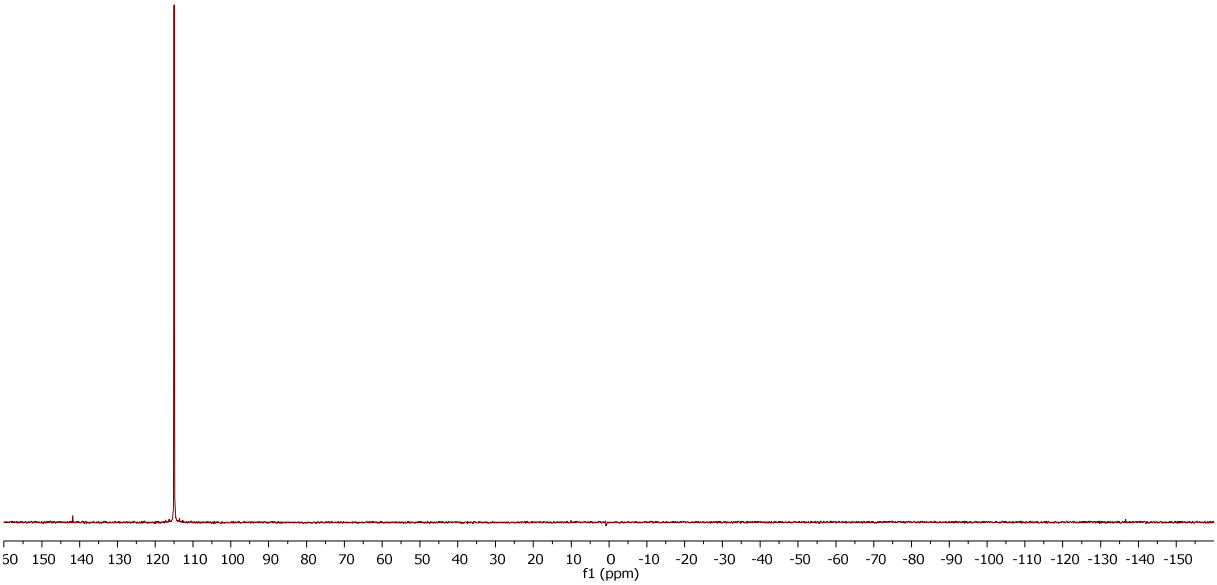

Figure S45. $^{31}P\{^{1}H\}$ NMR spectrum (162 MHz, $CDCl_3$) of **3**.

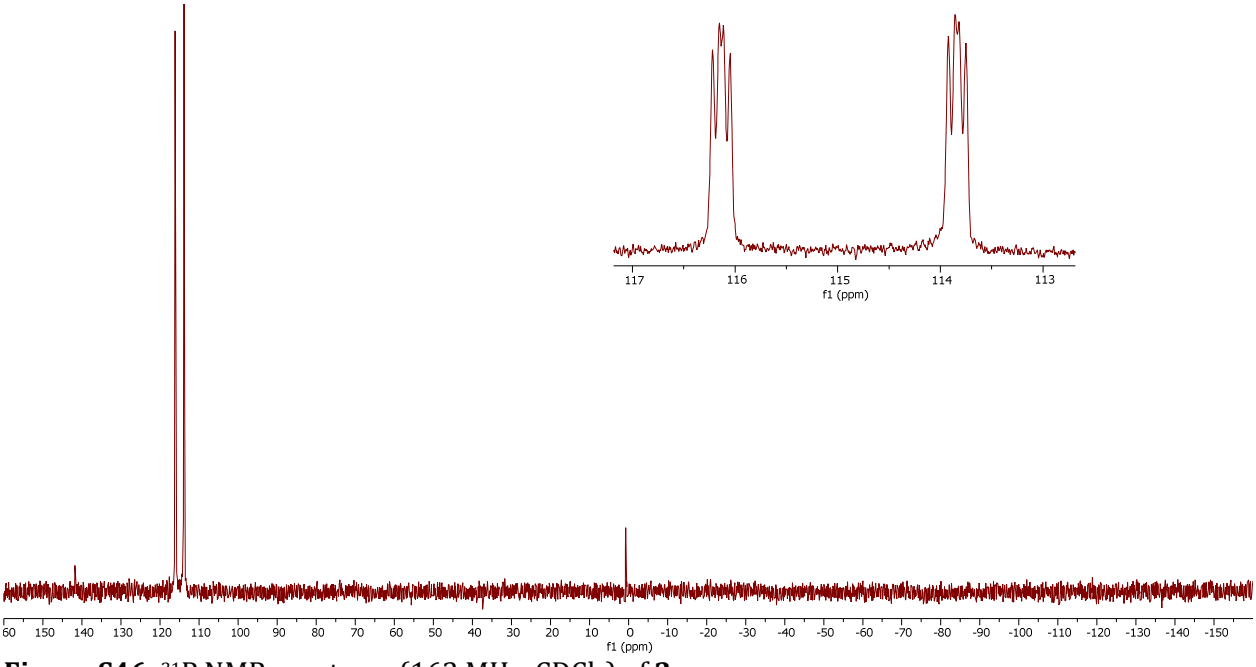

Figure S46. ^{31}P NMR spectrum (162 MHz, $CDCl_3$) of **3**.

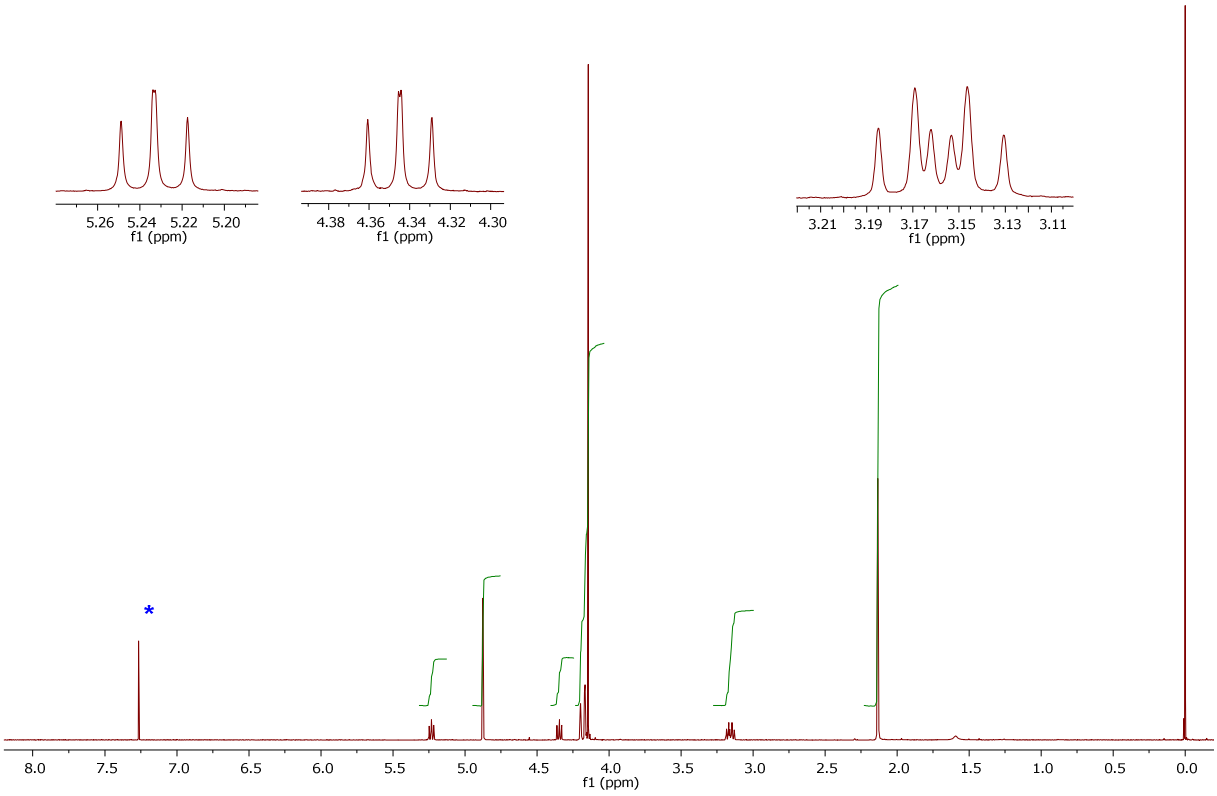

Figure S47. ^{1}H NMR spectrum (400 MHz, $CDCl_3$) of **4**.

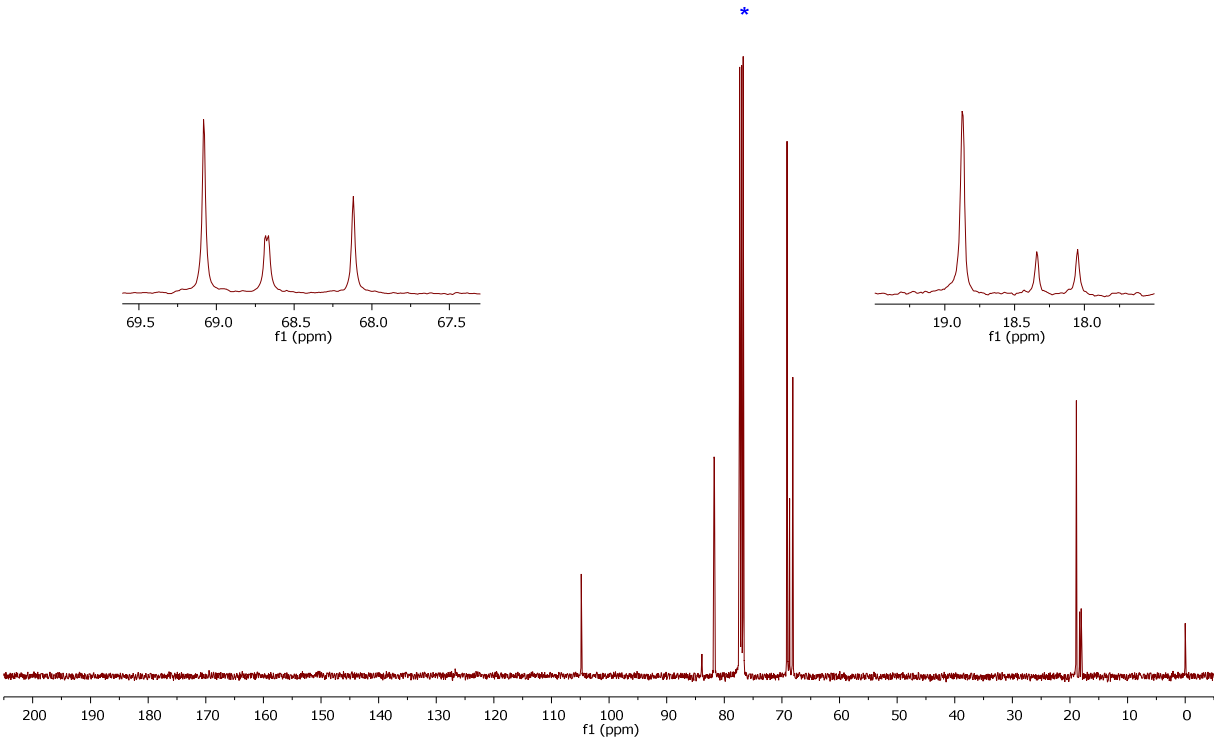

Figure S48. $^{13}C\{^{1}H\}$ NMR spectrum (101 MHz, $CDCl_3$) of **4**.

Figure S49. $^{31}P\{^{1}H\}$ NMR spectrum (162 MHz, $CDCl_3$) of **4**.

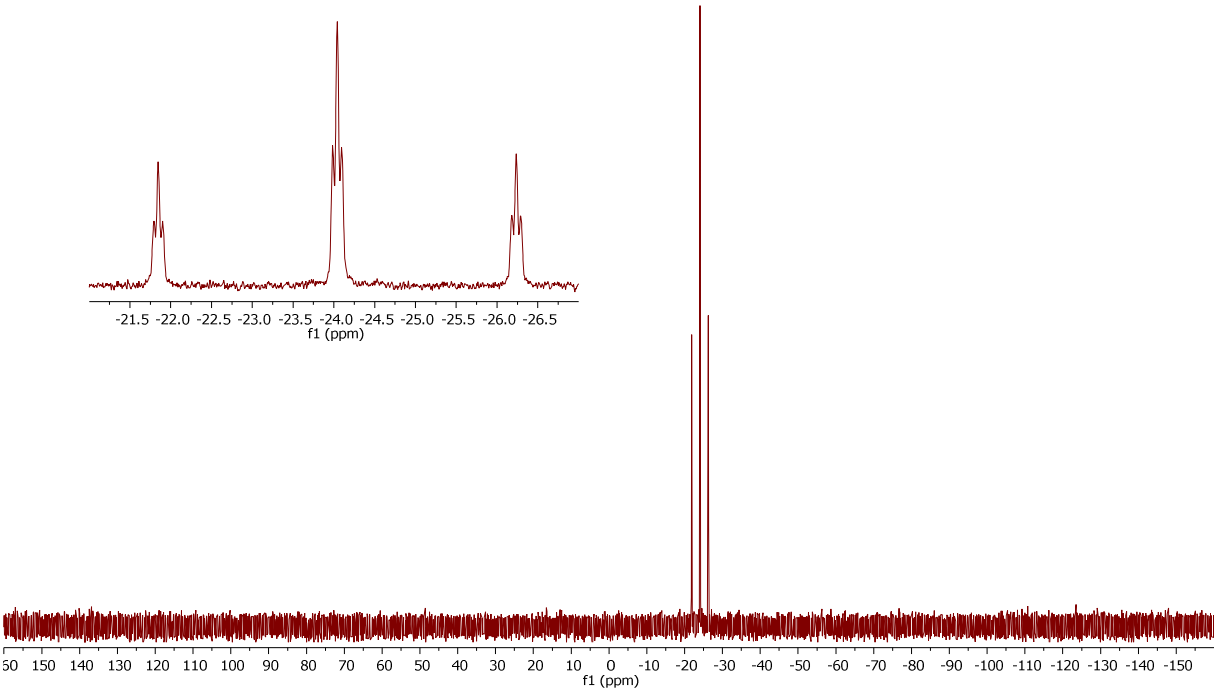

Figure S50. ^{31}P NMR spectrum (162 MHz, $CDCl_3$) of **4**.

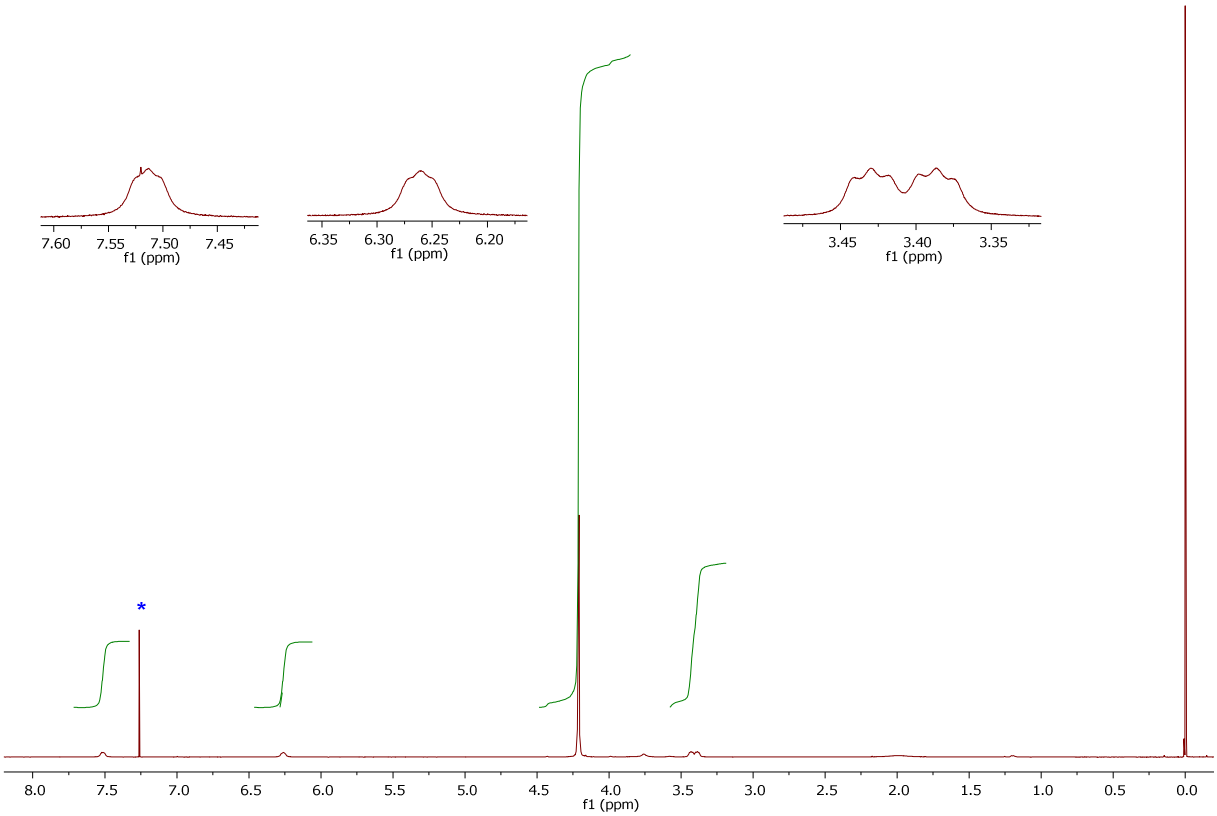

Figure S51. ^{1}H NMR spectrum (400 MHz, $CDCl_3$) of **5**.

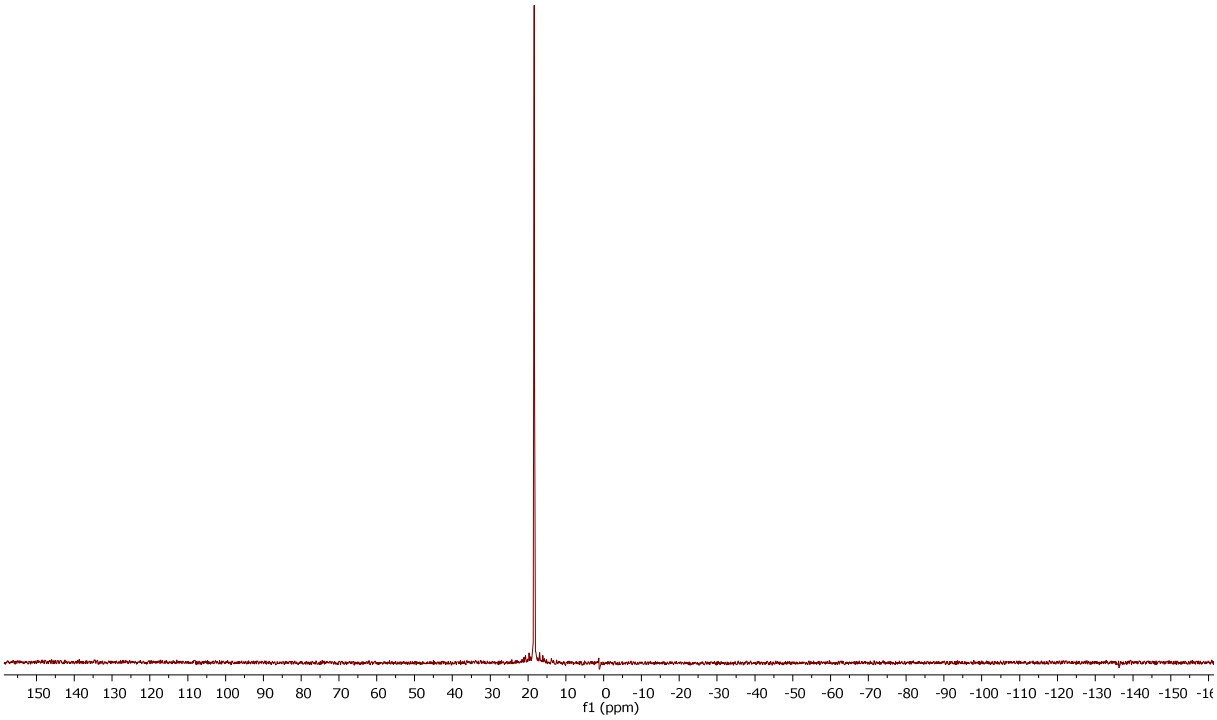

Figure S52. $^{31}P\{^{1}H\}$ NMR spectrum (162 MHz, $CDCl_3$) of **5**.

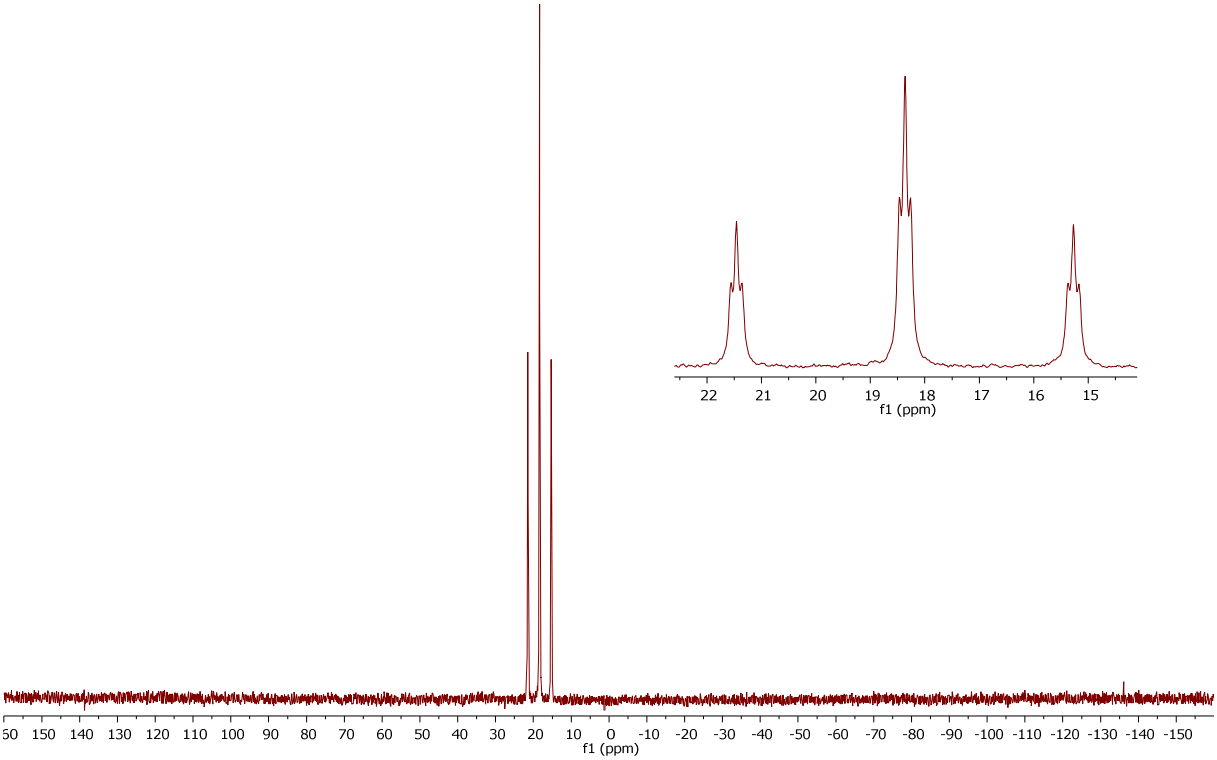

Figure S53. ^{31}P NMR spectrum (162 MHz, $CDCl_3$) of **5**.

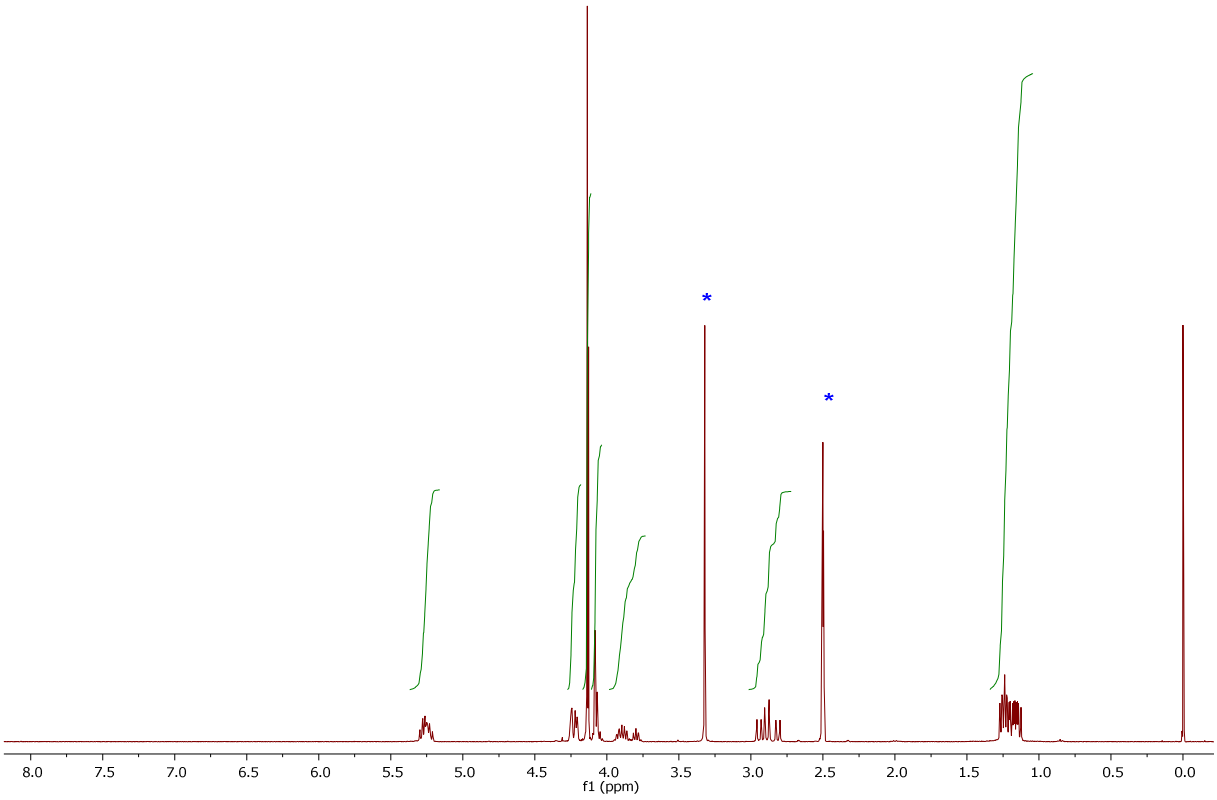

Figure S54. ^{1}H NMR spectrum (400 MHz, dmso-d_6) of **6a**.

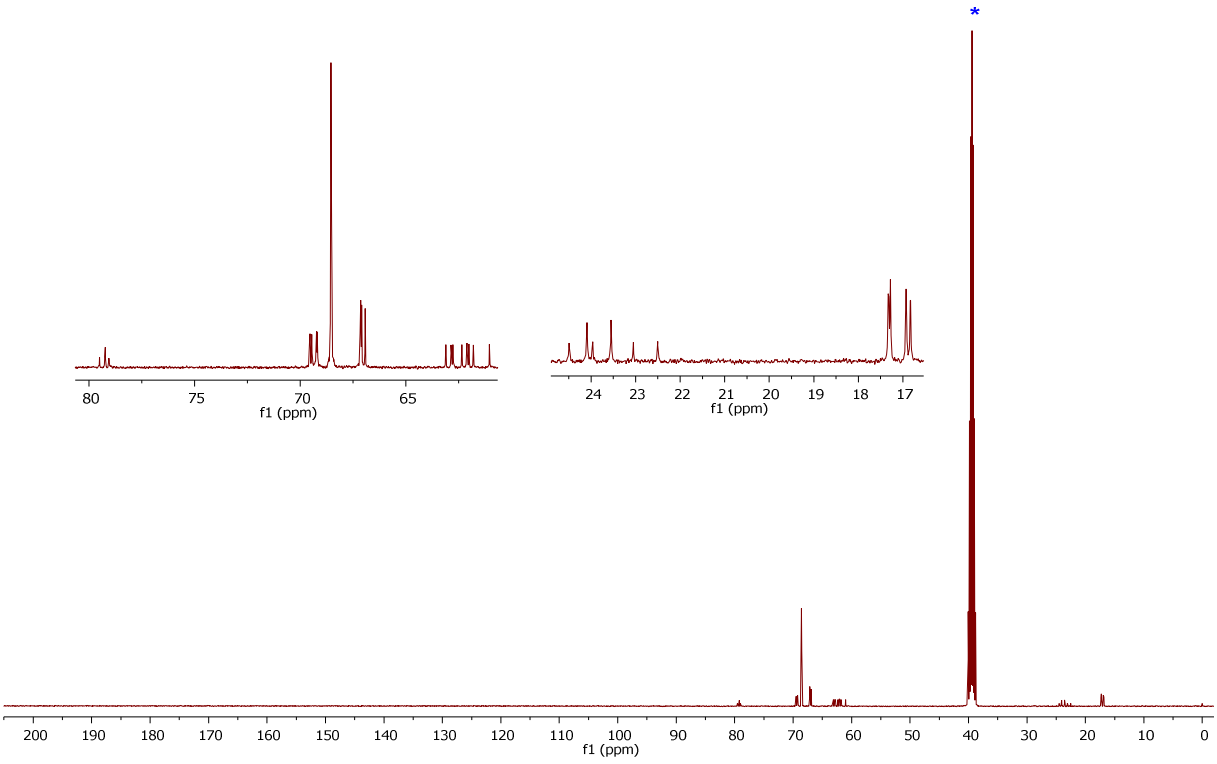

Figure S55. $^{13}C\{^{1}H\}$ NMR spectrum (101 MHz, dmso-d_6) of **6a**.

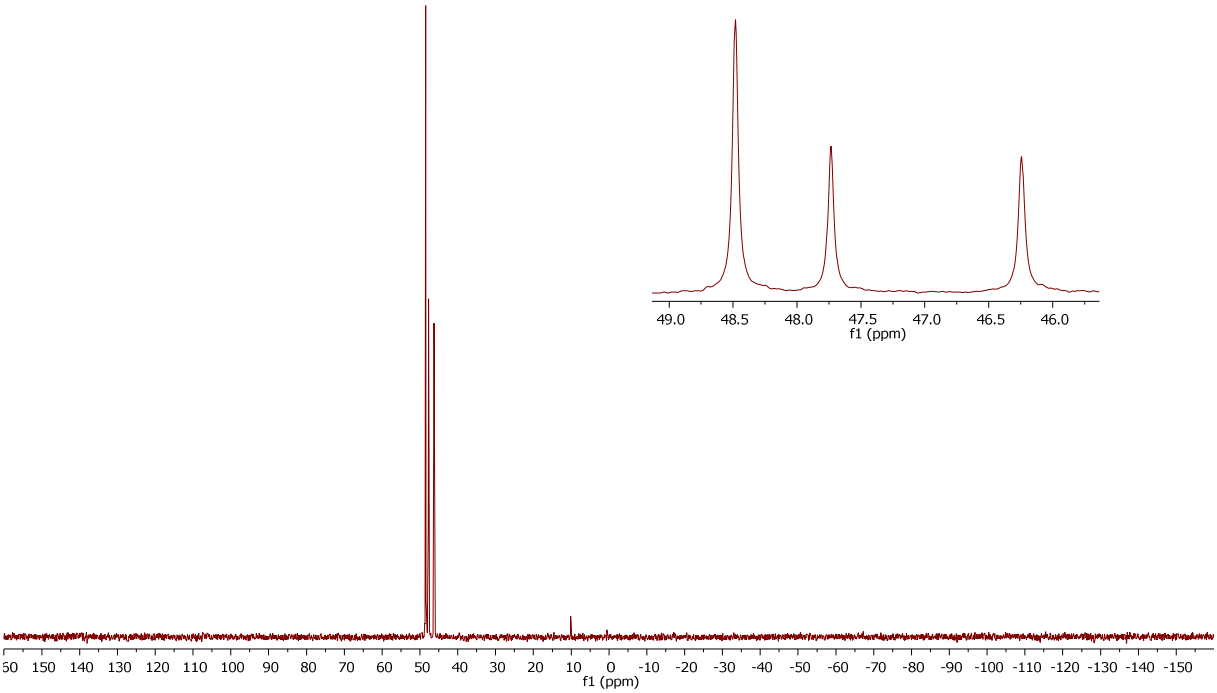

Figure S56. $^{31}P\{^{1}H\}$ NMR spectrum (162 MHz, dmso-d_6) of **6a**.

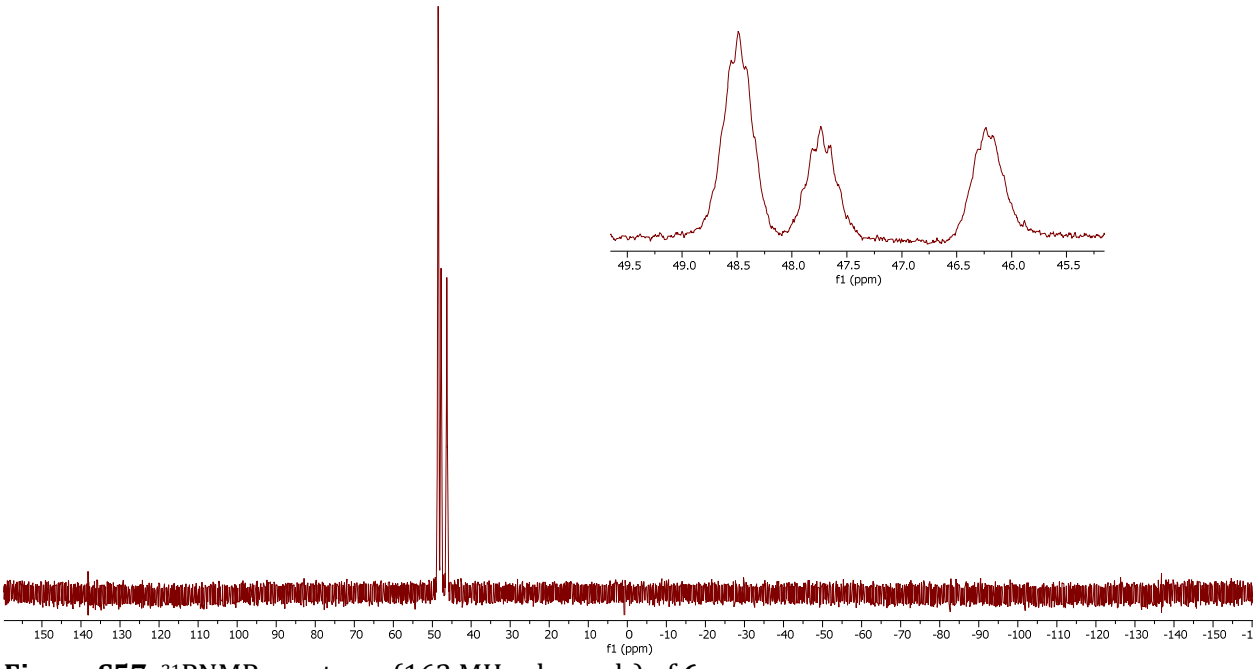

Figure S57. ^{31}PNMR spectrum (162 MHz, dmso-d_6) of **6a**.

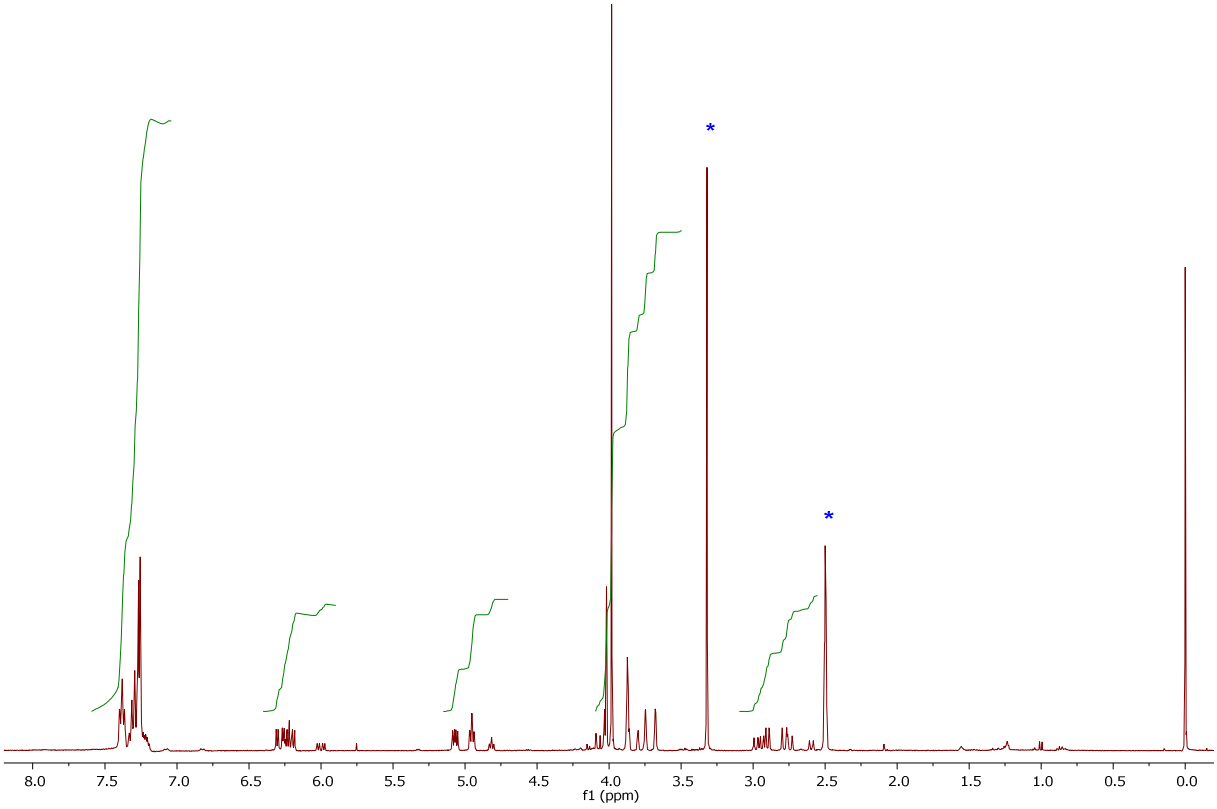

Figure S58. ^{1}H NMR spectrum (400 MHz, dmso-d_6) of **6b**.

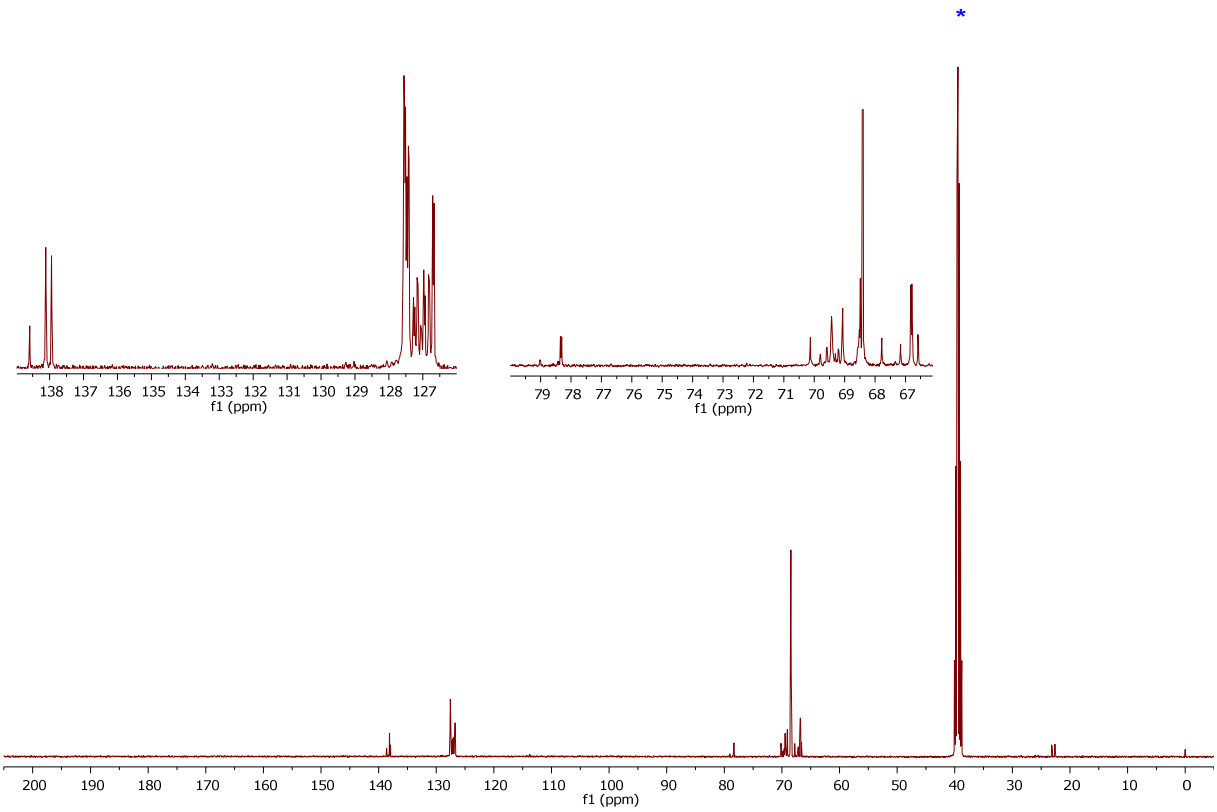

Figure S59. $^{13}C\{^{1}H\}$ NMR spectrum (101 MHz, dmso-d_6) of **6b**.

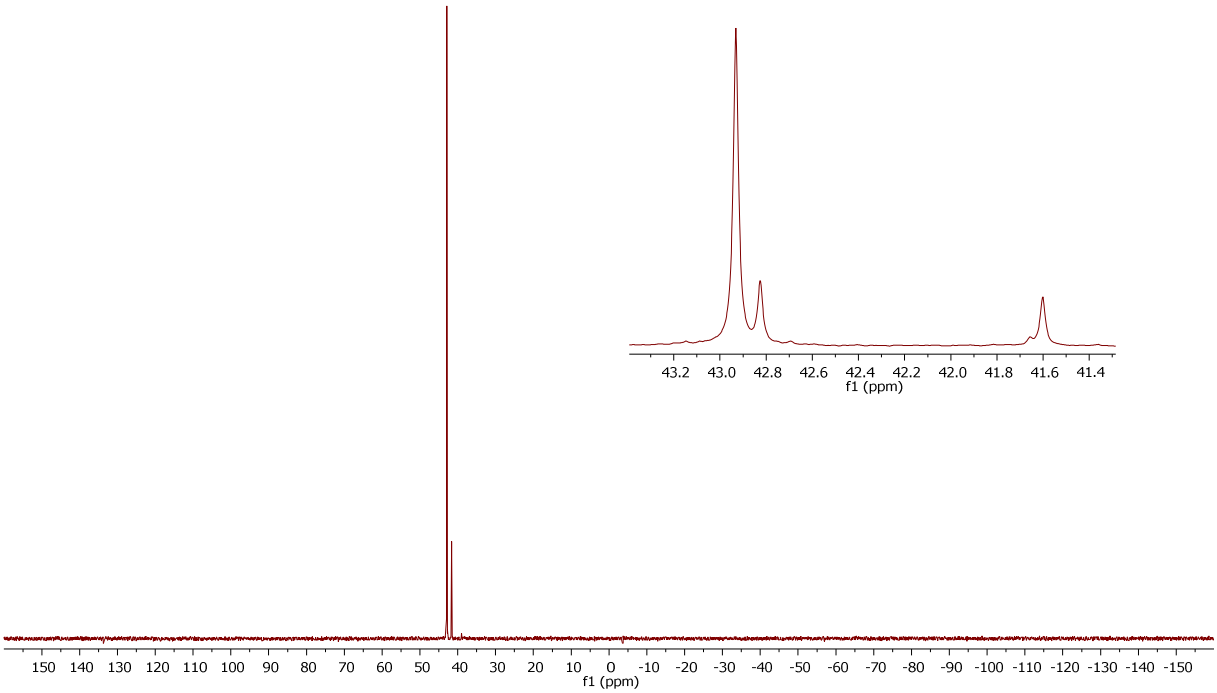

Figure S60. $^{31}P\{^{1}H\}$ NMR spectrum (162 MHz, dmso-d_6) of **6b**.

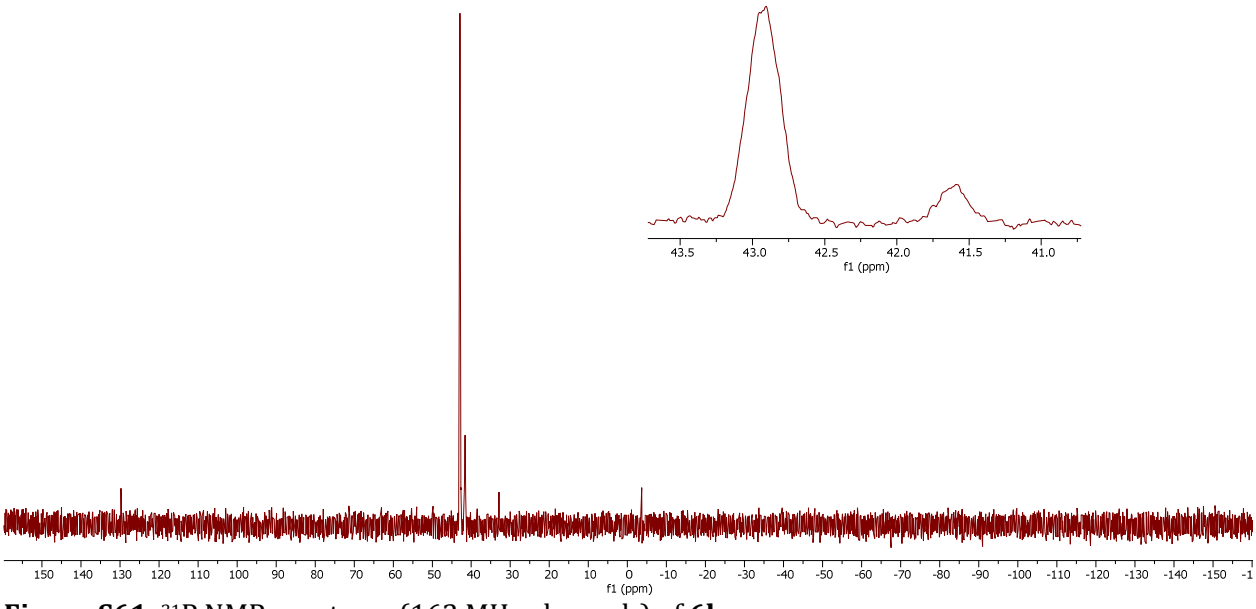

Figure S61. ^{31}P NMR spectrum (162 MHz, dmso-d_6) of **6b**.

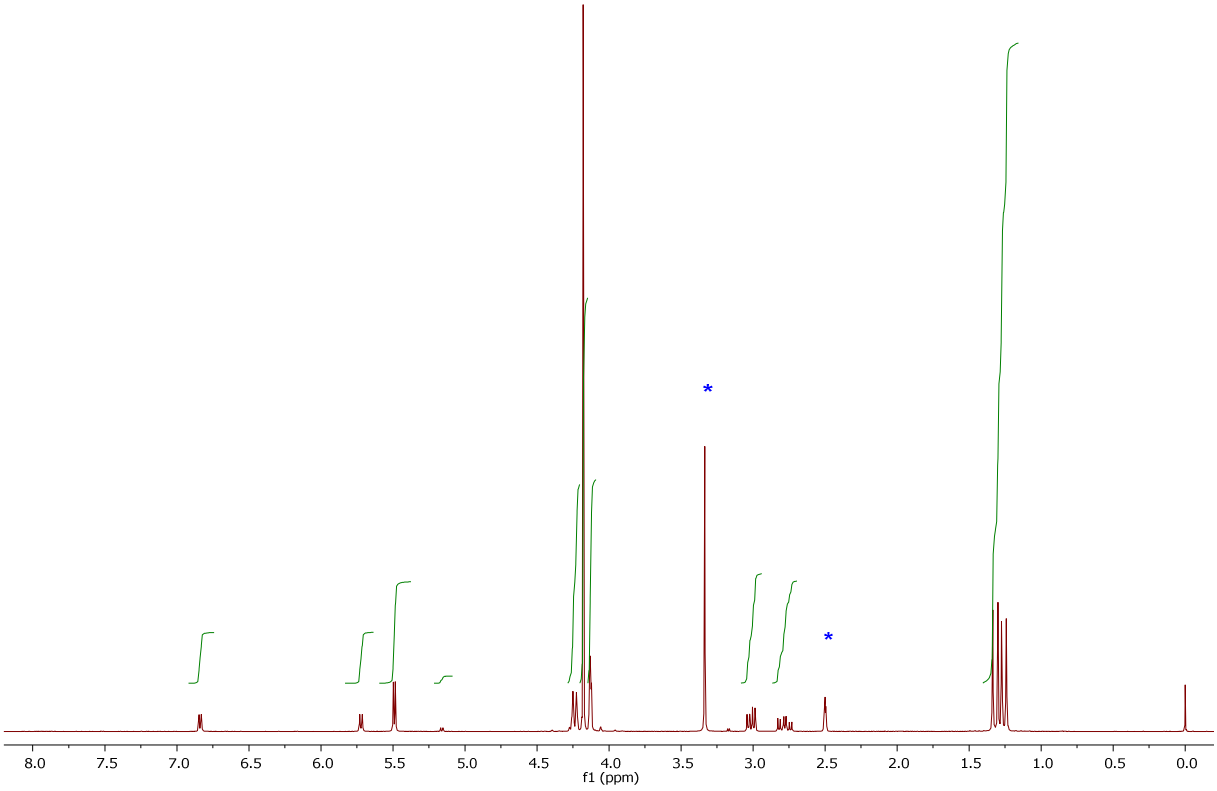

Figure S62. ^{1}H NMR spectrum (400 MHz, dmso-d_6) of **7a**.

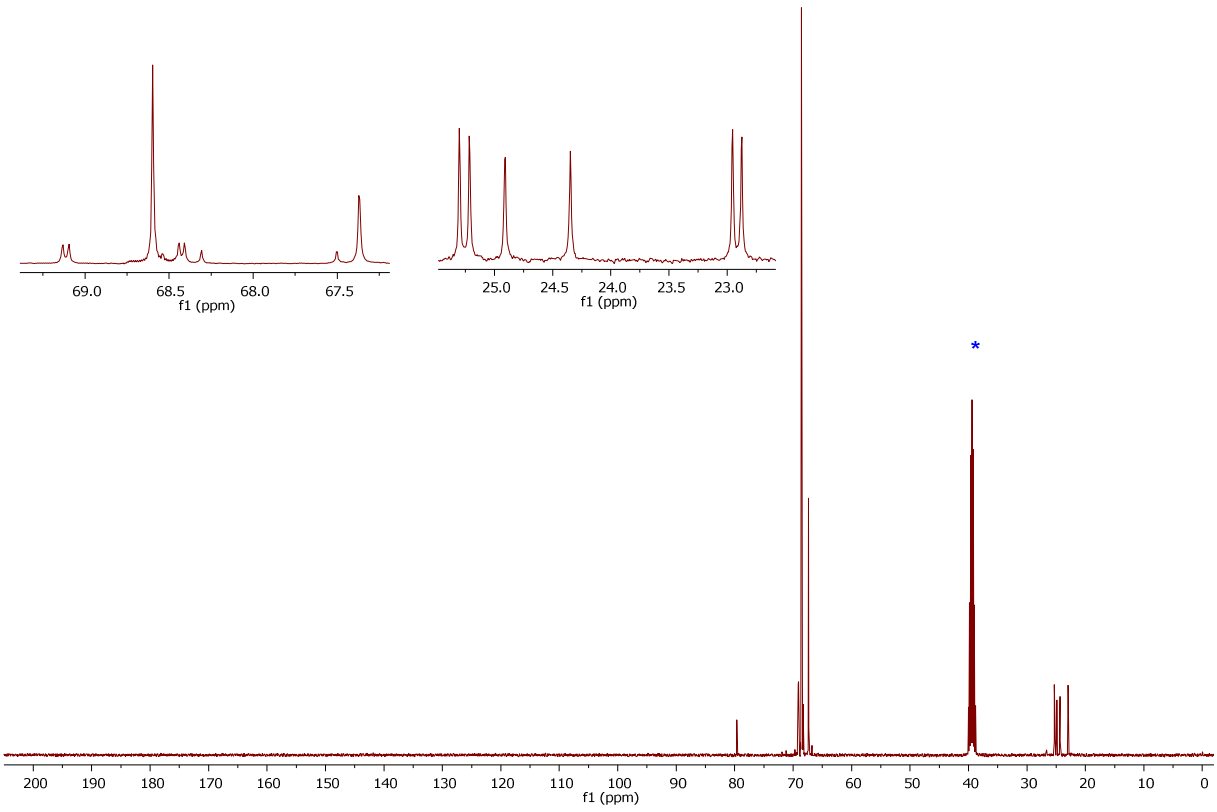

Figure S63. $^{13}C\{^{1}H\}$ NMR spectrum (101 MHz, dmso-d_6) of **7a**.

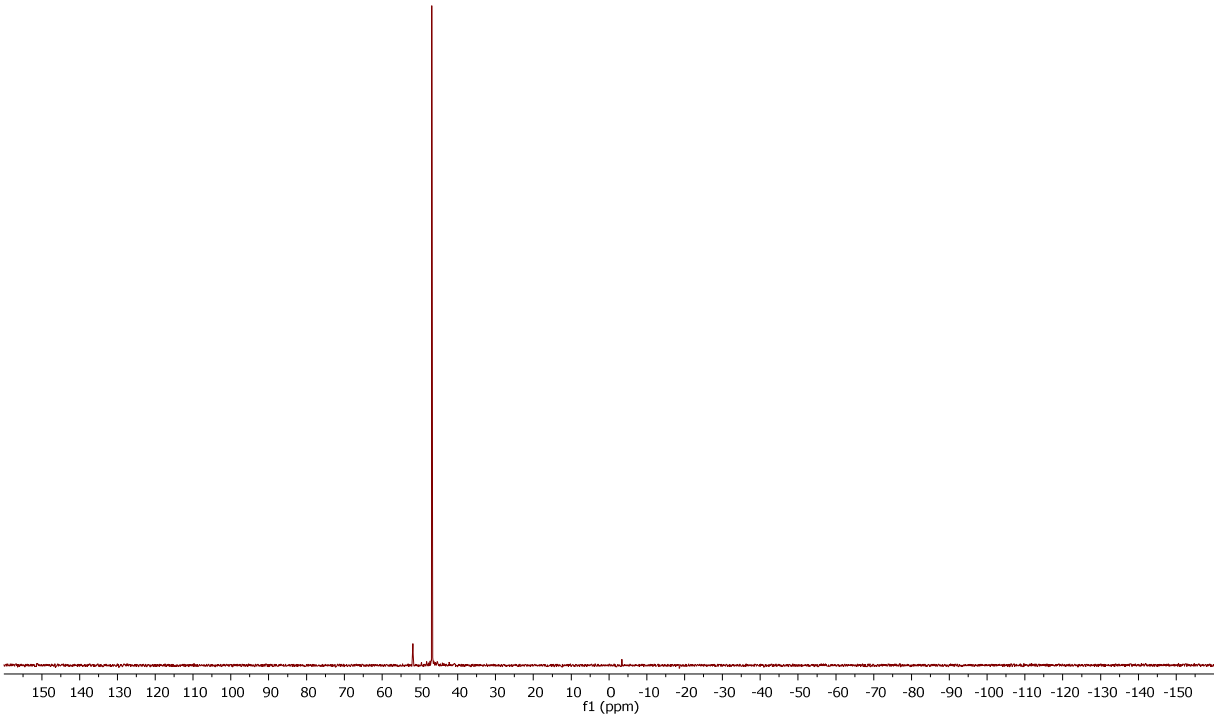

Figure S64. $^{31}P\{^{1}H\}$ NMR spectrum (162 MHz, dmso-d_6) of **7a**.

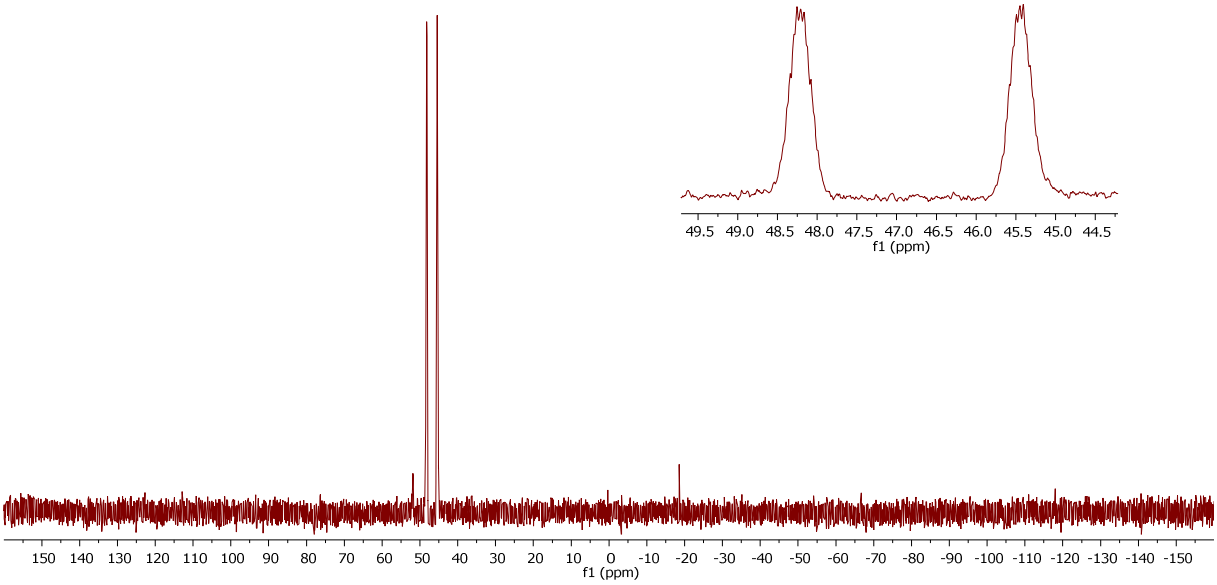

Figure S65. ^{31}P NMR spectrum (162 MHz, dmso-d_6) of **7a**.

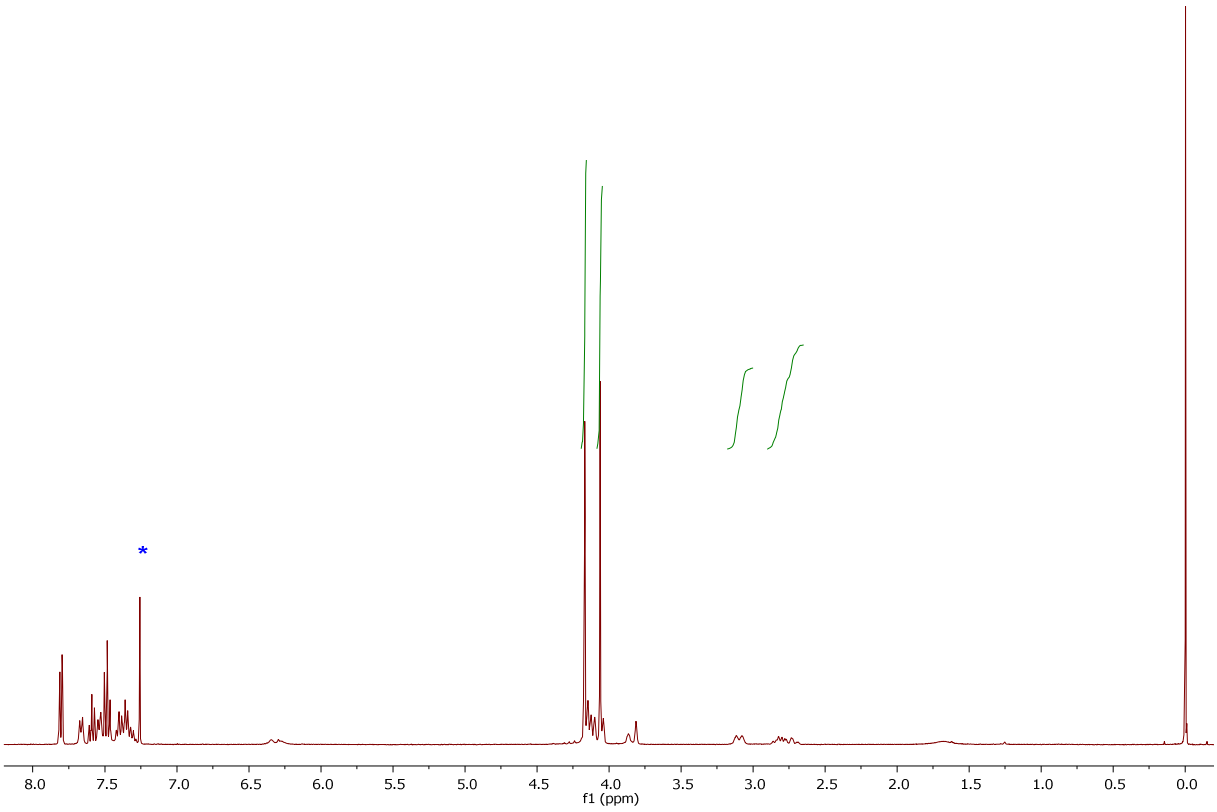

Figure S66. ^{1}H NMR spectrum (400 MHz, $CDCl_3$) of **7b** (reaction mixture).

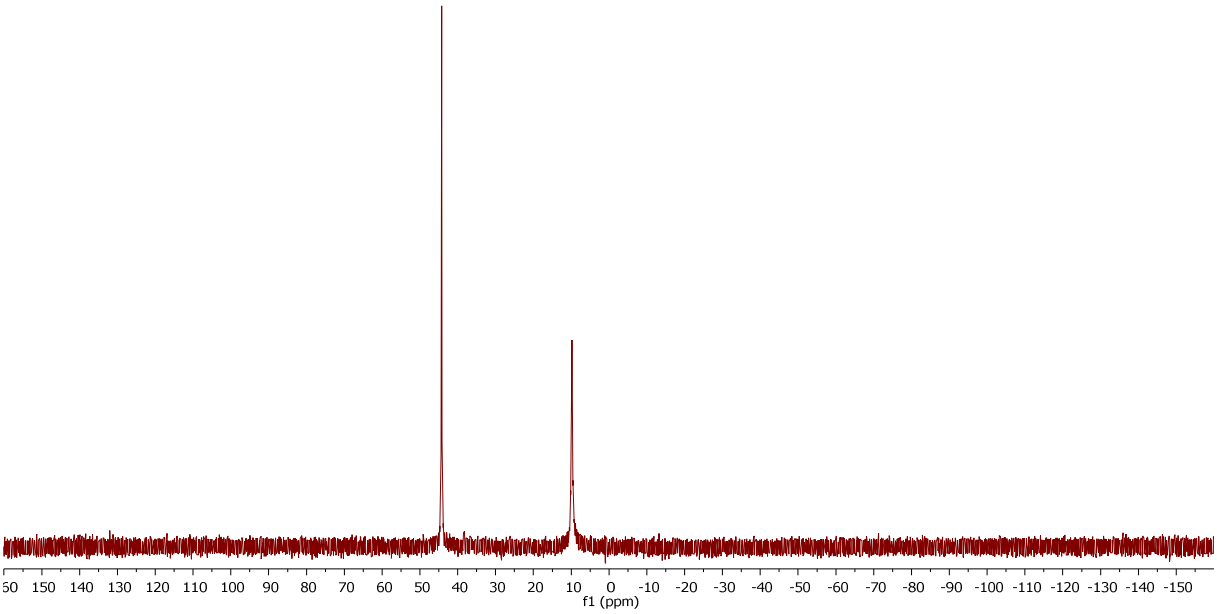

Figure S67. $^{31}P\{^{1}H\}$ NMR spectrum (162 MHz, $CDCl_3$) of **7b** (reaction mixture).

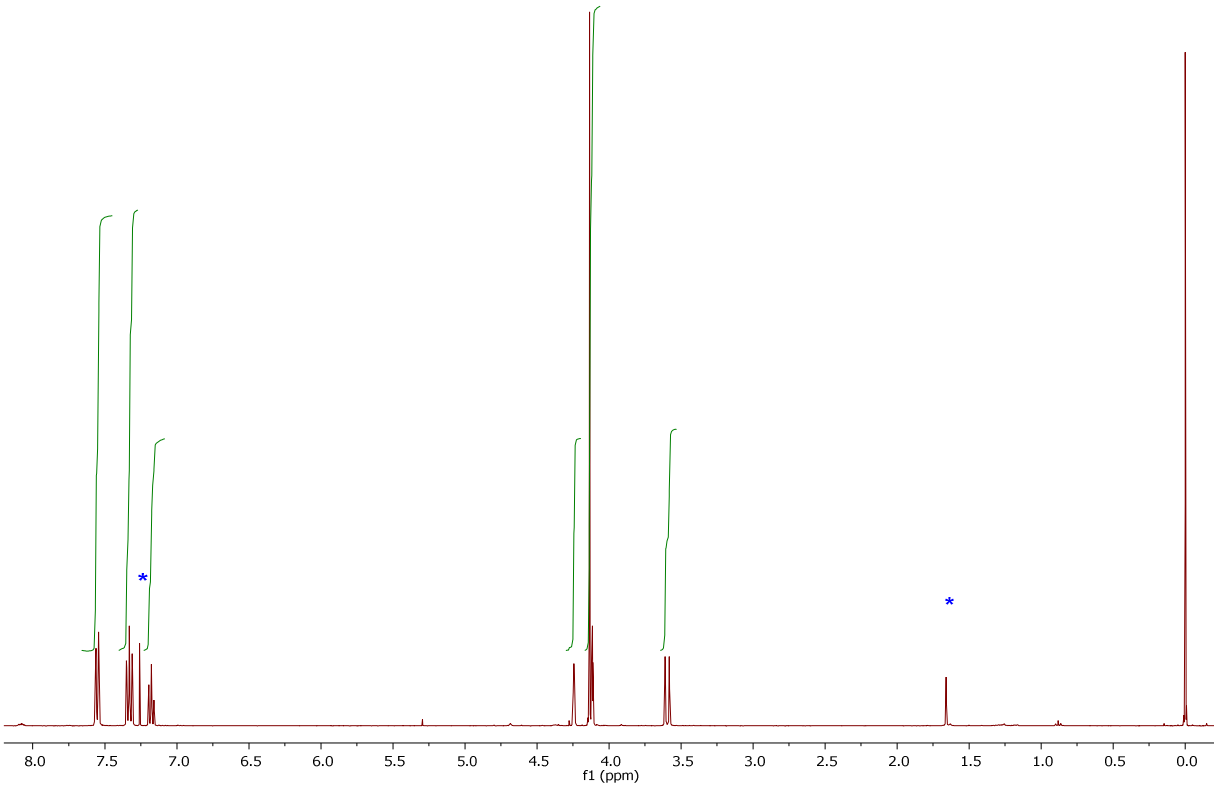

Figure S68. ^{1}H NMR spectrum (400 MHz, $CDCl_3$) of **8a**.

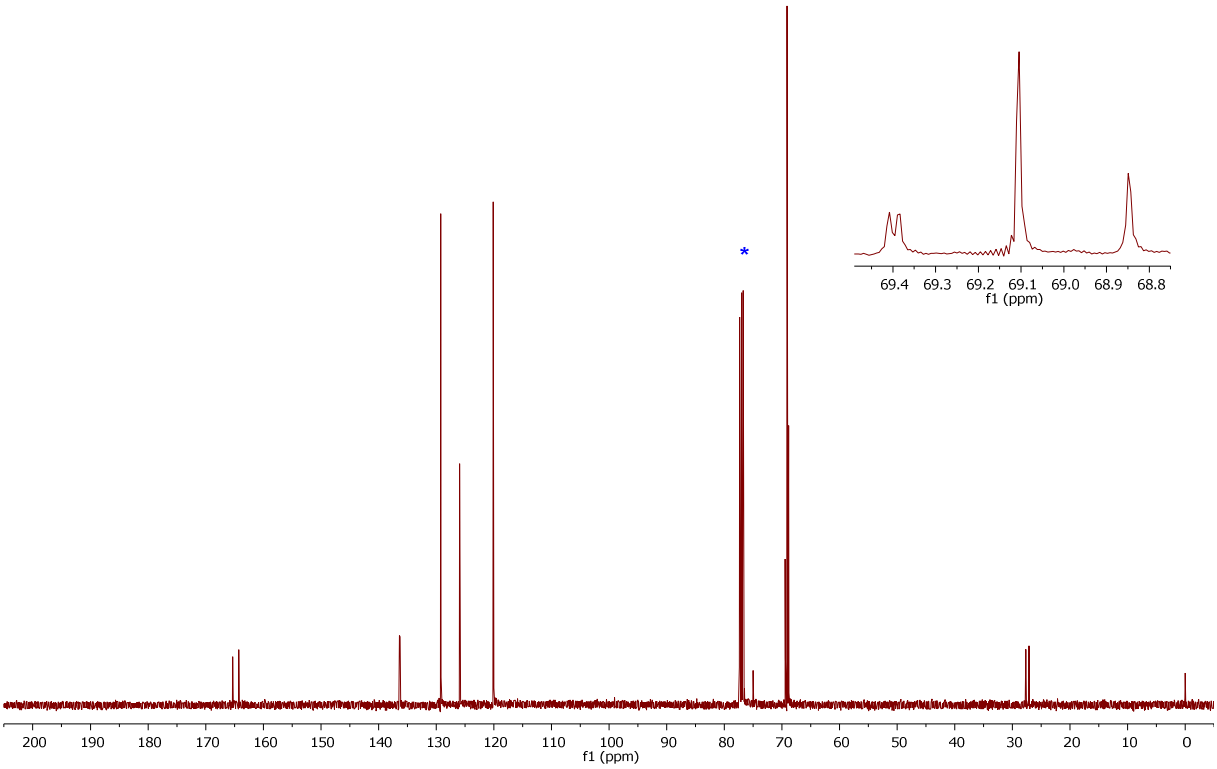

Figure S69. $^{13}C\{^{1}H\}$ NMR spectrum (101 MHz, $CDCl_3$) of **8a**.

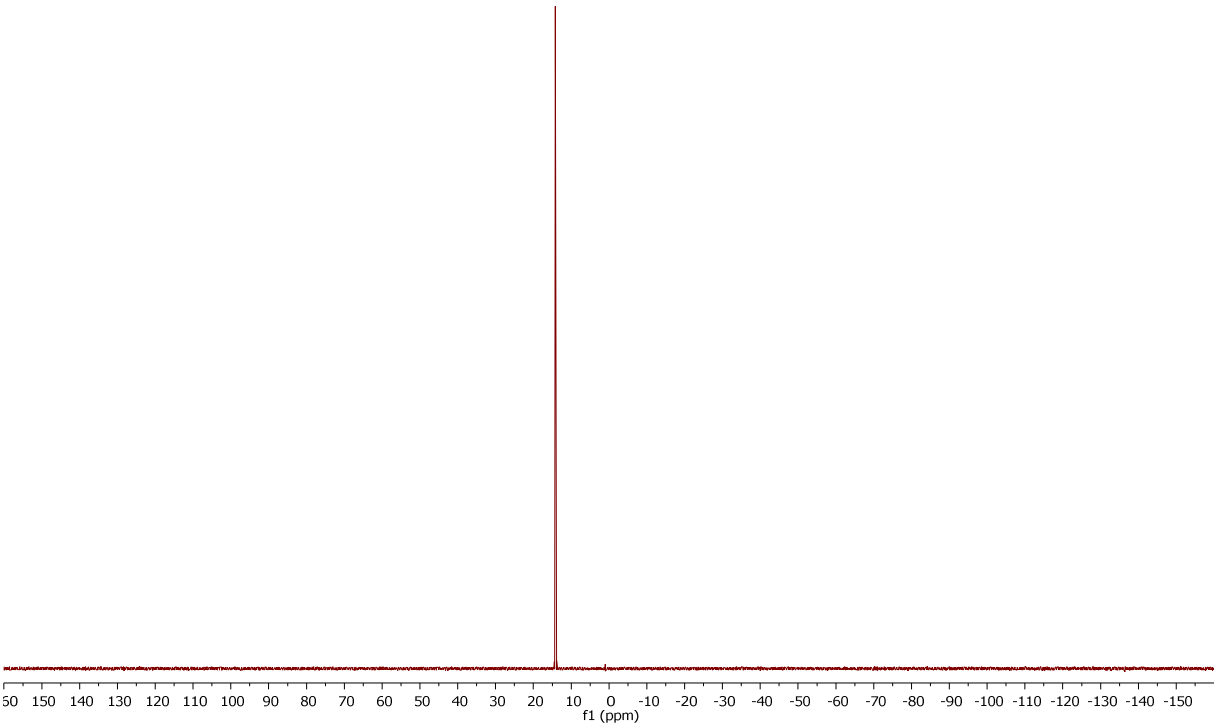

Figure S70. $^{31}P\{^{1}H\}$ NMR spectrum (162 MHz, $CDCl_3$) of **8a**.

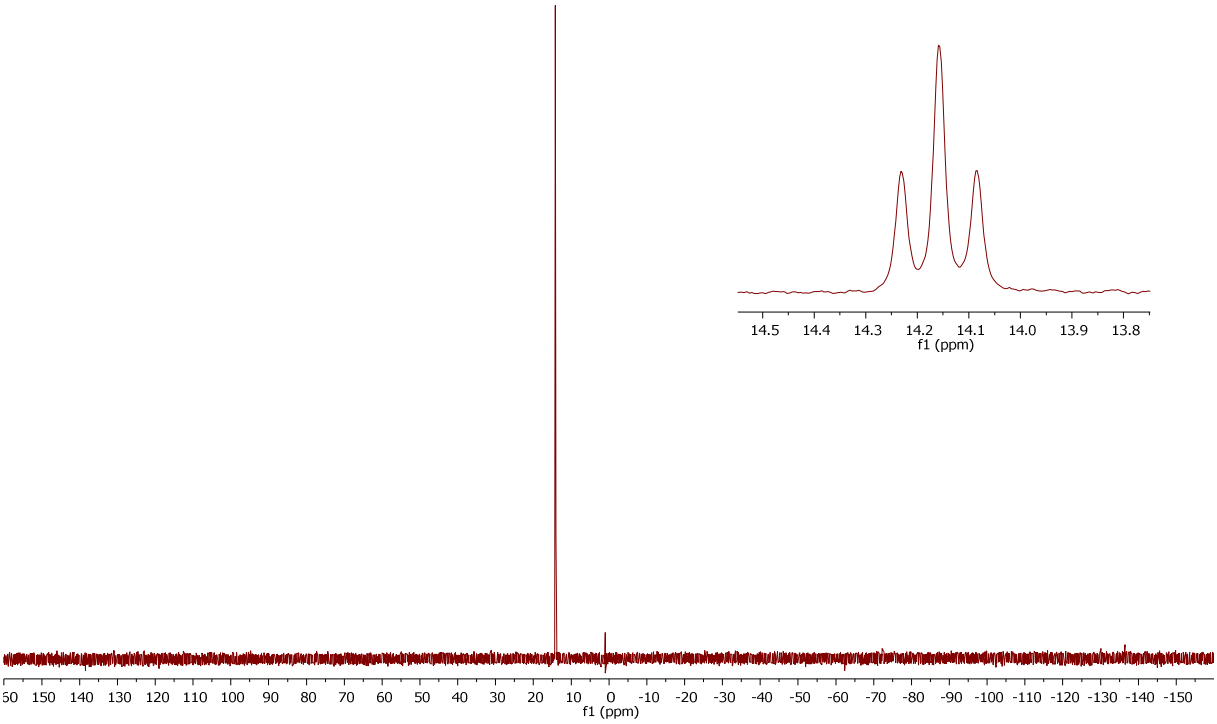

Figure S71. ^{31}P NMR spectrum (162 MHz, $CDCl_3$) of **8a**.

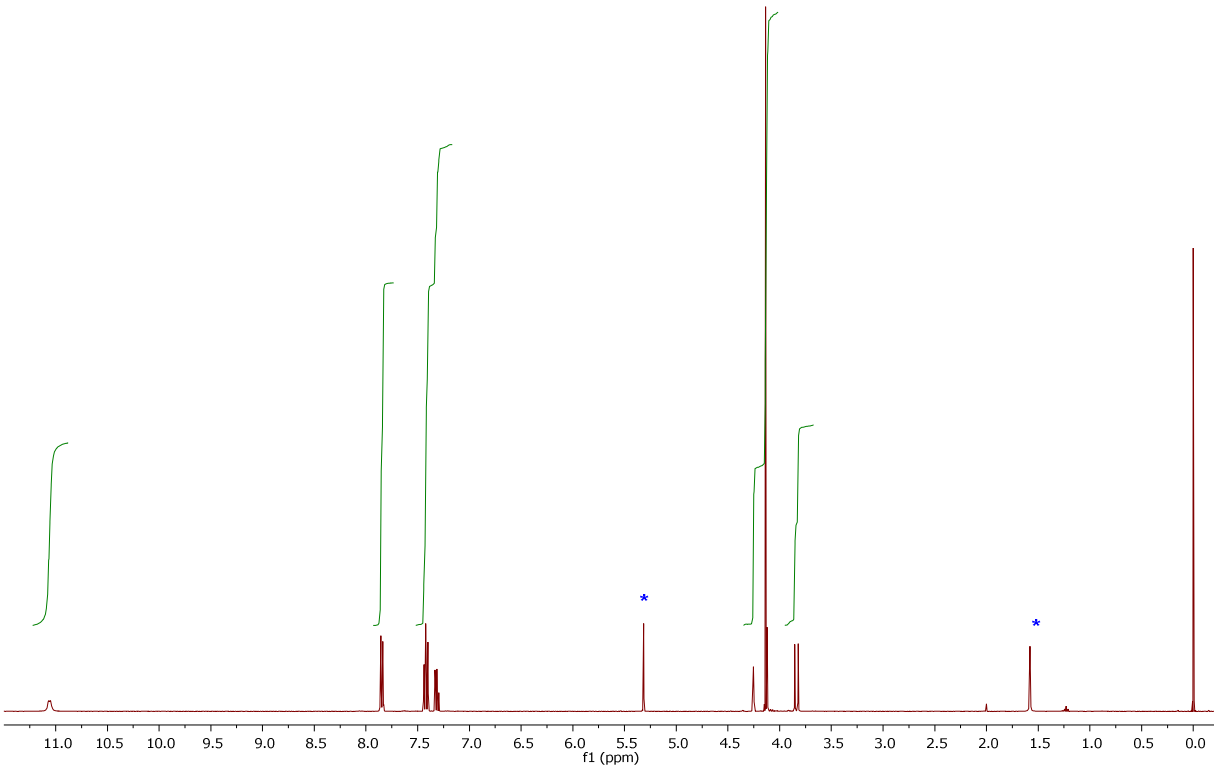

Figure S72. ^{1}H NMR spectrum (400 MHz, CD_2Cl_2) of **8b**.

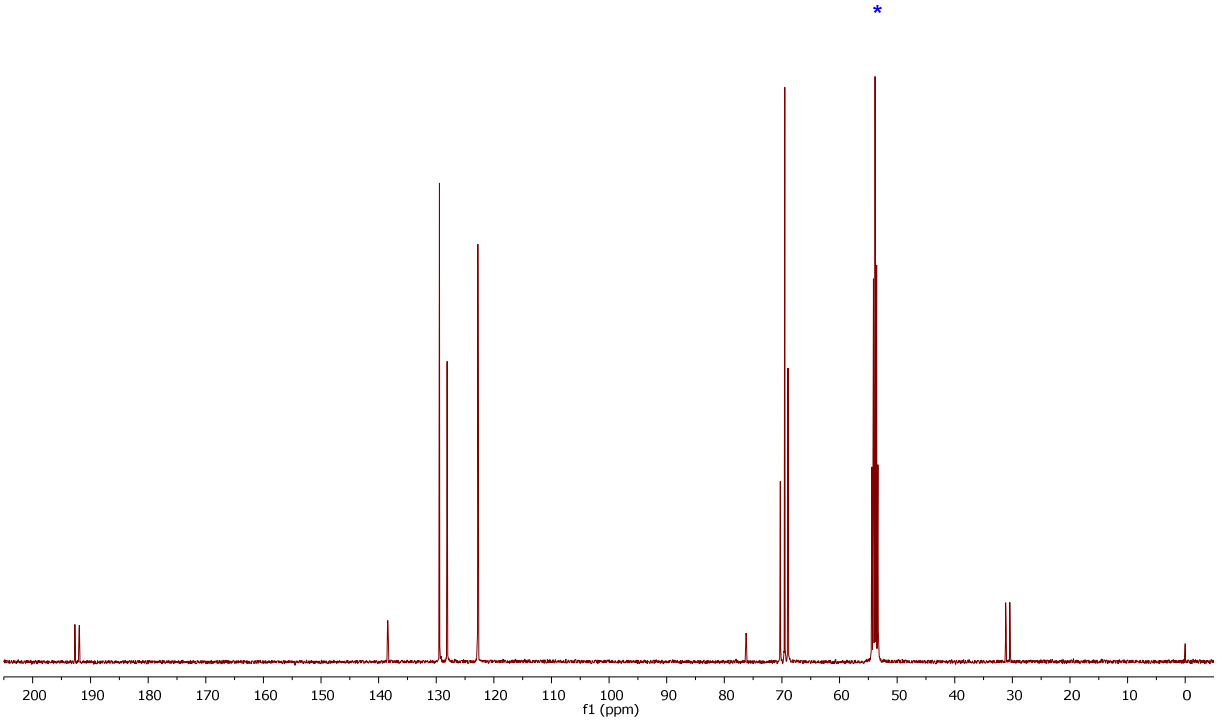

Figure S73. $^{13}C\{^{1}H\}$ NMR spectrum (101 MHz, CD_2Cl_2) of **8b**.

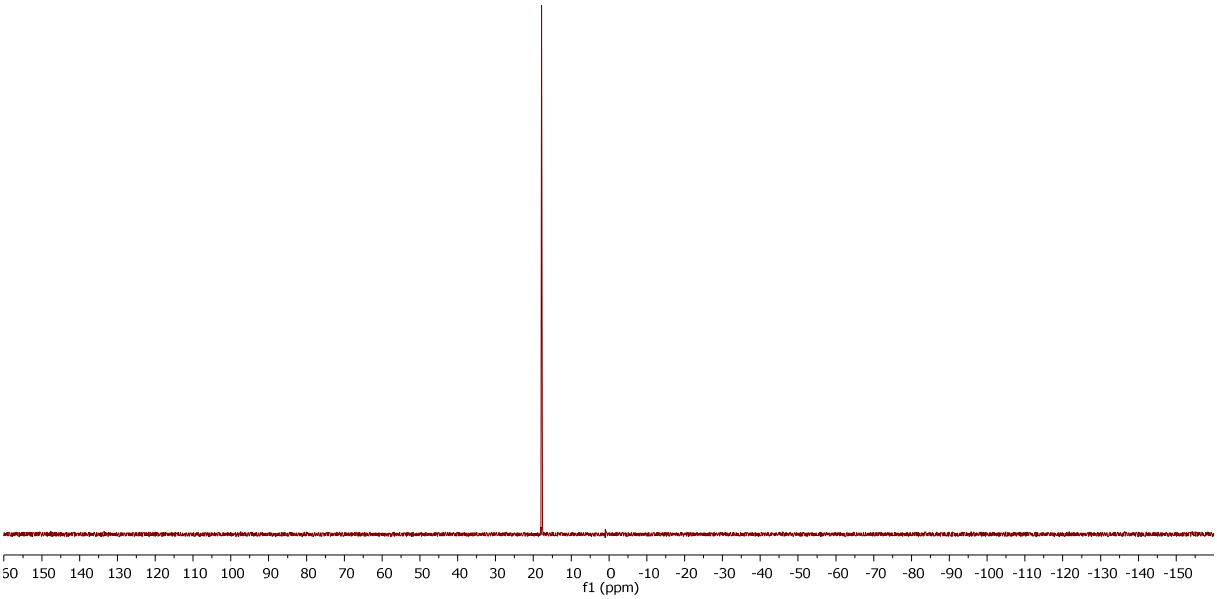

Figure S74. $^{31}P\{^{1}H\}$ NMR spectrum (162 MHz, CD_2Cl_2) of **8b**.

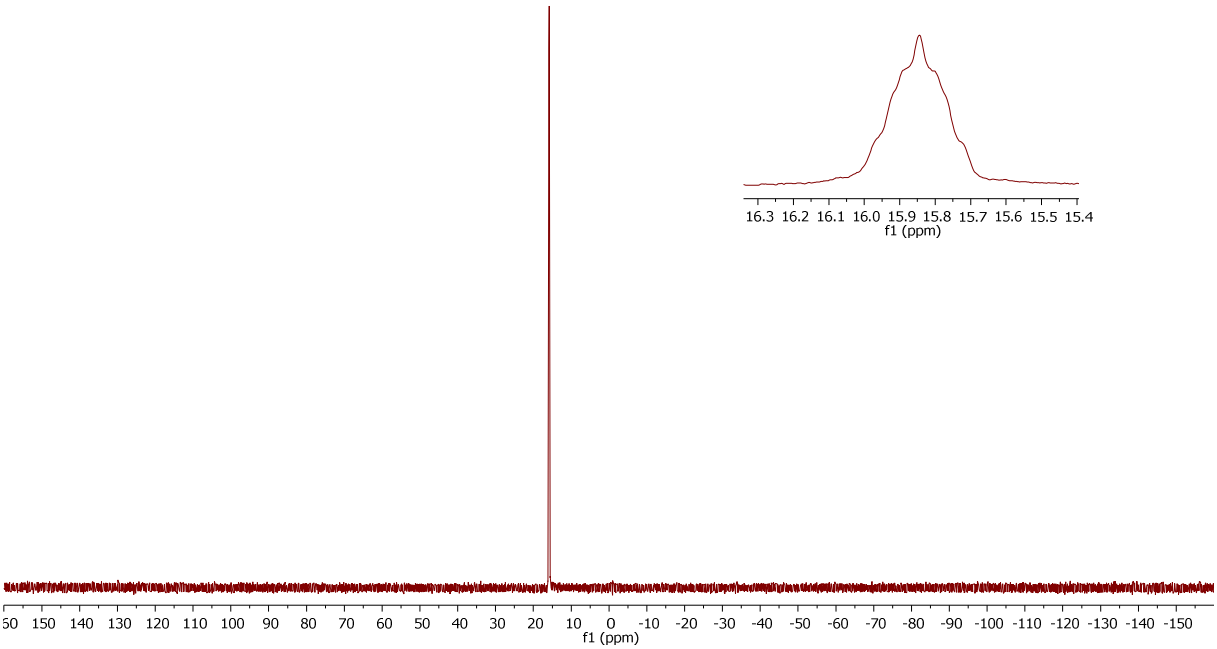

Figure S75. ^{31}P NMR spectrum (162 MHz, CD_2Cl_2) of **8b**.

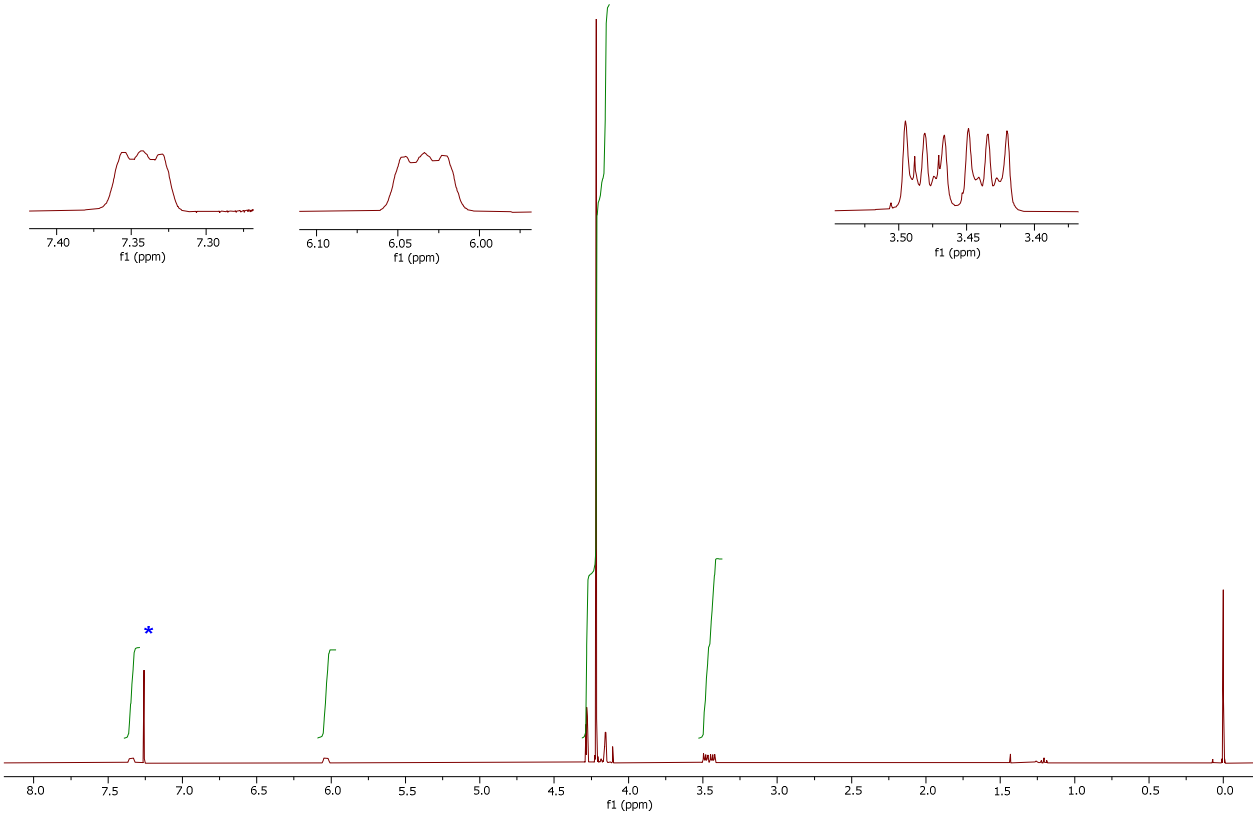

Figure S76. ^{1}H NMR spectrum (400 MHz, $CDCl_3$) of **9**.

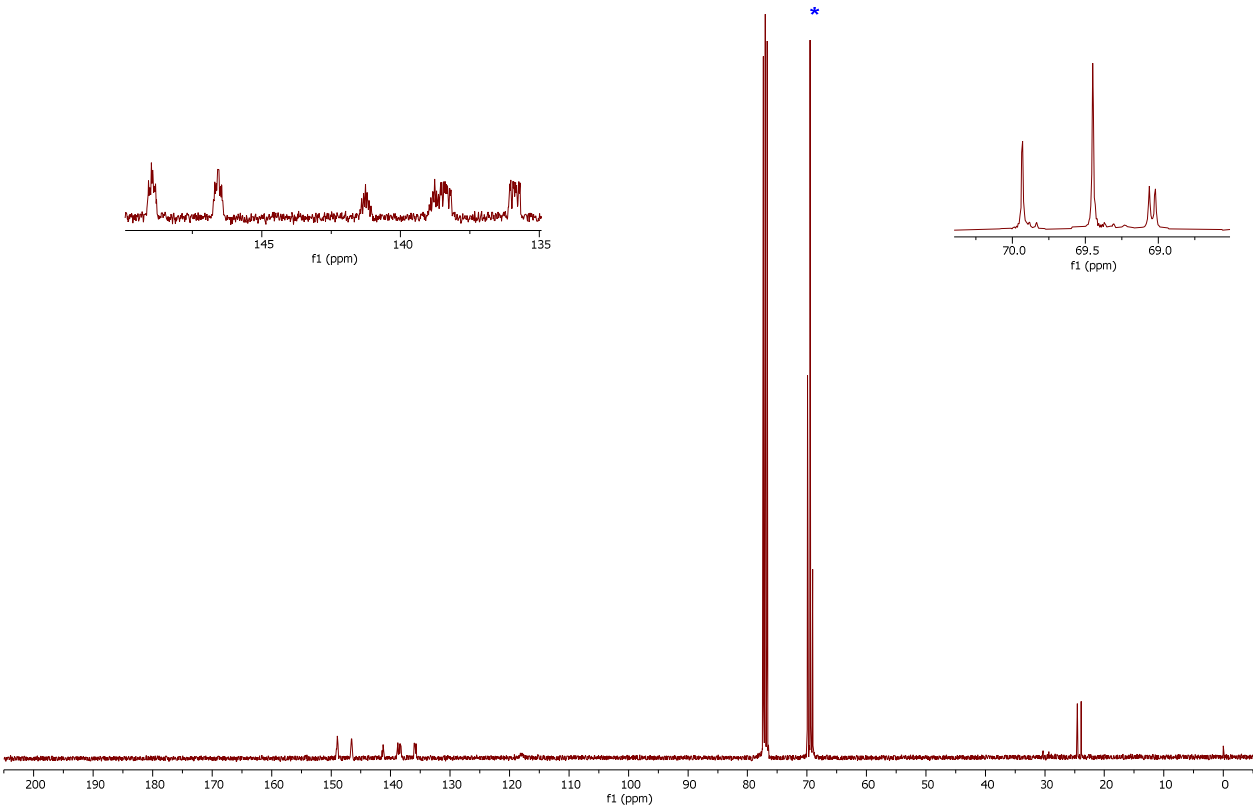

Figure S77. $^{13}C\{^{1}H\}$ NMR spectrum (101 MHz, $CDCl_3$) of **9**.

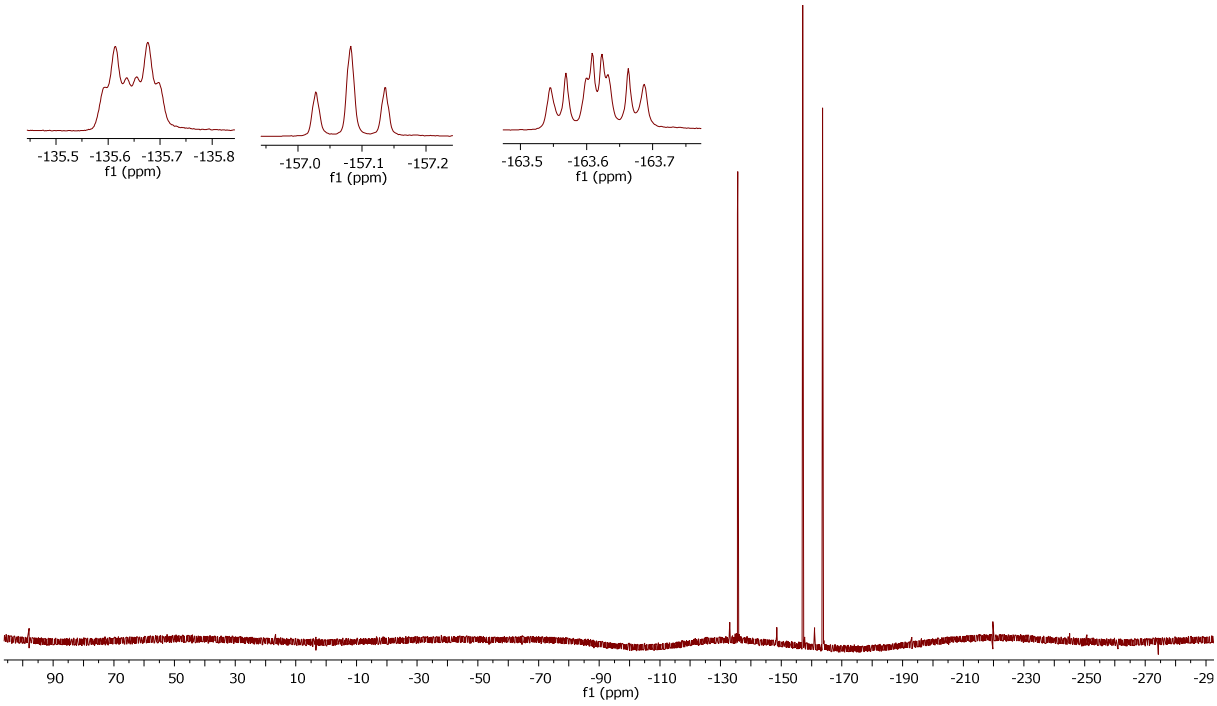

Figure S78. ^{19}F NMR spectrum (376 MHz, $CDCl_3$) of **9**.

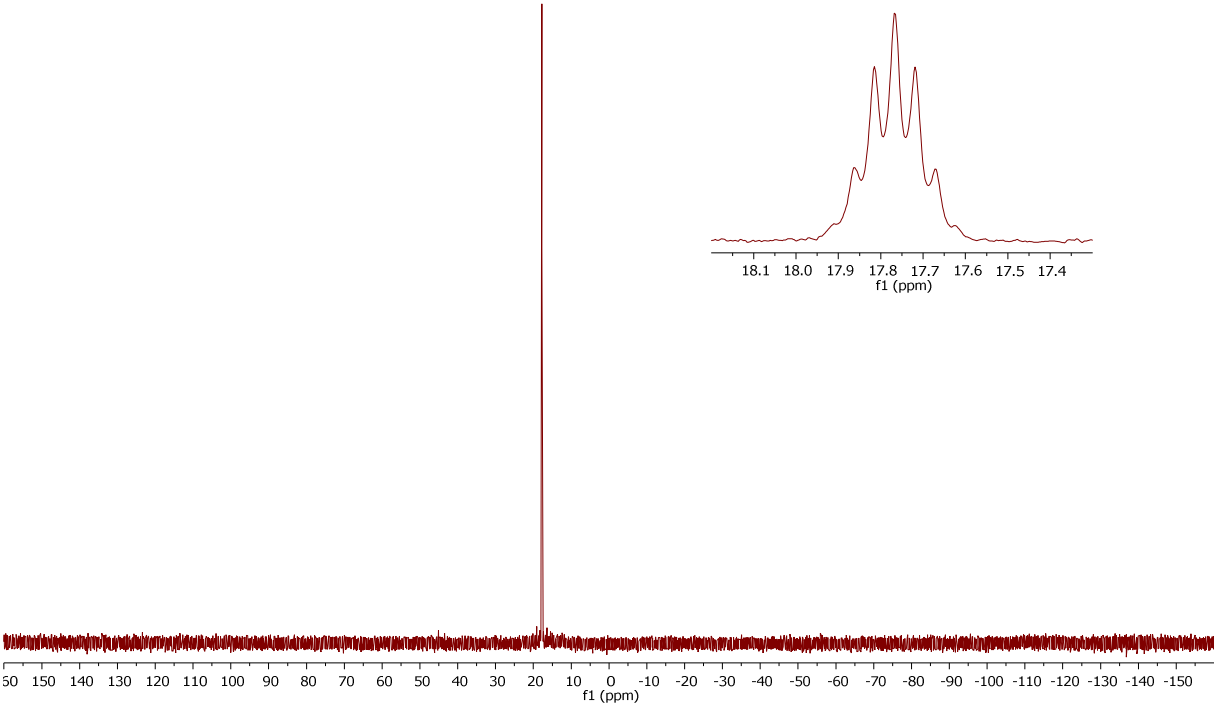

Figure S79. $^{31}P\{^1H\}$ NMR spectrum (162 MHz, $CDCl_3$) of **9**.

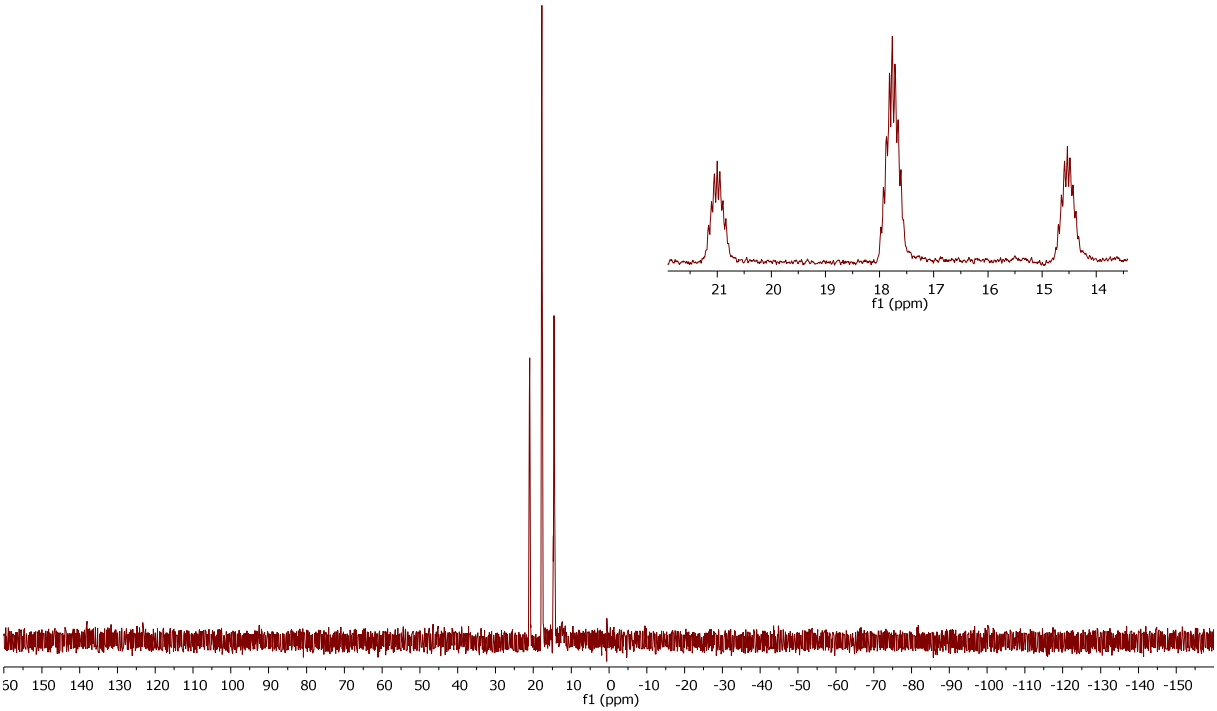

Figure S80. ^{31}P NMR spectrum (162 MHz, $CDCl_3$) of **9**.

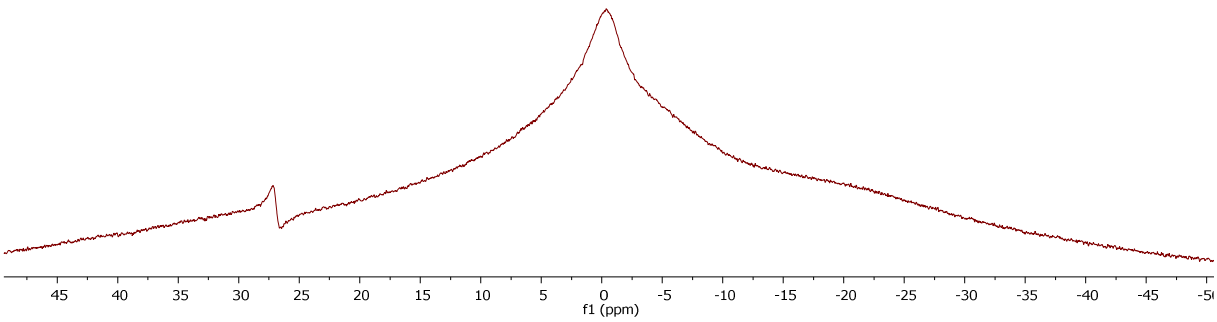

Figure S81. ^{11}B NMR spectrum (128 MHz, $CDCl_3$) of **9**.

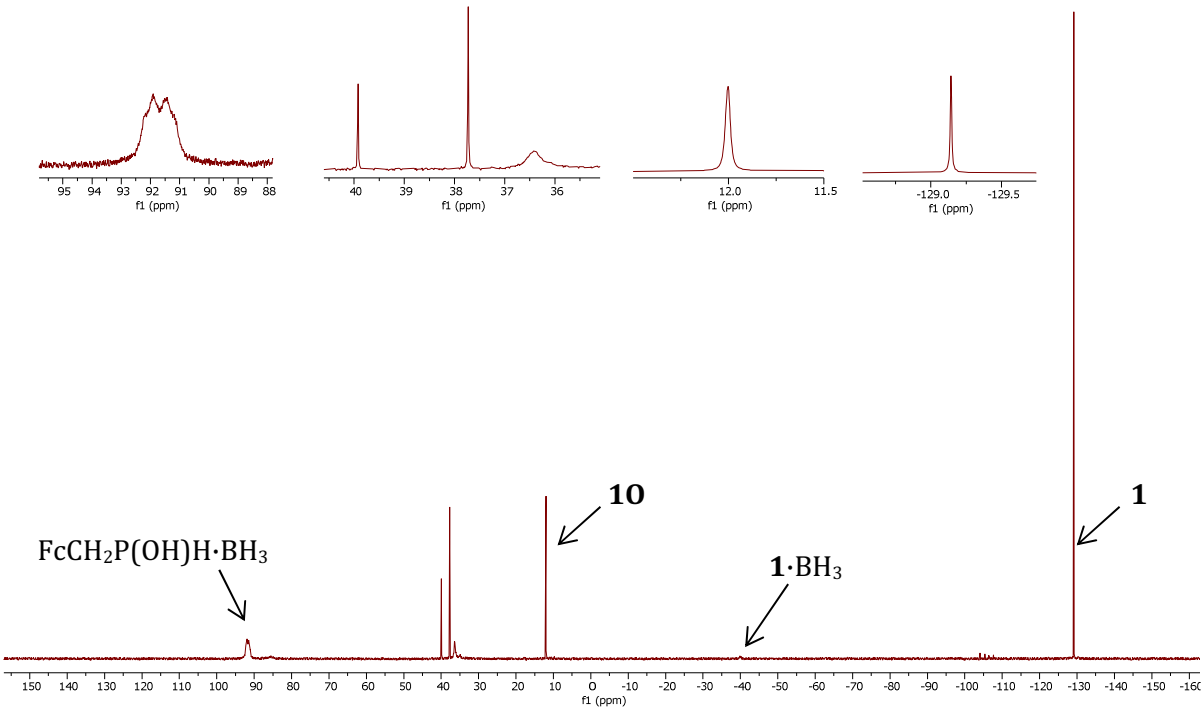

Figure S82. $^{31}P\{^{1}H\}$ NMR spectrum (162 MHz, $CDCl_3$) of the **1O**–BH_3 reaction mixture.

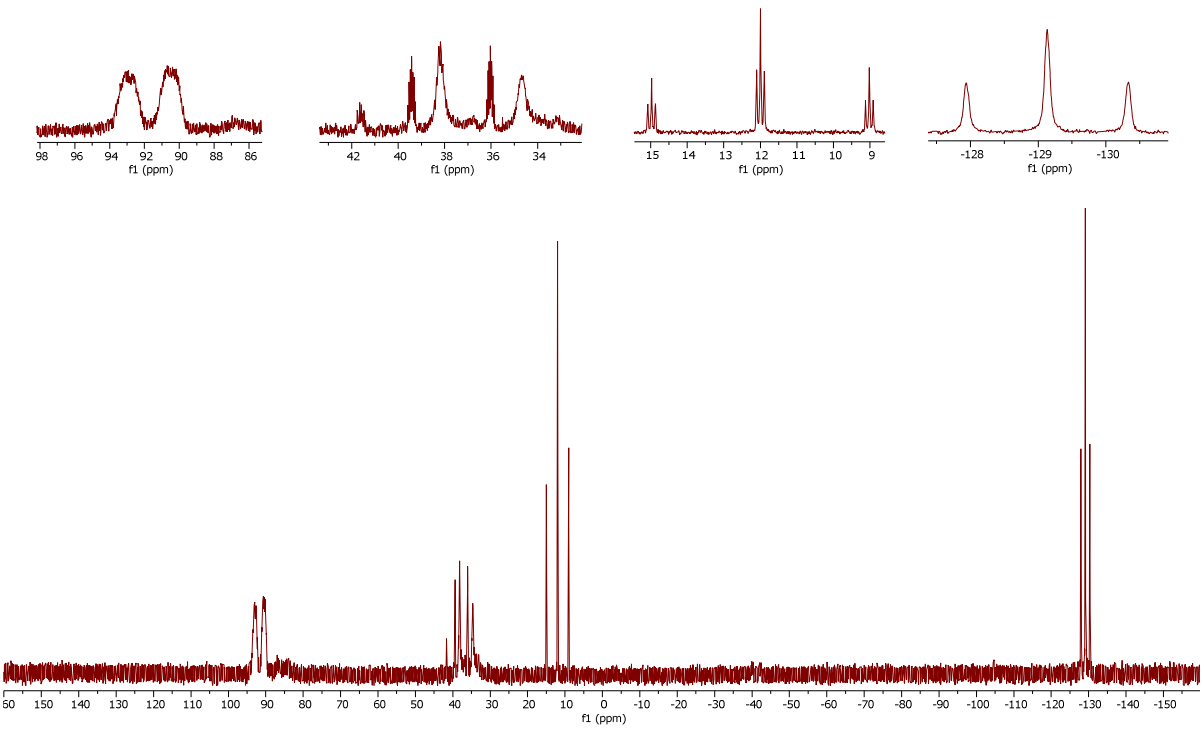

Figure S83. ^{31}P NMR spectrum (162 MHz, $CDCl_3$) of the **1O**–BH_3 reaction mixture.

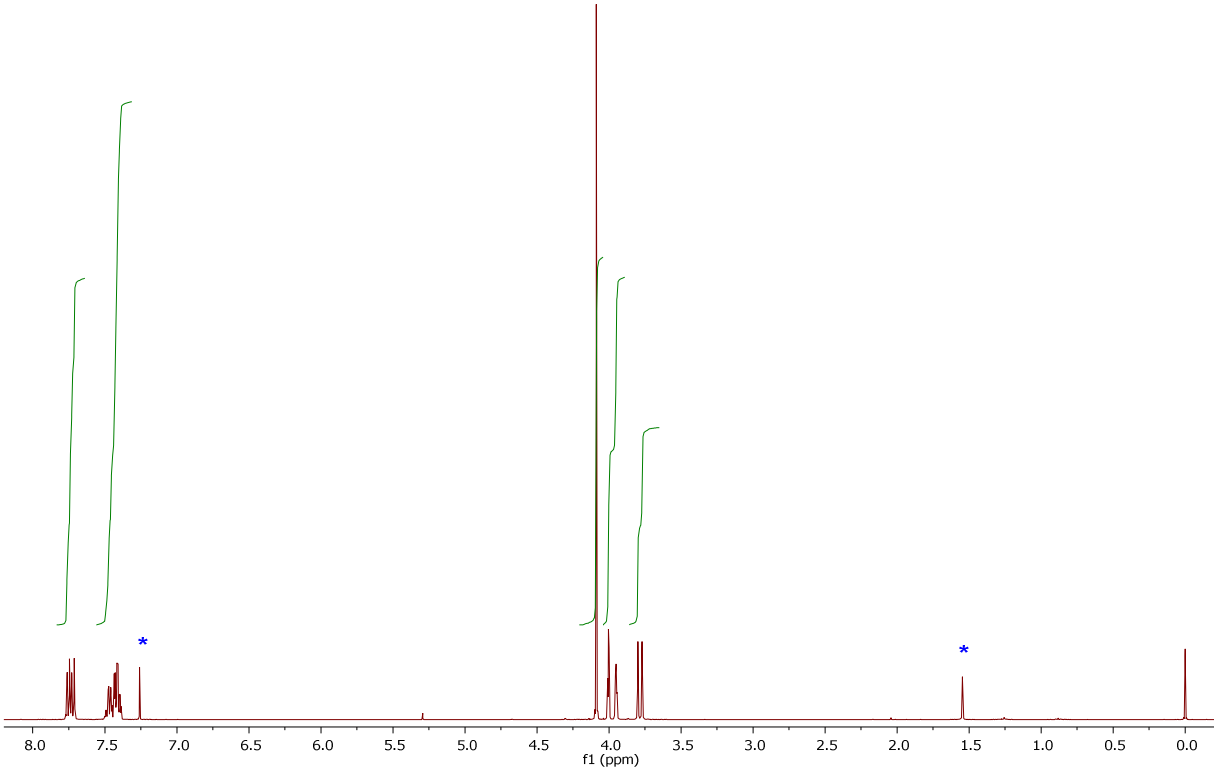

Figure S84. ^{1}H NMR spectrum (400 MHz, $CDCl_3$) of **$FcCH_2P(Se)Ph_2$**.

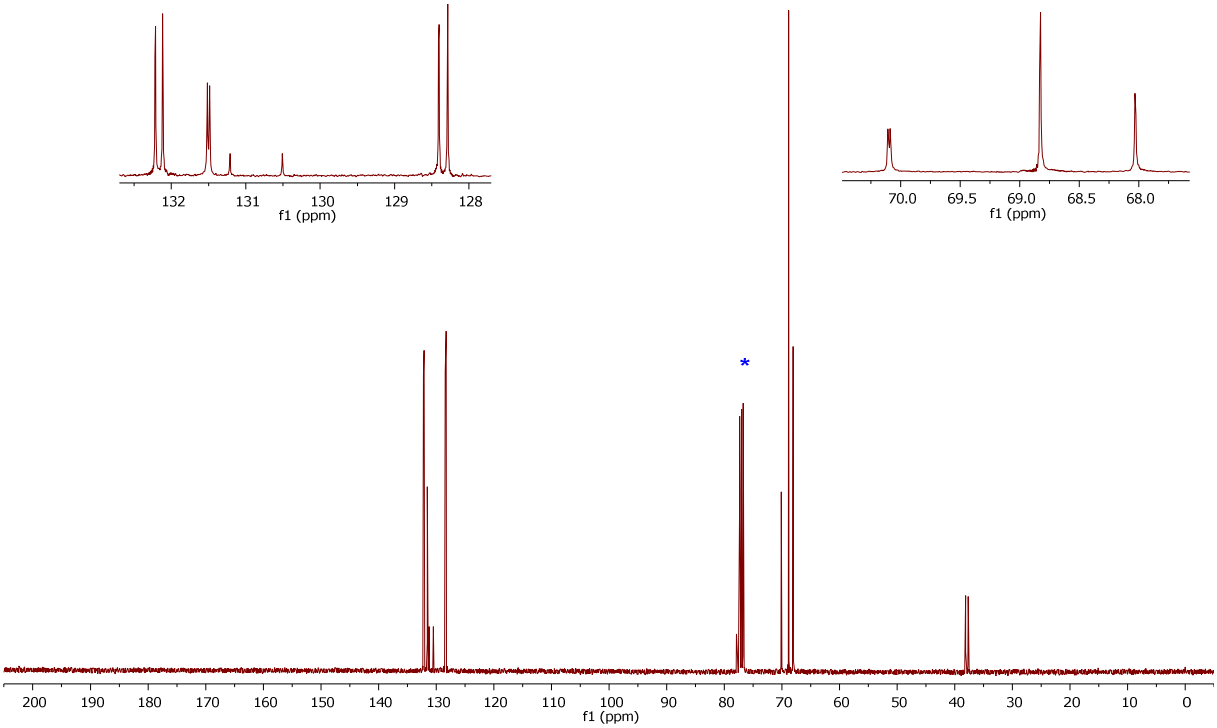

Figure S85. $^{13}C\{^{1}H\}$ NMR spectrum (101 MHz, $CDCl_3$) of **$FcCH_2P(Se)Ph_2$**.

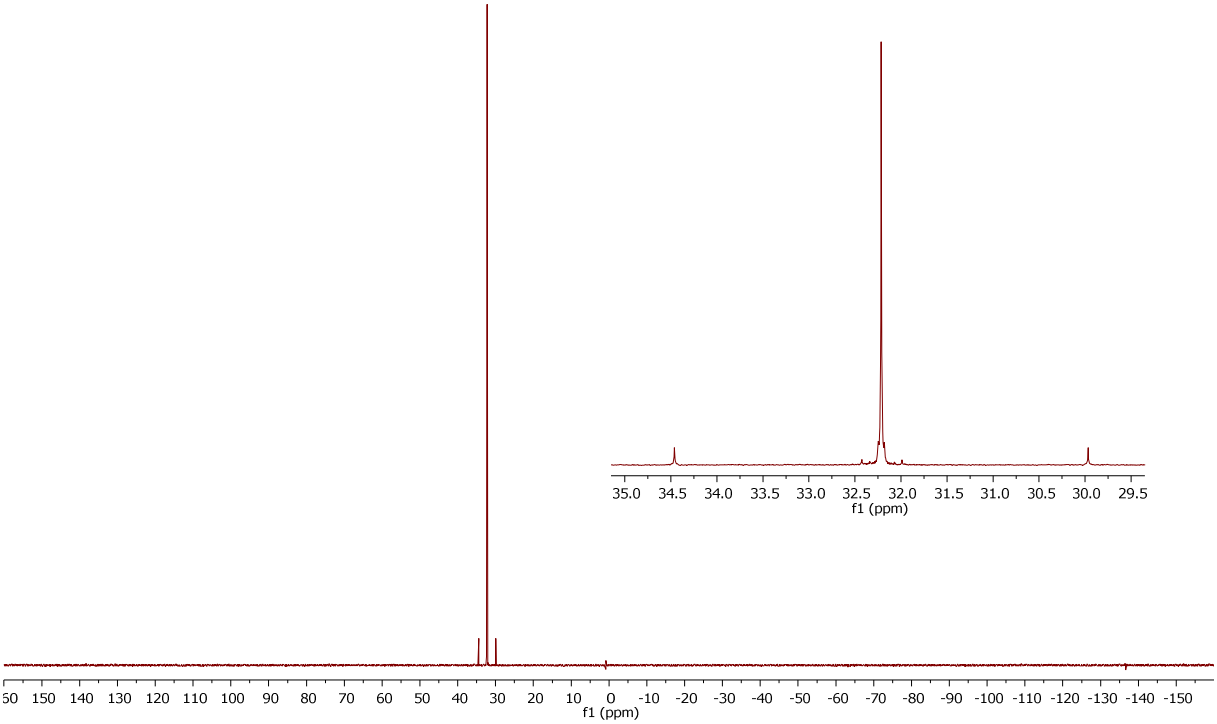

Figure S86. $^{31}P\{^{1}H\}$ NMR spectrum (162 MHz, $CDCl_3$) of **$FcCH_2P(Se)Ph_2$**.

REFERENCES

[1] P. Štěpnička, I. Císařová, *Dalton Trans.* 2013, **42**, 3373-3389.

[2] S.-J. Jong, J.-M. Fang, C.-H. Lin, *J. Organomet. Chem.* 1999, **590**, 42-45.

[3] R. J. Barney, R. M. Richardson, D. F. Wiemer, *J. Org. Chem.* 2011, **76**, 2875-2879.

[4] S. Zheng, S. Barlow, T. C. Parker, S. R. Marder, *Tetrahedron Lett.* 2003, **44**, 7989-7992.

[5] N. J. Goodwin, W. Henderson, B. K. Nicholson, J. Fawcett, D. R. Russell, *J. Chem. Soc., Dalton Trans.* 1999, **11**, 1785-1794.

[6] M. A. Pet, M. F. Cain, R. P. Cainn, R. P. Hughes, D. S. Glueck, J. A. Golen, A. L. Rheingold, *J. Organomet. Chem.* 2009, **694**, 2279-2289.

[7] N. J. Goodwin, W. Henderson, B. K. Nicholson, *Inorg. Chim. Acta* **1999**, *295*, 18-24.

[8] G. M. Sheldrick, *Acta Crystallogr., Sect. A: Found. Adv*. **2015**, *71*, 3-8.

[9] G. M. Sheldrick, *Acta Crystallogr., Sect. C: Struct. Chem*. **2015**, *71*, 3-8.

[10] a) A. L. Spek, *J. Appl. Crystallogr*. **2003**, *36*, 7-13; b) A. L. Spek, *Acta Crystallogr. D, Biol. Crystallogr*. **2009**, *65*, 148-155.

[11] J. Bruckmann, C. Kruger, C. W. Lehmann, W. Leitner, J. Rust, C. Six, *Acta Crystallogr., Sect. C: Cryst. Struct. Commun*. **1999**, *55*, 695-696.

[12] S. I. M. Paris, F. R. Lemke, R. Sommer, P. Lönnecke, E. Hey-Hawkins, *J. Organomet. Chem.* **2005**, *690*, 1807-1813.

[13] N. J. Goodwin, W. Henderson, B. K. Nicholson, *Inorg. Chim. Acta* **1999**, *295*, 18-24.

[14] Y. Nie, H. Pritzkow, H. Wadepohl, W. Siebert, *J. Organomet. Chem.* **2005**, *690*, 4531-4536.

[15] L. Yang, D. R. Powell, R. P. Houser, *Dalton Trans*. **2007**, 955-964.

[16] S. Härling, J. Greiser, T. M. A. Al-Shboul, H. Görls, S. Krieck, M. Westerhausen, *Aust. J. Chem.* **2013**, *66*, 1264-1273.

[17] M. Ernzerhof, G. E. Scuseria, *J. Chem. Phys.* **1999**, *110*, 5029-5036.

[18] (a) S. Grimme, J. Antony, S. Ehrlich, H. Krieg, *J. Chem. Phys.* **2010**, *132*, 154104; (b) S. Grimme, S. Ehrlich, L. Goerigk, *J. Comput. Chem.* **2011**, *32*, 1456-1465.

[19] F. Weigend, R. Ahlrichs, *Phys. Chem. Chem. Phys.* **2005**, *7*, 3297-3305.

[20] D. Andrae, U. Haeussermann, M. Dolg, H. Stoll, H. Preuss, *Theor. Chim. Acta* **1990**, *77*, 123–141.

[21] Gaussian 16, Revision A.03, M. J. Frisch, G. W. Trucks, H. B. Schlegel, G. E. Scuseria, M. A. Robb, J. R. Cheeseman, G. Scalmani, V. Barone, G. A. Petersson, H. Nakatsuji, X. Li, M. Caricato, A. V. Marenich, J. Bloino, B. G. Janesko, R. Gomperts, B. Mennucci, H. P. Hratchian, J. V. Ortiz, A. F. Izmaylov, J. L. Sonnenberg, D. Williams-Young, F. Ding, F. Lipparini, F. Egidi, J. Goings, B. Peng, A. Petrone, T. Henderson, D. Ranasinghe, V. G. Zakrzewski, J. Gao, N. Rega, G. Zheng, W. Liang, M. Hada, M. Ehara, K. Toyota, R. Fukuda, J. Hasegawa, M. Ishida, T.

Nakajima, Y. Honda, O. Kitao, H. Nakai, T. Vreven, K. Throssell, J. A. Montgomery, Jr., J. E. Peralta, F. Ogliaro, M. J. Bearpark, J. J. Heyd, E. N. Brothers, K. N. Kudin, V. N. Staroverov, T. A. Keith, R. Kobayashi, J. Normand, K. Raghavachari, A. P. Rendell, J. C. Burant, S. S. Iyengar, J. Tomasi, M. Cossi, J. M. Millam, M. Klene, C. Adamo, R. Cammi, J. W. Ochterski, R. L. Martin, K. Morokuma, O. Farkas, J. B. Foresman, and D. J. Fox, Gaussian, Inc., Wallingford CT, 2016.

[22] F. Barrière, W. E. Geiger, *J. Am. Chem. Soc.* **2006**, *128*, 3980-3989.

Appendix C

Horký, F.; Císařová, I.; Štěpnička, P. Stable Pd(0) Complexes with Ferrocene Bisphosphanes Bearing Phosphatrioxaadamantyl Substituents Efficiently Catalyze Selective C-H Arylation of Benzoxazoles by Aryl Chlorides. *ChemCatchem* **2021**, accepted manuscript, https://doi.org/10.1002/cctc.202101013.

ChemCatChem

The European Society Journal for Catalysis

Chemistry Europe

European Chemical Societies Publishing

Supported by

GECATS GERMAN CATALYSIS SOCIETY

Accepted Article

Title: Stable Pd(0) Complexes with Ferrocene Bisphosphanes Bearing Phosphatrioxaadamantyl Substituents Efficiently Catalyze Selective C-H Arylation of Benzoxazoles by Aryl Chlorides

Authors: Filip Horký, Ivana Císařová, and Petr Stepnicka

To be cited as: *ChemCatChem* 10.1002/cctc.202101013

Link to VoR: https://doi.org/10.1002/cctc.202101013

WILEY-VCH

Stable Pd(0) Complexes with Ferrocene Bisphosphanes Bearing Phosphatrioxaadamantyl Substituents Efficiently Catalyze Selective C-H Arylation of Benzoxazoles by Aryl Chlorides

Filip Horký,[a] Ivana Císařová[a] and Petr Štěpnička*[a]

Dedicated to Christian Bruneau in recognition of his outstanding contributions to organometallic chemistry and catalysis.

[a] F. Horký, Dr. I. Císařová and Prof. Dr. P. Štěpnička
Department of Inorganic Chemistry
Faculty of Science, Charles University
Hlavova 2030, 128 40 Prague, Czech Republic
E-mail address: petr.stepnicka@natur.cuni.cz

Supporting information for this article is given via a link at the end of the document.

Abstract: Versatile applications and unique performance of 1,1'-bis(diphenylphosphanyl)ferrocene (dppf) in coordination chemistry and catalysis prompted the search for its analogs. This contribution describes the synthesis of the first donor-unsymmetric dppf congeners bearing bulky and rigid 1,3,5,7-tetramethyl-2,4,6-trioxa-8-phosphaadamantyl (CgP) donor groups, *viz*. $Ph_2PfcPCg$ (**1**) and Ph_2PfcCH_2PCg (**2**; fc = ferrocene-1,1'-diyl). Bis-phosphanes **1** and **2** were converted into air-stable Pd(0) complexes, [Pd(ma)(L^L)] (L^L = **1** and **2**; ma = maleic anhydride). Together with [Pd(ma)(dppf)], these complexes were applied as catalysts in Pd-catalyzed C-H arylation of benzoxazoles with aryl chlorides in *n*-butanol as an environmentally benign solvent. Among all catalysts tested in this study, complex [Pd(ma)(**2**)] performed the best, providing a high-yield and selective synthesis of 2-arylbenzoxazoles from a range of the generally less reactive chloroarenes at low catalyst loading (typically 1 mol.%). Under similar conditions, the structurally related heterocycles (*e.g.,* 1-methylbenzimidazole and benzothiazole) did not react.

Introduction

Although the formation of phosphatrioxaadamantanes, frequently referred to as cage phosphanes (CgPR) due to their shape, by acid-catalyzed condensation of PH_3 and primary phosphanes with acetylacetone (Hacac) has already been reported in the 1960s,[1] ligands featuring 1,3,5,7-tetramethyl-2,4,6-trioxa-8-phosphatricyclo[3.3.1.1^{3,7}]decane-8-yl groups (hereafter denoted as CgP; Scheme 1) and their applications emerged only decades later,[2] triggered by the discovery of reliable synthetic routes toward suitable precursors (*e.g.*, CgPH, $CgPH{\cdot}BH_3$ and CgPBr).[3] Soon after, the unique characteristics of the CgP moiety were identified, including an unparalleled combination of specific steric properties, electron-poor nature, comparable with that of a $P(OR)_2$ group, and high chemical robustness.[2] These properties were advantageously exploited in the design of new ligands for catalysis. In particular, phosphanes bearing CgP substituents display favorable properties in Pd-catalyzed carbonylation (*e.g.*, hydroformylation and alkoxycarbonylation)[4] and cross-coupling reactions,[5] whereas nickel complexes supported by CgP ligands efficiently mediate C-N and C-O bond formation.[6]

Encouraged by successful applications of ditopic phosphane ligands combining conventional (PR_2) and CgP donor groups (**A** in Scheme 1),[6] we prepared analogous ferrocene-based compounds and investigated their catalytic potential. Despite the enormous practical success of ferrocene phosphanes,[7] compounds combining ferrocene and CgP fragments in their structures remained limited to a handful of bis-phosphanes of type **B** (Scheme 1) used in metal-catalyzed alkoxycarbonylation of vinylic substrates.[8]

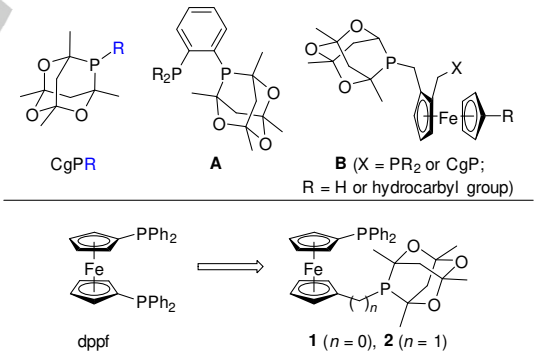

Scheme 1. (top) Examples of phosphane ligands with CgP substituents; (bottom) dppf and the newly prepared CgP ferrocene phosphanes

In this contribution, we report the synthesis of ferrocene bis-phosphanes **1** and **2** (Scheme 1), formally analogous to the widely used 1,1'-bis(diphenylphosphanyl)ferrocene (dppf).[9] Together with dppf, for comparative purposes, compounds **1** and **2** were used to prepare stable Pd(0) complexes, which were subsequently tested as defined catalysts for selective C-H arylation of benzoxazoles with aryl chlorides.

Results and Discussion

Synthesis of phosphane ligands and their Pd(0) complexes

Compound **1** was prepared by stepwise lithiation and functionalization of 1,1'-dibromoferrocene (**3**).[10] Of the two alternative routes, differing in the order in which the functional substituents were introduced (Scheme 2), the route employing **5** as an intermediate proved more efficient because lithiation and phosphanylation of this compound proceeded with a better yield and resulted in a cleaner product, which was easier to purify and required no final crystallization (*N.B.* compounds **1** and **4** are more difficult to separate from each other than **1** and **5** and even **3** and **5**).

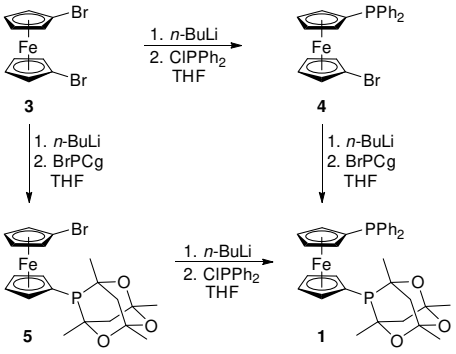

Scheme 2. Alternative synthetic routes toward bis-phosphane **1**

The semi-homologous[11] bis-phosphane **2** was synthesized by acid-catalyzed condensation of air-stable primary phosphane **6**[12] with acetylacetone (Scheme 3), similarly to the original preparation of CgPR (R = H, alkyl, Ph) reported by Epstein and Buckler.[1]

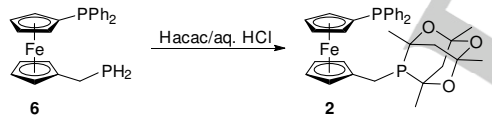

Scheme 3. Synthesis of bis-phosphane **2** (Hacac = acetylacetone)

Bis-phosphanes **1** and **2** and compound **5** were obtained in good yields as air-stable, orange crystalline solids and characterized by elemental analysis, spectroscopic methods (multinuclear NMR, IR and ESI-MS) and X-ray crystallography. Their ^{1}H and $^{13}C\{^{1}H\}$ NMR spectra are consistent with the proposed structures, but rather complicated due to the inherent chirality of the CgP cage, which renders the ferrocene CH groups and the CH_2 protons diastereotopic and anisochronic. Nevertheless, by using 2D and ^{31}P decoupled NMR spectra, we were able to identify all NMR signals and to distinguish between H-H and P-H couplings, albeit without attempting full assignment, including distinguishing individual C, CH_2 and CH_3 fragments.

The $^{31}P\{^{1}H\}$ NMR spectra of **1** and **2** (Table 1) display pairs of singlets attributable to two phosphorus substituents: the signal due to the CgP substituent in **2** (δ_P –26.1) appears downfield shifted with respect to **1** (δ_P –31.7), whereas the position the PPh_2 signals practically does not change ($\delta_P \approx -17$; *cf.* δ_P –16.2 for $FcPPh_2$; Fc = ferrocenyl).[13]

Table 1. Selected ^{31}P NMR data[a]

Compound	^{31}P NMR parameters (δ_P [$^{1}J_{PSe}$] (assignment))
1	–31.7 (CgP), –16.8 (PPh_2)
1-Se	30.4 [766] (PCg), 31.6 [738] (PPh_2)
2	–26.1 (PCg), –16.5 (PPh_2)
2-Se	33.9 [757] (PCg), 32.4 [731] (PPh_2)
7	23.6 (PPh_2)
8	13.8/14.6 (PCg), 23.6/23.7 (PPh_2)[b]
9	4.3/6.0 (PCg), 20.8/20.9 (PPh_2)[b]

[a] Spectra of the phosphines and their selenides were recorded in $CDCl_3$, and spectra of the complexes in CD_2Cl_2. Data for **5**: $\delta_P = -32.4$ ppm; data for **5-Se**: $\delta_P = 30.6$ ppm, $^{1}J_{PSe} = 766$ Hz. [b] Complexes **8** and **9** are mixtures of two stereoisomers. Their $^{31}P\{^{1}H\}$ NMR signals are observed as doublets owing to scalar interactions of the two different P-donor groups.

Compounds **1**, **2** and **5** were further converted into the respective phosphane selenides **1-Se**, **2-Se** and **5-Se** by treatment with potassium selenocyanate[14] (Scheme 4). The formation of P-selenides results in a down-field shift of ^{31}P NMR resonances and in characteristic ^{77}Se satellites (Table 1). The $^{1}J_{PSe}$ value determined for the $P(Se)Ph_2$ group in **2** is the same as that of $FcP(Se)Ph_2$ (731 Hz in $CDCl_3$),[13] and lower than the $^{1}J_{PSe}$ value of compound **1** bearing the electron-withdrawing CgP(Se) substituent directly at the ferrocene unit. The CgP(Se) moieties show significantly larger $^{1}J_{PSe}$ coupling constants, in line with the lower basicity of their phosphorus atoms and narrower C-P-C angles.[15]

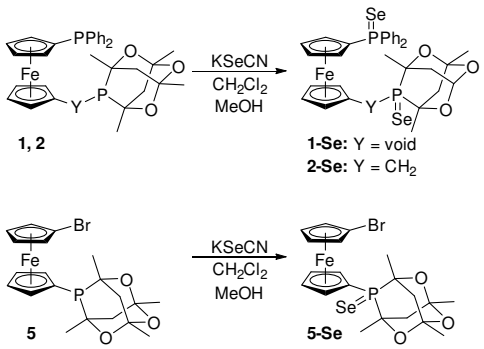

Scheme 4. Synthesis of phosphane selenides **1-Se**, **2-Se** and **5-Se**

Solid-state structures of bis-phosphanes **1** and **2** are displayed in Figure 1; structural diagrams for **1-Se** and **2-Se** and the crystal structures of **5** and **5-Se** are presented in Supporting Information. All compounds crystallize in centrosymmetric space groups, which underscores their racemic nature. Structural parameters compiled in Table 2, particularly the smaller tilt angles and closer positions of the substituents at the ferrocene core, suggest a smaller steric crowding in compounds with a spacer inserted between the ferrocene unit and the PCg group and in compounds with no additional substituent at the phosphorus (phosphanes *vs.* phosphane selenides). The P-Se bond distances are within the expected margins (*cf.* 2.103(6) Å

for dppfSe$_2$,[16] and 2.06-2.10 Å for CgP(Se)X, where X = F-I[17]). However, the oxidation of the phosphane moieties results in a characteristic shortening of the P-C bonds with a concomitant opening of the C-P-C angles.

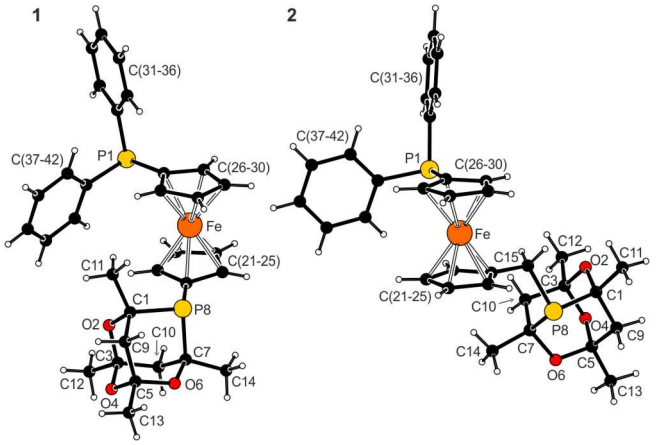

Figure 1. Molecular structures of **1** and **2** (additional structural diagrams are available in Supporting Information).

Table 2. Selected distances and angles for **1**, **2**, **1-Se** and **2-Se** (in Å and °)

Param[a]	**1**[c]	**2**[d]	**1-Se**[e]	**2-Se**[f]
P1-C26	1.813(1)	1.811(1)	1.797(2)	1.788(2)
P1-C31/37	1.836(1)/1.843(2)	1.833(1)/1.838(1)	1.814(2)/1.817(2)	1.816(2)/1.814(2)
P8-C*n*[b]	1.815(2)	1.861(2)	1.787(2)	1.843(2)
P8-C1/7	1.878(2)/1.891(2)	1.880(1)/1.884(2)	1.864(2)/1.870(2)	1.858(2)/1.870(2)
Fe-C	2.034(2)-2.058(2)	2.037(1)-2.059(1)	2.034(2)-2.073(2)	2.033(2)-2.053(2)
tilt	4.56(9)	1.28(8)	5.81(1)	1.1(1)
τ	−122.4(2)	79.0(1)	−165.4(1)	161.2(2)

[a] Tilt is the dihedral angle of the least-squares cyclopentadienyl planes and τ is the torsion angle C21-Cg1-Cg2-C26, where Cg1 and Cg2 stand for the centroids of the cyclopentadienyl rings C(21-25) and C(26-30), respectively. [b] *n* = 21 for **1** and **1-Se**, *n* = 15 for **2** and **2-Se**. [c] Parameters pertaining to the CgP cage in the dominating orientation are given. [d] Further data: P8-C15-C21 = 112.14(9)°. [e] Further data: P1-Se1 = 2.1100(5) Å, P8-Se2 = 2.0988(6) Å. [f] Additional parameters: P1-Se1 = 2.1081(6) Å, P8-Se2 = 2.1013(6) Å, P8-C15-C21 = 115.5(2)°.

Compounds **1**, **2** and dppf readily displaced the chelating diimine ligand in [Pd(ma)(N^N)] (ma = maleic anhydride, N^N = *N,N*-di-*t*-butylethanedialdimine)[18] to produce Pd(0) complexes **7**-**9** (Scheme 5), which were isolated as air-stable orange solids (the compounds did not decompose when purified by column chromatography in air and stored as solids under ambient conditions for months, no decomposition was observed even when allowing a CD_2Cl_2 solution to stand in the air overnight[19]) and characterized similarly to the free ligands. Complexes **8** and **9**, result as mixtures of diastereoisomers differing in chirality at the CgP cage (*R* or *S*) *and* in the mutual positioning of the substituents at the ferrocene unit (formally R_p and S_p isomers; *N.B.* orientation of the ferrocene substituents determines the placement of the η^2-ma ligand). Although crystals used for structure determination (*vide infra*) contained only one diastereoisomeric form, their dissolution produced the same isomer mixtures as those resulting from synthesis. This in turn indicates a facile interconversion between the R_p and S_p isomers, while the chirality of the CgP cage remains expectedly unchanged. The ratios of the isomers were similar for both compounds (53:47 for **8**, and 51:49 for **9**).

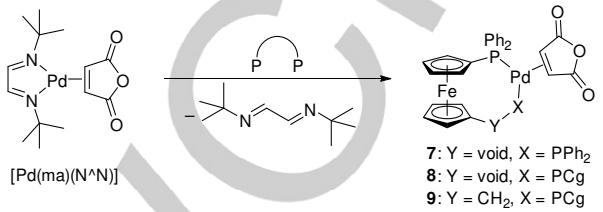

Scheme 5. Synthesis of Pd(0) complexes **7**-**9** (P^P = dppf, **1** and **2**)

Coordination of the phosphane ligands leads to downfield shifts of the $^{31}P\{^1H\}$ NMR signals and, in **8** and **9**, to their splitting into doublets by mutual coupling of the phosphane moieties (Table 1). In addition, characteristic signals of the η^2-ma ligand are observed in ^1H and ^{13}C NMR spectra, namely signals due to the C=O groups ($\delta_C \approx 171$) and to the η^2-coordinated double bond (δ_H 3.4-4.1/δ_C 52-58), whereas IR spectra display strong carbonyl stretching bands at approximately 1740 and 1800 cm^{-1}. Molecular structures of **7**-**8** are displayed in Figure 2. All compounds crystallize racemic (space groups *P*–1 or *Pbca*) and with one complex molecule in the asymmetric unit (some in solvated form). The Pd atoms are ligated by the η^2-ma ligand and two phosphane groups, whose proper positioning is ensured by twisting of the ferrocene scaffold (see τ angles in Table 3). The π-bound double bond lies in the PdP_2 plane, and the alkene ligand is coordinated in a side-on manner, oriented nearly perpendicularly to the PdP_2 plane and with the ring oxygen diverted from the Pd atom (Table 3). The Pd-donor distances are similar to those determined for [{PhP(O)(2-C_6H_4P*i*Pr_2-κ*P*)$_2$}Pd(η^2-ma)],[20] and, in line with the Dewar-Chatt-Duncanson model,[21] the π-coordinated C=C bond in **7**-**9** is elongated with respect to uncoordinated ma (1.3322(9) Å).[22] The different steric demands of the P-donor moieties affect the P-Pd-C(C=C) angles, which are wider for CgP donor groups and in complexes containing more rigid ligands (**8** > **9**). Whereas the ligand bite angles are similar in **7** and **8**, complex **9**, featuring the homologated ligand **2**, shows a wider bite angle.

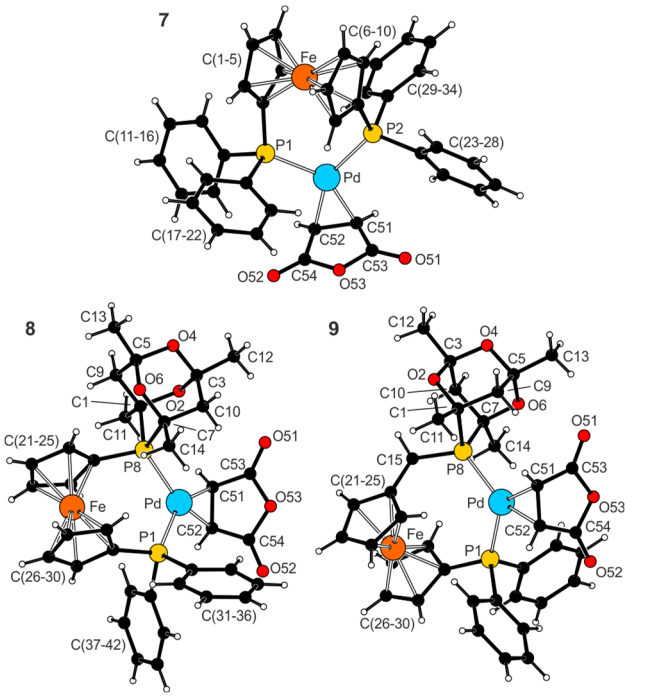

Figure 2. Views of the complex molecules in the structures of **7**·3CHCl$_3$, **8**·½C$_2$H$_4$Cl$_2$ and **9** (for displacement ellipsoid plots, see Supporting Information)

Table 3. Selected distances and angles for **7**·3CHCl$_3$, **8**·½C$_2$H$_4$Cl$_2$ and **9** (in Å and °)

Parameter[a]	**7**·3CHCl$_3$	**8**·½C$_2$H$_4$Cl$_2$	**9**
Pd-P1/P*n*[b]	2.3174(6)/2.3208(6)	2.3342(6)/2.3047(5)	2.3242(9)/2.3406(8)
P1-Pd-P*n*[b]	104.73(2)	103.84(2)	112.34(3)
P1-Pd-C52	106.47(7)	106.47(5)	96.6(8)
P*n*-Pd-C51	109.76(7)	110.18(5)	112.11(8)
Pd-C51/C52	2.134(2)/2.120(2)	2.133(2)/2.119(2)	2.158(3)/2.097(3)
C51-Pd-C52	39.04(9)	39.19(7)	39.0(1)
C51-C52	1.422(3)	1.426(3)	1.420(4)
φ[c]	1.2(1)	8.8(1)	4.6(2)
ψ[d]	81.4(1)	70.50(8)	75.4(1)
τ	45.5(2)	–28.9(1)	64.4(2)
tilt	2.6(2)	2.6(1)	3.3(2)

[a] The parameters are defined as for the free ligands (see Table 2). [b] n = 2 for **7**·3CHCl$_3$, n = 8 for **8**·½C$_2$H$_4$Cl$_2$ and **9**. [c] φ is the angle at which the C51=52 bond intersects the {Pd,P1,P*n*} plane. [d] ψ is the dihedral angle of the {Pd,P1,P*n*} and {O53, C51-C54} least-square planes.

C-H arylation of benzoxazoles

2-Arylbenzoxazole motifs are central parts of naturally occurring and biologically active compounds including pharmaceuticals[23] and materials.[24] Although they can be synthesized using various conventional methods, approaches based on selective C-H bond activation have recently emerged as attractive, atom-economic alternatives.[25] Early studies into Pd-catalyzed arylation of azoles exploited aryl bromides and iodides.[26] In contrast, the reaction employing less reactive aryl chlorides were enabled only after applying tailored Pd,[27] Cu,[28] Pd/Cu,[29] and Ni[30] catalysts, albeit still at rather high metal loadings.

In view of recent studies suggesting that electron-poor phosphanes can give rise to active catalysts for heterocycle arylation,[31] we applied the newly prepared Pd(0) complexes featuring electronically dissymmetric bis-phosphanes **1** and **2** as defined catalysts to these challenging reactions. For an initial assessment and screening of the reaction conditions, we chose benzoxazole (**10a**) arylation with chlorobenzene (**11a**), affording 2-phenylbenzoxazole (**12aa**; Scheme 6). The results are outlined in Table 4.

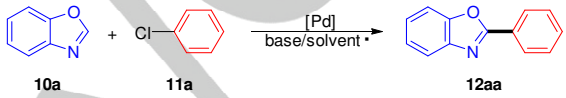

Scheme 6. Arylation of benzoxazole (**10a**) with chlorobenzene (**11a**) used to screen reaction conditions

Table 4. Screening of the reaction conditions[a]

Entry	Catalyst (loading)	Solvent	Base (equiv.)	Conversion [%]
1	[Pd(ma)(N^N)] (1.5%)	*n*-BuOH	K_2CO_3 (2)	25
2	**7** (1.5%)	*n*-BuOH	K_2CO_3 (2)	53
3	**8** (1.5%)	*n*-BuOH	K_2CO_3 (2)	48
4	**9** (1.5%)	*n*-BuOH	K_2CO_3 (2)	75
5	**9** (1%)	*n*-BuOH	Na_2CO_3 (2)	8
6	**9** (1%)	*n*-BuOH	K_2CO_3 (2)	26
7	**9** (1%)	*n*-BuOH	Cs_2CO_3 (2)	100
8	**9** (1%)	*n*-BuOH	NaOAc (2)	0
9	**9** (1%)	*n*-BuOH	KOAc (2)	<5
10	**9** (1%)	*n*-BuOH	CsOAc (2)	11
11	**9** (1%)	*n*-BuOH	$KHCO_3$ (2)	34
12	**9** (1%)	*n*-BuOH	K_3PO_4 (2)	100
13	**9** (1%)	*n*-BuOH	KOH (2)	decomp.
14	**9** (0.5%)	*n*-BuOH	K_3PO_4 (2)	100
15	**9** (0.5%)	*t*-BuOH	K_3PO_4 (2)	73
16	**9** (0.5%)	PhMe	K_3PO_4 (2)	13
17	**9** (0.5%)	PhMe/H_2O	K_3PO_4 (2)	0
18	**9** (0.5%)	DMF	K_3PO_4 (2)	24
19	**9** (0.5%)	*n*-BuOH	K_3PO_4 (1.5)	100[b]
20	**9** (0.5%)	*n*-BuOH	K_3PO_4 (1.1)	59

21	**9** (0.5%)	*n*-BuOH	K_3PO_4 (1.5)	23[c]

[a] Conditions: benzoxazole (**10a**; 1.0 mmol) and chlorobenzene (**11a**; 1.5 mmol) were reacted in the presence of catalyst in 3 mL of solvent at 125°C for 18 h. Conversions were determined by integrating ^{1}H NMR spectra and represent an average of two independent runs. [b] The same result was found when using only 1 mL of the solvent. [c] Reaction at 100°C

Gratifyingly, the model arylation reaction proceeded selectively, producing the 2-arylated product **12aa** as the sole product. As illustrated in Table 4, the catalyst based on bis-phosphane **2** performed better than the catalysts containing **1** or dppf as the supporting ligand and the precursor [Pd(N^N)(ma)]. The conversions were significantly affected by the base and the solvent (Table 4). When combining inexpensive K_3PO_4 and *n*-butanol as an environmentally benign solvent,[32] which consistently led to the best results, catalyst loading and the amount of base could be reduced to 0.5 mol.% and 1.5 equiv., respectively, without losing full conversion of the starting material. Lowering the reaction temperature below ca. 120°C, however, had a detrimental effect on the reaction.

After screening the reaction conditions, we performed a series of reaction scope tests. The results, summarized in Scheme 7, indicate that the arylation of the parent benzoxazole **10a** proceeds satisfactorily with electron-poor and electron-rich aryl chlorides except when sterically hindered (see attempted synthesis of **12ae** as an example). As a representative heterocyclic reagent, 2-chloropyridine also reacted smoothly, unlike aryl chlorides bearing unprotected reactive functional groups, such as 4-nitrochlorobenzene, 4-chloroaniline and 4-chlorobenzoic acid, which did not observably react.

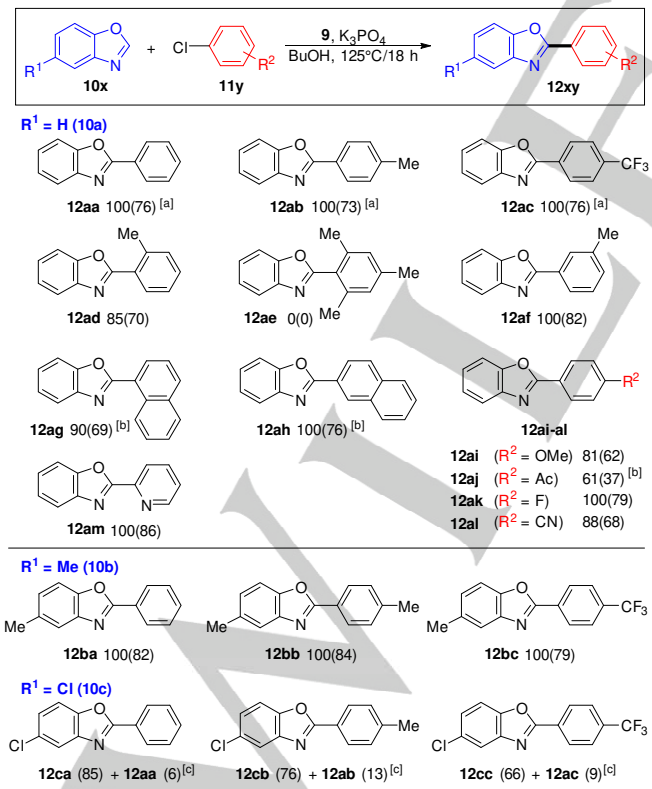

Scheme 7. Reaction scope experiments. Conversions determined by ^{1}H NMR spectroscopy are given, followed by isolated yields, in parentheses. The values are an average of two independent results. Conditions: benzoxazole **10** (1.0 mmol) and chlorobenzene **11** (1.5 mmol) were reacted in the presence of catalyst **9** (usually 1 mol.%) and K_3PO_4 (1.5 mmol) in 1 mL of *n*-butanol at 125°C for 18 h. n.a. = not available. [a] Reaction in the presence of 0.5 mol.% Pd catalyst. [b] 1.0 mmol of aryl chloride was used to avoid problems with compound isolation. [c] 2.0 mmol of aryl chloride and 1.5 mmol of K_3PO_4 were employed.

Introduction of methyl group into position 5 of the benzoxazole scaffold (substrate **10b**) had virtually no effect on the reaction yields and selectivity, whereas arylations of the chloride-substituted substrate **10c** were accompanied by partial dehalogenation, leading to (separable) mixtures of the expected arylation products **12ca-cc** and their dechlorinated analogs **12aa-ac** (*ca.* 10%; see Scheme 7).

The possibility of multiple C-H arylation was subsequently tested using dichloroarene substrates (Scheme 8). Thus, the reaction of 1,4-dichlorobenzene (**11n**) with **10a** used in excess to avoid monoarylation (4 equiv. or 2 equiv. *per* the C–Cl bond) produced the poorly soluble 1,4-bis(benzoxazol-2-yl)benzene (**12an**) in 90% isolated yield. 2,5-Bis(benzoxazol-2-yl)thiophene (**12ao**), commercially known as Fluorescent brightener 185, was similarly obtained in 74% yield from the reaction between 2,5-dichlorothiophene (**11o**) and **10a**. When the amount of **10a** was reduced to 3 equiv., the yields of **12an** and **12ao** decreased to 64% and 48%, respectively.

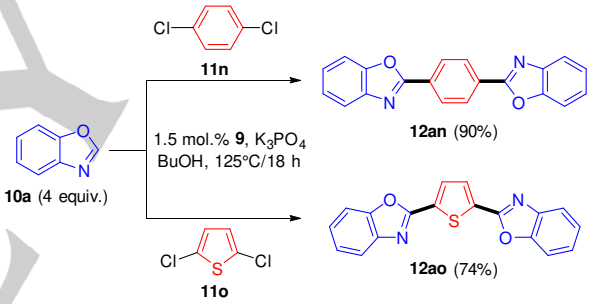

Scheme 8. Double C-H arylation using dichloroarenes **11n** and **11o**. Isolated yields given in parentheses are an average of two independent runs.

Subsequent experiments revealed that similar reactions proceed with oxazole, but the yields of the isolated arylated products were only low (ca. 10%), most likely due to the high volatility of the substrate (b.p. 69°C). 4,4-Dimethyloxazoline did not react under similar conditions. Even so, our attempts to apply the developed approach toward arylation of benzothiazole and 1-methylbenzimidazole as structurally related substrated failed. Under the standard conditions (1 mol.%Pd/K_3PO_4/125°C), these heterocycles did not appreciably react with chlorobenzene. Further reaction tests employing benzothiazole as the more stable substrate were also unsuccessful: no arylation was observed with bromo- and iodobenzene (under the standard conditions), and even increasing the reaction temperature (reaction in 1-pentanol at 145°C), using different bases (Cs_2CO_3, Ag_2CO_3 of Ag_2O) or adding a CuI co-catalyst had no beneficial effect.

Conclusion

Compounds **1** and **2** are novel dppf congeners, which continue to attract considerable research attention for their tunable coordination properties and wide catalytic applications.[9, 33] Owing to the presence of the CgP moiety with specific steric and electronic properties, bis-phosphines **1** and **2** are markedly sterically and electronically dissymmetric. Compounds **1**, **2** and dppf (for a comparison) were used to prepare benchtop stable Pd(0) complexes [Pd(ma)(L^L)] (L^L = **1**, **2** and dppf), which were applied as catalysts for selective C-H bond arylation of benzoxazoles with chloroarenes. By using the defined Pd(0) complexes, particularly the most catalytically active compound **9** containing the homologated ligand **2**, these challenging arylation reactions could be efficiently performed even with the poorly reactive chloroarenes, under low catalyst loading and in *n*-butanol as an environmentally innocuous solvent. The arylation reactions proceeded selectively to produce 2-arylated products in good yields except when prevented by steric bulk or *partly* compromised by the competing dehalogenation of the benzoxazole substrate (*e.g.*, when using educt **10c**). Notably, the structurally related substrates such as benzothiazole and 1-methylimidazole did not react under similar conditions.

Experimental Section

Materials and Methods

All syntheses were performed in an inert atmosphere using standard Schlenk techniques and oven-dried glassware. Compounds **4**,[34] **6**,[12] BrPCg,[3] and [Pd(ma)(N^N)][35] were prepared according to the literature procedures. Syntheses of other starting materials and all phosphane selenides are described in Supporting Information. Other chemicals were purchased from commercial suppliers (Sigma-Aldrich or Alfa-Aesar) and used as received. Anhydrous dichloromethane, tetrahydrofuran and methanol used for syntheses were obtained from a PureSolv MD5 solvent purification system (Innovative Technology, USA). Acetone was dried over anhydrous potassium carbonate and distilled under nitrogen. *n*-Butanol was dried with sodium metal and distilled under nitrogen. Anhydrous K_3PO_4 was obtained by drying at 250°C under vacuum for 5 h. Solvents used for crystallizations and chromatography (reagent-grade; Lach-Ner, Czech Republic) were utilized without additional purification. NMR spectra were recorded at 25°C on a Varian Unity Inova 400 spectrometer operating at 400, 101, and 162 MHz for ^{1}H, ^{13}C, and ^{13}P, respectively. Chemical shifts (δ in ppm) are given relative to internal $SiMe_4$ (^{1}H and ^{13}C) and to external 85% aqueous H_3PO_4 (^{13}P). FTIR spectra were acquired with a Thermo Nicolet 6700 instrument over the 400-4000 cm^{-1} range. Electrospray ionization (ESI) mass spectra were recorded on a Compact QTOF-MS spectrometer (Bruker Daltonics). Elemental analyses were performed on a PE 2400 Series II CHNS/O Elemental Analyzer (PerkinElmer). Details about structure determination are provided in Supporting Information.

Syntheses

Synthesis of 5. Under argon, *n*-BuLi (13.6 mL of 2.5 M in hexanes, 33.9 mmol) was added to a solution of 1,1′-dibromoferrocene (**3**; 11.65 g, 33.9 mmol) in tetrahydrofuran (250 mL) at –78°C. After stirring for 30 min, the solution of CgPBr (11.10 g, 37.6 mmol) in tetrahydrofuran (20 mL) was slowly introduced, and the reaction mixture was stirred at –78°C for 15 min and then at room temperature overnight. The resulting solution was washed with brine (100 mL), dried over $MgSO_4$ and evaporated. The crude product was purified by column chromatography (silica gel, hexane-ethyl acetate, 8:1), collecting the second, major orange band. Subsequent evaporation and crystallization from hot heptane afforded **5** as an orange crystalline solid. Yield: 10.96 g (68%).

^{1}H NMR (400 MHz, $CDCl_3$): δ = 1.22 (d, $^3J_{PH}$ = 12.9 Hz, 3H, Me), 1.30 (s, 3H, Me), 1.31 (dd, $^2J_{HH}$ = 13.1 Hz, $^3J_{PH}$ = 4.2 Hz, 1H, CH_2), 1.38 (s, 3H, Me), 1.47 (d, $^2J_{HH}$ = 13.1 Hz, 1H, CH_2), 1.78 (d, $^3J_{PH}$ = 11.9 Hz, 3H, Me), 1.87 (dd, $^3J_{PH}$ = 24.5 Hz, $^2J_{HH}$ = 13.2 Hz, 1H, CH_2), 2.04 (dd, $^2J_{HH}$ = 13.2 Hz, $^3J_{PH}$ = 7.0 Hz, 1H, CH_2), 4.11 (td, *J′* = 2.5, 1.4 Hz, 1H, fc), 4.14 (td, *J′* = 2.6, 1.4 Hz, 1H, fc), 4.26 (tt, *J′* = 2.6, 1.2 Hz, 1H, fc), 4.35 (tdd, *J′* = 2.5, 1.2, 0.7 Hz, 1H, fc), 4.41-4.43 (m, 2H, fc), 4.44 (dt, *J′* = 2.5, 1.3 Hz, 1H, fc), 4.65 (dtd, *J′* = 2.5, 1.2, 0.5 Hz, 1H, fc) ppm. ^{13}C{^{1}H} NMR (101 MHz, $CDCl_3$): δ = 27.46 (d, $^2J_{PC}$ = 22 Hz, Me), 27.80 (s, Me), 27.95 (s, Me), 28.26 (d, $^2J_{PC}$ = 11 Hz, Me), 36.85 (d, $^2J_{PC}$ = 2 Hz, CH_2), 45.07 (d, $^2J_{PC}$ = 18 Hz, CH_2), 68.87 (s, CH of fc), 69.00 (s, CH of fc), 71.19 (s, CH of fc), 71.45 (s, CH of fc), 72.23 (d, J_{PC} = 5 Hz, CH of fc), 73.10 (d, $^1J_{PC}$ = 22 Hz, C of PCg), 73.10 (d, $^1J_{PC}$ = 8 Hz, C^{ipso} of fc), 73.80 (s, CH of fc), 73.98 (d, J_{PC} = 7 Hz, CH of fc), 74.07 (d, $^1J_{PC}$ = 24 Hz, C of PCg), 77.93 (s, C^{ipso} of fc), 96.02 (s, C of PCg), 96.47 (s, C of PCg) ppm; signal due to CH of fc is obscured by the solvent resonance. ^{31}P{^{1}H} NMR (162 MHz, $CDCl_3$): δ = –32.4 (s) ppm. IR (Nujol): ν_{max} = 3096 m, 3006 m, 2723 w, 2360 w, 1805 w, 1774 w, 1722 w, 1677 w, 1647 w, 1449 s, 1430 s, 1413 s, 1389 s, 1349 s, 1264 m, 1184s, 1170 s, 1154 s, 1134 s, 1086 m, 1067 m, 1029 s, 1010 s, 979 s, 960 m, 947 m, 896 s, 875 m, 829 s, 823 s, 813 s , 795 s, 688 m, 663 w, 642 w, 616 w, 590 w, 572 m, 549 w, 498 s, 484 s, 461 s, 444 s cm^{-1}. ESI-MS: *m/z* = 495 ([M + H + O]$^+$). Anal. Calc. for $C_{20}H_{24}O_3BrFeP$ (479.1): C 50.14, H 5.05%. Found: C 50.28, H 4.86%.

Synthesis of 1. An oven-dried reaction flask was charged with 1′-(diphenylphosphanyl)-1-bromoferrocene (**4**; 898 mg, 2.0 mmol), flushed with argon and sealed with a rubber septum. The solid educt was dissolved in THF (30 mL), and the solution was cooled to –78°C. *n*-BuLi (1.3 mL of 1.6 M in hexanes, 2.1 mmol) was added, and the mixture was stirred at –78°C for 15 min before a solution of CgPBr (649 mg, 2.2 mmol) in toluene (15 mL) was gradually introduced. Next, the reaction mixture was stirred for 15 min at –78°C and then at room temperature overnight. All volatiles were removed under reduced pressure, and the orange solid residue was dissolved in dichloromethane (ca. 20 mL) and evaporated with chromatographic silica gel (ca. 15 mL). The crude, pre-adsorbed product was transferred onto a top of chromatographic column packed in ethyl acetate-hexane (1:3). Elution with the same solvent mixture provided a single orange band, which was collected and evaporated to give **1**. The compound was further crystallized from hot ethanol (ca. 75 mL), producing analytically pure **1** as orange crystals. Yield: 461 mg (42%).

Alternatively, a solution of phosphane **5** (240 mg, 0.50 mmol) in tetrahydrofuran (15 mL) was lithiated with *n*-BuLi (0.35 mL of 1.6 M in hexanes, 0.56 mmol) at –78°C under argon. After stirring for 15 minutes, neat chloro-diphenylphosphane (124 mg, 0.56 mmol) was added and the mixture was stirred for another 15 min at –78°C and then at room temperature for 9 hours. After solvent removal, the crude product was dissolved in dichloromethane (ca. 20 mL), pre-adsorbed onto silica gel (ca. 15 mL) and further purified as described above. Yield of **1**: 206 mg (70%).

^{1}H NMR (400 MHz, $CDCl_3$): δ = 1.19 (d, $^3J_{PH}$ = 12.9 Hz, 3H, Me), 1.28 (dd, $^2J_{HH}$ = 13.1 Hz, $^3J_{PH}$ = 4.1 Hz, 1H, CH_2), 1.28 (s, 3H, Me), 1.36 (s, 3H, Me), 1.46 (d, $^2J_{HH}$ = 13.1 Hz, 1H, CH_2), 1.70 (d, $^3J_{PH}$ = 11.9 Hz, 3H, Me), 1.83 (dd, $^3J_{PH}$ = 24.5 Hz, $^2J_{HH}$ = 13.2 Hz, 1H, CH_2), 2.01 (dd, $^2J_{HH}$ = 13.2 Hz, $^3J_{PH}$ = 7.0 Hz, 1H, CH_2), 4.10 (ddt, *J′* = 2.4, 1.8, 1.3 Hz, 1H, fc), 4.16-4.15 (m, 2H, fc), 4.23 (tdd, *J′* = 2.4, 1.2, 0.6 Hz, 1H, fc), 4.25 (tt, *J′* = 2.3, 1.1 Hz, 1H, fc), 4.36 (td, *J′* = 2.4, 1.2 Hz, 1H, fc), 4.40 (td, *J′* = 2.4, 1.2 Hz, 1H, fc), 4.48 (dtd, *J′* = 2.4, 1.2, 0.5 Hz, 1H, fc), 7.30-7.38 (m, 10H, PPh_2) ppm. ^{13}C{^{1}H} NMR (101 MHz, $CDCl_3$): δ = 27.48 (d, $^2J_{PC}$ = 22 Hz, Me), 2.70 (s, Me), 27.94 (s, Me), 28.3 (d, $^2J_{PC}$ = 11 Hz, Me), 36.87 (d, $^2J_{PC}$ = 2 Hz, CH_2), 45.12 (d, $^2J_{PC}$ = 18 Hz, CH_2), 71.41 (d, J_{PC} = 5 Hz, CH of fc), 71.80 (dd, J_{PC} = 6, 2 Hz, CH of fc), 72.01 (d, J_{PC} = 2 Hz, CH of fc), 72.62 (d, J_{PC} = 3 Hz, CH of fc), 72.81 (dd, J_{PC} = 4, 2 Hz, CH of fc), 73.05 (d, $^1J_{PC}$ = 22 Hz, C of PCg), 73.12 (d, $^1J_{PC}$ = 9 Hz, C^{ipso} of fc), 73.28 (d, $^1J_{PC}$ = 24 Hz, C of PCg), 73.72 (d, J_{PC} = 14 Hz, CH of fc), 73.80 (d, J_{PC} = 14 Hz, CH of fc), 74.91 (d, J_{PC} = 29 Hz, CH of fc), 77.15 (d, $^1J_{PC}$ = 11 Hz, C^{ipso} of fc), 95.98 (s, C of PCg), 96.46 (s, C of PCg), 128.16 (d, J_{PC} = 7

Hz, CH of PPh_2), 128.18 (d, J_{PC} = 7 Hz, CH of PPh_2), 128.56 (s, CH of PPh_2), 128.58 (s, CH of PPh_2), 133.43 (d, J_{PC} = 19 Hz, CH of PPh_2), 133.49 (d, J_{PC} = 20 Hz, CH of PPh_2), 138.70 (d, $^1J_{PC}$ = 10 Hz, C^{ipso} of PPh_2), 138.78 (d, $^1J_{PC}$ = 10 Hz, C^{ipso} of PPh_2) ppm. $^{31}P\{^1H\}$ NMR (162 MHz, $CDCl_3$): δ = –31.7 (s, PCg), –16.8 (s, PPh_2) ppm. IR (Nujol): ν_{max} = 3080 m, 3065 m, 1648 w, 1455 m, 1432 m, 1391 s, 1379 s, 1368 s, 1344 s, 1306 w, 1264 m, 1218 s, 1188 s, 1170 s, 1163 m, 1137 s, 1089 s, 1071 m, 1061 m, 1035 m, 1025 s, 981 s, 965 w, 951 w, 897 s, 864 w, 855 w, 830 s, 815 m, 796 m, 745 m, 739 s, 698 s, 642 w, 588 w, 573 m, 551 w, 525 w, 515 w, 497 m, 488 m, 469 m, 452 m, 441 m, 420 w cm^{-1}. ESI-MS: *m/z* = 617 ($[M + 2O + H]^+$), 623 ($[M + O + Na]^+$), 639 ($[M + 2O + Na]^+$). Anal. Calc. for $C_{32}H_{34}O_3FeP_2$ (584.4): C 65.77, H 5.86%. Found: C 65.54, H 5.75%.

Synthesis of 2. A Schlenk tube was charged with bis-phosphane **6** (832 mg, 2.0 mmol), acetylacetone (2.5 mL) and hydrochloric acid (3.5 mL of 35% aqueous solution), and the resulting mixture was stirred overnight. Then, the mixture was diluted with ethyl acetate, water (75 mL each) and sodium hydroxide (25 mL of 1 M solution), and the aqueous layer was separated and back-extracted with ethyl acetate (2× 50 mL). The combined organic layers were dried over $MgSO_4$ and evaporated, leaving a crude product which was purified by chromatography (SiO_2, AcOEt). The major orange band was collected and evaporated, leaving an orange oil. Subsequent crystallization from hot hexane produced **2** as a light-orange crystalline solid. Yield: 726 mg (61%). Crystals suitable for structure determination were grown from ethanol/2-propanol mixture.

^1H NMR (400 MHz, $CDCl_3$): δ = 1.10 (d, $^3J_{PH}$ = 12.6 Hz, 3H, Me), 1.26 (d, $^3J_{PH}$ = 11.9 Hz, 3H, Me), 1.34 (s, 3H, Me), 1.40 (s, 3H, Me), 1.57 (dd, $^2J_{HH}$ = 13.3 Hz, $^3J_{PH}$ = 3.9 Hz, 1H, CH_2), 1.71 (d, $^2J_{HH}$ = 13.2 Hz, 1H, CH_2), 1.79 (dd, $^3J_{PH}$ = 21.7 Hz, $^2J_{HH}$ = 13.1, 1H, CH_2), 1.90 (dd, $^2J_{HH}$ = 13.1 Hz, $^3J_{PH}$ = 6.5 Hz, 1H, CH_2), 2.14 (dd, $^2J_{HH}$ = 14.7 Hz, $^2J_{PH}$ = 3.4 Hz, 1H, CH_2P), 2.58 (d, $^2J_{HH}$ = 14.7 Hz, 1H, CH_2P), 3.97 (td, *J'* = 2.4, 1.3 Hz, 1H, fc), 3.98-4.02 (m, 3H, fc), 4.05 (tt, *J'* = 2.1, 1.3 Hz, 1H, fc), 4.12 (dt, *J'* = 2.7, 1.4 Hz, 1H, fc), 4.30-4.38 (m, 2H, fc), 7.29-7.40 (m, 10H, PPh_2) ppm. $^{13}C\{^1H\}$ NMR (101 MHz, $CDCl_3$): δ = 22.00 (d, $^1J_{PC}$ = 25 Hz, CH_2P), 26.81 (d, $^2J_{PC}$ = 12 Hz, Me), 27.77 (s, Me), 28.04 (s, Me), 28.10 (d, $^2J_{PC}$ = 22 Hz, Me), 36.98 (d, $^2J_{PC}$ = 2 Hz, CH_2), 44.49 (d, $^2J_{PC}$ = 15 Hz, CH_2), 68.65 (s, CH of fc), 69.10 (s, CH of fc), 70.09 (d, J_{PC} = 4 Hz, CH of fc), 70.18 (d, J_{PC} = 5 Hz, CH of fc), 71.82 (d, J_{PC} = 4 Hz, CH of fc), 71.86 (d, J_{PC} = 4 Hz, CH of fc), 72.21 (d, $^1J_{PC}$ = 24 Hz, C of PCg), 72.21 (d, $^1J_{PC}$ = 10 Hz, C of PCg), 73.64 (d, J_{PC} = 10 Hz, CH of fc), 73.79 (d, J_{PC} = 9 Hz, CH of fc), 76.02 (d, $^1J_{PC}$ = 5 Hz, C^{ipso} of fc), 85.68 (d, $^2J_{PC}$ = 17 Hz, C^{ipso} of fc), 95.74 (s, C of PCg), 96.53 (s, C of PCg), 128.13 (d, J_{PC} = 7 Hz, CH of PPh_2), 128.15 (d, J_{PC} = 7 Hz, CH of PPh_2), 128.49 (s, CH of PPh_2), 128.54 (s, CH of PPh_2), 133.46 (d, J_{PC} = 20 Hz, CH of PPh_2), 133.56 (d, J_{PC} = 19 Hz, CH of PPh_2), 138.97 (d, J_{PC} = 9 Hz, C^{ipso} of PPh_2), 139.09 (d, J_{PC} = 9 Hz, C^{ipso} of PPh_2) ppm. $^{31}P\{^1H\}$ NMR (162 MHz, $CDCl_3$): δ = –26.1 (s, PCg), –16.5 (s, PPh_2) ppm. IR (Nujol): ν_{max} = 3318 w, 3087 w, 3053 w, 2360 s, 2342 s, 1958 w, 1889 w, 1772 w, 1734 w, 1717 w, 1507 w, 1465 s, 1458 s, 1436 s, 1340 m, 1310 w, 1261 m, 1217 s, 1193 s, 1171 m, 1164 m, 1133 s, 1091 s, 1070 w, 1057 w, 1034 m, 980 s, 959 m, 926 m, 901 m, 895 m, 867 m, 855 m, 836 m, 830 m, 812 s, 793 m, 747 s, 724 s, 698 s, 685 m, 669 m, 659 w, 636 w, 619 w, 600 w, 581 w, 568 w, 537 w, 525 w, 498 s, 457 m, 442 w, 435 w, 421 w cm^{-1}. ESI-MS: *m/z* = 599 ($[M + H]^+$). Anal. Calc. for $C_{33}H_{36}FeO_3P_2$ (598.4): C 66.23, H 6.06%. Found: C 66.27, H 6.19%.

Synthesis of the Pd(0) complexes. (*N,N'*-Di-*t*-butyl-ethanedialdimine-κ^2*N,N'*)(η^2-2,5-furandione)palladium(0) ([Pd(ma)(N^N)]; 74 mg, 0.20 mmol) and dppf (111 mg, 0.20 mmol) were mixed in dry tetrahydrofuran (20 mL) under argon at room temperature, and the resulting solution was stirred for 6 hours. The volatiles were removed under vacuum, and the residue was filtered over a short silica gel column, eluting with dichloromethane-methanol (50:1). The single orange band was collected and evaporated, leaving complex **7** as an orange solid. Yield: 147 mg (97%). X-ray quality crystals were obtained from chloroform/diethyl ether.

^1H NMR (400 MHz, CD_2Cl_2): δ = 4.06-4.09 (m, 2H, ma), 4.18 (dt, *J'* = 2.4, 1.2 Hz, 2H, fc), 4.22 (dt, *J'* = 2.4, 1.2 Hz, 2H, fc), 4.32-4.34 (m, 2H, fc), 4.34-4.36 (m, 2H, fc), 7.37-7.45 (m, 12H, PPh_2), 7.49-7.55 (m, 4H, PPh_2), 7.62-7.68 (m, 4H, PPh_2) ppm. $^{13}C\{^1H\}$ NMR (101 MHz, CD_2Cl_2): δ = 53.94 (d, $^2J_{PC}$ = 12 Hz, CH of ma), 72.94 (m, CH of fc), 75.05 (m, CH of fc), 77.41 (m, C^{ipso} of fc), 128.52 (m, 2×CH of PPh_2), 130.43 (s, CH of PPh_2), 130.67 (s, CH of PPh_2), 133.93 (t, J_{PC} = 8 Hz, CH of PPh_2), 134.55 (t, J_{PC} = 7 Hz, CH of PPh_2), 134.56 (m, C^{ipso} of PPh_2), 137.11 (m, C^{ipso} of PPh_2), 170.81 (m, CO) ppm. $^{31}P\{^1H\}$ NMR (162 MHz, CD_2Cl_2): δ = 23.6 (s) ppm. IR (Nujol): ν_{max} = 3053 w, 1797 s, 1732 s, 1480 w, 1435 m, 1352 w, 1306 w, 1221 s, 1198 w, 1166 w, 1095 m, 1054 m, 1027 w, 884 m, 836 m, 745 m, 697 s, 638 w, 619 w, 591 w, 541 m, 511 m, 489 s, 466 m, 431 m cm^{-1}. ESI-MS: *m/z* = 781 ($[M + Na]^+$). Anal. Calc. for $C_{38}H_{30}FeO_3P_2Pd \cdot 1/4CH_2Cl_2$ (780.1): C 58.89, H 3.94%. Found: C 59.27, H 3.89%.

The same procedure employing [Pd(ma)(N^N)] (74 mg, 0.20 mmol), bis-phosphane **1** (111 mg, 0.20 mmol) and 15 mL of the solvent and 8 h reaction time produced complex **8** as a yellow powder in quantitative yield (158 mg). Crystals used for structure determination were obtained from 1,2-dichlorethane/hexane.

^1H NMR (400 MHz, CD_2Cl_2): δ = 1.26 (s, 3H, Me), 1.26 (s, 3H, Me), 1.33 (d, $^3J_{PH}$ = 14.8 Hz, 3H, Me), 1.40 (d, $^3J_{PH}$ = 14.4 Hz, 3H, Me), 1.50-1.55 (m, 5H, CH_2), 1.52 (s, 3H, Me), 1.57 (s, 3H, Me), 1.70-1.79 (m, 1H, CH_2), 1.78 (d, $^3J_{PH}$ = 13.6 Hz, 3H, Me), 1.83 (d, $^3J_{PH}$ = 13.2 Hz, 3H, Me), 2.22 (dd, $^2J_{HH}$ = 13.7 Hz, $^3J_{PH}$ = 5.6 Hz, 1H, CH_2), 2.45 (dd, $^2J_{HH}$ = 13.3 Hz, $^3J_{PH}$ = 5.5 Hz, 1H, CH_2), 3.79 (td, $^3J_{PH}$ = 8.9 Hz, $^3J_{HH}$ = 4.4 Hz, 1H, ma), 3.95-3.97 (m, 1H, fc), 3.99 (td, $^3J_{PH}$ = 9.0 Hz, $^3J_{HH}$ = 4.2 Hz, 1H, ma), 4.02-4.06 (m, 1H, ma), 4.03-4.04 (m, 1H, fc), 4.18 (tt, *J'* = 2.5, 1.3 Hz, 1H, fc), 4.21 (tt, *J'* = 2.5, 1.3 Hz, 1H, fc), 4.27 (tt, *J'* =2.5, 1.2 Hz, 1H, fc), 4.29-4.35 (m, 5H, fc), 4.48-4.50 (m, 1H, fc), 4.51-4.53 (m, 1H, fc), 4.62 (td, $^3J_{PH}$ = 9.8 Hz, $^3J_{HH}$ = 4.3 Hz, 1H, ma), 4.65 (tt, *J'* = 2.5, 1.2 Hz, 1H, fc), 4.72 (tt, *J'* = 2.5, 1.3 Hz, 1H, fc), 4.79 (dtd, *J'* = 2.5, 1.3, 0.8 Hz, 1H, fc), 4.82 (dtd, *J'* = 2.6, 1.3, 0.8 Hz, 1H, fc), 7.30-7.38 (m, 8H, PPh_2), 7.43-7.58 (m, 8H, PPh_2), 7.62-7.70 (m, 4H, PPh_2) ppm. $^{13}C\{^1H\}$ NMR (101 MHz, CD_2Cl_2): δ = 26.92 (s, Me), 27.14 (d, $^2J_{PC}$ = 13 Hz, Me), 27.40 (d, $^2J_{PC}$ = 13 Hz, Me), 27.63 (s, Me), 27.80 (s, Me), 27.85 (s, Me), 29.14 (d, $^2J_{PC}$ = 7 Hz, Me), 29.48 (d, $^2J_{PC}$ = 7 Hz, Me), 38.42 (d, $^2J_{PC}$ = 16 Hz, 2×CH_2), 42.57 (d, $^2J_{PC}$ = 13 Hz, CH_2), 43.65 (d, $^2J_{PC}$ = 13 Hz, CH_2), 52.01 (dd, $^2J_{PC}$ = 28, 4 Hz, CH of ma), 52.43 (dd, $^2J_{PC}$ = 27, 4 Hz, CH of ma), 53.85 (dd, $^2J_{PC}$ = 29, 4 Hz, CH of ma), 56.29 (dd, $^2J_{PC}$ = 27, 4 Hz, CH of ma), 70.97 (d, J_{PC} = 7 Hz, CH of fc), 71.01 (d, J_{PC} = 6 Hz, CH of fc), 71.44 (d, J_{PC} = 10 Hz, CH of fc), 71.46 (d, J_{PC} = 10 Hz, CH of fc), 73.17 (d, J_{PC} = 7 Hz, CH of fc), 73.30 (d, J_{PC} = 7 Hz, CH of fc), 73.63 (s, CH of fc), 73.79 (s, CH of fc), 73.88 (d, $^1J_{PC}$ = 20 Hz, C^{ipso} of fc), 73.89 (d, $^1J_{PC}$ = 20 Hz, C^{ipso} of fc), 74.17-74.88 (m, 5×CH of fc, 2×C of PCg and C^{ipso} of fc), 74.87 (dd, J_{PC} = 20, 4 Hz, C^{ipso} of fc), 75.32 (d, J_{PC} = 8 Hz, CH of fc), 76.58 (dd, J_{PC} = 42, 2 Hz, C of PCg), 77.65 (dd, J_{PC} = 42, 2 Hz, C of PCg), 78.61 (d, J_{PC} = 21 Hz, CH of fc), 79.00 (d, J_{PC} = 22 Hz, CH of fc), 96.59 (s, C of PCg), 96.7 (s, C of PCg), 96.79 (s, C of PCg), 97.49 (s, C of PCg), 128.59 (d, J_{PC} = 9 Hz, CH of PPh_2), 128.64 (d, J_{PC} = 9 Hz, CH of PPh_2), 128.98 (d, J_{PC} = 10 Hz, CH of PPh_2), 129.02 (d, J_{PC} = 11 Hz, CH of PPh_2), 129.52 (d, J_{PC} = 2 Hz, CH of PPh_2), 129.84 (d, J_{PC} = 2 Hz, CH of PPh_2), 131.23 (d, J_{PC} = 2 Hz, CH of PPh_2), 131.67 (d, J_{PC} = 2 Hz, CH of PPh_2), 131.98 (d, J_{PC} = 13 Hz, CH of PPh_2), 133.19 (d, J_{PC} = 13 Hz, CH of PPh_2), 135.21 (d, J_{PC} = 16 Hz, CH of PPh_2), 136.05 (d, J_{PC} = 17 Hz, CH of PPh_2), 133.22 (d, $^1J_{PC}$ = 38 Hz, C^{ipso} of PPh_2), 135.31 (dd, $^1J_{PC}$ = 37, 1 Hz, C^{ipso} of PPh_2), 135.85 (d, $^1J_{PC}$ = 32 Hz, C^{ipso} of PPh_2), 138.98 (dd, $^1J_{PC}$ = 32, 2 Hz, C^{ipso} of PPh_2), 170.19 (m, 2×CO), 171.11 (m, CO), 171.41 (m, CO) ppm. $^{31}P\{^1H\}$ NMR (162 MHz, CD_2Cl_2): δ = 13.8 (d, $^2J_{PP}$ = 18 Hz, PCg), 14.6 (d, $^2J_{PP}$ = 17 Hz, PCg), 23.6 (d, $^2J_{PP}$ = 17 Hz, PPh_2), 23.7 (d, $^2J_{PP}$ = 18 Hz, PPh_2) ppm. IR (DRIFTS): ν_{max} = 2988 w, 2919 w, 1801 s, 1736 s, 1481 w, 1435 m, 1390 m, 1379 m, 1351 m, 1298 w, 1264 m, 1223 s, 1196 m, 1185 s, 1134 s, 1090 m, 1059 w, 1033 w, 980 s, 894 m, 838 m, 796 w, 744 m, 698 s, 644 w, 619 w, 592 m, 575 w, 537 w, 515 w, 490 s, 476 m, 443 m, 432 m cm^{-1}. ESI-MS: *m/z* = 811 ($[M + Na]^+$). Anal. Calc. for $C_{36}H_{36}FeO_6P_2Pd \cdot 1/5CH_2Cl_2$ (805.9): C 53.95, H 4.55%. Found: C 54.09, H 4.44%.

Complex **9** was obtained similarly using [Pd(ma)(N^N)] (74 mg, 0.20 mmol), bis-phosphane **2** (120 mg, 0.20 mmol) in 20 mL of THF and was isolated as a yellow solid. Yield: 154 mg (96%). Crystals suitable for structure determination were obtained from chloroform/hexane.

^{1}H NMR (400 MHz, CD_2Cl_2): δ = 1.22 (d, $^3J_{PH}$ = 14.6 Hz, 3H, Me), 1.27 (d, $^3J_{PH}$ = 15.0 Hz, 3H, Me), 1.28 (d, $^3J_{PH}$ = 13.9 Hz, 6H, Me), 1.35 (s, 3H, Me), 1.35 (s, 3H, Me), 1.45 (s, 3H, Me), 1.47 (s, 3H, Me), 1.69-1.90 (m, 6H, CH_2), 2.65 (dd, $^2J_{HH}$ = 16.8 Hz, $^2J_{PH}$ = 8.1 Hz, 1H, CH_2P), 2.76 (dd, $^2J_{HH}$ = 17.0 Hz, $^2J_{PH}$ = 7.9 Hz, CH_2P), 2.85 (dd, $^2J_{HH}$ = 13.5 Hz, $^3J_{PH}$ = 4.8 Hz, 1H, CH_2), 2.9 (dd, $^2J_{HH}$ = 13.8 Hz, $^3J_{PH}$ = 4.9 Hz, 1H, CH_2), 3.20 (dd, $^2J_{HH}$ = 16.9 Hz, $^2J_{PH}$ = 11.5 Hz, 1H, CH_2P), 3.28 (dd, $^2J_{HH}$ = 17.0 Hz, $^2J_{PH}$ = 12.0 Hz, 1H, CH_2P), 3.35 (ddd, $^3J_{PH}$ = 8.4, 5.0 Hz, $^3J_{HH}$ = 4.4 Hz, 1H, ma), 3.72 (ddd, $^3J_{PH}$ = 8.3, 5.1 Hz, $^3J_{HH}$ = 4.3 Hz, 1H, ma), 3.73 (m, 1H, fc), 3.83 (tt, J' = 2.5, 1.3 Hz, 1H, fc), 3.90 (ddt, J' = 2.5, 2.0, 1.2 Hz, 1H, fc), 4.00 (td, J' = 2.5, 1.3 Hz, 1H, fc), 4.06 (tt, J' = 2.5, 1.2 Hz, 1H, fc), 4.13-4.16 (m, 2H, fc), 4.22-4.28 (m, 1H, ma), 4.26-4.28 (m, 1H, fc), 4.31-4.34 (m, 2H, fc), 4.35-4.37 (m, 2H, fc), 4.35-4.41 (m, 1H, ma), 4.42-4.44 (m, 1H, fc), 4.58 (tt, J' = 2.4, 1.2 Hz, 1H, fc), 4.59-4.61 (m, 1H, fc), 4.71-4.72 (m, 1H, fc), 7.33-7.59 (m, 20H, PPh_2) ppm. ^{13}C{^{1}H} NMR (101 MHz, CD_2Cl_2): δ = 22.30 (d, $^1J_{PC}$ = 6 Hz, CH_2P), 23.09 (d, $^1J_{PC}$ = 7 Hz, CH_2P), 26.21 (d, $^2J_{PC}$ = 9 Hz, Me), 26.80 (s, Me), 27.16 (d, $^2J_{PC}$ = 8 Hz, Me), 27.54 (s, Me), 27.81 (s, Me), 27.85 (s, Me), 28.87 (d, $^2J_{PC}$ = 7 Hz, Me), 29.01 (d, $^2J_{PC}$ = 7 Hz, Me), 38.34 (d, $^2J_{PC}$ = 2 Hz, 2×CH_2), 41.06 (d, $^2J_{PC}$ = 10 Hz, CH_2), 41.54 (d, $^2J_{PC}$ = 10 Hz, CH_2), 53.58 (dd, $^2J_{PC}$ = 29, 4 Hz, CH of ma), 56.20 (dd, $^2J_{PC}$ = 26, 4 Hz, CH of ma), 58.27 (dd, $^2J_{PC}$ = 26, 4 Hz, CH of ma), 69.12-69.16 (m, 4xCH of fc), 70.03 (d, J_{PC} = 4 Hz, CH of fc), 70.31 (d, J_{PC} = 9 Hz, CH of fc), 71.43 (d, J_{PC} = 9 Hz, CH of fc), 71.77 (d, J_{PC} = 5 Hz, CH of fc), 72.46 (d, J_{PC} = 7 Hz, CH of fc), 73.07 (d, J_{PC} = 7 Hz, CH of fc), 73.24 (d, J_{PC} = 4 Hz, CH of fc), 73.48 (dd, J_{PC} = 10, 2 Hz, CH of fc), 73.54 (d, J_{PC} = 8 Hz, CH of fc), 73.57 (d, $^1J_{PC}$ = 45 Hz, C of PCg), 73.77 (d, $^1J_{PC}$ = 45 Hz, C of PCg), 74.68 (dd, J_{PC} = 9, 5 Hz, C^{ipso} of fc), 74.89 (dd, J_{PC} = 7, 4 Hz, C^{ipso} of fc), 75.48 (d, $^1J_{PC}$ = 41 Hz, C of PCg), 76.88 (d, $^1J_{PC}$ = 42 Hz, C of PCg), 76.92 (dd, J_{PC} = 11, 4 Hz, CH of fc), 77.53 (d, J_{PC} = 16 Hz CH of fc), 78.08 (d, J_{PC} = 18 Hz CH of fc), 83.33 (d, $^1J_{PC}$ = 38 Hz, C^{ipso} of fc), 83.39 (d, $^1J_{PC}$ = 38 Hz, C^{ipso} of fc), 96.14 (s, C of PCg), 96.28 (s, C of PCg), 97.35 (s, C of PCg), 97.72 (s, C of PCg), 128.52 (d, J_{PC} = 9 Hz, CH of PPh_2), 128.66 (d, J_{PC} = 10 Hz, CH of PPh_2), 128.69 (d, J_{PC} = 9 Hz, CH of PPh_2), 129.03 (d, J_{PC} = 10 Hz, CH of PPh_2), 129.67 (d, J_{PC} = 13 Hz, CH of PPh_2), 129.69 (d, J_{PC} = 13 Hz, CH of PPh_2), 130.94 (d, J_{PC} = 30 Hz, CH of PPh_2), 130.96 (d, J_{PC} = 30 Hz, CH of PPh_2), 131.85 (d, J_{PC} = 12 Hz, CH of PPh_2), 132.29 (d, J_{PC} = 12 Hz, CH of PPh_2), 133.49 (d, $^1J_{PC}$ = 32 Hz, C^{ipso} of PPh_2), 133.71 (d, $^1J_{PC}$ = 32 Hz, C^{ipso} of PPh_2), 134.56 (d, J_{PC} = 15 Hz, CH of PPh_2), 135.21 (d, J_{PC} = 16 Hz, CH of PPh_2), 136.23 (dd, J_{PC} = 32, 3 Hz, C^{ipso} of PPh_2), 137.31 (dd, J_{PC} = 32, 2 Hz, C^{ipso} of PPh_2), 169.87-170.05 (m, 2×CO), 170.84-170.91 (m, CO), 171.19-171.26 (m, CO) ppm; a signal due to CH of ma is overlapped by the solvent resonance. ^{31}P{^{1}H} NMR (162 MHz, CD_2Cl_2): δ = 4.3 (d, $^2J_{PP}$ = 9 Hz, PCg), 6.0 (d, $^2J_{PP}$ = 8 Hz, PCg), 20.8 (d, $^2J_{PP}$ = 9 Hz, PPh_2), 20.9 (d, $^2J_{PP}$ = 8 Hz, PPh_2) ppm. IR (Nujol): ν_{max} = 2989 w, 2960 w, 2917 w, 1804 s, 1759 m, 1741 s, 1480 w, 1436 m, 1390 w, 1363 w, 1346 w, 1298 w, 1264 w, 1224 s, 1197 m, 1133 m, 1088 m, 1061 w, 1025 w, 977 m, 894 m, 848 m, 833 m, 808 m, 791 w, 746 m, 698 m, 673 w, 631 w, 596 w, 580 w, 536 w, 519 m, 507 m, 499 m, 467 m, 437 w cm^{-1}. ESI-MS: *m/z* = 825 ([M + Na]$^+$). Anal. Calc. for $C_{37}H_{38}FeO_6P_2Pd{\cdot}1/2CH_2Cl_2$ (845.4): C 53.28, H 4.65%. Found: C 53.35, H 4.54%.

General procedure for the catalytic reactions

Schlenk flask was charged with catalyst **9** (0.5 or 1.0 mol.% with respect to **10**), benzoxazole **10** (1.0 mmol), dry K_3PO_4 (318 mg, 1.5 mmol), chloroarene (1.5 mmol) and a magnetic stirring bar, flushed with argon and sealed with a rubber septum. *n*-Butanol (1 mL) was introduced, the septum was replaced for a glass stopper, and the flask was transferred to an oil bath maintained at 125°C. After stirring for 18 h, the reaction vessel was cooled to room temperature and small aliquot of the reaction mixture was analyzed by ^{1}H NMR spectroscopy to determine the conversion. Then, water and diethyl ether (20 mL each) were added, the organic layer was separated, and the aqueous layer was extracted with diethyl ether (20 mL). The combined organic extracts were dried over anhydrous magnesium sulfate and evaporated under reduced pressure with chromatographic silica gel (ca. 10 mL). The crude, pre-adsorbed product was transferred onto the top of a chromatographic column and eluted with an ethyl acetate-hexane mixture. Typically, a second band was collected and evaporated to produce the coupling product **12**.

Details of screening experiments and analytical data of the coupling products are provided in Supporting Information.

Acknowledgements

This work was supported by Charles University Research Centre program (project UNCE/SCI/014) and by the Grant Agency of Charles University (project no. 920119).

Keywords: metallocenes • phosphane ligands • palladium complexes • C-H activation • heterocycle arylation

[1] M. Epstein, S. A. Buckler, *J. Am. Chem. Soc.* **1961**, *83*, 3279-3292.

[2] P. G. Pringle, M. B. Smith in *Phosphorus(III) Ligands in Homogeneous Catalysis: Design and Synthesis* (Eds.: P. C. J. Kamer, P. W. N. M. van Leeuwen), Wiley, Chichester, 2012, ch. 13, pp 400-413.

[3] J. H. Downing, J. Floure, K. Heslop, M. F. Haddow, J. Hopewell, M. Lusi, H. Phetmung, A. G. Orpen, P. G. Pringle, R. I. Pugh, D. Zambrano-Williams, *Organometallics* **2008**, *27*, 3216-3224.

[4] Selected examples: a) R. A. Baber, M. L. Clarke, K. M. Heslop, A. C. Marr, A. G. Orpen, P. G. Pringle, A. Ward, D. E. Zambrano-Williams, *Dalton Trans.* **2005**, 1079-1085; b) J. A. Fuentes, A. M. Z. Slawin, M. L. Clarke, *Catal. Sci. Technol.* **2012**, *2*, 715-718; c) T. Fanjul, G. Eastham, J. Floure, S. J. K. Forrest, M. F. Haddow, A. Hamilton, P. G. Pringle, A. G. Orpen, M. Waugh, *Dalton Trans.* **2013**, 42, 100-115; d) T. A. Shuttleworth, A. M. Miles-Hobbs, P. G. Pringle, H. A. Sparkes, *Dalton Trans.,* **2017**, 46, 125-137.

[5] G. Adjabeng, T. Brenstrum, J. Wilson, C. Frampton, A. Robertson, J. Hillhouse, J. McNulty, A. Capretta, *Org. Lett.* **2003**, *5*, 953-955.

[6] Representative examples: a) C. M. Lavoie, P. M. MacQueen, N. L. Rotta-Loria, R. S. Sawatzky, A. Borzenko, A. J. Chisholm, B. K. V. Hargreaves, R. McDonald, M. J. Ferguson, M. Stradiotto, *Nat. Commun.* **2016***, 7*, 11073; b) P. M. MacQueen, J. P. Tassone, C. Diaz, M. Stradiotto, *J. Am. Chem. Soc.* **2018**, *140*, 5023-5027; c) R. T. McGuire, J. F. J. Paffile, Y. Zhou, M. Stradiotto, *ACS Catal.* **2019**, *9*, 9292-9297; d) J. P. Tassone, E. V. England, P. M. MacQueen, M. J. Ferguson, M. Stradiotto, *Angew. Chem. Int. Ed.* **2019**, *58*, 2485-2489; e) J. S. K. Clark, M. J. Ferguson, R. McDonald, M. Stradiotto, *Angew. Chem. Int. Ed.* **2019**, *58*, 6391-6395; f) R. T. McGuire, C. M. Simon, A. A. Yadav, M. J. Ferguson, M. Stradiotto, *Angew. Chem. Int. Ed.* **2020**, *59*, 8952-8956.

[7] a) *Ferrocenes: Homogeneous Catalysis, Organic Synthesis, Materials Science* (Eds.: A. Togni, T. Hayashi), VCH, Weinheim, **1995**; b) *Ferrocenes: Ligands, Materials and Biomolecules* (Ed.: P. Štěpnička), Wiley, Chichester, **2008**; c) R. Gómez Arrayás, J. Adrio, J. C. Carretero, *Angew. Chem. Int. Ed.* **2006**, *45*, 7674-7715; d) L. Cunningham, A. Benson, P. J. Guiry, *Org. Biomol. Chem.* **2020**, *18*, 9329-9370.

[8] For examples, see: a) G. Eastham, World Patent WO 2004024322, **2004**; b) G. Eastham, World Patent WO 2005079981, **2005**; c) G. Eastham, World Patent WO 2005118519, **2005**.

[9] K.-S. Gan, T. S. A. Hor in *Ferrocenes: Homogeneous Catalysis, Organic Synthesis Materials Science* (Eds.: A. Togni, T. Hayashi), Wiley-VCH, Weinheim, **1995**, ch. 1, pp. 3-104; b) S. W. Chien, T. S. A. Hor in *Ferrocenes: Ligands, Materials and Biomolecules* (Ed.: P. Štěpnička), Wiley, Chichester, **2008**, ch. 2, pp. 33-116; c) G. Bandoli, A. Dolmella, *Coord. Chem. Rev.* **2000**, *209*, 161-196; d) D. J. Young, S. W. Chien, T. S. A. Hor, *Dalton Trans.* **2012**, *41*, 12655-12665.

[10] P. Štěpnička in *Ferrocenes: Ligands, Materials and Biomolecules* (Ed.: P. Štěpnička), Wiley, Chichester, **2008**, ch. 5, pp. 177-204.
[11] Representative examples: a) P. Štěpnička, J. Schulz, T. Klemann, U. Siemeling, I. Císařová, *Organometallics* **2010**, *29*, 3187-3200; b) P. Štěpnička, I. Císařová, J. Schulz, *Organometallics* **2011**, *30*, 4393-4403; c) P. Štěpnička, I. Císařová, *Dalton Trans.* **2013**, *42*, 3373-3389; d) M. Zábranský, A. Machara, I. Císařová, P. Štěpnička, *Eur. J. Inorg. Chem.* **2017**, 4850-4860; e) O. Bárta, I. Císařová, P. Štěpnička *Eur. J. Inorg. Chem.* **2017**, 489-495; f) P. Vosáhlo, I. Císařová, P. Štěpnička, *J. Organomet. Chem.* **2018**, *860*, 14-29.
[12] F. Horký, I. Císařová, P. Štěpnička, *Organometallics* **2021**, *40*, 427-441.
[13] A. Muller, S. Otto, A. Roodt, *Dalton Trans.* **2008**, 650-657.
[14] P. Nicpon, D. W. Meek, *Inorg. Chem.* **1966**, *5*, 1297-1298.
[15] a) C. A. Tolman, *Chem. Rev.* **1977**, *77*, 313-348; b) U. Beckmann, D. Süslüyan, P. C. Kunz, *Phosphorus, Sulfur, Silicon, Rel. Elem.* **2011**, *186*, 2061-2070.
[16] G. Pilloni, B. Longato, G. Bandoli, B. Corain, *J. Chem. Soc., Dalton Trans.* **1997**, 819-825.
[17] J. P. Hopewell, C. L. McMullin, P. G. Pringle, T. A. Shuttleworth, C. H. Woodall, *Eur. J. Inorg. Chem.* **2014**, 1843-1849.
[18] K. J. Cavell, D. J. Stufkens, K. Vrieze, *Inorg. Chim. Acta* **1981**, *47*, 67-76.
[19] The related Pd(0) complex [Pd(dba)(CgPPh)$_2$] containing monodentate CgPPh ligand (dba = dibenzylideneacetone) undergoes dissociation of the dba ligand in solution: G. Adjabeng, T. Brenstrum, C. S. Frampton, A. J. Robertson, J. Hillhouse, J. McNulty, A. Capretta, *J. Org. Chem.* **2004**, *69*, 5082-5086.
[20] E. J. Derrah, C. Martin, S. Mallet-Ladeira, K. Miqueu, G. Bouhadir, D. Bourissou, *Organometallics* **2013**, *32*, 1121-1128.
[21] a) M. J. S. Dewar, *Bull. Soc. Chem. Fr.* **1951**,*18*, C71-C79, b) J. Chatt, L. A. Duncanson, *J. Chem. Soc.* **1953**, 2939-2947.
[22] M. Lutz, *Acta Crystallogr., Sect. E: Struct. Rep. Online* **2001**, *57*, o1136-o1138.
[23] a) H.-Z. Zhang, Z.-L. Zhao, C.-H. Zhou, *Eur. J. Med. Chem.* **2018**, *144*, 444-492; b) V. S. C. Yeh, *Tetrahedron* **2004**, *60*, 11995-12042; c) U. Kamal, N. M. Javed, K. Arun, *Asian J. Pharm. Clinic. Res.* **2020**, *13*, 28-41; d) S. Pal, B. Manjunath, S. Ghorai, S. Sasmal in *The Alkaloids: Chemistry and Biology Vol. 79* (Ed.: H.-J. Knölker), Elsevier, Cambridge, MA, **2018**, pp. 71-137.
[24] Representative examples: a) Colin A. Scholes, *Aust. J. Chem.* **2016**, *69*, 601-611; b) C. Carayona, S. Fery-Forgues, *Photochem. Photobiol. Sci.* **2017**, *16*, 1020-1035; c) X. Huang, E. Meggers, *Acc. Chem. Res.* **2019**, *52*, 833-847; d) S.-H. Chen, K. Jiang, Y, Xiao, X.-Y. Cao, M. Arulkumar, Z.-Y. Wang, X. Huang, *Dyes Pigm.* **2020**, *175*, 108157.
[25] a) *Chemistry of Heterocyclic Compounds, vol. 60, Oxazoles: Synthesis, Reactions, and Spectroscopy* (Ed.: D. C. Palmer), Wiley, Hoboken, **2003**; b) C. A. Zificsak, D. J. Hlasta, Tetrahedron **2004**, *60*, 8991-9016; c) C. Verrier, P. Lassalas, L. Théveau, G. Quéguiner, F. Trécourt, F. Marsais, C. Hoarau, *Beil. J. Org. Chem.* **2011**, *7*, 1584-1601; d) S. Rajasekhar, B. Maiti, K. Chanda, *Synlett* **2017**, 521-541; e) S. Chen, P. Ranjan, L. G. Voskressensky, E. V. Van der Eycken, U. K. Sharma, *Molecules* **2020**, *25*, 4970.
[26] For early examples, see: a) A. Ohta, Y. Akita, T. Ohkuwa, M. Chiba, R. Fukunaga, A. Miyafuji, T. Nakata, N. Tani, Y. Aoyagi, *Heterocycles* **1990**, *31*, 1951-1958; b) S. Pivsa-Art, T. Satoh, Y. Kawamura, M. Miura, M. Nomura, *Bull. Chem. Soc. Jpn.* **1998**, *71*, 467-473.
[27] a) H. A. Chiong, O. Daugulis, *Org. Lett.* **2007**, *9*, 1449-1451; b) F. Derridj, S, Djebbara, O. Benali-Baitich, H. Doucet, *J. Organomet. Chem.* **2008**, *693*, 135-144; c) S. Yanagisawa, K. Ueda, H. Sekizawa, K. Itami, *J. Am. Chem. Soc.* **2009**, *131*, 14622-14623; d) D. T. Gryko, O. Vakuliuk, D. Gryko, B. Koszarna, *J. Org. Chem.* **2009**, *74*, 9517-9520; e) F. Shibahara, E. Yamaguchi, T. Murai *Chem. Commun.* **2010**, *46*, 2471-2473; f) L. Chen, J. Roger, C. Bruneau, P. H. Dixneuf, H. Doucet, *Adv. Synth. Catal.* **2011**, *353*, 2749-2760; g) X.-B. Shen, Y. Zhang, W.-X. Chen, Z.-K. Xiao, T.-T. Hu, L.-X. Shao, *Org. Lett.* **2014**, *16*,1984-1987; h) J. Ahmed, S. C. Sau, P. Sreejyothi, P. K. Hota, P. K. Vardhanapu, G. Vijaykumar, S. K. Mandal, *Eur. J. Org. Chem.* **2017**, 1004-1011.
[28] H.-Q. Do, O. Daugulis, *J. Am. Chem. Soc.* **2007**, *129*, 12404-12405.
[29] L. L. Zheng, B. Yin, X.-C. Tian, M.-Y. Yuan, X.-H. Li, F. Gao, *Tetrahedron Letters* **2019**, *60*, 151316.
[30] H. Larson, D. Schultz, D. Kalyani, *J. Org. Chem.* **2019**, *84*, 13092-13103.
[31] a) O. René, K. Fagnou, *Adv. Synth. Catal.* **2010**, *352*, 2116-2120; b) T. Korenaga, R. Sasaki, K. Shimada, *Dalton Trans.* **2015**, *44*, 19642-19650; c) A. Jakab, Z. Dalicsek, T. Soós, *Eur. J. Org. Chem.* **2015**, 56-59.
[32] a) B. Ndaba, I. Chiyanzu, S. Marx, *Biotechnol. Rep.* **2015**, *8*, 1-9; b) F. P. Byrne, S. Jin, G. Paggiola, T. H. M. Petchey, J. H. Clark, T. J. Farmer, A. J. Hunt, C. R. Mc Elroy, J. Sherwood, *Sustainable Chem. Process.* **2016**, *4*, 7.
[33] a) S. Dey, R.Pietschnig, *Coord. Chem. Rev.* **2021**, *437*, 213850; b) T. J. Colacot, S. ebastien Parisel in in *Ferrocenes: Ligands, Materials and Biomolecules* (Ed.: P. Štěpnička), Wiley, Chichester, **2008**, ch. 3, pp. 117-140.
[34] I. R. Butler, R. L. Davies, *Synthesis*, **1996**, 1350-1354.
[35] S. Raoufmoghaddam, S. Mannathan, A. J. Minnaard, J. G. de Vries, J. N. H. Reek, *ChemCatChem* **2018**, *10*, 266-272.

Entry for the Table of Contents

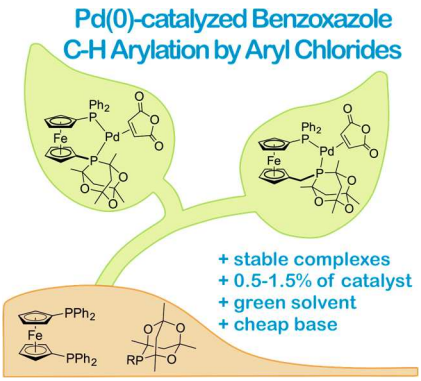

New donor-asymmetric ferrocene bis-phosphanes structurally related to the ubiquitous 1,1'-bis(diphenylphosphanyl)ferrocene (dppf) equipped with bulky and electron-poor phosphatrioxaadamantyl substituents have been synthesized and converted into stable Pd(0) complexes. The complexes were applied as potent catalysts for Pd-mediated C-H bond arylation of benzoxazoles with aryl chlorides under low catalyst loading in an environmentally benign solvent.

Institute and/or researcher Twitter usernames: @InorgChemCUNI

Contents

Syntheses

Synthesis of 1,3,5,7-tetramethyl-4,6,8-trioxa-2-phosphaadamantane (CgPH)[1]

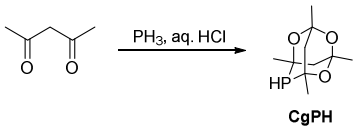

Safety Note. ***Caution!*** *PH_3 gas is a highly toxic and flammable gas. It should be handled with extreme care in an efficient hood and under constant supervision.*

An apparatus was set up according to Figure S1. Grease was applied to all glass joints, and connections were secured with joint clips. Argon was passed through the apparatus for 10 min, and then acetylacetone (50 mL, 0.49 mmol), water (50 mL) and hydrochloric acid (37%, 50 mL) were introduced to the reaction flask. Dropping funnel was filled with hydrochloric acid (ca. 15%, 300 mL), the sidearm flask was charged with zinc phosphide (Sigma-Aldrich; 19% active phosphorus basic, ca. 50 g), and argon was passed through the apparatus for another 5 hours to ensure complete oxygen removal. Subsequently, the reaction flask was cooled in an ice bath, and argon flow was reduced to keep only a small overpressure in the apparatus (this prevents blocking of the frit as the product is being formed). The gas bubbler and the beaker were filled with a solution of sodium hypochlorite solution (ca. 5%, 2× 200 mL; commercial household bleach was used), and phosphine gas was evolved by slowly adding HCl to the phosphide during 8 hours, whereupon white crystals separated in the reaction flask. After the reaction subsided, sodium hypochlorite solution was replenished in the beaker, and argon was bubbled through the mixture for 2 hours to eliminate all phosphine. Finally, the product was filtered off in air, washed with water (3× 50 mL) and dried under vacuum. Yield: 24 g (45%), an air-stable, white crystalline solid.

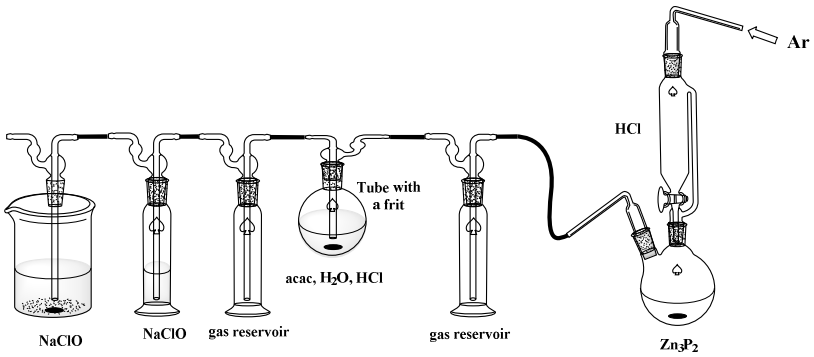

Figure S1. Apparatus for the synthesis of CgPH

^{1}H NMR (400 MHz, $CDCl_3$): δ = 1.38 (s, 3H, Me), 1.39 (s, 3H, Me), 1.46 (d, $^{3}J_{PH}$ = 13.7 Hz, 3H, Me), 1.48 (d, $^{3}J_{HH}$ = 13.8 Hz, 3H, Me), 1.73 (d, $^{2}J_{HH}$ = 12.8 Hz, 1H, CH_2), 1.78-1.84 (m, 2H, CH_2), 1.91 (dd, $^{2}J_{HH}$ = 12.8 Hz, $^{3}J_{PH}$ = 2.7 Hz, 1H, CH_2), 3.08 (dm, $^{1}J_{PH}$ = 190 Hz, 1H, PH) ppm. ^{31}P{^{1}H} NMR (162 MHz, $CDCl_3$): δ = −49.5 (s) ppm. The data are in agreement with the literature.[1]

Synthesis of 1,3,5,7-tetramethyl-2-bromo-4,6,8-trioxa-2-phosphaadamantane (CgPBr)[1]

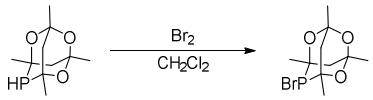

CgPH CgPBr

In a Schlenk flask under an inert atmosphere, bromine was dissolved in dichloromethane to give a solution of a known concentration (4.39 g, 27.5 mmol of Br_2 in 100 mL of the solvent). CgPH (5.0 g, 23.1 mmol) was dissolved in a second Schlenk flask in dichloromethane (100 mL), and the resulting solution was cooled in an ice bath to 0°C. Then, the bromine solution slowly added with vigorous stirring (93 mL, 25.4 mmol, 1.1 ekv.), subsequently continuing stirring for another hour and removing the solvent under vacuum (*Caution! The volatiles contain Br_2 and HBr*). Toluene (120 mL) was added to the solid residue, and the suspension was filtered under argon. The filtrate was evaporated under reduced pressured to produce CgPBr as a yellowish solid, which can be stored in a fridge for months. Yield: 6.37 g (93%).

^{1}H NMR (400 MHz, $CDCl_3$): δ = 1.38 (s, 3H, Me), 1.40 (d, $^{3}J_{PH}$ = 0.9 Hz, 3H, Me), 1.42 (s, 3H, Me), 1.43 (d, $^{3}J_{PH}$ = 1.6 Hz, 3H, Me), 1.64 (dd, $^{2}J_{HH}$ = 13.6 Hz, $^{3}J_{PH}$ = 4.5 Hz, 1H, CH_2), 2.01-2.08 (m, 2H, CH_2), 2.43 (d, $^{2}J_{HH}$ = 13.6 Hz, 1H, CH_2) ppm. ^{31}P{^{1}H} NMR (162 MHz, $CDCl_3$): δ = 54.9 (s) ppm. The NMR spectra match the literature ones.[1]

Synthesis of (*N*,*N*'-di-*t*-butylethanedialdimine-κ^2*N*,*N*')[(3,4-η)-2,5-furandione]-palladium(0), [Pd(ma)(N^N)][2]

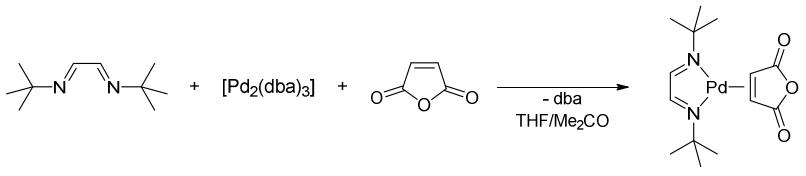

[Pd(ma)(N^N)]

A flame-dried flask was charged with tris(dibenzylideneacetone)dipalladium(0)−chloroform (1:1) (1.036 g, 1.0 mmol), maleic anhydride (216 mg, 2.2 mmol), *N*,*N*'-di-*t*-butylethanediimine[3] (370 mg, 2.2 mmol), tetrahydrofuran (50 mL) and acetone (30 mL), and the resulting mixture was stirred for 3 h. The black-yellow suspension was concentrated under reduced pressure to approximately 10 mL and filtered (in air) using a PTFE syringe filter (0.45 μm pore size). The filter was washed with tetrahydrofuran (3× 10 mL), and the filtrate was evaporated under vacuum. The crude product was triturated with diethyl ether (5 mL), collected on a frit, washed

with diethyl ether (5 mL) and dried under vacuum to afford [Pd(ma)(N^N)] as a yellow solid. Yield: 400 mg (54%). The compound can be stored in a fridge for months.

^{1}H NMR (400 MHz, $CDCl_3$): δ = 1.44 (s, 18H, *t*-Bu), 3.88 (s, 2H, N=CH), 8.12 (s, 2H, ma) ppm.

Synthesis of 1-Se

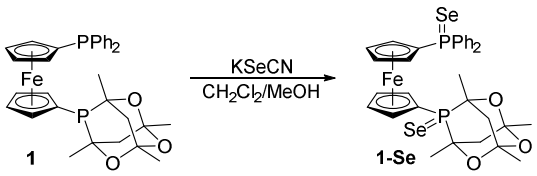

Compound **1** (175 mg, 0.3 mmol) and potassium selenocyanate (115 mg, 0.8 mmol) were mixed in methanol (20 mL) and dichloromethane (10 mL), and the resulting mixture was stirred at room temperature overnight and then evaporated. The crude product was purified by chromatography over a silica gel column, eluting with hexane-ethyl acetate (3:1). A single orange band was collected and evaporated, leaving **1-Se** as an orange solid. Yield: 133 mg (60%). Crystals suitable for structure determination were obtained by liquid-phase diffusion of diethyl ether into an acetonitrile solution of the bis-selenide.

^{1}H NMR (400 MHz, $CDCl_3$): δ = 1.17 (d, $^3J_{PH}$ = 15.0 Hz, 3H, Me), 1.31 (s, 3H, Me), 1.41 (s, 3H, Me), 1.63-1.74 (m, 3H, CH_2), 1.66 (d, $^3J_{PH}$ = 14.4 Hz, 3H, Me), 3.02 (dd, $^2J_{HH}$ = 13.7 Hz, $^3J_{PH}$ = 4.2 Hz, 1H, CH_2), 4.47 (tt, *J′* = 2.6, 1.3 Hz, 1H, fc), 4.57 (tt, *J′* = 2.5, 1.3 Hz, 1H, fc), 4.58-4.61 (m, 2H, fc), 4.70 (dtd, *J′* = 2.5, 1.2, 0.5 Hz, 1H, fc), 4.78 (tt, *J′* = 2.6, 1.3 Hz, 1H, fc), 4.90 (tt, *J′* = 2.6, 1.4 Hz, 1H, fc), 4.93 (tt, *J′* = 2.6, 1.4 Hz, 1H, fc), 7.38-7.54 (m, 6H, PPh_2), 7.61-7.68 (m, 2H, PPh_2), 7.71-7.79 (m, 2H, PPh_2) ppm. ^{13}C{^{1}H} NMR (101 MHz, $CDCl_3$): δ = 22.31 (d, $^2J_{PC}$ = 2 Hz, Me), 23.29 (d, $^2J_{PC}$ = 2 Hz, Me), 27.39 (s, 2×Me), 39.24 (d, $^2J_{PC}$ = 6 Hz, CH_2), 39.98 (d, $^2J_{PC}$ = 3 Hz, CH_2), 71.05 (d, $^1J_{PC}$ = 65 Hz, C^{ipso} of fc), 72.76 (d, $^1J_{PC}$ = 43 Hz, C of PCg), 73.67 (d, J_{PC} = 6 Hz, CH of fc), 73.92 (d, J_{PC} = 10 Hz, CH of fc), 74.53 (d, J_{PC} = 11 Hz, CH of fc), 74.84 (d, J_{PC} = 14 Hz, CH of fc), 75.00 (d, J_{PC} = 13 Hz, CH of fc), 75.48 (d, J_{PC} = 7 Hz, CH of fc), 75.63 (d, $^1J_{PC}$ = 42 Hz, C of PCg), 75.79 (d, $^1J_{PC}$ = 87 Hz, C^{ipso} of fc), 75.83 (d, J_{PC} = 9 Hz, CH of fc), 76.74 (d, J_{PC} = 10 Hz, CH of fc), 96.31 (d, $^3J_{PC}$ = 2 Hz, C of PCg), 96.50 (d, $^3J_{PC}$ = 2 Hz, C of PCg), 128.28 (d, J_{PC} = 13 Hz, CH of PPh_2), 128.37 (d, J_{PC} = 13 Hz, CH of PPh_2), 131.43 (d, J_{PC} = 3 Hz, CH of PPh_2), 131.60 (d, J_{PC} = 3 Hz, CH of PPh_2), 131.85 (d, J_{PC} = 11 Hz, CH of PPh_2), 132.13 (d, J_{PC} = 11 Hz, CH of PPh_2), 132.30 (d, $^1J_{PC}$ = 79 Hz, C^{ipso} of PPh_2), 133.46 (d, $^1J_{PC}$ = 79 Hz, C^{ipso} of PPh_2) ppm. ^{31}P{^{1}H} NMR (162 MHz, $CDCl_3$): δ = 30.4 (s with ^{77}Se satellites, $^1J_{PSe}$ = 766 Hz, PCg), 31.6 (s with ^{77}Se satellites, $^1J_{PSe}$ = 738 Hz, PPh_2) ppm. IR (Nujol): ν_{max} = 1437 w, 1343 w, 1305 w, 1266 w, 1231 w, 1213 m, 1192 m, 1172 m, 1138 m, 1100 m, 1090 m, 1026 m, 982 m, 897 m, 855 w, 835 m, 794 w, 750 w, 713 w, 690 w, 633 w, 604 m, 584 w, 570 m, 533 w, 503 w, 478 m, 470 m, 445 w, 430 w cm^{-1}. ESI-MS: *m/z* = 745 ($[M + H]^+$). Anal. Calc. for $C_{32}H_{34}FeO_3P_2Se_2$ (742.3): C 51.78, H 4.62%. Found: C 51.74, H 4.38%.

Synthesis of 2-Se

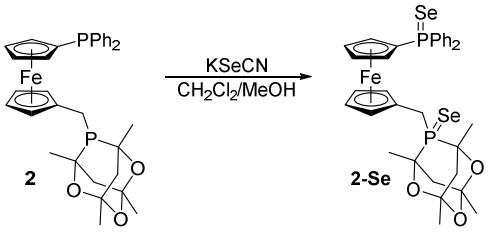

Bis-phosphane **2** (120 mg, 0.2 mmol) and potassium selenocyanate (72 mg, 0.5 mmol) were dissolved in methanol and dichloromethane (10 mL each) under argon, and the mixture was stirred overnight. On the following day, the mixture was concentrated under vacuum, and the residue was purified by chromatography over silica gel column using hexane-ethyl acetate (3:1) as the eluent. Evaporation of a single orange band afforded pure **2-Se** as an orange powdery solid. Yield: 32 mg (21%). Crystals for structure determination were obtained from dichloromethane/hexane.

^{1}H NMR (400 MHz, $CDCl_3$): δ = 1.01 (d, $^{3}J_{PH}$ = 14.6 Hz, 3H, Me), 1.38 (d, $^{3}J_{PH}$ = 14.6 Hz, 3H, Me), 1.40 (s, 3H, Me), 1.52 (s, 3H, Me), 1.68 (dd, $^{3}J_{PH}$ = 23.2 Hz, $^{2}J_{HH}$ = 13.5 Hz, 1H, CH_2), 2.05 (dd, $^{3}J_{PH}$ = 21.4 Hz, $^{2}J_{HH}$ = 13.9 Hz, 1H, CH_2), 2.34 (dd, $^{2}J_{HH}$ = 13.9 Hz, $^{3}J_{PH}$ = 1.7 Hz, 1H, CH_2), 2.87 (dd, $^{2}J_{HH}$ = 13.5 Hz, $^{3}J_{PH}$ = 3.6 Hz, 1H, CH_2), 3.32 (dd, $^{2}J_{HH}$ = 14.4 Hz, $^{2}J_{PH}$ = 13.1 Hz, 1H, PCH_2), 3.84 (dd, $^{2}J_{HH}$ = 14.4 Hz, $^{2}J_{PH}$ = 9.2 Hz, 1H, PCH_2), 3.99 (td, J' = 2.5, 1.3 Hz, 1H, fc), 4.09 (td, J' = 2.5, 1.6 Hz, 1H, fc), 4.23 (tt, J' = 2.4, 1.3 Hz, 1H, fc), 4.39 (tt, J' = 2.5, 1.3 Hz, 1H, fc), 4.51 (tt, J' = 2.5, 1.3 Hz, 1H, fc), 4.55 (dq, J' = 2.0. 1.1 Hz, 1H, fc), 4.60 (tt, J' = 2.6, 1.4 Hz, 1H, fc), 4.66 (dq, J' = 2.3, 1.2 Hz, 1H, fc), 7.38-7.53 (m, 6H, PPh_2), 7.63-7.70 (m, 2H, PPh_2), 7.72-7.78 (m, 2H, PPh_2) ppm. ^{13}C{^{1}H} NMR (101 MHz, $CDCl_3$): δ = 22.03 (d, $^{2}J_{PC}$ = 2 Hz, Me), 23.73 (d, $^{2}J_{PC}$ = 2 Hz, Me), 27.39 (s, Me), 27.60 (s, Me), 28.05 (d, $^{1}J_{PC}$ = 30 Hz, PCH_2), 38.72 (d, $^{2}J_{PC}$ = 4 Hz, CH_2), 40.88 (d, $^{2}J_{PC}$ = 3 Hz, CH_2), 69.45 (s, CH of fc), 70.03 (s, CH of fc), 71.92 (d, J_{PC} = 2 Hz, CH of fc), 72.17 (d, $^{1}J_{PC}$ = 36 Hz, C of PCg), 72.35 (d, J_{PC} = 10 Hz, CH of fc), 72.80 (d, J_{PC} = 10 Hz, CH of fc), 73.33 (d, J_{PC} = 2 Hz, CH of fc), 73.70 (d, J_{PC} = 12 Hz, CH of fc), 74.45 (d, $^{1}J_{PC}$ = 37 Hz, C of PCg), 75.09 (d, $^{1}J_{PC}$ = 89 Hz, C^{ipso} of fc), 75.52 (d, J_{PC} = 13 Hz, CH of fc), 79.92 (s, C^{ipso} of fc), 96.37 (d, $^{3}J_{PC}$ = 2 Hz, C of PCg), 96.62 (d, $^{3}J_{PC}$ = 2 Hz, C of PCg), 128.28 (d, J_{PC} = 13 Hz, 2× CH of PPh_2), 131.34 (d, J_{PC} = 3 Hz, CH of PPh_2), 131.46 (d, J_{PC} = 3 Hz, CH of PPh_2), 131.97 (d, J_{PC} = 11 Hz, CH of PPh_2), 132.09 (d, J_{PC} = 12 Hz, CH of PPh_2), 132.52 (d, $^{1}J_{PC}$ = 79 Hz, C^{ipso} of PPh_2), 133.67 (d, $^{1}J_{PC}$ = 79 Hz, C^{ipso} of PPh_2) ppm. ^{31}P{^{1}H} NMR (162 MHz, $CDCl_3$): δ = 32.4 (s with ^{77}Se satellites, $^{1}J_{PSe}$ = 731 Hz, PPh_2), 33.9 (s with ^{77}Se satellites, $^{1}J_{PSe}$ = 757 Hz, PCg) ppm. IR (DRIFTS): ν_{max} = 1482 w, 1437 m, 1383 m, 1370 m, 1343 w, 1311 w, 1265 w, 1233, 1216 s, 1199 s, 1178 s, 1137 s, 1100 s, 1041 w, 1028 m, 979 m, 926 w, 904 m, 893 m, 859 m, 826 m, 790 w, 757 m, 747 m, 711 w, 703 m, 695 s, 682 w, 631 w, 604 w, 584 s, 571 w, 553 s, 510 m, 500 m, 478 s, 467 m, 449 w, 434 m, 427 m, 402 w cm^{-1}. ESI-MS: *m/z* = 781 ($[M + Na]^+$). Anal. Calc. for $C_{33}H_{36}FeO_3P_2Se_2$ (758.0): C 52.40, H 4.80%. Found: C 52.45, H 4.82%.

Synthesis of 5-Se

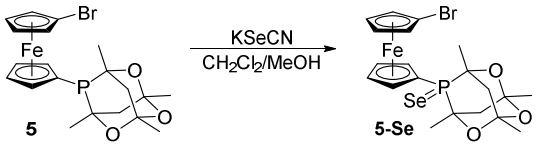

Phosphane **5** (96 mg, 0.2 mmol) and potassium selenocyanate (43 mg, 0.3 mmol) were mixed in methanol (20 mL) and dichloromethane (5 mL) under argon, and the resulting mixture was stirred overnight. On the next day, the mixture was concentrated under vacuum, and the residue was purified by chromatography over silica gel, eluting with hexane-ethyl acetate (3:1). Evaporation of a single orange band afforded a pure product **5-Se** as an orange solid. Yield: 50 mg (45%). Crystals used for structure determination were grown from dichloromethane/hexane.

^{1}H NMR (400 MHz, $CDCl_3$): δ = 1.25 (d, $^{3}J_{PH}$ = 14.9 Hz, 3H, Me), 1.34 (s, 3H, Me), 1.44 (s, 3H, Me), 1.72 (dd, $^{2}J_{HH}$ = 13.7 Hz, $^{3}J_{PH}$ = 11.7 Hz, 1H, CH_2), 1.76 (d, $^{2}J_{HH}$ = 13.7 Hz, 1H, CH_2), 1.78-1.80 (m, 1H, CH_2), 1.81 (d, $^{3}J_{PH}$ = 14.6 Hz, 3H, Me), 3.07 (dd, $^{2}J_{HH}$ = 13.6 Hz, $^{3}J_{PH}$ = 4.2 Hz, 1H, CH_2), 4.39 (dt, J' = 2.6, 1.4 Hz, 1H, fc), 4.42 (dt, J' = td, 2.6, 1.4 Hz, 1H, fc), 4.48 (tt, J' = 2.6, 1.3 Hz, 1H, fc), 4.52 (dt, J' = 2.6, 1.3 Hz, 1H, fc), 4.57 (tt, J' = 2.6, 1.3 Hz, 1H, fc), 4.63 (dt, J' = 2.6, 1.3 Hz, 1H, fc), 4.72 (tt, J' = 2.6, 1.3 Hz, 1H, fc) 4.86 (dtd, J' = 2.5, 1.2, 0.5 Hz, 1H, fc) ppm. ^{13}C{^{1}H} NMR (101 MHz, $CDCl_3$): δ = 22.37 (d, $^{2}J_{PC}$ = 3 Hz, Me), 23.30 (d, $^{2}J_{PC}$ = 2 Hz, Me), 27.43 (s, Me), 27.46 (s, Me), 39.33 (d, $^{2}J_{PC}$ = 7 Hz, CH_2), 40.09 (d, $^{2}J_{PC}$ = 3 Hz, CH_2), 70.91 (s, CH of fc), 71.00 (s, CH of fc), 71.97 (d, $^{1}J_{PC}$ = 67 Hz, C^{ipso} of fc), 72.19 (s, CH of fc), 72.20 (s, CH of fc), 72.81 (d, $^{1}J_{PC}$ = 43 Hz, C of PCg), 73.96 (d, J_{PC} = 7 Hz, CH of fc), 75.33 (d, J_{PC} = 16 Hz, CH of fc), 75.42 (d, J_{PC} = 13 Hz, CH of fc), 75.54 (d, $^{1}J_{PC}$ = 42 Hz, C of PCg), 75.85 (d, J_{PC} = 14 Hz, CH of fc), 78.25 (s, C^{ipso} of fc), 96.39 (d, $^{3}J_{PC}$ = 1 Hz, C of PCg), 96.55 (d, $^{3}J_{PC}$ = 2 Hz, C of PCg) ppm. ^{31}P{^{1}H} NMR (162 MHz, $CDCl_3$): δ = 30.6 (s with ^{77}Se satellites, $^{1}J_{SeP}$ = 766 Hz) ppm. IR (Nujol): ν_{max} = 1344 m, 1266 w, 1232 w, 1212 m, 1193 m, 1138 m, 1091 m, 1027 m, 982 m, 899 m, 869 m, 855 w, 837 w, 794 w, 684 w, 602 m, 584 w, 552 w, 493 m, 460 w cm^{-1}. ESI-MS: *m/z* = 559 ([M + H]$^{+}$). Anal. Calc. for $C_{20}H_{24}BrFeO_3PSe$ (558.1): C 43.04, H 4.33%. Found: C 43.03, H 4.33%.

X-Ray crystallography

Full-sphere diffraction data were collected on a Bruker D8 VENTURE Kappa Duo diffractometer equipped with a PHOTON detector and a Cryostream Cooler (Oxford Cryosystems), using Mo Kα radiation (λ = 0.71073 Å). The structures were solved using direct methods (SHELXT, recent version [4]) and subsequently refined by full-matrix least-squares routine based on F^2 (SHELXL, recent version[5]). The nonhydrogen atoms were refined with anisotropic displacement parameters. Hydrogen atoms were included in their theoretical positions with their U_{iso}(H) set to a multiple of U_{eq}(C) (1.2-times for CH and CH_2 hydrogens, 1.5-times for methyl groups). Relevant crystallographic data and structure refinement parameters are collected in Table S1. Particular details on structure refinement are described below.

The CgP moiety in the structure of **1** was disordered by rotation of its bonding cyclopentadienyl ring and of the phosphatrioxaadamantane cage along the pivotal C(Cp)–P bond. The two contributing orientations occupy essentially the same space and have refined occupancies 93.5:6.5. The cage in the less abundant position has been refined with the same geometry as the dominating one (command SAME in SHELXL) and with constrained isotropic displacement parameters for all atoms. The disordered cyclopentadienyl ring was refined similarly but without using the SAME restraint. Conversely, in the structure of **5-Se**, the bulky CgP fragment acted as a pivotal moiety for disordered bromoferrocenyl group, which appeared in two orientations mutually rotated along the P8-C21 bond and, simultaneously, along the axis of the ferrocene unit (*i.e.*, with the Br atoms in approximately opposite positions). Even in this case, most cyclopentadienyl carbon atoms at the less populated site were refined isotropically. The refined occupancies were 92.5:7.5.

The solvent molecules in the structure of **7**·3$CHCl_3$ were disordered and, consequently, modelled over two positions for the chlorine and, in one molecule, for the carbon atoms as well. Even so, the 1,2-dichloroethane molecule in the structure of **8**·½$C_2H_4Cl_2$ was disordered over two positions near the crystallographic inversion center.

All geometric data and structural diagrams were obtained using a recent version of the PLATON program.[6] The numerical values were rounded to one decimal place with respect to the respective estimated standard deviations (ESDs).

Complete crystallographic data were deposited with the Cambridge Crystallographic Data Centre and can be obtained free of charge at www.ccdc.cam.ac.uk/data_request/cif, by email at data_request@ccdc.cam.ac.uk, or by contacting The Cambridge Crystallographic Data Centre, 12 Union Road, Cambridge CB2 1EZ, UK; fax: +44 1223 336033. Deposition numbers are quoted in Table S1.

Table S1. Selected crystallographic data and structure refinement parameters[a]

Compound	**1**	**2**	**5**
Formula	$C_{32}H_{34}FeO_3P_2$	$C_{33}H_{36}FeO_3P_2$	$C_{20}H_{24}BrFeO_3P$
M	584.38	598.41	479.12
T [K]	120(2)	120(2)	150(2)
Crystal system	triclinic	triclinic	orthorhombic
Space group	*P*–1 (no. 2)	*P*–1 (no. 2)	*Pbca* (no. 61)
a [Å]	7.4725(3)	11.4996(4)	18.8415(8)
b [Å]	8.8970(3)	11.5036(5)	7.7017(4)
c [Å]	21.2978(8)	12.2183(5)	26.542(1)
α [°]	101.614(1)	70.276(1)	90
β [°]	91.934(1)	70.557(1)	90
γ [°]	90.217(1)	84.019(1)	90
V [Å]^3	1386.08(9)	1434.7(1)	3851.6(3)
Z	2	2	8
μ(Mo Kα) [mm^{-1}]	0.692	0.670	2.958
Diffrns collected	27954	47244	121786
Independent diffrns	6364	6586	4425
Observed[a] diffrns	5885	6171	3869
R_{int}[b] [%]	2.33	2.58	5.31
No. of parameters	415	356	239
R[b] obsd diffrns [%]	2.62	2.49	2.99
R, *wR*[b] all data [%]	2.93, 6.70	2.71, 6.45	3.71, 8.21
Δρ [e Å^{-3}]	0.46, −0.40	0.39, −0.31	0.49, −1.00
CCDC no.	2092779	2092780	2092781

[a] Diffractions with $I > 2\sigma(I)$. [b] Definitions: $R_{int} = \Sigma \left| F_o^2 - F_o^2(\text{mean}) \right| / \Sigma F_o^2$, where F_o^2(mean) is the average intensity of symmetry-equivalent diffractions. $R = \Sigma \left| \left| F_o \right| - \left| F_c \right| \right| / \Sigma \left| F_o \right|$, $wR = [\Sigma\{w(F_o^2 - F_c^2)^2\}/\Sigma w(F_o^2)^2]^{1/2}$.

Table S1 continued

Compound	**1-Se**	**2-Se**	**5-Se**
Formula	$C_{32}H_{34}FeO_3P_2Se_2$	$C_{33}H_{36}FeO_3P_2Se_2$	$C_{20}H_{24}BrFeO_3PSe$
M	742.30	756.33	558.08
T [K]	120(2)	120(2)	120(2)
Crystal system	triclinic	triclinic	monoclinic
Space group	$P\bar{1}$ (no. 2)	$P\bar{1}$ (no. 2)	$P2_1/c$ (no. 14)
a [Å]	10.3844(3)	7.4820(5)	20.291(1)
b [Å]	12.3624(5)	14.707(1)	7.4043(4)
c [Å]	13.1944(5)	14.743(1)	14.3314(8)
α [°]	63.430(1)	97.185(2)	90
β [°]	88.824(1)	90.247(2)	106.526(2)
γ [°]	81.698(1)	102.657(2)	90
V [Å]^3	1497.22(9)	1569.6(2)	2064.2(2)
Z	2	2	4
μ(Mo Kα) [mm^{-1}]	3.075	2.934	4.525
Diffrns collected	34543	28872	50166
Independent diffrns	6873	7202	4753
Observed[a] diffrns	6191	6846	4512
R_{int}[b] [%]	2.69	2.25	2.77
No. of parameters	366	375	278
R[b] obsd diffrns [%]	2.19	6.31	2.41
R, wR[b] all data [%]	2.72, 5.41	2.88, 6.37	2.58, 5.89
Δρ [e Å^{-3}]	0.43, −0.52	0.64, −0.52	0.73, −0.81
CCDC no.	2092782	2092783	2092784

Table S1 continued

Compound	**7**·3$CHCl_3$	**8**·½$C_2H_4Cl_2$	**9**
Formula	$C_{41}H_{33}Cl_9FeO_3P_2Pd$	$C_{37}H_{38}ClFeO_6P_2$ Pd	$C_{37}H_{38}FeO_6P_2Pd$
M	1116.91	838.31	802.86
T [K]	120(2)	120(2)	120(2)
Crystal system	triclinic	triclinic	orthorhombic
Space group	*P*–1 (no. 2)	*P*–1 (no. 2)	*Pbca* (no. 61)
a [Å]	13.7542(5)	9.0584(4)	15.2761(3)
b [Å]	14.1021(5)	9.3904(4)	17.7022(3)
c [Å]	14.2855(5)	20.5137(8)	24.8572(5)
α [°]	109.605(1)	83.823(1)	90
β [°]	96.953(1)	87.645(1)	90
γ [°]	116.536(1)	79.915(1)	90
V [Å]^3	2211.3(1)	1707.6(1)	6721.9(2)
Z	2	2	8
μ(Mo Kα) [mm^{-1}]	1.389	1.170	1.109
Diffrns collected	45924	37683	54289
Independent diffrns	10105	7798	7697
Observed[a] diffrns	9558	7642	6548
R_{int}[b] [%]	2.08	1.69	5.36
No. of parameters	583	441	428
R[b] obsd diffrns [%]	2.83	2.45	3.43
R, wR[b] all data [%]	3.03, 6.96	2.51, 5.98	4.57, 7.20
Δρ [e Å^{-3}]	1.52, –0.85	1.79, –0.86	0.56, –0.50
CCDC no.	2092785	2092786	2092787

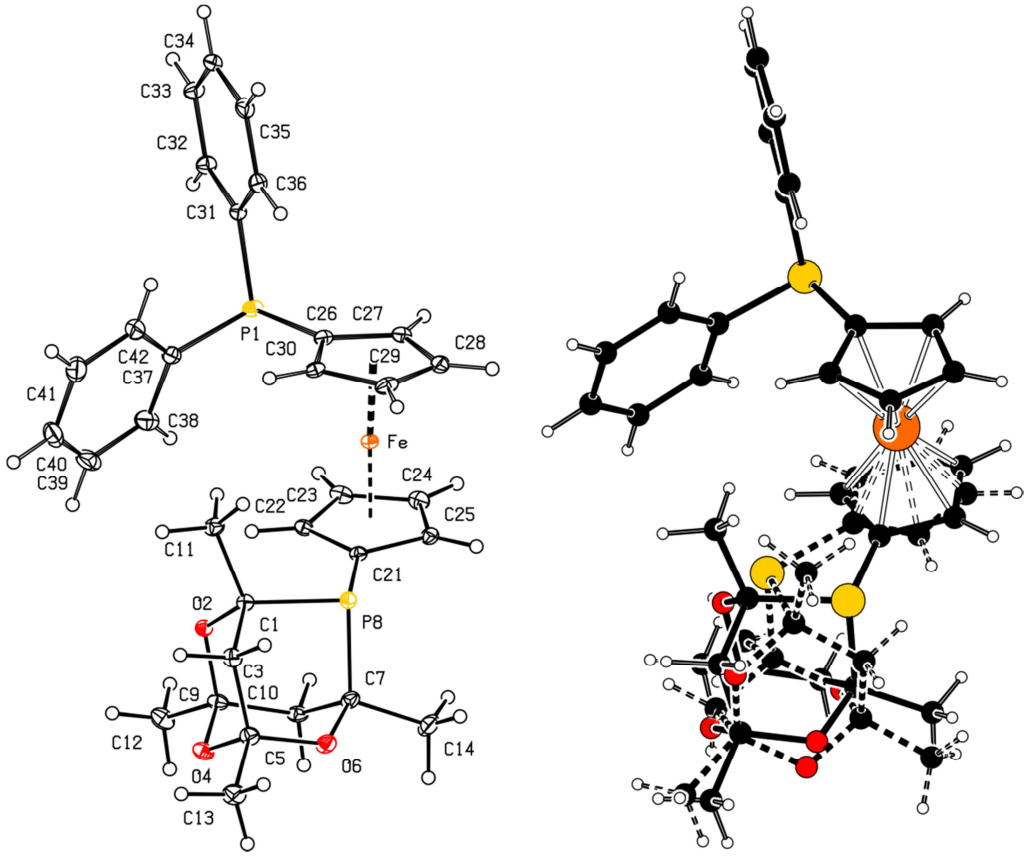

Figure S1. (left) PLATON plot of the molecular structure of **1** with displacement ellipsoids at the 30% probability level. For clarity, only one position of the disordered CgP cage is shown (right). Structure diagram illustrating the disorder of the CgP cage.

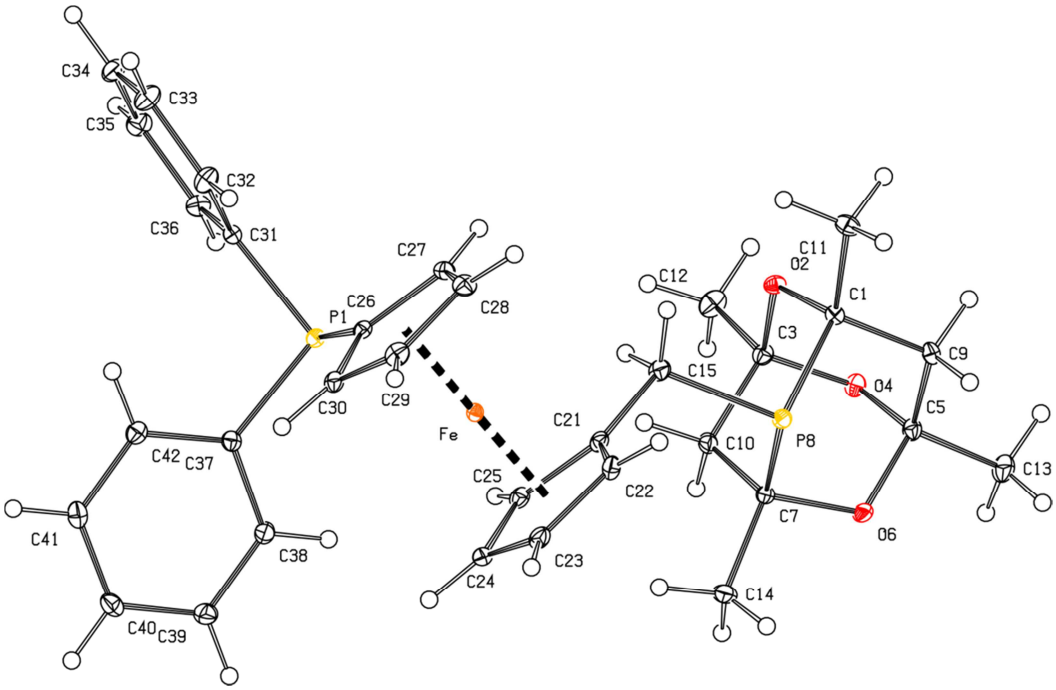

Figure S2. PLATON plot of the molecular structure of **2** with displacement ellipsoids at the 30% probability level

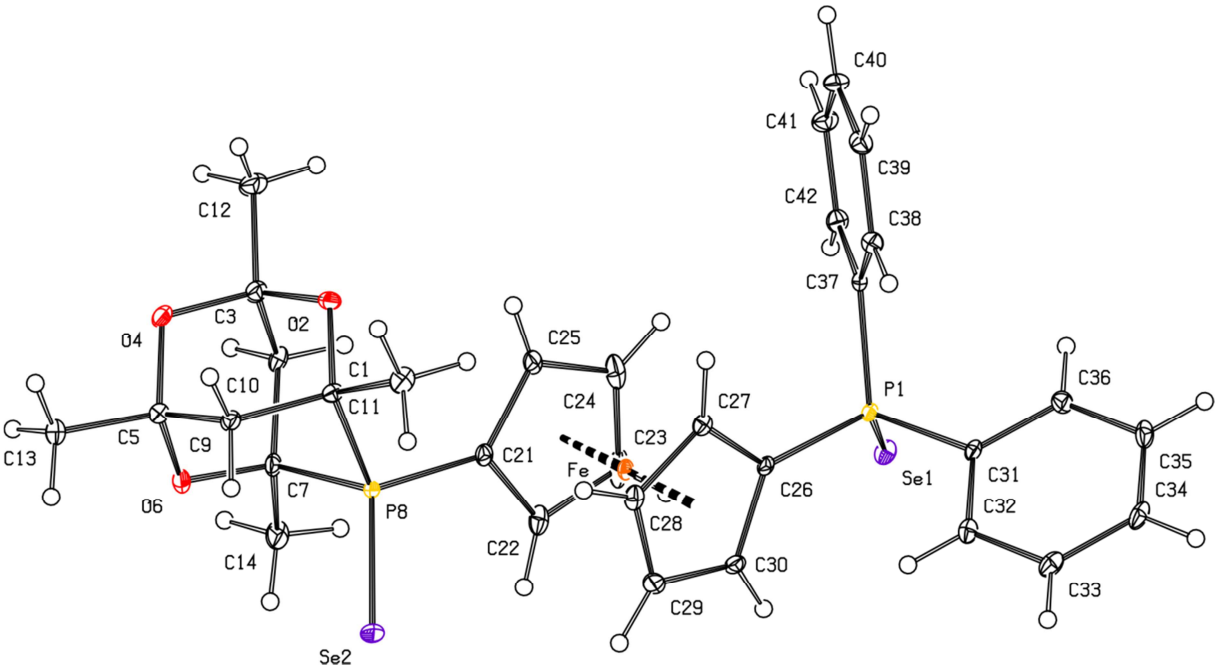

Figure S3. PLATON plot of the molecular structure of **1-Se** with displacement ellipsoids at the 30% probability level

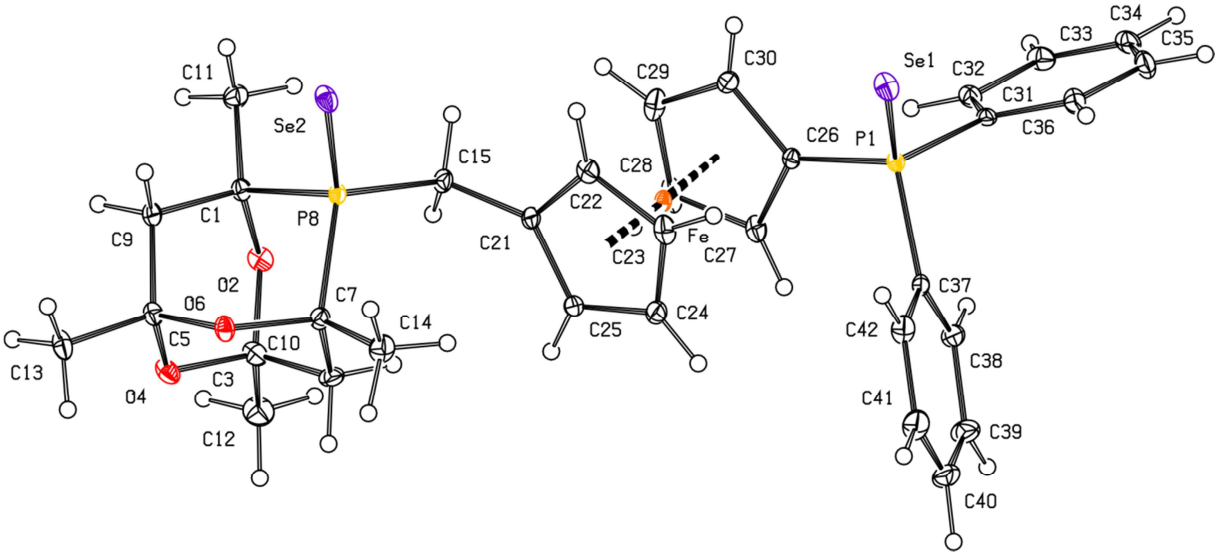

Figure S4. PLATON plot of the molecular structure of **2-Se** with displacement ellipsoids at the 30% probability level

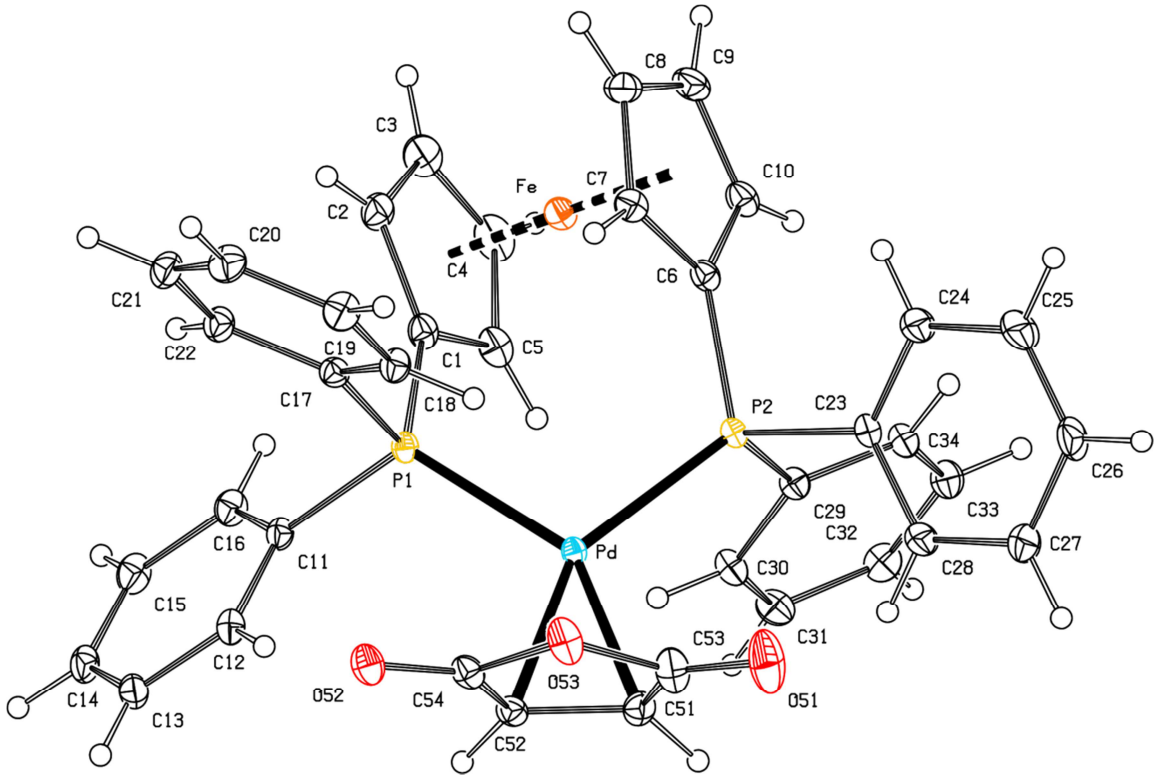

Figure S5. PLATON plot of the complex molecule in the structure of **7**·3$CHCl_3$ with displacement ellipsoids at the 30% probability level

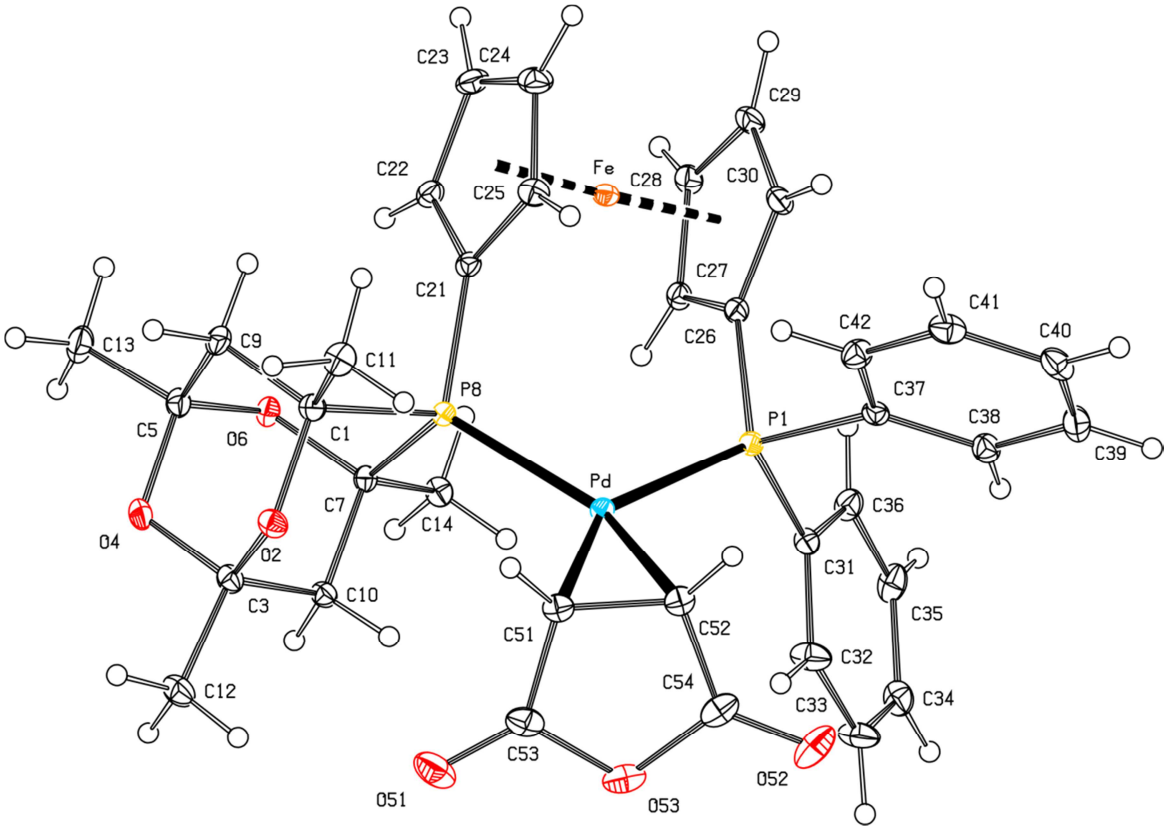

Figure S6. PLATON plot of the complex molecule in the structure of **8**·½$C_2H_4Cl_2$ with displacement ellipsoids at the 30% probability level

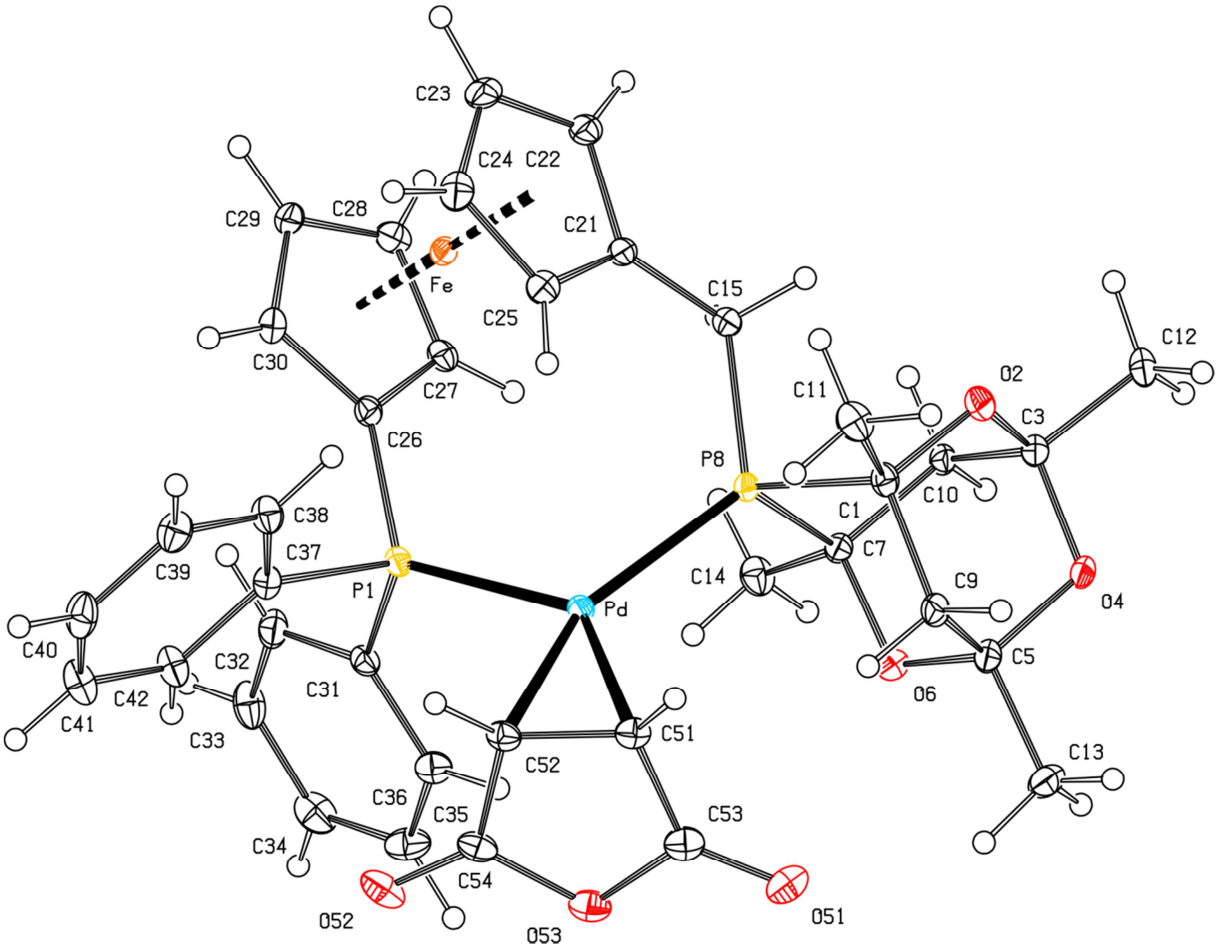

Figure S7. PLATON plot of the molecular structure of **9** with displacement ellipsoids at the 30% probability level

Molecular structures of **5** and **5-Se** and presented in Figures S8 and S9, and the pertinent geometric parameters are outlined in Table S2.

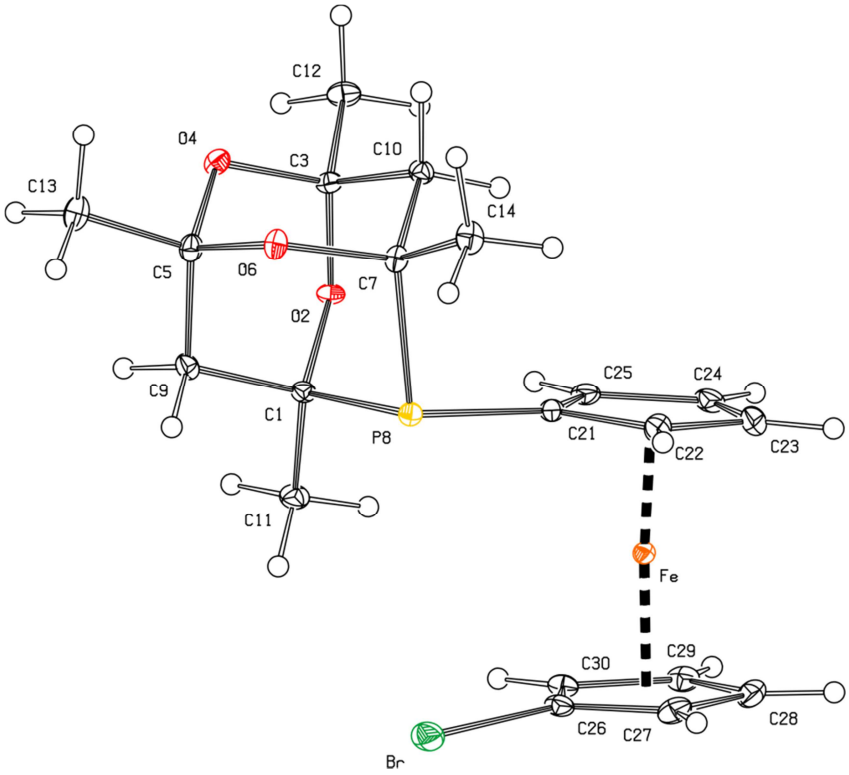

Figure S8. PLATON plot of the molecular structure of **5** with displacement ellipsoids at the 30% probability level

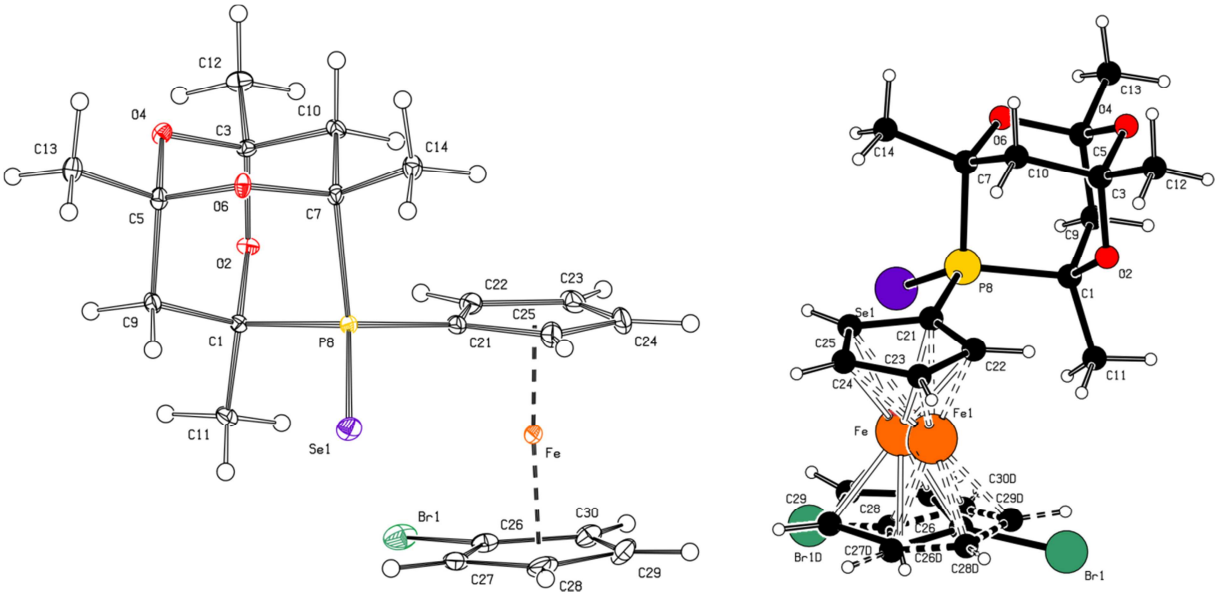

Figure S9. (left) PLATON plot of the molecular structure of **5-Se** showing the more abundant orientation of the disordered ferrocenyl moiety. The displacement ellipsoids enclose the 30% probability level. (right) Molecular diagram illustrating the disorder of the ferrocene unit.

Table S2. Selected distances and angles for **5** and **5-Se** (in Å and °)

Parameter[a]	**5**	**5-Se**[b]
P8-C21	1.812(2)	1.790(2)
P8-C1/7	1.879(2)/1.886(2)	1.859(2)/1.871(2)
Br-C26	1.878(2)	1.881(3)
Fe-C (range)	2.033(2)-2.066(2)	2.021(2)-2.065(2)
tilt	4.5(2)	4.1(2)
τ	−12.8(2)	80.0(2)
P8=Se1	n.a.	2.1051(6)

[a] Tilt is the dihedral angle of the least-square cyclopentadienyl planes, and τ is the torsion angle C21-Cg1-Cg2-C26, where Cg1 and Cg2 stand for the centroids of the cyclopentadienyl rings C(21-25) and C(26-30), respectively. n.a. = not applicable [b] Parameters of the ferrocene unit are given in the dominating orientation.

Copies of the NMR spectra

(Note: solvent signals in the NMR spectra are denoted by an asterisk.)

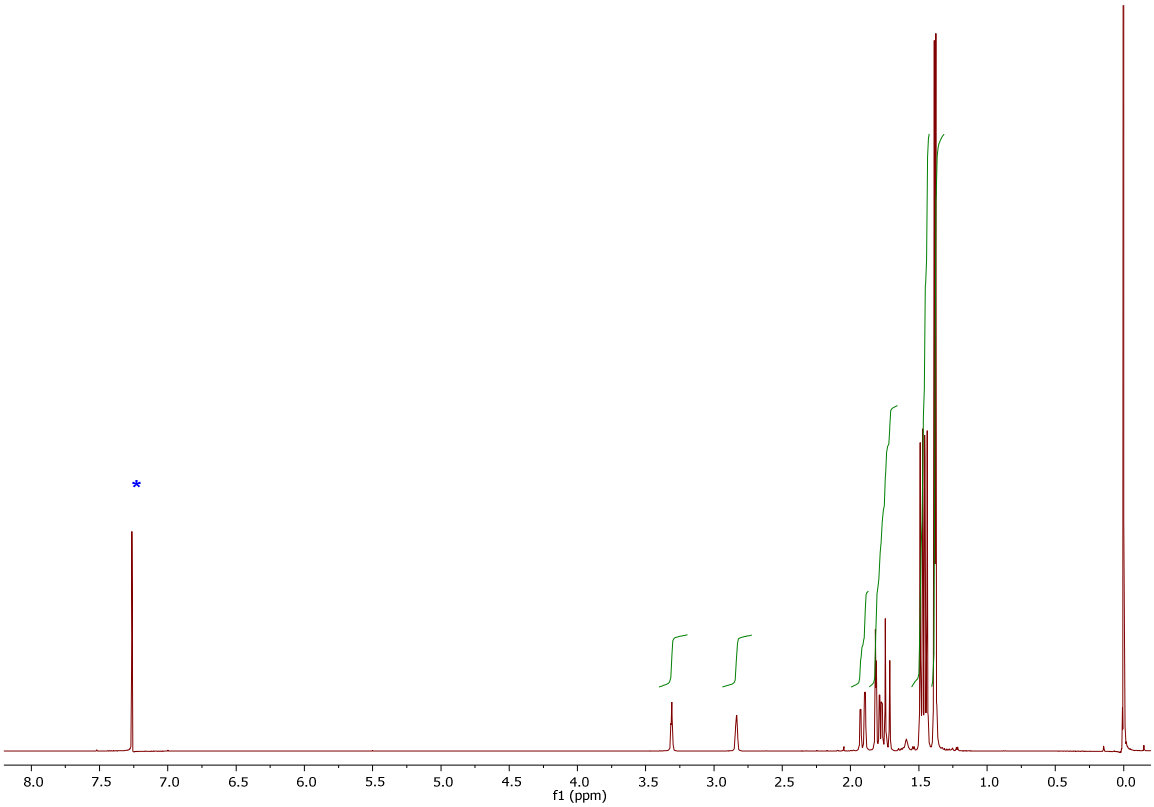

Figure S10. ^{1}H NMR spectrum (400 MHz, $CDCl_3$) of **CgPH**

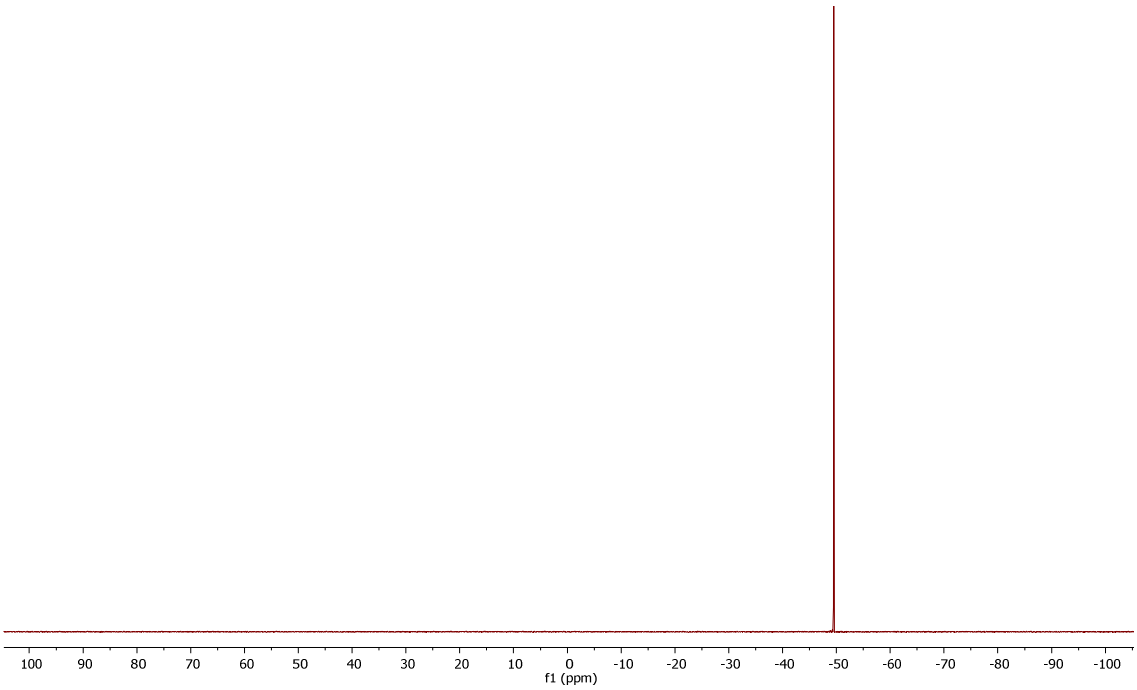

Figure S11. $^{31}P\{H\}$ NMR spectrum (162 MHz, $CDCl_3$) of **CgPH**

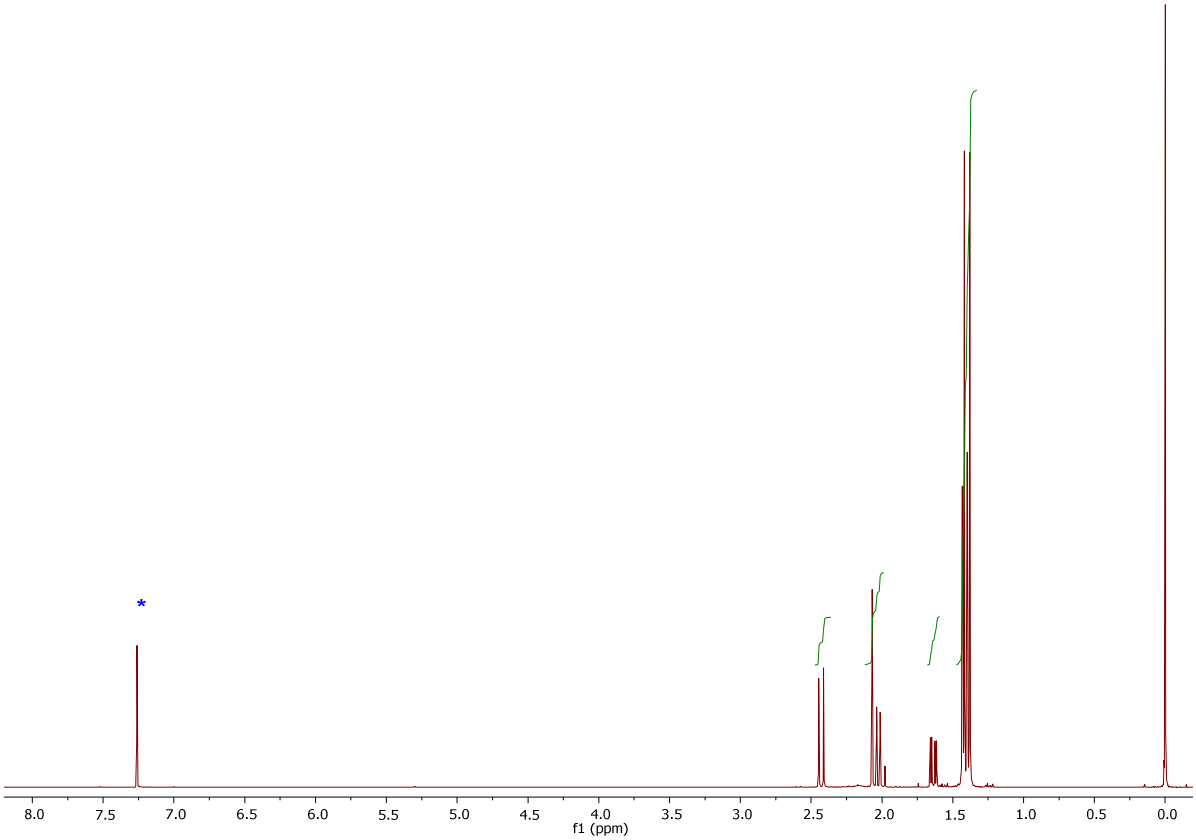

Figure S12. ^{1}H NMR spectrum (400 MHz, $CDCl_3$) of **CgPBr**

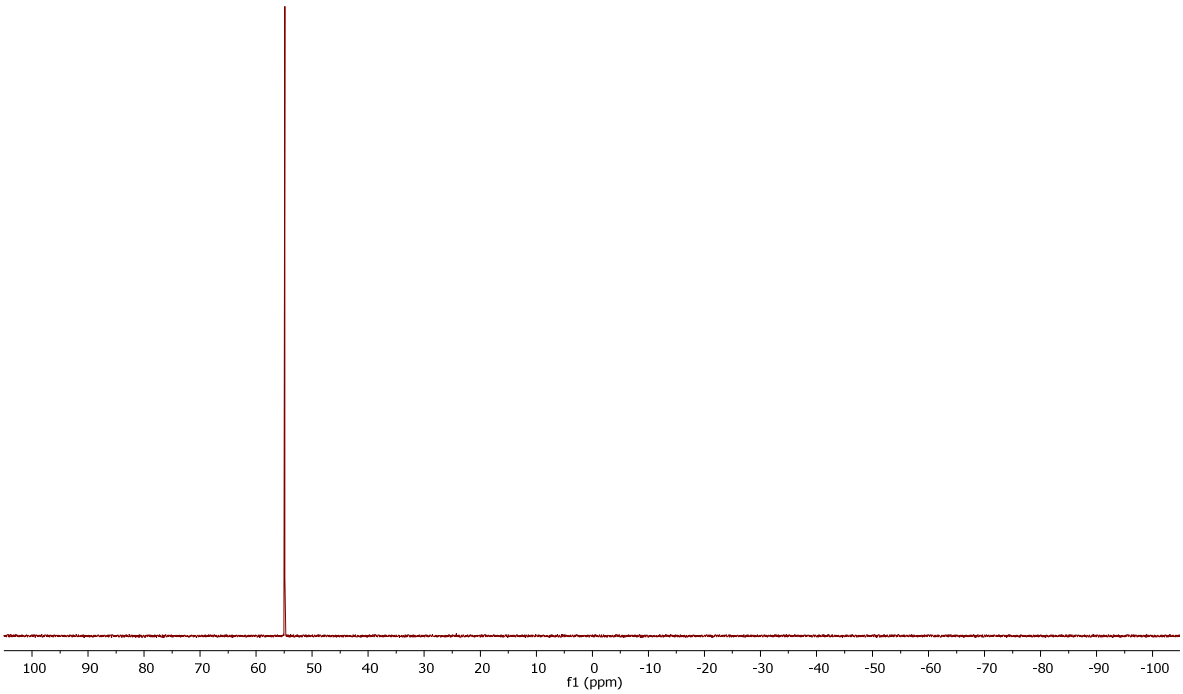

Figure S13. $^{31}P\{H\}$ NMR spectrum (162 MHz, $CDCl_3$) of **CgPBr**

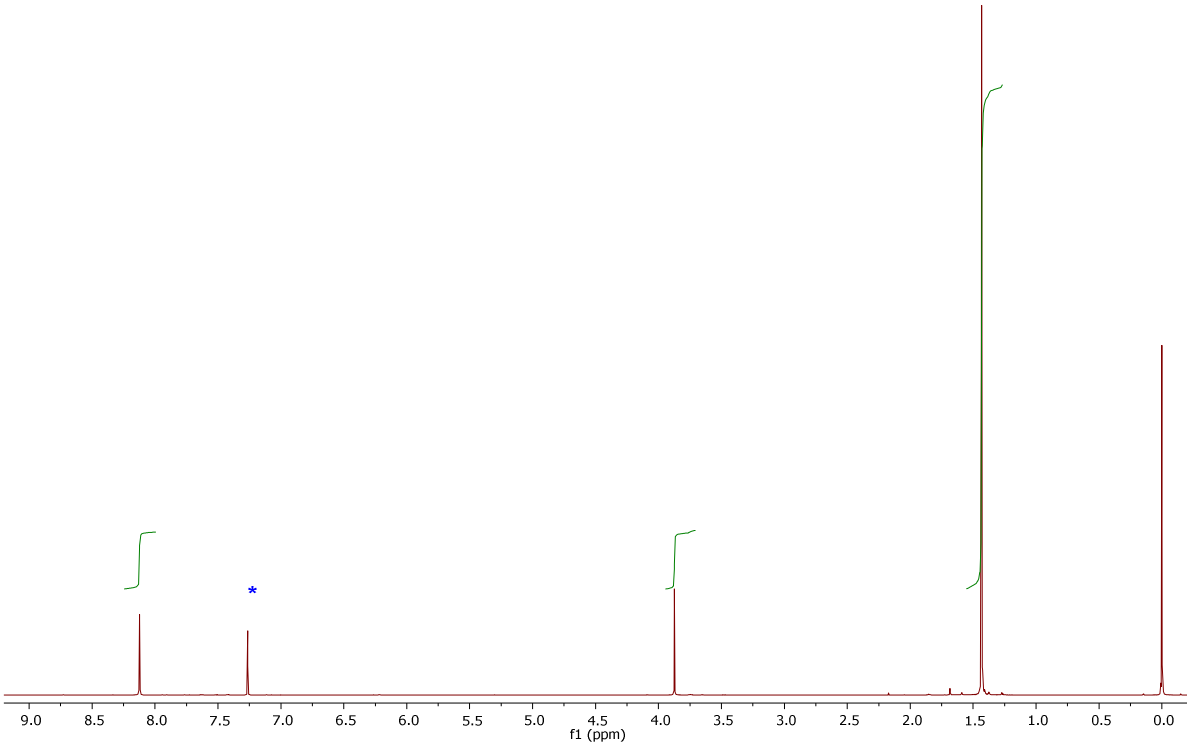

Figure S14. ^{1}H NMR spectrum (400 MHz, $CDCl_3$) of **[Pd(ma)(N^N)]**

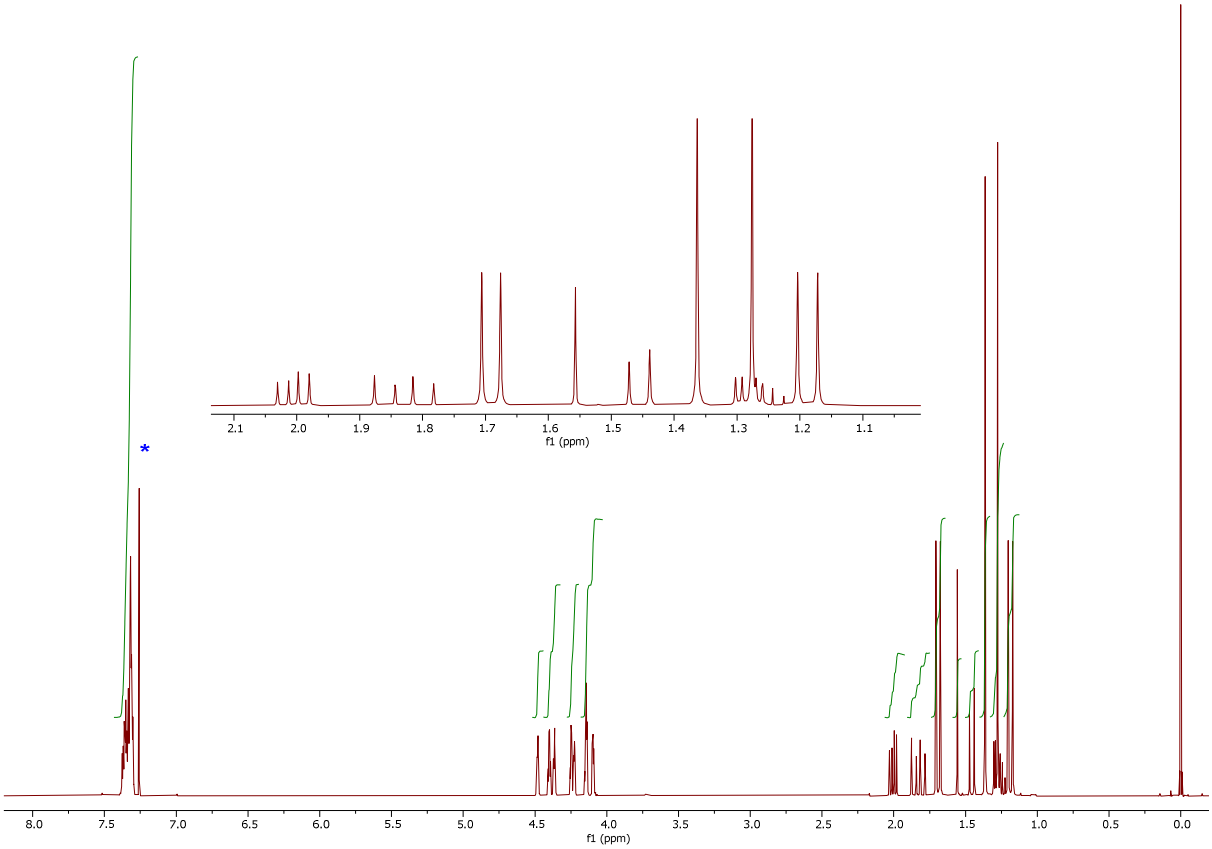

Figure S15. ^{1}H NMR spectrum (400 MHz, $CDCl_3$) of **1**

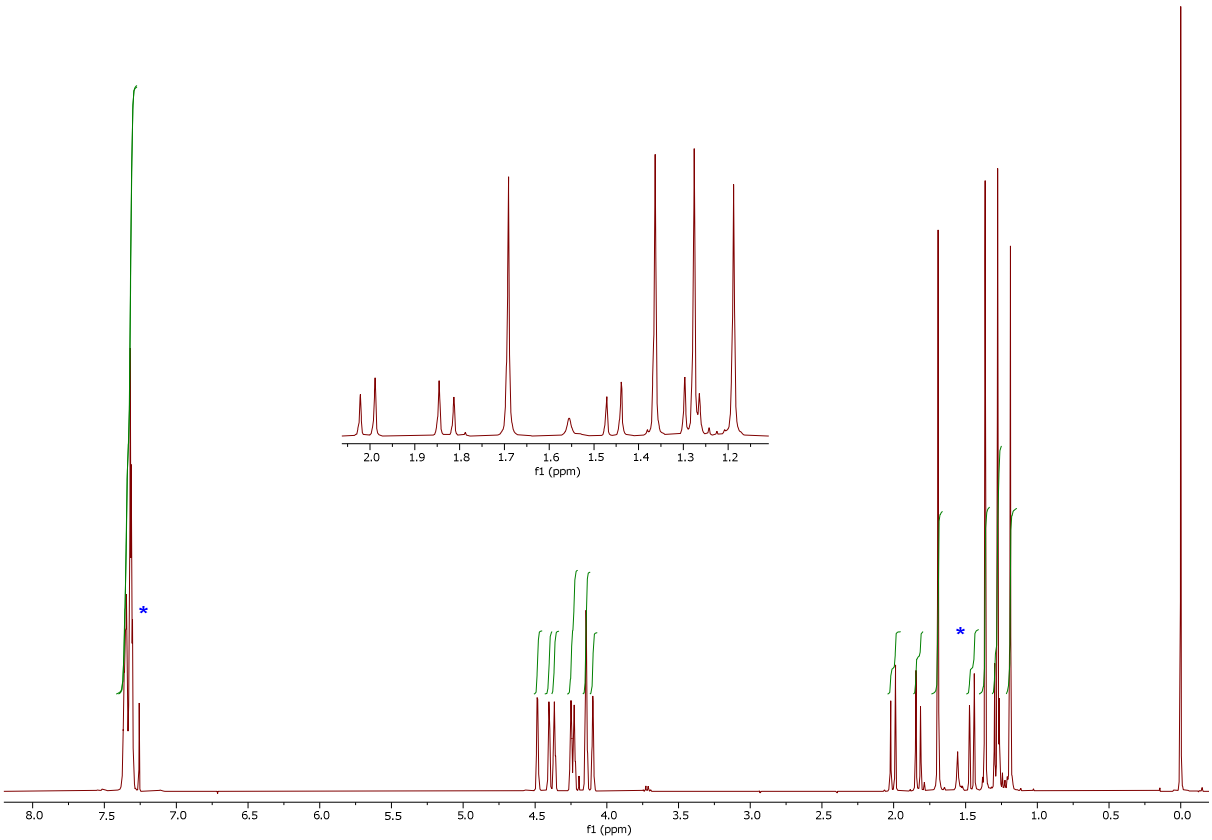

Figure S16. $^{1}H\{^{31}P\}$ NMR spectrum (400 MHz, $CDCl_3$) of **1**

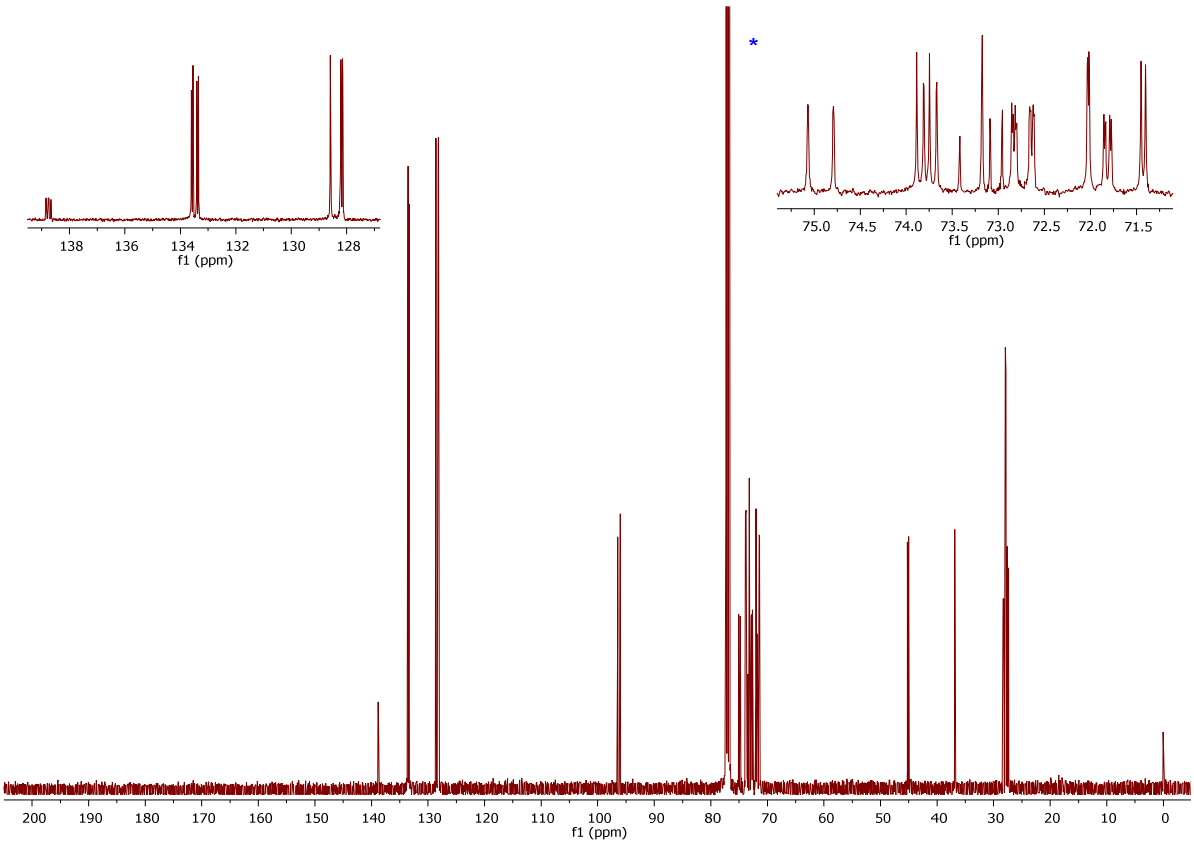

Figure S17. $^{13}C\{^{1}H\}$ NMR spectrum (101 MHz, $CDCl_3$) of **1**.

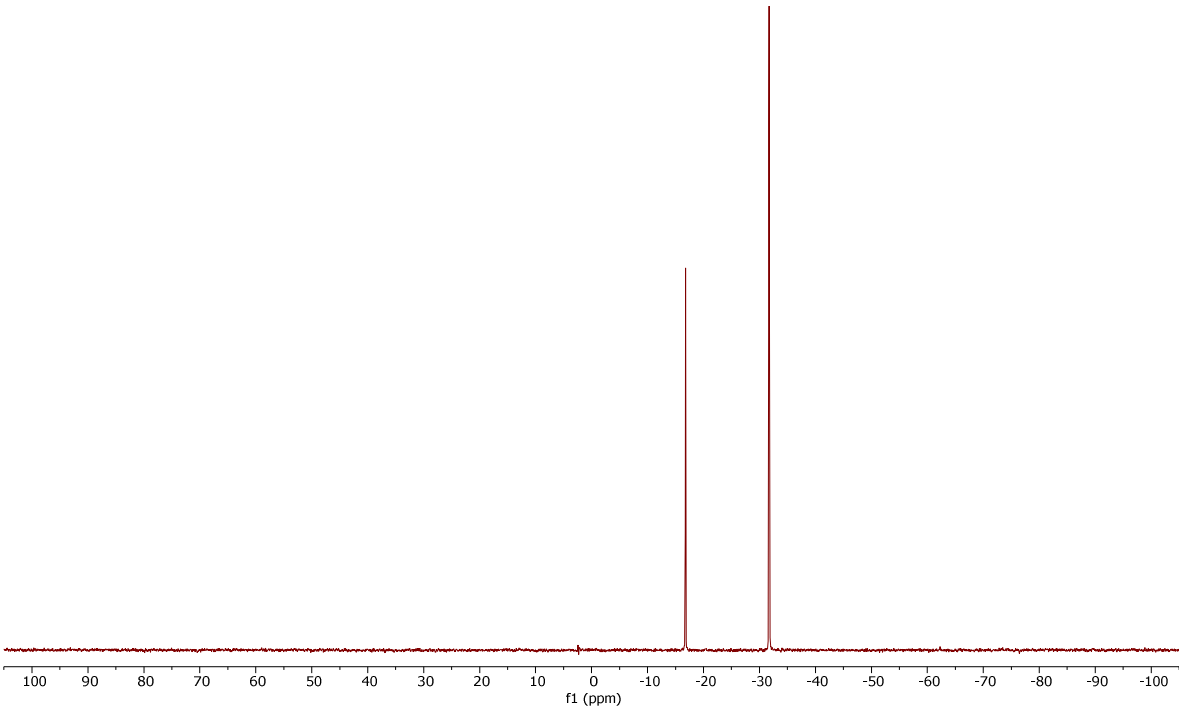

Figure S18. $^{31}P\{H\}$ NMR spectrum (162 MHz, $CDCl_3$) of **1**

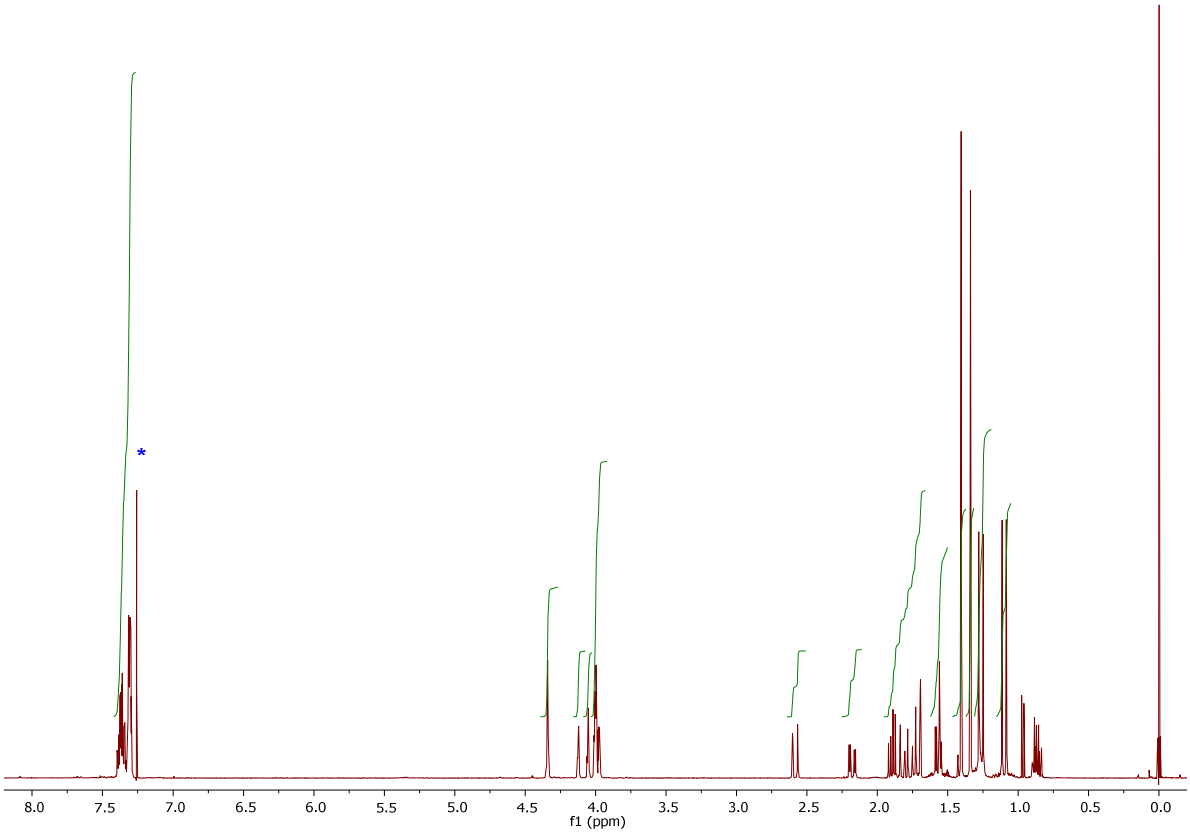

Figure S19. ^{1}H NMR spectrum (400 MHz, $CDCl_3$) of **2**

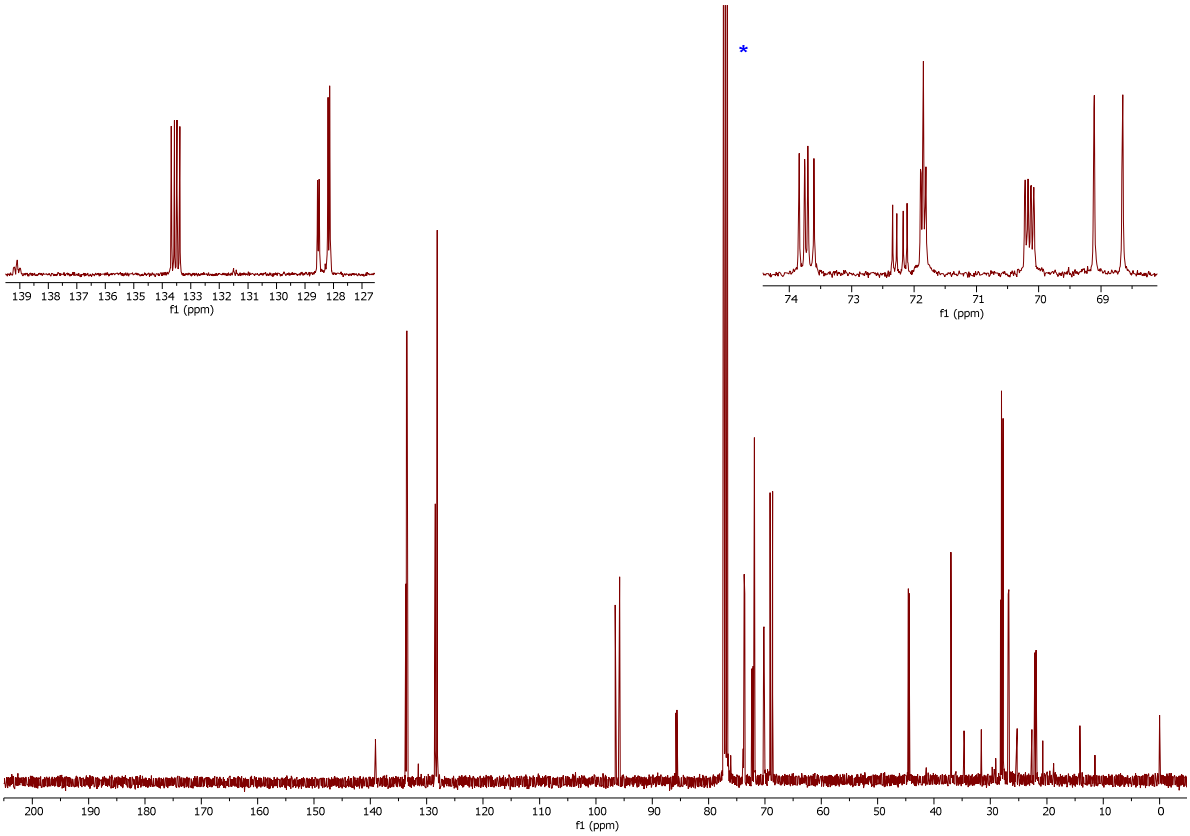

Figure S20. $^{13}C\{^{1}H\}$ NMR spectrum (101 MHz, $CDCl_3$) of **2**

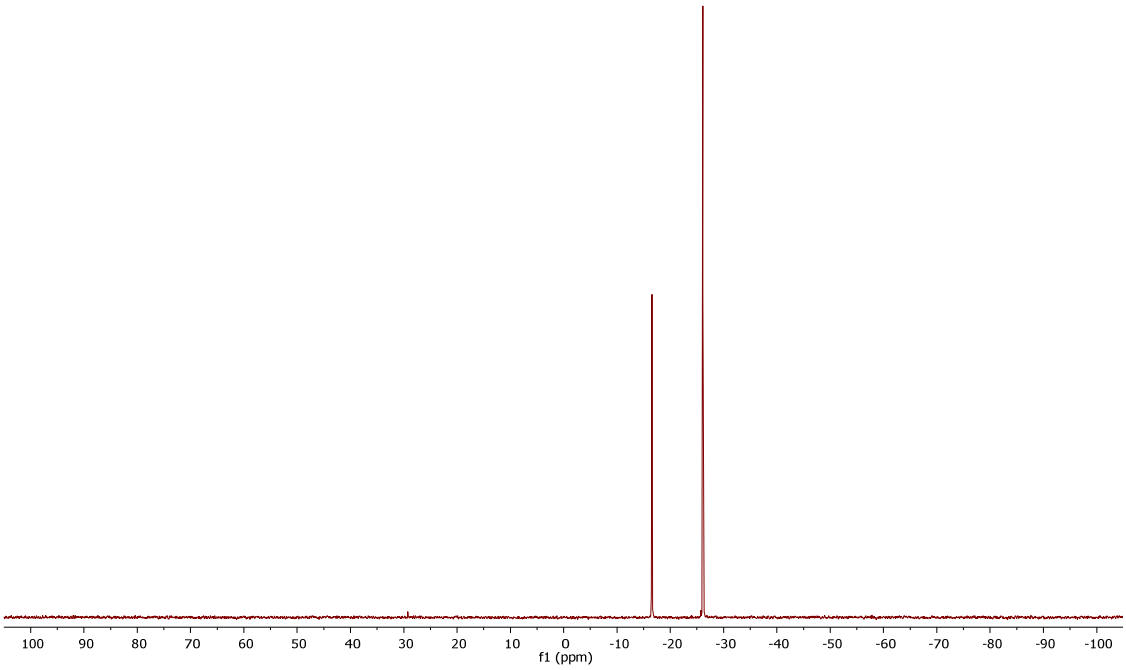

Figure S21. $^{31}P\{H\}$ NMR spectrum (162 MHz, $CDCl_3$) of **2**

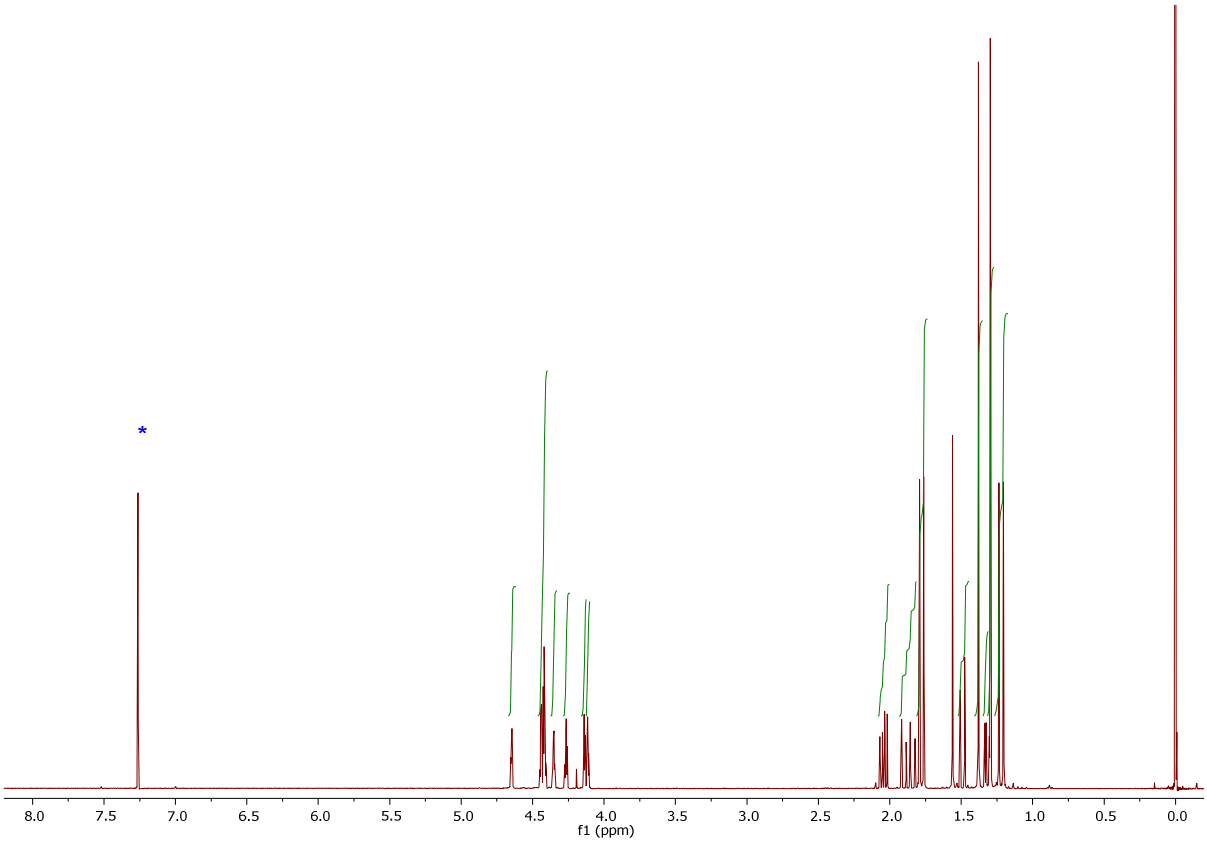

Figure S22. ^{1}H NMR spectrum (400 MHz, $CDCl_3$) of **5**.

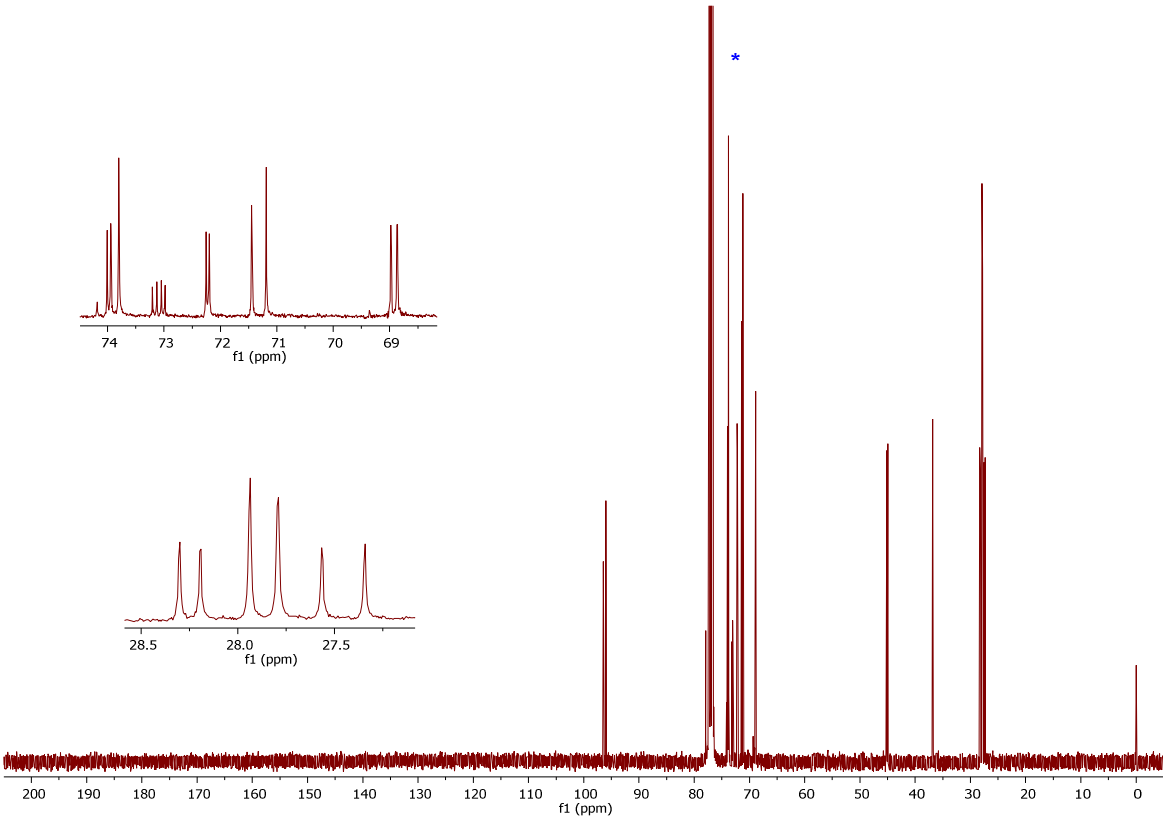

Figure S23. $^{13}C\{^{1}H\}$ NMR spectrum (101 MHz, $CDCl_3$) of **5**

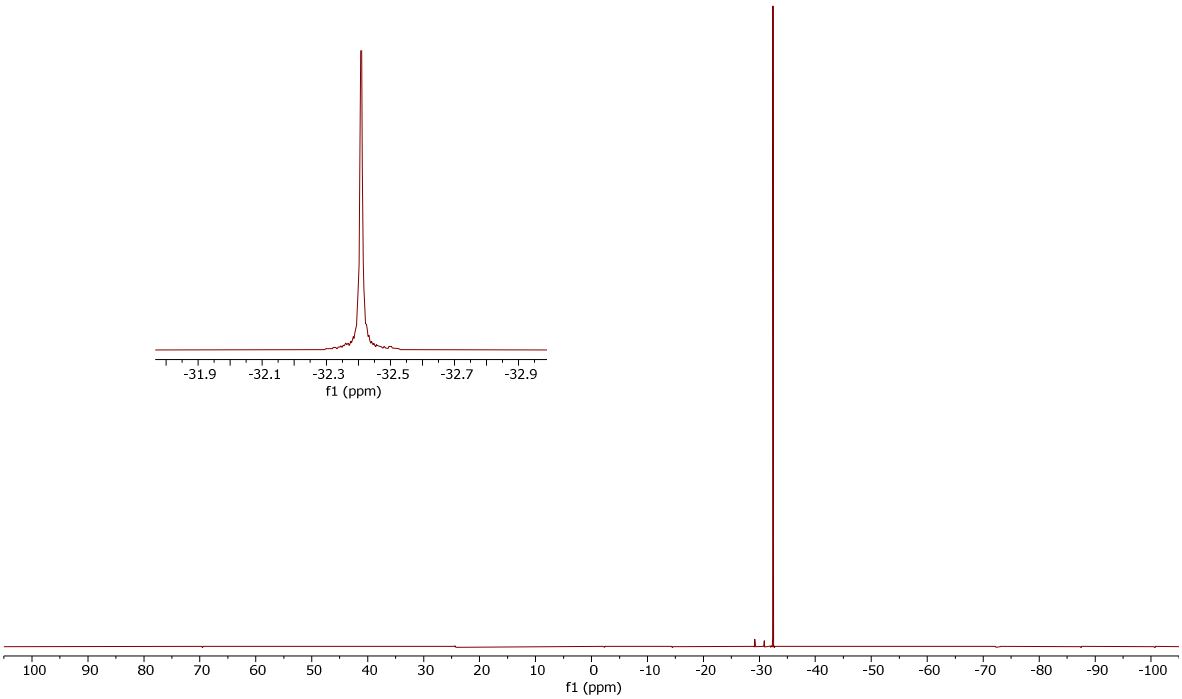

Figure S24. $^{31}P\{H\}$ NMR spectrum (162 MHz, $CDCl_3$) of **5**

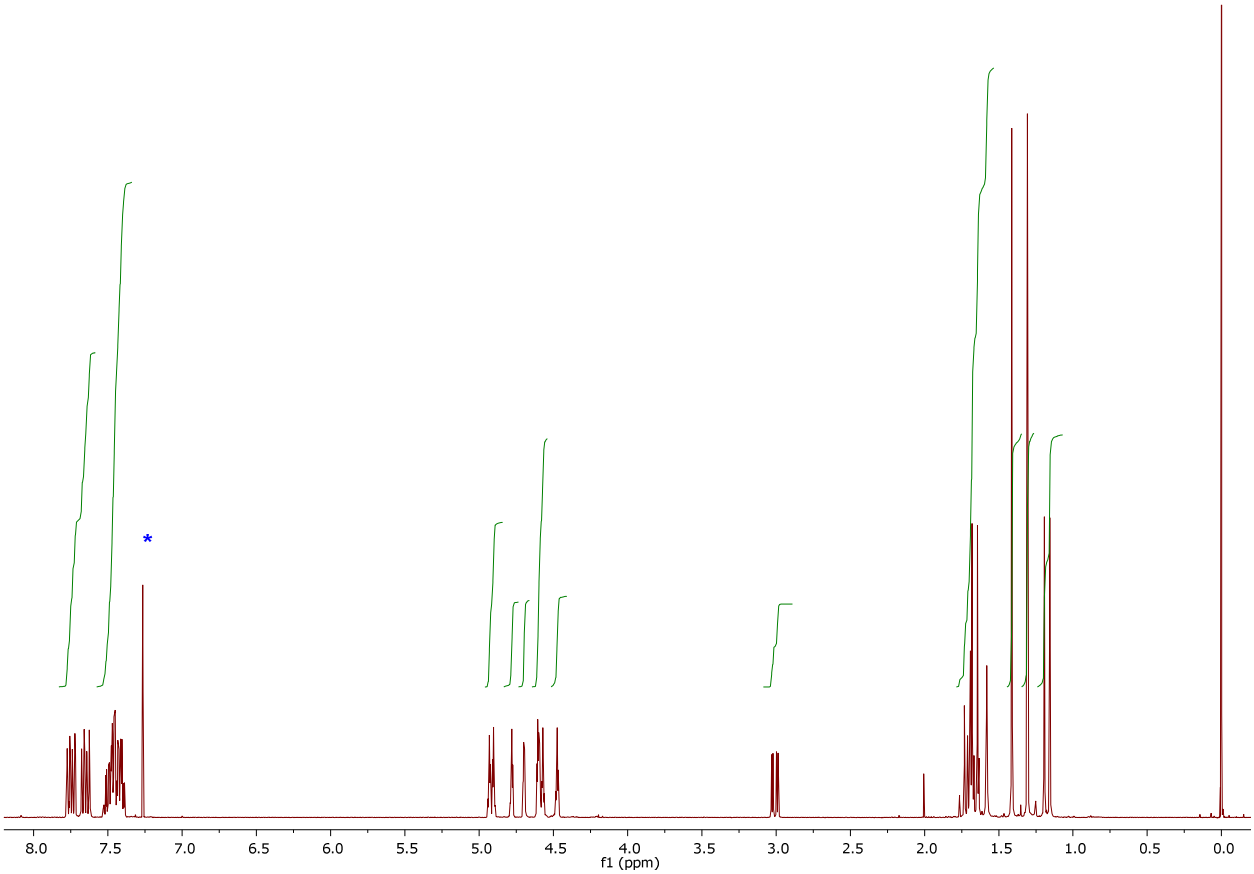

Figure S25. ^{1}H NMR spectrum (400 MHz, $CDCl_3$) of **1-Se**

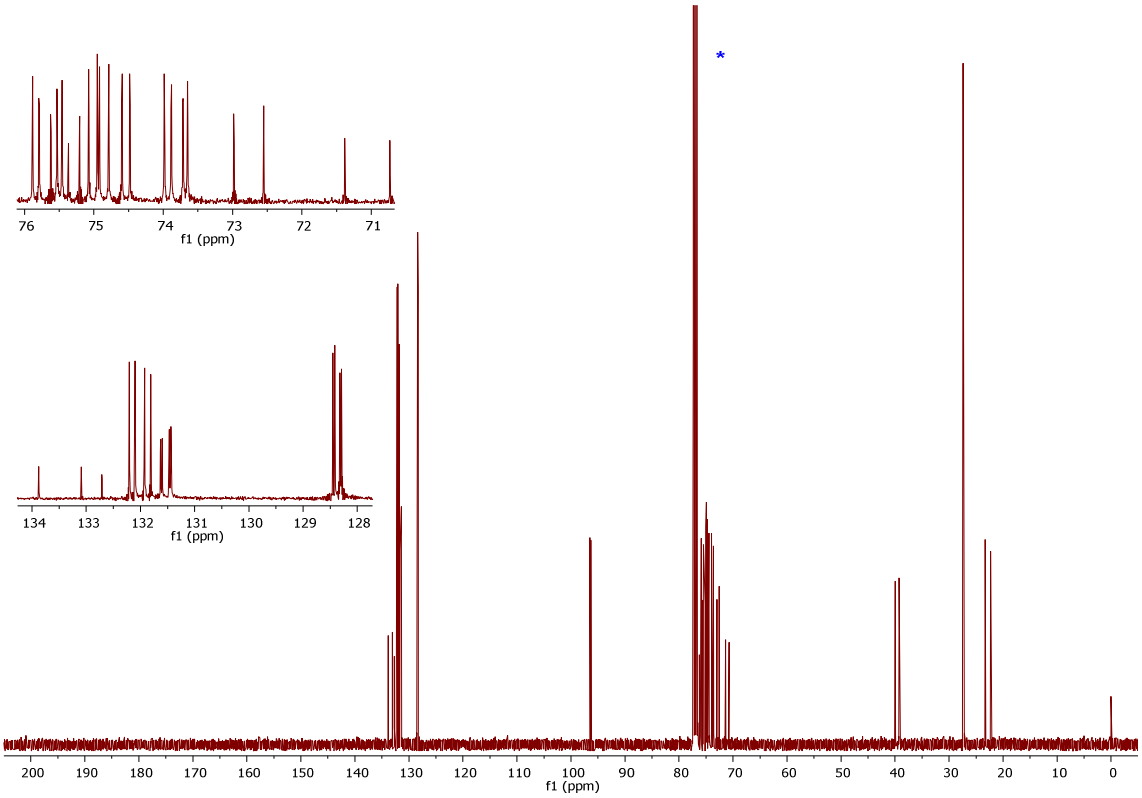

Figure S26. $^{13}C\{^{1}H\}$ NMR spectrum (101 MHz, $CDCl_3$) of **1-Se**

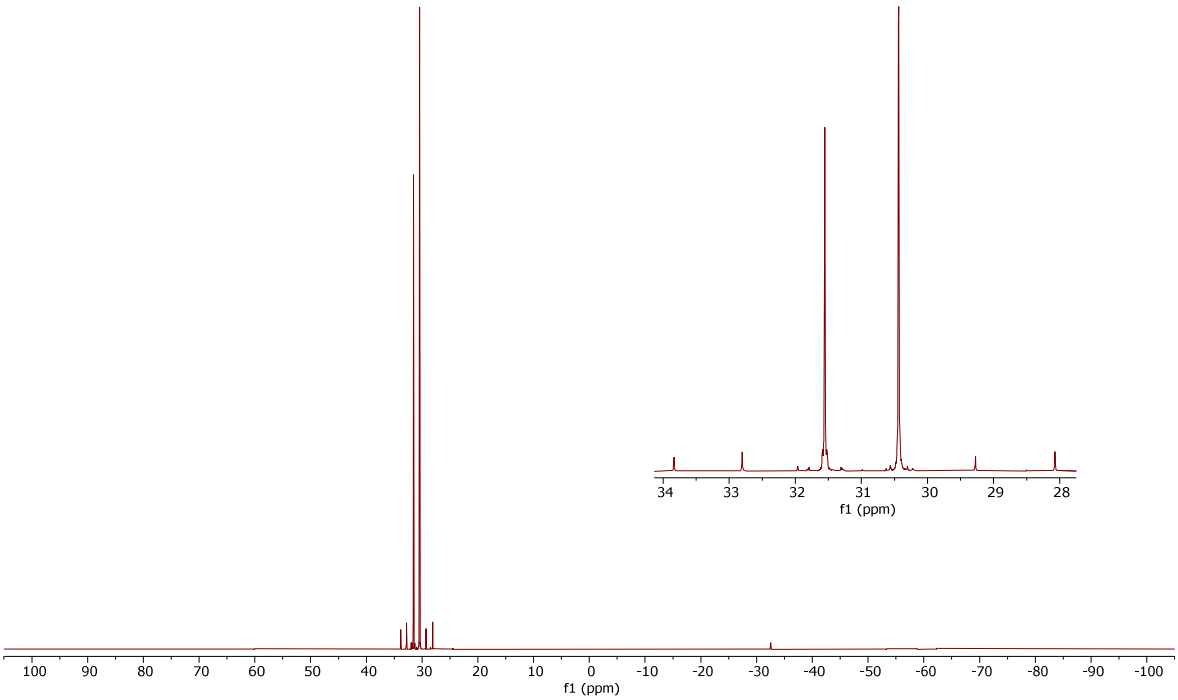

Figure S27. $^{31}P\{H\}$ NMR spectrum (162 MHz, $CDCl_3$) of **1-Se**

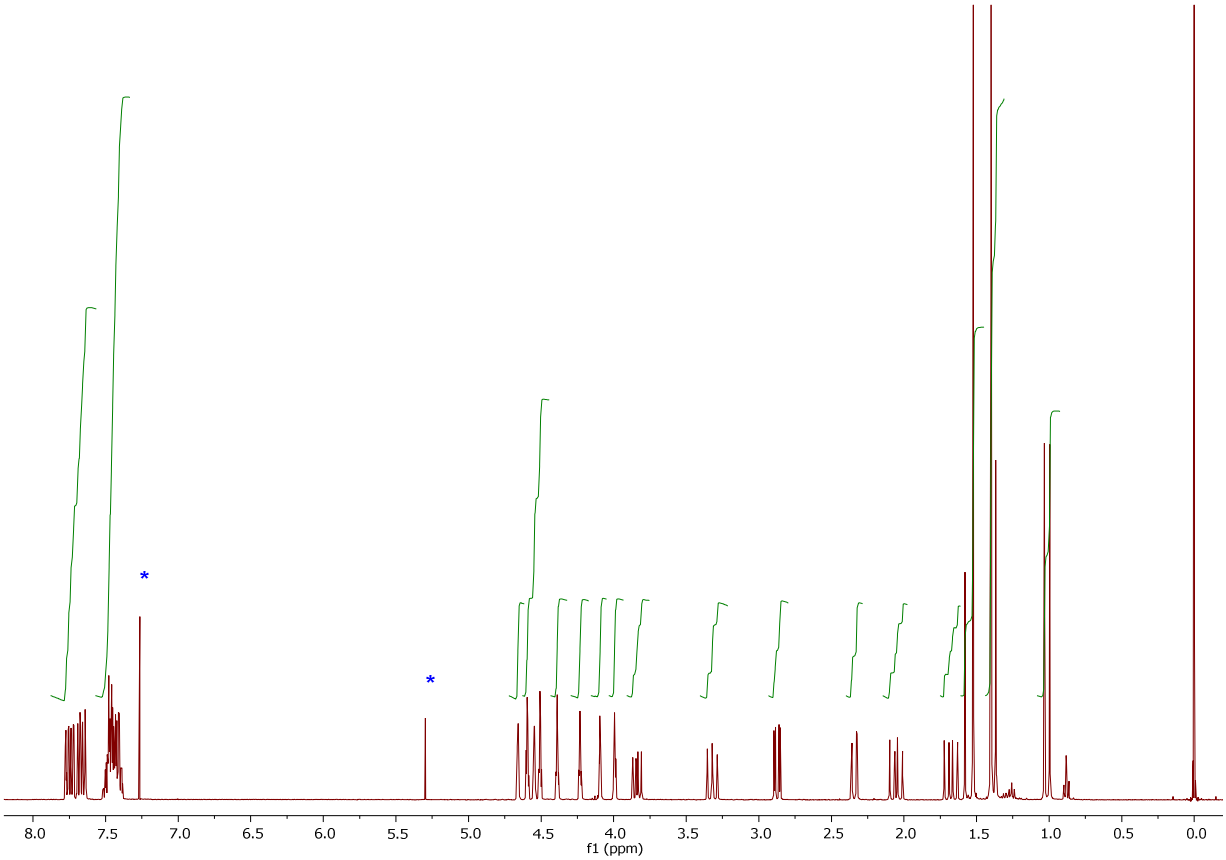

Figure S28. ^{1}H NMR spectrum (400 MHz, $CDCl_3$) of **2-Se**.

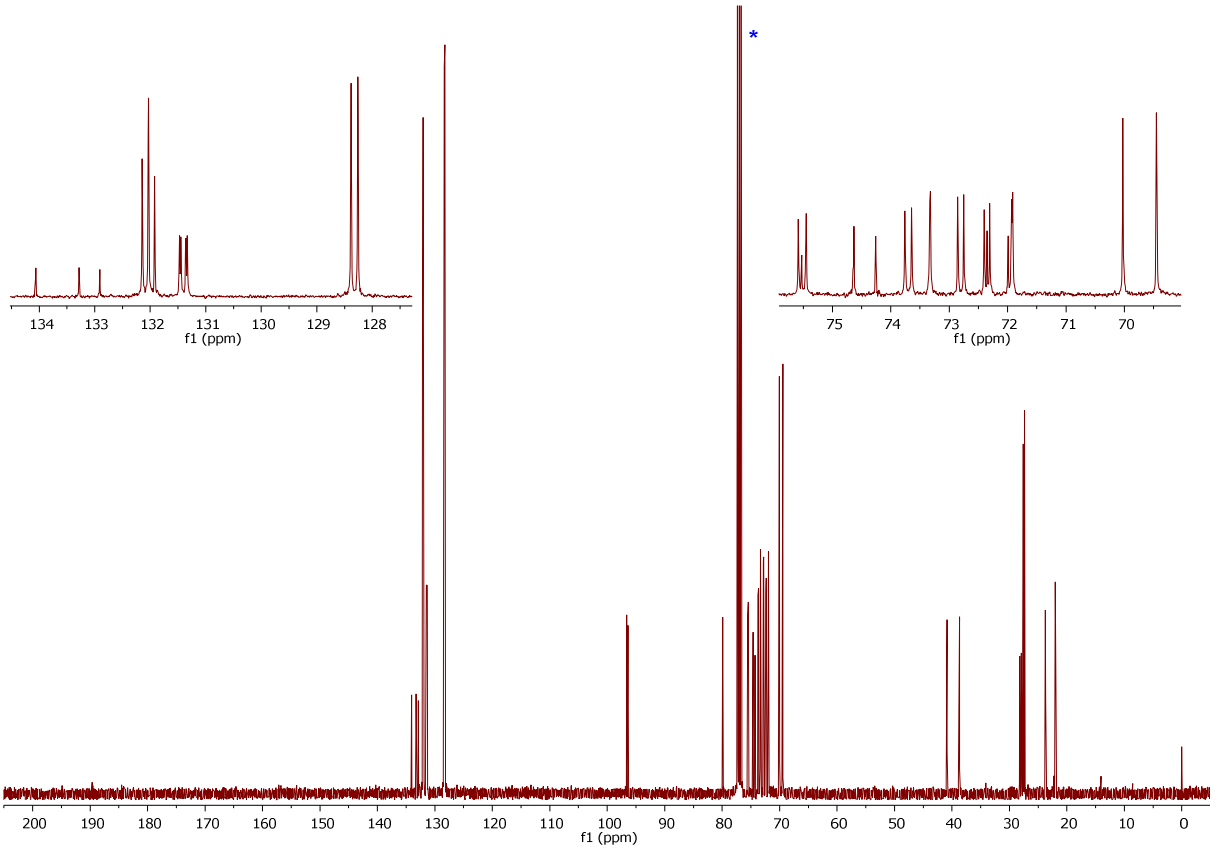

Figure S29. $^{13}C\{^{1}H\}$ NMR spectrum (101 MHz, $CDCl_3$) of **2-Se**

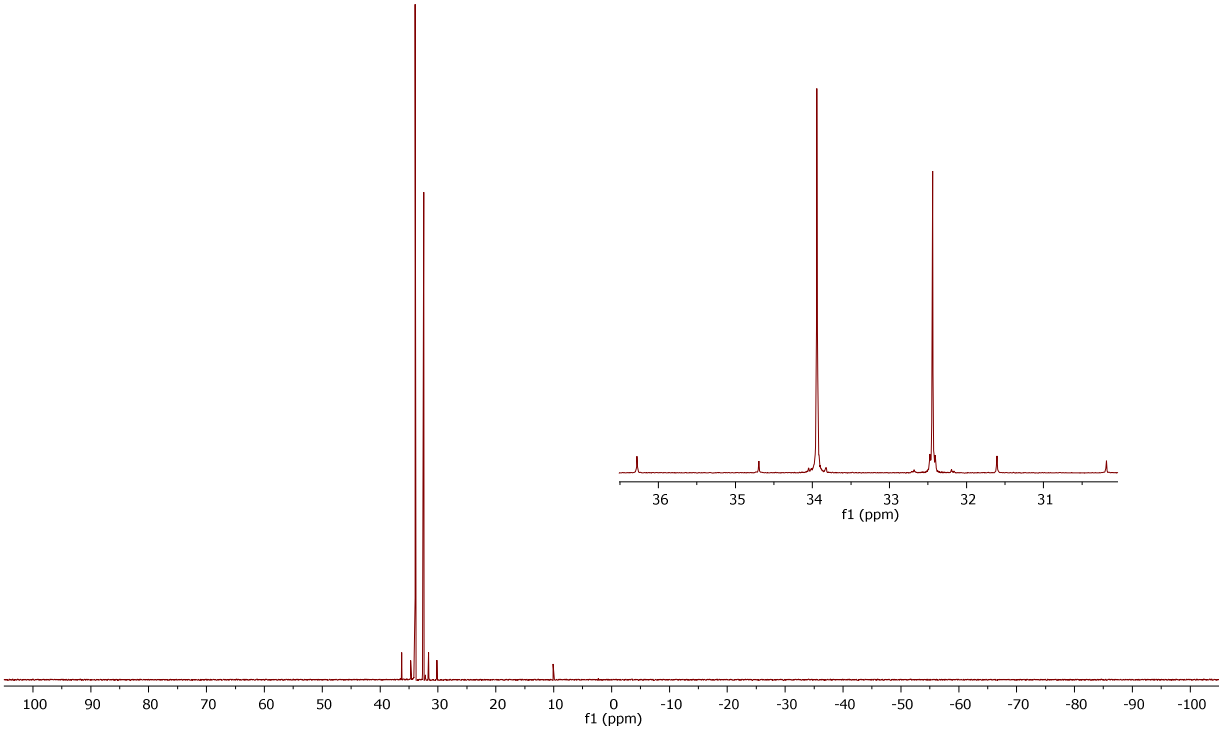

Figure S30. $^{31}P\{H\}$ NMR spectrum (162 MHz, $CDCl_3$) of **2-Se**

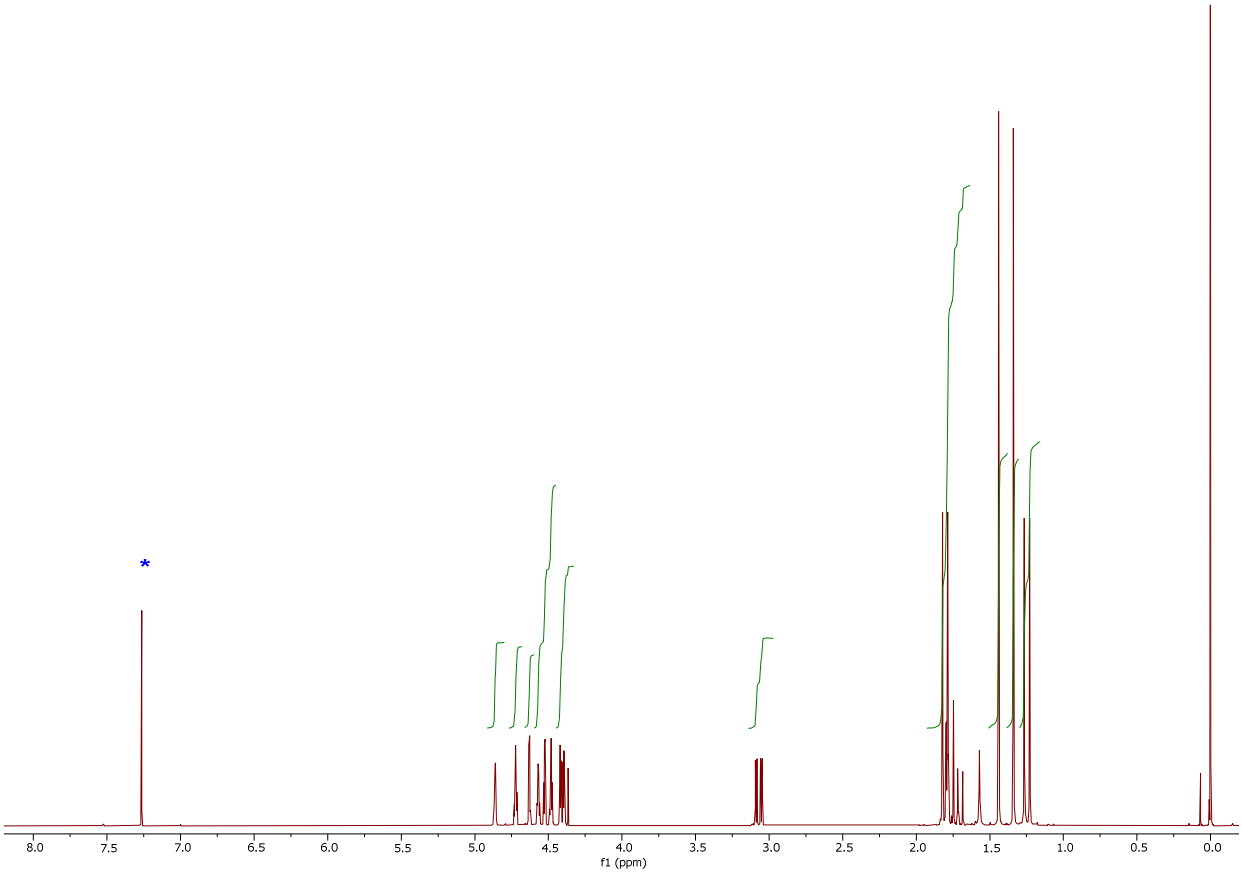

Figure S31. ^{1}H NMR spectrum (400 MHz, $CDCl_3$) of **5-Se**

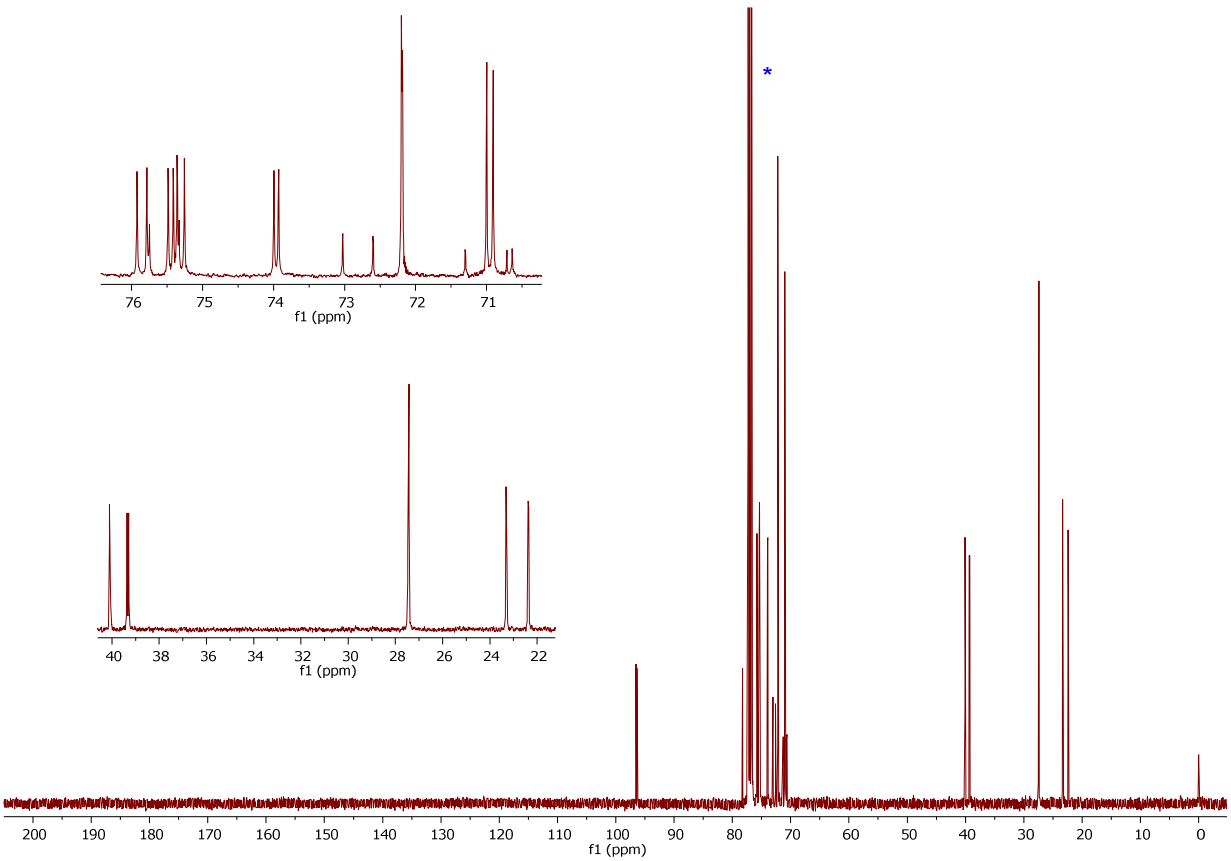

Figure S32. $^{13}C\{^{1}H\}$ NMR spectrum (101 MHz, $CDCl_3$) of **5-Se**

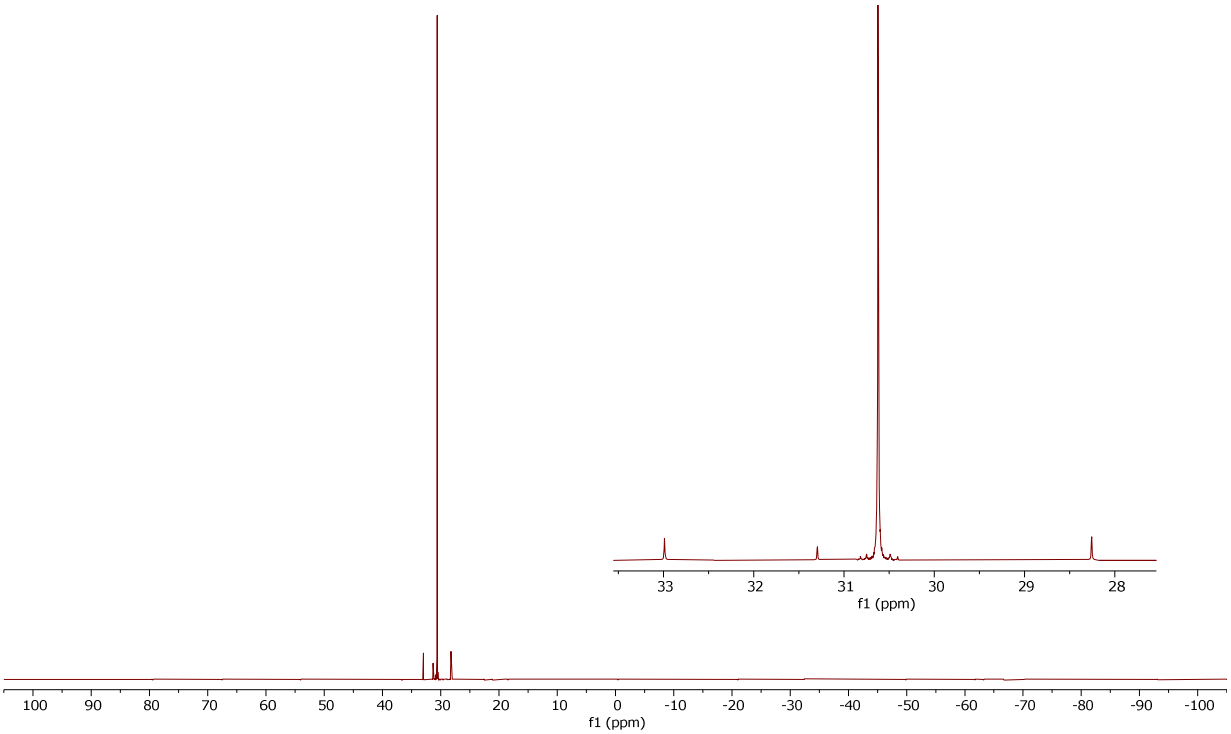

Figure S33. $^{31}P\{H\}$ NMR spectrum (162 MHz, $CDCl_3$) of **5-Se**

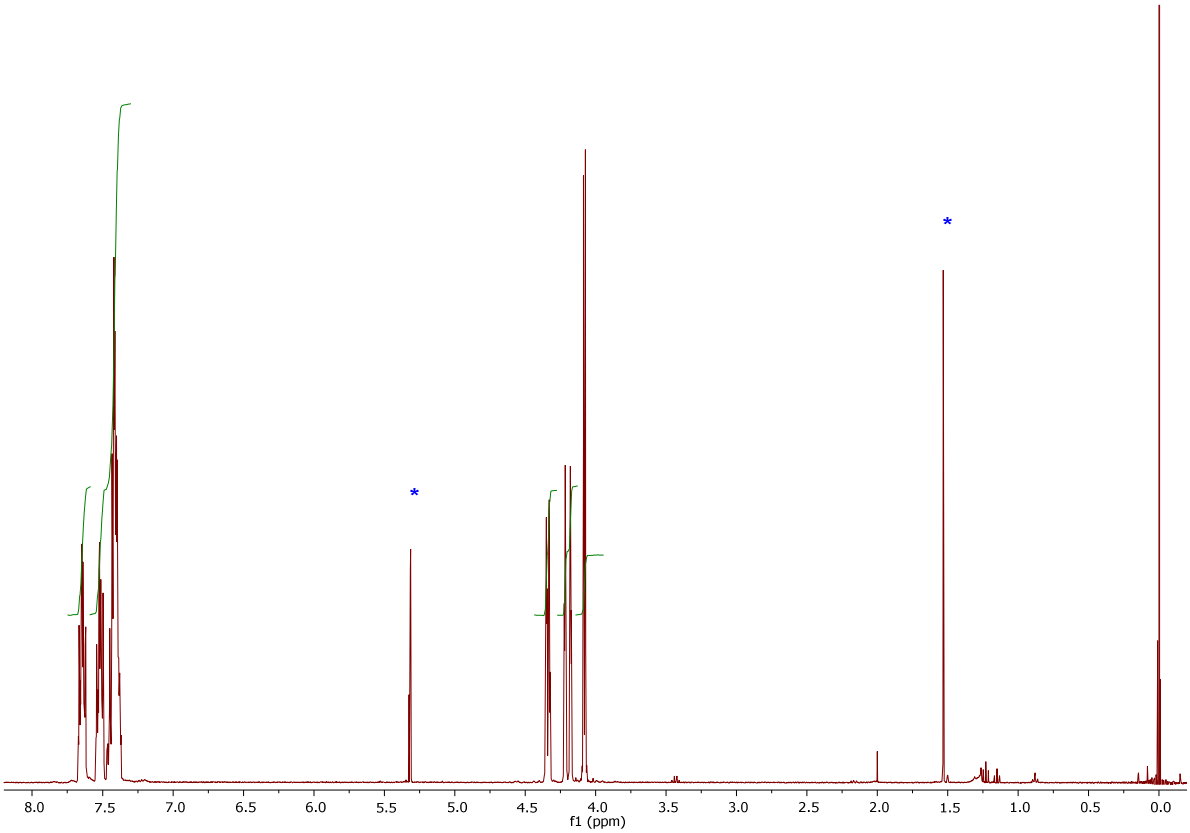

Figure S34. ^{1}H NMR spectrum (400 MHz, CD_2Cl_2) of **7**.

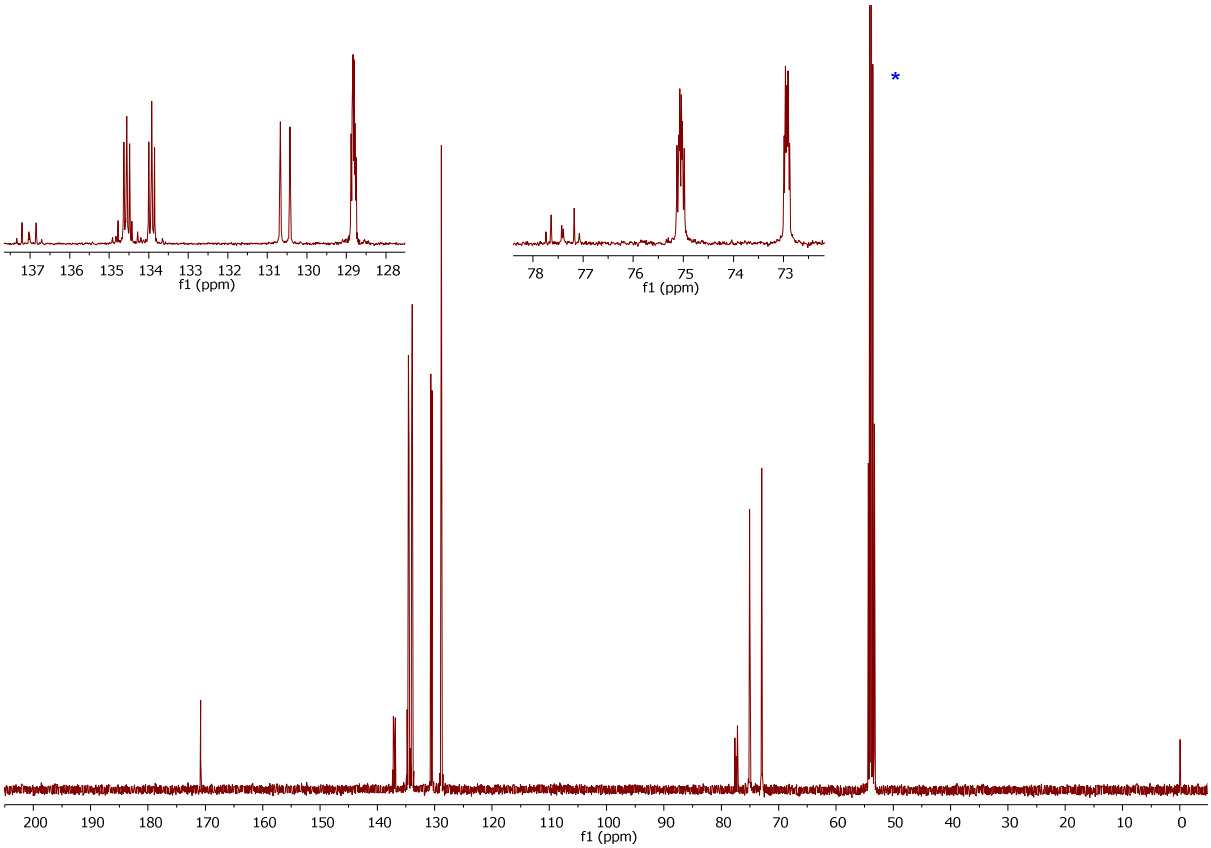

Figure S35. $^{13}C\{^{1}H\}$ NMR spectrum (101 MHz, CD_2Cl_2) of **7**

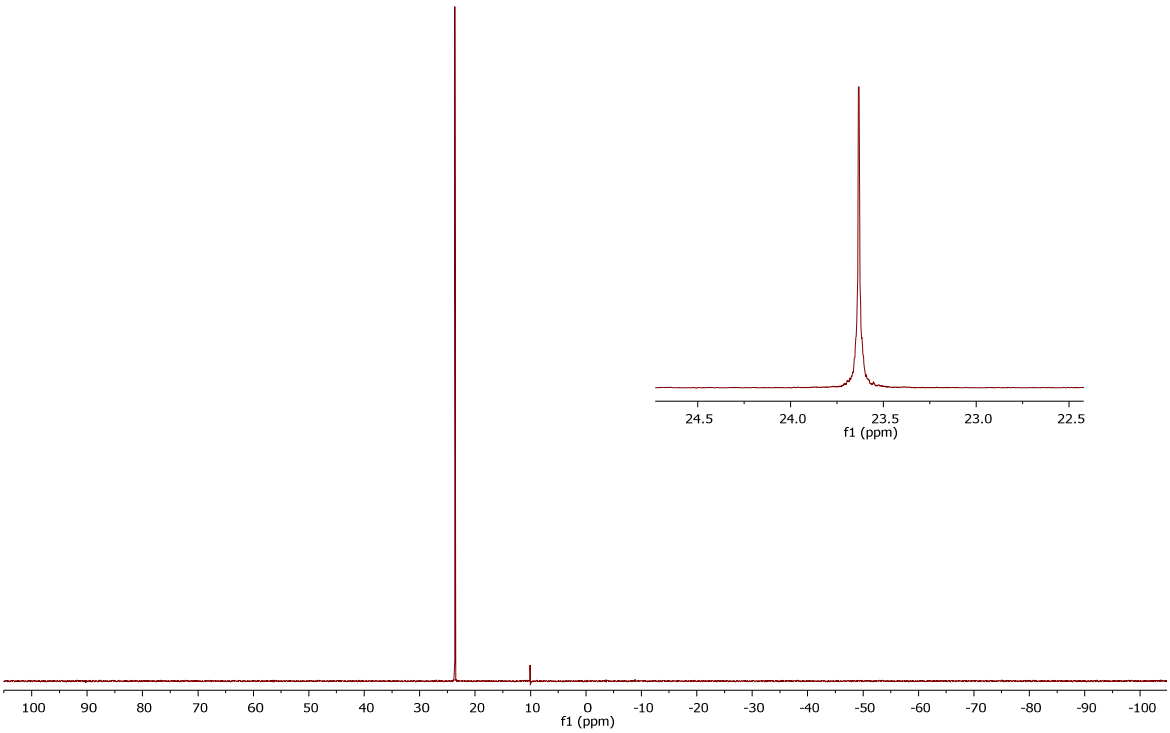

Figure S36. $^{31}P\{H\}$ NMR spectrum (162 MHz, CD_2Cl_2) of **7**

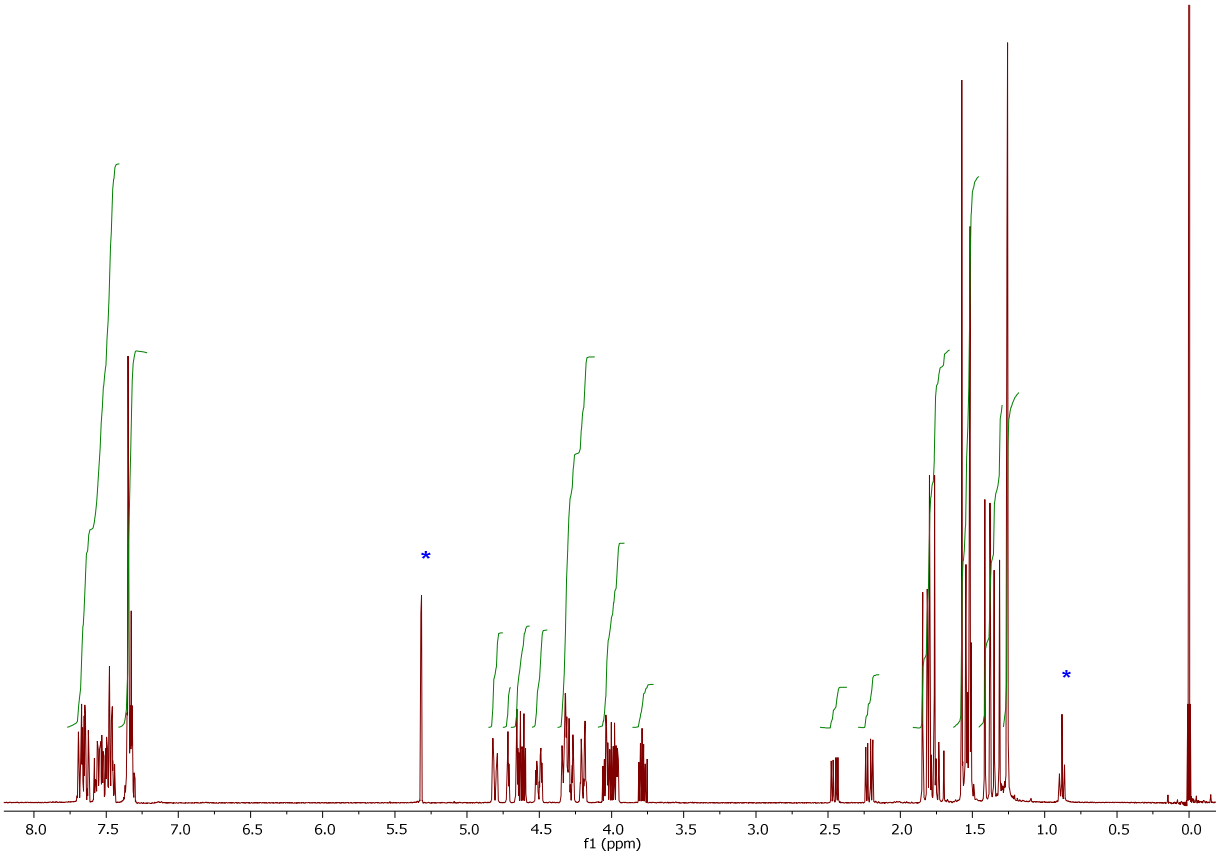

Figure S37. ^{1}H NMR spectrum (400 MHz, CD_2Cl_2) of **8**

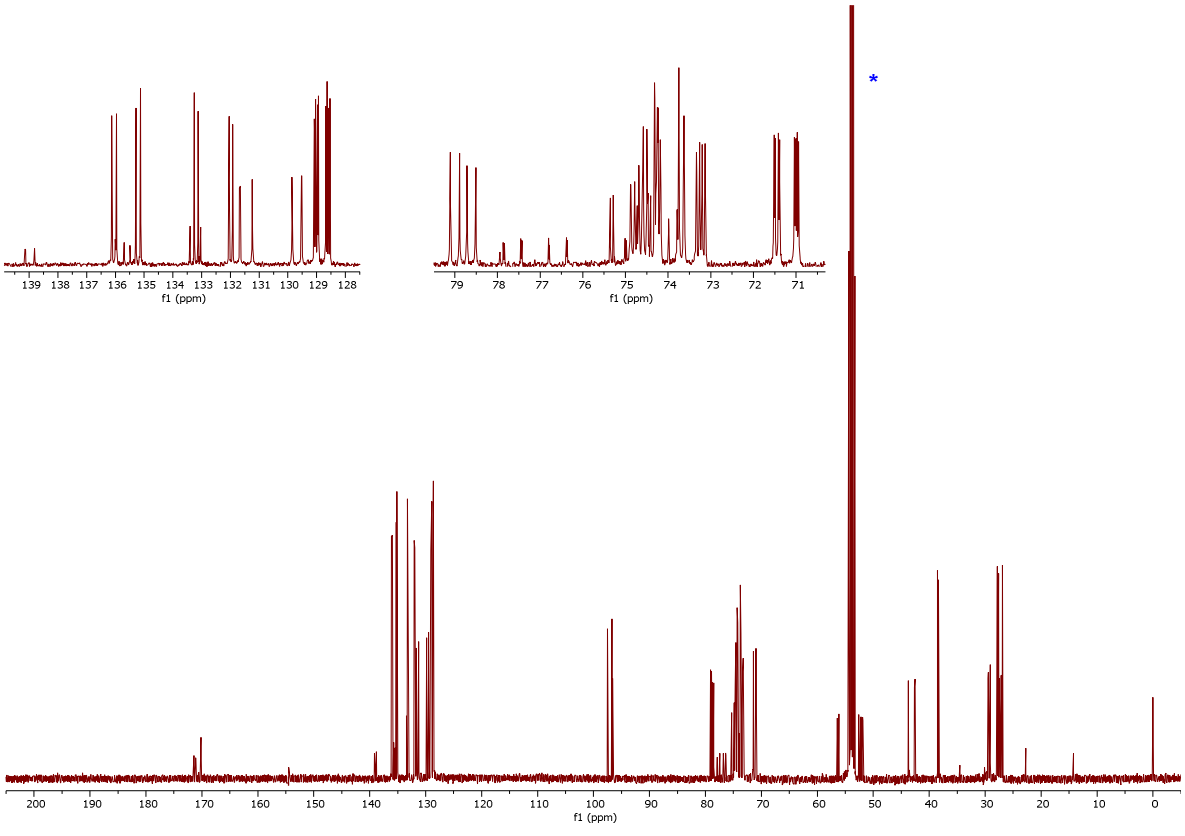

Figure S38. $^{13}C\{^{1}H\}$ NMR spectrum (101 MHz, CD_2Cl_2) of **8**

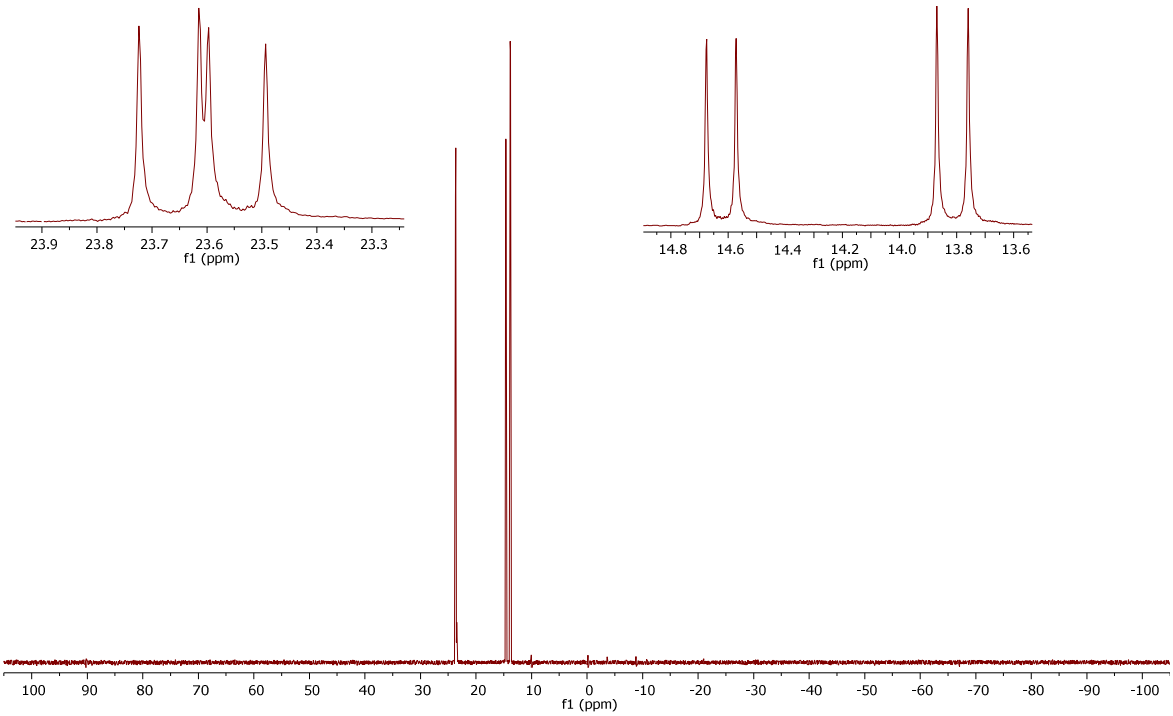

Figure S39. $^{31}P\{H\}$ NMR spectrum (162 MHz, CD_2Cl_2) of **8**

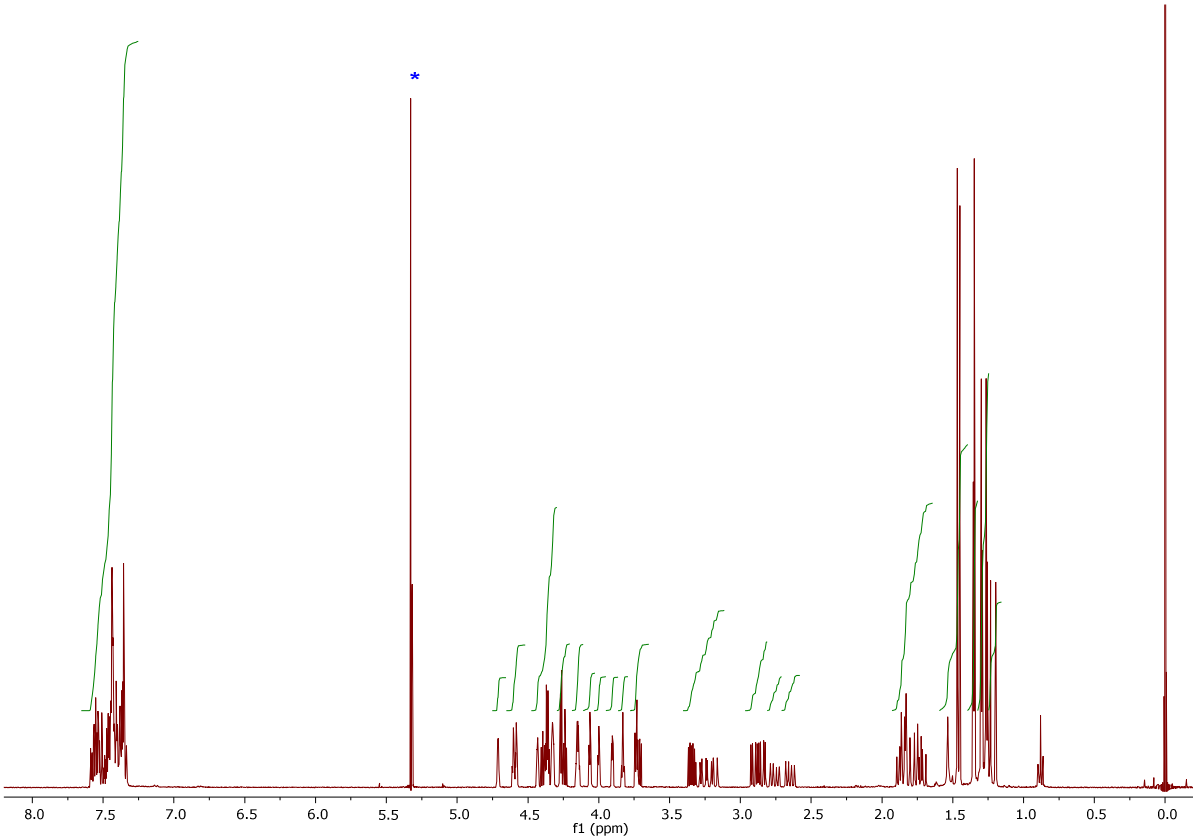

Figure S40. ^{1}H NMR spectrum (400 MHz, CD_2Cl_2) of **9**

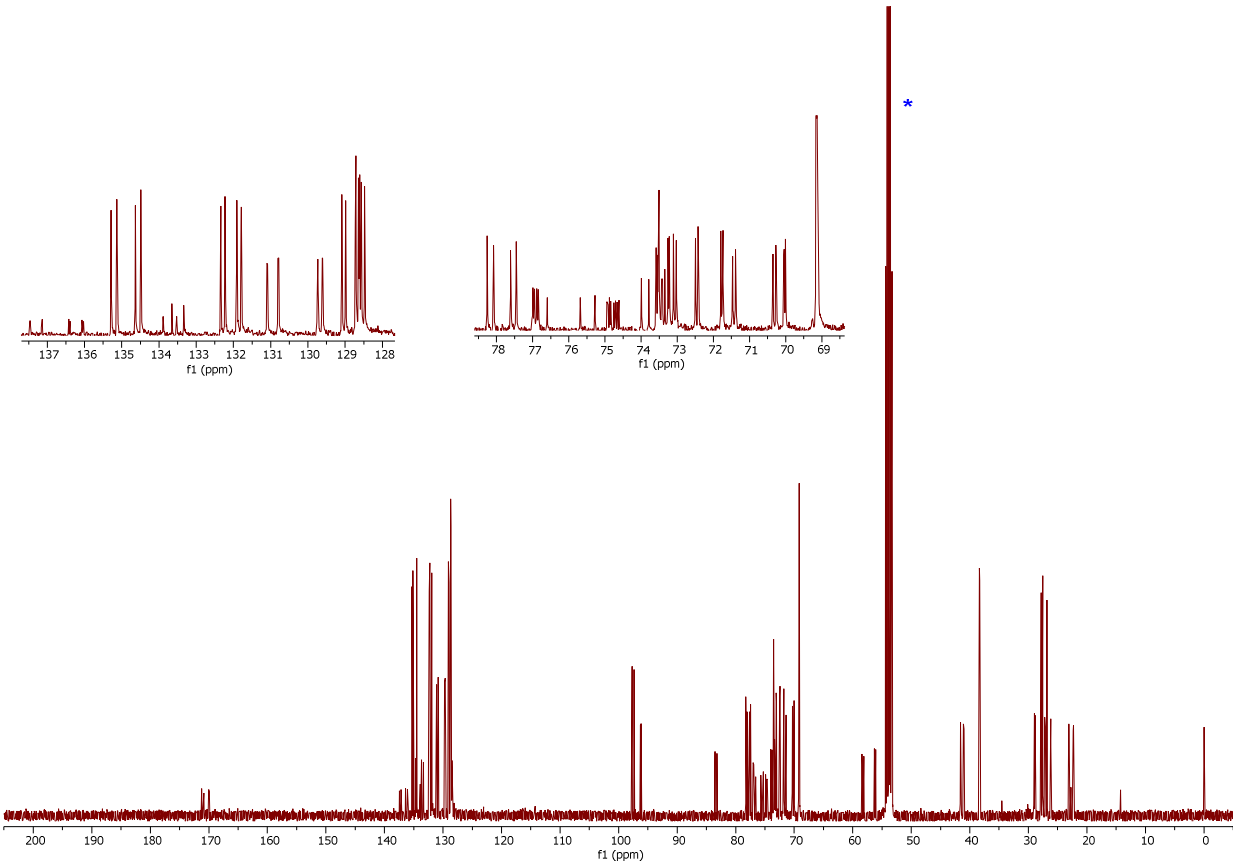

Figure S41. $^{13}C\{^{1}H\}$ NMR spectrum (101 MHz, CD_2Cl_2) of **9**

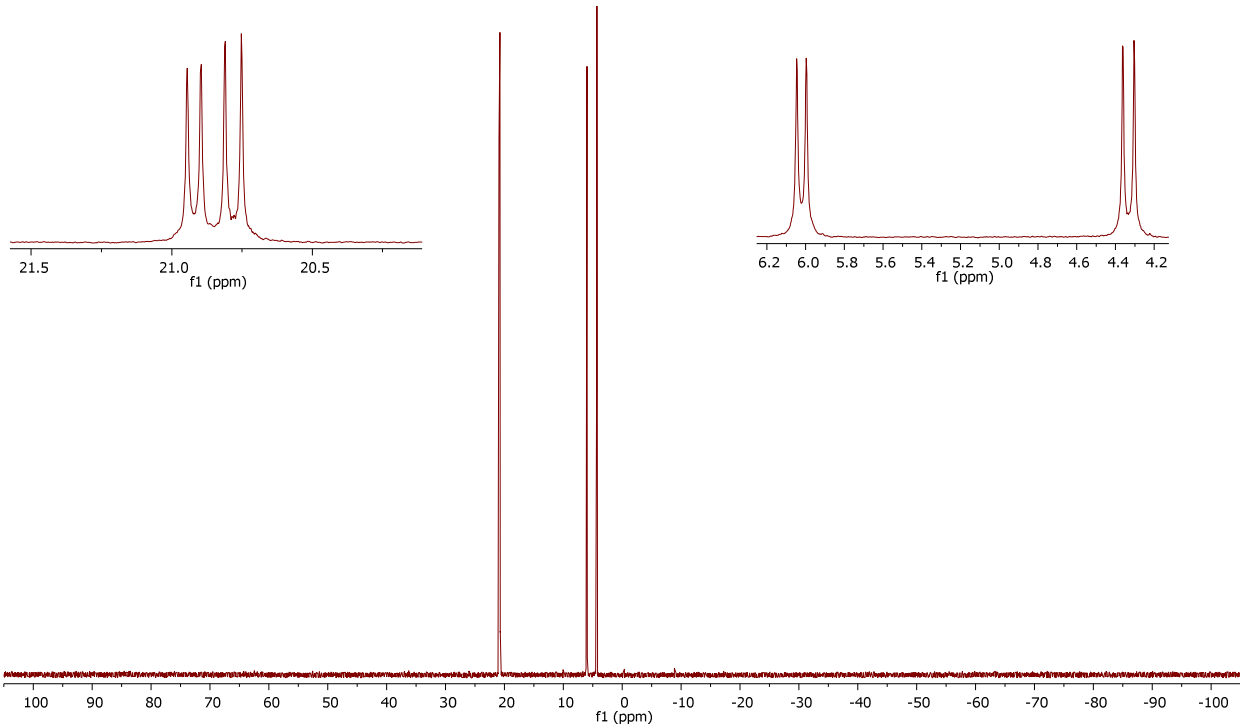

Figure S42. $^{31}P\{H\}$ NMR spectrum (162 MHz, CD_2Cl_2) of **9**

Catalytic experiments and analytical data of the coupling products

Screening experiments. A Schlenk flask was charged with the respective catalyst (1.5, 1.0 or 0.5 mol.% relative to **10**), benzoxazole **10a** (119 mg, 1.0 mmol), a base (2.0 mmol), chlorobenzene (169 mg, 1.5 mmol) and a magnetic stirring bar, flushed with argon and sealed with a rubber septum. *n*-Butanol (3 mL) was introduced, the septum was replaced for a glass stopper, and the flask was transferred to an oil bath maintained at 125°C. After stirring for 18 h, the reaction vessel was cooled to room temperature, and a small aliquot of the reaction mixture was analyzed by ^{1}H NMR spectroscopy to determine the conversion rate.

Preparative experiments. The reactions were performed as described above using catalyst **9** (0.5 or 1.0 mol.%), benzoxazole (1.0 mmol), aryl chloride (1.5 mmol), K_3PO_4 (1.5 mmol) and *n*-butanol (1 mL; N.B. a smaller amount of the solvent facilitates product isolation). After heating the mixture at 125°C for 18 h, the reaction mixture was cooled and diluted with water and diethyl ether (20 mL each). The organic layer was separated, and the aqueous layer was extracted with diethyl ether (20 mL). The combined organic extracts were dried over $MgSO_4$ and evaporated under reduced pressure with chromatographic silica gel (ca. 10 mL) to adsorb the crude product. Subsequent chromatographic purification was performed with a Reveleris® PREP Purification System (UV-vis detection: 254 nm, 265 nm, 280 nm) using silica gel columns (80 g column, 30 μm) and ethyl acetate-hexane mixtures with gradually increasing amount of the more polar solvent. Typically, a second band was collected and evaporated to produce the coupling product **12**. The eluent and other particular details are given below.

A: hexane-ethyl acetate (2% → 15%)
B: hexane-ethyl acetate (5% → 30%)
C: hexane-ethyl acetate (5% → 35%)
D:hexane-ethyl acetate (10% → 50%)

2-Phenylbenzoxazole (12aa)

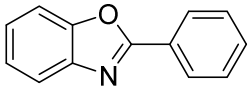

Eluent **A**. White crystalline solid. ^{1}H NMR (400 MHz, $CDCl_3$): δ = 7.33-7.38 (m, 2H, aromatics), 7.51-7.55 (m, 3H, aromatics), 7.58-7.62 (m, 1H, aromatics), 7.76-7.81 (m, 1H, aromatics), 8.24-8.29 (m, 2H, aromatics) ppm. ^{13}C{^{1}H} NMR (101 MHz, $CDCl_3$): δ = 111.6 ,120.0, 124.6, 125.1, 127.2, 127.6, 128.9, 131.5, 142.1, 150.8, 163.0 (s, aromatics) ppm.[7]

2-(4-Methylphenyl)benzoxazole (12ab)

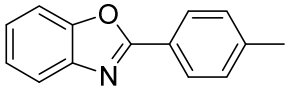

Eluent **A**. White crystalline solid. ^{1}H NMR (400 MHz, $CDCl_3$): δ = 2.44 (s, 3H, Me), 7.32-7.36 (m, 4H, aromatics), 7.57-7.59 (m, 1H, aromatics), 7.73-7.78 (m, 1H, aromatics), 8.13-8.16 (m, 2H, aromatics) ppm. ^{13}C{^{1}H} NMR (101 MHz, $CDCl_3$): δ = 21.7 (s, Me), 110.5, 119.8, 124.3, 124.5, 124.9, 127.6, 129.6, 142.1, 150.7, 163.3 (s, aromatics) ppm.[8]

2-[4-(Trifluoromethyl)phenyl]benzoxazole (12ac)

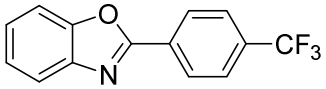

Eluent **A**. White crystalline solid. This compound is known. **[2]** ^{1}H NMR (400 MHz, $CDCl_3$): δ = 7.37-7.43 (m, 2H, aromatics), 7.59-7.64 (m, 1H, aromatics), 7.78-7.83 (m, 3H, aromatics), 8.37-8.39 (m, 2H, aromatics) ppm. ^{13}C{^{1}H} NMR (101 MHz, $CDCl_3$): δ = 110.8, 120.4, 122.4, 124.9, 125.0, 125.1, 125.8 (s, aromatics), 125.9 (q, $^{2}J_{FC}$ = 4 Hz, aromatics), 127.9, 128.9 (s, aromatics), 133.05 (s, aromatics), 146.4 (q, $^{1}J_{FC}$ = 901 Hz, CF_3) ppm. ^{19}F NMR (376 MHz, $CDCl_3$): δ = −63.0 (s) ppm.[8]

2-[2-(Methyl)phenyl]benzoxazole (12ad)

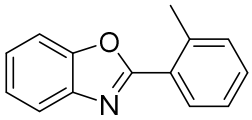

Eluent **A**. White crystalline solid. ^{1}H NMR (400 MHz, $CDCl_3$): δ = 2.82 (s, 3H, Me), 7.32-7.43 (m, 5H, aromatics), 7.57-7.61 (m, 1H, aromatics), 7.78-7.83 (m, 1H, aromatics), 8.16-8.19 (m, 1H, aromatics) ppm. ^{13}C{^{1}H} NMR (101 MHz, $CDCl_3$): δ = 22.2 (s, Me), 110.5, 120.1, 124.4, 125.0, 126.1, 126.2, 129.9, 130.9, 131.8, 138.8, 142.1, 150.3, 163.4 (s, aromatics) ppm.[8]

2-(3-Methylphenyl)benzoxazole (12af)

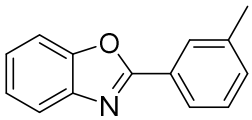

Eluent **A**. White crystalline solid. ^{1}H NMR (400 MHz, $CDCl_3$): δ = 2.46 (s, 3H, Me), 7.33-7.37 (m, 3H, aromatics), 7.41 (t, $^{3}J_{HH}$ = 7.6 Hz, 1H, aromatics), 7.56-7.60 (m, 1H, aromatics), 7.75-7.79 (m, 1H, aromatics), 8.04-8.07 (m, 1H, aromatics), 8.10-8.11 (br s, 1H, aromatics) ppm. ^{13}C{^{1}H} NMR (101 MHz, $CDCl_3$): δ = 21.4 (s, Me), 110.6, 120.0, 124.5, 124.8, 125.0, 127.0, 128.2, 128.8, 132.4, 138.7, 142.1, 150.7, 163.3 (s, aromatics) ppm.[8]

2-(1-Naphthyl)benzoxazole (12ag)

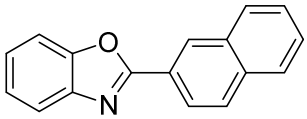

Eluent **A**. White crystalline solid. ^{1}H NMR (400 MHz, $CDCl_3$): δ = 7.35-7.40 (m, 2H, aromatics), 7.54-7.65 (m, 3H, aromatic), 7.79-7.83 (m, 1H, aromatics), 7.88-7.91 (m, 1H, aromatics), 7.96-8.00 (m, 2H, aromatics), 8.32 (dd, $^{3}J_{HH}$ = 8.8, 4.9 Hz, 1H, aromatics), 8.77-8.79 (m, 1H, aromatics) ppm. ^{13}C{^{1}H} NMR (101 MHz, $CDCl_3$): δ = 110.6, 120.0, 124.0, 124.4, 124.6, 125.2, 126.9, 127.8, 127.9, 128.1, 128.8, 129.0, 133.0, 134.8, 142.2, 150.9, 163.2 (s, aromatics) ppm.[9]

2-(2-Naphthyl)benzoxazole (12ah)

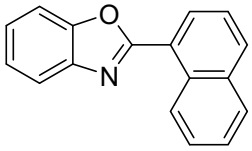

Eluent **A**. White crystalline solid. ^{1}H NMR (400 MHz, $CDCl_3$): δ = 7.37-7.42 (m, 2H, aromatics), 7.57-7.66 (m, 3H, aromatics), 7.70-7.73 (m, 1H, aromatics), 7.86-7.90 (m, 1H, aromatics), 7.93 (d, $^{3}J_{HH}$ = 8.2 Hz, 1H, aromatics), 8.03 (d, $^{3}J_{HH}$ = 8.2 Hz, 1H, aromatics), 8.43 (dd, $^{3}J_{HH}$ = 13, 7.3 Hz, 1H, aromatics), 9.47 (d, $^{3}J_{HH}$ = 8.6 Hz, 1H, aromatics) ppm. ^{13}C{^{1}H} NMR (101 MHz, $CDCl_3$): δ = 110.5, 120.3, 123.6, 124.5, 124.9, 125.3, 126.3, 126.4, 127.9, 128.7, 129.3, 130.7, 132.3, 134.0, 142.3, 150.2, 162.8 (s, aromatics) ppm.[9]

2-(4-methoxyphenyl)benzoxazole (12ai)

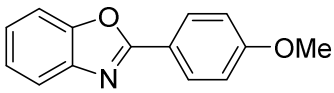

Eluent **A**. White crystalline solid. ^{1}H NMR (400 MHz, $CDCl_3$): δ = 3.89 (s, 3H, Me), 7.01-7.05 (m, 2H, aromatics), 7.29-7.35 (m, 2H, aromatics), 7.53-7.57 (m, 1H, aromatics), 7.72-7.76 (m, 1H, aromatics), 8.18-8.22 (m, 2H, aromatics) ppm. ^{13}C{^{1}H} NMR (101 MHz, $CDCl_3$): δ = 55.5 (s, Me), 110.4, 114.4, 119.6, 119.7, 124.4, 124.6, 129.4, 142.3, 150.7, 162.3, 163.2 (s, aromatics) ppm.[8]

2-(4-Acetylphenyl)benzoxazole (12aj)

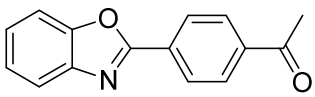

Eluent **B**. White crystalline solid. ^{1}H NMR (400 MHz, $CDCl_3$): δ = 2.68 (s, 3H, Me), 7.31-7.43 (m, 2H, aromatics), 7.60-7.64 (m, 1H, aromatics), 7.79-7.83 (m, 1H, aromatics), 8.09-8.12 (m, 2H, aromatics), 8.35-8.38 (m, 2H, aromatics) ppm. ^{13}C{^{1}H} NMR (101 MHz, $CDCl_3$): δ = 26.8 (s, Me),

110.8, 120.4, 124.9, 125.8, 127.7, 128.8, 131.1, 138.96, 142.0, 150.9, 161.9 (s, aromatics), 197.3 (s, CO) ppm.[9]

2-(4-Fluorophenyl)benzoxazole (12ak)

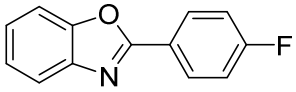

Eluent **A**. White crystalline solid. ^{1}H NMR (400 MHz, $CDCl_3$): δ = 7.18-7.25 (m, 2H, aromatics), 7.33-7.38 (m, 2H, aromatics), 7.55-7.60 (m, 1H, aromatics) 7.74- 7.79 (m, 1H, aromatics), 8.23-8.29 (m, 2H, aromatics) ppm. ^{13}C{^{1}H} NMR (101 MHz, $CDCl_3$): δ = 110.6 (s, aromatics), 116.2 (d, J_{FC} = 22 Hz, aromatics), 119.9, (s, aromatics), 123.4 (d, J_{FC} = 3 Hz, aromatics), 124.7, 125.1 (s, aromatics), 129.8 (d, J_{FC} = 9 Hz, aromatics), 142.1, 150.8, 162.2 (s, aromatics), 164.8 (d, J_{FC} = 253 Hz, aromatics) ppm. ^{19}F NMR (376 MHz, $CDCl_3$): δ = −107.5 (tt, J = 9, 5 Hz) ppm.[8]

2-(4-Cyanophenyl]benzoxazole (12al)

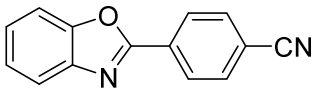

Eluent **B**. White crystalline solid. ^{1}H NMR (400 MHz, $CDCl_3$): δ = 7.38-7.45 (m, 2H, aromatics), 7.60-7.64 (m, 1H, aromatics), 7.79-7.83 (m, 3H, aromatics), 8.35-8.42 (m, 2H, aromatics) ppm. ^{13}C{^{1}H} NMR (101 MHz, $CDCl_3$): δ = 110.9, 114.8 (s, aromatics), 118.2 (s, CN), 120.6, 125.1, 126.2, 128.0, 131.1, 132.7, 141.9, 150.9, 160.9 (s, aromatics) ppm.[8]

2-(2-Pyridyl)benzoxazole (12am)

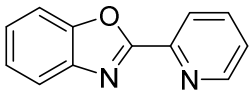

Eluent **C**. Chromatography was performed on alumina (80 g, 30 μm). White crystalline solid. ^{1}H NMR (400 MHz, $CDCl_3$): δ = 7.37-7.48 (m, 3H, aromatics), 7.65-7.70 (m, 1H, aromatics), 7.81-7.86 (m, 1H, aromatics), 7.87-7.92 (m, 1H, aromatics), 8.37 (dt, $^{3}J_{HH}$ = 7.9, 1.1 Hz, 1H, aromatic), 8.83 (ddd, $^{3}J_{HH}$ = 4.8, 1.8, 0.9 Hz, 1H, aromatic) ppm. ^{13}C{^{1}H} NMR (101 MHz, $CDCl_3$): δ = 111.2, 120.7, 123.5, 124.9, 125.6, 126.0, 137.1, 141.8, 146.1, 150.3, 151.1, 161.5 (s, aromatics) ppm.[10]

2-Phenyl-5-methylbenzoxazole (12ba)

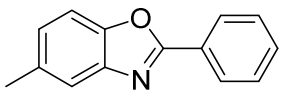

Eluent **A**. White crystalline solid. This compound is known. **[3]** ^{1}H NMR (400 MHz, $CDCl_3$): δ = 2.49 (s, 3H, Me), 7.16-7.14 (m, 1H, aromatics), 7.45 (d, $^{3}J_{HH}$ = 8.3 Hz, 1H, aromatics), 7.50-7.56 (m,

4H, aromatics), 8.22-8.26 (m, 2H, aromatics) ppm. $^{13}C\{^1H\}$ NMR (101 MHz, $CDCl_3$): δ = 21.5 (s, Me), 109.9, 119.3, 126.2, 127.3, 127.5, 128.9, 131.4, 134.4, 142.3, 149.0, 163.1 (s, aromatics) ppm.[9]

2-[4-Methylphenyl]-5-methylbenzoxazole (12bb)

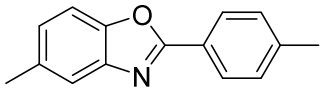

Eluent **A**. White crystalline solid. ^1H NMR (400 MHz, $CDCl_3$): δ = 2.43 (s, 3H, Me), 2.48 (s, 3H, Me), 7.12-7.15 (m, 1H, aromatics), 7.30-7.34 (m, 2H, aromatics), 7.43 (d, J_{HH} = 8.3 Hz, 1H, aromatics), 7.53 (br s, 1H, aromatics), 8.11-8.14 (m, 2H, aromatics) ppm. $^{13}C\{^1H\}$ NMR (101 MHz, $CDCl_3$): δ = 21.5, 21.6 (s, Me), 109.8, 119.8, 124.6, 126.0, 127.5, 129.6, 134.3, 141.9, 142.4, 148.9, 163.4 (s, aromatics) ppm. [9]

2-[4-(Trifluoromethyl)phenyl]-5-methylbenzoxazole (12bc)

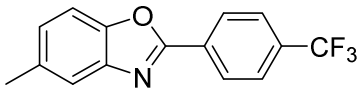

Eluent **A**. White crystalline solid. ^1H NMR (400 MHz, $CDCl_3$): δ = 2.50 (s, 3H, Me), 7.19-7.22 (m, 1H, aromatics), 7.47 (d, $^3J_{HH}$ = 8.3 Hz, 1H, aromatics), 7.57-7.58 (m, 1H, aromatics), 7.76-7.79 (m, 2H, aromatics), 8.34-8.37 (m, 2H, aromatics) ppm. $^{13}C\{^1H\}$ NMR (101 MHz, $CDCl_3$): δ = 21.5 (s, Me), 110.1, 120.2 (s, aromatics), 123.7 (q, $^1J_{FC}$ = 272 Hz, CF_3), 125.9 (q, $^2J_{FC}$ = 4 Hz, aromatics), 127.0, 127.8, 130.5 (s, aromatics), 132.9 (q, $^2J_{FC}$ = 33 Hz, aromatics), 134.9, 141.9, 149.1, 161.6 (s, aromatics) ppm. ^{19}F NMR (376 MHz, $CDCl_3$): δ = −63.0 (s) ppm. [9]

2-Phenyl-5-chlorobenzoxazole (12ca)

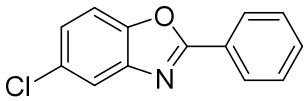

Eluent **A**. White crystalline solid. ^1H NMR (400 MHz, $CDCl_3$): δ = 7.32 (dd, $^3J_{HH}$ = 8.6, 2.1 Hz, 1H, aromatics), 7.49-7.56 (m, 4H, aromatics), 7.75 (dd, $^3J_{HH}$ = 2.1, 0.4 Hz, 1H, aromatics), 8.21-8.27 (m, 2H, aromatics) ppm. $^{13}C\{^1H\}$ NMR (101 MHz, $CDCl_3$): δ = 111.3, 120.0, 125.4, 126.7, 127.8, 129.0, 130.0, 131.9, 143.3, 149.4, 164.4 (s, aromatics) ppm.[11]

2-[4-Methylphenyl]-5-chlorobenzoxazole (12cb)

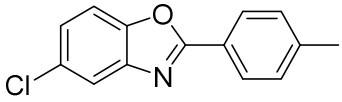

Eluent **A**. White crystalline solid. ^{1}H NMR (400 MHz, $CDCl_3$): δ = 2.44 (s, 3H, Me), 7.30 (dd, $^{3}J_{HH}$ = 8.6, 2.1 Hz, 1H, aromatics), 7.32-7.34 (m, 2H, aromatics), 7.47 (d, $^{3}J_{HH}$ = 8.6 Hz, 1H, aromatics), 7.72 (d, $^{3}J_{HH}$ = 2.1 Hz, 1H, aromatics), 8.10-8.13 (m, 2H, aromatics) ppm. ^{13}C{^{1}H} NMR (101 MHz, $CDCl_3$): δ = 21.7 (s, Me), 111.2, 119.8, 123.9, 125.1, 127.7, 129.7, 129.9, 142.6, 143.4, 149.3, 164.6 (s, aromatics) ppm.[9]

2-[4-(Trifluoromethyl)phenyl]-5-chlorobenzoxazole (12cc)

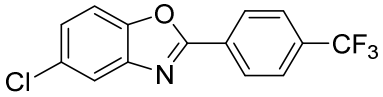

Eluent **A**. White crystalline solid. ^{1}H NMR (400 MHz, $CDCl_3$): δ = 7.37 (dd, $^{3}J_{HH}$ = 8.6, 2.1 Hz, 1H, aromatics), 7.53 (dd, $^{3}J_{HH}$ = 8.7, 0.5 Hz, 1H, aromatics), 7.78-7.81 (m, 3H, aromatics), 8.34-8.37 (m, 2H, aromatics) ppm. ^{13}C{^{1}H} NMR (101 MHz, $CDCl_3$): δ = 111.5, 120.4, (s, aromatics), 123.7 (q, $^{1}J_{FC}$ = 273 Hz, CF_3), 126.0 (q, J_{FC} = 4 Hz, aromatics), 126.1, 128.0, 130.0, 130.5 (s, aromatics), 133.4 (q, J_{FC} = 33 Hz, aromatics), 143.0, 149.4, 162.8 (s, aromatics) ppm. ^{19}F NMR (376 MHz, $CDCl_3$): δ = −63.1 (s) ppm. [9]

1,4-Bis(benzoxazol-2-yl)benzene (12an)

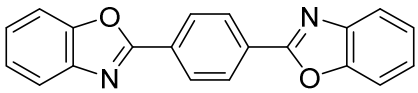

Given the extremely low solubility of this compound, a different purification procedure was applied: the reaction mixture was cooled to room temperature and diluted with water (50 mL) and dichloromethane (100 mL). The organic layer was separated, and aqueous layer was extracted with dichloromethane (3× 50 mL). The organic extracts were combined and evaporated, leaving a crude product, which was washed with methanol (3× 50 mL), diethyl ether (3× 50 mL) and dried in vacuum. Average yield of **12an**: 90%, an off-white solid. ^{1}H NMR (400 MHz, dmso-d_6, **100°C**): δ = 7.41-7.48 (m, 4H, aromatics), 7.77-7.84 (m, 4H, aromatics), 8.41 (s, 4H, C_6H_4) ppm.[12] HR ESI-MS calc. for $C_{20}H_{13}N_2O_2$ ([M + H]$^{+}$): 313.0977, found 313.0971.

2,5-Bis(benzoxazol-2-yl)thiophene (12ao)

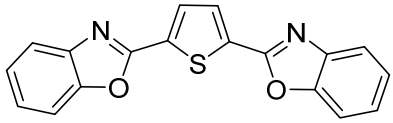

Four equivalents of **10a** (476 mg, 4.0 mmol) were reacted with 2,5-dichlorothiophene (153 mg, 1.0 mmol in the presence of catalyst **9** (1.5 mol.%) and K_3PO_4 (637 mg, 3.0 mmol) in 2 mL of butanol at 125°C for 18 h. The reaction mixture was extracted with dichloromethane. Eluent **D**. White crystalline solid. ^1H NMR (400 MHz, $CDCl_3$): δ = 7.35-7.42 (m, 4H, aromatics), 7.57-7.62 (m, 2H, aromatics), 7.75-7.81 (m, 2H, aromatics), 7.95 (s, 2H, C_4H_2S) ppm. $^{13}C\{^1H\}$ NMR (101 MHz, $CDCl_3$): δ = 110.6, 120.2, 125.0, 125.7, 130.4, 133.3, 142.0, 150.6, 158.0 (s, aromatics) ppm.[13]

NMR spectra of the coupling products

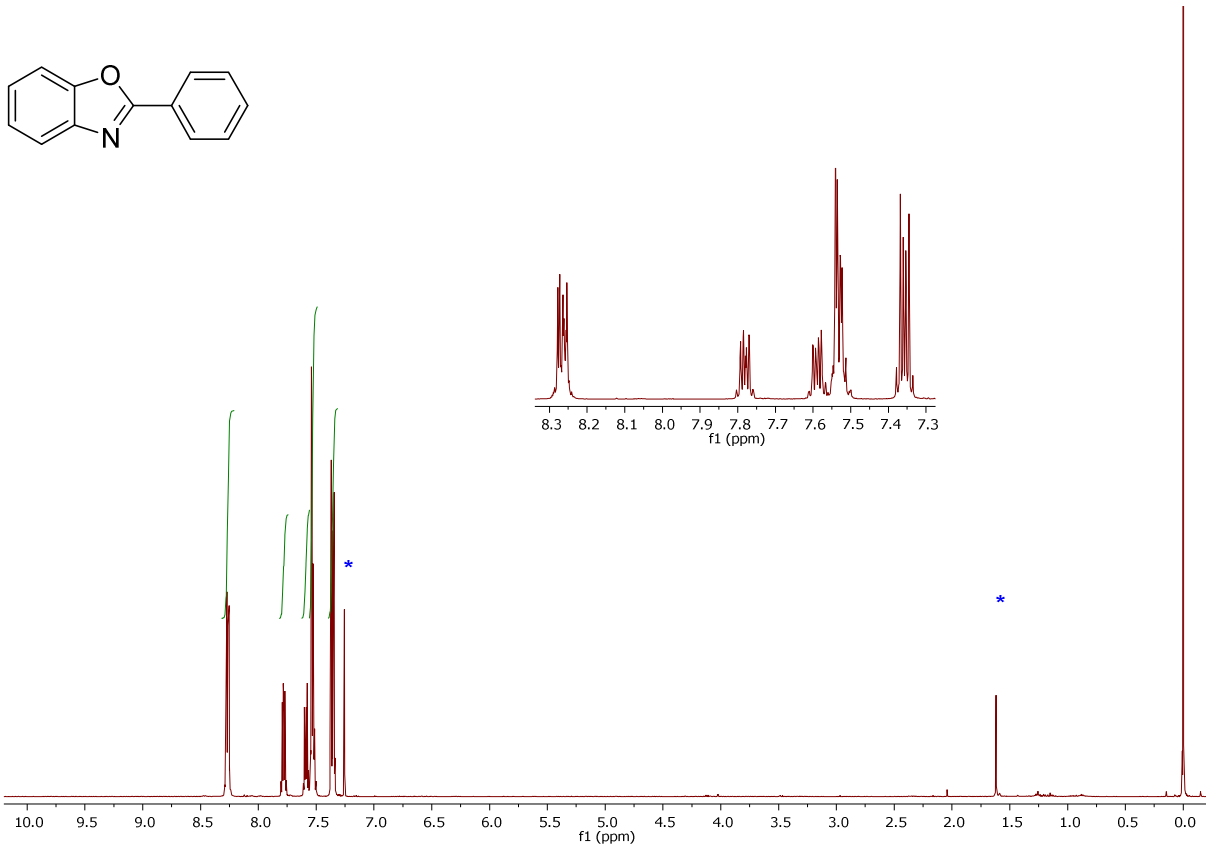

Figure S43. ^{1}H NMR spectrum (400 MHz, $CDCl_3$) of **12aa**

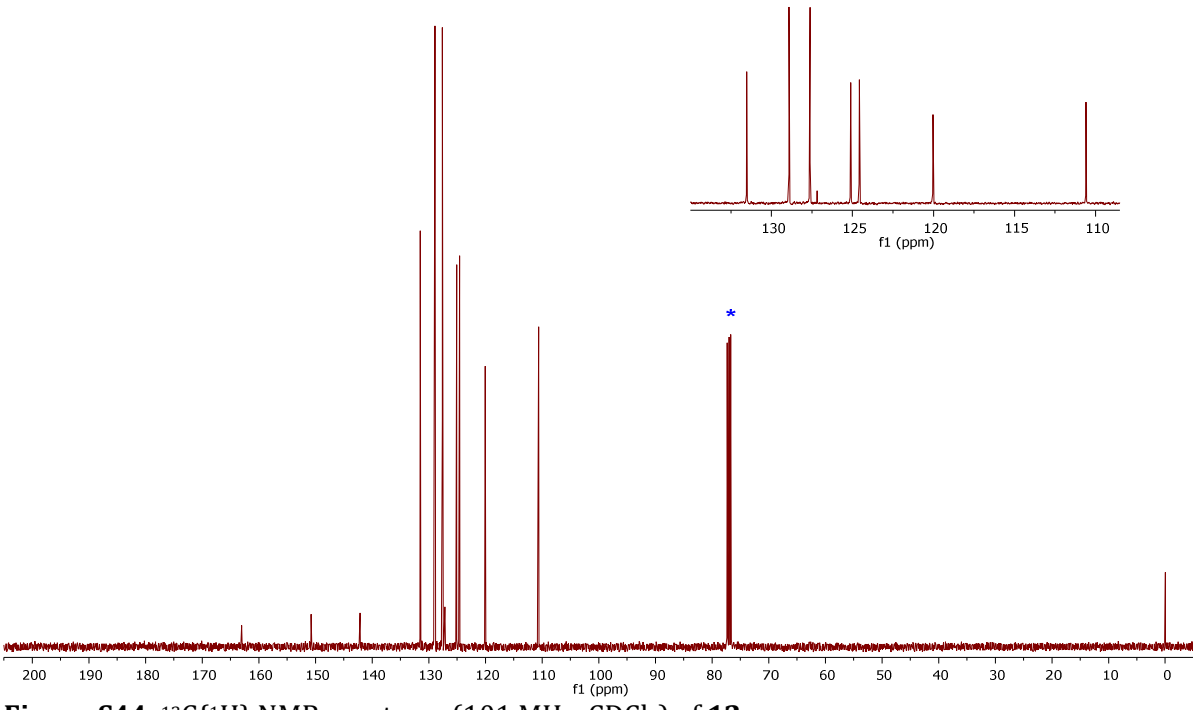

Figure S44. $^{13}C\{^{1}H\}$ NMR spectrum (101 MHz, $CDCl_3$) of **12aa**

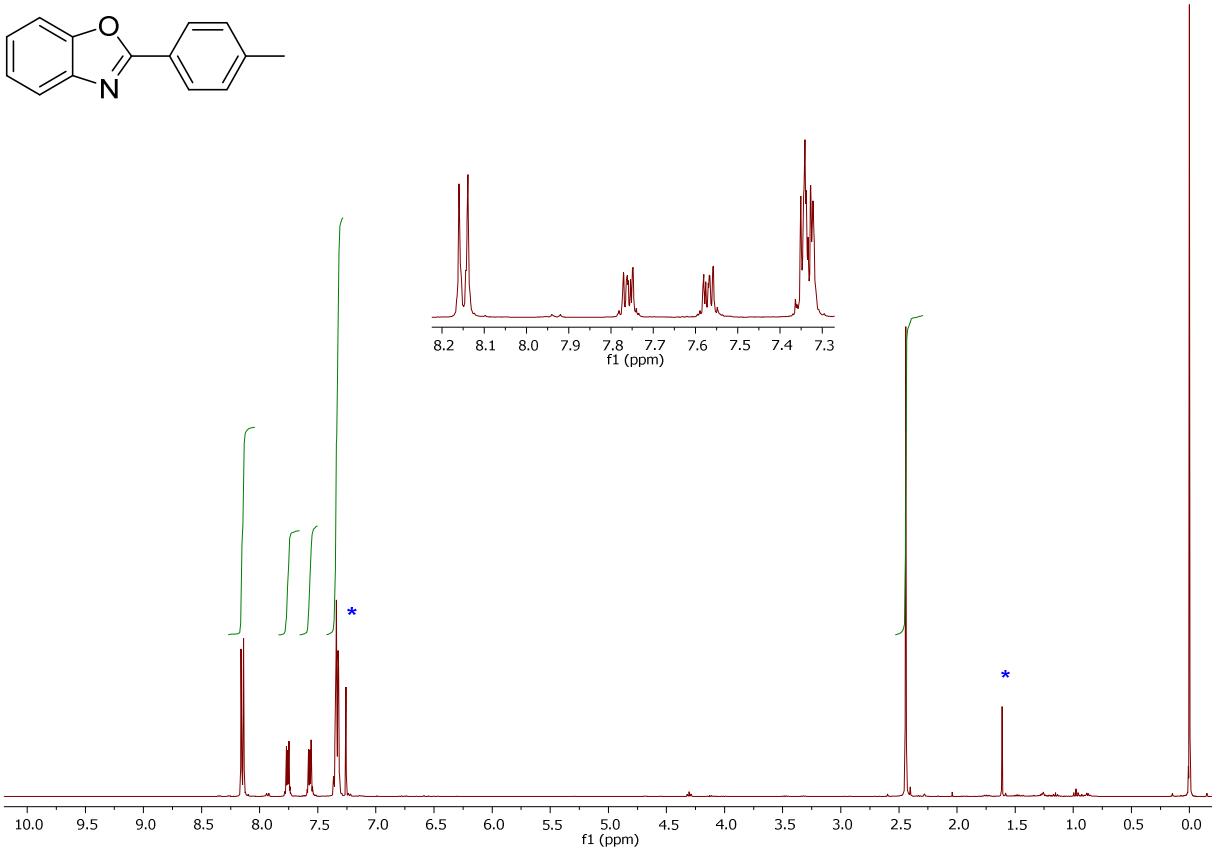

Figure S45. ^{1}H NMR spectrum (400 MHz, $CDCl_3$) of **12ab**

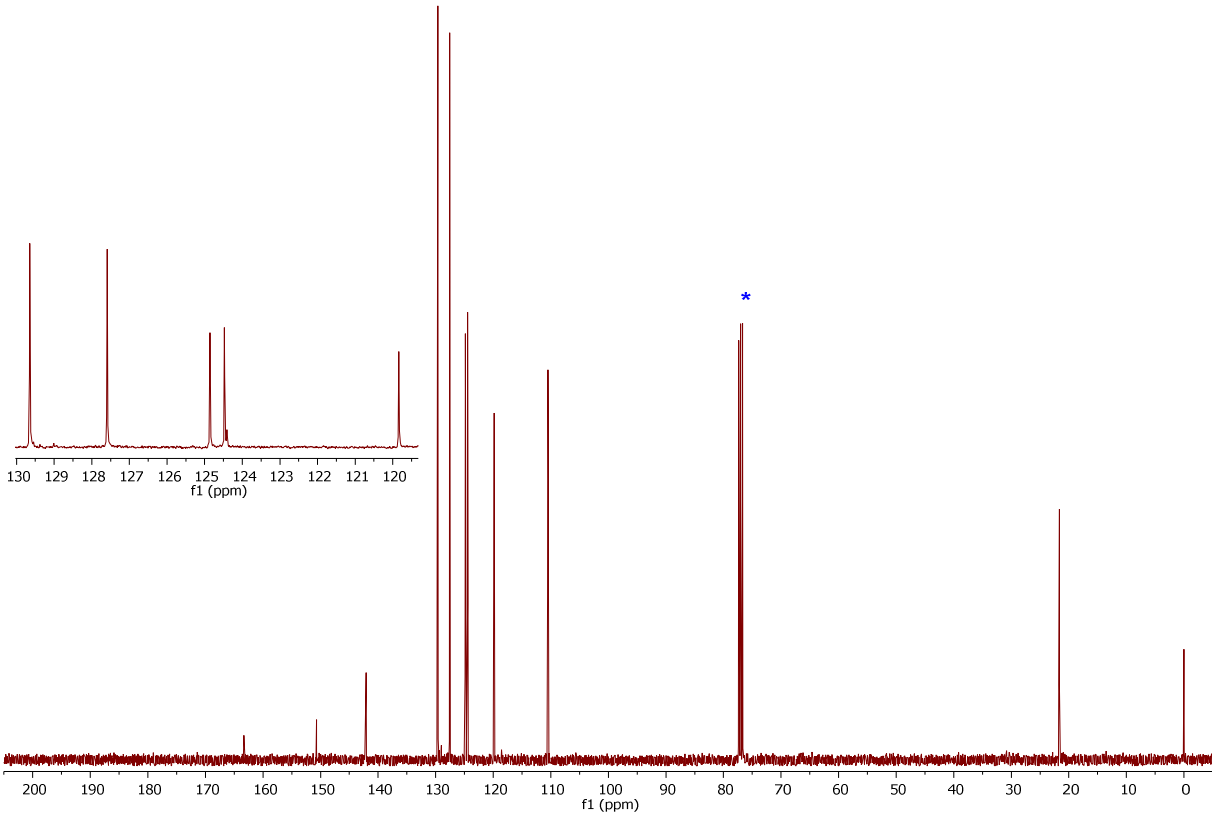

Figure S46. $^{13}C\{^{1}H\}$ NMR spectrum (101 MHz, $CDCl_3$) of **12ab**

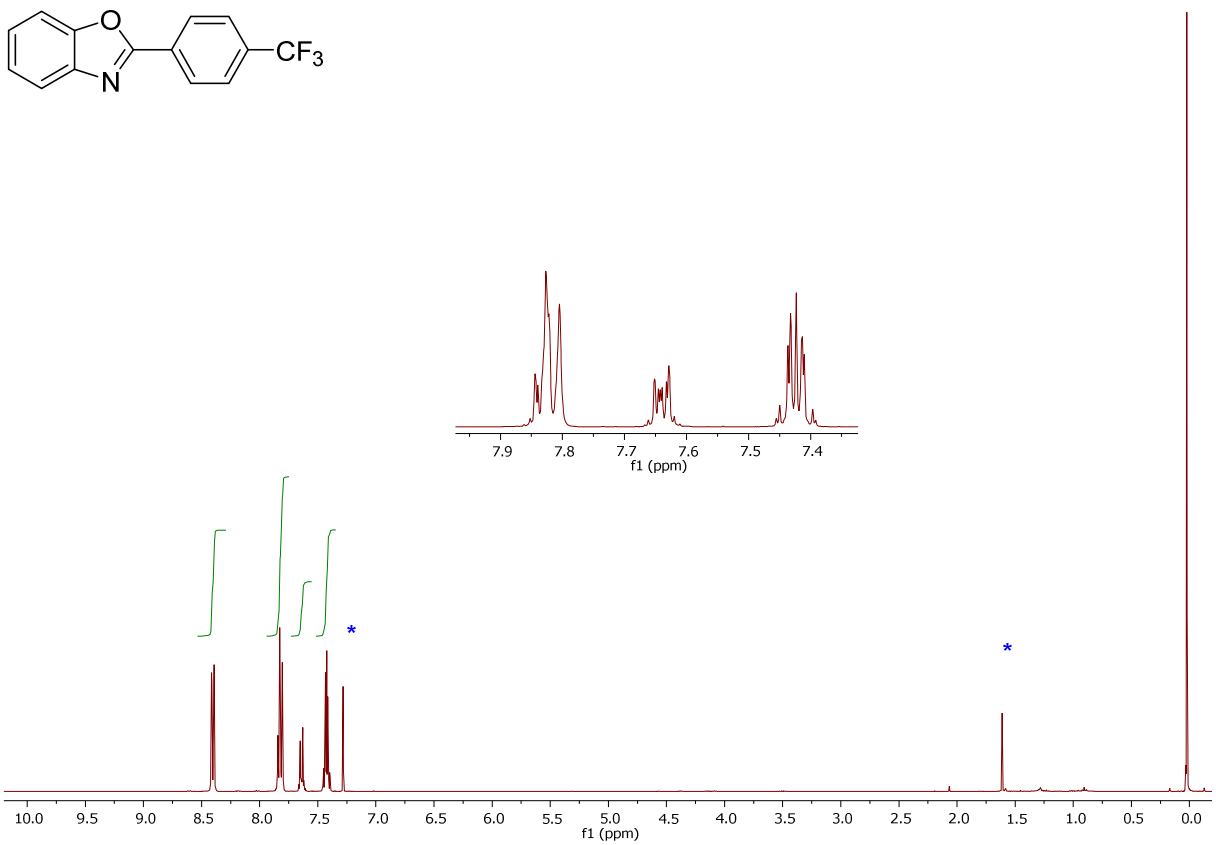

Figure S47. ^{1}H NMR spectrum (400 MHz, $CDCl_3$) of **12ac**

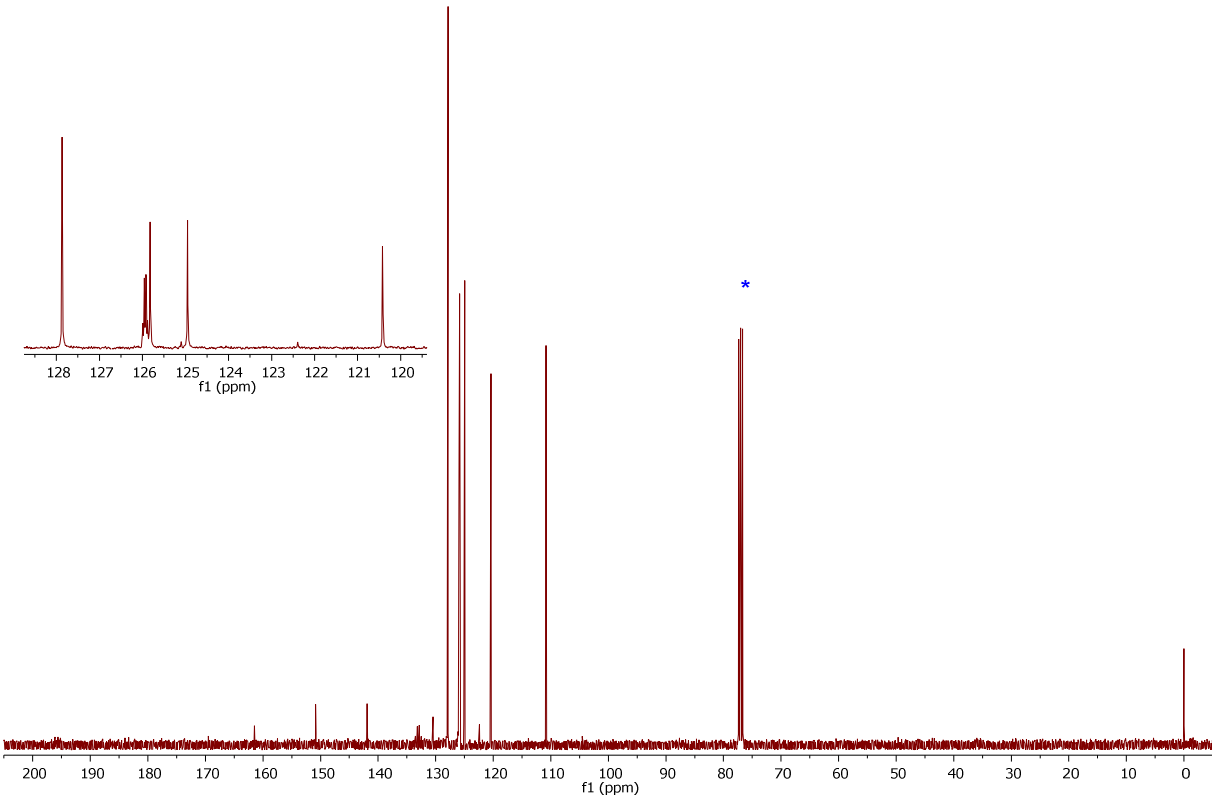

Figure S48. $^{13}C\{^{1}H\}$ NMR spectrum (101 MHz, $CDCl_3$) of **12ac**

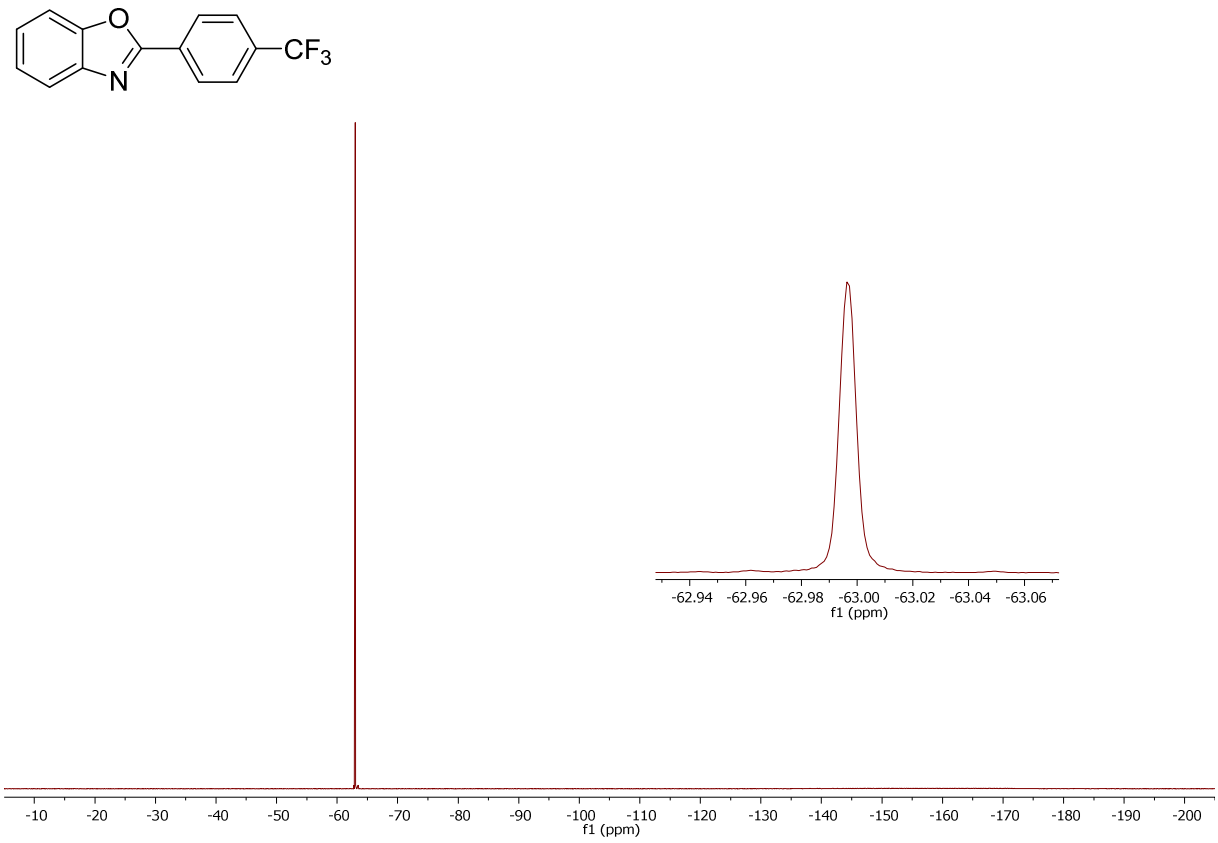

Figure S49. ^{19}F NMR spectrum (376 MHz, $CDCl_3$) of **12ac**

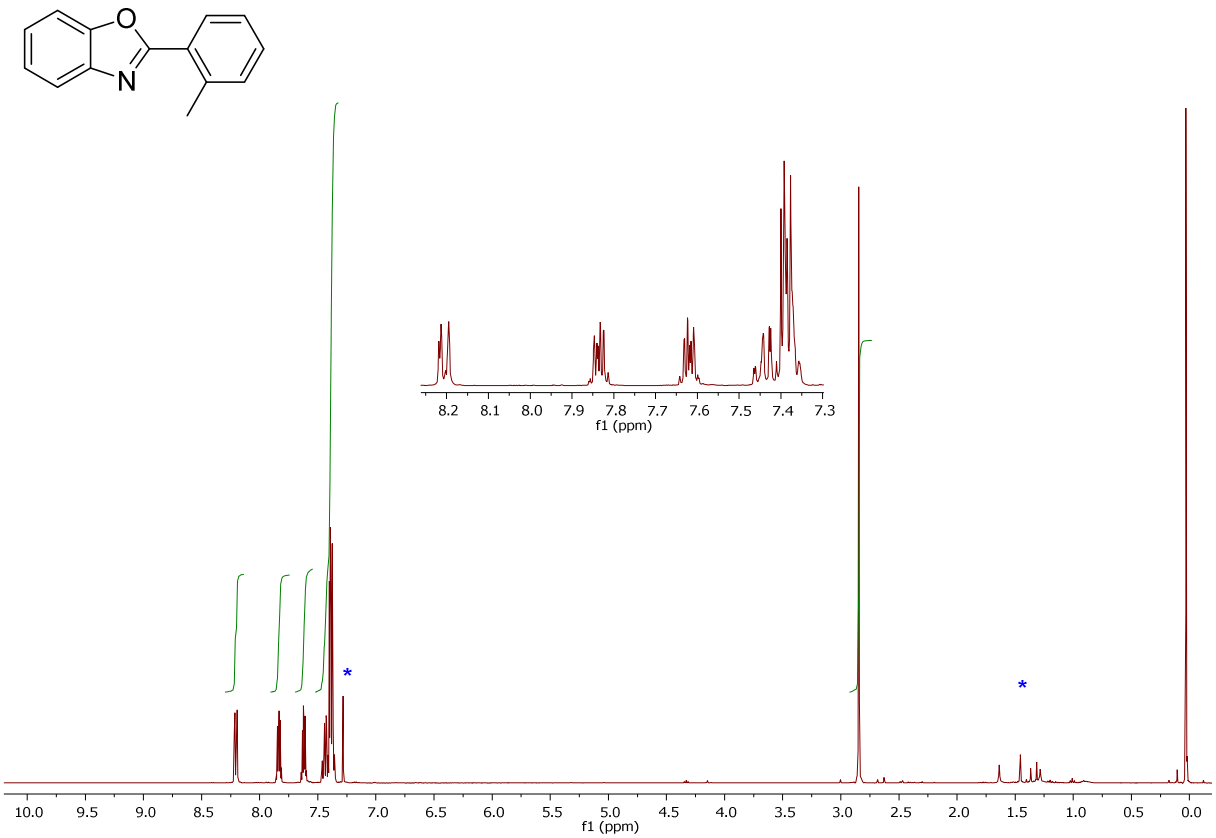

Figure S50. ^{1}H NMR spectrum (400 MHz, $CDCl_3$) of **12ad**

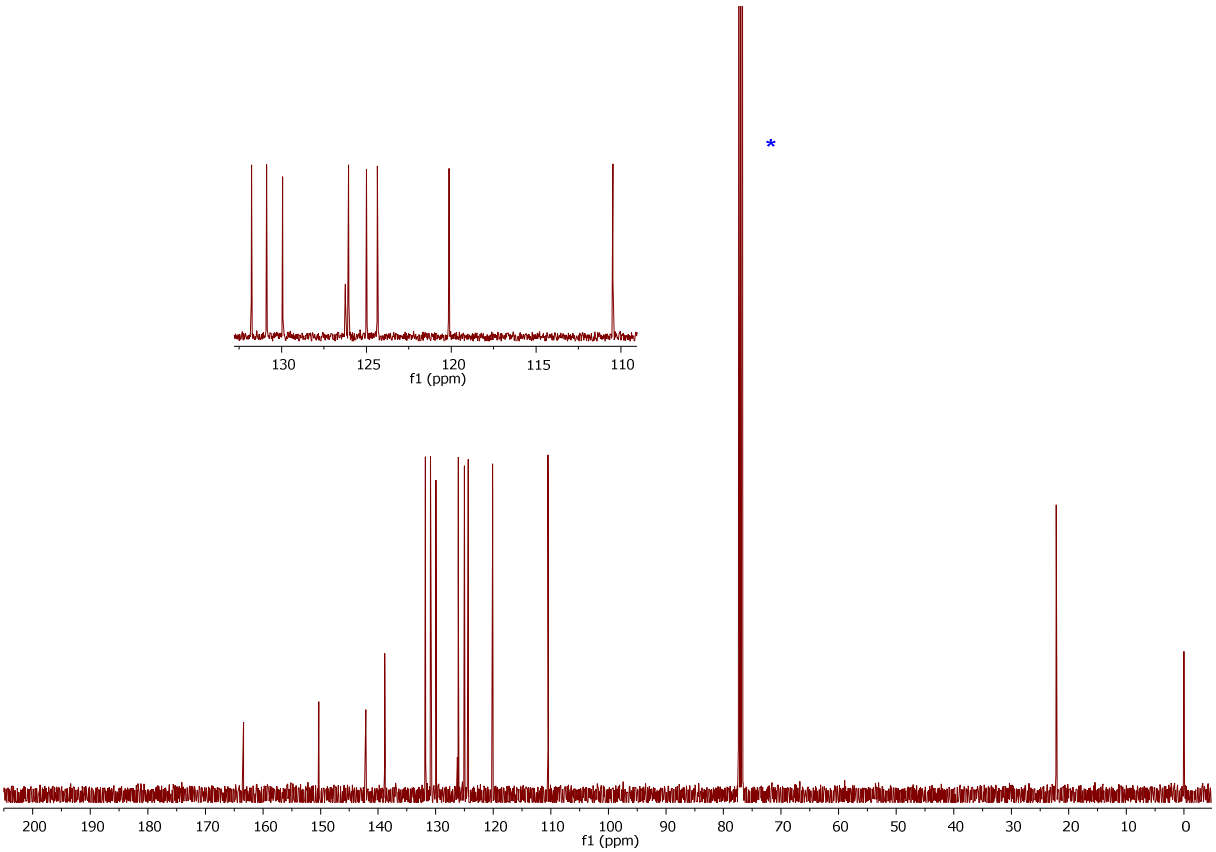

Figure S51. $^{13}C\{^{1}H\}$ NMR spectrum (101 MHz, $CDCl_3$) of **12ad**

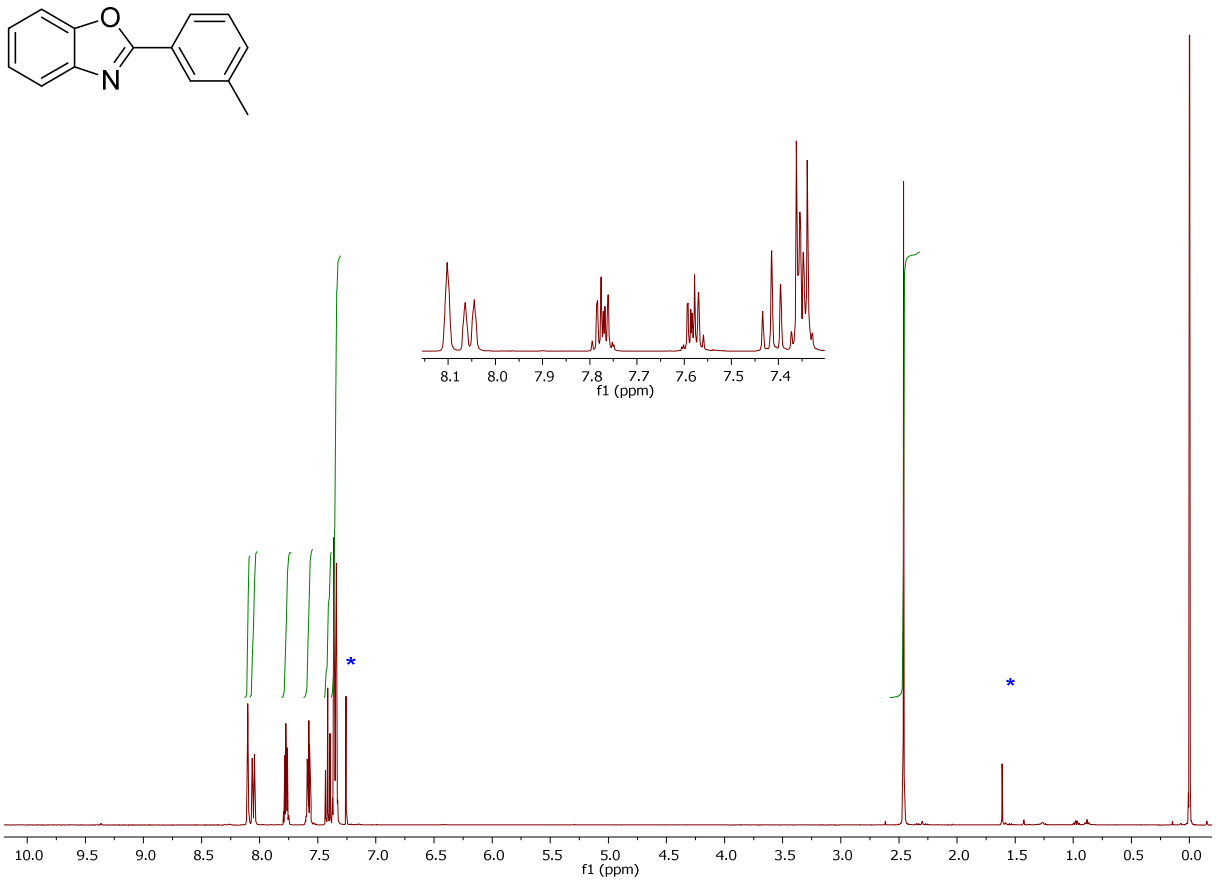

Figure S52. ^{1}H NMR spectrum (400 MHz, $CDCl_3$) of **12af**

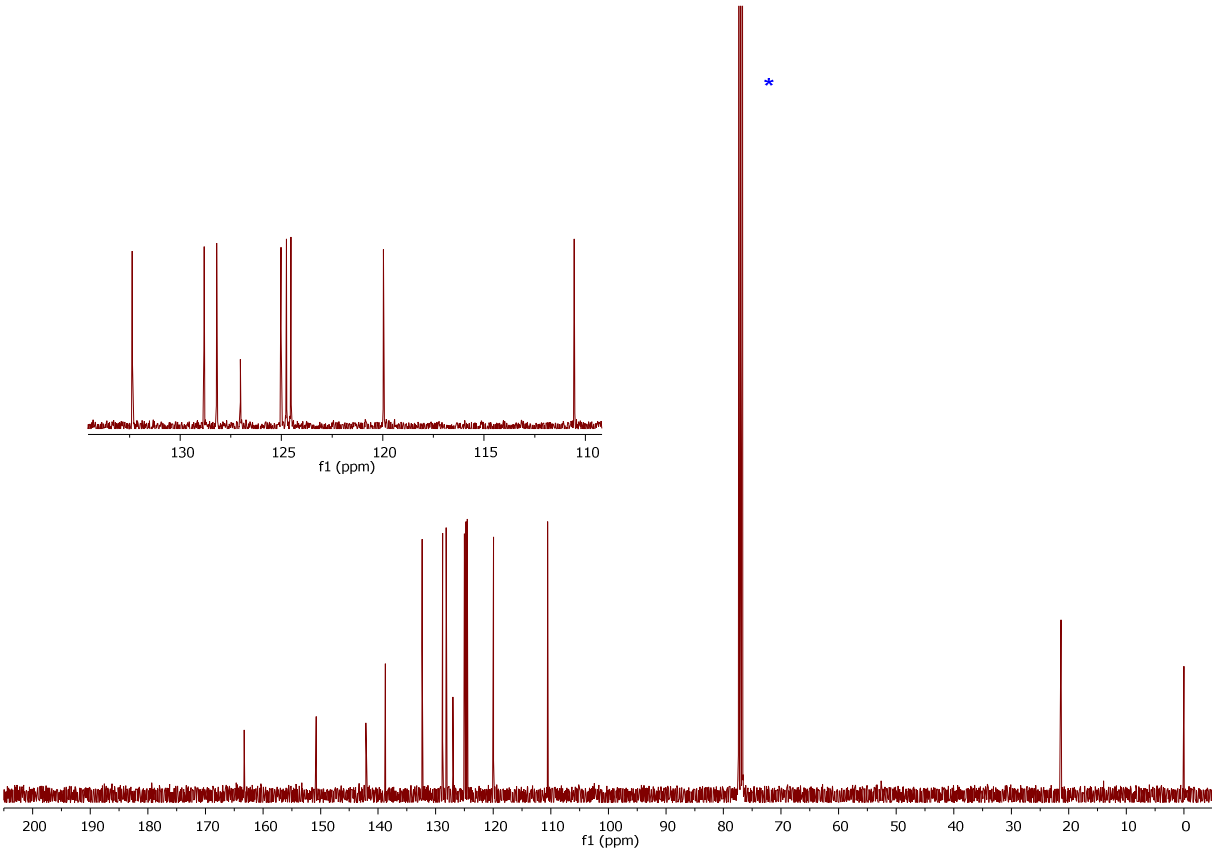

Figure S53. $^{13}C\{^{1}H\}$ NMR spectrum (101 MHz, $CDCl_3$) of **12af**

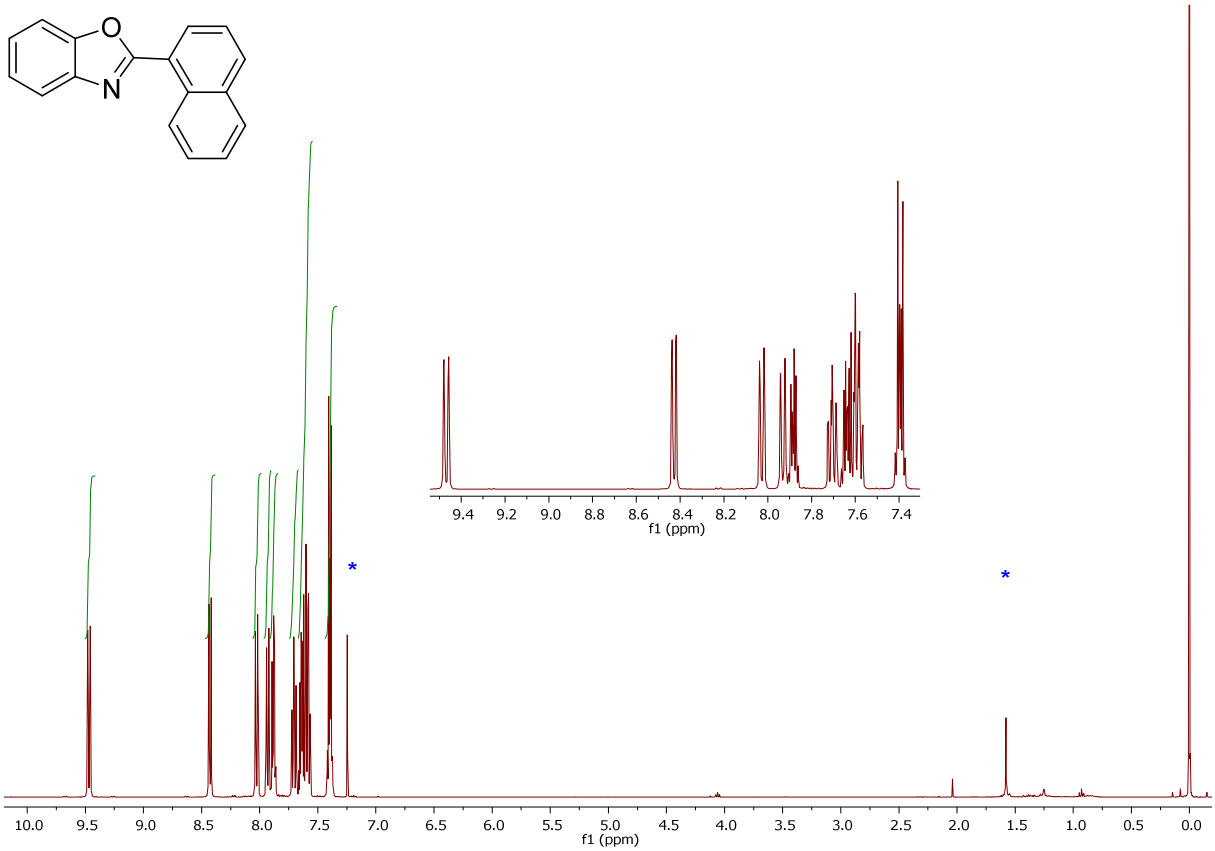

Figure S54. ^{1}H NMR spectrum (400 MHz, $CDCl_3$) of **12ag**

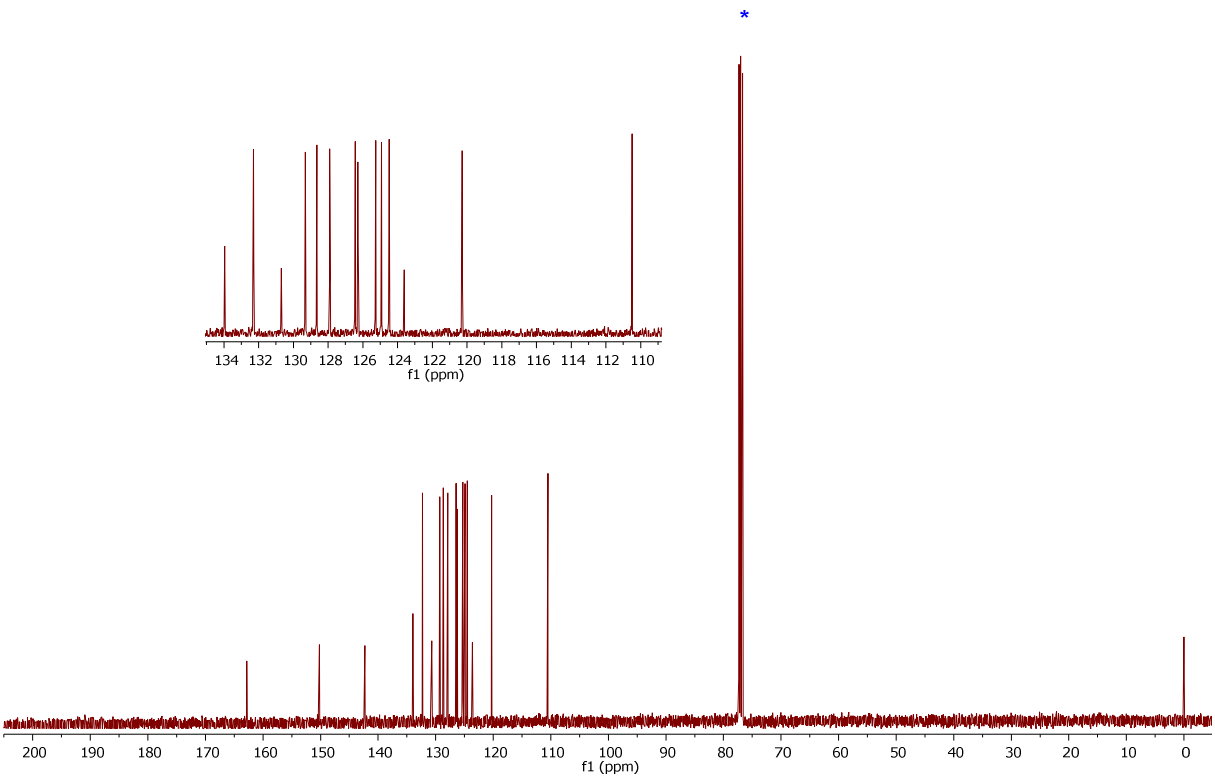

Figure S55. $^{13}C\{^{1}H\}$ NMR spectrum (101 MHz, $CDCl_3$) of **12ag**

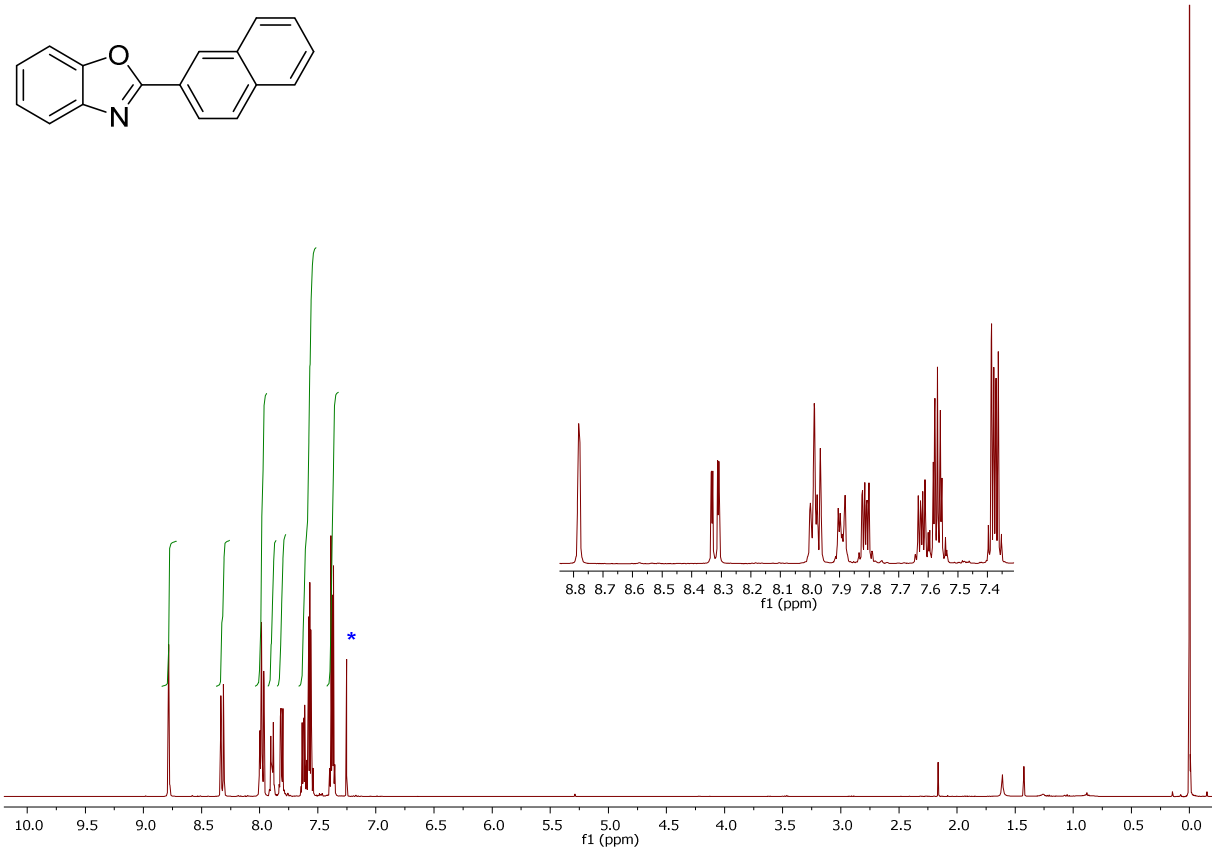

Figure S56. ^{1}H NMR spectrum (400 MHz, $CDCl_3$) of **12ah**

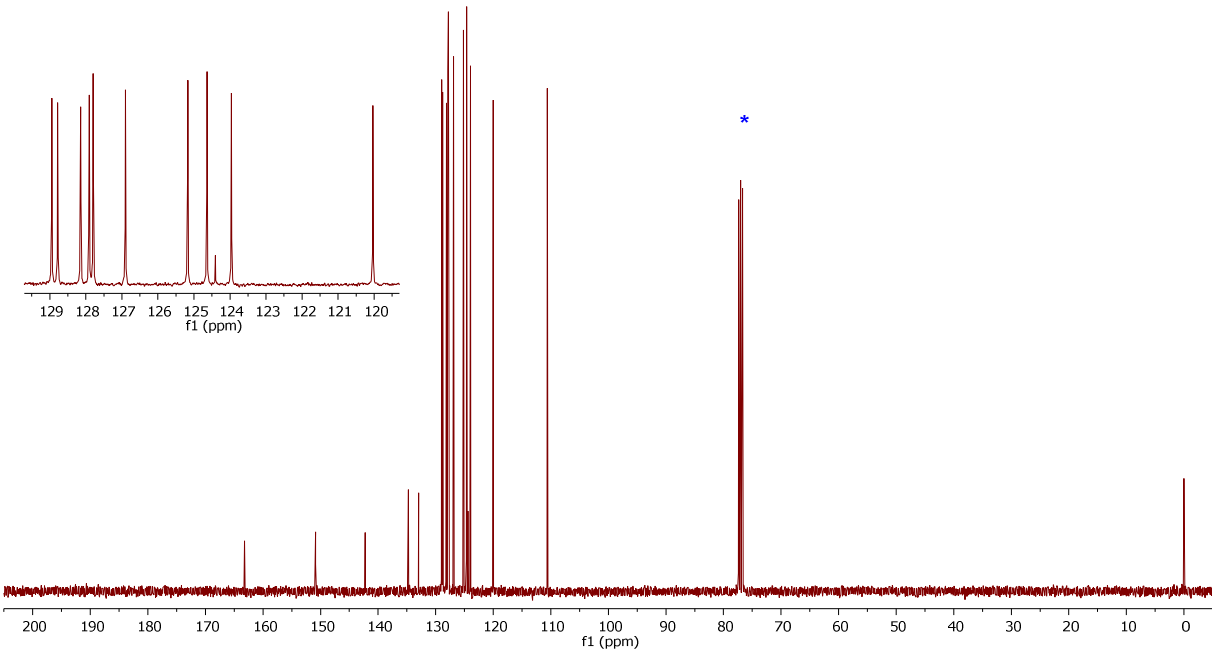

Figure S57. $^{13}C\{^{1}H\}$ NMR spectrum (101 MHz, $CDCl_3$) of **12ah**

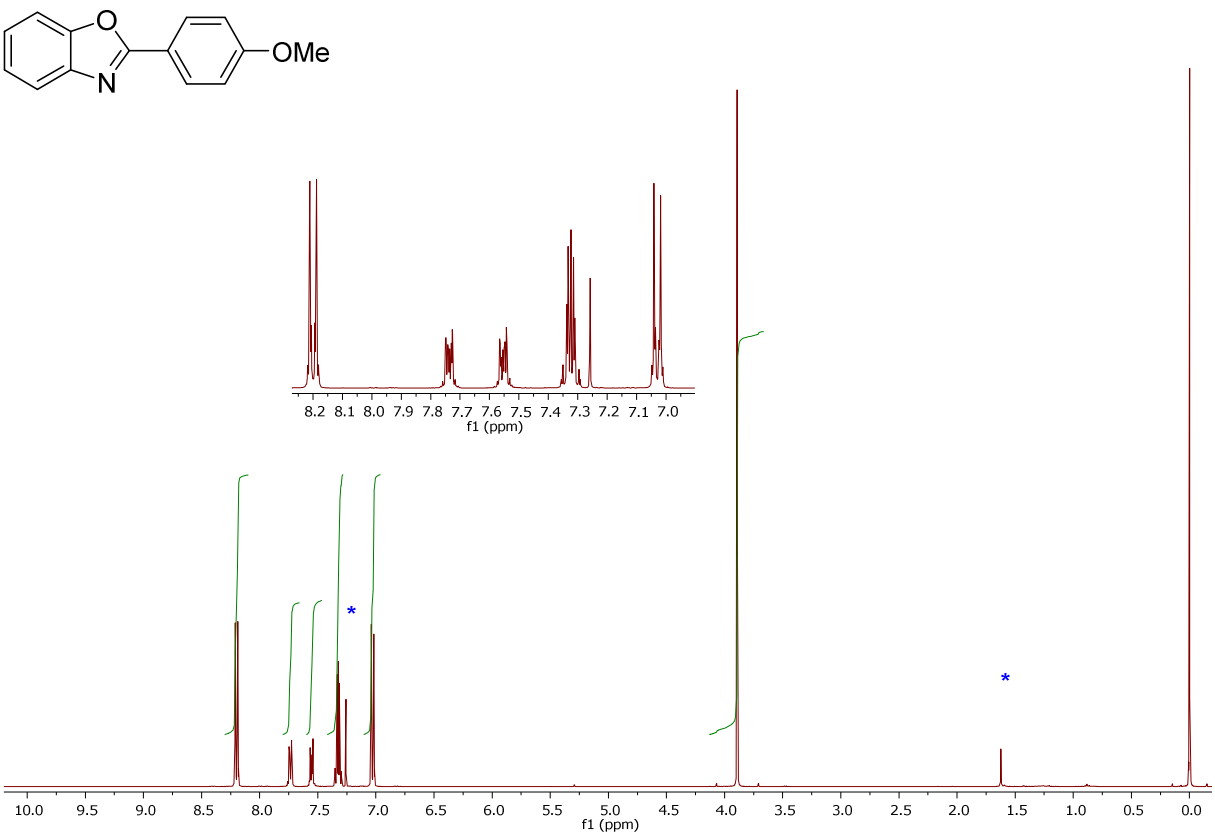

Figure S58. ^{1}H NMR spectrum (400 MHz, $CDCl_3$) of **12ai**

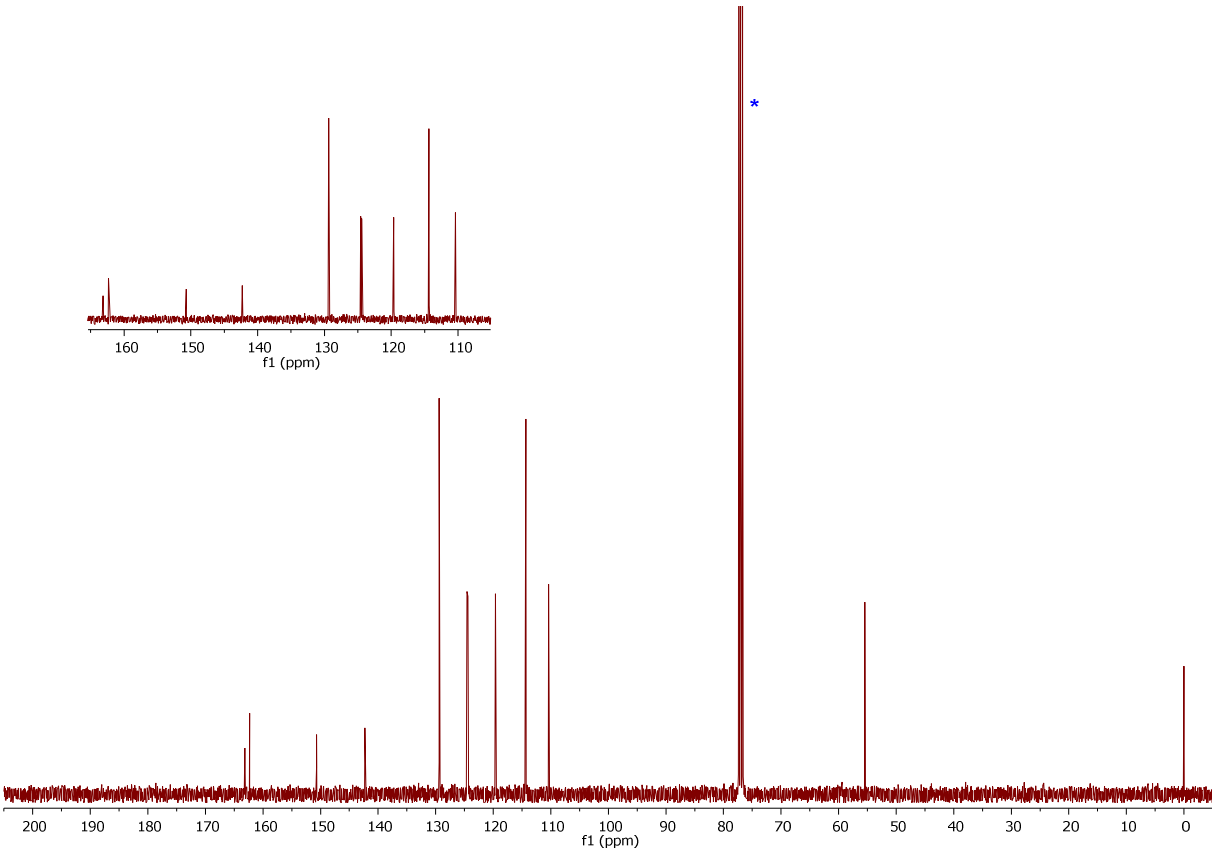

Figure S59. $^{13}C\{^{1}H\}$ NMR spectrum (101 MHz, $CDCl_3$) of **12ai**

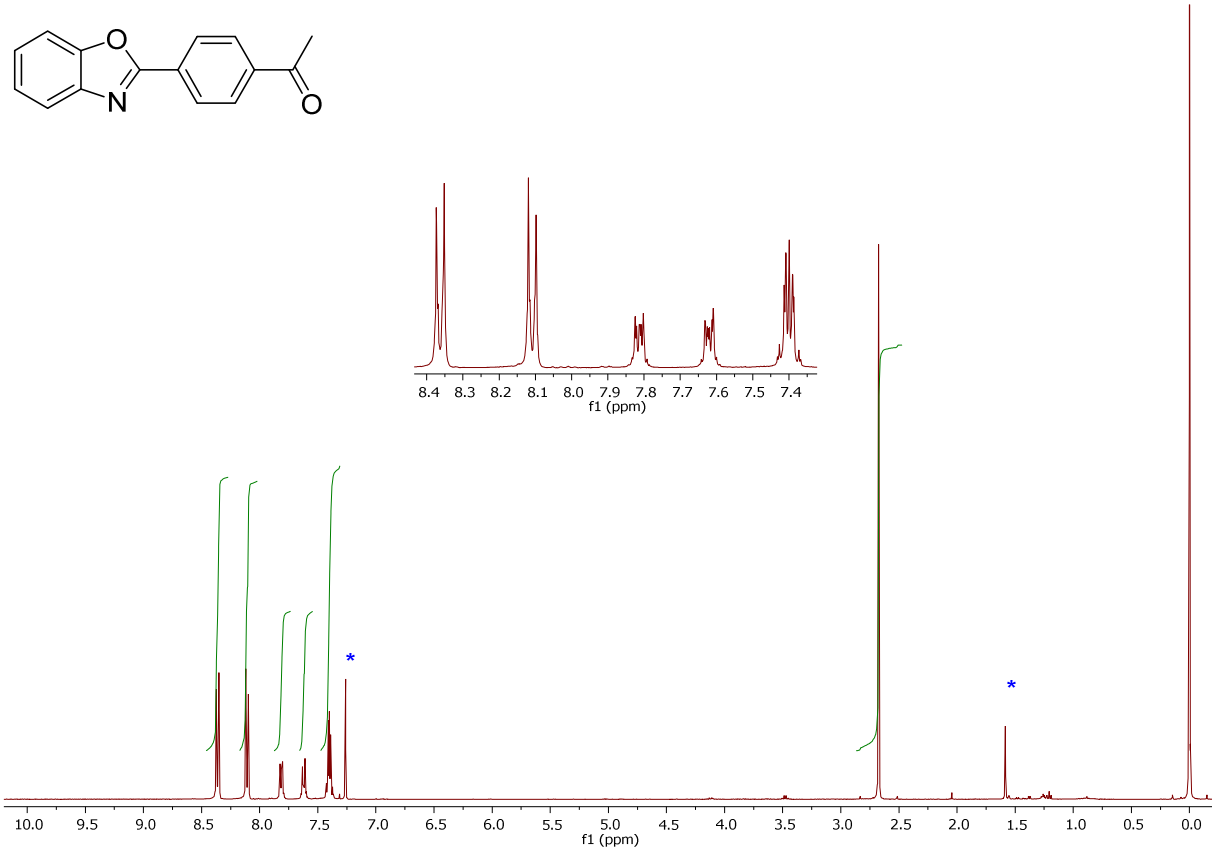

Figure S60. ^{1}H NMR spectrum (400 MHz, $CDCl_3$) of **12aj**

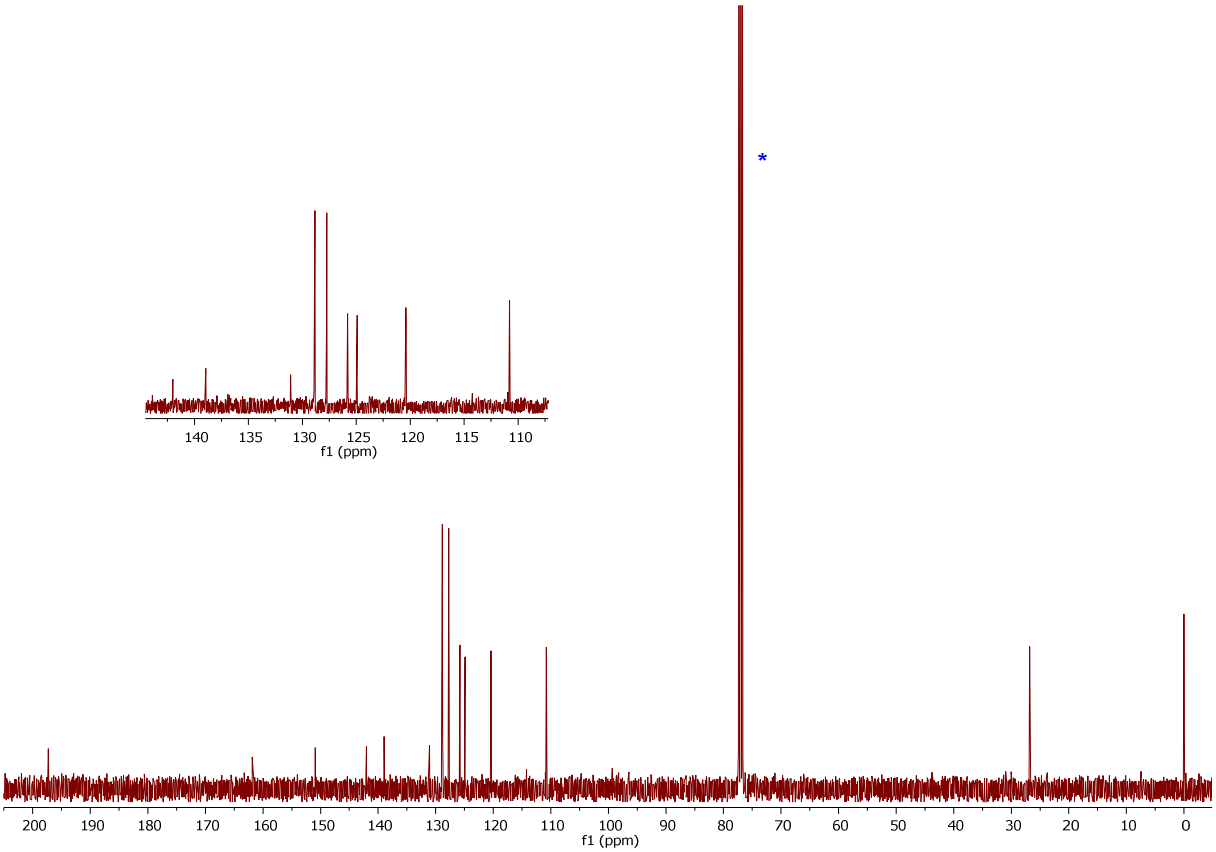

Figure S61. $^{13}C\{^{1}H\}$ NMR spectrum (101 MHz, $CDCl_3$) of **12aj**

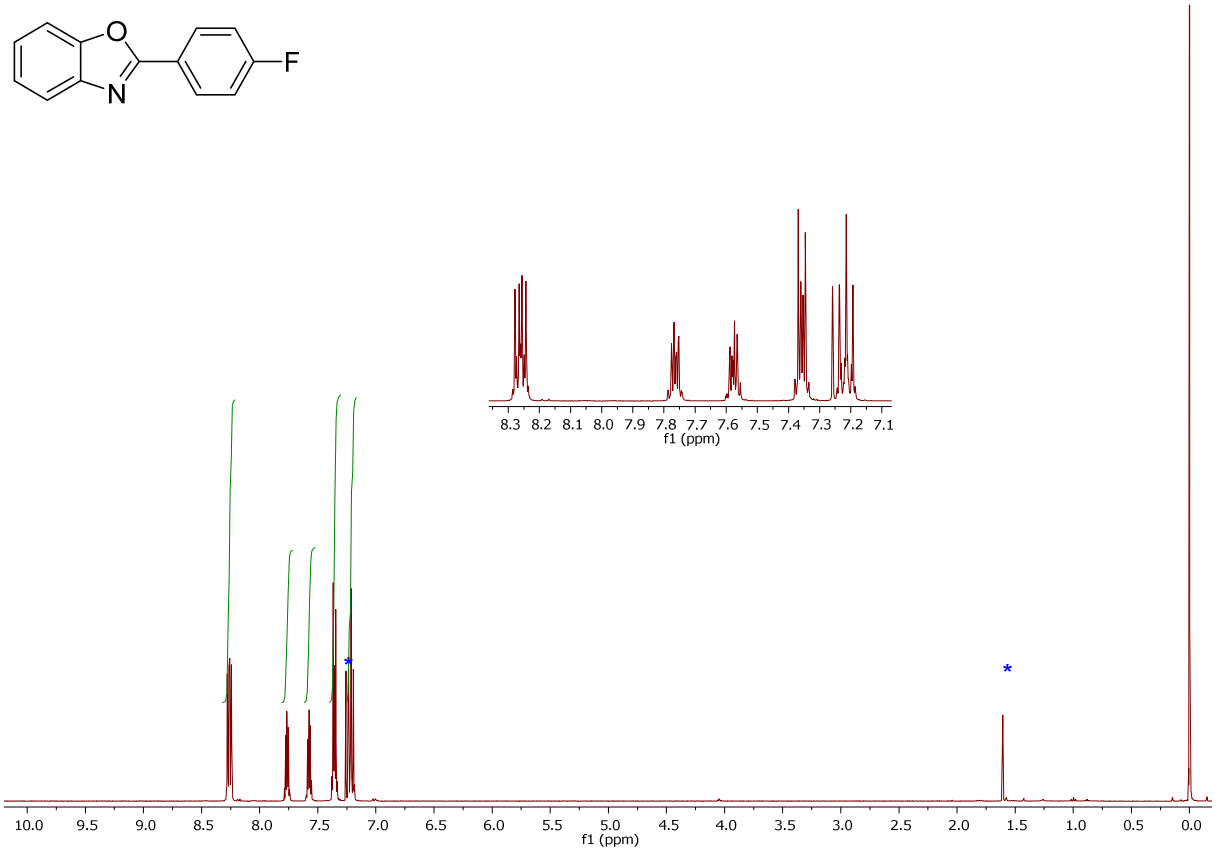

Figure S62. ^{1}H NMR spectrum (400 MHz, $CDCl_3$) of **12ak**

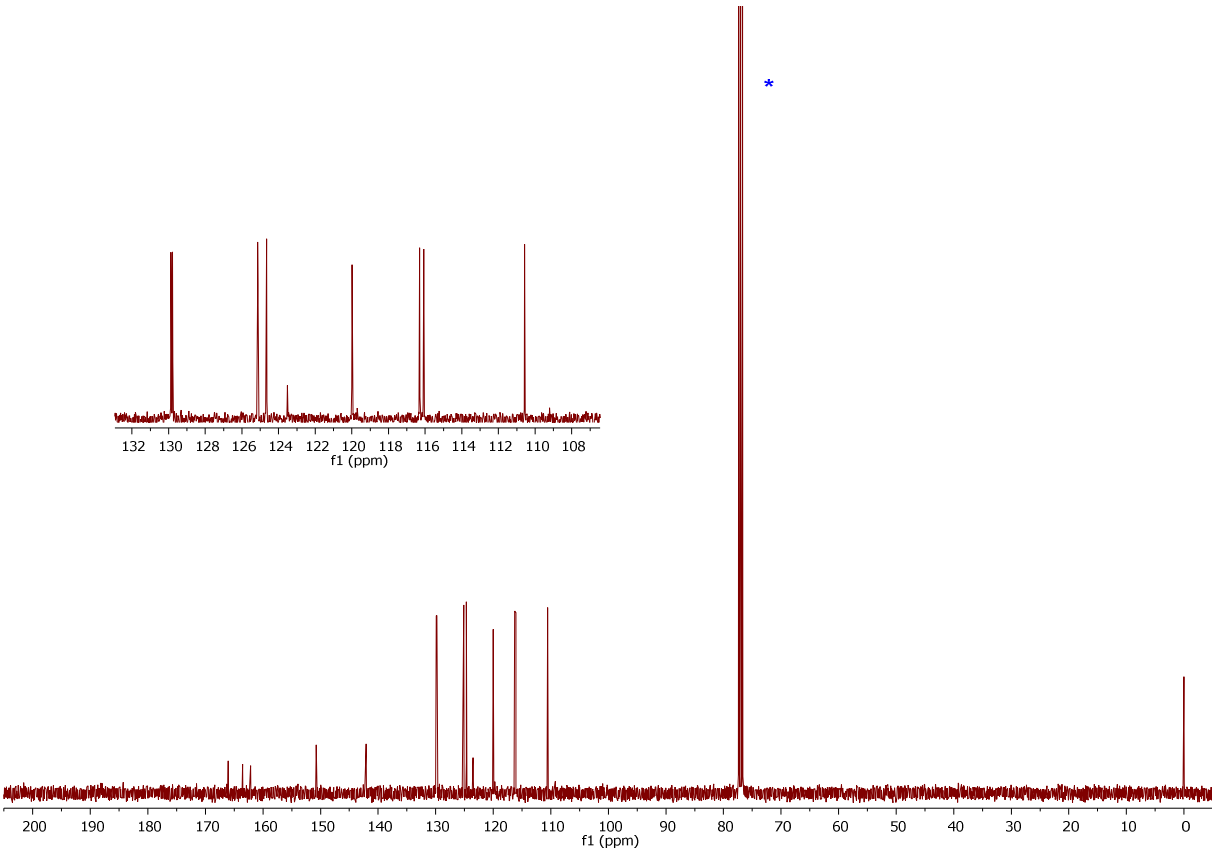

Figure S63. $^{13}C\{^{1}H\}$ NMR spectrum (101 MHz, $CDCl_3$) of **12ak**

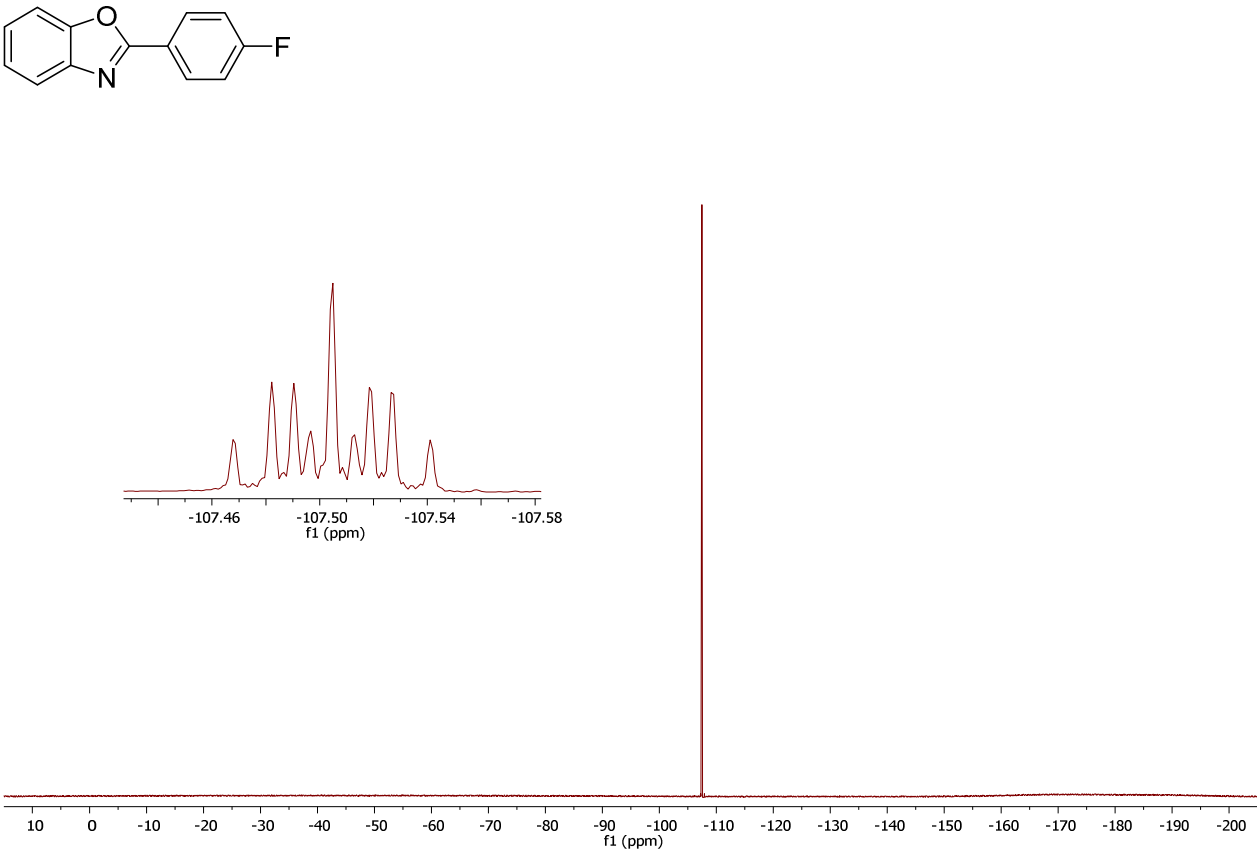

Figure S64. ^{19}F NMR spectrum (376 MHz, $CDCl_3$) of **12ak**

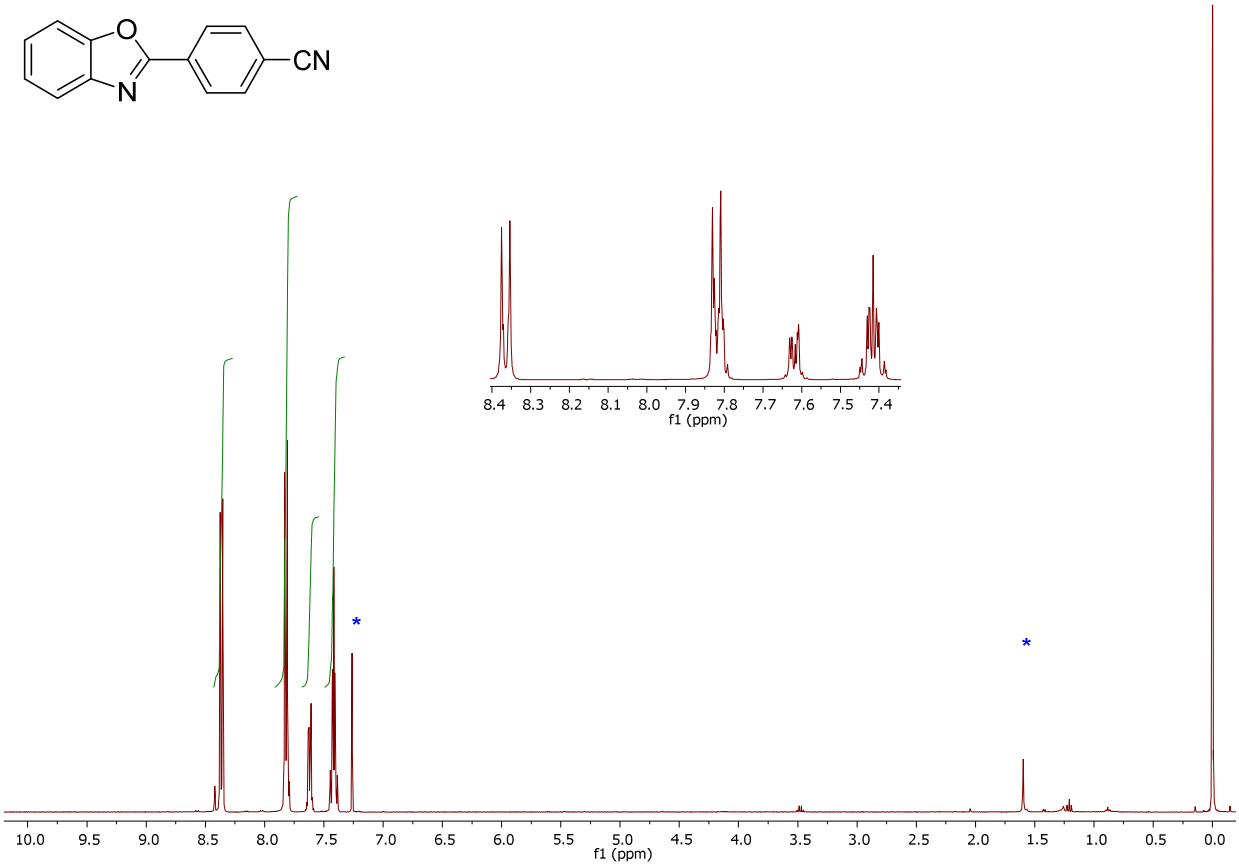

Figure S65. ^{1}H NMR spectrum (400 MHz, $CDCl_3$) of **12al**

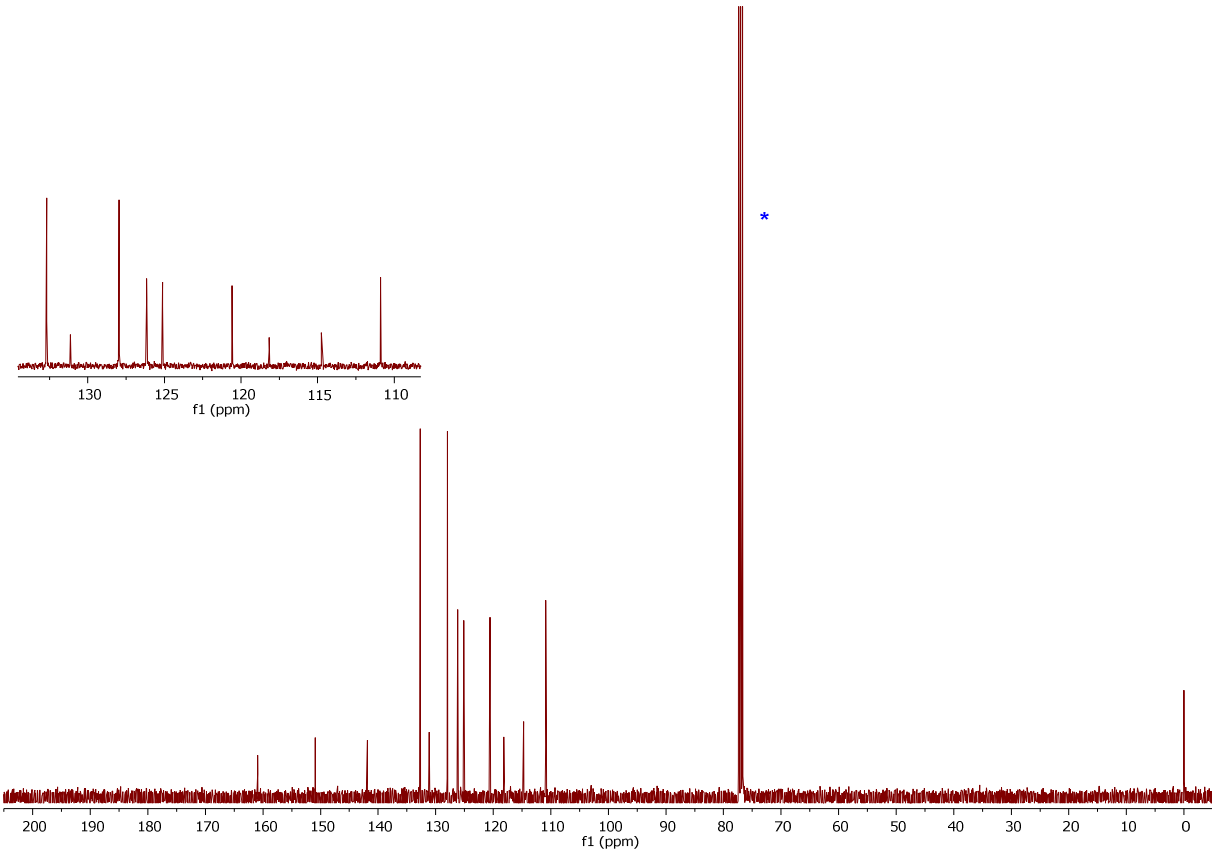

Figure S66. $^{13}C\{^{1}H\}$ NMR spectrum (101 MHz, $CDCl_3$) of **12al**.

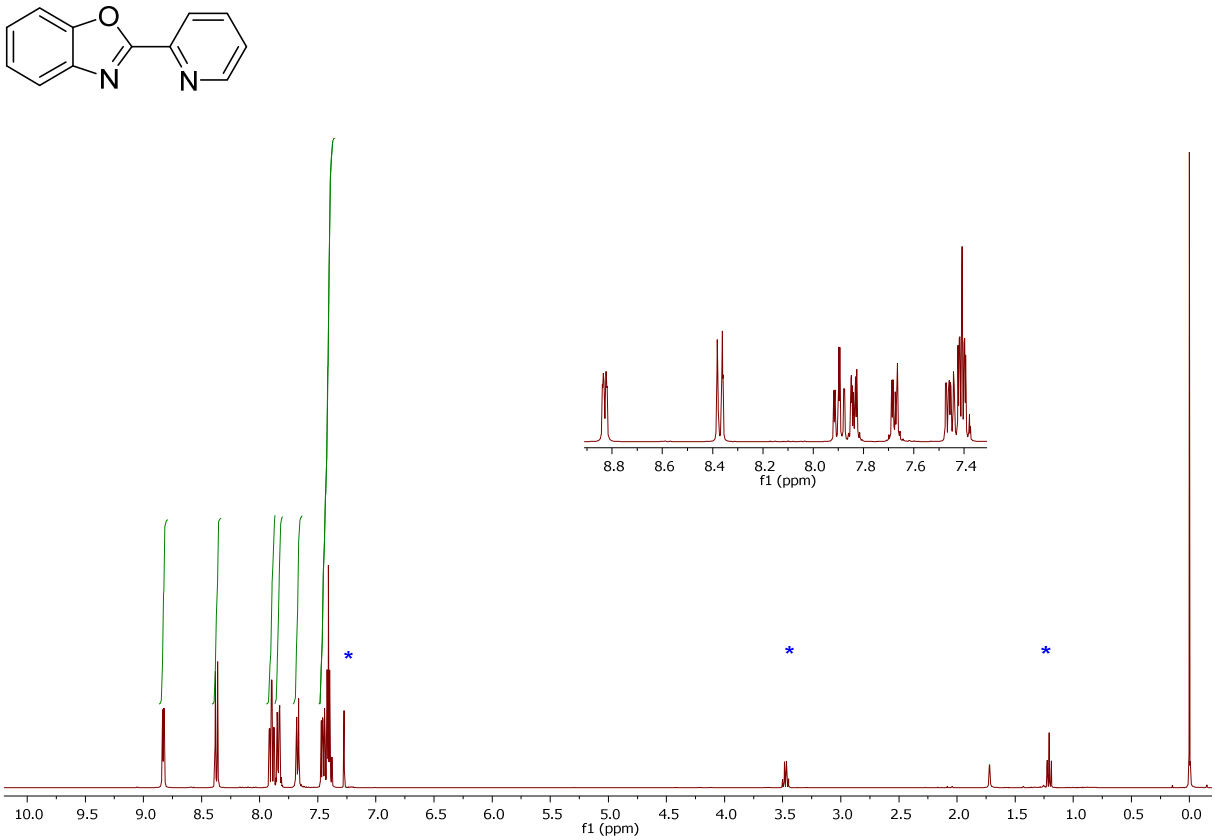

Figure S67. ^{1}H NMR spectrum (400 MHz, $CDCl_3$) of **12am**

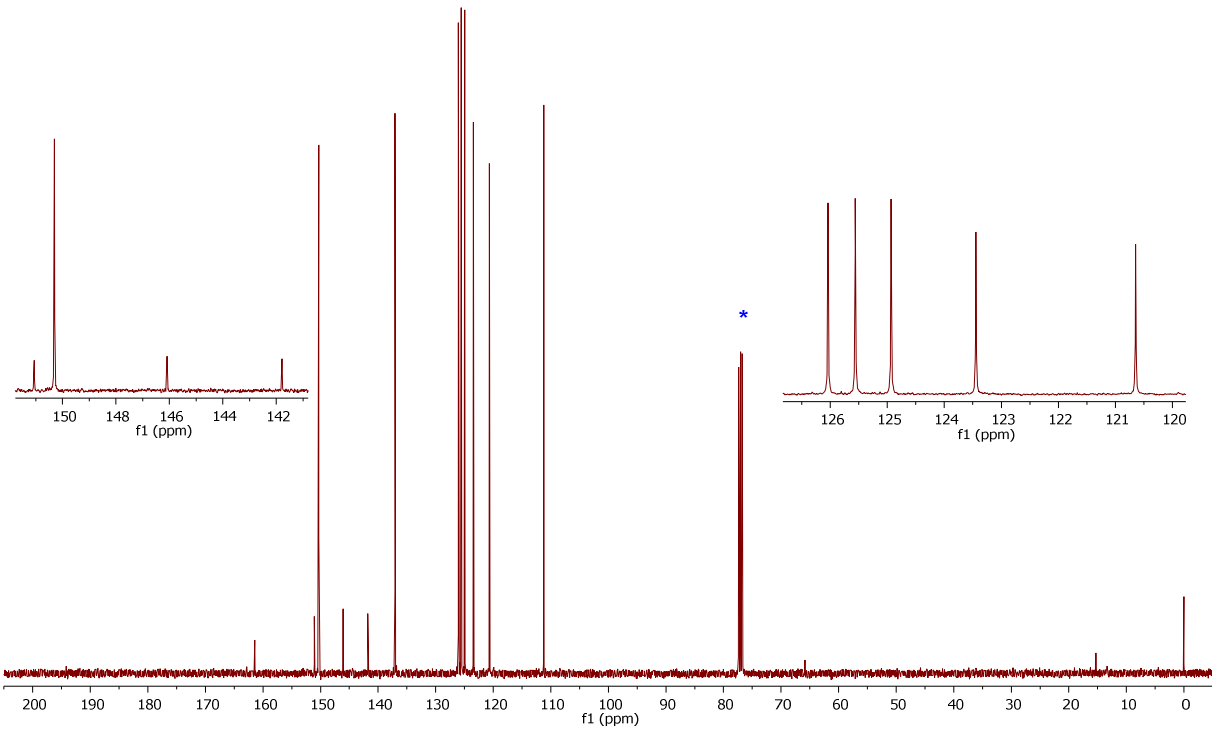

Figure S68. $^{13}C\{^{1}H\}$ NMR spectrum (101 MHz, $CDCl_3$) of **12am**.

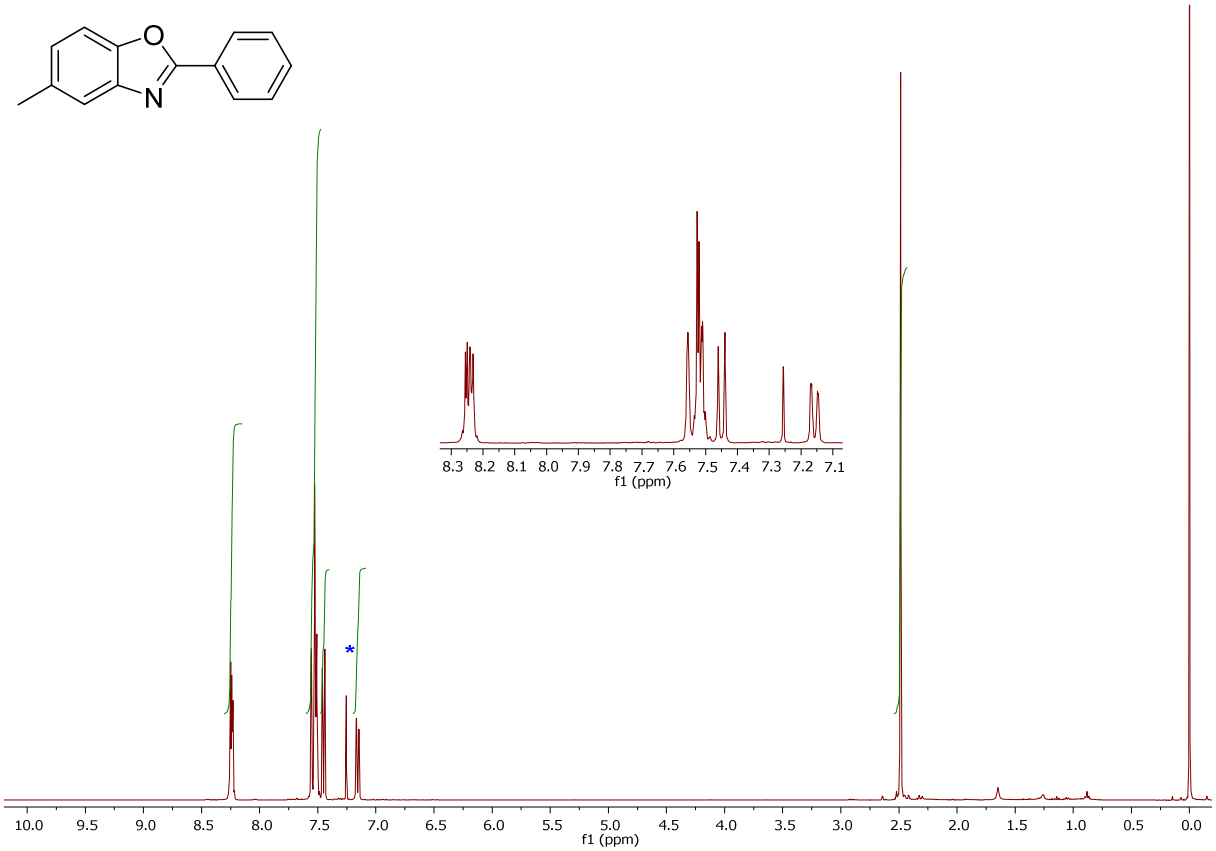

Figure S69. ^{1}H NMR spectrum (400 MHz, $CDCl_3$) of **12ba**

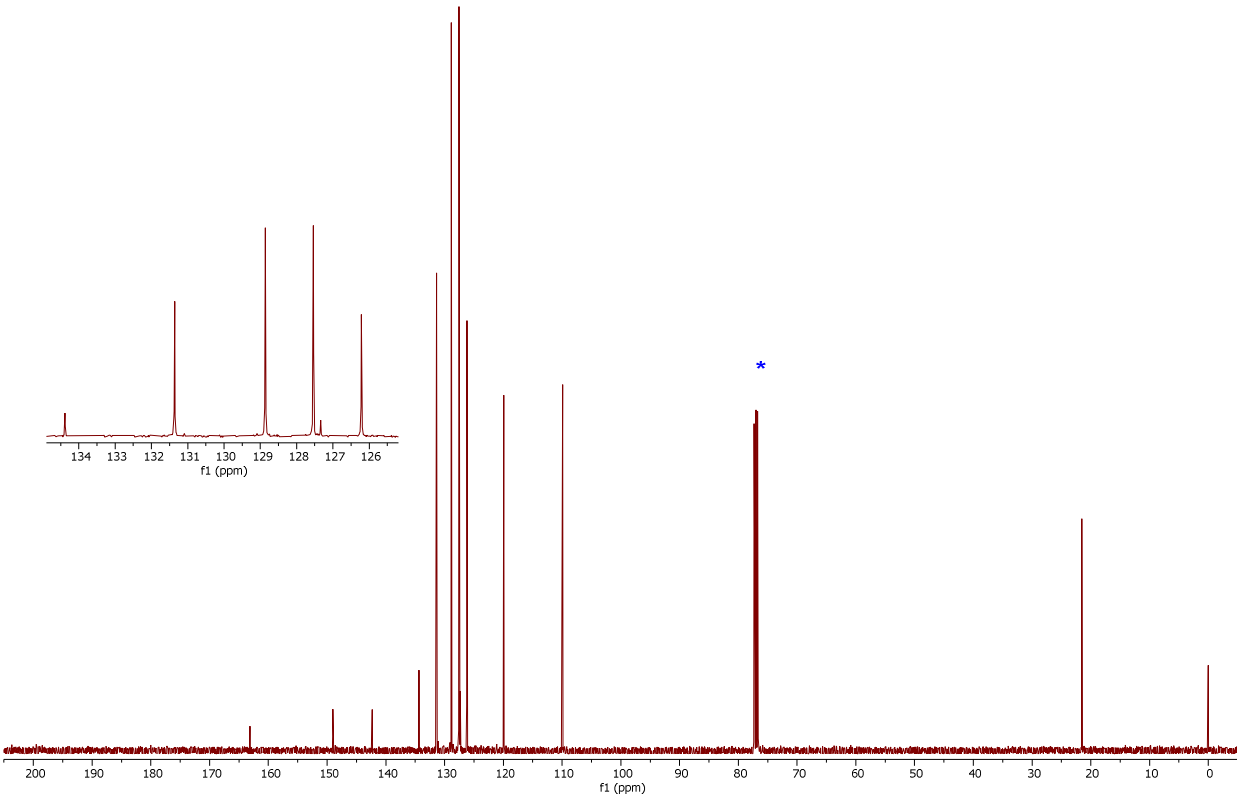

Figure S70. $^{13}C\{^{1}H\}$ NMR spectrum (101 MHz, $CDCl_3$) of **12ba**

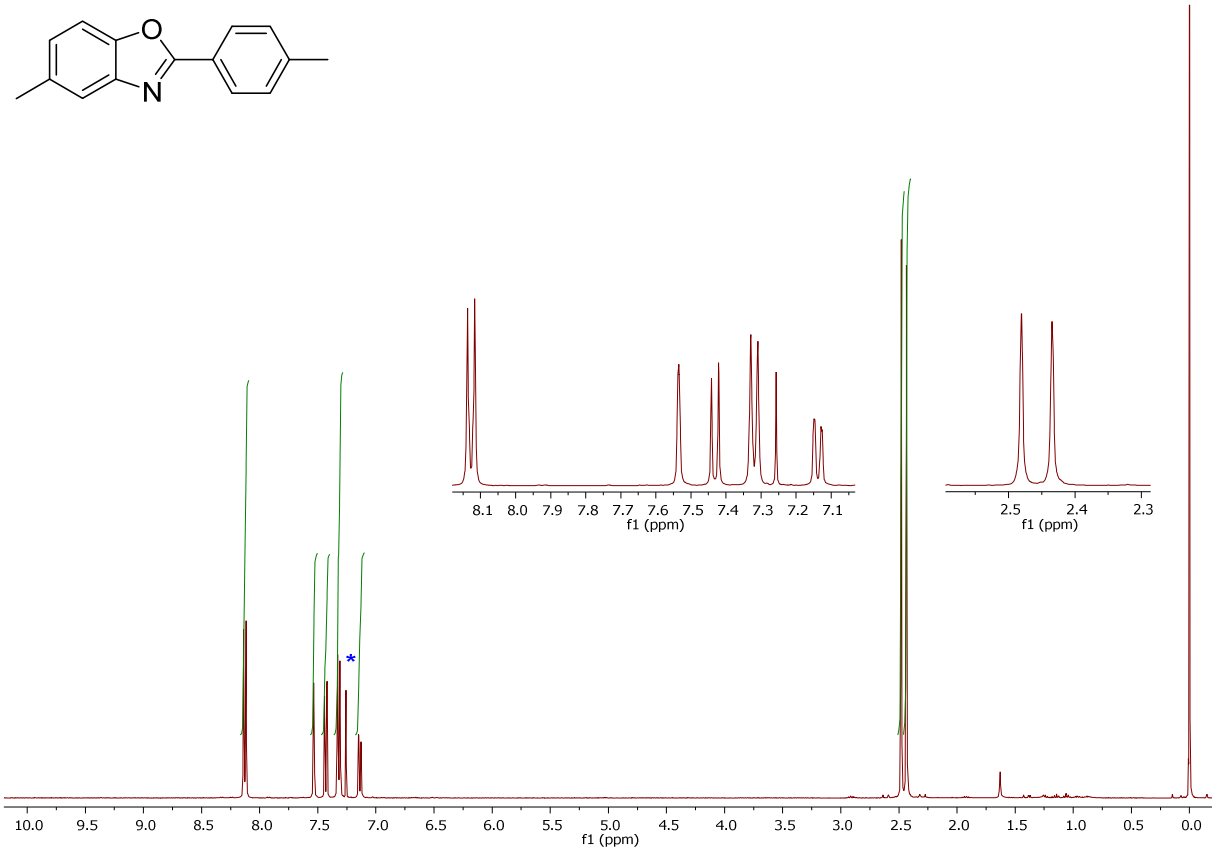

Figure S71. ^{1}H NMR spectrum (400 MHz, $CDCl_3$) of **12bb**

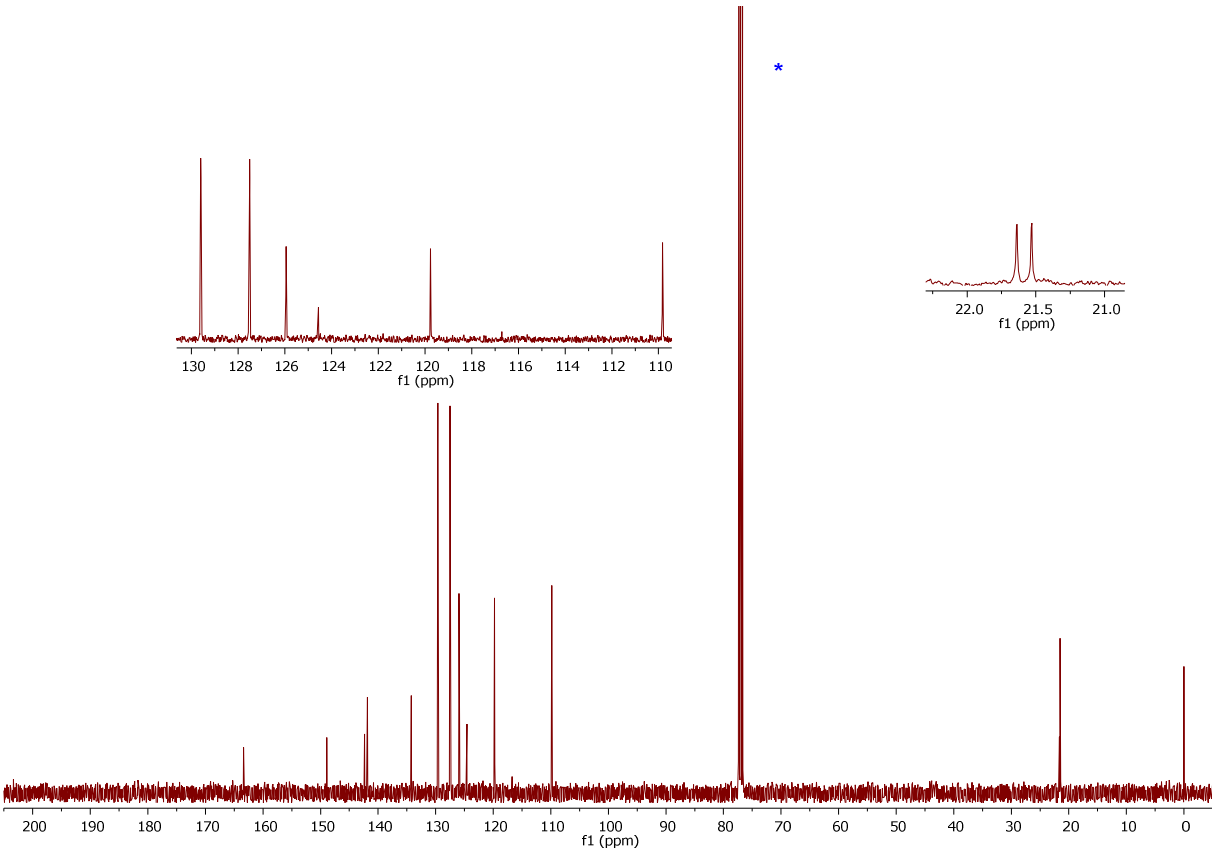

Figure S72. $^{13}C\{^{1}H\}$ NMR spectrum (101 MHz, $CDCl_3$) of **12bb**

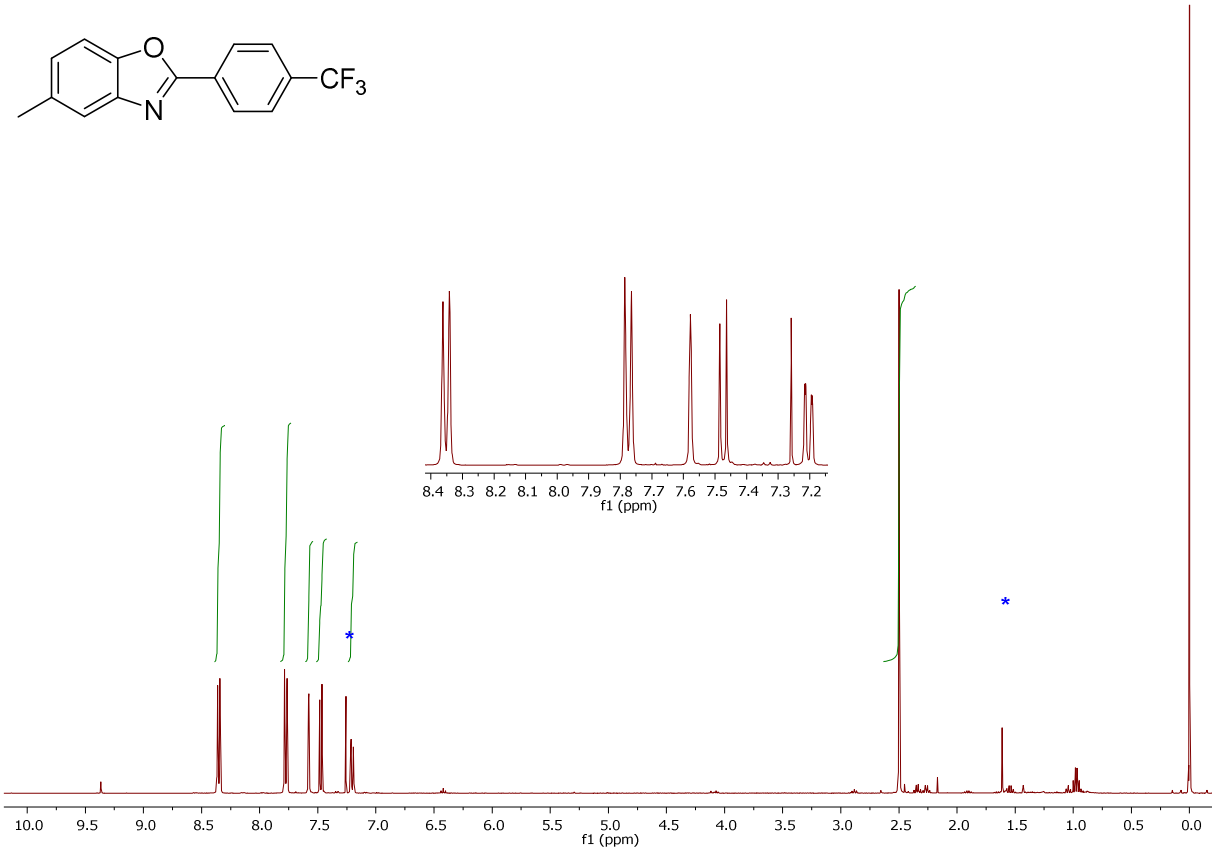

Figure S73. ^{1}H NMR spectrum (400 MHz, $CDCl_3$) of **12bc**

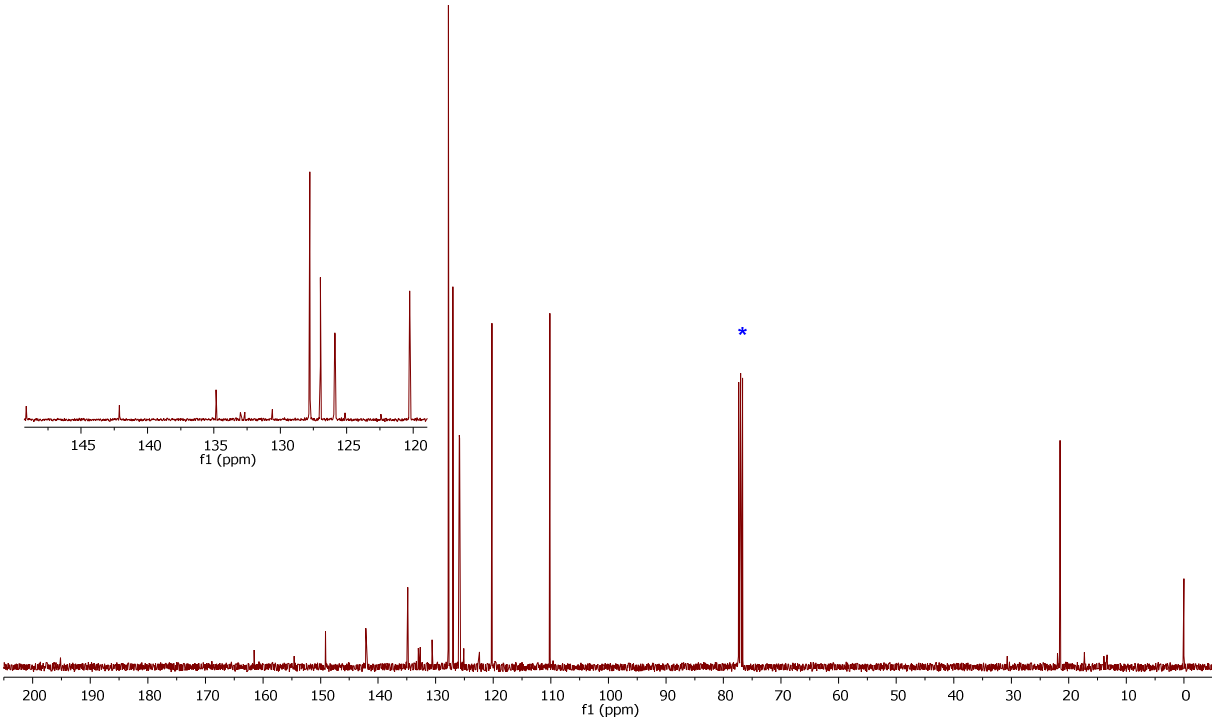

Figure S74. $^{13}C\{^{1}H\}$ NMR spectrum (101 MHz, $CDCl_3$) of **12bc**

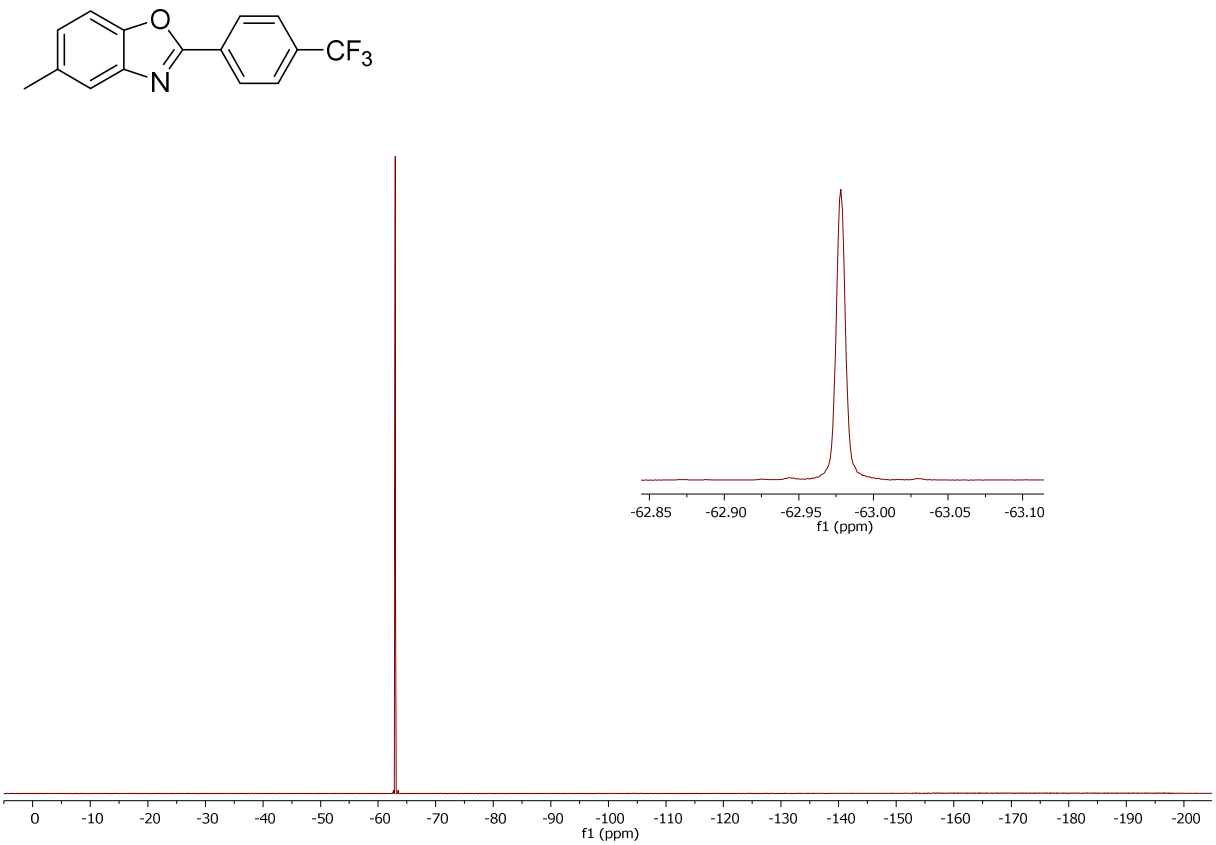

Figure S75. ^{19}F NMR spectrum (376 MHz, $CDCl_3$) of **12bc**

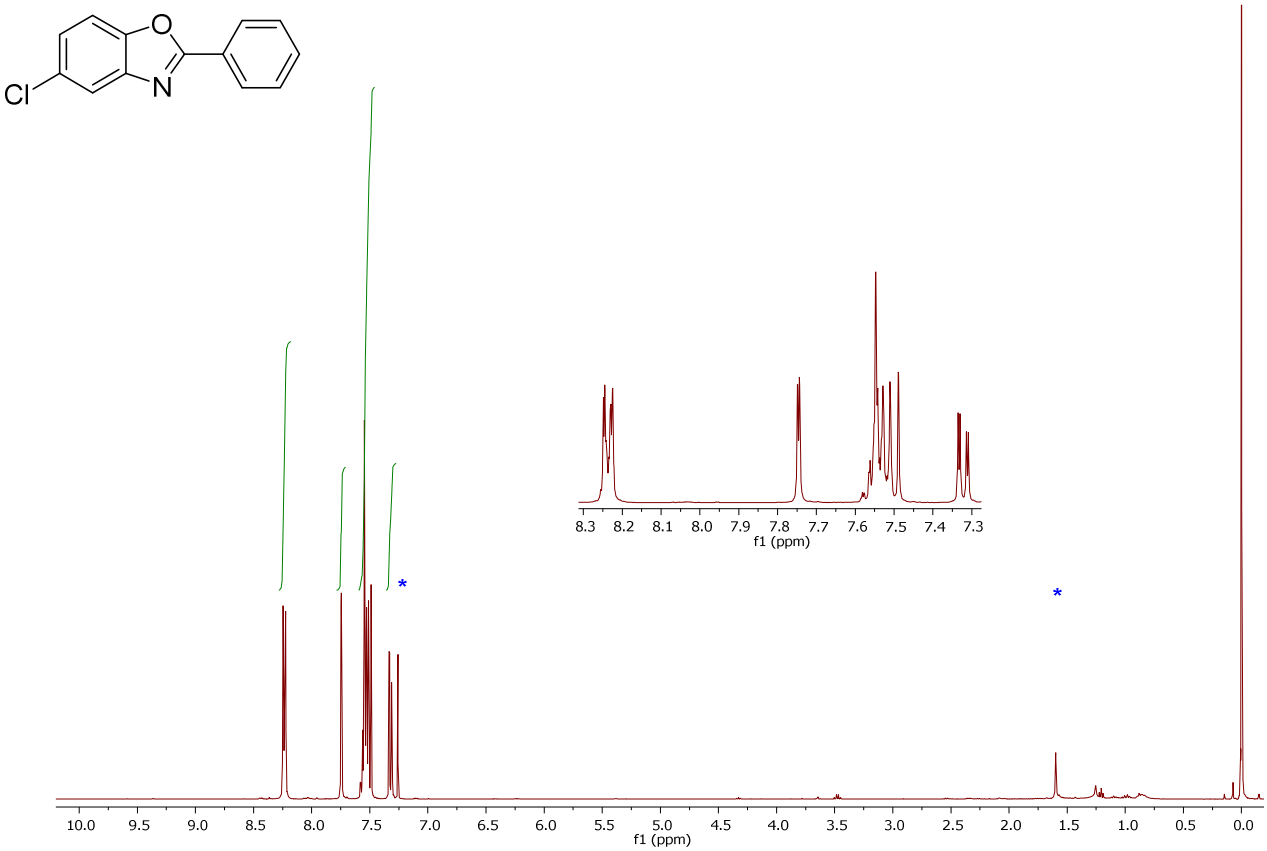

Figure S76. ^{1}H NMR spectrum (400 MHz, $CDCl_3$) of **12ca**

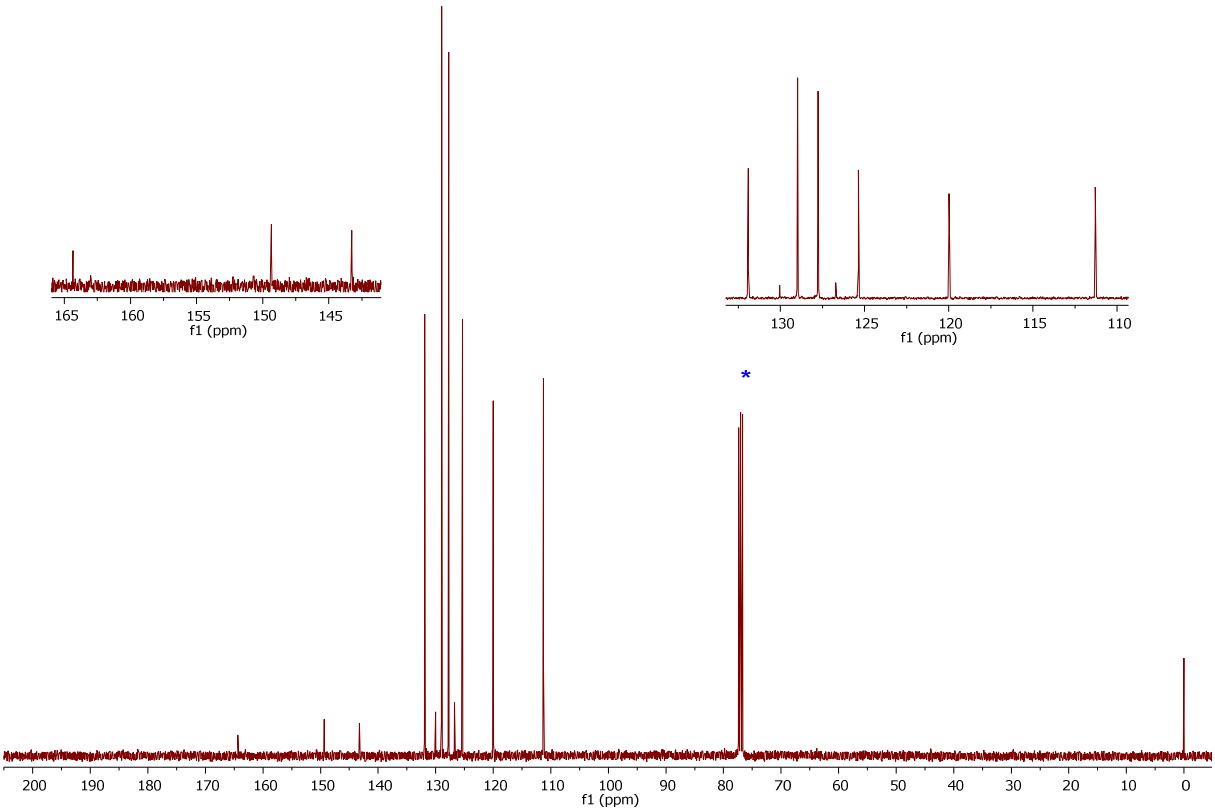

Figure S77. $^{13}C\{^{1}H\}$ NMR spectrum (101 MHz, $CDCl_3$) of **12ca**

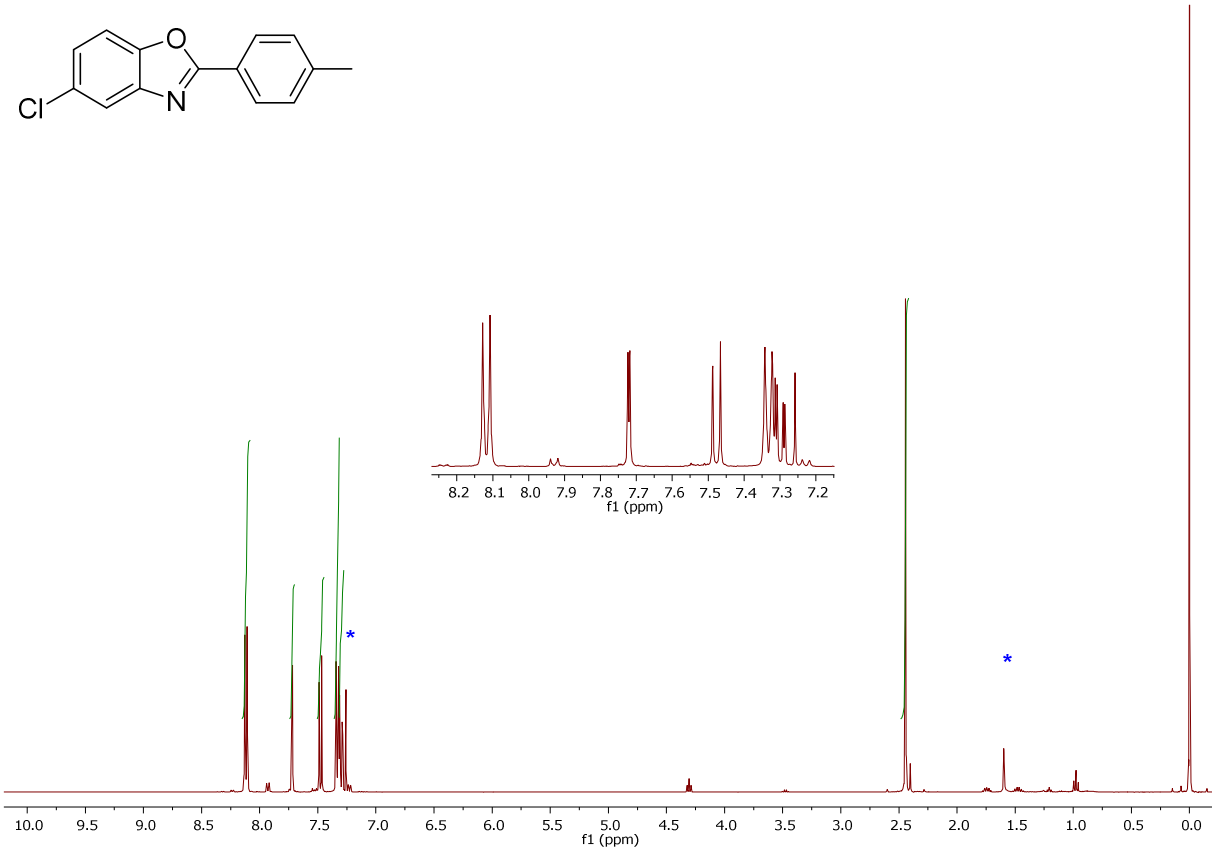

Figure S78. ^{1}H NMR spectrum (400 MHz, $CDCl_3$) of **12cb**

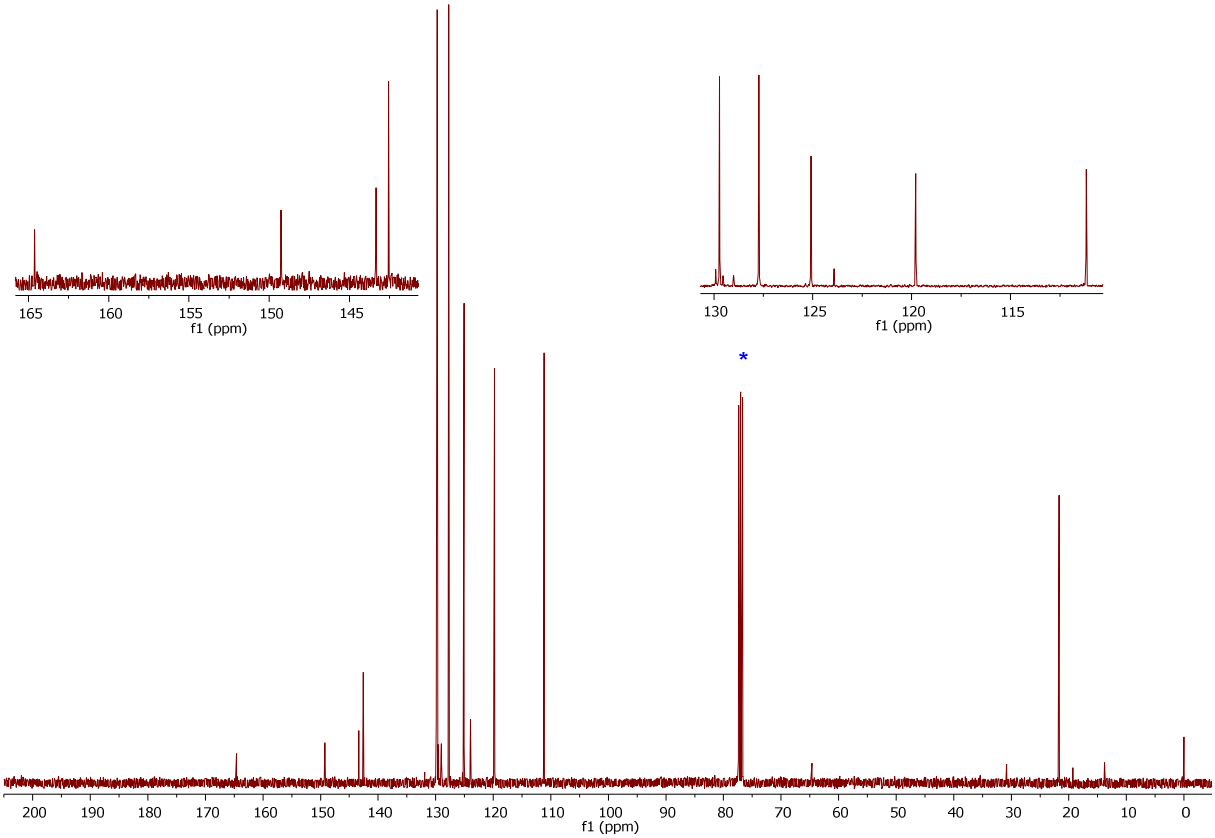

Figure S79. $^{13}C\{^{1}H\}$ NMR spectrum (101 MHz, $CDCl_3$) of **12cb**

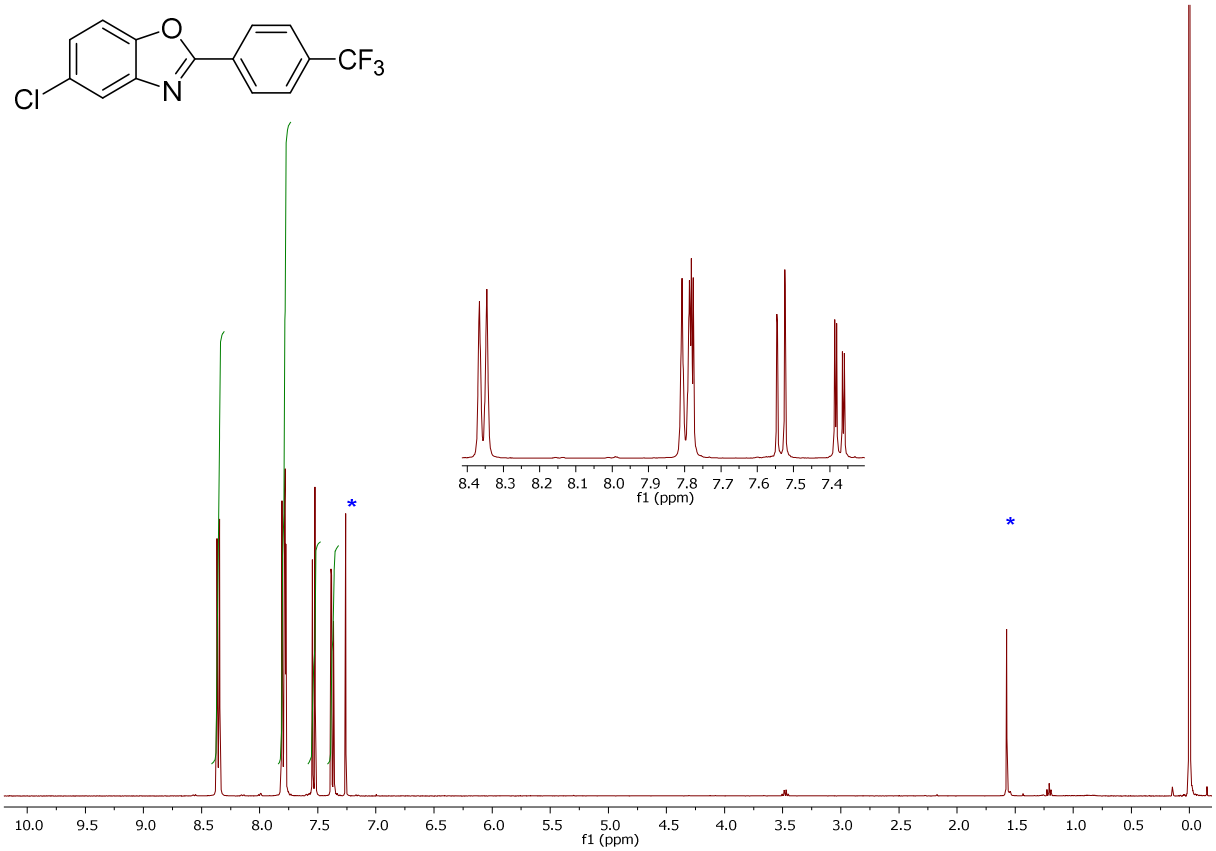

Figure S80. ^{1}H NMR spectrum (400 MHz, $CDCl_3$) of **12cc**

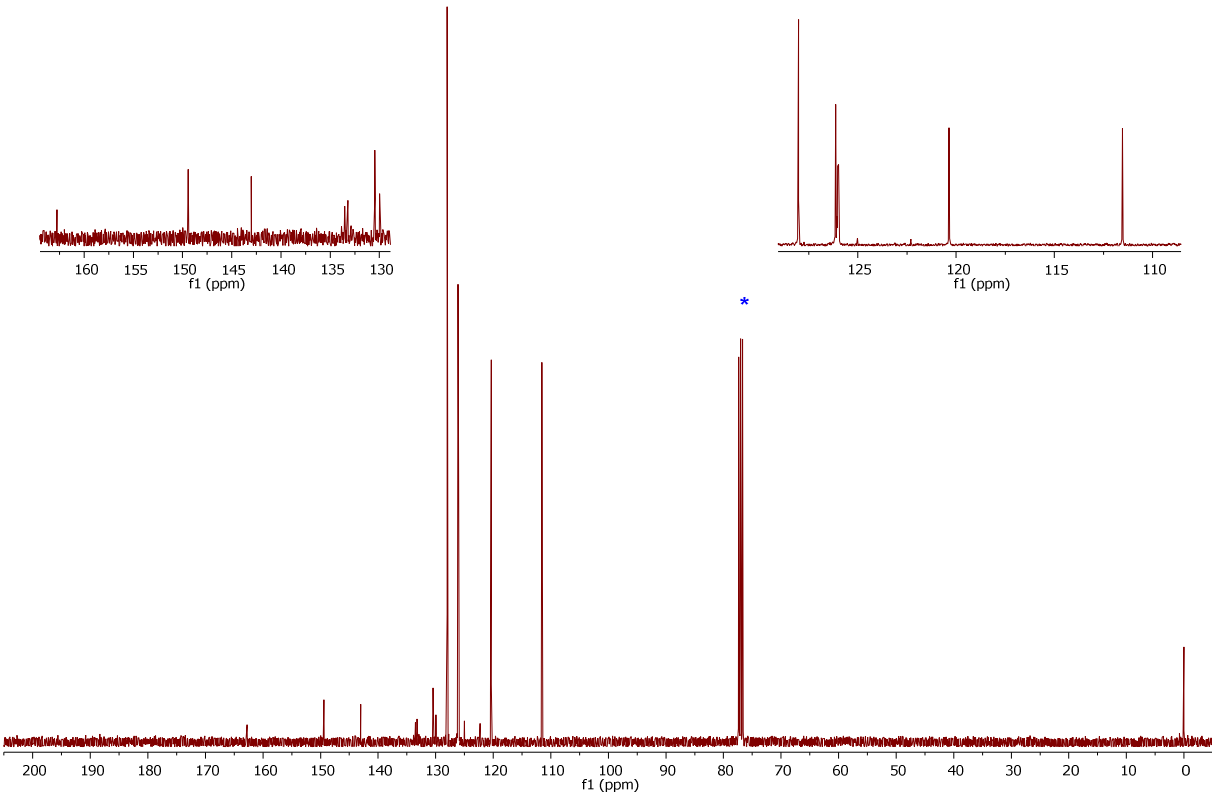

Figure S81. $^{13}C\{^{1}H\}$ NMR spectrum (101 MHz, $CDCl_3$) of **12cc**

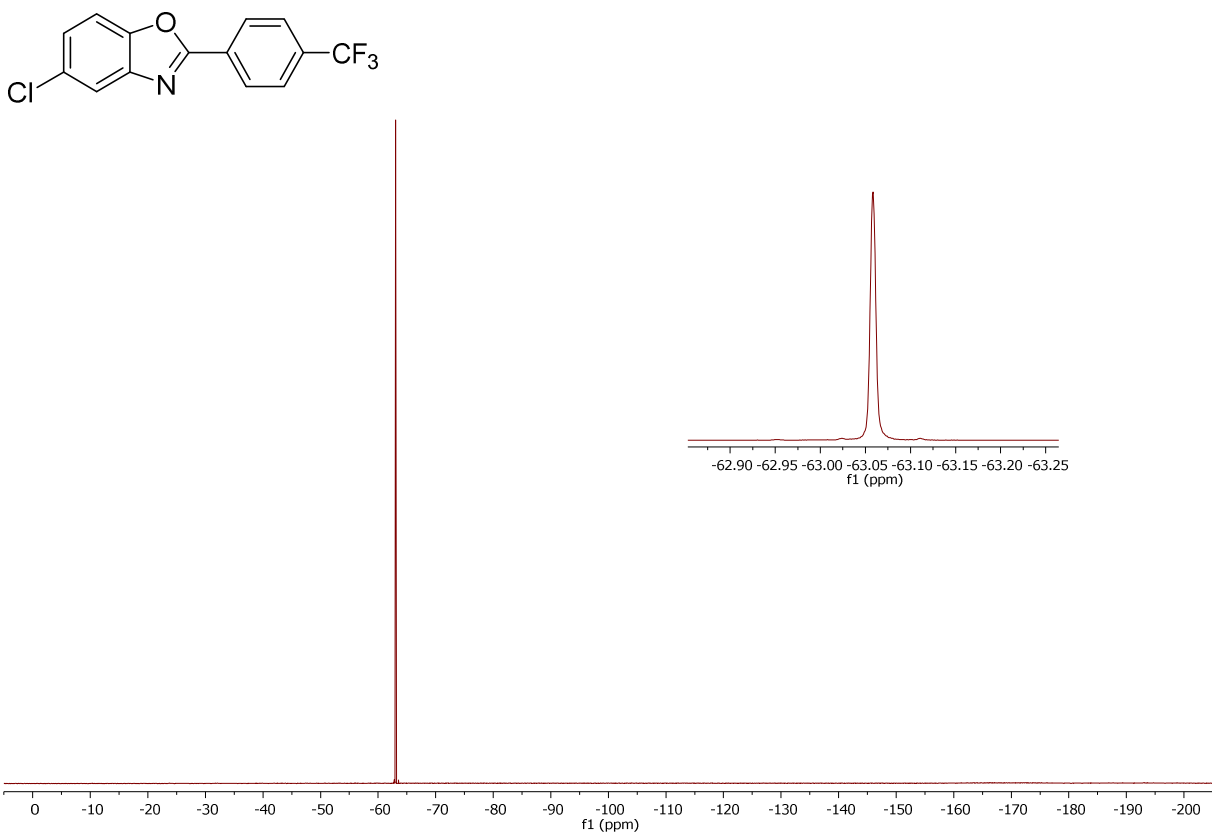

Figure S82. ^{19}F NMR spectrum (376 MHz, $CDCl_3$) of **12cc**

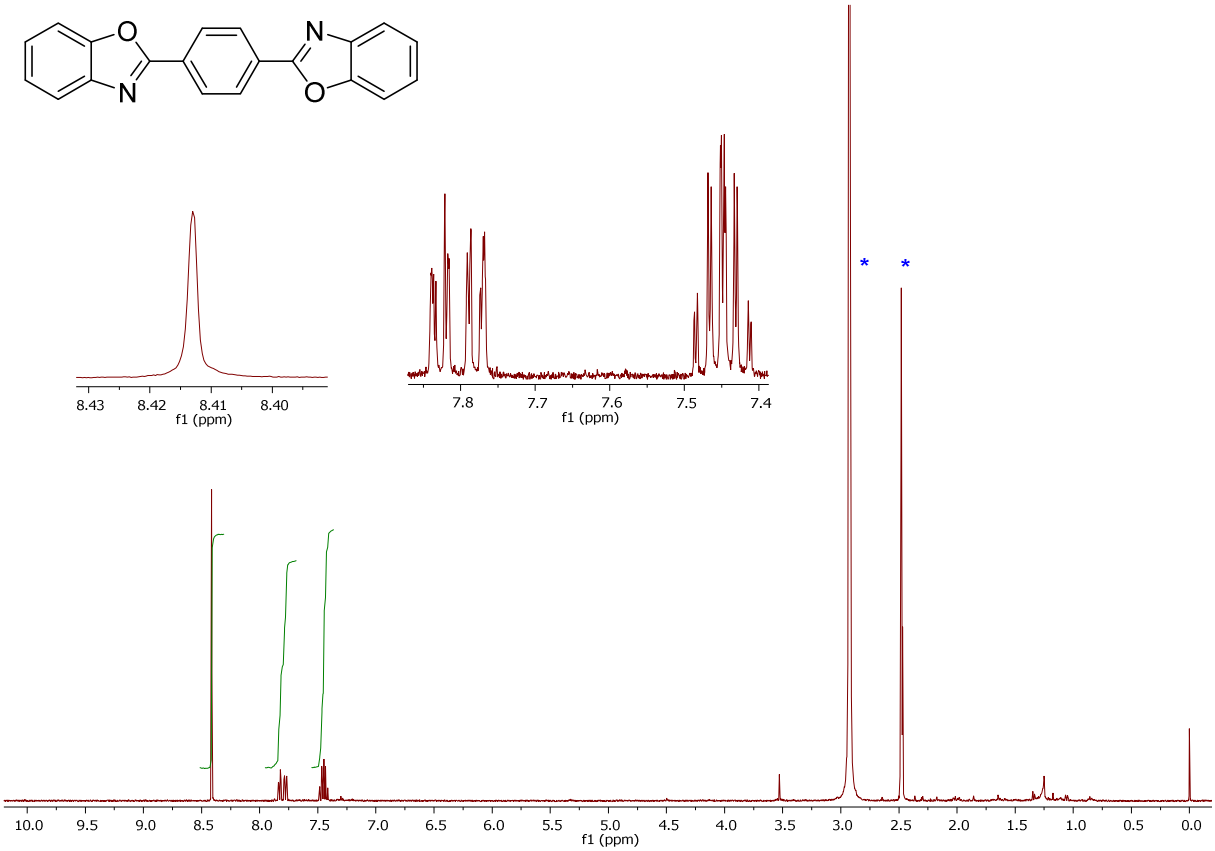

Figure S83. ^{1}H NMR spectrum (400 MHz, dmso-d_6, **100°C**) of **12an**

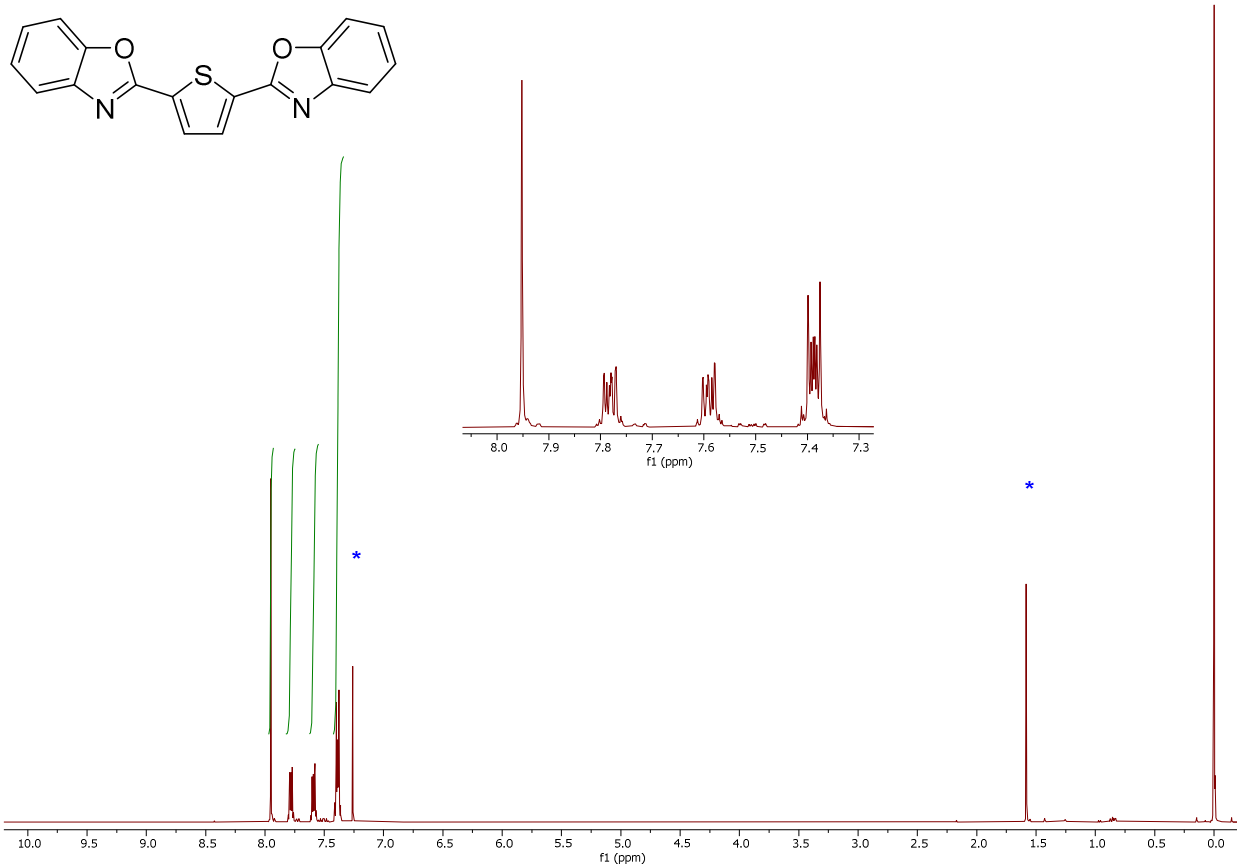

Figure S84. ^{1}H NMR spectrum (400 MHz, $CDCl_3$) of **12ao**

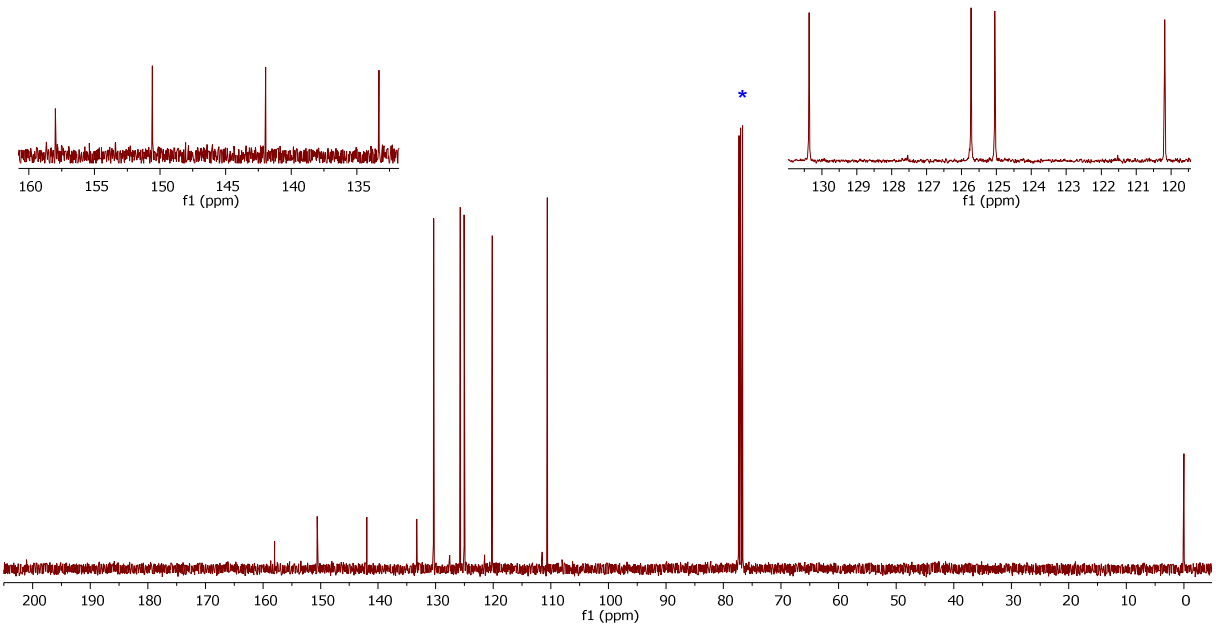

Figure S85. $^{13}C\{^{1}H\}$ NMR spectrum (101 MHz, $CDCl_3$) of **12ao**

References

[1] J. H. Dowing, J. Floure, K. Heslop, M. F. Haddow, J. Hopewell, M. Lusi, H. Phetmung, A. G. Orpen, P. G. Pringle, R. I. Plugh, *Organometallics* **2008**, *27*, 3216-3224.

[2] S. Raoufmoghaddam, S. Mannathan, A. J. Minnaard, J. G. de Vries, J. N. H. Reek, *ChemCatChem* **2018**, *10*, 266-272.

[3] Y.-C. Chang, Y.-C. Lee, M.-F. Chang, F.-E. Hong, *J. Organomet. Chem.* **2016**, *808*, 23-33.

[4] G. M. Sheldrick, *Acta Crystallogr., Sect. A: Found. Adv*. **2015**, *71*, 3-8.

[5] G. M. Sheldrick, *Acta Crystallogr., Sect. C: Struct. Chem*. **2015**, *71*, 3-8.

[6] a) A. L. Spek, *J. Appl. Crystallogr.* **2003**, *36*, 7-13; b) A. L. Spek, *Acta Crystallogr. D, Biol. Crystallogr.* **2009**, *65*, 148-155.

[7] S. P. Marsden, A. E. McGonagle, B. McKeever-Abbas, *Org. Lett.* **2008**, *10*, 2589-2591.

[8] L. Wang, Z. G. Ma, X.-J. Wei, Q.-Y. Meng, D.-T. Yang, S.-F. Du, Z.-F. Chen, L.-Z. Wu, Q. Liu, *Green Chem.* **2014**, *16*, 3752-3757.

[9] M. Zhang, S. Zhang, M. Liua, J. Cheng, *Chem. Commun*. **2011**, *47*, 11522-11524.

[10] S. Haneda, Z. Gan, K. Eda, M. Hayashi, *Organometallics* **2007**, *26*, 6551-6555.

[11] J. Lee, J. Kim, Y. M. Jun, B. M. Lee, B. H. Kim, *Tetrahedron* **2009**, *65*, 8821-8831.

[12] A. Kremer, C. Aurisicchio, F. De Leo, B. Ventura, J. Wouters, N. Armaroli, A. Barbieri, D. Bonifazi, *Chem. Eur. J*. **2015**, *21*, 15377-15387.

[13] F. Shibahara, E. Yamaguchi, T. Murai, *Chem. Commun.* **2010**, *46*, 2471-2473.

Appendix D

Horký, F.; Císařová, I.; Štěpnička, P. Synthesis, coordination and catalytic use of phosphinoferrocene ligands bearing 6-phospha-2,4,6-trioxaadamantane P-donor moieties. *J. Organomet. Chem.* **2021**, submitted manuscript.

Synthesis, coordination and catalytic use of phosphinoferrocene ligands bearing 6-phospha-2,4,6-trioxaadamantane P-donor moieties

Filip Horký, Ivana Císařová and Petr Štěpnička*

Department of Inorganic Chemistry, Faculty of Science, Charles University, Hlavova 2030, 128 40 Prague, Czech Republic

* Corresponding author. E-mail address: petr.stepnicka@natur.cuni.cz

Abstract. 1,1'-bis(Diphenylphosphino)ferrocene (dppf) and structurally related ferrocene bis-phosphines are indispensable ligands for coordination chemistry and catalysis. This contribution focuses on the coordination behaviour and catalytic properties of two dppf congeners bearing 1,3,5,7-tetramethyl-2,4,6-trioxa-8-phosphatricyclo[3.3.1.1^{3,7}]decane-8-yl groups (CgP) as the P-donor moieties, viz. $Ph_2PfcCgP$ (**1**) and its semi-homologous counterpart Ph_2PfcCH_2CgP (**2**; fc = ferrocene-1,1'-diyl). In reactions with a $PdCl_2$ source, compound **1** produced exclusively the *cis*-chelate complex [$PdCl_2$(**1**-κ^2*P*,*P*')], while the homologated ligand **2** afforded a complex mixture of compounds which equilibrated upon heating in methanol in favour of the symmetrical dimeric complexes *trans*-[(μ-**2**)$PdCl_2$]$_2$ as a mixture of racemic and *meso* isomers. Notably, in aqueous Pd-catalysed cyanation of aryl bromides and Suzuki-Miyaura-type cross-coupling of benzoyl chlorides with boronic acids producing benzophenones, catalysts generated *in situ* from bis-phosphine **1** and Pd(II) sources were more active than their counterparts resulting from dppf and **2**.

1. Introduction

Phosphine derivatives featuring 6-phospha-2,4,6-trioxaadamantane cages (or 1,3,5,7-tetramethyl-2,4,6-trioxa-8-phosphatricyclo[3.3.1.1^{3,7}]decane-8-yl groups; henceforth denoted as CgP or cage phosphines) have emerged as attractive auxiliary ligands for transition metal catalysis [1]. In particular, their catalytic applications capitalise on the unique properties of the P-donor sites derived from a specific combination of steric rigidity of the phosphabicyclic system, the narrow C-P-C angle and low basicity of its phosphorus atoms, comparable with that of phosphites. Yet, ferrocene-based ligands containing CgP moieties remain rare [2]. For this reason, we have recently prepared two CgP-ferrocene bis-phosphines [3], structurally related to the widely used 1,1'-bis(diphenylphosphino)ferrocene (dppf) [4] (Scheme 1). Compounds **1** and **2** were applied as ligands in the synthesis of stable Pd(0) complexes, which were in turn used as defined active Pd (pre)catalysts for C−H arylation of benzoxazole with aryl chlorides [3].

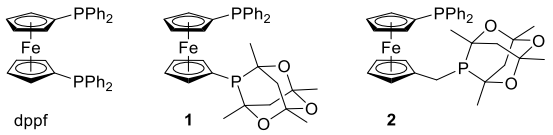

Scheme 1. Dppf and the analogous, donor-unsymmetric phosphinoferrocene ligands with CgP donor groups.

Encouraged by the successful applications of other CgP phosphines in Pd- and Ni-catalysed cross-coupling reactions [5], we decided to extend our research focused on ferrocene phosphines with CgP substituents to such reactions. This contribution describes the comparison of bis-phosphines **1** and **2** and the widely studied dppf as supporting ligands in Pd-catalysed cyanation of aryl bromides and Suzuki-Miyaura-type cross-coupling of arylboronic acids with benzoyl chlorides yielding benzophenones, both performed in biphasic aqueous reaction media. Besides, we report the preparation and structural characterisation of Pd(II) complexes with both ferrocene-based CgP bis-phosphines.

2. Results and discussion

*2.1 Synthesis and characterisation of Pd(II) complexes with ligands **1** and **2***

Compound **1** reacted cleanly with $[PdCl_2(MeCN)_2]$ in dichloromethane to produce chelate complex **3** (Scheme 2). The complex was conveniently isolated by crystallisation from chloroform/hexane, resulting in a stoichiometric solvate, **3**·2$CHCl_3$. However, this solvate partly loses the solvent of crystallisation upon prolonged storage or under vacuum. Based on the NMR data, the compound was formulated as a *cis*-chelate complex, analogous to the well-known *cis*-$[PdCl_2(dppf\text{-}\kappa^2P,P')]$. In particular, the compound displays a pair of doublets in the $^{31}P\{^1H\}$ NMR spectrum attributable to the different P-donor moieties, at δ_P 29.4 (PCg) and 37.1 (PPh_2), while the relatively small $^2J_{PP}$ coupling constant (12 Hz) suggests their *cis* arrangement. The ^1H and $^{13}C\{^1H\}$ NMR further corroborate the formulation by showing only one set of signals due to the CgP cage and to the phosphinoferrocene unit. Given the inherent chirality of the CgP cage, the ferrocene CH groups become diastereotopic and give rise to eight resonances in both spectra. The signals of the phenyl ring carbons in the ^{13}C NMR spectrum are similarly affected.

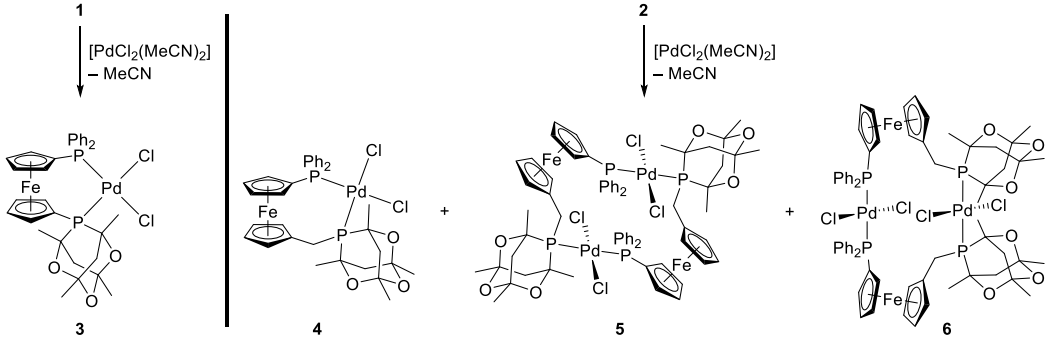

Scheme 2. Preparation of Pd(II) complexes with ligands **1** and **2** (the chirality of the CgP page is neglected to simplify the overall picture).

An analogous reaction involving bis-phosphine **2** was much more complicated, producing an intractable product mixture. Most ^{31}P NMR signals were, nevertheless, downfield shifted, suggesting coordination of the phosphine moieties. Furthermore, among the numerous signals, we were able to identify two pairs attributable to symmetrical dimers $[(\mu\text{-}\mathbf{2})PdCl_2]_2$ (**5**) in which

the phosphines occupy *trans* positions [6]: δ_P 4.7 and 17.6 (2× d, $^2J_{PP}$ = 551 Hz); 6.7 and 15.9 (2× br d, $^2J_{PP}$ = 550 Hz). Apparently, the CH_2 linker reduces the tendency of **2** to form chelate complexes due the overall higher molecular flexibility and destabilisation of the larger and more flexible chelate rings. These findings are in line with our previous observations, suggesting that homologated dppf congeners form equilibrium mixtures of P,P-chelate monopalladium and P,P-bridged dipalladium complexes under similar conditions [6]. In the present case, however, the situation is further complicated by chirality of the CgP cage, which contains four stereogenic carbon atoms, whose configuration cannot change independently [7]. As a result, the cage can exist in two enantiomeric forms, formally **A** and **B** (Scheme 3). Thus, while **3** results as a simple racemate, each ligand-bridged dipalladium complex can exist in racemic (**AA** or **BB**) and *meso* (**AB** and **BA**) form.

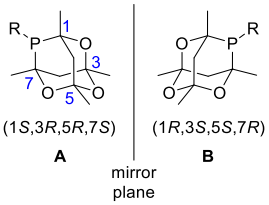

Scheme 3. Depiction of the two enantiomeric forms of the CgP cage

Gratifyingly, upon changing the reaction solvent to methanol and heating the reaction mixture at 40°C for 6 h or overnight, the reaction of **2** with $[PdCl_2(MeCN)_2]$ produced a mixture of *two* major products, most likely stereoisomers of the aforementioned complexes $[(\mu\text{-}\mathbf{2})PdCl_2]_2$ (see Supporting Information). By comparison to the NMR data of $[(\mu\text{-}R_2PfcCH_2PPh_2)PdCl_2]_2$ (R = *i*-Pr, *t*-Bu, Cy) [6] and to the results of structure determination (*vide infra*), we formulated these products as racemic (**AA** + **BB**, major) and *meso* (**AB**, minor) forms of the symmetrical (head-to-tail) dimer **5**. The formation of the analogous unsymmetrical (head-to-head) dimers **6**, other isomers (e.g., dimers with *cis* positioned P-donor groups) and the chelate complex **4**, which we were unable to unambiguously identify by ^{31}P NMR spectroscopy in the crude reaction mixture, is probably disfavoured for steric reasons.

As indicated above, complex **3** crystallised in solvated form. Figure 1 shows its molecular structure, and Table 1 outlines the relevant distances and angles. Additional structural diagrams are available in Supporting Information.

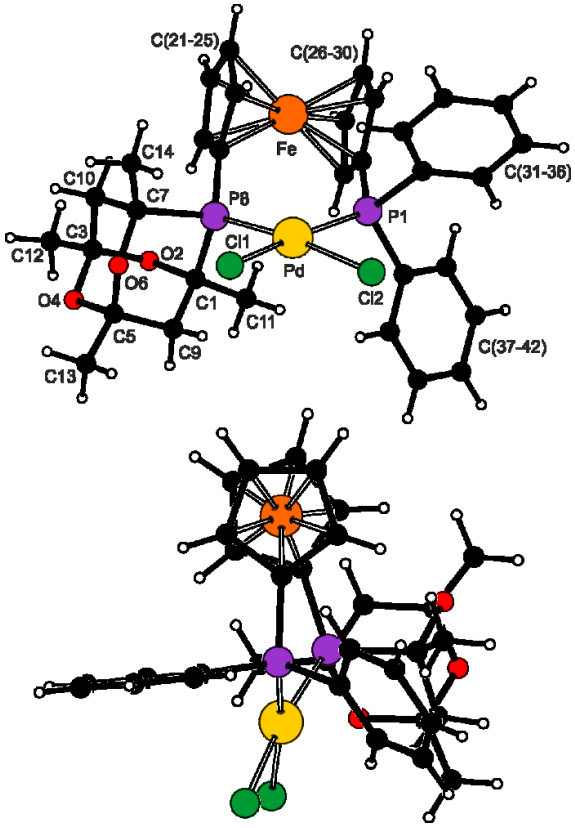

Figure 1. A general (top) and side (bottom) view of the complex molecule in the structure of **3**·2$CHCl_3$.

Table 1. Selected distances and angles for **3**·2$CHCl_3$ (in Å and °)[a]

Distances		Angles	
Pd-P1	2.2909(7)	P1-Pd-P8	98.97(3)
Pd-P8	2.2799(7)	P1-Pd-Cl2	82.70(2)
Pd-Cl1	2.3335(7)	P8-PdCl1	91.36(2)
Pd-Cl2	2.3600(7)	Cl1-Pd-Cl2	87.32(2)
Fe···Pd	4.3327(6)	tilt	1.5(2)
Fe-C	2.016(2)-2.056(3)	τ	−21.2(2)

[a] Fe-C is the range of Fe-C(21-30) bond lengths, tilt is the dihedral angles of the least square cyclopentadienyl planes, and τ is the torsion angle C21-Cg1-Cg2-C26, where Cg1 and Cg2 denote the centroids of the cyclopentadienyl rings C(21-25) and C(26-30), respectively.

The Pd-P and Pd-Cl distances determined for **3**·2$CHCl_3$ are similar to those determined for the analogous dppf complex, [$PdCl_2$(dppf-κ²*P*,*P*')]·CH_2Cl_2 at 173 K [8] or [$PdCl_2$(dppf-κ²*P*,*P*')]·$CHCl_3$, at ambient temperature [9]. As in [$PdCl_2$(dppf-κ²*P*,*P*')], the ligand bite angle in **3**·2$CHCl_3$, P1-Pd-P8 of 99°, is the widest of the interligand angles. This wide angle is, nevertheless, compensated for by closing of other interligand angles, mainly P1-Pd-Cl2, albeit without substantial distortion of the planar coordination sphere: the palladium and its four ligating atoms remain coplanar within ca. 0.1 Å (*cf*. the maximum deviation from the mean plane of −0.110(1) Å for atom Cl2), and the coordination "half-planes" {Pd,P1,P8} and {Pd,Cl1,Cl2} are mutually tilted by 7.09(3)°.

The CgP fragment in the structure of **3**·2$CHCl_3$ is positioned so that the P8-C1 bond is oriented parallel to the bonding cyclopentadienyl ring C(21-25) (angle 3.3(1)°), while the P8-C7 bond is almost perpendicular (82.8(1)°). Due to the rigidity and steric bulk of the CgP moiety, the pivotal atom P8 is displaced by 0.128(1) Å from the C(21-25) plane; no such distortion is detected in the PPh_2 moiety (the distance of P1 from the C(21-25) plane is only 0.025(1) Å). The ferrocene cyclopentadienyls are tilted by 2° and rotated from an eclipsed conformation by approximately 21°.

Crystallisation of the Pd-**2** reaction mixture containing mostly *rac*- and *meso*-**5** from methanol/diethyl ether produced single crystals of the solvated *racemic* isomer, *rac*-**5**·2MeOH·Et_2O. Unfortunately, the crystals suffered from twinning, and the chloride ligands and solvent molecules were partly disordered (see Section 4.6). Figure 2 displays a view of the molecular structure, and Table 2 provides main geometric parameters.

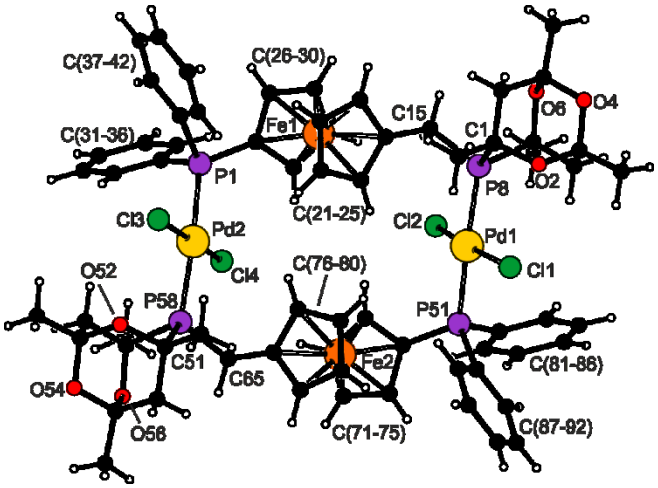

Figure 2. View of the complex molecule in the structure of *rac*-**5**·2MeOH·Et_2O. For clarity, only one position of the disordered chlorine atoms Cl1 and Cl3 is shown.

Table 2. Selected distances and angles for *rac*-**5**·2MeOH·Et_2O (in Å and °).[a]

Pd1-P51	2.304(2)	Pd2-P1	2.315(2)
Pd1-P8	2.326(2)	Pd2-P58	2.335(2)
Pd1-Cl1	2.284(3)	Pd2-Cl3	2.296(3)
Pd1-Cl2	2.310(2)	Pd2-Cl4	2.306(2)
P8-Pd1-Cl1	91.66(7)	P58-Pd2-Cl3	93.49(7)
P8-Pd1-Cl2	88.96(5)	P58-Pd2-Cl4	87.78(5)
P51-Pd1-Cl1	91.45(7)	P1-Pd2-Cl3	92.39(7)
P51-Pd1-Cl2	87.15(5)	P1-Pd2-Cl4	85.76(5)
Fe1-C(21-30)	2.024(5)-2.051(5)	Fe2-C(71-80)	2.020(7)-2.052(6)
tilt(Fe1)	6.2(3)	tilt(Fe2)	4.4(3)
τ(Fe1)	162.5(4)	τ(Fe2)	162.7(4)

[a] The parameters are defined as for **3**·3$CHCl_3$ (see footnote to Table 1). The parameters involving the disordered chlorine atoms (Cl1 and Cl3) pertain to the more populated position.

Compound *rac*-**5**·2MeOH·Et_2O crystallises with the symmetry of the orthorhombic space group $Pna2_1$ as a racemic twin (each molecule of the complex thus contains two CgP fragments of the

same configuration). The crystal structure corroborates the formulation of the complex as a "symmetrical" (or head-to-tail) dimer. Because of changed distribution of the donor moieties, which differ not only by steric demands but also in *trans* influence of the donor atoms (P > Cl) [10], the compound displays longer Pd-P and shorter Pd-Cl bonds than the *cis*-chelate complex mentioned above, where the P and Cl donor atoms occupy mutually *trans* positions. This also affects the interligand angles, which are closer to the ideal 90° (within approximately 4°). The two ferrocene units adopt similar, opened conformations ($\tau \approx 163°$), which are better suited for bridging two metal ions, albeit showing a higher tilting than **2**. The solvating methanol molecule, which was unambiguously included in the structure model, forms a hydrogen bond towards oxygen atom in the CgP cage (O1S···O52 = 2.926(8) Å).

2.2 Catalytic experiments

Two reactions of practical relevance were used to assess the catalytic properties of the Pd-L complexes (L = **1** and **2**), *viz*. the Pd-catalysed Suzuki-Miyaura-type cross-coupling of benzoyl chlorides with arylboronic acids selectively producing substituted benzophenones [11] and Pd-catalysed cyanation of aryl bromides [12] employing $K_4[Fe(CN)_6]$ as a non-toxic cyanide source [13]. Considering the complicated coordination behaviour of ligand **2**, the catalytic reactions were performed with catalysts generated *in situ* by pre-mixing the ligand and the respective palladium source (palladium acetate and $[PdCl_2(cod)]$, where cod = η^5:η^5-cycloocta-1,5-diene) in dichloromethane. To probe the influence of substituents, a pair of substrates, bearing electron-donating (MeO) and electron-withdrawing (CF_3) moieties in position 4 of the benzene ring, was used in both reactions.

The reaction conditions were adopted from our previous studies focused on such reactions. Thus, the cyanation of aryl bromides (Scheme 4) was performed in dioxane-water mixture (1:1), using 0.5 molar equiv. of $K_4[Fe(CN)_6]$ and K_2CO_3 (1 equiv.) as the base at 100°C [14]. The cyanation of **7a** was completed within 8 h when applying 0.4 mol.% of Pd of *in situ* formed catalyst generated from **1** and both palladium(II) acetate and $[PdCl_2(cod)]$ (higher Pd loading

ensued in smooth and complete conversions), while catalysts based on dppf and **2** led to relatively poorer conversions. For the electron-poor substrate **7b**, the conversions were generally lower. Even in this reaction, ligand **1** provided the best results, but the catalysts based on $Pd(OAc)_2$ performed consistently better than the corresponding catalyst resulting from $[PdCl_2(cod)]$ (Table 3).

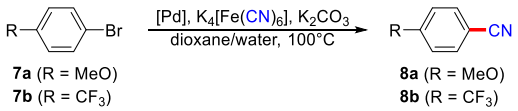

Scheme 4. Pd-catalysed cyanation of aryl bromides with $K_4[Fe(CN)_6]$

Table 3. Summary of the catalytic results for cyanation of aryl bromides with $K_4[Fe(CN)_6]$[a]

Substrate	dppf	**1**	**2**
	Yield of the coupling product **8** [%] (palladium source = $Pd(OAc)_2$)		
7a	60	100	62
7b	73	82	27
	Yield of the coupling product **8** [%] (palladium source = $[PdCl_2(cod)]$)		
7a	62	100	81
7b	21	16	53

[a] Conditions: Aryl bromide **7** (2.0 mmol) was mixed with $K_4[Fe(CN)_6]$ (1.0 mmol) in the presence of 0.4 mol.% of Pd catalyst (Pd:L = 1:1) and K_2CO_3 (2.0 mmol) in dioxane/water (2 + 2 mL) at 100°C for 8 h. The yields were determined by integration of ^1H NMR spectra and are an average of two independent runs.

The coupling of benzoyl chlorides **9** with phenylboronic acid (Scheme 5) producing benzophenones **10** was conducted in a toluene/water mixture at 50°C for 1 h using 0.1 mol.% of Pd catalyst and Na_2CO_3 as the base (1 equiv.) [15]. Once again, the catalysts obtained from bis-phosphine **1** gave better yields than those supported by dppf and **2** with both palladium precursors, and reactions mediated by $Pd(OAc)_2$/L catalysts proceed with higher conversions

than those performed in the presence of the corresponding [$PdCl_2$(cod)]/L catalysts (L = dppf, **1** and **2**) (Table 4).

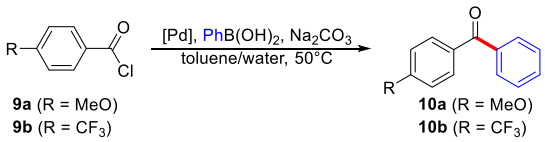

Scheme 5. Cross-coupling of benzoyl chlorides with phenylboronic acid to give benzophenones **10**

Table 4. Summary of the catalytic results for the cross-coupling of benzoyl chlorides with phenylboronic acid[a]

Substrate	dppf	**1**	**2**
Yield of the coupling product **10** [%] (palladium source = $Pd(OAc)_2$)			
8a	53	100	20
8b	92	100	100
Yield of the coupling product **10** [%] (palladium source = [$PdCl_2$(cod)])			
9a	44	100	20
9b	53	100	93

[a] Conditions: Benzoyl chloride **8** (3.0 mmol) was mixed with $PhB(OH)_2$ (2.5 mmol) in the presence of 0.1 mol.% of Pd catalyst (Pd:L = 1:1), Na_2CO_3 (2.5 mmol) and anisole (2.5 mmol; internal standard) in toluene/water (2 + 2 mL) at 50°C for 1 h. The yields were determined by integration of ^{1}H NMR spectra and are an average of two independent runs.

3. Conclusion

The coordination properties of the homologous pair of ligands **1** and **2** in Pd(II) complexes seem to be influenced more significantly by introducing flexible linker [16] than by replacing the conventional phosphine moiety (PR_2) for a CgP unit. While the reaction of **1** with a $PdCl_2$ surrogate affords the *cis*-chelate complex **3** as the sole product, the coordination behaviour of the more flexible, homologated ligand **2** is substantially more complicated. Among the possible

products reflecting the preference of Pd(II) for square planar coordination and the presence of two firmly bound chloride ligands (*viz.*, a monopalladium chelate and two types of dimers), the preferred products appear to be the symmetrical P,P-bridged dipalladium complex **5**, resulting as a mixture of diastereoisomers differing stereochemically at the CgP unit. Compared to the widely studied dppf [4], its electronically and sterically dissymmetric congener **1** gives rise to considerably more active catalysts for Pd-catalysed cyanation of aryl bromides and for Suzuki-Miyaura-type cross-coupling of benzoyl chlorides with boronic acids, producing benzophenones.

4. Experimental

4.1 Materials and methods

All manipulations were performed under nitrogen atmosphere using standard Schlenk techniques. Compounds **1** and **2** were prepared as previously reported [3]. Other chemicals were purchased from commercial suppliers and used without additional purification (TCI, Sigma-Aldrich). Anhydrous dichloromethane and methanol were obtained from a PureSolv MD5 solvent purification system (Innovative Technology). Dioxane and toluene were distilled from sodium metal, and water was degassed and distilled under nitrogen atmosphere before use. Other solvents (analytical grade from Lach-Ner) were used without further purification.

NMR spectra were recorded on a Varian Unity Inova 400 spectrometer at 25°C. Chemical shifts (δ in parts per million) are expressed relative to internal $SiMe_4$ (^1H and ^{13}C) and to external 85% aqueous H_3PO_4 (^{13}P). FTIR spectra were acquired on a Thermo Nicolet 6700 FT-IR spectrometer. Electrospray ionization (ESI) mass spectra were recorded on a Compact QTOF-MS spectrometer (Bruker Daltonics). Elemental analyses were performed using a PE 2400 Series II CHNS/O Elemental Analyser (PerkinElmer).

*4.2 Synthesis of **3***

Bis(acetonitrile)dichloropalladium(II) (26 mg, 0.10 mmol) and bis-phosphine **1** (58 mg, 0.10 mmol) were dissolved in dry dichloromethane (10 mL) under argon, and the mixture was stirred

overnight. Subsequent evaporation and crystallization by layering a chloroform solution of the crude product with hexane afforded **3**·2$CHCl_3$ as red crystalline solid. Yield: 70 mg (70%).

^{1}H NMR (CD_2Cl_2): δ 1.25 (s, 3H, Me), 1.40 (dd, $^3J_{PH}$ = 16.1 Hz, $^2J_{HH}$ = 13.9 Hz, 1H, CH_2), 1.42 (s, 3H, Me), 1.67 (dd, $^2J_{HH}$ = 13.9 Hz, $^3J_{PH}$ = 1.4 Hz, 1H, CH_2), 1.68 (d, $^3J_{PH}$ = 15.4 Hz, 3H, Me), 1.84 (d, $^3J_{PH}$ = 14.8 Hz, 3H, Me), 1.86 (dd, $^3J_{PH}$ = 25.1 Hz, $^2J_{HH}$ = 13.7 Hz, 1H, CH_2), 3.29 (dd, $^2J_{HH}$ = 13.8 Hz, $^3J_{PH}$ = 4.9 Hz, 1H, CH_2), 3.89 (ddt, *J′* = 2.6, 1.8, 1.3 Hz, 1H, fc), 4.22 (tdt, *J′* = 2.6, 1.3, 0.7 Hz, 1H, fc), 4.31 (tt, *J′* = 2.6, 1.3 Hz, 1H, fc), 4.37 (dq, *J′* = 2.8, 1.4 Hz, 1H, fc), 4.51 (tt, *J′* = 2.5, 1.2 Hz, 1H, fc), 4.77 (tt, *J′* = 2.6, 1.3 Hz, 1H, fc), 4.91 (tt, *J′* = 3.5, 1.2 Hz, 1H, fc), 5.21 (ddd, *J′* = 2.5, 2.1, 1.2 Hz, 1H, fc), 7.46-7.60 (m, 6H, PPh_2), 7.78-7.86 (m, 2H, PPh_2), 8.08-8.16 (m, 2H, PPh_2). ^{13}C{^{1}H} NMR (CD_2Cl_2): δ 25.55 (d, $^2J_{PC}$ = 6 Hz, Me), 27.26 (s, Me), 27.49 (s, Me), 29.61 (d, $^2J_{PC}$ = 6 Hz, Me), 41.53 (d, $^2J_{PC}$ = 10 Hz, CH_2), 41.75 (s, CH_2), 71.55 (dd, J_{PC} = 4, 1 Hz, CH of fc), 71.76 (d, J_{PC} = 6 Hz, CH of fc), 74.67 (d, J_{PC} = 7 Hz, CH of fc), 75.10 (d, $^1J_{PC}$ = 19 Hz, C of PCg), 75.33 (d, J_{PC} = 17 Hz, CH of fc), 75.70 (d, J_{PC} = 9 Hz, CH of fc), 76.22 (d, J_{PC} = 10 Hz, CH of fc), 76.62 (dd, $^1J_{PC}$ = 53 Hz, $^3J_{PC}$ = 5 Hz, C^{ipso} of fc), 77.82 (d, J_{PC} = 8 Hz, CH of fc), 78.15 (d, $^1J_{PC}$ = 25 Hz, C of PCg), 78.33 (s, CH of fc), 79.11 (dd, $^1J_{PC}$ = 36 Hz, $^3J_{PC}$ = 8 Hz, C^{ipso} of fc), 96.53 (s, C of PCg), 96.79 (s, C of PCg), 128.53 (s, CH of PPh_2), 128.64 (d, J_{PC} = 2 Hz, CH of PPh_2), 130.72 (d, J_{PC} = 3 Hz, CH of PPh_2), 131.07 (d, $^1J_{PC}$ = 54 Hz, C^{ipso} of PPh_2), 132.23 (d, J_{PC} = 3 Hz, CH of PPh_2), 132.37 (d, J_{PC} = 11 Hz, CH of PPh_2), 134.71 (d, $^1J_{PC}$ = 63 Hz, C^{ipso} of PPh_2), 137.55 (d, $^1J_{PC}$ = 12 Hz, CH of PPh_2). ^{31}P{^{1}H} NMR (CD_2Cl_2): δ 29.4 (d, $^2J_{PP}$ = 12 Hz, PCg), 37.1 (d, $^2J_{PP}$ = 13 Hz, PPh_2). IR (Nujol): ν_{max} 3123 w, 3077 m, 2725 w, 1684 w, 1459 s, 1438 s, 1338 w, 1307 w, 1267 m, 1230 w, 1209 m, 1196 m, 1181 m, 1167 m, 1134 m, 1095 s, 1070 w, 1039 m, 1027 w, 986 m, 959 w, 899 m, 853 w, 837 w, 830 w, 798 w, 756 s, 722 w, 699 s, 691 w, 646 w, 634 w, 593 w, 574 w, 555 m, 543 m, 526 w, 514 w, 499 w, 476 w, 469 m, 450 m, 433 m cm^{-1}. ESI+ MS: *m/z* 785 ($[M + Na]^+$). Anal. Calc. for $C_{32}H_{34}O_3Cl_2FeP_2Pd$·1/3$CHCl_3$ (801.5): C 48.45, H 4.32%. Found: C 48.24, H 4.08% (dried sample).

*4.3 Reaction of [$PdCl_2(MeCN)_2$] with **2***

Ligand **2** (48 mg, 0.08 mmol), bis(acetonitrile)dichloropalladium(II) (21 mg, 0.08 mmol) and methanol (25 mL) were introduced to a Schlenk tube under nitrogen atmosphere, and the resulting mixture was heated to 40°C for 6 hours. Then, the reaction flask was allowed to cool to room temperature, and the solvents were evaporated under vacuum. The crude product was washed twice with diethyl ether (10 ml) and dried under vacuum to give 62 mg of a red solid (quantitative yield). The product mixture contains 90% of racemic dinuclear complex **5** and 10% of other diastereoisomers, presumably the corresponding *meso* form. Crystals used for structure determination were obtained from methanol/diethyl ether.

Analytical data for *rac*-**5**. ^{1}H NMR (CD_2Cl_2): δ 1.15 (d, $^{3}J_{PH}$ = 13.5 Hz, 6H, Me), 1.29 (s, 6H, Me), 1.40 (s, 6H, Me), 1.57 (d, $^{3}J_{PH}$ = 12.3 Hz, 6H, Me), 1.69 (td, $^{2}J_{HH}$ = 13.5 Hz, $^{3}J_{PH}$ = 3.9 Hz, 2H, CH_2), 1.85 (dd, $^{3}J_{PH}$ = 21.9 Hz, $^{2}J_{HH}$ = 13.3 Hz, 2H, CH_2), 2.10 (dd, $^{2}J_{HH}$ = 13.5 Hz, $^{3}J_{PH}$ = 1 Hz, 2H, CH_2), 2.55 (td, $^{2}J_{HH}$ = 14.1 Hz, $^{2}J_{PH}$ = 8.1 Hz, 2H, PCH_2), 2.79 (dd, $^{2}J_{HH}$ = 13.2 Hz, $^{3}J_{PH}$ = 4.3 Hz, 2H, CH_2), 3.78 (br s, 2H, fc), 4.18 (br s, 2H, fc), 4.31 (tt, *J*' = 2.6, 1.3 Hz, 2H, fc), 4.32 (dt, *J*' = 2.4, 1.2 Hz, 2H, fc), 4.54 (td, *J*' = 2.5, 1.2 Hz, 2H, fc), 4.63 (dd, $^{2}J_{HH}$ = 14.1 Hz, $^{2}J_{PH}$ = 6.2 Hz, 2H, PCH_2), 5.40-5.44 (m, 4H, fc), 5.70 (br s, 2H, fc), 7.36-7.57 (m, 20H, PPh_2). ^{13}C{^{1}H} NMR (CD_2Cl_2): δ 17.19 (dd, J_{PC} = 11, 2 Hz, PCH_2), 26.82 (d, $^{2}J_{PC}$ = 7 Hz, Me), 26.92 (d, $^{2}J_{PC}$ = 5 Hz, Me), 27.47 (s, Me), 27.87 (s, Me), 41.74 (d, $^{2}J_{PC}$ = 4 Hz, CH_2), 41.92 (d, $^{2}J_{PC}$ = 8 Hz, CH_2), 69.98 (s, CH of fc), 71.04 (dd, J_{PC} = 53, 5 Hz, C^{ipso} of fc), 71.39 (s, CH of fc), 72.18 (d, J_{PC} = 8 Hz, CH of fc), 72.23 (d, J_{PC} = 10 Hz, CH of fc), 73.35 (dd, J_{PC} = 11, 4 Hz, C of PCg), 73.56 (s, CH of fc), 74.46 (dd, J_{PC} = 16, 4 Hz, C of PCg), 75.55-75.63 (m, CH of fc), 77.55 (d, J_{PC} = 11 Hz, CH of fc), 78.32 (d, $^{2}J_{PC}$ = 8 Hz, CH of fc), 82.65 (d, J_{PC} = 3 Hz, C^{ipso} of fc), 96.58 (s, C of PCg), 96.65 (s, C of PCg), 127.71 (d, J_{PC} = 10 Hz, CH of PPh_2), 128.52 (d, J_{PC} = 10 Hz, CH of PPh_2), 129.50 (dd, J_{PC} = 48, 5 Hz, C^{ipso} of fc), 130.76 (s, CH of fc), 130.78 (s, CH of fc), 132.54 (dd, J_{PC} = 46, 4 Hz, C^{ipso} of fc), 134.05 (d, J_{PC} = 11 Hz, CH of PPh_2), 135.08 (d, J_{PC} = 9 Hz, CH of PPh_2). ^{31}P{^{1}H} NMR (CD_2Cl_2): δ 4.7 (d, $^{2}J_{PP}$ = 551 Hz, PCg), 17.6 (d, $^{2}J_{PP}$ = 551 Hz, PPh_2). IR (Nujol): ν_{max} 1263 w, 1214 m, 1135 m, 1097 m, 1027 m, 979 m, 896 m, 856 m, 837 m, 748 m, 722 m, 695 m,

542 m, 521 m, 506 m, 467 m, 439 w cm^{-1}. ESI+ MS: *m/z* 740 ($[M - Cl]^+$), 761 ($[M - HCl + Na]^+$). Anal. Calc. for $C_{33}H_{36}O_3Cl_2FeP_2Pd \cdot 1/8CH_2Cl_2$ (786.8): C 50.51, H 4.65%. Found: C 50.68, H 4.54%.

4.4 Pd-catalysed cyanation of aryl bromides

A solution of the respective ligand (0.40 mol.% with respect to aryl bromide) in dry dichloromethane (5 mL) was added to the solid palladium precursor in an equimolar amount (0.40 mol.%). The resulting mixture was stirred for 5 min and then evaporated under vacuum. Anhydrous potassium hexacyanoferrate(II) (368 mg, 1.0 mmol), potassium carbonate (276 mg, 2.0 mmol) and aryl bromide **7** (2.0 mmol) were successively introduced to the reaction vessel, which was then equipped with a magnetic stirring bar, flushed with nitrogen and sealed with a septum. 1,4-Dioxane and water (2 mL each) were introduced, and the flask was stoppered and transferred to an oil bath maintained at 100°C. After stirring for 8 h, the reaction mixture was cooled and extracted with ethyl acetate (2×25 mL). The combined organic layers were washed with brine (25 mL), dried over anhydrous magnesium sulfate, and evaporated under reduced pressure. Conversion was determined by integration of the ^{1}H NMR spectrum of the crude product.

Analytical data for 4-methoxybenzonitrile (**8a**). ^{1}H NMR (dmso-d_6): δ 3.84 (s, 3H, MeO), 7.09-7.13 (m, 2H, C_6H_4), 7.76-7.79 (m, 2H, C_6H_4). Analytical data for 4-(trifluoromethyl)benzonitrile (**8b**). ^{1}H NMR (dmso-d_6): δ 7.70-7.72 (m, 2H, C_6H_4), 7.83-7.86 (m, 2H, C_6H_4). The data match those reported in the literature [17].

4.5 Pd-catalysed cross-coupling of aryl bromides with boronic acids

Palladium precursor (0.10 mol.% with respect to boronic acid) and the ligand (0.10 mol.%) were placed in a Schlenk tube and dissolved in dichloromethane (2 mL) under nitrogen. The mixture was stirred for 5 min and evaporated under vacuum. Then, acyl chloride **9** (3.0 mmol), boronic acid (2.5 mmol) and anisole (270 mg, 2.5 mmol, internal standard), Na_2CO_3 (2.5 mmol) were added to the Schlenk tube, and the reaction flask was flushed with nitrogen and sealed with a

rubber septum. Degassed water (3 mL) and toluene (3 mL) were introduced, and the reaction flask was placed into a preheated oil bath (50°C). After stirring for 1 h, the reaction was terminated by cooling on ice and adding diethyl ether (50 mL) and brine (25 mL). The organic layer was separated, dried over $MgSO_4$ and evaporated under reduced pressure. Conversion was determined by ^{1}H NMR spectroscopy.

Analytical data for 4-methoxybenzophenone (**10a**). ^{1}H NMR ($CDCl_3$): δ 3.81 (s, 3H, OMe), 6.88 (dd, $^3J_{HH}$ = 8.8 Hz, 2H, aromatics), 7.40 (t, $^3J_{HH}$ = 7.8 Hz, 2H, aromatics), 7.49 (t, $^3J_{HH}$ = 7.1 Hz,1H, aromatics), 7.68 (d, $^3J_{HH}$ = 7.8 Hz, 2H, aromatics), 7.81 (d, $^3J_{HH}$ = 8.8 Hz, 2H, aromatics). Analytical data for 4-(trifluoromethyl)benzophenone (**10b**). ^{1}H NMR ($CDCl_3$): δ 7.50 (d, $^3J_{HH}$ = 8.0 Hz, 2H), 7.61 (d, $^3J_{HH}$ = 8.5 Hz, 2H), 7.63 (t, $^3J_{HH}$ = 7.6 Hz, 2H), 7.75 (d, $^3J_{HH}$ = 8.5 Hz, 1H), 8.71 (t, $^3J_{HH}$ = 7.6 Hz, 2H) (all aromatics). The analytical data are in line with the literature [18].

4.6 X-ray crystallography

Full-sphere diffraction data ($\pm h \pm k \pm l$, θ_{max} = 26 or 27°) were collected at 120 K on a D8 VENTURE Kappa Duo diffractometer (Bruker) equipped with a PHOTON detector and a Cryostream Cooler (Oxford Cryosystems), using Mo Kα radiation (λ = 0.71073 Å). The structures were solved using direct methods (SHELXT 2014 [19]) and refined with a full-matrix least-squares routine based on F^2 (SHELXL-2017 [20]). All non-hydrogen atoms were refined with anisotropic displacement parameters. Hydrogen atoms were included in their theoretical positions with their U_{iso}(H) set to a multiple of U_{eq}(C) (1.2-times for CH and CH_2 hydrogens, 1.5-times for methyl groups). The OH hydrogen was located on the difference electron density map and refined similarly. Relevant crystallographic data and structure refinement parameters are collected in Table 5.

Both complexes were isolated in solvated form. While crystallisation of **3** from chloroform/hexane produced crystals of the defined stoichiometric solvate **3**·2$CHCl_3$, compound *rac*-**5** resulted in the form *rac*-**5**·2CH_3OH·Et_2O with partly disordered solvent molecules and as a racemic twin (space group $Pna2_1$; refined contributions of the two domains were approximately 95:5). The diethyl ether and one methanol molecule could not be reliably included in the

structure model; hence, their contribution to the overall scattering was removed by PLATON SQUEEZE [21]. In addition, one of the chloride ligands at each metal centre was disordered and was therefore modelled over two positions with refined occupancies 79:21 (Cl1···Cl1d = 0.74(1) Å, Cl3···Cl3d = 0.68(1) Å). Geometric data and structural diagrams were obtained using a recent version of the PLATON program [22]. All numerical values were rounded to one decimal place with respect to their estimated standard deviations.

Complete crystallographic data were deposited with the Cambridge Crystallographic Data Centre and are available free of charge from www.ccdc.cam.ac.uk/data_request/cif, by email at data_request@ccdc.cam.ac.uk, or by contacting The Cambridge Crystallographic Data Centre, 12 Union Road, Cambridge CB2 1EZ, UK; fax: +44 1223 336033. The deposition numbers are quoted in Table 5.

Table 5. Selected crystallographic data and structure refinement parameters[a]

Compound	**3**·2CHCl$_3$	*rac*-**5**·2CH$_3$OH·Et$_2$O
Formula	$C_{32}H_{34}Cl_2FeO_3P_2Pd$·2CHCl$_3$	$C_{66}H_{72}Cl_4Fe_2O_6P_4Pd_2$·2CH$_4$O·C$_4H_{10}$O
M [g mol^{-1}]	1000.42	1689.61
Crystal system	Monoclinic	orthorhombic
Space group	$P2_1/n$ (no. 14)	$Pna2_1$ (no. 33)
a [Å]	14.7918(7)	22.682(1)
b [Å]	13.4902(7)	16.0780(9)
c [Å]	20.714(1)	20.046(1)
α [°]	90	90
β [°]	106.892(2)	90
γ [°]	90	90
V [Å]^3	3955.0(3)	7310.6(7)
Z	4	4
μ(Mo Kα) [mm^{-1}]	1.477	1.162
Diffrns collected	58707	70414
Independent diffrns	8669	14330
Observed[a] diffrns	6927	12588
R_{int}[b] [%]	4.90	5.58
No. of parameters	446	792
R[b] obsd diffrns [%]	2.91	3.28
R, wR[b] all data [%]	4.58, 6.50	4.25, 7.33
Δρ [e Å^{-3}]	−1.10, 0.83	−0.75, 0.45
CCDC no.	2092777	2092778

[a] Diffractions with $I > 2\sigma(I)$. [b] Definitions: $R_{int} = \Sigma \left| F_o^2 - F_o^2(\text{mean}) \right| / \Sigma F_o^2$, where F_o^2(mean) is the average intensity of symmetry-equivalent diffractions. $R = \Sigma \left| \left| F_o \right| - \left| F_c \right| \right| / \Sigma \left| F_o \right|$, $wR = [\Sigma\{w(F_o^2 - F_c^2)^2\}/\Sigma w(F_o^2)^2]^{1/2}$.

Declaration of competing interest

The authors declare that they have no known competing financial interests or personal relationships that could have influenced the work reported in this paper.

Acknowledgments

This work was supported by Charles University Research Centre program (project UNCE/SCI/014) and by the Grant Agency of Charles University (project no. 920119).

Supplementary materials

Supplementary material associated with this article can be found, in the online version, at doi: 10.1016/j.jorganchem.2021.XXX

References

[1] P. G. Pringle, M. B. Smith in *Phosphorus(III) Ligands in Homogeneous Catalysis: Design and Synthesis* (Eds.: P. C. J. Kamer, P. W. N. M. van Leeuwen), Wiley, Chichester, 2012, ch. 13, pp 400-413.

[2] For examples, see: a) G. Eastham, World Patent WO 2004024322 (2004); b) G. Eastham, World Patent WO 2005079981 (2005); c) G. Eastham, World Patent WO 2005118519 (2005).

[3] F. Horký, I. Císařová, P. Štěpnička, ChemCatChem, doi: 10.1002/cctc.202101013.

[4] K.-S. Gan, T. S. A. Hor in *Ferrocenes: Homogeneous Catalysis, Organic Synthesis Materials Science* (Eds.: A. Togni, T. Hayashi), Wiley-VCH, Weinheim, 1995, ch. 1, pp. 3-104; b) S. W. Chien, T. S. A. Hor in *Ferrocenes: Ligands, Materials and Biomolecules* (Ed.: P. Štěpnička), Wiley, Chichester, 2008, ch. 2, pp. 33-116; c) G. Bandoli, A. Dolmella, *Coord. Chem. Rev.* 209 (2000) 161; d) D. J. Young, S. W. Chien, T. S. A. Hor, *Dalton Trans.* 41 (2012) 12655.

[5] Selected examples: a) G. Adjabeng, T. Brenstrum, J. Wilson, C. Frampton, A. Robertson, J. Hillhouse, J. McNulty, A. Capretta, Org. Lett. 5 (2003) 953; b) C. M. Lavoie, P. M. MacQueen, N. L. Rotta-Loria, R. S. Sawatzky, A. Borzenko, A. J. Chisholm, B. K. V. Hargreaves, R. McDonald, M. J. Ferguson, M. Stradiotto, Nat. Commun. 7 (2016) 11073; c) P. M. MacQueen, J. P. Tassone, C. Diaz, M. Stradiotto, J. Am. Chem. Soc. 140 (2018) 5023; d) R. T. McGuire, J. F. J. Paffile, Y. Zhou, M. Stradiotto, ACS Catal. 9 (2019) 9292; e) J. P. Tassone, E. V. England,

P. M. MacQueen, M. J. Ferguson, M. Stradiotto, Angew. Chem. Int. Ed. 58 (2019) 2485; f) J. S. K. Clark, M. J. Ferguson, R. McDonald, M. Stradiotto, Angew. Chem. Int. Ed. 58 (2019) 6391; g) R. T. McGuire, C. M. Simon, A. A. Yadav, M. J. Ferguson, M. Stradiotto, Angew. Chem. Int. Ed. 59 (2020) 8952.

[6] P. Vosáhlo, I. Císařová, P. Štěpnička, J. Organomet. Chem. 860 (2018) 14.

[7] For resolution of racemic CgPH, see: J. Hopewell, P. Jankowski, C. L. McMullin, A. G. Orpen, P. G. Pringle, Chem. Commun .46 (2010) 100-102.

[8] R. S. Chauhan, D. B. Cordes, A. M. Z. Slawin, S. Yadav, C. Dash, Inorg. Chim. Acta 478 (2018) 125.

[9] T. Hayashi, M. Konishi, Y. Kobori, M. Kumada, T. Higuchi, K. Hirotsu, J. Am. Chem. Soc. 106 (1984) 158.

[10] a) T. G. Appleton, H. C. Clark, L. E. Manzer, Coord. Chem. Rev. 10 (1973) 335; b) F. R. Hartley, Chem. Soc. Rev. 2 (1973) 163.

[11] M. Blangetti, H. Rosso, C. Prandi, A. Deagostino, P. Venturello, Molecules 18 (2013) 1188.

[12] P. Anbarasan, T. Schareinaa, M. Beller, Chem. Soc. Rev. 40 (2011) 5049.

[13] T. Schareina, A. Zapf, M. Beller, Chem. Commun. (2004) 1388.

[14] a) J. Schulz, F. Horký, P. Štěpnička, Catalysts 6 (2016) 182; b) J. Schulz, F. Horký, I. Císařová, P. Štěpnička, Catalysts 7 (2017) 167; c) K. Škoch, I. Císařová, P. Štěpnička, Organometallics 34 (2015) 1942; d) J. Schulz, I. Císařová, P. Štěpnička, Organometallics 31 (2012) 729.

[15] a) O. Bárta, I. Císařová, E. Mieczyńska, A. M. Trzeciak, P. Štěpnička, Eur. J. Inorg. Chem. (2019) 4846; b) M. Zábranský, I. Císařová, P. Štěpnička, Organometallics 37 (2018) 1615; c) K. Škoch, I. Císařová, P. Štěpnička, Organometallics 35 (2016) 3378; d) H. Charvátová, I. Císařová, P. Štěpnička, Eur. J. Inorg Chem. (2017) 288; e) H. Charvátová, I. Císařová, P. Štěpnička, Organometallics 33 (2014) 4131.

[16] Representative examples: a) P. Štěpnička, J. Schulz, T. Klemann, U. Siemeling, I. Císařová, Organometallics 29 (2010) 3187; b) P. Štěpnička, I. Císařová, J. Schulz, Organometallics 30 (2011) 4393; c) P. Štěpnička, I. Císařová, Dalton Trans. 42 (2013) 3373; d) O. Bárta, I.

Císařová, P. Štěpnička, Eur. J. Inorg. Chem. (2017) 489; e) M. Zábranský, A. Machara, I. Císařová, P. Štěpnička, Eur. J. Inorg. Chem. (2017) 4850 and ref. [6].

[17] M. Hatsuda, M. Seki, Tetrahedron Lett. 61 (2005) 9908.

[18] V. P. Mehta, A. Sharma, E. Van der Eycken, Adv. Synth. Catal. 350 (2008) 2174.

[19] G. M. Sheldrick, Acta Crystallogr., Sect. A: Found. Adv. 71 (2015) 3.

[20] G. M. Sheldrick, Acta Crystallogr., Sect. C: Struct. Chem. 71 (2015) 3.

[21] A. L. Spek, Acta Crystallogr., Sect. C: Struct. Sci. 71 (2015) 9.

[22] a) A. L. Spek, J. Appl. Crystallogr. 36 (2003) 7; b) A. L. Spek, Acta Crystallogr. D, Biol. Crystallogr. 65 (2009) 148.

Synthesis, coordination and catalytic use of phosphinoferrocene ligands bearing 6-phospha-2,4,6-trioxaadamantane P-donor moieties

Filip Horký, Ivana Císařová and Petr Štěpnička*

SUPPORTING INFORMATION

Additional structural diagrams

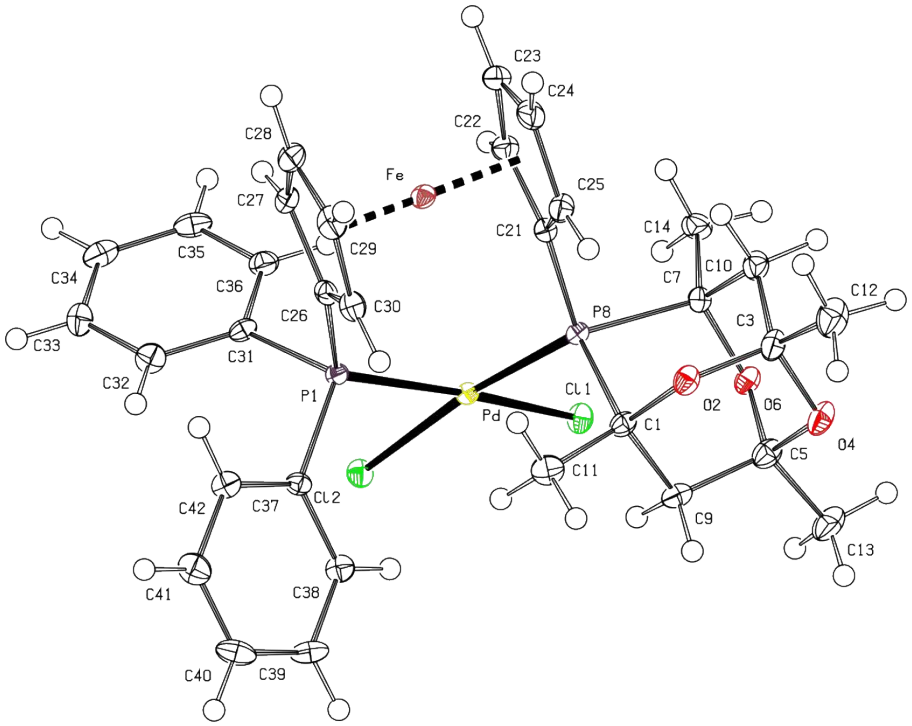

Figure S1. PLATON plot of the complex molecule in the structure of **3**·2$CHCl_3$ showing the displacement ellipsoids at the 30% probability level.

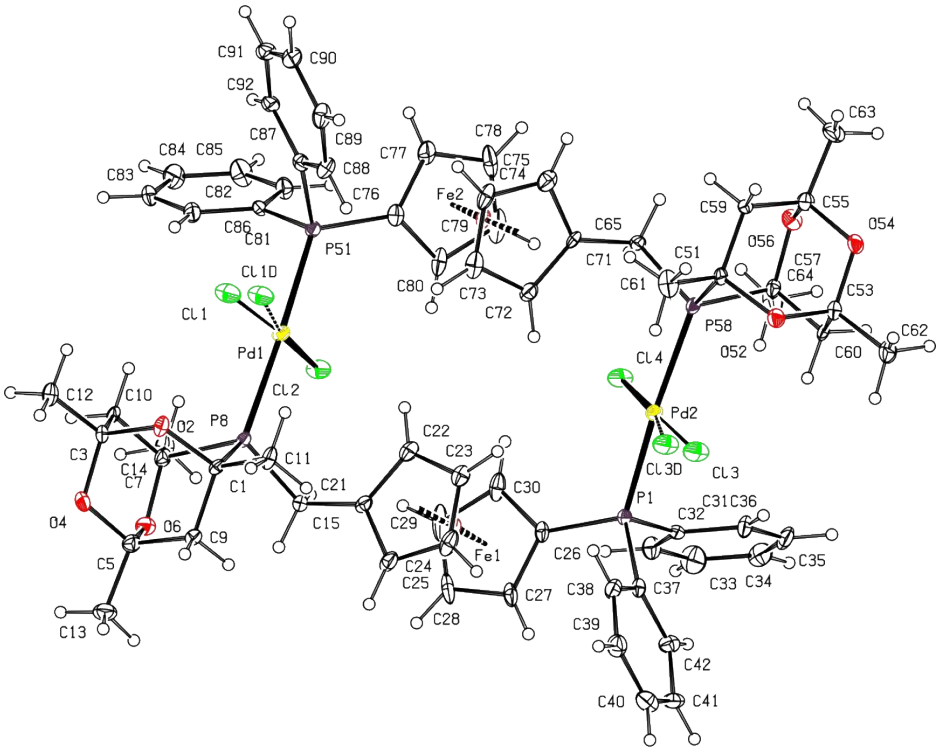

Figure S2. PLATON plot of the complex molecule in the structure of *rac*-**5**·3$CHCl_3$ showing the displacement ellipsoids at the 30% probability level.

Copies of the NMR spectra

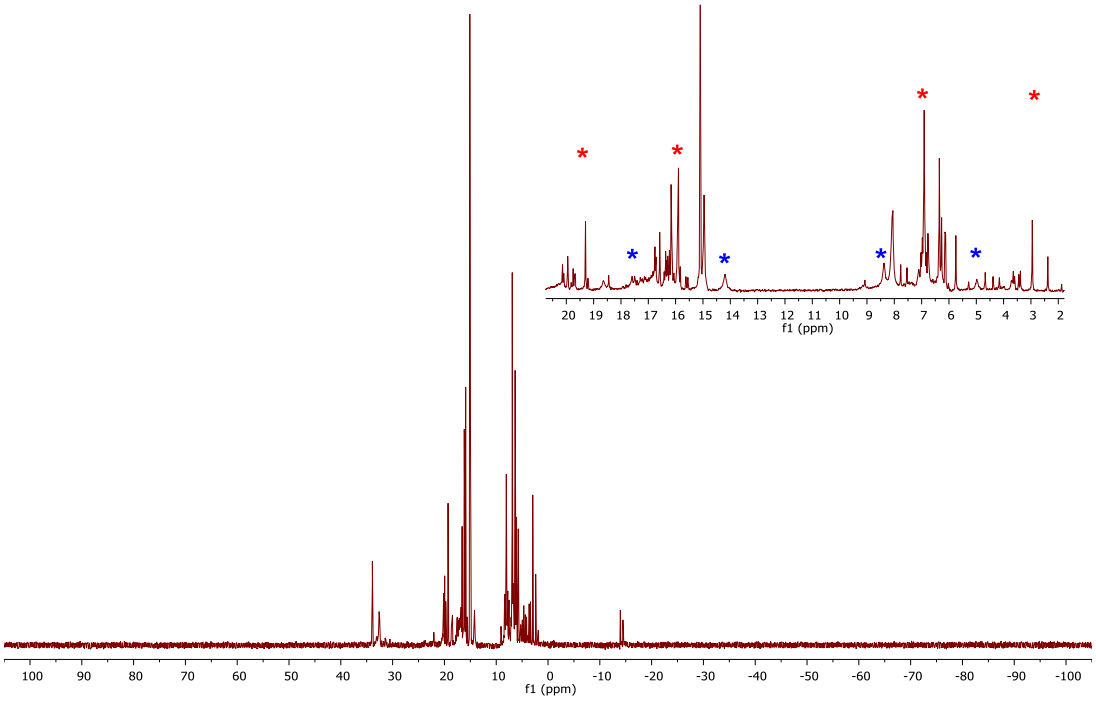

Figure S3. $^{31}P\{^{1}H\}$ NMR spectrum (162 MHz, CD_2Cl_2) of the reaction mixture obtained by mixing $[PdCl_2(MeCN)_2]$ with **2** (Pd:**2** = 1:1) in CH_2Cl_2. Red asterisks: δ_P 4.7 and 17.6 (2× d, $^2J_{PP}$ = 551 Hz, PPh_2); blue asterisks: δ_P 6.7 and 15.9 (2× br d, $^2J_{PP}$ = 550 Hz, PPh_2). Note that after refluxing the crude product in methanol/dichloromethane (approximately 9:1) overnight, the composition of the product mixture changes in favour of the symmetrical dimer *rac*-**5**. The spectrum is shown in Figure S9.

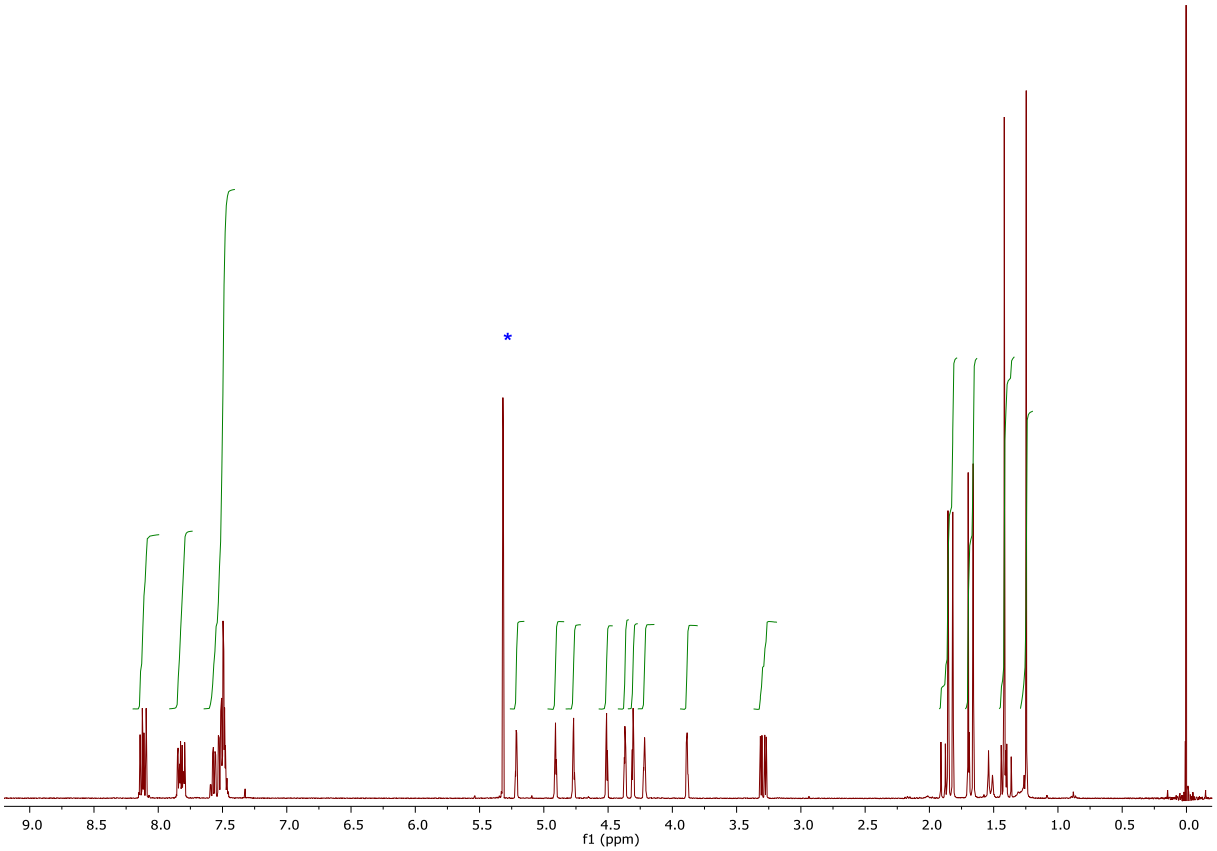

Figure S4. ^{1}H NMR spectrum (400 MHz, CD_2Cl_2) of **3**.

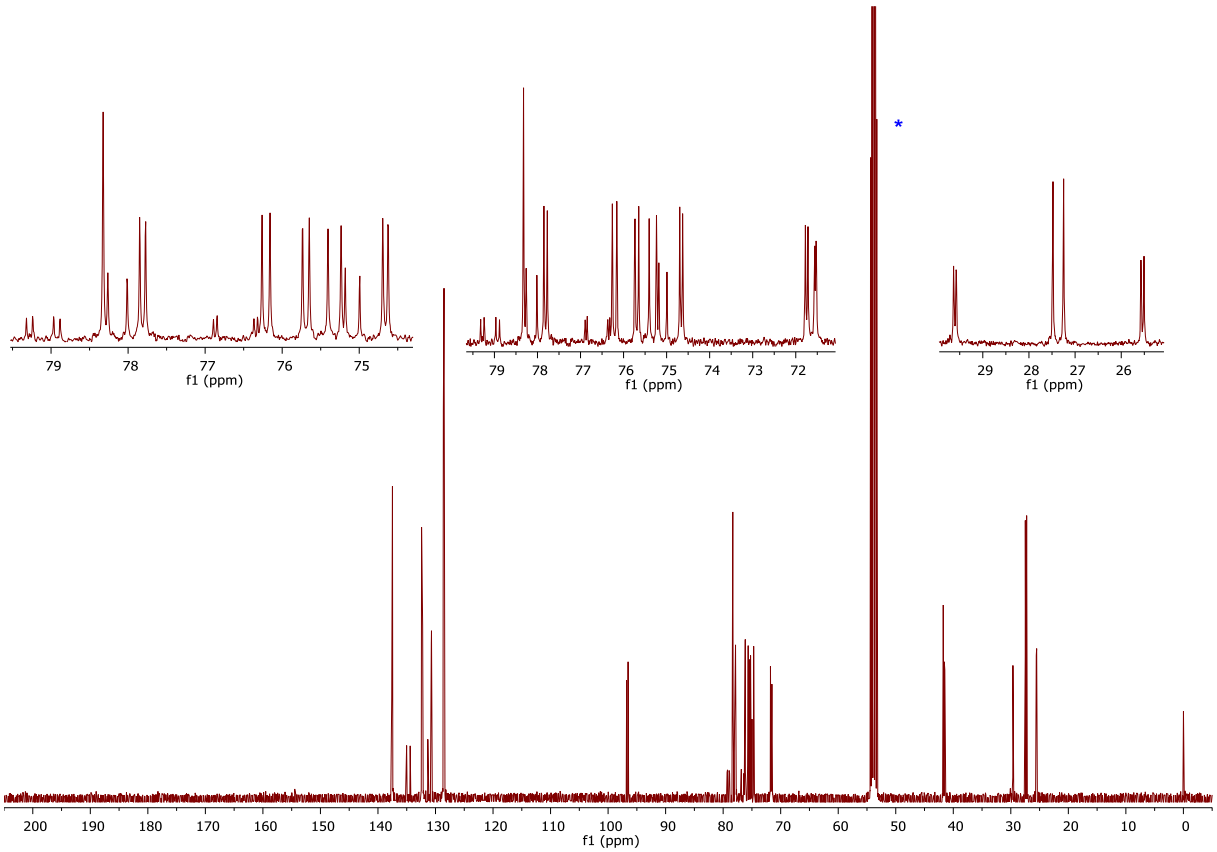

Figure S5. $^{13}C\{^{1}H\}$ NMR spectrum (101 MHz, CD_2Cl_2) of **3**.

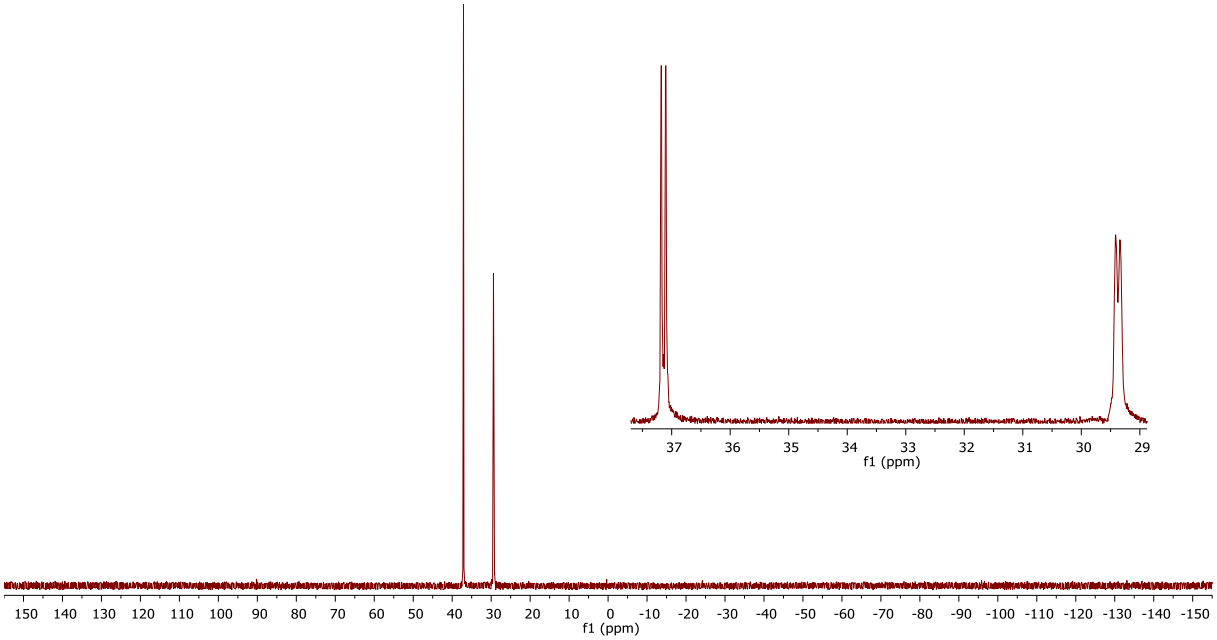

Figure S6. $^{31}P\{H\}$ NMR spectrum (162 MHz, CD_2Cl_2) of **3**.

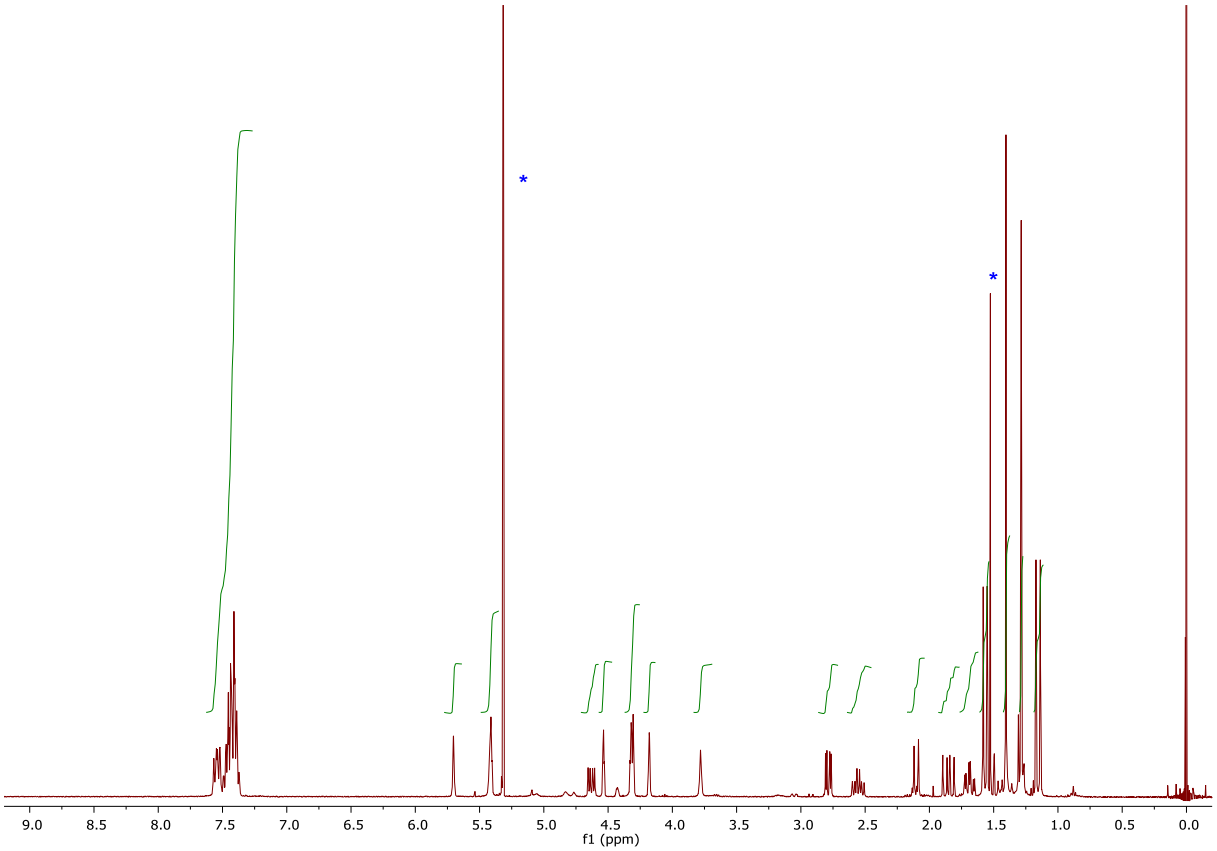

Figure S7. ^{1}H NMR spectrum (400 MHz, CD_2Cl_2) of *rac*-**5**.

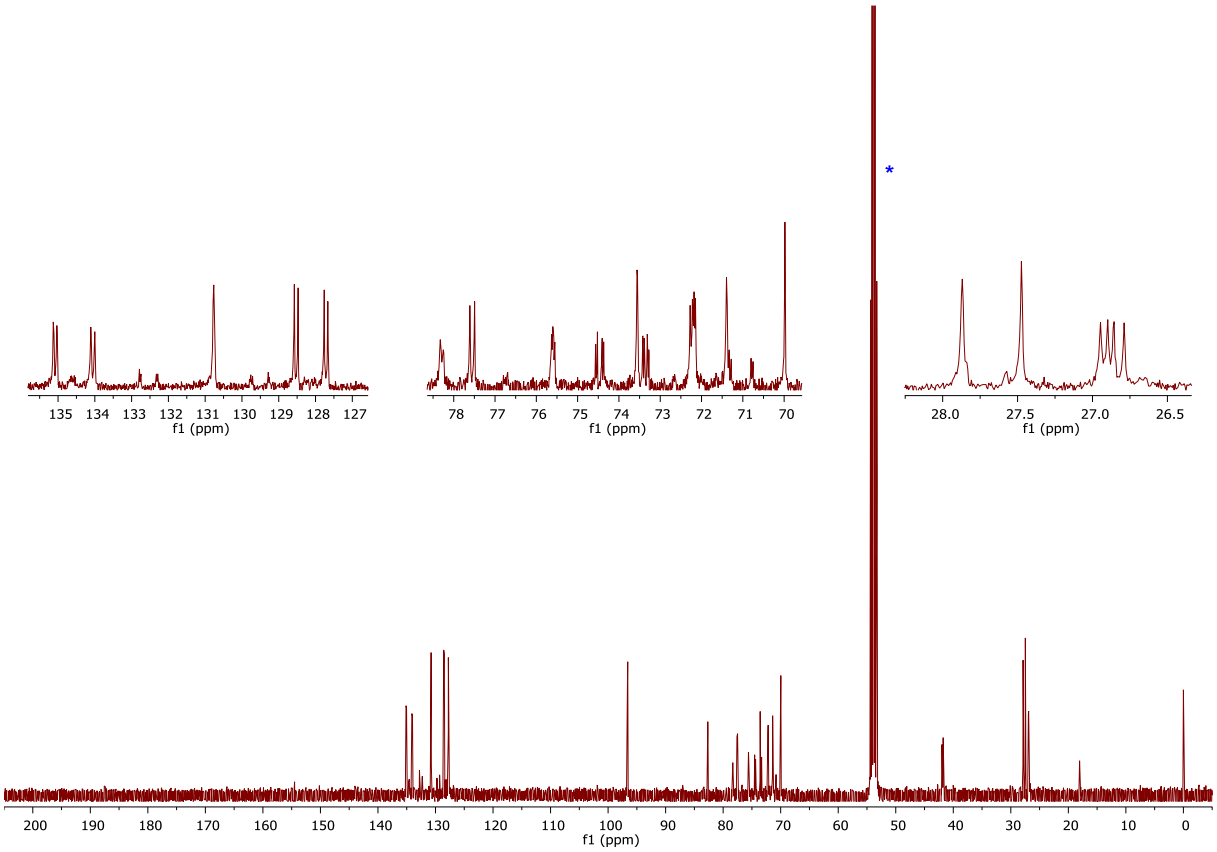

Figure S8. $^{13}C\{^{1}H\}$ NMR spectrum (101 MHz, CD_2Cl_2) of *rac*-**5**.

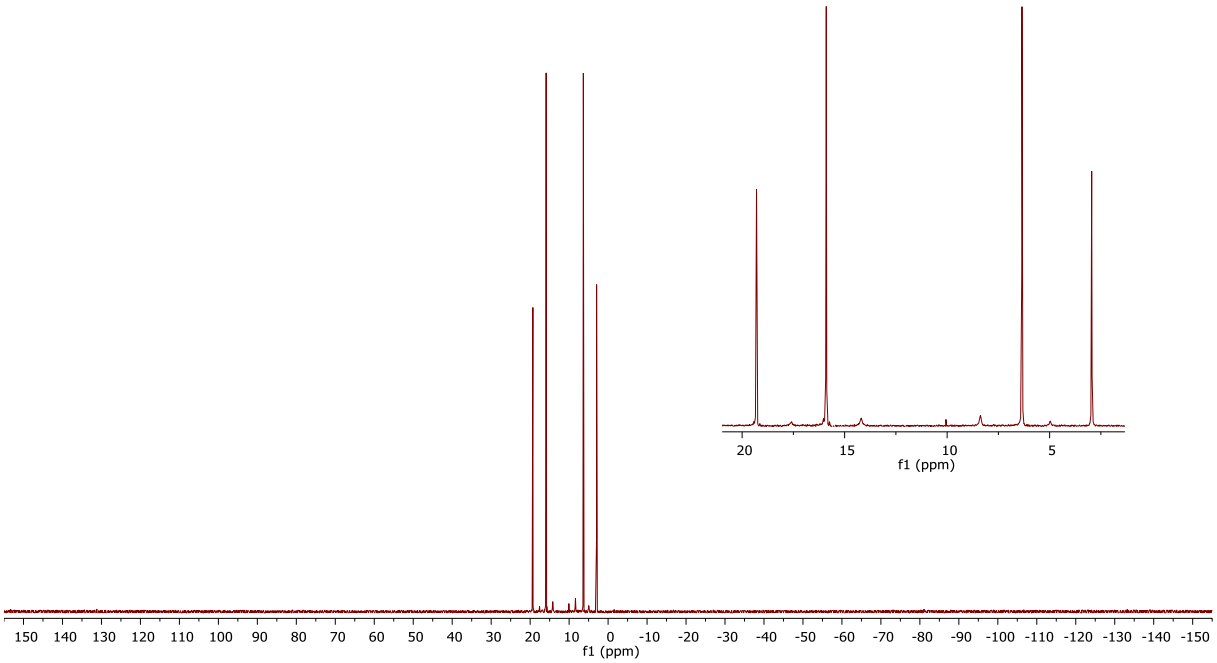

Figure S9. $^{31}P\{H\}$ NMR spectrum (162 MHz, CD_2Cl_2) of *rac*-**5**.

Appendix E

Horký, F.; Císařová, I.; Schulz, J.; Štěpnička, P. Synthesis and structural characterization of 1'-(diphenylphosphino)ferrocene-1-phosphonic acid, its ammonium salts and Pd(II) complexes. *J. Organomet. Chem.* **2019**, *891*, 44.

Journal of Organometallic Chemistry 891 (2019) 44–53

Contents lists available at ScienceDirect

Journal of Organometallic Chemistry

journal homepage: www.elsevier.com/locate/jorganchem

Synthesis and structural characterisation of 1'-(diphenylphosphino) ferrocene-1-phosphonic acid, its ammonium salts and Pd(II) complexes

Filip Horký, Ivana Císařová, Jiří Schulz, Petr Štěpnička*

Department of Inorganic Chemistry, Faculty of Science, Charles University, Hlavova 2030, 12840, Prague, Czech Republic

ARTICLE INFO

Article history:
Received 1 March 2019
Received in revised form
28 March 2019
Accepted 11 April 2019
Available online 17 April 2019

Keywords:
Ferrocene
Phosphine ligands
Phosphonates
Palladium complexes
Structure elucidation
DFT computations

ABSTRACT

A new polar phosphinoferrocene ligand, viz. 1'-(diphenylphosphino)ferrocene-1-phosphonic acid (H_2**L**), was prepared by hydrolysis of the corresponding phosphonate ethyl ester. However, the compound is relatively unstable, gradually decomposing upon prolonged storage, ultimately affording phosphine oxide H_2**L**O. When the phosphine moiety was protected (*e.g.*, in phosphine oxide H_2**L**O and adduct H_2**L**·BH_3), no decomposition was observed. An alternative approach to prepare more stable H_2**L** surrogates by converting the phosphonic acid into ammonium salts (dabcoH)(**HL**) and [$(OHCH_2CH_2)_2NH_2$](**HL**) (dabco = 1,4-diazabicyclo[2.2.2]octane) resulted in no significant stabilisation. H_2**L** reacted with [$PdCl_2$(cod)] (cod = cycloocta-1,5-diene), producing the bis(phosphine) complex, *trans*-[$PdCl_2$(H_2**L**-κ*P*)$_2$]. When mixed with Pd(II)-acetylacetonate (acac) complexes with *ortho*-metallated auxiliary ligands, [(L^{CY})Pd(acac)] (L^{CY} = 2-[(dimethylamino-κ*N*)methyl]phenyl-κC^1 and 2-[(methylthio-κ*S*)methyl]phenyl-κC^1), H_2**L** gave rise to bis-chelate complexes of the [(L^{CY})Pd(**HL**-κ^2*O*,*P*)] type. H_2**L**, the ammonium salts featuring the HL^- anion, and all Pd(II) complexes were structurally characterised by single-crystal X-ray diffraction analysis. Variations in phosphonate P-O bond lengths observed in the crystal structures were rationalised by DFT computations.

1. Introduction

Introducing polar moieties into phosphine molecules is a time-tested and efficient approach for the design of new hydrophilic ligands [1]. In this regard, acidic functional groups such as carboxylate, phosphonate and especially sulfonate are among the most frequently used polar moieties. Their incorporation into phosphine molecules results in structurally versatile hybrid phosphine ligands with diverse coordination modes and pH-dependent behaviour [2]. However, this approach has been used less often in the chemistry of otherwise ubiquitous phosphinoferrocene ligands [3]. Examples of functional ferrocene phosphines structurally analogous to the widely studied 1,1′-bis(diphenylphosphino) ferrocene (dppf, Scheme 1) [4], include 1'-(diphenylphosphino)-1-ferrocenecarboxylic acid (Hdpf) [5] and the recently reported phosphinoferrocene sulfonate **A** [6] (Scheme 1). The analogous 1-(diphenylphosphino)-1-ferrocenephosphonic acid (H_2**L**) has not yet been reported, although diethyl 1'-(diphenylphosphino)-1-ferrocenephosphonate, the obvious precursor of H_2**L**, has already been prepared, used as a synthetic intermediate [7] and studied as a ligand in Group 12 metal complexes [8]. To expand the series of dppf-like phosphinoferrocene ligands featuring polar acidic functional groups, we prepared H_2**L**, an organometallic analogue of the triphenylphosphine derivative **B** (Scheme 1) [9]. The synthesis and characterisation of H_2**L**, its ammonium salts and palladium(II) complexes are reported in this paper.

2. Results and discussion

2.1. Synthesis and characterisation of H_2L, its derivatives and salts

Acid H_2**L** was obtained from a reaction of phosphonate ester **2** [8] with Me_3SiBr followed by hydrolysis [10] (Scheme 2). Even when carefully purified, the acid gradually decomposed at room temperature and at 4 °C. Decomposition is first manifested as sample darkening and broadening of ^{1}H NMR signals. Later, the ^{31}P NMR spectra show resonances due to the corresponding phosphine oxide (δ_P 16.5 and 31.7 in dmso-d_6). Partly decomposed samples of

* Corresponding author.
E-mail address: petr.stepnicka@natur.cuni.cz (P. Štěpnička).

https://doi.org/10.1016/j.jorganchem.2019.04.012
0022-328X/

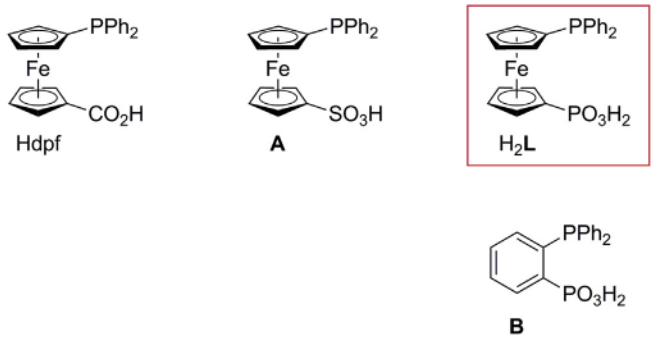

Scheme 1. Polar phosphines relevant to this study.

H_2**L** could be purified by column chromatography (silica gel, chloroform-methanol 10:1), which removed a faster eluting brown band containing unknown decomposition products, followed by an orange band due to H_2**L** and, finally, a slowly moving band containing phosphine oxide H_2**L**O. H_2**L** was also crystallised from ethyl acetate. However, this crystallisation was associated with a substantial loss of crude material and produced easily decomposing, orange crystals.

Attempts to stabilise the phosphino-phosphonate by converting it into crystalline ammonium salts were only partly successful. H_2**L** neutralisation with 1 or 2.5 equiv. of 1,4-diazabicyclo[2.2.2]octane (dabco) and diethanolamine (*i.e.*, 2,2′-iminodiethanol) uniformly led to salts containing the singly deprotonated anion H**L**$^-$, (dabcoH)(H**L**) (**5**) and ((OHCH$_2$CH$_2$)$_2$NH$_2$)(H**L**) (**6**), respectively. Only such salts were obtained, irrespective of the amount of base added, in line with the large differences between the first and second dissociation constants of phosphonic acids (*cf.* pK_{a1} 2.3, pK_{a2} 7.6 for PhCH$_2$PO$_3$H$_2$ [11]). Salts **5** and **6** were spectroscopically and crystallographically characterised, but they nevertheless decomposed upon prolonged storage.

Notably, spontaneous decomposition of ferrocenephosphonic acids, such as FcCH$_2$PO$_3$H$_2$, most likely a self-catalysed oxidation, has already been reported [12]. However, the spontaneous decomposition of the phosphine-substituted derivative H_2**L** may be further complicated by processes involving the phosphine moiety in which the primary decomposition products are converted into the phosphine oxide H_2**L**O. To confirm this assumption, the phosphine oxide H_2**L**O and the phosphine-borane adduct H_2**L**·BH$_3$ were prepared via H_2O_2-oxidation of H_2**L** and analogously to H_2**L** from the P-protected precursor **3**, respectively (Scheme 2). Both H_2**L**O and H_2**L**·BH$_3$ showed no signs of decomposition when stored at room temperature for weeks.

In the ^{1}H NMR spectra, H_2**L** and its P-modified derivatives display four signals due to chemically non-equivalent ferrocene CH groups. These signals broaden into unresolved signals in the spectra of H_2**L** and H_2**L**O, which also show multiplets due to the PPh$_2$ moieties. The presence of the phosphonate moiety is manifested as ^{31}P NMR resonances at $\delta_P \approx 17$ ppm (in dmso-d$_6$). The signal of the phosphine moiety in H_2**L** is observed at δ_P −17.4, whereas this signal appears characteristically shifted to lower field in H_2**L**O and H_2**L**·BH$_3$ (δ_P 31.7 and 15.6 ppm, respectively). H_2**L**, its phosphine oxide, and the borane adduct display the corresponding pseudomolecular ions ([M + H]$^+$) in their ESI mass spectra.

The molecular structure of H_2**L** is depicted in Fig. 1. The compound crystallises unsolvated, with the symmetry of the monoclinic space group $P2_1/n$ and with one formula unit in the asymmetric unit. The individual molecules in the crystal structure assemble *via* O-H···O hydrogen bonds, forming one-dimensional chains along the crystallographic *b* axis (Fig. 2).

Parameters describing the molecular geometry of H_2**L** match those of the respective monofunctional ferrocene derivatives,

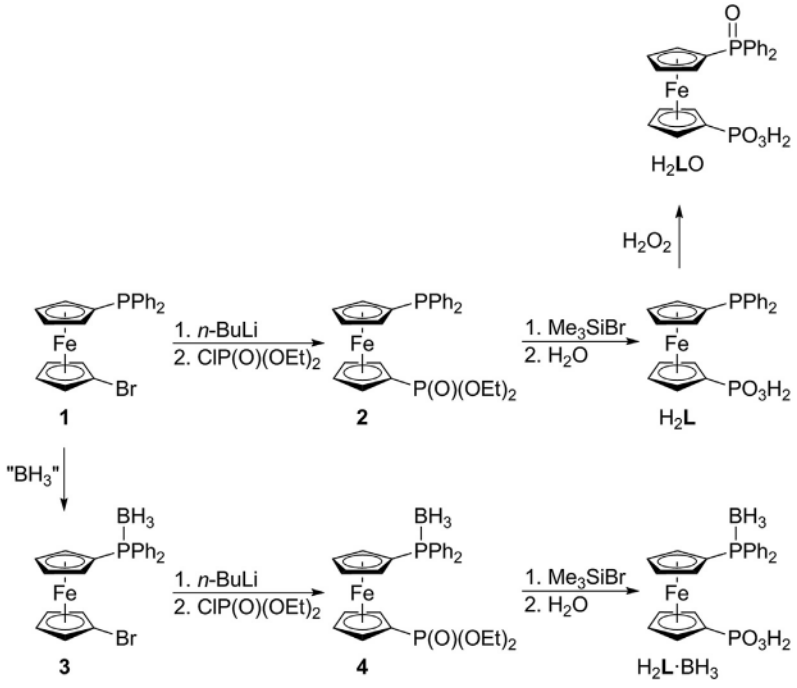

Scheme 2. Synthesis of H_2**L**, its borane adduct H_2**L**·BH$_3$ and phosphine oxide H_2**L**O.

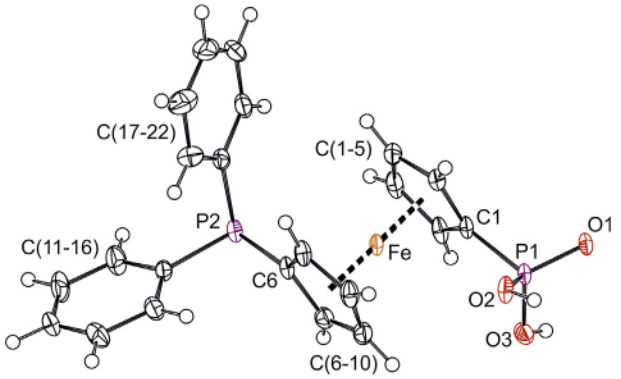

Fig. 1. PLATON plot of the molecular structure of H_2**L** showing atom labelling and displacement ellipsoids at the 50% probability level.

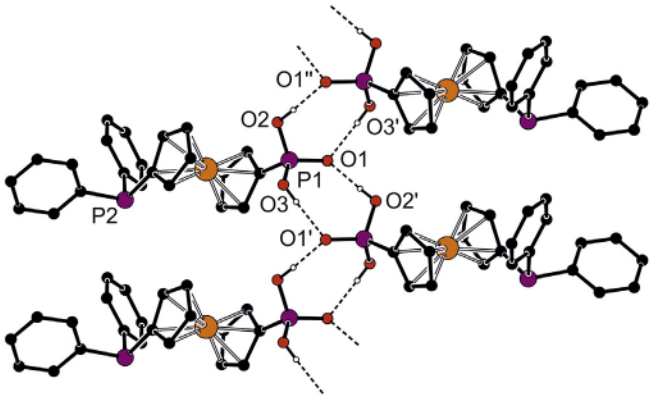

Fig. 2. Section of the hydrogen-bonded assembly in the structure of H_2**L**; for clarity, only OH hydrogens are shown. H-bond parameters: O2···O1 = 2.572(2) Å, O3···O1 = 2.630(2) Å.

$FcPO_3H_2$ [13] and $FcPPh_2$ [14] (Fc = ferrocenyl). The cyclopentadienyl rings in the H_2**L** molecule are essentially parallel (tilt angle: 0.8(1)°), indicating only minor variations in individual Fe-C distances (2.033(2)-2.062(2) Å), and adopt an intermediate conformation between anticlinal eclipsed and antiperiplanar staggered [4b] that brings the substituents to approximately opposite (*anti*) positions, as shown by the τ angle (−165.7(1)°; N.B. τ is the dihedral angle C1-Cg1-Cg2-C6, where Cg1 and Cg2 are the centroids of the cyclopentadienyl rings C(1-5) and C(6-10), respectively).

In addition to free H_2**L**, the crystal structures of salts **5** and **6** were also solved. The molecular structures of the salts are depicted in Fig. 3, and the selected geometric parameters are outlined in Table 1. The ferrocene moieties in the structures of **5** and **6** adopt their regular geometries, showing only insignificant tilting (2.8(2)° in **5**, and 2.9(1)° in **6**). However, they have different conformations. While the ferrocene substituents in **5** adopt rather distant positions, those in **6** are rotated closer to each other (*cf.* the τ angles in Table 1). Notably, the deprotonation of the phosphonate groups markedly differentiates the P-O bonds, presumably due to charge delocalisation. In both salts, the bonds formally attributable to P=O and P-O$^-$ units (P1-O1 and P1-O2) are substantially shorter than the bonds towards the OH groups (P1-O3). On the contrary, the P-O bond lengths of the free acid H_2**L** suggest the presence of one P=O (1.51 Å) and two P-O bonds (1.55 Å). Similar features can be observed when converting phenylphosphonic acid [15] into ammonium salts of the $(R_2NH_2)(PhPO_3H)$ type [16]. In addition,

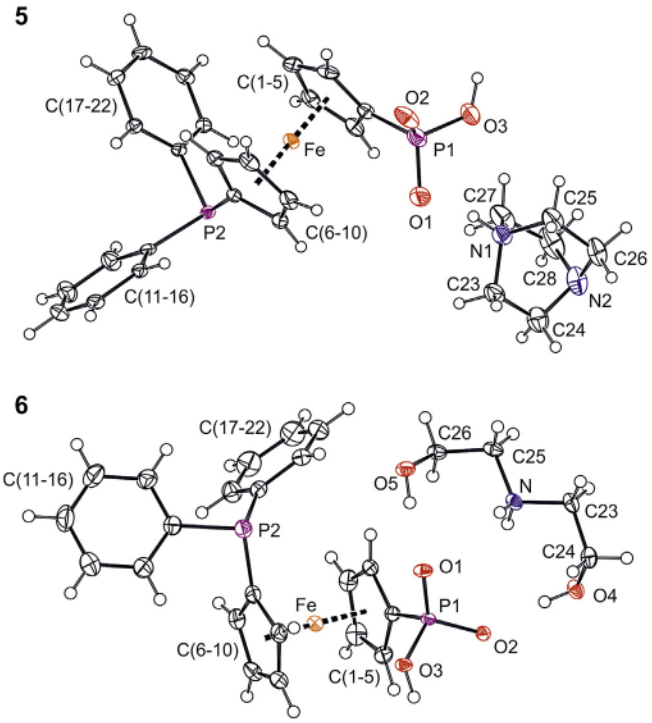

Fig. 3. PLATON plots of the molecules structures of **5** (top) and **6** (bottom); displacement ellipsoids correspond to the 50% probability level.

Table 1
Selected distances and angles for H_2**L**, **5** and **6** (in Å and deg).

Parameter	H_2L	5[a]	6[b]
P-O1	1.510(1)	1.505(3)	1.498(1)
P-O2	1.550(1)	1.509(2)	1.519(1)
P-O3	1.554(2)	1.578(3)	1.577(1)
O1-P1-O2	111.35(7)	116.4(2)	115.48(6)
O1-P1-O3	111.30(8)	106.5(2)	108.53(6)
O2-P1-O3	108.08(8)	111.5(1)	109.01(6)
P1-C1	1.753(2)	1.800(3)	1.787(1)
P2-C6	1.818(2)	1.810(3)	1.820(2)
P2-C11	1.832(2)	1.837(3)	1.839(2)
P2-C17	1.840(2)	1.840(3)	1.835(2)
τ	−165.7(1)	−139.6(2)	85.4(1)

[a] Further data: N-C distance range in $(dabcoH)^+$ = 1.457(6)-1.499(5) Å.
[b] Further data: N-C23 1.492(2), N-C25 1.496(2), O4-C24 1.429(2), O5-C26 1.417(2), C23-N-C25 113.8(1).

deprotonation of the phosphonate moiety results in a shortening of the pivotal C1-P1 bond so that the sum of the C1-P1 and P1-O2 bond lengths remains virtually constant.

The shortening of the P-O2 bond distance, which can be attributed to resonance stabilization of the negative charge by delocalization over the O1-P-O2 moiety, is well reproduced by DFT computations (Table 2). The Mayer bond indices (MBIs) calculated for ferrocenylphosphonic acid and the corresponding monoanion as model compounds at the M06/def-TZVP:sdd(Fe) level of theory support this explanation, revealing the significantly increased bond order of the P-O2 bond (1.863) and the slightly decreased bond order of the P-O1 bond (1.818). Consequently, P-O1 and P-O2 bonds have very similar lengths, shorter than the remaining P-OH bond. The calculated charges, which are very similar at the three oxygen atoms in $FcPO_3H_2$, somewhat differentiate upon deprotonation. The largest negative charge in $FcPO_3H^-$ is found at the O2 oxygen atom, as expected.

Table 2
Calculated bond distances, Mayer bond indices (MBIs) and Merz-Kollman charges (MKs) at the oxygen atoms.

Compound	Bond	Bond distance [Å]	MBIs	MKs
$FcPO_3H_2$	P-O1	1.462	1.961	−0.63
	P-O2	1.602	1.153	−0.62
	P-O3	1.590	1.169	−0.58
$FcPO_3H^-$	P-O1	1.481	1.818	−0.73
	P-O2	1.485	1.863	−0.79
	P-O3	1.649	0.982	−0.69

Salts **5** and **6** incorporated molecules of halogenated solvents, used during the crystallisation, in their structures. Unfortunately, the solvent molecules were severely disordered within the structural voids and had to be eliminated from the structure model (see Experimental). Notably, the crystal assembly of the ions that form the structure of salt **5** is relatively simple (Fig. 4), reflecting the prevalence of H-bond acceptors over conventional H-bond donors (OH, NH). Specifically, the anions HL^- associate into dimers around crystallographic inversion centres through charge-supported O-H···O^- hydrogen bonds (O2···O3 = 2.533(4) Å), while the phosphoryl oxygens O1 form additional hydrogen bonds with the NH groups of the adjacent cations $(dabcoH)^+$ (O1···N1 = 2.597(4) Å). Conversely, the supramolecular assembly of **6** is relatively complex due to the presence of additional H-bond donors in the structure (Fig. 5). Similarly to **5**, the phosphonate moieties form dimeric units *via* the O3-H···O2 interactions, whose midpoints coincide with the crystallographic inversion centres (O2···O3 = 2.554(1) Å). Furthermore, each phosphonate moiety acts as a hydrogen bond acceptor for a proximal ammonium cation, forming two O-H···O bonds (O4···O2 = 2.669(2) Å, O5···O1 = 2.696(1) Å) and one relatively longer N-H···O hydrogen bond (N2···O1 = 3.054(2) Å). The resulting $\{(HOCH_2CH_2)_2NH_2\}_2\{HL\}_2$ motifs are interlinked into a two-dimensional array by additional N-H···O interactions towards the P=O oxygen (N···O1 = 2.853(2) Å) and by N-H···OH interactions (N···O4 = 2.902(2) Å).

2.2. Preparation and characterisation of Pd(II) complexes

A series of Pd(II) complexes [17] was prepared and structurally characterised to study the coordination behaviour of H_2L. Various Pd(II) precursors were used in the testing reactions, differing in supporting ligands and in the number of accessible coordination sites at the central Pd(II) ion, including those that may possibly

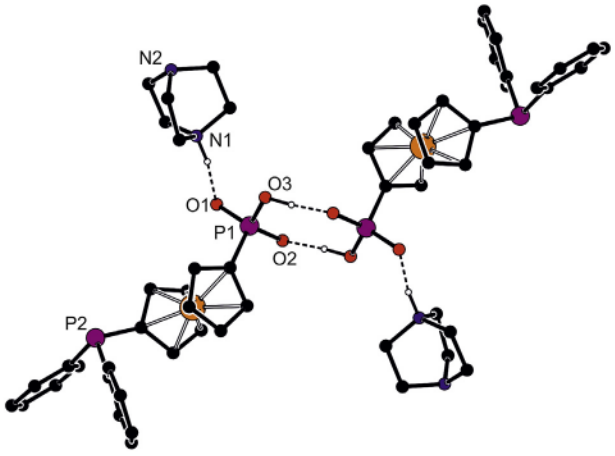

Fig. 4. Hydrogen-bonded dimers in the crystal structure of **5**; only NH hydrogens are shown for clarity.

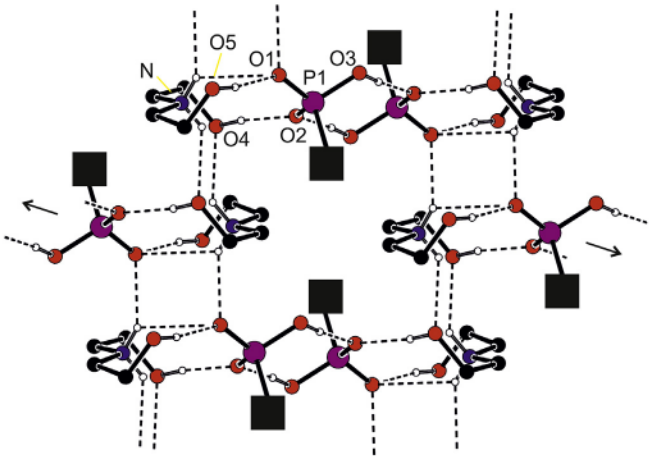

Fig. 5. Section of the hydrogen-bonded assembly in the crystal structure of **6**; for clarity, the bulky phosphinoferrocenyl moieties are replaced with black boxes, and only the NH and OH hydrogens are shown. The arrows indicate lateral propagation of the columnar arrays.

assist in the H_2L conversion into a phosphino-phosphonate anion. Thus, the reaction of H_2L with $[PdCl_2(cod)]$ (cod = cycloocta-1,5-diene) produced the bis(phosphine) complex **7** (Scheme 3). The compound is relatively unstable, readily decomposing in solution, which in turn complicates the characterisation of the compound and its purification. For instance, attempts to purify **7** by crystallization typically resulted in massive losses of the material.

The ^1H NMR spectra of **7** display broad signals due to the ferrocene and PPh_2 fragments at the expected positions, and the coordination of the phosphine moiety is manifested as a shift of the ^{31}P NMR resonance to a lower field (δ_P 17.0 ppm; N.B. the signals due to the phosphonate moiety is observed as a broad singlet at δ_P 18.0). Repeated attempts to obtain crystalline material suitable for X-ray diffraction analysis eventually afforded crystals of the stoichiometric solvate **7**·3EtOH from ethanol/diethyl ether (Fig. 6). The geometry of the coordination sphere around Pd(II) is similar to that of the formally parent compound *trans*-$[PdCl_2(FcPPh_2\text{-}\kappa P)_2]$ [6a], and the parameters of the independent but chemically equivalent halves of the complex molecule differ only marginally. The bulky phosphinoferrocene ligands occupy mutually opposite positions, highlighting the near centrosymmetric arrangement of the complex (accordingly, the phosphonate units are directed away from the ligated metal centre with τ(Fe1) and τ(Fe2) of −145.0(1)° and 139.7(1)°). In turn, this suggests that the relatively lower symmetry of the complex molecule results from intermolecular interactions and from the overall symmetry of the crystal array rather than from any intrinsic asymmetry (*e.g.*, in ligand coordination).

In the crystal, ferrocene ligands from different complex molecules pair into dimers through $(O\text{-}H\cdots O{=}P)_2$ interactions involving their uncoordinated phosphonate groups. These fragments further assemble into infinite chains *via* interactions between the remaining phosphonate OH moieties and the solvating ethanol

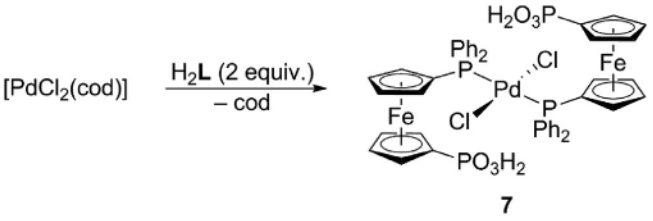

7

Scheme 3. Synthesis of the bis(phosphine) complex **7** (cod = cycloocta-1,5-diene).

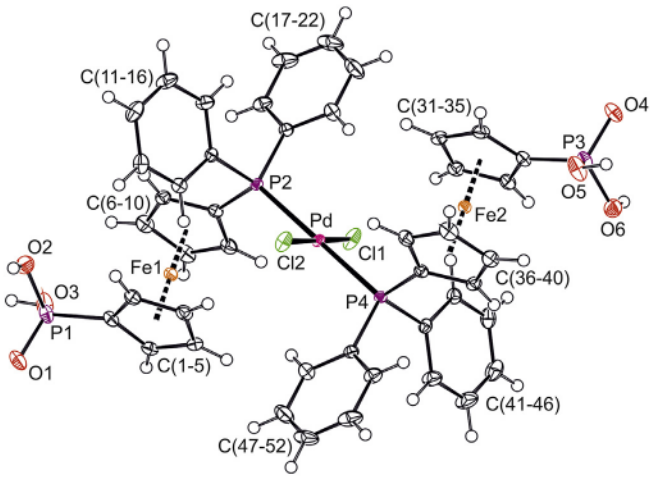

Fig. 6. View of the complex molecule in the structure of **7**·3EtOH. Displacement ellipsoids at the 50% probability level. Selected distances and angles (in Å and deg): Pd-Cl1 2.2989(5), Pd-Cl2 2.2980(5), Pd-P2 2.3440(4), Pd-P4 2.3328(4), Cl1-Pd-P2 88.04(2), Cl1-Pd-P4 92.19(2), Cl2-Pd-P2 92.90(2), Cl2-Pd-P4 86.87(2), P1-O1 1.502(1), P1-O2 1.556(1), P1-O3 1.547(1), P1-C1 1.768(2), P2-C6 1.802(1), P2-C11 1.830(1), P2-C17 1.818(1), P3-O4 1.501(1).

molecules (Fig. 7). The phosphoryl oxygen atoms (P=O) serve as additional H-bond acceptors for these interactions. When combined, hydrogen bond interactions give rise to layers oriented parallel to the crystallographic (1 1 1) planes.

When mixed with Pd(II) acetylacetonate (acac) complexes containing supporting *ortho*-palladated ligands, *viz.* [(L^{CY})Pd(acac)], where L^{CY} = 2-[(dimethylamino-κ*N*)methyl]phenyl-κC^1 and 2-[(methylthio-κ*S*)methyl]phenyl-κC^1, H_2**L** produced the neutral bis-chelate complexes **8** and **9** (Scheme 4), formed through proton transfer from H_2**L** to the acetylacetonate ligand and through O,P-chelating coordination of the formed anion H**L**$^-$.

Compounds **8** and **9** result as yellow solids and are stable under ambient conditions. Their ^{1}H and ^{13}C NMR spectra display signals attributable to the ferrocene phosphino-phosphonate and to the respective *ortho*-metallated ligand. The resonances of the CH_2SMe/CH_2NMe_2 arms are split into ^{31}P-coupled doublets, thus suggesting a *trans*-P,N/S relationship for both compounds. The ^{31}P NMR signals attributable to the Pd-bound phosphine moieties are identified (in $CDCl_3$) as singlets at δ_P 29.1 and 26.2 ppm for **8** and **9**, respectively, whereas the resonances of the O-coordinated PO_3H^- units are found at δ_P 19.2 (**8**) and 19.9 ppm (**9**) (*i.e.*, shifted to a higher field in relation to H_2**L** itself; δ_P 26.7 ppm in $CDCl_3$). ESI MS spectra further

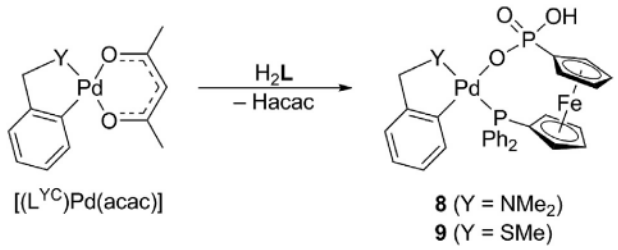

Scheme 4. Synthesis of Pd(II) complexes with supporting *ortho*-metallated ligands (Hacac = acetylacetone).

corroborate the formulation of **8** and **9**, showing $[M + H]^+$ ions.

Complexes **8** and **9** crystallise relatively willingly but tend to incorporate disordered solvent molecules in their crystals (see Experimental). In addition, compound **8** crystallizes with two structurally independent but otherwise very similar molecules in the asymmetric unit (space group *P*–1; for an overlap, see the Supporting Information, Figure S1). Views of the molecular structures of **8** (molecule 1) and **9** are presented in Fig. 8, and the relevant structural parameters are outlined in Table 3. The Pd-donor distances and the interligand angles determined for **8** and **9** are generally similar to those found in analogous complexes featuring O,P-chelating phosphinoferrocene sulfonate ligand $Ph_2PfcSO_3^-$ [6a]. Similarly to phosphino*sulfonate* complexes, the Pd-P bond length in **9** is significantly longer than in **8**, thus reflecting a stronger *trans* influence of the sulfur donor [18]. The coordination environments of the palladium(II) ions in **8** and **9** are distorted due to variations in individual Pd-donor distances and to steric demands of the chelate rings. However, the degree of distortion differs between the complexes. In **9**, which features the larger sulfur donor atom, the angle associated with the L^{CY} chelating ligand is larger (*i.e.*, departs less from the ideal 90°) but the coordination plane is more severely twisted than in **8**, as shown by the dihedral angle of the {Pd,O,P} and {Pd,C,S} "half-planes" associated with the two chelate rings (16.09(7)°). The analogous angles subtended by the {Pd,O,P} and {Pd,C,N} planes in **8** are only 6.28(9)° (Pd1) and 8.60(9)° (Pd2).

O,P-chelating coordination requires that the donor moieties of the phosphinophosphonate anion H**L**$^-$ be rotated into positions closer than those found in the crystal structures discussed above (H_2**L**, its salts and complex **7**). Consequently, the conformations of the 1,1′-disubstituted ferrocene units in **8** and **9** are between synclinal staggered (ideal value: 36°) and synclinal eclipsed (ideal value: 72°), characterised by τ angles of 53.2(2)° (**8**, molecule 1), 42.9(2)° (**8**, molecule 2), and 39.6(1)° (**9**). In addition, the

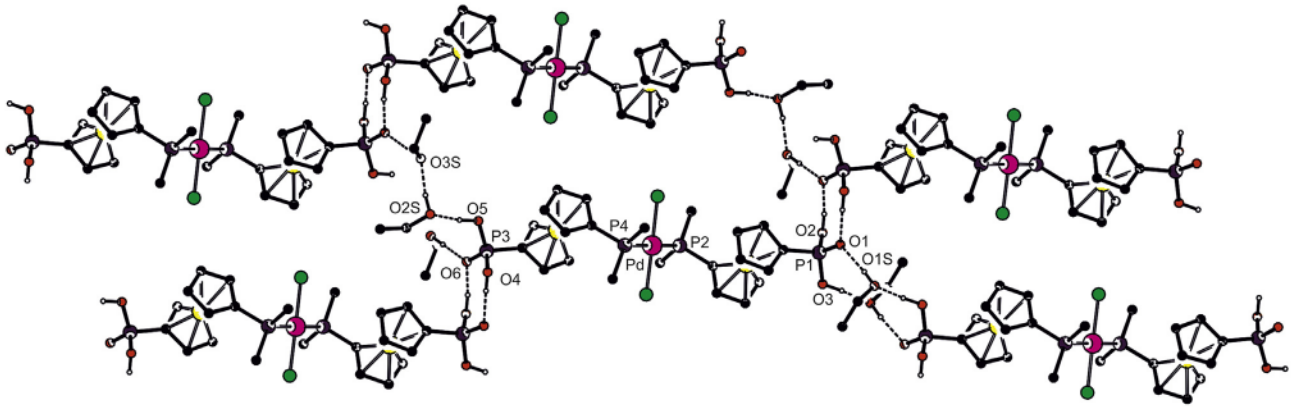

Fig. 7. Section of the hydrogen-bonded assembly in the structure of **7**·3EtOH. Only the OH hydrogens and the pivotal atoms from the phenyl rings are shown for clarity. Hydrogen bond parameters (in Å): O2···O4 2.559(2) Å, O3···O1S 2.502(2), O5···O2S 2.488(2), O6···O1 2.616(2), O1S···O1 2.669(2), O2S···O3S 2.622(2), O3S···O4 2.712(2).

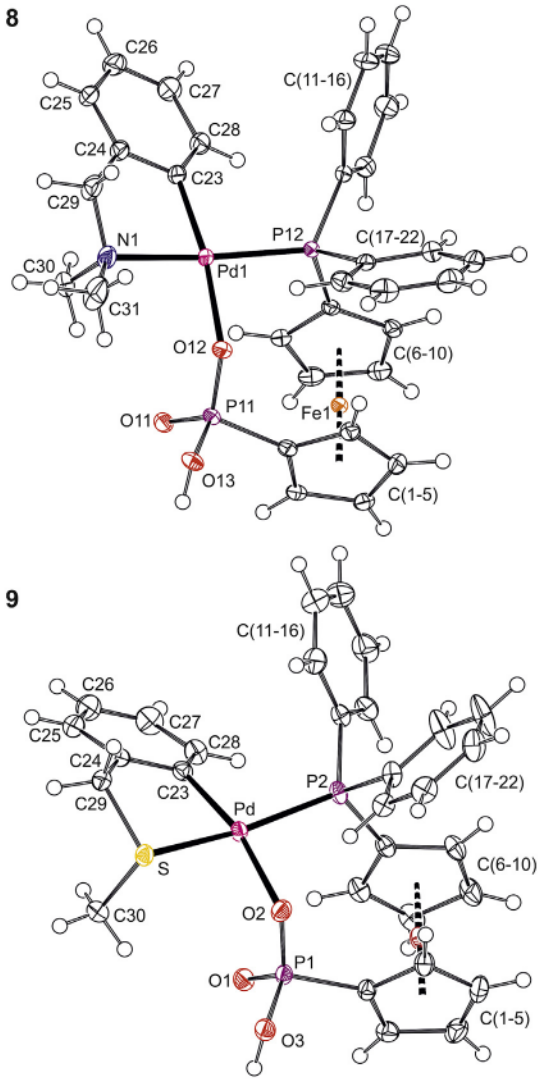

Fig. 8. PLATON plots of the molecular structures of **8** (molecule 1) and **9** (molecule 2); displacement ellipsoids at the 50% probability level.

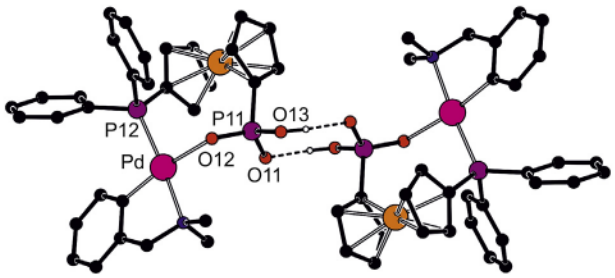

Fig. 9. Hydrogen-bonded dimeric motif in the structure of **8** (molecule 1 interacts with its inversion image); only OH hydrogens are shown for clarity.

deprotonation and coordination of the phosphonate group results in the differentiation of the P-O distances, as observed in salts **5** and **6**. In particular, the P=O and P-O(Pd) bonds of **8** and **9** are shorter than the P-OH bond involved in hydrogen bonding interactions.

In the crystals of **8** and **9**, the complex associates through pairs of O-H···O=P hydrogen bonds into dimers around the crystallographic inversion centres (in **8**, the dimers are formed between molecules 1 or 2 separately). The intermolecular O···O distances are 2.588(2) Å (O13···O11), 2.522(2) Å (O23···O21) for **8**, and 2.584(2) Å (O3 ···O1) for **9**. Notably, both the symmetry of the crystal lattice (space group $P2_1/c$) and even the particular supramolecular interactions indicate that complex **9**, which contains a stereogenic sulfur atom, is obtained in racemic form (Fig. 9).

Table 3
Selected distances and angles for **8** and **9** (in Å and deg).

Parameter	8 (molecule 1, Z = N)	8 (molecule 2, Z = N)	9 (Z = S)
Pd-P	2.2644(6)	2.2494(6)	2.3126(6)
Pd-O	2.137(2)	2.132(2)	2.145(2)
Pd-C	2.001(2)	1.988(2)	2.007(2)
Pd-Z	2.142(2)	2.144(2)	2.3292(6)
P-Pd-O	90.68(4)	89.28(5)	93.34(4)
P-Pd-C	97.05(6)	96.88(7)	97.87(6)
Z-Pd-O	91.36(7)	92.86(7)	85.67(4)
Z-Pd-C	81.18(8)	81.25(8)	84.98(6)
P=O	1.506(2)	1.504(2)	1.504(2)
P-O(Pd)	1.510(2)	1.511(2)	1.512(2)
P-OH	1.579(2)	1.573(2)	1.579(2)

3. Conclusion

1'-(Diphenylphosphino)ferrocene-1-phosphonic acid (H_2**L**), a new addition into the family of polar phosphinoferrocene ligands, can be prepared in a conventional manner from the corresponding phosphonate ester. Although the compound is relatively unstable and spontaneously decomposes upon storage, it can be converted into acidic ammonium salts containing the anion HL^- and used to prepare transition metal complexes. While in its native form compound H_2**L** coordinates soft Pd(II) ions as a P-monodentate donor, deprotonation to HL^- (*e.g.*, by proton transfer to a suitable Pd-bound ligand) opens a convenient access to O,P-chelated complexes. The phosphonate moieties in the free acid H_2**L**, its salts and even the Pd(II) complexes participate in intermolecular (or interionic) hydrogen-bonding interactions. In turn, these interactions give rise to discrete or polymeric solid-state assemblies, whose complexity changes with the number of the available hydrogen bond donors and acceptors. Overall, the coordination behaviour of H_2**L** resembles that of phosphinoferrocene sulfonate **A** rather than the behaviour of the analogous phosphinocarboxylic ligand Hdpf, except that anion HL^- resulting by monodeprotonation of H_2**L** retains one of its OH groups and can thus enter into hydrogen bonding interactions as a H-bond donor.

4. Experimental

4.1. Materials and methods

All preparations were performed under an argon atmosphere using standard Schlenk techniques. Compounds **2** [8], **3** [19], [(L^{NC})Pd(acac)] [20], and [(L^{YC})Pd(acac)] [21] were prepared according to literature procedures. Other chemicals were purchased from commercial suppliers (Sigma-Aldrich, Alfa-Aesar) and used as received. Anhydrous dichloromethane and THF were obtained using a PureSolv MD5 solvent purification system (Innovative Technology, Inc., Amesbury, MA, USA). Solvents for chromatography and crystallisations were of reagent grade (Lach-Ner, Czech Republic) and used without any additional purification step.

^{1}H, ^{31}P{^{1}H}, and ^{13}C{^{1}H} NMR spectra were recorded at 25 °C with a Varian Unity Inova 400 spectrometer operating at 400, 101 and 162 MHz for ^{1}H, ^{13}C and ^{31}P, respectively. Chemical shifts (δ in ppm) are given relative to internal tetramethylsilane (^{1}H and ^{13}C) and to external 85% aqueous H_3PO_4 (^{31}P). In addition to the

standard notation of signal multiplicity (s = singlet, d = doublet, t = triplet, etc.) [22], vt and vq are used to distinguish virtual triplet and quartets arising from the second-order spin systems formed by cyclopentadienyl hydrogens. FTIR spectra were acquired on a Thermo Nicolet 6700 instrument over the 400–4000 cm^{-1} range. Electrospray ionization (ESI) mass spectra were recorded on a Compact QTOF-MS spectrometer (Bruker Daltonics) using samples dissolved in HPLC-grade methanol. Elemental analyses were performed with a PE 2400 Series II CHNS/O Elemental Analyser (Perkin Elmer). The amount of clathrated solvent (if present) was confirmed by NMR analysis.

4.2. Synthesis of [1'-(diphenylphosphino)ferrocenyl]phosphonic acid (H_2**L**)

Neat bromo-trimethylsilane (1.3 mL, 10 mmol) was added dropwise to a solution of ester **2** (1.67 g, 3.3 mmol) in dichloromethane (60 mL). The resulting mixture was stirred for 4 h and then evaporated under vacuum. The residue was dissolved in dichloromethane (10 mL) and treated with water (0.5 mL) under vigorous stirring for 30 min. The resulting mixture was dried over $MgSO_4$, filtered and evaporated under vacuum to afford an orange oily residue, which was purified by column chromatography over silica gel using chloroform-methanol (10:1) as eluent. A single orange band was collected and concentrated. The product was dissolved in chloroform (3 mL) and precipitated by adding an excess of hexane. The separated solid was filtered off, washed with hexane and dried under vacuum, yielding H_2**L**·0.5H_2O as a pale orange powder (1.02 g, 67%). Crystals of unsolvated H_2**L** suitable for X-ray diffraction analysis were obtained from ethyl acetate-hexane.

^{1}H NMR (dmso-d_6): δ 3.75 (very br s, 2 H, PO_3H_2), 4.02 (br s, 2 H, fc), 4.11 (br s, 2 H, fc), 4.24 (br s, 2 H, fc), 4.57 (br s, 2 H, fc) 7.25–7.38 (m, 10 H, PPh_2). ^{13}C{^{1}H} NMR (dmso-d_6): δ 71.13 (d, J_{PC} = 11 Hz, CH of fc), 71.50 (d, J_{PC} = 15 Hz, CH of fc), 73.25 (d, J_{PC} = 3 Hz, CH of fc), 73.44 (d, J_{PC} = 15 Hz, CH of fc), 75.80 (br d, J_{PC} = 6 Hz, *C*-PPh_2 of fc), 128.25 (d, J_{PC} = 7 Hz, CH of PPh_2), 128.55 (s, CH of PPh_2), 133.00 (d, J_{PC} = 20 Hz, CH of PPh_2), 138.73 (d, J_{PC} = 11 Hz, C_{ipso} of PPh_2). The signal due to ferrocene *C*–PO_3H_2 was not observed. ^{31}P{^{1}H} NMR (dmso-d_6): δ −17.4 (s, PPh_2), 17.3 (br s, PO_3H_2). ^{31}P{^{1}H} NMR ($CDCl_3$): δ −16.0 (s, PPh_2), 26.7 (br s, PO_3H_2). IR (Nujol): ν_{max} 1654 br m, 1586 m, 1437 m, 1309 m, 1195 s, 1161 m, 1122 w, 1070 w, 1034 s, 997s, 641 w, 573 s, 487 s, 455 m cm^{-1}. EI + MS: *m/z* 451 ($[M + H]^+$). Anal. Calc. for $C_{22}H_{20}O_3FeP_2$·0.5H_2O (459.2): C 57.54, H 4.61%. Found: C 57.60, H 4.55%.

4.3. Synthesis of diethyl [1'-(diphenylphosphino)ferrocenyl] phosphonate–borane (1/1) (**4**)

A stirring solution of 1-(diphenylphosphino)-1′-bromferrocene–borane (**3**; 1.85 g, 4.0 mmol) in dry THF (150 mL) was cooled in a dry ice/ethanol bath to −78 °C and treated with *n*-butyllithium (1.6 mL of 2.5 M in hexanes, 0.44 mmol). After stirring the reaction mixture for 15 min, neat diethyl chlorophosphate (0.8 mL, 0.55 mmol) was introduced, and the mixture was stirred at −78 °C for another 15 min and then at room temperature for 3 h. Then, it was evaporated under reduced pressure, and the residue was purified by column chromatography over alumina. Chloroform-diethyl ether (2:3) was used to remove non-polar byproducts (mostly FcPPh_2·BH_3). Subsequent elution with chloroform-diethyl ether (3:2) eluted ester **4**. Yield: 1.39 g (60%), an orange oil.

^{1}H NMR ($CDCl_3$): δ 1.20 (br s, 3 H, BH_3), 1.30 (t, $^3J_{HH}$ = 7.1 Hz, 6 H, CH_3), 4.06 (q, $^3J_{HH}$ = 7.0 Hz, 4 H, CH_2), 4.38 (br s, 4 H, fc), 4.52 (vq, J' = 1.7 Hz, 2 H, fc), 4.74 (vq, J' = 1.0 Hz, 2 H, fc), 7.39–7.44 (m, 4 H, PPh_2), 7.45–7.51 (m, 2 H, PPh_2), 7.54–7.61 (m, 4 H, PPh_2). ^{31}P{^{1}H} NMR ($CDCl_3$): δ 16.3 (br d, J_{PH} = 55 Hz, PPh_2BH_3), 24.8 (s, PO_3Et_2). ^{13}C{^{1}H}: δ 16.43 (d, $^3J_{PC}$ = 6 Hz, CH_3), 61.82 (d, $^2J_{PC}$ = 6 Hz, CH_2), 70.54 (d, J_{PC} = 67 Hz, *C*-PO_3Et_2), 72.78 (d, J_{PC} = 15 Hz, CH of fc), 73.84 (d, J_{PC} = 13 Hz, CH of fc), 74.05 (d, J_{PC} = 10 Hz, CH of fc), 74.74 (d, J_{PC} = 7 Hz, CH of fc), 128.50 (d, J_{PC} = 10 Hz, CH of PPh_2), 130.82 (d, $^1J_{PC}$ = 82 Hz, C_{ipso} of PPh_2), 131.04 (d, J_{PC} = 2 Hz, CH of PPh_2), 132.60 (d, J_{PC} = 9 Hz, CH of PPh_2). The signal due to ferrocene *C*-PPh_2 was not observed. IR (Nujol): ν_{max} 3460 br s, 3077 m, 3056 s, 2386 s, 2254 m, 1653 m, 1589 w, 1574 w, 1484 m, 1437 s, 1390 s, 1370 s, 1313 m, 1248 s, 1189 s, 1106 s, 1033 s, 962 s, 834 s, 795 m, 739 s, 700 s, 639 m, 623 m, 595 s, 527 s, 490 s cm^{-1}. ESI + MS: *m/z* 519 ($[M - H]^+$), 521 ($[M + H]^+$). Anal. Calc. for $C_{26}H_{31}BFeO_3P_2$·2/3CH_2Cl_2 (576.6): C 55.53, H 5.65%. Found: C 55.34, 5.55%.

4.4. Synthesis of [1'-(diphenylphosphino)ferrocenyl]phosphonic acid–borane (1/1) (H_2**L**·BH_3)

Bromo-trimethylsilane (1.1 mL, 8.0 mmol) was added dropwise to a solution of adduct **4** (1.39 g, 2.7 mmol) in dichloromethane (60 mL), and the mixture was stirred for 4 h before evaporation under vacuum. The residue was taken up with dichloromethane (10 mL), and the solution was treated with water (0.5 mL) under stirring for 30 min. The resulting mixture was dried over $MgSO_4$, filtered and evaporated under vacuum to give an orange oily residue, which was purified by column chromatography over silica gel using a dichloromethane-methanol (10:1) as eluent. A single orange band was collected and evaporated. The product was redissolved in chloroform (3 mL) and precipitated by adding an excess of hexane. The separated solid was filtered off, washed with hexane and dried under vacuum to give H_2**L**·BH_3 as an orange solid (0.91 g, 73%).

^{1}H NMR (dmso-d_6): δ 1.20 (very br s, 3 H, BH_3), 4.04 (vq, J' = 1.8 Hz, 2 H, fc), 4.20 (vq, J' = 2.2 Hz, 2 H, fc), 4.25 (very br s, 2 H, OH), 4.49 (vq, J' = 1.8 Hz, 2 H, fc), 4.72 (br d, J' = 1.4 Hz, 2 H, fc), 7.47–7.58 (m, 10 H, PPh_2). ^{13}C{^{1}H} NMR (dmso-d_6): δ 68.80 (d, J_{PC} = 68 Hz, *C*-PPh_2 of fc), 71.93 (d, J_{PC} = 15 Hz, CH of fc), 72.19 (d, J_{PC} = 13 Hz, CH of fc), 73.40 (d, J_{PC} = 10 Hz, CH of fc), 74.55 (d, J_{PC} = 8 Hz, CH of fc), 74.89 (d, J_{PC} = 202 Hz, *C*-PO_3H_2 of fc), 128.73 (d, J_{PC} = 10 Hz, CH of PPh_2), 130.64 (d, J_{PC} = 60 Hz, C_{ipso} of PPh_2), 131.21 (d, J_{PC} = 2 Hz, CH of PPh_2), 132.10 (d, J_{PC} = 10 Hz, CH of PPh_2). ^{31}P{^{1}H} NMR (dmso-d_6): δ 15.6 (br s, PPh_2), 17.8 (s, PO_3H_2). IR (Nujol): IR (Nujol): ν_{max} 2725 w, 2383 s, 1683 w, 1588 w, 1467 s, 1377 s, 1312 w, 1256 w, 1197 s, 1174 s, 1107 s, 1059 s, 1036 s, 999 s, 943 m, 886 m, 837 s, 739 s, 698 s, 639 m, 624 m, 610 w, 576 m, 527 m, 475 s cm^{-1}. ESI + MS: *m/z* 487 ($[M + H]^+$). Anal. Calc. for $C_{22}H_{23}BFeO_3P_2$ (464.0): C 56.94, H 5.00%. Found: C 56.65, H 5.08%.

4.5. Synthesis of [1'-(diphenylphosphinoyl)ferrocenyl]phosphonic acid (H_2**L**O)

Hydrogen peroxide in excess (0.2 mL, 30% in H_2O) was added dropwise to a solution of H_2L (90 mg, 0.20 mmol) in acetone (5 mL). The resulting mixture was stirred for 1 h, dried over $MgSO_4$, filtered and evaporated under vacuum. The product was dissolved in dichloromethane (3 ml) and precipitated by adding excess of hexane. The separated solid was filtered off, washed with hexane and dried under vacuum, yielding H_2LO·H_2O as an orange solid (50 mg, 52%).

^{1}H NMR (dmso-d_6): δ 4.24 (br s, 2 H, fc), 4.37 (br s, 2 H, fc), 4.51 (br s, 2 H, fc), 4.73 (br s, 2 H, fc), 7.53–7.73 (m, 10 H, P(O)Ph_2). ^{13}C{^{1}H} NMR (dmso-d_6): δ 71. 52 (d, J_{PC} = 13 Hz, CH of fc), 71.63 (d, J_{PC} = 115 Hz, *C*-PPh_2 of fc), 72.53 (d, J_{PC} = 15 Hz, CH of fc), 73.48 (d, J_{PC} = 6 Hz, CH of fc), 73.60 (d, J_{PC} = 9 Hz, CH of fc), 74.50 (d, J_{PC} = 198 Hz, C-PO_3H_2 of fc), 128.71 (d, J_{PC} = 12 Hz, CH of PPh_2), 130.77 (d, J_{PC} = 10 Hz, CH of PPh_2), 132.19 (d, J_{PC} = 3 Hz, CH of PPh_2), 132.58 (d, $^1J_{PC}$ = 107 Hz, C_{ipso} of PPh_2). ^{31}P {^{1}H} NMR (dmso-d_6):

δ 16.5 (s, PO_3H_2), 31.7 (s, P(O)Ph_2). IR (Nujol): ν_{max} 1706 m, 1591 w, 1310 w, 1152 s, 1122 s, 1098 m, 1072 m, 998 w, 941 w, 539 m, 752 m, 571 s, 534 m, 497 m cm^{-1}. ESI + MS: *m/z* 467 ($[M + H]^+$), 489 ($[M + Na]^+$). Anal. Calc. for $C_{22}H_{20}FeO_4P_2 \cdot H_2O$ (484.2): C 54.57, H 4.58%. Found: C 54.62, 4.17%.

4.6. Synthesis of (dabcoH)(H**L**) (**5**)

H_2**L** (67.5 mg, 0.15 mmol) and dabco (16.8 mg, 0.15 mmol) were dissolved in a mixture of dichloromethane (7 mL) and methanol (4 mL). After stirring for 30 min, the volatiles were removed under vacuum to produce salt **5** as an orange solid in quantitative yield (84.3 mg). The crystals used for structure determination were obtained by recrystallisation from chloroform/hexane.

^{1}H NMR ($CDCl_3$): δ 3.00 (s, 12 H, CH_2), 4.03 (s, 2 H, fc), 4.18 (s, 2 H, fc), 4.42 (s, 2 H, fc), 4.63 (s, 2 H, fc), 5.79 (very br s, 1 H, OH), 7.26–7.37 (m, 10 H, PPh_2). $^{13}C\{^1H\}$ NMR (dmso-d_6): δ 44.83 (s, CH_2 dabco), 70.54 (d, J_{PC} = 11 Hz, CH of fc), 71.56 (d, J_{PC} = 14 Hz, CH of fc), 73.27 (d, J_{PC} = 16 Hz, CH of fc), 73.35 (br s, CH of fc), 75.16 (d, J_{PC} = 7 Hz, *C*-PPh_2 of fc), 78.46 (d, J_{PC} = 199 Hz, *C*-PO_3H of fc), 128.19 (d, J_{PC} = 7 Hz, CH of PPh_2), 128.46 (s, CH of PPh_2), 132.99 (d, J_{PC} = 19 Hz, CH of PPh_2), 138.95 (d, J_{PC} = 11 Hz, C_{ipso} of PPh_2). $^{31}P\{^1H\}$ NMR (dmso-d_6): δ −17.1 (s, PPh_2), 14.8 (br s, PO_3H). ESI + MS: *m/z* 113 ($[C_6H_{13}N_2]^+$), 451 ($[H_2$**L** + H$]^+$). IR (Nujol): ν_{max} 3393 br m, 3051 w, 2725 w, 1981 w, 1697 w, 1585 w, 1568 w, 1541 w, 1318 m, 1230 m, 1208 w, 1192 w, 1181 m, 1139 s, 1060 s, 1027 m, 995 m, 972 m, 917 s, 881 s, 830 m, 784 w, 746 s, 698 s, 669 w, 650 w, 607 m, 583 s, 529 w, 502 s, 483 m, 457 m, 441 m, 423 w cm^{-1}. HR − MS: *m/z* 449 ($[PPh_2fcPO_3H]^-$). Anal. Calc. for $C_{28}H_{32}O_3N_2FeP_2 \cdot 0.5CH_2Cl_2$ (604.8): C 56.60, H 5.50, N 4.63%. Found: C 56.14, H 5.47, N 4.79%.

4.7. Synthesis of ((HOCH$_2$CH$_2$)$_2$NH$_2$)(H**L**) (**6**)

H_2**L** (90.0 mg, 0.20 mmol) and bis(2-hydroxyethyl)amine (21.0 mg, 0.20 mmol) were dissolved in acetone (5 mL), and the mixture was stirred for 15 min. Subsequent evaporation under vacuum left salt **6** as a yellow powder in quantitative yield (111 mg). Crystals suitable for X-ray diffraction analysis were obtained after layering the solution of the salt in dichloromethane-THF (1:1) with hexane.

^{1}H NMR (dmso-d_6): δ 2.91 (br s, 4 H, NCH_2), 3.64 (br s, 4 H, OCH_2), 3.93 (vq, *J'* = 1.8 Hz, 2 H, fc), 4.07 (vq, *J'* = 1.8 Hz, fc), 4.17 (vq, *J'* = 2.2 Hz, fc), 4.53 (vt, *J'* = 1.8 Hz, fc), 4.86 (very br s, 2 H, CH_2OH), 7.25–7.36 (m, 10 H, PPh_2). $^{13}C\{^1H\}$ NMR (dmso-d_6): δ 49.91 (s, NCH_2), 57.12 (s, OCH_2), 70.46 (d, J_{PC} = 12 Hz, CH of fc), 71.39 (d, J_{PC} = 14 Hz, CH of fc), 73.18 (d, J_{PC} = 15 Hz, CH of fc), 73.23 (d, J_{PC} = 5 Hz, CH of fc), 75.17 (d, J_{PC} = 7 Hz, *C*-PPh_2 of fc), 78.92 (d, J_{PC} = 195 Hz, *C*-PO_3H of fc), 128.20 (d, J_{PC} = 7 Hz, CH of PPh_2), 128.46 (s, CH of PPh_2), 132.99 (d, J_{PC} = 19 Hz, CH of PPh_2), 138.95 (d, J_{PC} = 11 Hz, C_{ipso} of PPh_2). $^{31}P\{^1H\}$ NMR (dmso): δ −17.1 (s, PPh_2), 15.0 (s, PO_3H). IR (Nujol): ν_{max} 2041 m, 1932 m, 1683 w, 1653 w, 1558 w, 1540 w, 1307 m, 1169 m, 1073 m, 1035 m, 971 m, 833 m, 695 m, 608 m, 569 m, 483 m cm^{-1}. ESI + MS: *m/z* 451 ($[H_2$**L** + H$]^+$). Anal. Calc. for $C_{26}H_{31}O_5NFeP_2$ (555.3): C 56.23, H 5.63, N 2.52%. Found: C 56.01, H 5.47, N 2.37%.

4.8. Synthesis of trans-[PdCl$_2$(H$_2$**L**-κP)$_2$] (**7**)

H_2**L** (90.0 mg, 0.20 mmol) and [$PdCl_2$(cod)] (28.5 mg, 0.10 mmol) were dissolved in dichloromethane (30 mL), and the resulting mixture was stirred for 1 h. Then, the solvent was evaporated under reduced pressure, the residue was dissolved in methanol-dichloromethane (1:1, 10 mL), and the solution was precipitated by adding an excess of pentane-diethyl ether (1:1, 40 mL). The separated solid was filtered off, washed with pentane and dried under vacuum, affording **7**·0.5CH_2Cl_2 as a brown powder (88 mg, 79%). The crystals of **7**·3EtOH used for structure determination were grown by liquid-phase diffusion of diethyl ether into an ethanolic solution of the complex.

^{1}H NMR (dmso-d_6): δ 4.11 (very br s, 4 H, OH), 4.55 (br s, 8 H, fc), 4.70 (br s, 4 H, fc), 4.75 (br s, 4 H, fc), 7.38–7.60 (m, 20 H, PPh_2). $^{31}P\{^1H\}$ NMR (dmso-d_6): δ 17.0 (s, PPh_2), 18.0 (br s, PO_3H_2). IR (Nujol): ν_{max} 2726 w, 1653 br w, 1481 w, 1437 s, 1196 s, 1166 s, 1099 s, 1061 w, 1035 s, 1000 s, 932 s, 884 m, 872 w, 841 m, 814 w, 748 m, 708 w, 696 s, 669 w, 644 w, 627 w, 580 m, 541 m, 507 s, 465 m, 455 w cm^{-1}. EIS + MS: *m/z* 1049 ($[PdL_2Na_2 + H]^+$). Anal. Calc. for $C_{44}H_{40}O_6Cl_2Fe_2P_4Pd \cdot 0.5CH_2Cl_2$ (1120.2): C 47.71, H 3.69%. Found: C 47.73, H 3.72%.

4.9. Synthesis of [(L^{NC})Pd(H**L**-κ^2*O*,*P*)] (**8**)

H_2**L** (36.0 mg, 0.08 mmol) and [(L^{NC})Pd(acac)] (27.2 mg, 0.08 mmol) were dissolved in dichloromethane (5 mL), and the reaction mixture was stirred for 30 min. Subsequent solvent removal produced **8**·0.25CH_2Cl_2 as a yellow solid. Yield: 50.0 mg (88%). Crystals of **8**·2CH_2Cl_2 suitable for X-ray diffraction analysis were obtained from dichloromethane/ethyl acetate/hexane.

^{1}H NMR ($CDCl_3$): δ 2.88 (s, 6 H, NMe_2), 3.99 (br s, 2 H, NCH_2), 4.02 (br s, 2 H, fc), 4.25 (br s, 2 H, fc), 4.57 (br s, 2 H, fc), 4.74 (br s, 2 H, fc), 5.85 (t, *J* = 7.1 Hz, 1 H, C_6H_4), 6.17 (t, *J* = 7.3 Hz, 1 H, C_6H_4), 6.66 (t, *J* = 7.32 Hz, 1 H, C_6H_4), 6.84 (t, *J* = 7.2 Hz, 1 H, C_6H_4), 7.22–7.29 (m, 4 H, PPh_2), 7.30–7.37 (m, 2 H, PPh_2), 7.55–7.64 (m, 4 H, PPh_2). $^{13}C\{^1H\}$ NMR ($CDCl_3$): 50.03 (br s, NMe_2), 70.59 (br s, CH of fc), 71.76 (d, J_{PC} = 53 Hz, *C*-PPh_2 of fc), 72.44 (br s, NCH_2), 72.52 (s, CH of fc), 74.23 (br d, *J* = 13 Hz, CH of fc), 76.53 (br s, partly overlapping with the solvent signal, CH of fc), ≈77.5 (d, *C*-PO_3H of fc; overlapping with the solvent resonance), 122.06 (s, CH of C_6H_4), 123.27 (s, CH of C_6H_4), 124.50 (d, J_{PC} = 5 Hz, CH of C_6H_4), 127.88 (d, J_{PC} = 11 Hz, PPh_2), 130.12 (s, CH of PPh_2), 133.59 (d, J_{PC} = 52 Hz, C_{ipso} of PPh_2), 134.62 (d, J_{PC} = 12 Hz, CH of PPh_2), 137.37 (d, J_{PC} = 10 Hz, CH of C_6H_4), 146.21 (s, C_{ipso} of C_6H_4), 148.38 (s, C_{ipso} of C_6H_4). $^{31}P\{^1H\}$ NMR ($CDCl_3$): δ 19.2 (s, PO_3H), 29.1 (s, PPh_2). IR (Nujol): ν_{max} 1168 br m, 1073 m, 1032 m, 930 m, 887 m, 844 m, 743 m, 696 m, 584 m, 485 m cm^{-1}. ESI + MS: *m/z* 690 ($[M + H]^+$). Anal. Calcd. for $C_{31}H_{31}FeNO_3P_2Pd \cdot 0.25CH_2Cl_2$ (711.0): C 52.79, H 4.47, N 1.97%. Found: C 52.79, H 4.56, 1.99%.

4.10. Synthesis of [(L^{SC})Pd(H**L**-κ^2*O*,*P*)] (**9**)

H_2**L** (36.0 mg, 0.08 mmol) and [(L^{SC})Pd(acac)] (27.5 mg, 0.08 mmol) were dissolved in dichloromethane (5 mL), and the resulting mixture was stirred for 30 min. Subsequent solvent removal afforded analytically pure **9** as a yellow solid. Yield 47.7 mg (86%). Recrystallization from dichloromethane-hexane gave single-crystals suitable for X-ray diffraction analysis.

^{1}H NMR ($CDCl_3$): δ 2.64 (d, J_{PH} = 3.6 Hz, 3 H, SMe), 4.05 (br s, 4 H, SCH_2 and fc), 4.31 (br s, 2 H, fc), 4.60 (br s, 2 H, fc), 4.79 (br s, 2 H, fc), 6.11 (br m, 2 H, C_6H_4), 6.59 (br t, *J* = 7.5 Hz, 1 H, C_6H_4), 6.84 (br d, *J* = 7.5 Hz, 1 H, C_6H_4), 7.20–7.28 (m, 4 H, PPh_2), 7.29–7.35 (m, 2 H, PPh_2), 7.51–7.60 (m, 4 H, PPh_2). $^{13}C\{^1H\}$ NMR ($CDCl_3$): δ 20.41 (s, SMe), 46.23 (s, SCH_2), 70.61 (br s, CH of fc), 71.64 (d, J_{PC} = 51 Hz, *C*-PPh_2 of fc), 72.58 (d, J_{PC} = 8 Hz, CH of fc), 74.25 (d, J_{PC} = 13 Hz, CH of fc), 76.66 (d, overlapping with the solvent resonance, CH of fc), ≈78.5 (d, *C*-PO_3H of fc, partly overlapped by the solvent signal), 123.20 (s, CH of C_6H_4), 123.83 (s, CH of C_6H_4), 125.01 (d, J_{PC} = 6 Hz, CH of C_6H_4), 127.94 (d, J_{PC} = 11 Hz, CH of PPh_2), 130.15 (s, CH of PPh_2), 133.00 (d, J_{PC} = 50 Hz, C_{ipso} of PPh_2), 134.54 (d, J_{PC} = 12 Hz, CH of PPh_2), 139.46 (d, J_{PC} = 13 Hz, CH of C_6H_4), 147.26 (s, C_{ipso} of C_6H_4), 149.80 (s, C_{ipso} of C_6H_4). $^{31}P\{^1H\}$ NMR ($CDCl_3$): δ 19.9 (s, PO_3H), 26.2 (s, PPh_2). IR (Nujol): ν_{max} 3056 m, 1717 br m, 1573 m, 1483 m, 1436 s,

1312 m, 1260 m, 1196 s, 1166 m, 1148 s, 1095 m, 1068 s, 1046 w, 1029 m, 998 w, 971 w, 924 s, 889 m, 826 m, 751 m, 735 m, 694 s, 653 w, 626 w, 584 s, 539 m, 519 m, 482 s, 470 s, 449 w cm^{-1}. ESI + MS: *m/z* 693 ($[M + H]^+$). Anal. Calc. for $C_{30}H_{28}FeO_3P_2PdS$ (692.8): C 52.01, H 4.07%. Found: C 51.96, H 4.10%.

4.11. X-ray crystallography

Diffraction data ($\pm h \pm k \pm l$, $\theta_{max} = 27.5°$) were collected at 120(2) (for **5**) or 150(2) K (for all other compounds) using a Bruker D8 VENTURE Kappa Duo PHOTON100 instrument equipped with a IμS micro-focus X-ray tube (Mo Kα radiation, $\lambda = 0.71073$ Å). The structures were solved using direct methods (SHELXT [23]) and then refined using the full-matrix least-squares routine based on F^2 using SHELXL-2014 or SHELXL-2016 [24]. The non-hydrogen atoms were refined with anisotropic displacement parameters. The OH and NH hydrogens were identified on difference density maps and refined either freely (only for H_2**L**) or as riding atoms with U_{iso}(H) set to a 1.2U_{eq} of their bonding atom. Hydrogens at carbon atoms were included in their theoretical positions and refined analogously. In some cases, the analysed crystals contained disordered molecules of halogenated solvents used during the crystallisation (**5**: chloroform; **6**, **8** and **9**: dichloromethane). The contributions of these molecules to the overall scattering were numerically eliminated by PLATON SQUEEZE [25]. A recent version of the PLATON program [26] was used to perform all geometric calculations and to prepare the structural diagrams.

Selected crystallographic data, data collection and structure refinement parameters are available in Supporting Information. CCDC 1899917-1899922 contains supplementary crystallographic data on this paper. These data are available, free of charge from The Cambridge Crystallographic Data Centre via www.ccdc.cam.ac.uk/data_request/cif.

4.12. DFT computations

DFT calculations have been performed using the M06 density functional [27] and SDD (Fe) [28] and def2-TZVP (C, H, O and P) [29] basis sets together with Grimme's D3 dispersion correction [30], as implemented in the Gaussian 16 program package [31]. The solid-state structure of $FcPO_3H_2$ determined by X-ray diffraction analysis [13] was used as a starting point for geometry optimization. Mayer bond indices [32] and Merz-Kollman charges [33] were obtained using the software package Multiwfn [34].

Acknowledgements

This work was supported by the Charles University Research Centre program (project no. UNCE/SCI/014). Computational resources were provided by the CESNET (project LM2015042) and by the CERIT Scientific Cloud (project LM2015085), supported within the programme “Projects of Large Research, Development, and Innovations Infrastructures”.

Appendix A. Supplementary data

Supplementary data related to this article can be found at https://doi.org/10.1016/j.jorganchem.2019.04.012.

References

[1] a) N. Pinault, D.W. Bruce, Coord. Chem. Rev. 241 (2003) 1;
b) K.H. Shaughnessy, Chem. Rev. 109 (2009) 643;
c) F. Joó, Aqueous Organometallic Catalysis, Kluwer, Dordrecht, 2001;
d) B. Cornils, W.A. Herrmann (Eds.), Aqueous-Phase Organometallic Chemistry, second ed., Wiley-VCH, Weinheim, 2004.
[2] a) A. Bader, E. Lindner, Coord. Chem. Rev. 108 (1991) 27;
b) C.S. Slone, D.A. Weinberger, C.A. Mirkin, Prog. Inorg. Chem. 48 (1999) 233.
[3] a) Ferrocenes, in: A. Togni, T. Hayashi (Eds.), Homogeneous Catalysis, Organic Synthesis, Materials Science, VCH, Weinheim, 1995;
b) Ferrocenes, in: P. Štěpnička (Ed.), Ligands, Materials and Biomolecules, Wiley, Chichester, 2008;
c) R.C.J. Atkinson, V.C. Gibson, N.J. Long, Chem. Soc. Rev. 33 (2004) 313;
d) R. Gómez Arrayás, J. Adrio, J.C. Carretero, Angew. Chem. Int. Ed. 45 (2006) 7674.
[4] a) S.W. Chien, T.S.A. Hor, in: P. Štěpnička (Ed.), Ferrocenes: Ligands, Materials and Biomolecules, Wiley, Chichester, 2008, pp. 33–116, ch. 2;
b) K.-S. Gan, T.S.A. Hor, in: A. Togni, T. Hayashi (Eds.), Ferrocenes: Homogeneous Catalysis, Organic Synthesis, Materials Science, Wiley-VCH, Weinheim, 1995, pp. 3–104, ch. 1;
c) G. Bandoli, A. Dolmella, Coord. Chem. Rev. 209 (2000) 161.
[5] a) J. Podlaha, P. Štěpnička, J. Ludvík, I. Císařová, Organometallics 15 (1996) 543;
b) P. Štěpnička, Eur. J. Inorg. Chem. (2005) 3787.
[6] a) M. Zábranský, I. Císařová, P. Štěpnička, Organometallics 37 (2018) 1615;
b) M. Zábranský, I. Císařová, A.M. Trzeciak, W. Alsalahi, P. Štěpnička, Organometallics 38 (2019) 479.
[7] S. Basra, J.G. de Vries, D.J. Hyett, G. Harrison, K.M. Heslop, A.G. Orpen, P.G. Pringle, K. von der Luehe, Dalton Trans. (2004) 1901.
[8] P. Štěpnička, I. Císařová, R. Gyepes, Eur. J. Inorg. Chem. (2006) 926.
[9] a) T.L. Schull, J.C. Fettinger, D.A. Knight, Inorg. Chem. 35 (1996) 6717;
b) C.M. Reisinger, R.J. Nowack, D. Volkmer, B. Rieger, Dalton Trans. (2007) 272;
c) A. Labed, F. Jiang, I. Labed, A. Lator, M. Peters, M. Achard, A. Kabouche, Z. Kabouche, G.V.M. Sharma, C. Bruneau, ChemCatChem 7 (2015) 1090.
[10] a) O. Oms, F. Maurel, F.J. Le Bideau, A. Vioux, D. Leclercq, J. Organomet. Chem. 689 (2004) 2654;
b) C.E. McKenna, M.T. Higa, N.H. Cheung, M.-C. McKenna, Tetrahedron Lett. (1977) 155.
[11] L.D. Freedman, G.O. Doak, Chem. Rev. 57 (1957) 479.
[12] S.R. Alley, W. Henderson, J. Organomet. Chem. 637–639 (2001) 216.
[13] B.-Z. Yang, C. Xu, T.-K. Duan, W. Chen, Q.-F. Zhang, Acta Crystallogr. E: Struct. Rep. Online 67 (2011) m1087.
[14] J.A. Adeleke, L.-K. Liu, Acta Crystallogr. C: Struct. Chem. 49 (1993) 680.
[15] T.J.R. Weakley, Acta Crystallogr. Sect. B Struct. Crystallogr. Cryst. Chem. 32 (1976) 2889;
b) A.H. Mahmoudkhani, V. Langer, J. Mol. Struct. 609 (2002) 97.
[16] a) G. Ferguson, C. Glidewell, R.M. Gregson, P.R. Meehan, Acta Crystallogr. Sect. B Struct. Sci. 51 (1998) 129;
b) J. Beckmann, D. Dakternieks, A. Duthie, Appl. Organomet. Chem. 17 (2003) 817;
c) T. Diop, L. Diop, T. Maris, H. Stoeckli-Evans, Acta Crystallogr. E: Struct. Rep. Online 68 (2012) o1432;
d) M. Sarr, M.S. Boye, A. Diasse-Sarr, A. Grosjean, P. Guionneau, Acta Crystallogr. E: Struct. Rep. Online 68 (2012) o3087.
[17] C.F.J. Barnard, M.H.J. Russel, in: G. Wilkinson, R.D. Gillard, J.A. McCleverty (Eds.), Comprehensive Coordination Chemistry 5, Pergamon Press, Oxford, 1987, pp. 1099–1130;
b) A.T. Hutton, C.P. Morley, in: G. Wilkinson, R.D. Gillard, J.A. McCleverty (Eds.), Comprehensive Coordination Chemistry 5, Pergamon Press, Oxford, 1987, pp. 1157–1170;
c) F.R. Hartley, The Chemistry of Platinum and Palladium, Applied Science, London, 1973.
[18] a) T.G. Appleton, H.C. Clark, L.E. Manzer, Coord. Chem. Rev. 10 (1973) 335;
b) F.R. Hartley, Chem. Soc. Rev. 2 (1973) 163.
[19] K. Škoch, I. Císařová, J. Schulz, U. Siemeling, P. Štěpnička, Dalton Trans. 46 (2017) 10339.
[20] R. Navarro, J. García, E.P. Urriolabeitia, C. Cativiela, M.D. Diaz-de-Villegas, J. Organomet. Chem. 490 (1995) 35.
[21] M. Zábranský, I. Císařová, P. Štěpnička, Eur. J. Inorg. Chem. (2017) 2557.
[22] R.M. Silverstein, F.X. Webster, D.J. Kiemle, Spectrometric Identification of Organic Compounds, seventh ed., Wiley, Hoboken, 2005.
[23] G.M. Sheldrick, Acta Crystallogr. A: Found. Adv. 71 (2015) 3.
[24] G.M. Sheldrick, Acta Crystallogr., Sect. C, Struct. Chem. 71 (2015) 3.
[25] A.L. Spek, Acta Crystallogr. C: Struct. Chem. 71 (2015) 9.
[26] A.L. Spek, J. Appl. Crystallogr. 36 (2003) 7.
[27] Y. Zhao, D.G. Truhlar, Theor. Chem. Acc. 120 (2008) 215.
[28] D. Andrae, U. Haeussermann, M. Dolg, H. Stoll, H. Preuss, Theor. Chim. Acta 7 (1990) 123.
[29] F. Weigend, R. Ahlrichs, Phys. Chem. Chem. Phys. 7 (2005) 3297.
[30] a) S. Grimme, J. Antony, S. Ehrlich, H. Krieg, J. Chem. Phys. 132 (2010) 154104;
b) S. Grimme, S. Ehrlich, L. Goerigk, J. Comput. Chem. 32 (2011) 1456.
[31] Gaussian 16, Revision A. 03, M.J. Frisch, G.W. Trucks, H.B. Schlegel, G.E. Scuseria, M.A. Robb, J.R. Cheeseman, G. Scalmani, V. Barone, G.A. Petersson, H. Nakatsuji, X. Li, M. Caricato, A.V. Marenich, J. Bloino, B.G. Janesko, R. Gomperts, B. Mennucci, H.P. Hratchian, J.V. Ortiz, A.F. Izmaylov, J.L. Sonnenberg, D. Williams-Young, F. Ding, F. Lipparini, F. Egidi, J. Goings, B. Peng, A. Petrone, T. Henderson, D. Ranasinghe,

V.G. Zakrzewski, J. Gao, N. Rega, G. Zheng, W. Liang, M. Hada, M. Ehara, K. Toyota, R. Fukuda, J. Hasegawa, M. Ishida, T. Nakajima, Y. Honda, O. Kitao, H. Nakai, T. Vreven, K. Throssell, J.A. Montgomery Jr., J.E. Peralta, F. Ogliaro, M.J. Bearpark, J.J. Heyd, E.N. Brothers, K.N. Kudin, V.N. Staroverov, T.A. Keith, R. Kobayashi, J. Normand, K. Raghavachari, A.P. Rendell, J.C. Burant, S.S. Iyengar, J. Tomasi, M. Cossi, J.M. Millam, M. Klene, C. Adamo, R. Cammi, J.W. Ochterski, R.L. Martin, K. Morokuma, O. Farkas, J.B. Foresman, D.J. Fox, Gaussian, Inc., Wallingford CT, 2016.

[32] a) I. Mayer, Chem. Phys. Lett. 97 (1983) 270;
(b) I. Mayer, Int. J. Quantum Chem. 26 (1984) 151.

[33] a) U.C. Sing, P.A. Kollman, J. Comput. Chem. 5 (1984) 129;
(b) B.H. Besler, K.M. Merz, P.A. Kollman, J. Comput. Chem. 11 (1990) 431.

[34] T. Lu, F. Chen, J. Comput. Chem. 33 (2012) 580.

Supporting Information

for

Synthesis and structural characterisation of 1'-(diphenylphosphino)ferrocene-1-phosphonic acid, its ammonium salts and Pd(II) complexes

Filip Horký, Ivana Císařová, Jiří Schulz and Petr Štěpnička*

Department of Inorganic Chemistry, Faculty of Science, Charles University, Hlavova 2030, 128 40 Prague, Czech Republic

Table S1. Selected crystallographic data and structure refinement parameters.

Compound	H_2**L**	**5**	**6**
Formula	$C_{22}H_{20}FeO_3P_2$	$C_{28}H_{32}FeN_2O_3P_2$	$C_{26}H_{31}FeNO_5P_2$
M/g mol^{-1}	450.17	562.34	555.31
Crystal system	monoclinic	triclinic	triclinic
Space group	$P2_1/n$	P-1	P-1
T/K	150(2)	120(2)	150(2)
a/Å	14.9624(6)	8.3083(5)	8.2429(3)
b/Å	5.9603(3)	11.2991(6)	8.8410(3)
c/Å	22.7194(9)	15.1555(8)	20.9101(9)
α/deg	90.00	80.930(2)	88.5080(10)
β/deg	97.5170(10)	81.395(2)	82.0300(10)
γ/deg	90.00	78.525(2)	64.5540(10)
V/Å^3	2008.71(15)	1366.55(13)	1361.76(9)
Z	4	2	2
μ(Mo Kα)/mm^{-1}	0.931	0.701	0.707
F(000)	928	588	580
Diffrns collected	36403	27998	28569
Independent diffrns	4620	6298	6268
Observed diffrns[a]	4204	4798	5584
R_{int}[b]/%	3.09	5.15	2.66
No. of parameters	255	325	316
R[c] obsd diffrns/%	3.21	3.95	2.74
R, wR[c] all data /%	3.64, 7.87	5.22, 14.24	3.27, 7.12
Δρ/e Å^{-3}	0.48, −0,40	1.85, -0.69	0.67, -0.47

[a] Diffractions with $I > 2\sigma(I)$. [b] Definitions: $R_{int} = \Sigma|F_o^2 - F_o^2(\text{mean})|/\Sigma F_o^2$, where $F_o^2(\text{mean})$ denotes the average intensity of symmetry-equivalent diffractions. [c] $R = \Sigma||F_o| - |F_c||/\Sigma|F_o|$, w$R = [\Sigma\{w(F_o^2 - F_c^2)^2\}/\Sigma w(F_o^2)^2]^{½}$.

Table S1 continued

Compound	**7**·3EtOH	**8** (solv.)	**9** (solv.)
Formula	$C_{50}H_{58}Cl_2Fe_2O_9P_4Pd$	$C_{32}H_{33}Cl_2FeNO_3P_2Pd$	$C_{30}H_{28}FeO_3P_2PdS$
M/g mol^{-1}	1215.84	774.68	692.77
Crystal system	triclinic	triclinic	monoclinic
Space group	*P*-1	*P*-1	$P2_1/c$
T/K	150(2)	150(2)	150(2)
a/Å	9.6772(4)	11.5515(5)	17.9423(9)
b/Å	15.9811(7)	15.8140(6)	8.7396(4)
c/Å	17.5576(7)	19.4555(8)	19.3436(10)
α/deg	80.8680(10)	81.9980(10)	90.00
β/deg	79.6250(10)	87.8830(10)	111.257(2)
γ/deg	78.1640(10)	72.5970(10)	90.00
V/Å^3	2593.15(19)	3358.3(2)	2826.9(2)
Z	2	2	4
μ(Mo Kα)/mm^{-1}	1.175	1.254	1.367
F(000)	1244	1568	1400
Diffrns collected	81100	73276	60315
Independent diffrns	11904	15419	6500
Observed diffrns[a]	10701	13674	5675
R_{int}[b]/%	2.47	2.66	2.90
No. of parameters	616	765	344
R[c] obsd diffrns/%	2.13	6.93	2.29
R, wR[c] all data /%	2.53, 5.50	3.33, 7.24	3.04, 5.80
Δρ/e Å^{-3}	0.38, -0.75	0.78, -1.30	0.37, -0.67

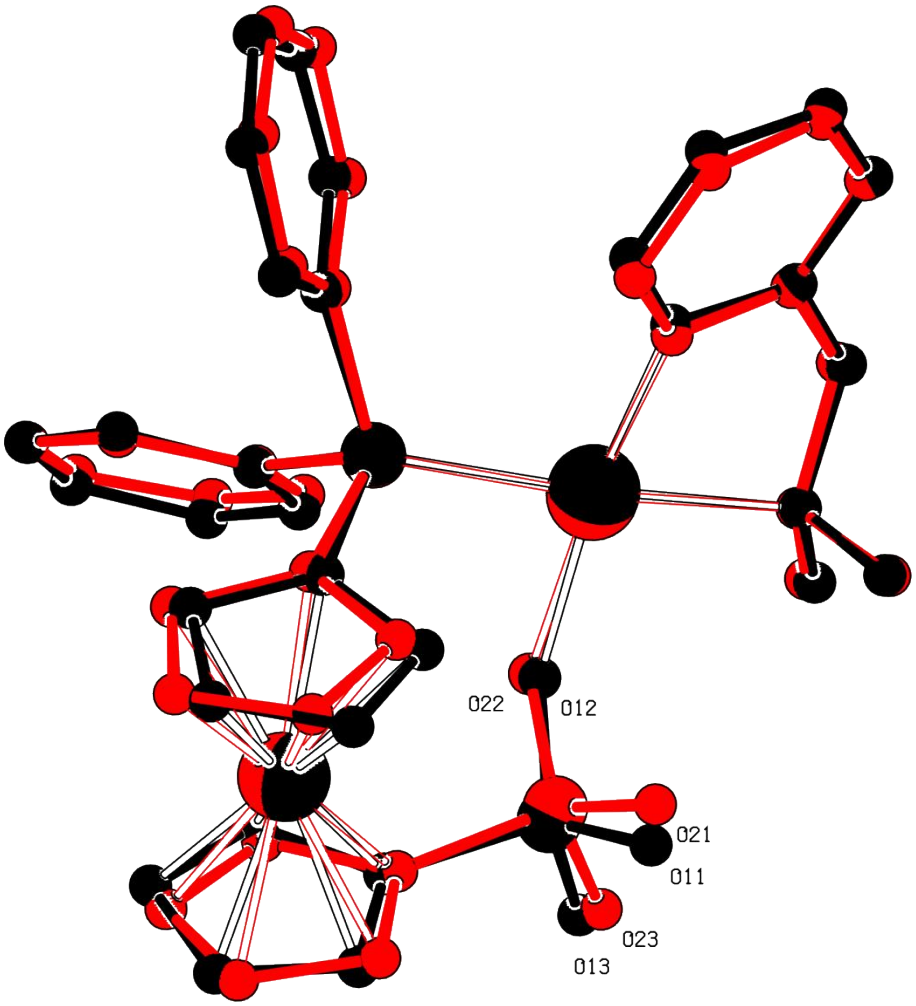

Figure S1. Least-squares overlap of the two independent complex molecules in the crystal structure of compound **8** (molecule 1 in black, molecule 2 in red).